N67-18911

EXP 462

27 May 1966

LUNAR GEOPHYSICAL SURFACE & SUBSURFACE PROBES FOR APOLLO APPLICATIONS PROGRAM

VOLUME I
DETAILED TECHNICAL REPORT

TP-277

Work Performed Under
NASA CONTRACT NO. NAS8-20085

Submitted to
RESEARCH PROJECTS LABORATORY
MARSHALL SPACE FLIGHT CENTER
HUNTSVILLE, ALABAMA

TEXACO EXPERIMENT INCORPORATED
RICHMOND, VIRGINIA

FOREWORD

The final report for a study of Lunar Geophysical Surface and Subsurface Probes for Apollo Applications Program, NASA Contract NAS8-20085, was prepared and submitted by Texaco Experiment Incorporated in three volumes:

Volume I - Detailed Technical Report
Volume II - Summary Technical Report
Volume III - Developmental and Unit Cost Estimates

The study was organized on a project basis. The following were major contributors in the various measurement areas:

Program Manager	R. H. Clinard, Jr.
Nuclear Measurements	R. H. Clinard, Jr. Dr. G. H. Miller
Thermal Measurements	C. M. Slough Dr. P. L. Goodfriend I. R. King W. V. Evans, Jr.
Seismic, Magnetic and Gravity Measurements	R. W. Aiken
Electrical Measurements	R. E. Canup C. L. Epley
Miscellaneous Measurements	N. E. Flournoy C. M. Slough Dr. P. L. Goodfriend I. R. King
Resource Planning	J. L. Peramplе
Mechanical Design	N. E. Flournoy
Technical Editing	J. C. Kennedy

R. H. Clinard, Jr.
Program Manager

Approved:

W. N. Gilmer
Director of Engineering

ABSTRACT

A study has been carried out to determine the optimum integrated instrument probes to be used for manned lunar exploration with the Apollo Applications Program. The contract was awarded on 28 June 1965, and expired on 27 May 1966. This, the final Detailed Technical Report, presents the findings of the study.

A Lunar Probes System is recommended consisting of: an Optimum Subsurface Probe, a Subsurface Neutron-Gamma Probe, a Subsurface Television Probe, and Integrated Surface Probe, a Supporting Electronics Package, a Deployment and Cable Assembly, and an Acoustic Source Holder. This system is described in detail with the justifications, instruments characteristics, and operations requirement of the selected experiments given. Information is also included on experiments considered in the study, which do not appear in the recommended system.

Non-functional mockup hardware of the recommended probes was constructed and submitted to NASA for use in system integration studies and time-and-motion-study testing. Developmental and unit cost estimates for follow-on equipment and other resources planning information is included in Volume III. Volume II contains the Summary Technical Report.

CONTENTS

		Page
	FOREWORD	i
	ABSTRACT	iii
I.	INTRODUCTION	1
	A. Apollo Applications Program Mission	1
	B. Study Objectives	2
	C. Guidelines and Restraints	3
	D. Study Philosophy	6
	E. Study Approach	6
	F. Study Organization	9
	G. Summary of Findings	10
II.	RECOMMENDED PROBE SYSTEM	13
	A. System Description	13
	B. Optimum Subsurface Probe	16
	1. Probe Configuration	16
	2. Probe Description	16
	3. Mechanical Design	21
	4. Measurement Discussion	22
	5. Supporting Surface Measurements	23
	C. Subsurface Neutron-Gamma Probe	24
	D. Subsurface Television Probe	24
	E. Integrated Surface Probe	28
	1. Probe Description	28
	2. Measurement Discussion	31
	F. Supporting Electronics Package	31
	G. Subsurface Probe Deployment	31
	H. Experiment Scheduling, Sequencing, and Switching	34
	1. Experiment Scheduling and Sequencing	35
	2. Experiment Switching	40
III.	EXPERIMENT DESCRIPTIONS	45
	A. Recommended Experiments	45
	1. Nuclear Measurements	45
	a. Natural Radioactivity (Natural and Spectral Gamma)	45
	b. Bulk Density (Gamma-Gamma Technique)	56
	c. Neutron Irradiation Experiments (Neutron-Gamma)	65
	2. Thermal Measurements	75
	a. Temperature	76
	b. Thermal Diffusivity	90
	3. Seismic Measurements	103
	4. Electrical Measurements	116
	5. Atmospheric Pressure and Compositional Analysis	126

	Page
6. Borehole Television System	135
7. Centralizer - Caliper Experiment	145
B. Other Possible Experiments	150
1. Neutron-Neutron (Hydrogen Log)	150
2. Resistivity	151
3. Formation Tester	158
4. Total Pressure Gage	164
C. Rejected Experiments	171
1. Nuclear Experiments	171
2. Thermal Experiments	174
3. Gravity and Magnetic Experiments	177
4. Electrical Experiments	180
5. Soil Mechanics and Soil Properties Experiments	181
6. Compositional Experiments	181
IV. ENVIRONMENTAL CONSIDERATIONS	183
A. Thermal/Meteoroid Shield Design	183
B. Thermal Analysis - Probe in Borehole	189
V. EXPERIMENT RATING TECHNIQUE	193
REFERENCES	200
BIBLIOGRAPHY	201

APPENDIXES

I Lunar Experiment List
II Temperature Accuracy and Probe Requirements
III A Thermal-Meteoroid Shield Design Study for the Lunar Thermal Probe
IV Analysis of Heat Transfer Between Subsurface Probe and Borehole Wall
V Experiment Scheduling and Sequencing Plans and Methodology
VI Control System Optimization and Preliminary Panel Design for Subsurface Probe
VII Contact Temperature Measurements
VIII Neutron-Gamma Experiment Results
IX Specification Sheets
Hall-Sears Geophone
Line Heater
EAI Series 210 Residual Gas Analyzer
STEM Device

FIGURES

		Page
1.	Lunar Probes' Mock-up Hardware	11
2.	Deployed Lunar Probe System	14
3.	Optimum Subsurface Probe	17
4.	Subsurface Neutron-Gamma Probe	25
5.	Subsurface Television Probe	27
6.	Integrated Surface Probe	29
7.	STEM Deployment Device	33
8.	Switch Panel Design	44
9.	Switching Diagram - 79-min Optimum Plan	44
10.	Efficiency and Photofraction of a Sodium-Iodide Crystal	50
11.	Block Diagram - Natural- and Spectral-Gamma Systems	51
12.	Subassembly - Scintillation Detector (Phoswich Arrangement)	53
13.	Response Curve - Gamma-Gamma (Density) Instrument	60
14.	Block Diagram - Gamma-Gamma (Density) System	61
15.	Subassembly - Gamma-Gamma (Density) System	62
16.	Timing of Neutron Activation Events	69
17.	Block Diagram - Fast-Neutron-Gamma System	71
18.	Subassembly - Interferometer Spectrometer	78
19.	Block Diagram - Interferometer Spectrometer	80
20.	Effects of Thermal Conductivity on Contact-Temperature Measurement Error	83
21.	Block Diagram - Contact Temperature System	84
22.	Subassembly - Contact Temperature Sensor	86
23.	Subassembly - Thermal Diffusivity Instrument	93

		Page
24.	Response Curve - Subsurface Thermal Diffusivity Instrument	94
25.	Block Diagram - Subsurface Thermal Diffusivity Instrument	95
26.	Block Diagram - Surface Thermal Diffusivity Instrument	97
27.	Subsurface Acoustic Velocity Techniques	105
28.	Block Diagram - Acoustic Velocity Experiment	109
29.	Subassembly - Subsurface Geophone and Actuator	110
30.	Seismic Source Holder	112
31.	Shot Pattern for Seismic Experiments	113
32.	Response Curve - Surveyor-Type Magnetic Susceptibility Instrument	119
33.	Block Diagram - Magnetic Susceptibility/Induction Log Experiment	121
34.	Subassembly - Magnetic Susceptibility/Induction Log Instrument	122
35.	Operational Schematic - RF and Quadrupole Mass Spectrometer	129
36.	Block Diagram - Quadrupole Mass Spectrometer	131
37.	Subassembly - Quadrupole Mass Spectrometer Sensor	133
38.	Subsurface Television Probe System Link	137
39.	Block Diagram - Subsurface Television System	140
40.	Subassembly - Centralizer-Caliper	146
41.	Block Diagram - Centralizer-Caliper	148
42.	Block Diagram - Neutron-Neutron System	152
43.	Subassembly - Neutron-Neutron System	153
44.	Block Diagram - Scratcher-Electrode Resistivity Experiment	155
45.	Block Diagram - Q Resistivity Experiment	156

		Page
46.	Subassembly - Change-of-Q Coil Section	157
47.	Formation Tester Configurations	159
48.	Experiment Geometry - Formation Tester	161
49.	Response Curves - Formation Tester	162
50.	Block Diagram - Formation Tester	165
51.	Subassembly - Atmospheric Pressure Gage	168
52.	Block Diagram - Atmospheric Pressure Gage	169
53.	Thermal/Meteoroid Shield Design	186
54.	Theoretical Temperature Variations - Shielded Probe	187
55.	Probe Temperature vs. Time - Lunar Noon	190
56.	Probe Temperature vs. Time - Lunar Night	191
57.	Probe Effects on Borehole Temperature	192

TABLES

		Page
I.	Optimum Subsurface Probe Complement	19
II.	Experiment Characteristics	35
III.	Experiment Scheduling Plans - 10-Ft Holes	38
IV.	Summary of Measurements In 10-Ft Holes	39
V.	Experiment Scheduling Plans - 100-Ft Hole	41
VI.	Summary Of Measurements In 100-Ft Hole	42
VII.	Experiment Switching Requirements	43
VIII.	Thorium, Uranium, and Potassium In Igneous Rocks	47
IX.	Natural Radioactivity Experiment Characteristics	55
X.	Bulk Density Experiment Characteristics	63
XI.	Neutron Cross Sections of Lunar Elements	66
XII.	Elements Detectable By Neutron-Gamma Techniques	70
XIII.	Neutron-Gamma Experiment Characteristics	74
XIV.	Interferometer Spectrometer Characteristics	88
XV.	Contact Temperature Experiment Characteristics	89
XVI.	Subsurface Thermal Diffusivity Characteristics	101
XVII.	Surface Thermal Diffusivity Instrument Characteristics	102
XVIII.	Acoustic Velocity Experiment Characteristics	115
XIX.	Subsurface Magnetic Susceptibility/Induction Log Characteristics	124
XX.	Surface Magnetic Susceptibility/Induction Log Characteristics	125

TABLES (Cont.)

		Page
XXI.	Quadrupole Mass Spectrometer Characteristics	134
XXII.	Subsurface Television Characteristics	144
XXIII.	Centralizer - Caliper Experiment Characteristics	149
XXIV.	Probe Temperature Limits	188
XXV.	Meteoroid Puncture Probability	188
XXVI.	Final Experiment Ratings	199

I. INTRODUCTION

A. APOLLO APPLICATIONS PROGRAM MISSION

The proposed Apollo Applications Program (AAP) (formerly designated Apollo Extension System) concept is an efficient and effective means for carrying out scientific exploration of the moon. The AAP will extend the capabilities of the Apollo system by allowing for longer stay times on the moon and by providing mobility aids to increase the range and scope of the scientific surveys.

The AAP concept includes earth-and-lunar-orbital, and lunar-surface missions. However, for the purpose of this study we will restrict reference to the AAP as being those missions which can be carried out on the lunar surface by two astronaut-scientists in a nominal 14-day period. The AAP mission will consist of two Saturn V launches. The first launch will be an unmanned logistics type payload utilizing a modified LEM (LEM/Shelter). This payload will include an environmental shelter, locomotion aids such as a Lunar Surface Survey Module (LSSM), and the scientific equipment. The second launch will be that of a manned LEM (LEM/Taxi). The LEM/Taxi may not carry any scientific equipment, but will be capable of returning lunar samples, photographs, and other scientific data back to earth.

Experiments associated with the AAP mission will normally fall into one of three general categories:

1. Manned geological - and geophysical - reconnaissance investigations made on lunar surface traverses requiring mobile equipment.

2. Scientific equipment that will be contained within the LEM/Shelter or will be directly dependent on this payload for support.

3. An automatic package of scientific apparatus to be deployed by the astronauts and then remain as a permanently emplaced scientific station.

This report concerns the study of Lunar Surface and Subsurface Probes which will constitute a portion of the experiments in category 1 above. These surface and subsurface probes along with their supporting equipment make up the Lunar Probe System.

B. STUDY OBJECTIVES

The general purpose of this study may best be described by quoting from the statement of work. "The purpose of this investigation is to perform a preliminary design study of a family of instruments for observing specific properties of lunar surface and subsurface materials. This investigation will provide nonfunctional mock-ups of the scientific instruments to be used for future design integration testing." And more specifically the study is..."to provide engineering estimates of surface and subsurface logging equipment for incorporation into the overall lunar surface payload design and feasibility studies."

Expressed requirements, pertaining to the rather general objectives just stated,are given in the tasks outlined below. Provide:

1. A survey-in-depth of probe experiments which might be performed, including the basic theory and proposed operational scheme, with a listing and functional description of the instruments required and their interrelationships.

2. A number of alternate concepts for the lunar geophysical probes, including for each a listing of experiments and the various sensors that may be complexed into a single probe.

3. A <u>single</u>, <u>integrated</u>, <u>multiple</u> experiment probe which is considered optimum for the intended use.

4. An individual, comprehensive summary statement explaining why experiments which were not included in the recommended optimum probe (3 above) were excluded.

5. A preliminary design of each of the instruments recommended.

6. A preliminary systems design to integrate each of the individual instruments into a complete complex.

7. Development time and cost estimates.

8. Nonfunctional, mock-up hardware.

These specific requirements were further qualified according to the guidelines and restraints which are given in the next section.

C. GUIDELINES AND RESTRAINTS

The Lunar Probe System Study has been conducted within the general guidelines and restraints indicated below. These conditions were, for the most part, specifically delineated in the contract statement of work and are lifted from that document. Others evolved during pre-planning and other conferences with the sponsor.

1. Individual experiments are to be considered for deployment in:

   a. A Lunar Subsurface Geophysical Probe.

   b. A Lunar Surface Geophysical Probe.

It is intended that such surface measurements as may be made will be for the purpose of increasing the usefulness of the subsurface probe measurements and will exclude such measurements as extensive seismic surveys, gravity surveys, magnetometer surveys, and related effort.

2. Typical experiments to be considered for probe integration are included in the following groupings:

   a. Radioactivity (alpha, beta, and gamma-ray intensities).

   b. Thermal (infrared radiation, thermal conductivity and diffusivity, and temperature).

   c. Acoustic (surface and subsurface velocity, and wave transmission characteristics).

   d. Electrical (impedance, permeability, relative permittivity, resistance, and telluric currents).

   e. Physical characteristics (density) (soil properties and soil mechanics experiments are to be excluded).

   f. Scanning spectrometers.

Note: This experiment list was to be considered as exemplary. Experiments could be added or deleted should it appear necessary or desirable.

3. For the purpose of this study, it can be assumed that a small, lunar-surface vehicle (LSSM) will be available to support the geological field studies. This vehicle

will probably be designed to house the power supply, data conditioning and handling equipment, and telemetry systems to support the surface and subsurface probe experiments. However, it shall be assumed that all equipment necessary for operation of the probes will be in self-contained, complete packages which will be transported by the small vehicle, but which can be deployed and used in locations not directly accessible to the surface vehicle.

4. The subsurface probe must be capable of being inserted in a two-inch (51-mm) hole. The small vehicle will carry a 10-ft (3-m) core drill, and a 100-ft (30-m) core drill operation will be conducted at the LEM/Shelter site. The subsurface probe will be employed to log both size holes.

5. The surface geophysical probe must measure the required parameters on the lunar surface or, if practical, from the small roving vehicle while the vehicle is in motion. The surface instruments and principles may be the same as for the downhole units if feasible; otherwise, different techniques and configurations may be used.

6. A package may contain one or a combination of related instruments, with separate packages as necessary for others. It is desirable to contain as many experiments as possible in a single probe unit, but not if the sensors or experiments interact with each other and limit experimental accuracy.

7. Cables and mechanisms for the deployment and operation of the probes will be considered within the scope of this contract.

8. Weight and size considerations are extremely important in the design of the surface and subsurface probes (no restrictions were placed on size and weight nor on permissible power consumption).

9. The resulting instruments must be rugged enough to withstand Apollo launch, transit, landing dynamic loads and rough surface handling.

10. The acoustic velocity measurements will require an acoustic source on the lunar surface. Means of

implanting the source in addition to drilling of a shot charge hole should be investigated.

11. The "International System of Units" shall be used in all final reports and at presentations.

12. As a restraint, contracts with NASA members of the Apollo Science Planning Committees shall be prohibited. Information and indirect contacts concerning instruments under their cognizance shall be obtained from the MSFC Technical Supervisor.

13. Maximum use of applicable existing hardware and designs will be made, such as instrumentation developed for unmanned exploration (Ranger, Surveyor, etc.).

14. It is not regarded that telemetering equipment is part of the scope of this study, except that signal conditioning equipment may be required. Specifications such as number of channels and bandwidths that may be required of the telemetering equipment are, however, within the scope of this study.

15. Mock-up hardware shall, so far as possible, represent the true external configuration, mass, volume, and operating characteristics, in order that system design and integration testing may be realistically manipulated.

16. The design of surface and subsurface probes and supporting equipment shall recognize the limitation imposed on the astronaut by his spacesuit.

17. Justification for inclusion of experiments in the integrated surface and subsurface probes shall be based on the following criteria (shown in decreasing order of importance):

    a. The measurement will contribute to a better understanding of the moon's composition or of the age, origin, or history of the earth-moon system.

    b. The measurement will assist in sample selection.

    c. The measurement will provide data concerning the engineering aspects of lunar basing.

18. Recommendations of the NASA 1965 Summer Conference on Lunar Exploration and Science held in July 1965 at

Falmouth, Massachusetts, should be given thorough consideration.

D. STUDY PHILOSOPHY

The basic philosophy used in this study of surface and subsurface probes gave major emphasis to those scientific measurements which would be most useful and informative when made below the lunar surface. The two most important ways in which the AAP can extend the exploration capability of Apollo are: (1) through the ability to carry out more lengthy investigations of a much greater area of the moon, and (2) by providing means for sampling and measuring the lunar, subsurface, physical parameters and environment.

Accordingly, experiments were considered first for their usefulness and suitability for exploring the lunar subsurface, and then for their desirability to be used also for surface measurements. Emphasis was given those experiments which measure, in situ, parameters likely to vary when made on samples returned to the earth. In certain cases it was found that, because of the geometry of the subsurface equipment, the same device could not readily be used on the surface. When it could be shown that the surface measurement was important in terms of both its scientific merit and as support for the subsurface measurement, a different geometry was recommended for the surface instrument.

A third type of experiment has also been briefly mentioned in this study. Under certain circumstances, equipment necessary for performing one experiment (such as deployment) can also be used as part of a second experiment. When little modification to the equipment is required, and additional instrumentation is minor, this experiment group is also discussed. These are referred to as bonus measurements. The three categories, then, in decreasing order of importance, are: (1) subsurface measurements, (2) surface measurements, and (3) bonus measurements.

E. STUDY APPROACH

In order to achieve the objective of the Lunar Surface and Subsurface Probes' study, previously outlined, the overall program was divided into a group of definable tasks. These tasks are such that a definite sequence of performance is required. The tasks, in their proper sequence, are:

1. To make a detailed survey of all experiments which might provide useful information about the composition or environment of the moon, or aid in determining the age, origin, or history of the earth-moon system. Also to

be considered are experiments which assist in the sample selection process and/or are useful in determining information about lunar materials, which information is necessary to the construction and support of a lunar base.

2. To determine, from the points of view of justification and feasibility of the individual measurements, those experiments from the above survey which best fit the proposed concept of the AAP and the Study Philosophy.

3. Then to provide an instrument description and operational procedure outline for those justified and feasible experiments, which will promote a complete understanding of the instrument specification and how it will be used in lunar exploration.

4. To recommend the optimum probe configuration (or probes, if necessary, from which a choice may be made) to best accomplish the AAP.

5. To make a detailed design of the probes and accompanying electronics, deployment devices, and instrumentation from which the various units can be developed.

6. To supply hardware mock-ups for astronaut time and motion studies and system-integration tests.

The study contract was divided by the sponsor such that Tasks 1 through 4 above were designated as Phase I, with the remaining two tasks making up Phase II. Phase I was originally scheduled for completion in 4 months but this was amended by mutual consent to 5-1/2 months. The total effort was completed in 11 months from date of contract award.

Phase I Effort

The approach in the Phase I Study was to initially consider the various possible experiments from the experiment point of view rather than from the mission point of view. This was done in order that experiment feasibility determinations would not be overly influenced by mission constraints, but would instead be based on the justification for the measurement per se.

The procedure then for the Phase I effort was to survey the instrumentation field and prepare as complete a listing as possible of candidate experiments (see Appendix I for this listing). The justification, both scientific and engineering, was then outlined for each experiment included in the list. This listing of

candidate experiments -- and their justification -- was then closely examined, and those experiments not suited to the probe concept (discussed under "Study Philosophy" above) were discarded and the remaining experiments considered as feasible.

The next step was to make a thorough analysis of the instrument requirements and operational procedures for the feasible experiments. Preliminary design information was developed to determine size, weight, and power requirements.

With the foregoing information prepared, it was then necessary to determine the optimum group of experiments from the feasible one. A ranking technique was developed of weighted questions to be considered concerning each instrument. Then each experiment was subjected to an "examination" from which an overall "worth" was determined. When considering candidate experiments for inclusion in the subsurface probe, primary consideration was given to their worth value and instrument length. Length was selected as the criteria because the other constraints such as weight and power were considered as closely related to length. Then, a figure of merit would be the experiments' W/L ratio (worth-to-length ratio). The optimum probe was then assembled of those experiments having the highest W/L ratios. The surface probe was determined primarily on the basis of experiment worth. To complement the Optimum Subsurface Probe and the Integrated Surface Probe, several supporting probes were also recommended.

These recommendations, along with the justification and instrument description material just discussed, made up the Phase I Interim Report which was submitted to NASA. This report was to be used by NASA as a basis for directing the completion of the study which was the Phase II effort discussed in the next section.

Phase II Effort

NASA chose to have all probes recommended in the Phase I effort carried through the detailed design work of Phase II. This effort included the examination of each experiment, as proposed for probe use, to determine probable characteristics, such as operating range and accuracy, size, weight, power requirements, etc. It also included description of setup, activiation, and operational requirements, telemetry requirements, thermal and other environmental control. From these descriptions of the basic experiment subsystem, a detailed mechanical design of the probes themselves evolved. The complete probe system was also analyzed to determine its capabilities. Experiment scheduling and sequencing plans were formulated to allow optimum utilization of the time available at the different drill holes. Switching plans were drawn up and a possible control panel designed to optimize utilization of the

astronaut's time and capabilities, remembering the limitations imposed by his spacesuit.

A Resources Plan, including time and cost estimates for follow-on programs, was submitted. This plan also included information on research and technology implications, delineating those areas wherein further development would be desirable based on the findings of this study.

And lastly, mock-up hardware of the Lunar Surface and Subsurface Probes was fabricated. This equipment was so constructed that it represents, to the best degree possible, the true size, earth weight, and center-of-gravity of the preliminary probe designs. It includes all devices which require manipulation by the astronaut.

Accomplishment of Phase II, including submission of all reports, required 5-1/2 months.

F. STUDY ORGANIZATION

The Study of Lunar Surface and Subsurface Probes for the Apollo Applications Program was carried out at Texaco Experiment Incorporated, Richmond, Virginia. The bulk of the work was centered within the Space and Instrumentation Group, but major contributions were made by members of other groups throughout the company; particularly the Chemistry and Physics Group. Supporting geophysical consultation was provided by Dr. Alex McKay of the Research and Technical Department of Texaco, Inc.

Subcontractors

In addition to the above groups, two subcontractors have contributed. Block Engineering Incorporated of Cambridge, Massachusetts, provided an analysis of non-contact temperature techniques and instrumentation, and preliminary design studies of an improved flight-weight interferometer spectrometer. A report covering this work may be found in Appendix II.

A second subcontractor has been the Northrop Space Laboratories, Huntsville Department. They have contributed in the areas of thermal analysis and control, experiment programming, and human factors considerations. They have also provided assistance in the preparation of the Resources Plan. Reports covering their specific task assignments are included in Appendixes III, IV, V, and VI.

Acknowledgments

Considerable assistance has been provided by several industrial and academic organizations. These were:

The Lawrence Radiation Laboratory
University of California
Livermore, California

Electronics Associates, Incorporated
Scientific Instruments Division
Palo Alto, California

Radio Corporation of America
Asto-Electronics Division
Princeton, New Jersey

Their cooperation and assistance is greatly appreciated.

G. SUMMARY OF FINDINGS

The study of surface and subsurface probes has resulted in a recommended Lunar Probes System. This system consists of an Optimum Subsurface Probe, a Subsurface Neutron-Gamma Probe, a Subsurface Television Probe, and an Integrated Surface Probe. These probes are supported by a surface electronics and control package, a deployment mechanism and cable assembly, and a seismic source holder. Figure 1 shows a photograph of the mock-up hardware representing these probes. All subsurface probes are capable of being deployed from the LSSM and operated in a 2-in. (51-mm) hole. Certain measurements can be made using the subsurface probes while attached to the LSSM either in the stationary or roving mode. Measurements may also be made with the subsurface probes deployed on the lunar surface. The surface probe is intended to be removed from the LSSM and placed on the surface. The total system has an estimated combined weight of 90.5 lbs. and a volume of 3.15 ft^3. (See page 15 for weight and volume breakdowns.)

Measurements which are possible using the Lunar Probes System include the following:

SURFACE

1. Non-Contact Temperature
2. Infrared Spectral Analysis
3. Contact Temperature
4. Thermal Diffusivity
5. Magnetic Susceptibility
6. Formation Electrical Conductivity

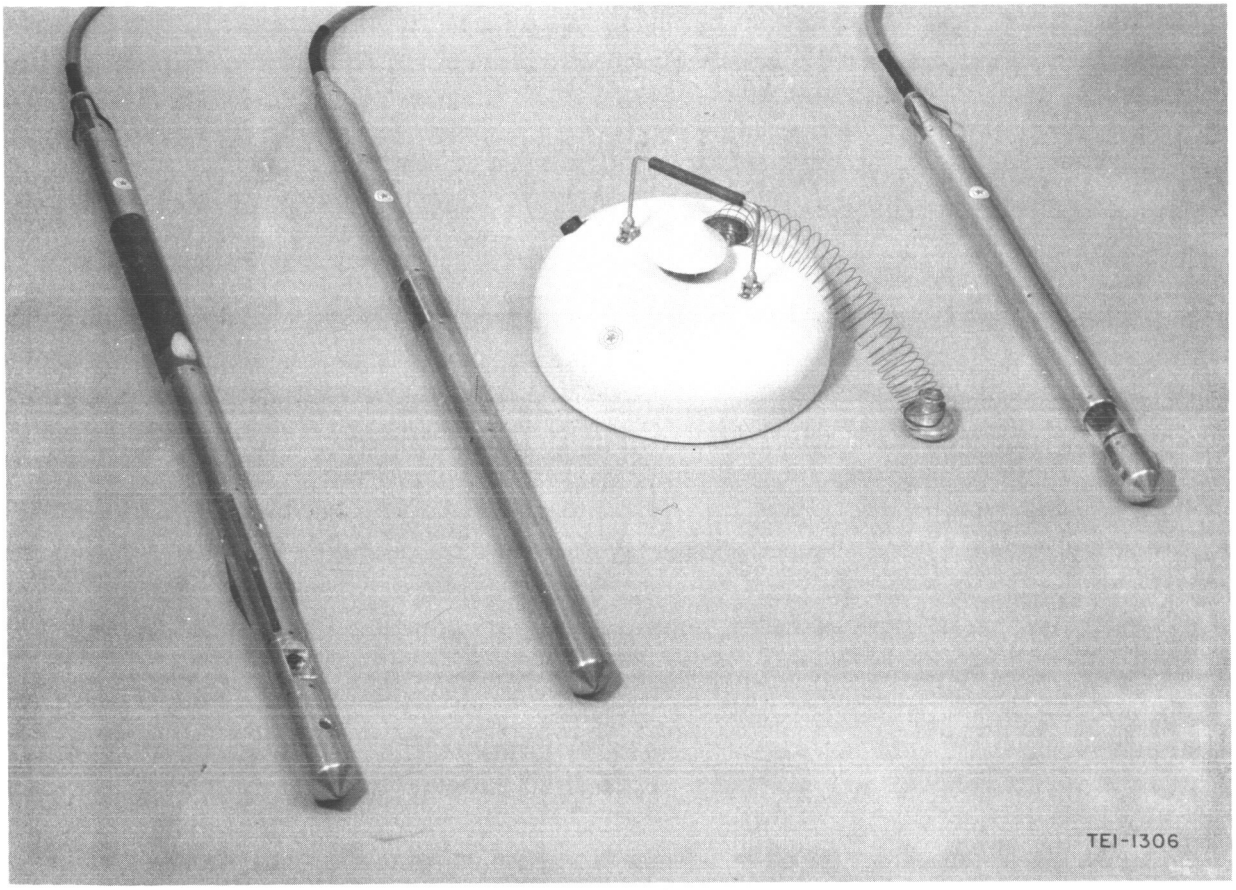

Fig. 1 Lunar Probes' Mock-up Hardware

7. Short-Spacing Acoustic Velocity

8. Natural Gamma Radioactivity

9. Gamma Spectral Analysis

10. Elemental Analysis Using Neutron-Gamma Techniques

11. Gas Analysis

SUBSURFACE

1. Non-Contact Temperature

2. Infrared Spectral Analysis

3. Thermal Diffusivity

4. Contact Temperature

5. Borehole Caliper

6. Gas Analysis

7. Natural Gamma Radioactivity

8. Gamma Spectral Analysis

9. Formation Bulk Density

10. Magnetic Susceptibility

11. Formation Electrical Conductivity

12. Integrated Acoustic Velocity

13. Elemental Analysis Using Neutron-Gamma Techniques

14. Borehole Television Surveying

II. RECOMMENDED PROBE SYSTEM

A. SYSTEM DESCRIPTION

The results of this study indicate that the objectives of surface and subsurface measurements via probe devices can best be met by an instrument complex herein designated the Lunar Probes System. This system consists of an Optimum Subsurface Probe, a Subsurface Neutron-Gamma Probe, a Subsurface Television Probe, an Integrated Surface Probe, a Supporting Electronics Package, and a Deployment and Cable Assembly. Figure 1, page 11, is a photograph of the mock-ups of the surface and subsurface probes making up The Lunar Probes System. The probe on the extreme left is the Optimum Subsurface Probe. It contains instruments to measure temperature, by contact and non-contact means, thermal diffusivity, borehole diameter, residual-gas constituents, formation bulk density, natural and spectral gamma radioactivity, magnetic susceptibility, formation conductivity, and acoustic velocity. The second instrument is the Subsurface Neutron-Gamma Probe. It is used to perform elemental analysis of the lunar subsurface via the borehole. The central instrument is the Integrated Surface Probe. It includes devices to measure thermal conductivity, contact and non-contact temperature, magnetic susceptibility/electrical conductivity, and acoustic velocity. And finally, on the extreme right, is the Subsurface Television Probe. This instrument is to be used to obtain pictures of the borehole wall which will be relayed back to earth for analysis.

The total capability of the system, when utilized to the maximum extent, can be seen by the listing of experiments which follow. These include subsurface measurements by the borehole devices and surface measurements using both the subsurface probes deployed on the surface and the surface probe.

POSSIBLE SUBSURFACE MEASUREMENTS

1. Non-Contact Temperature
2. Infrared Spectral Analysis
3. Thermal Diffusivity
4. Contact Temperature
5. Borehole Caliper
6. Gas Analysis
7. Natural Gamma Radioactivity
8. Gamma Spectral Analysis
9. Formation Bulk Density
10. Magnetic Susceptibility
11. Formation Electrical Conductivity
12. Integrated Acoustic Velocity
13. Elemental Analysis Using Neutron-Gamma Techniques
14. Borehole Television Surveying.

POSSIBLE SURFACE MEASUREMENTS

1. Non-Contact Temperature
2. Infrared Spectral Analysis
3. Contact Temperature
4. Thermal Diffusivity
5. Magnetic Susceptibility
6. Formation Electrical Conductivity
7. Short-Spacing Acoustic Velocity
8. Natural Gamma Radioactivity
9. Gamma Spectral Analysis
10. Elemental Analysis Using Neutron-Gamma Techniques
11. Gas Analysis

Figure 2 is an artist's sketch of the probe system deployed from the LSSM. It depicts the Storable Tubular Extendable Member (STEM) Deployment Device attached to the roving vehicle and the Optimum Subsurface Probe being prepared for insertion in the borehole. The Integrated Surface Probe has been placed on the lunar surface but the other probe devices are still mounted to the LSSM. It is seen that the Supporting Electronics Package is capable of handling two or more probes at the same time - being fitted with several cable connectors. Multiple cables are also provided.

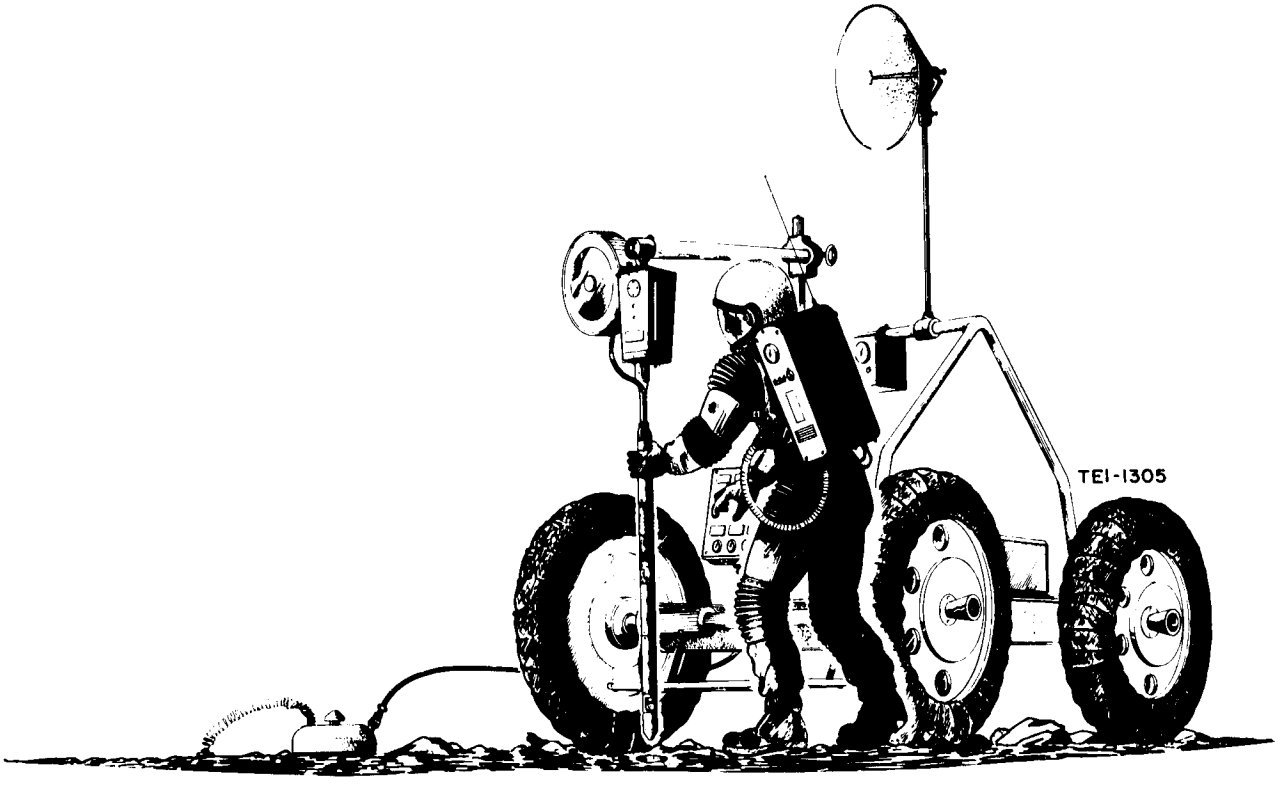

Fig. 2 Deployed Lunar Probe System

The input/output interfaces for the probe systems are defined, such that input power is received from an RTG-type power supply, attached to the LSSM, and properly conditioned output signals are fed to a telemetry system also attached to the roving vehicle. Power conditioning equipment is included in the Supporting Electronics Package to provide the needed input for each experiment.

Characteristics of the complete system are as follows:

Volume: 3.15 ft^3

Weight: 90.5 lbs.

Power Requirements: Maximum (under any operating condition) - 129.6 watts.

Mean (average system operation) - 28.8 watts.

The contributions of the various subsystems to these weight and volume estimates are shown below:

Subsystem	Weight (lbs.)	Volume ($in.^3$)
Optimum Subsurface Probe	10.90	100
Subsurface Neutron-Gamma Probe	8.67	93
Subsurface Television Probe	7.04	61
Integrated Surface Probe	5.35	500
Supporting Electronics Package	17.90	2760
(Pulse Height Analyzer)	4.00	1000
Deployment and Cable Assembly		
(Deployment Assembly)	8.00	180
(Cable - 120 ft., 2 ea. 20 ft.)	28.00	700
Seismic Source Holder	0.63	31
Total	90.49 lbs.	5425 $in.^3$
		(3.15 $ft.^3$)

B. OPTIMUM SUBSURFACE PROBE

1. Probe Configuration

The integrated subsurface probe, shown in Figure 3, is considered to contain the optimum combination of experiments for the AAP. The probe has an outside diameter of 1.75 in., with the centralizer springs compressed, an overall length of 44.2 in., and a weight, without cable, of 10.90 lbs. Total instantaneous required power is 134.1 watts, 6 watts of which is dissipated in the probe. The operating temperature range is 218° to 373°K.

Inclusion of experiments in the probe complement was based on the worth-to-length ratio determined from the rating test discussed in Section V, and a consensus of the study group. Experiments making up the optimum probe and the chargeable lengths and weights for each are shown in Table I.

2. Probe Description

At the lower end of the probe, Figure 3, is the non-contact temperature instrument [1], an interferometer-spectrometer (I.S.). This instrument will be used to determine borehole temperature by analysis of the emitted infrared spectra. It will also be used in the search for water vapor by observation of the absorption band in the 5-to-7-micron range.

A thermal-diffusivity instrument [2] is located directly above the interferometer-spectrometer. This instrument consists of: a heat source and reflector used to supply radiant energy to the formation; a radiation sensor, which is a forward-biased gallium-arsenide diode located at the focal point of a section of a parabolic mirror; and a second radiation sensor directed to the opposite wall and used to provide correlative data and information on surface conductance. Windows, transparent to infrared, cover the three devices. These windows protect the sensitive elements from dust and the like.

The next section houses a caliper-centralizer device [3] to provide centering of the probe in the hole during each of the measurements and to provide borehole gage data. Borehole diameter is measured using a linear-displacement potentiometer coupled to the centralizing springs. The spring assemblies are also used to house the contact-temperature sensors [4] and force them against the formation.

Above this is a mass spectrometer sensor [5] of the quadrupole type. It will be used to detect formation outgassing and to

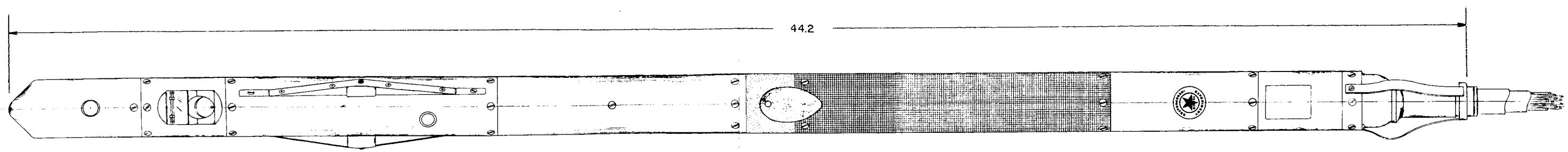

① INTERFEROMETER SPECTROMETER SENSOR ASS'Y
② THERMAL DIFFUSIVITY ASS'Y
③ CALIPER-CENTRALIZER ASS'Y
④ CONTACT TEMPERATURE SENSOR ASS'Y
⑤ MASS SPECTROMETER SENSOR ASS'Y
⑥ COLLIMATOR-SOURCE SHIELD ASS'Y
⑦ MAGNETIC SUSCEPTIBILITY/INDUCTION LOG ASS'Y
⑧ SCINTILLATION DETECTOR
⑨ ACOUSTIC SENSOR ASS'Y
⑩ FLEX JOINT ASS'Y
⑪ DEPLOMENT BOOM
⑫ ELECTRICAL CABLE

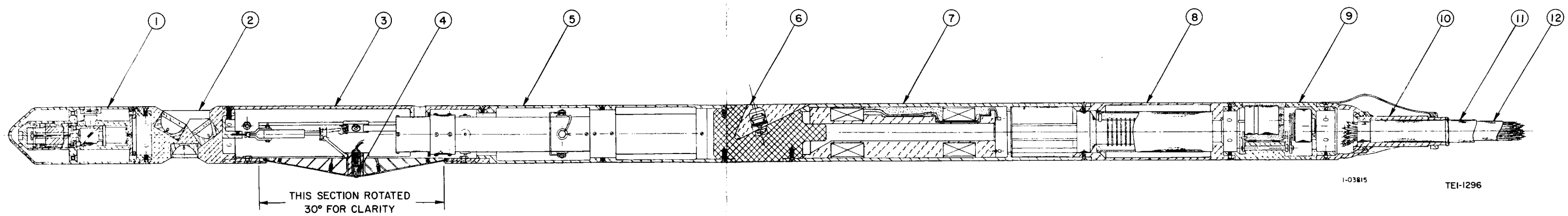

Fig. 3 Optimum Subsurface Probe

TABLE I

OPTIMUM SUBSURFACE PROBE COMPLEMENT

Experiment	Length (in.)	Weight (lbs.)
Non-Contact Temperature Instrument (Interferometer Spectrometer)	4.0	0.70
Thermal-Diffusivity Instrument	2.5	0.35
Caliper-Centralizer	4.7	0.80
Contact-Temperature Instrument	0.5*	0.10
Mass Spectrometer	9.8	1.50
Bulk Density Instrument	7.0**	4.25***
Magnetic Susceptibility/Induction Log	5.5	1.50
Natural And/Or Spectral Gamma Detector	3.5**	0.60***
Acoustic Velocity Detector	3.0	0.40
Flexure Joint	3.7	0.25
Internal Cabling	-	0.45
Total	44.2 in.	10.90 lbs.

Notes:

* The overall length of the caliper-centralizer is 5.2 in., since the contact temperature sensor is located on the contact arms, it is charged with 0.5 in.

** The density and natural/spectral gamma experiments share the same scintillation detector which is 7.0-in. long. Each experiment is charged 3.5 in.

*** The total weight of the scintillation detector is 1.20 lbs. The density and natural/spectral gamma experiments are each charged 0.60 lbs.

identify the constituent gases. Of particular interest will be the search for water vapor. The instrument can also be used to provide an indication of total atmospheric pressure if compared and calibrated against any surface pressure gage.

The gamma-ray source holder and collimator [6] of the density instrument is located in the next section. This section, fabricated of a tungsten alloy (Mallory 1000), is used to properly direct gamma rays into the borehole formation so that they may be detected by the scintillation counter [8]. The collimator plug is designed so that the source capsule can be easily installed in the instrument, by the astronaut, when the density measurement is to be made. The capsule is removed at other times so as not to interfere with the natural/spectral gamma experiment.

The next item is the sensor section of the magnetic susceptibility/induction log experiment [7]. It consists of a transmitter coil and a receiver coil wound on a stabilized epoxy-glass mandrel. The coils are positioned for minimum interference from the metal sections of the probe.

The scintillation detector [8], for the natural/spectral gamma measurement and the density determination, is located in the next section. This detector consists of a plastic and CsI crystal phoswich system attached to a photomultiplier tube-preamp assembly. Natural-gamma measurements are made using integral counting, whereas the spectral-gamma measurement requires use of a surface, multi-channel, pulse-height analyzer. A 512-channel unit is recommended in order to provide maximum resolution of natural emitters and to distinguish among the various induced emitters on the lunar surface. This pulse height analyzer will be shared with the Neutron-Gamma Probe.

Above the scintillation detector is the section containing the geophone and actuator assembly [9] for the acoustic velocity experiment. The geophone, a Hall-Sears Type HS-J, is mounted such that it can be pressed against the borehole wall during the measurement and retracted within the probe at other times. This is accomplished by using a rotary actuator and ratchet arrangement. A single power pulse will move the actuator to an extended position and a second pulse (of the same polarity) will return it. Acoustic isolation is provided by the compression springs which form the only contact between the geophone bracket and the probe when the geophone is in the measure position.

The uppermost section includes the flexure joint/centralizer assembly [10], which connects the deployment boom [11] to the probe, and the power and signal cable [12].

3. Mechanical Design

Since the Optimum Subsurface Probe is an instrument that is to be inserted into, and withdrawn from, a borehole, the strength of the probe in compression and in tension along the longitudinal axis, was the first structural design consideration. A suitable wall thickness was selected to provide the ruggedness necessary to prevent mechanical damage during prelaunch handling, environmental factors during launch, and handling during actual use. The wall thickness will give the probe a strength of several thousand pounds along the longitudinal axis which is many times greater than the expected force from the deployment mechanism. This force is limited by the lunar weight of the roving vehicle. The maximum deployment force is set at approximately 200 lbs.

A maximum extraction force of approximately 300 lb served as a design guide for the joints between each instrument. Considering the shear strength of the fasteners to be the factor most likely to cause failure, each joint has a design factor of safety of three as related to yield strength. Sufficient lapping of the external and internal members of each joint, required for the application of fasteners, gives a joint which is many times stronger than necessary for survival after any expected bending moments.

Extreme torsional or bending stresses are not expected, however the probe will withstand a twisting moment of 600 in.-lbs and a bending moment of 1,200 in.-lbs at the weakest point.

The maximum flexure will occur in the fiberglass-epoxy-laminate section of the probe which houses the magnetic susceptibility coils and scintillation crystal. This condition is caused by the difference in moduli of elasticity of aluminum and fiberglass-epoxy laminate. Since the bending deflection is inversely proportional to the product of the modulus of elasticity and the moment of inertia of area, the lower modulus of the fiberglass is compensated for by an increase in wall thickness. This thickness, however, could not be increased to the desired value without seriously decreasing the sensitivity of the magnetic susceptibility coils and the scintillation crystal. A final trade-off left this section slightly stronger than the remainder of the probe but more flexible. The wall thickness of the centralizer-caliper section was also increased to compensate for longitudinal slots which tend to weaken the section. All other sections are considered uniform except the thermal diffusivity unit which is stronger by virtue of the increased section modulus inherent in its non-tubular design.

2024-T4 aluminum was used where possible for the following reasons:

1. It maintains a good strength-density ratio throughout the required temperature range.

2. Its machineability is excellent, an important consideration on small and involved parts.

3. It is readily available

4. When anodized, a durable finish is obtained that will provide good thermal control in the lunar environment.

5. Aluminum ranks high when considering parameters which affect the buckling strength of hollow cylinders (1).

Wherever moving parts are found (collimator plug, both centralizers, seismic sensor), either coatings of tetrafluorethylene are used or the adjacent parts are made of dissimilar metals. This reduces the possibility of vacuum (cold) weldings. Protective windows for all the radiometric thermal devices are recessed in order to minimize scratching due to formation materials. Maintaining a centralized position for the probe in the hole also reduces scratching possibilities.

4. Measurement Discussion

Inspection of the experiment list will point out the wide variety of measurements made possible by use of the optimum probe. These measurements are divided into several different categories. The majority of the experiments included, measure parameters likely to be different if made in situ as compared to those obtained from analysis of returned samples. Obviously, we cannot bring the lunar temperature back to earth to measure, nor can a sample of the atmosphere be returned. Changes in the physical state of the lunar material can appreciably affect parameters such as thermal diffusivity, bulk density, and resistivity or conductivity; and therefore these should be measured in situ. Acoustic-velocity determinations cannot ordinarily be made on core samples and, therefore, the in situ measurement is the only suitable approach.

Many of the measurements are especially good for determining layering; a very important factor in the analysis of lunar tectonic history. These include density, the thermal measurements, magnetic susceptibility, natural gamma, and acoustic velocity. Other measurements are useful in defining the lunar environment, such as, again the temperature experiments, mass spectrometer, and radioactivity. With the determination of the presence of water so important, several experiments are directed toward this end. These are the interferometer-spectrometer, the mass spectrometer, and perhaps the induction log measurements.

Many of the experiments, in addition to providing direct measurement of a vital parameter, are also used in interpreting other measurements. For example, the acoustic-velocity information is used to analyze the natural or induced seismic records; the magnetic-susceptibility data are necessary to interpret the magnetic field instrument results; thermal-diffusivity data (along with density and specific heat capacity information) can lead to a calculation of thermal conductivity; residual-gas analysis data, provided by the mass spectrometer, can help in calibrating any total atmospheric pressure gage present and provide correlative information; and density data are also necessary to complement the gravity experiment to be conducted with other equipment.

In some cases, measurement of a given parameter is carried out using more than one technique. Temperature is determined by a contact sensor, an interferometer-spectrometer, and a total radiation detector, in order that information concerning this most important measurement will be available under the broadest set of conditions. As mentioned earlier, several water detectors are employed including the mass spectrometer, the interferometer-spectrometer and perhaps the induction log.

5. Supporting Surface Measurements

To increase its utility, the Optimum Subsurface Probe can also be used to carry out measurements on the lunar surface. These can be of the continuous type, while the probe is attached to the LSSM, or fixed-point measurements at selected locations. Continuous measurements will be limited to the natural-gamma and gas analysis experiments. This is because the sensors for these experiments do not have to be in intimate contact with the surface and the sampling times are compatible with vehicle speed. Fixed-point measurements would include natural/spectral gamma radioactivity, non-contact temperature, gas analysis, bulk density, and perhaps thermal diffusivity. These measurements can be made with the probe when properly positioned on the surface and when thermally controlled. Geometry considerations may preclude measurement of the contact temperature, thermal diffusivity, acoustic velocity, and magnetic susceptibility/induction log properties, by use of the subsurface probe on the surface. For example, the contact temperature sensors are located in the centralizer spring assemblies which may not be positioned normal to the surface. Also, when the probe is horizontal the geophone axis is perpendicular to that described. In the case of the magnetic susceptibility/induction log experiment, only a small portion of the field pattern of the instrument is intercepted by the formation when the probe is horizontally positioned on the lunar surface. Nevertheless, considerable information can be gained by use of the Optimum Subsurface Probe as a surface instrument. A separate surface probe containing those experiments which can not be adequately made via the subsurface probe is also recommended and discussed later in this section.

C. SUBSURFACE NEUTRON-GAMMA PROBE

A Subsurface Neutron-Gamma Probe, shown in Figure 4, is also recommended. This probe will be used to perform elemental analysis of the borehole formation, and of selected samples when the probe is placed on the lunar surface. It may also be used to make independent measurements of natural/spectral gamma radioactivity with its scintillation detector. The probe has a diameter of 1.75 in., a length of 40.9 in. and a total weight of 8.67 lbs. It requires 10 watts of power, 7 watts of which are dissipated in the probe itself (this does not include the power requirements for the pulse-height analyzer included with the Optimum Subsurface Probe). The operating temperature range is 218° to 343°K.

At the lower end of the probe is the transformer and electronics system [1] of the DC-DC voltage converter. This is followed by the voltage doubler [2], which increases the voltage to 80 kilovolts as required by the neutron generator.

The neutron generator [3] uses the 80 KV to accelerate deuterium ions, produced by a Penning-type ion source, into the tritium end-plate target; this reaction producing 14 MEV neutrons. High voltage insulation is provided between the generator tube and the probe case. An ion-source magnet [4] encircles the upper end of the neutron generator tube. This is followed by pulsing transformers [5] used to pulse the neutron source by means of ion pulsing.

A copper shield [6] is located above the source to protect the detector from direct neutrons and x-rays produced in the neutron generator. The gamma detector consists of a cesium-iodide scintillator crystal [7] and a photomultiplier-tube-preamp [8]. These are optically coupled and encapsulated in a single, epoxy-glass container.

The next section [9] contains certain critical electronics circuits required by the instrument. This section is followed by the flexure joint [10], which couples the probe to the deployment boom [11] and the cable [12].

D. SUBSURFACE TELEVISION PROBE

Figure 5 shows the Subsurface Television Probe, also recommended as part of the Lunar Probe System. It will be used to obtain and transmit back to earth image data of the walls of the borehole. With rapid turn-around time on earth, the astronaut will be able to direct special attention to measurement of areas of unusual appearance. The TV system is completely self-contained in the probe, with the cable providing input power and carrying the output signals to the telemetering system.

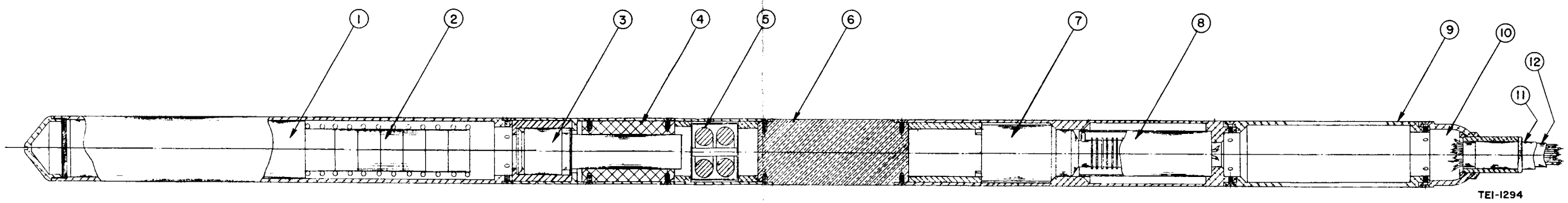

1-03802

1 ELECTRONICS
2 VOLTAGE DOUBLER
3 CONTROLATRON
4 MAGNET
5 PULSING TRANSFORMERS
6 COPPER SHIELD
7 SCINTILLATION CRYSTAL
8 PHOTOMULTIPLIER
9 ELECTRONIC SECTION
10 FLEXURE JOINT
11 DEPLOMENT BOOM
12 ELECTRICAL CABLE

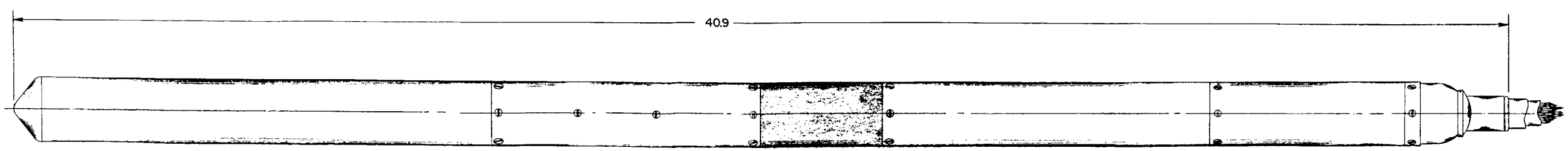

Fig. 4 Subsurface Neutron-Gamma Probe

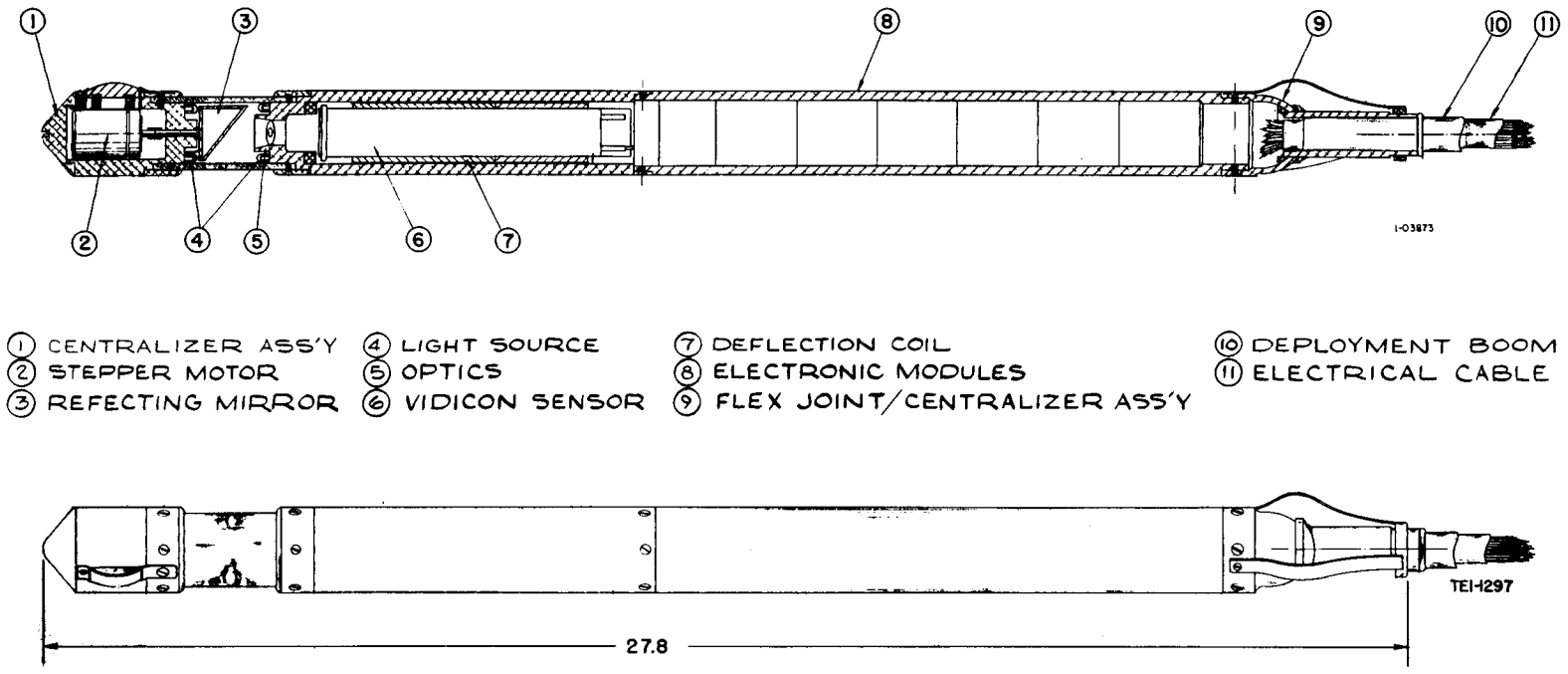

Fig. 5 Subsurface Television Probe

At the lower end of the probe is a centralizer assembly [1] to maintain proper positioning of the probe while in the hole. The mirror-stepping mechanism [2] is also located in this section. A rotary actuator is used to sweep the moving mirror [3], in a step-by-step manner, through a full 360° of azimuth, so that the complete borehole wall surface can be examined. Illumination is provided by the two rings of miniature lamps [4].

Above the scanning mirror is the optics assembly [5] which focuses the sidewall image on the vidicon face. The vidicon [6] and the deflection coil [7] follow. The vidicon is of the Apollo 1-in. type.

The majority of the remaining probe length contains the electronic circuit modules [8], and consists of the required power supply, deflection, amplifying, and conditioning circuits. The uppermost section includes the flexure-joint/centralizer assembly [9] which connects the deployment boom [10] to the probe, and the power and signal cable [11].

The probe has a diameter of 1.75 in., a length of 27.75 in. and a total weight of 7.04 lbs. Total required power is 8.5 watts. The operating temperature range is 273° to 313°K.

E. INTEGRATED SURFACE PROBE

1. Probe Description

Certain of the experiments contained in the Optimum Subsurface Probe cannot be effectively performed on the lunar surface because of the subsurface probe geometry. Figure 6 shows a surface probe which is recommended for measurement of these surface and near-surface parameters. It is an integrated unit, containing the following instruments: interferometer spectrometer, magnetic-susceptibility/induction log, thermal diffusivity, acoustic velocity detector, and contact temperature sensors. A thermal shield-radiator is provided for thermal control.

Performing these experiments will greatly enhance the value of the subsurface measurements because the two can be compared and the surface effects isolated. If a layer of unconsolidated material makes some sort of hole casing necessary, the use of this surface probe may be the only way to obtain surface and near-surface data because most instruments in the subsurface probe cannot work in a cased hole.

The surface probe has a diameter of 12.9 in. and a maximum height of 6.1 in., with handle folded. The weight is 5.35 lbs.

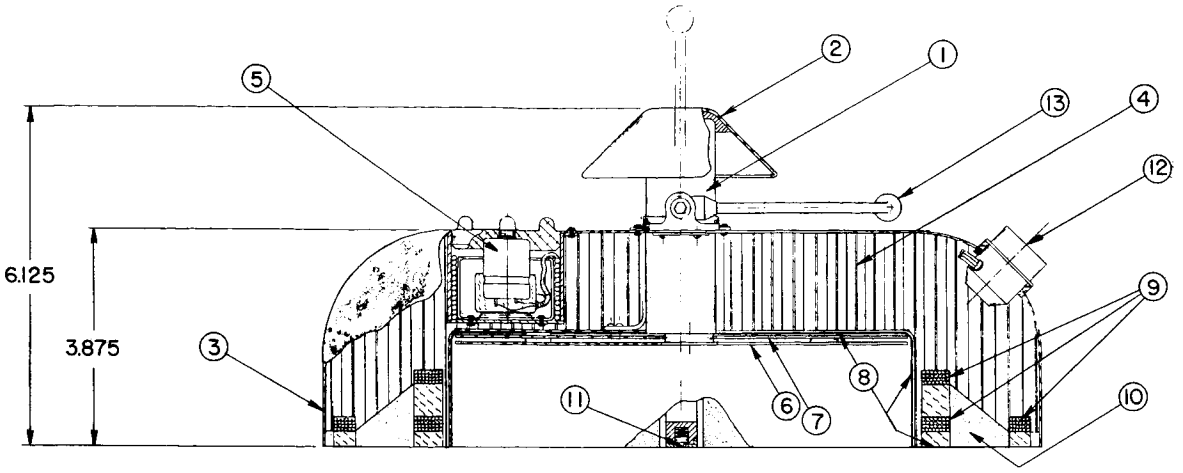

1. INTERFEROMETER-SPECTROMETER
2. THERMAL SHIELD
3. EPOXY-FIBERGLASS SHELL
4. HONEYCOMB STRUCTURE
5. ACOUSTIC SENSOR ASS'Y
6. HEATER PLATE
7. THERMAL SHIELD
8. REFLECTIVE MYLAR SURFACE
9. MAGNETIC SUSCEPTIBILITY/ INDUCTION LOG COILS
10. POTTING MATERIAL
11. CONTACT TEMPERATURE SENSORS
12. CONNECTOR
13. HANDLE

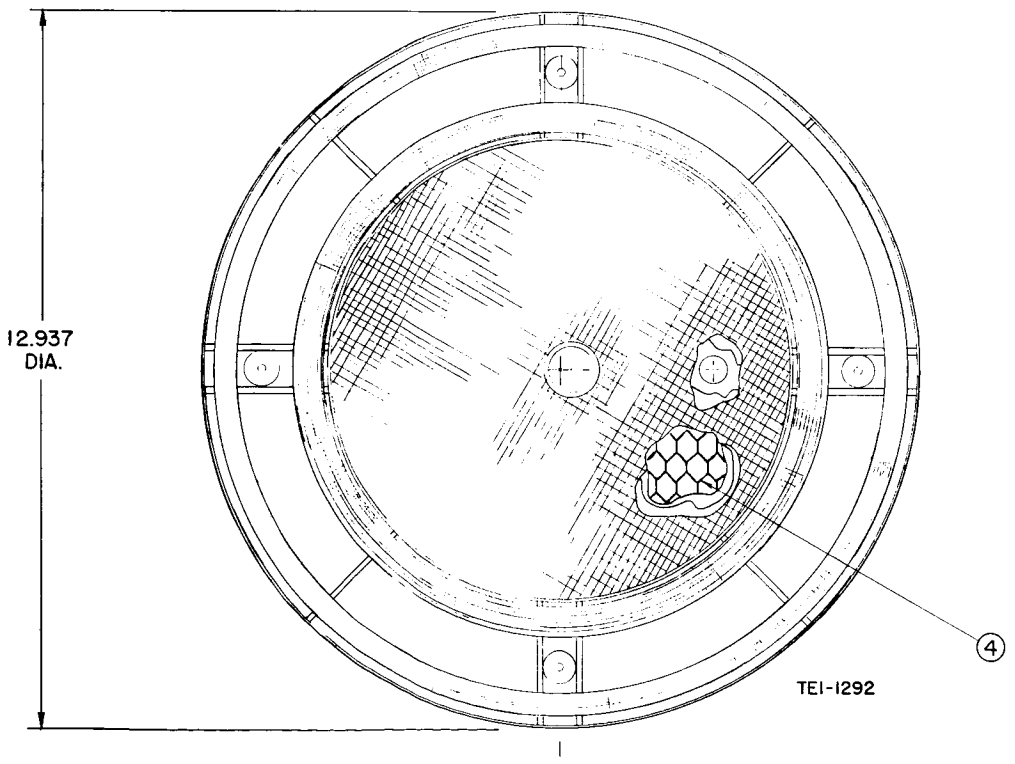

Fig. 6 Integrated Surface Probe

From Figure 6 it can be seen that the probe has the general shape of a curved shell ring with a central protuberance. The protuberance contains the interferometer-spectrometer [1]. This instrument will be used to measure the surface temperature and infrared spectra, and also serves as the temperature sensor for the thermal diffusivity instrument. The upper section of the I.S. case is protected with a thermal shield [2].

Thermal/meteoroid protection for the remainder of the probe is provided by a thermally-conductive, epoxy-fiberglass shell [3] covering a honeycomb structure [4]. The surface of the shell is painted white to provide the proper α/ε ratio for radioactive thermal control.

The acoustic-velocity, sensor assembly [5], consisting of a geophone, its surface contacting element, and a spring-wound cable, is located in a recessed well between the outer and inner epoxy-glass shells. It is designed so that it may be removed by the astronaut and placed on the lunar surface during the time of the measurement.

Below the inner shell is a thermostatically-controlled, spiral-wound, heater plate [6] which supplies heat energy to the lunar surface for thermal diffusivity measurements made during the lunar night. A thermal shield [7] is located above the heater plate to minimize heat flow to the probe body. A highly-reflective, gold-coated, mylar surface [8] covers the inner edge of the inner shell and minimizes heat transfer from the lunar surface to the probe.

The coils for the magnetic susceptibility/induction log [9] are located in the ring portion of the instrument and positioned so that, with the probe resting on the lunar surface, optimum coupling and response are obtained. The coils are encapsulated in a semi-rigid potting material [10].

Four contact-temperature sensors [11], of the resistance type, are located on the bottom surface of the probe in spring loaded assemblies. They provide additional temperature data to support the interferometer-spectrometer measurements.

The connector [12] brings power into the probe and carries the signals to the supporting electronics unit. A handle [13] is provided to allow deployment of the probe by the astronaut. This handle may be folded against the top of the unit during storage.

2. Measurement Discussion

The principle of operation of the various experiments making up the Integrated Surface Probe is the same as for the counterparts located in the subsurface probe. A complete description is found in Section III.

The important operational feature for the surface probe, is that measurements, with the exception of the acoustic-velocity experiment, can be made without further astronaut attendance once the probe is placed on the lunar surface. The sensor for the acoustic-velocity experiment is housed in such a way that it may be removed from the probe and placed in the most advantageous location available. This feature provides a firm contact with the surface for good coupling and good signal reception. Having the astronaut perform this important task will greatly enhance the probability of a successful acoustic-velocity measurement.

F. SUPPORTING ELECTRONICS PACKAGE

The power conditioning, control and signal conditioning circuits for the various probes are located in the Supporting Electronics Package. This unit has an estimated weight of 17.9 lbs and a volume of 2760 in.^{3} A pulse-height analyzer is also coupled with this package which has a weight of 4.0 lbs and a volume of 1000 in^3. A detailed design for the integrated Supporting Electronics Package was not included in this study because the overall volume requirements could be met in a number of dimensional combinations, and it was not known which general shape would best suit space available on the LSSM. The individual supporting requirements for each experiment are included in the experiment characteristics tables located in Section III. A possible layout for the control panel of the Supporting Electronics Package is shown in Figure 8.

G. SUBSURFACE PROBE DEPLOYMENT

In normal logging of boreholes on earth, the probe (or sonde) is usually of sufficient weight to slide down the borehole unaided. In certain cases when the sonde is light, it is pushed down the hole using the drill pipe. However, this requires that the logging cable be made of many sections, so that it can be broken as additional sections of pipe are added. Another method is to use an electro-mechanical crawler, which pulls the tool into the hole after it.

Probe insertion on the moon is affected by several additional factors:

1. Operation in a dry hole,

2. Small hole-to-probe-diameter ratio,

3. Probe is made with as small a mass as possible to minimize total weight.

4. Lunar gravity will make the effective force tending to pull the probe into the hole 1/6 that of earth, while most of the drag which will restrain the sonde will be the same as earthside.

For these reasons a mechanical means of probe insertion will be used. The proposed method makes use of a Storable Tubular Extendable Member (STEM), a development of DeHavilland Aircraft of Canada, Limited. This unit, normally used as a retractable antenna, consists of a thin-wall, prestressed, stainless-steel tape. This tape is similar to the ordinary, flexible, steel tape measure and is wound on a spool in a container in a similar fashion. When the tape is removed from its package, it bends to form a long, thin-wall cylinder or tube. Although the resultant tube has low torsional rigidity, it can exert a tremendous thrust along its axis.

Because the tape is flat as it comes from the package and then rolls along its length to form a cylinder, a funnel-shaped opening forms at the point where the tape is assuming a cylindrical shape. A cable, or conductors, can be fed continuously into this funnel as the cylinder is being formed. (See Figure 7 for schematic diagram).

The STEM unit consists of the extendable member, a storage drum, and a drive mechanism for extending and retracting the extendable member. A single unit can be used for both the 10- and the 100-ft holes. The total weight of a 1-in. diameter boom unit, including the drive mechanism, is about 8 lbs. These units have been used on other NASA space missions and have been fully qualified for space use.

The STEM system may be operated over the full range of temperatures expected on the moon (120° - 400°K). Thermal control may be required to limit the temperature excursions of the drive motor; the extendible member can withstand the full lunar temperature range.

An analysis shows that the STEM unit is sufficiently flexable so that it will follow any non-vertical drill holes which can be produced by any 2-in. drilling head having a length comparable with the surveying probe used. For a minimum straight section length of six feet and maximum bending (worst case), a driving force of 200 lbs. will produce a bending moment of 200 lb-in. The critical bending moment for a 1-inch STEM unit of 0.010 in. thickness is 1500 lb-in. Thus a considerable safety factor is provided.

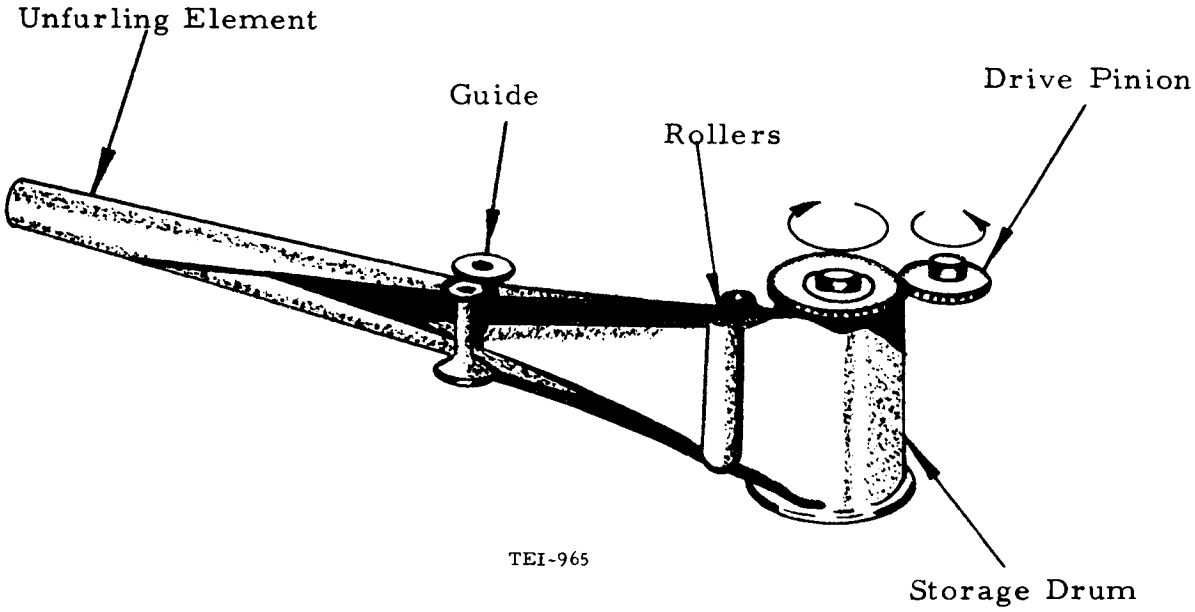

Fig. 7 STEM Deployment Device

This STEM system makes an ideal system for inserting and removing the probe from the hole. The cable to the probe can be inserted inside the extendable member, where it will be protected from abrasion in the hole, and will be used only for carrying signals and current. As it will not be used to retract the probe from the hole, the danger of breaking conductors from excessive pull will be minimized and, consequently, a lighter cable can be safely used.

Not included in the Lunar Probe System, but as a matter of interest, additional experiments, which otherwise could not be made or justified, may be provided by the probe deployment device.

The extendable member of the STEM device may possibly be used as a dipole to make certain RF measurements of the lunar surface and subsurface material. On the surface, the radiation properties of both a horizontal and vertical dipole can be measured by either extending the member horizontally or vertically. The addition of a small loop antenna and RF amplifier to the Lunar Probe System will allow the response of the dipole to be checked as a function of position.

H. EXPERIMENT SCHEDULING, SEQUENCING, AND SWITCHING

Experiment scheduling and switching plans are needed if optimum utilization is to be made of the astronaut and the probe system. The time available for logging the various boreholes, particularly the 10-ft holes, may be extremely limited and therefore the most effective use of the probes must be determined. Preliminary information has been prepared illustrating some of the trade-offs which can be made when a complex integrated probe is considered.

The material which follows pertains to the Optimum Subsurface Probe. This probe was chosen for the initial analysis because of the large number of experiments which it contains. Sufficient information was not available at the time of this report to allow a scheduling plan for the complete system to be formulated. The techniques which were used for the optimum probe would hold for the full system, however.

Detailed information concerning the theory and methodology used in this analysis is included in Appendixes V and VI.

1. Experiment Scheduling and Sequencing

The time which is to be available to carry out measurements, in the various 10-ft holes and in the 100-ft hole, is not known. Several times have been arbitrarily chosen for this scheduling and sequencing analysis, so that the level of information to be gained as a function of surveying time can be determined. The times are as follows:

10-ft Hole (min)	100-ft. Hole (min)
45	120
75	210
90	300

The experiments which are to be scheduled, pertinent information (such as measurement time) required, and interference problems, are shown in Table II.

Table II

EXPERIMENT CHARACTERISTICS

Experiment	Stationary/ Continuous	Measurement Time	Interferes with
1. Non-Contact Temp. (e_1)	S	1 min/point	-
2. Contact Temp. (e_2)	S	1 min/point	-
3. Thermal Diffusivity (e_3)	S	30 min/point	1,2
4. Mass Spectrometer (e_4)	S	10 sec/point	-
5. Natural Gamma (e_5)	C	5 ft/min	-
6. Density (e_6)	C	1 ft/min (10-ft hole) 5 ft/min (100-ft hole)	5,9
7. Magnetic Suscep/Ind. Log (e_7)	C	5 ft/min	-
8. Acoustic Velocity (e_8)	S	2 min/point	-
9. Spectral Gamma (e_9)	S	20 min/point	-
10. Caliper (e_{10})	C	5 ft/min	-

Minimization of Time Now, consider a set of experiments, E. If all elements of the set, e_1 through e_k, can be conducted simultaneously, the required time interval, to execute the entire set E, is equal to the time requirement of that e, of set E, whose execution time is the longest. If all elements of set E cannot be conducted simultaneously, the set E will have to be partitioned. Each partition will cost an element of time, since a partition means that the execution times for the partitioned sets cannot overlap. The total execution time for the set E will be the sum of the execution times of all partitioned sets. It is clear that in order to minimize the total execution time for the set E, the number of partitions must be minimized. Also, the partitions must be defined in such a way that the sum of their execution times is a minimum.

The partitioning procedure begins with the identification of the element e of set E whose execution time is maximum. Then all other elements of set E, which can be executed at the same time, are grouped with it. This defines the set X. Repeat this examination of set E-X, forming sets Y, Z, etc., until all experiments are included. Summation of the execution times for sets X, Y, Z, etc., will be the minimum execution time for the set E.

Scheduling The foregoing discussion demonstrates the grouping methodology to be used where the criterion for optimization is a minimum time. In our case we are concerned with the scheduling of the experiments such that the criterion for optimization is the maximum number of experiment replications in a given time.

The method is to initially schedule all experiments once. If any time is left for replication, as many experiment sets as there are time for, are scheduled for replication. As the resource of time is used, the group of experiments which fit within the given time frame diminishes. Once a set cannot be fit into the available time the set is examined and the experiment requiring the longest time is removed. With this done the complete set E must be examined to determine the new subsets X_1, Y_1, Z_1, etc., which require minimum total execution time for E. This process continues with replications of the X_1, Y_1, Z_1 sets and identification of X_2, Y_2, Z_2 sets until all time has been used or the remaining time available is not sufficient for any set X_k.

Scheduling Plans - 10-Ft Holes Examination of Table II reveals that certain experiments can be run on a continuous basis while others must be performed on a point-by-point basis. Therefore, the first subsets are determined by including those experiments which can be run on a continuous basis without interference. They are:

c_1 (continuous) = (e_5, e_7, e_{10}), time = 2 min.

c_2 = (e_6, e_7, e_{10}), time = 10 min.

Experiments e_7 and e_{10} can be run with either e_5 or e_6 and are included in both sets.

Next determine the minimum subsets of the stationary experiments. They are:

S_1 (stationary) = (e_3, e_4, e_8, e_9, e_{10}), time = 30 minutes

Note: certain continuous-type measurements are included but they do not extend the minimum execution time of the stationary set.

S_2 = (e_1, e_2, e_4, e_5, e_7, e_{10}), time = 1 min.

The set E, then, consists of C_1, C_2, S_1, and S_2. The execution time for E is 43 min.

It can also be shown that two additional subsets exist, S_3 and S_4, which are useful in the scheduling program as the time resource is utilized.

S_3 = (e_1, e_2, e_4, e_5, e_7, e_8, e_{10}), time = 2 min.

S_4 = (e_1, e_2, e_4, e_8, e_9, e_{10}), time = 20 min.

The limiting experiment in S_3 is e_8 (acoustic velocity), and the limiting experiment in S_4 is e_9 (spectral gamma). These sets are formed when the time remaining for replications falls below 30 minutes, the time required for execution of S_1.

Included in Table III below are scheduling plans suitable for surveying of the 10-ft. holes. Measurement times of 45, 75, and 90 minutes had been arbitrarily selected previously and three alternate plans for each time are included. In addition, a proposed optimum plan is shown. This plan includes the best features of the other three plans but is not constrained to a fixed time.

Table IV shows a summary of the number of times each measurement will be made for the different time allocations for the 10-ft. holes. It points out that significant information can be obtained with an allowed time of 79 minutes.

Table III

EXPERIMENT SCHEDULING PLANS - 10-FT HOLES

PLAN 1 - 45 min

No. of Replications	Set	Time (min)
1	C_1	2
1	C_2	10
1	S_1	30
1	S_2	1
		43
1	S_3	2
		45

PLAN 2 - 45 min

No. of Replications	Set	Time (min)
1	C_1	2
1	C_2	10
1	S_1	30
1	S_2	1
		43
2	S_2	2
		45

PLAN 1 - 75 min

No. of Replications	Set	Time (min)
1	C_1	2
1	C_2	10
1	S_1	30
1	S_2	1
		43
1	S_1	30
1	S_3	2
		75

PLAN 2 - 75 min

No. of Replications	Set	Time (min)
1	C_1	2
1	C_2	10
1	S_1	30
1	S_2	1
		43
1	S_4	20
3	S_3	6
6	S_2	6
		75

PLAN 3 - 75 min

No. of Replications	Set	Time (min)
1	C_1	2
1	C_2	10
1	S_1	30
1	S_2	1
		43
8	S_3	16
16	S_2	16
		75

PLAN 1 - 90 min

No. of Replications	Set	Time (min)
1	C_1	2
1	C_2	10
1	S_1	30
1	S_2	1
		43
1	S_1	30
4	S_3	8
9	S_2	9
		90

PLAN 2 - 90 min

No. of Replications	Set	Time (min)
1	C_1	2
1	C_2	10
1	S_1	30
1	S_2	1
		43
2	S_4	40
1	S_3	2
5	S_2	5
		90

PLAN 3 - 90 min

No. of Replications	Set	Time (min)
1	C_1	2
1	C_2	10
1	S_1	30
1	S_2	1
		43
1	S_4	20
7	S_3	14
13	S_2	13
		90

OPTIMUM PLAN - 79 min

No. of Replications	Set	Time (min)
1	C_1	2
1	C_2	10
1	S_1	30
1	S_2	1
		43
1	S_1	30
2	S_3	4
2	S_2	2
		79

Table IV

SUMMARY OF MEASUREMENTS IN 10-FT HOLES

Experiment	Time - min								
	45	45	75	75	75	79**	90	90	90
	Number of Measurements								
e_1 (Non-Contact Temp.)	3	2	2	11	25	5	14	9	22
e_2 (Contact Temp.)	3	2	2	11	25	5	14	9	22
e_3 (Thermal Diff.)	1	1	2	1	1	2	2	1	1
e_4 (Mass Spec.)	3	3	4	12	26	7	16	10	23
e_5 (Nat. Gamma)	3,1*	2,1*	2,1*	10,1*	25,1*	5,1*	14,1*	7,1*	21,1*
e_6 (Density)	1*	1*	1*	1*	1*	1*	1*	1*	1*
e_7 (Mag. Susc./Ind.)	3,2*	2,2*	2,2*	10,2*	25,2*	5,2*	14,2*	7,2*	21,2*
e_8 (Acoustic Vel.)	1	2	3	5	9	4	6	4	9
e_9 (Spectral Gamma)	1	1	2	2	1	2	2	3	2
e_{10} (Caliper)	4,2*	3,2*	4,2*	12,2*	26,2*	7,2*	16,2*	10,2*	23,2*

Notes:

* These are continuous runs
** Optimum Plan

Scheduling Plans - 100-ft Hole Scheduling plans were also prepared for the 100-ft hole (Table V). Surveying times of 120, 210, and 300 minutes were allocated. Three alternates for each time period and an optimum plan are given.

Table VI gives a summary of individual measurements in the 100-ft hole for the three time allocations and the optimum plan. Again, significant advantages are realized by the use of the optimum plan. It should be recognized that the choice of the number of times set S_2 or S_3 are run (the only difference is that S_3 includes the acoustic velocity experiment) is arbitrary. The alternate plans indicate the loss of additional replications by running an excessive number of velocity measurements.

2. Experiment Switching

The previous discussion has dealt with experiment scheduling, as pertains to maximizing the survey results as a function of time. A problem of equal magnitude is the proper sequencing of experiments, in order to minimize the switching operations required of the astronaut. Again, a "first cut" analysis has been performed only for the Optimum Subsurface Probe. The technique used is applicable to the complete system.

The switching optimization problem was to determine which of the sequencing plans just discussed, and those contained in Appendix V, would require a minimum of switching. A preliminary panel design was also required. Plans for both the 10-ft and 100-ft holes had to be analyzed to see if the switch panel designs would change if only 10-ft or 100-ft holes were included in the mission plan. The experiment switching requirements, included in Table VII, entered into the analysis.

The panel resulting from this preliminary analysis is shown in Figure 8. It can be seen that it contains switches that control experiment subsets, individual experiment switches, experiment readout devices, and supporting controls for the deployment device. Experiment subset switches were provided for the obvious reason that minimum switching movements would result if group activation was used. This was possible because the same six, experiment subsets serve both the 10-ft and 100-ft holes. Individual experiment activation switches were provided so that measurements could be made as desired after preliminary information about the formation had been obtained. These individual switches also serve as backup to the group switches to increase overall system reliability.

Table V

EXPERIMENT SCHEDULING PLANS - 100-FT HOLE

PLAN 1 - 120 min

No. of Replications	Set	Time (min)
1	C_1	20
1	C_2	20
1	S_1	30
1	S_2	1
		71
1	S_1	30
8	S_3	16
3	S_2	3
		120

PLAN 2 - 120 min

No. of Replications	Set	Time (min)
1	C_1	20
1	C_2	20
1	S_1	30
1	S_2	1
		71
1	S_4	20
12	S_3	24
5	S_2	5
		120

PLAN 3 - 120 min

No. of Replications	Set	Time (min)
1	C_1	20
1	C_2	20
1	S_1	30
1	S_2	1
		71
16	S_3	32
17	S_2	17
		120

PLAN 1 - 210 min

No. of Replications	Set	Time (min)
1	C_1	20
1	C_2	20
1	S_1	30
1	S_2	1
		71
3	S_1	90
16	S_3	32
17	S_2	17
		210

PLAN 2 - 210 min

No. of Replications	Set	Time (min)
1	C_1	20
1	C_2	20
1	S_1	30
1	S_2	1
		71
2	S_1	60
1	S_4	20
20	S_3	40
19	S_2	19
		210

PLAN 3 - 210 min

No. of Replications	Set	Time (min)
1	C_1	20
1	C_2	20
1	S_1	30
1	S_2	1
		71
1	S_1	30
3	S_4	60
16	S_3	32
17	S_2	17
		210

PLAN 1 - 300 min

No. of Replications	Set	Time (min)
1	C_1	20
1	C_2	20
1	S_1	30
1	S_2	1
		71
5	S_1	150
25	S_3	50
29	S_2	29
		300

PLAN 2 - 300 min

No. of Replications	Set	Time (min)
1	C_1	20
1	C_2	20
1	S_1	30
1	S_2	1
		71
5	S_1	150
3	S_4	60
5	S_3	10
9	S_2	9
		300

PLAN 3 - 300 min

No. of Replications	Set	Time (min)
1	C_1	20
1	C_2	20
1	S_1	30
1	S_2	1
		71
6	S_1	180
2	S_4	40
1	S_3	2
7	S_2	7
		300

OPTIMUM PLAN - 221 min

No. of Replications	Set	Time (min)
1	C_1	20
1	C_2	20
1	S_1	30
1	S_2	1
		71
4	S_1	120
10	S_3	20
10	S_2	10
		221

Table VI

SUMMARY OF MEASUREMENTS IN 100-FT HOLE

Experiment	Time - min									
	120	120	120	210	210	210	221**	300	300	300
	Number of Measurements									
e_1 (Non-Contact Temp.)	12	19	34	34	41	37	21	55	18	11
e_2 (Contact Temp.)	12	19	34	34	41	37	21	55	18	11
e_3 (Thermal Diff.)	2	1	1	4	3	2	5	6	6	7
e_4 (Mass Spec.)	14	20	35	38	42	39	26	61	24	18
e_5 (Nat. Gamma)	12,1*	18,1*	34,1*	34,1*	40,1*	34,1*	21,1*	55,1*	15,1*	9,1*
e_6 (Density)	1*	1*	1*	1*	1*	1*	1*	1*	1*	1*
e_7 (Mag. Susc./Ind.)	12,2*	18,2*	34,2*	34,2*	40,2*	34,2*	21,2*	55,2*	15,2*	9,2*
e_8 (Acoustic Vel.)	10	14	17	20	24	21	15	31	14	10
e_9 (Spectral Gamma)	2	2	1	4	4	5	5	6	9	9
e_{10} (Caliper)	14,2*	20,2*	35,2*	38,2*	42,2*	39,2*	26,2*	61,2*	24,2*	18,2*

Notes:

* These are continuous runs
** Optimum Plan

Table VII

EXPERIMENT SWITCHING REQUIREMENTS

	Experiment	Operations	Notes
1.	Non-Contact Temp.	Experiment On-Off	
2.	Contact Temp.	Experiment On-Off Meter Readouts	
3.	Thermal Diffusivity	Experiment On-Off Heater On-Off Meter Readout	
4.	Mass Spectrometer	Experiment On-Off Ionizer On Mass Filter On	Total Ion Density, total Ion neutral pressure, mass spectra
5.	Natural Gamma	Experiment On-Off Meter Readout	
6.	Gamma-Gamma Density	Experiment On-Off Meter Readout	
7.	Magnetic Susceptibility	Experiment On-Off Meter Readout	
8.	Acoustic Velocity	Experiment On-Off Geophone positioning out and in (momentary switch closure) Explosive charge initiation	For each measurement point
9.	Spectral Gamma	Energize pulse height analyzer	In addition to other circuits as in (5); no meter readout
10.	Caliper	Experiment On-Off Meter Readout	
11.	Probe Vertical Positioning	Up-Down Control speed control position readout	

Appendix VI shows that switching movements can range from 26 to 66 in the 10-ft holes and from 62 to 105 in the 100-ft hole. Therefore, much is to be gained by selection of the optimum plan. Figure 9 represents a flow diagram of the switching sequence required to carry out the 79-minute Optimum Plan for the 10-ft holes. A study of this diagram suggests that a great deal of astronaut attendance can be eliminated by the use of an automated programmer. This is recommended and is shown in the panel layout.

The analysis included in this report was not intended to produce final results but only to point out areas which must be considered during any follow-on program.

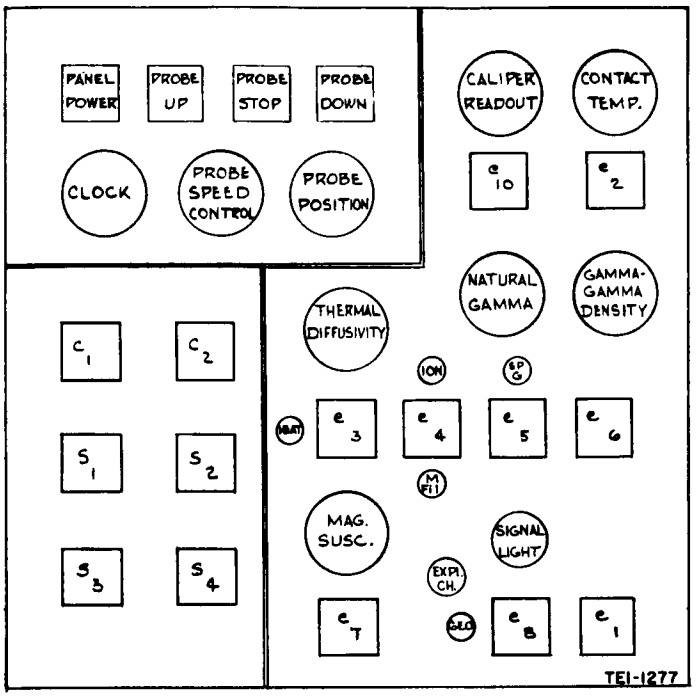

e_1 NON CONTACT TEMP.
e_2 CONTACT TEMP.
e_3 THEEMAL DIFFUSIVITY
e_4 MASS SPECTROMETER
e_5 NATURAL AND SPECTRAL GAMMA
e_6 GAMMA-GAMMA DENSITY
e_7 MAGNETIC SUSCEPTIBLITY
e_8 ACOUSTIC VELOSITY
e_{10} CALIPER

$C_1, C_2, S_1, S_2, S_3, S_4$ - EXPERIMENT GROUP SWITCHES

Fig. 8 Switch Panel Design

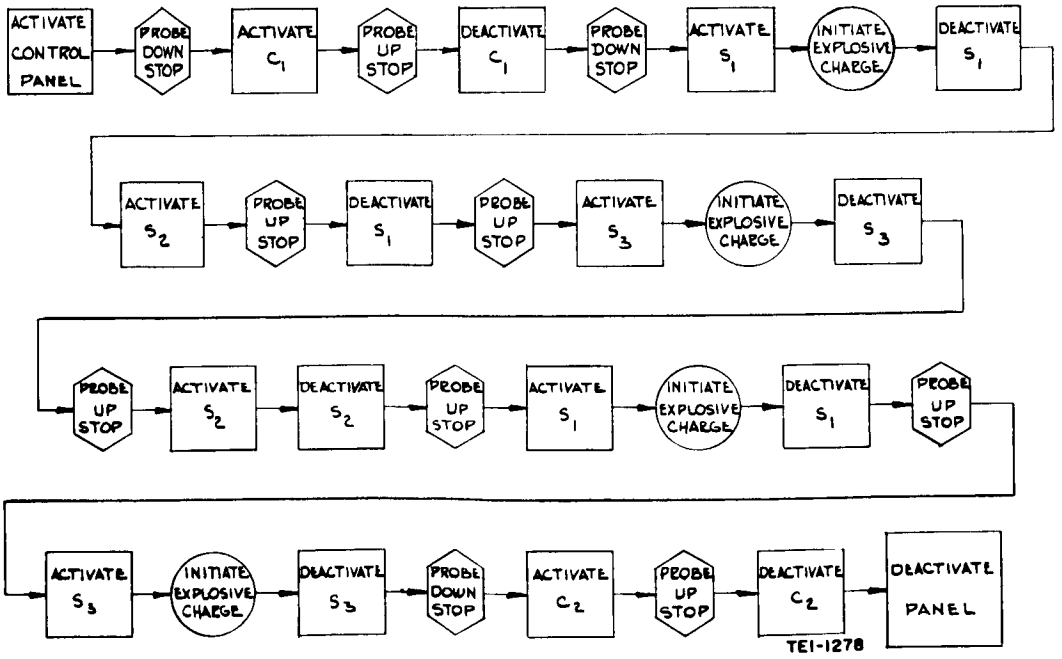

Fig. 9 Switching Diagram - 79-min Optimum Plan

III. EXPERIMENT DESCRIPTIONS

The previous section of this report dealt with a description of the various probes making up the Lunar Probe System. These descriptions were on a probe or systems basis and not on an individual experiment basis. This section examines the individual experiments considered in the study and shows why they were or were not included in the probe system. It also discusses the purpose and justification for the various measurements, the technique to be employed along with the expected measurement range and accuracy, the operational requirements, and the instrument state of development. A summary of instrument characteristics is included. It is hoped that this section may be used in other lunar system studies as an "Experiment Handbook" of probe devices.

A. RECOMMENDED EXPERIMENTS

1. Nuclear Measurements

Nuclear radiation measurements have proved to be of great value in the terrestrial search for radioactive minerals, petroleum, gas, and coal. Much has been learned about surface and subsurface geological features by highly-refined, measurement techniques of physical parameters. Applications of these techniques to lunar exploration provides a powerful tool, and, when combined with other physical measurements, can tell a great deal about the origin and character of the lunar crust. Parameters of major importance are:

- The measurement of natural radioactivity, especially the relative amounts of potassium-40 (K^{40}), thorium (Th), and uranium (U).
- The use of neutron irradiation to determine elemental composition.
- The use of gamma-ray scattering to determine structure density.

a. Natural Radioactivity (Natural and Spectral Gamma)

Background. The measurement of natural radioactivity in the lunar crust will be of major importance. It will produce useful evidence about the formation of the solar system and about the formation and thermal history of the moon.

The calculations of temperatures within the moon depend markedly on the concentrations of radioactive materials in the lunar-subsurface material. Urey writes (2) that the problem has caused great confusion during the last ten years or more, since variations in the concentration of these materials would cause considerable variation in the internal temperature of the moon. This, along with uncertainties in the values of specific heat, thermal conductivity, thermal diffusivity, etc., makes accurate calculations concerning the thermal properties of the moon impossible until first-hand data are available.

On earth, aerial radioactivity surveys are conducted, along with such other measurements as gravity and magnetic field, to provide preliminary information of regions worthy of more detailed examination using surface techniques. On the moon, these surveys can also prove beneficial, both from orbiting vehicles and by means of surface traverses utilizing a roving vehicle. Since the visual appearance of much of the lunar landscape may be similar in nature, measurement of the natural radioactivity will be most helpful in determining the extent of lithologic formations. This is possible because, for example, the natural radioactivity of materials normally associated with volcanic activity differs from that of materials of meteoritic origin by as much as two orders of magnitude (3). Thus thinly-covered, ash flows could be distinguished from earlier, meteoritic cover.

Natural-radioactivity surveys, in addition to helping distinguish volcanic material from meteorites, are also useful in distinguishing among the several, volcanic-rock types. See Table VIII. It can be seen that, in general, the radioactivity of igneous rocks increases with increasing acidity or silica content. The ultrabasic intrusives have the lowest; the granites, the highest; with the basalts and gabbros falling in between.

Subsurface measurements are especially important. From these one can determine the thickness of beds (if less than hole depth), and distinguish natural radioactivity from induced radioactivity. The latter is possible, because induced activity on the lunar surface should have a decreasing effect on total count rate as the instrument moves further below the surface, and should be negligible below one meter. Shielding properties, of the lunar material, may be determined by analysis of the change in count rate with depth (near the surface), and by correlation with data from the bulk density experiment. This will be helpful later in lunar basing considerations.

The major contributors to the radioactivity of rocks are the isotopes of the elements potassium, uranium, and thorium. If

TABLE VIII

THORIUM, URANIUM, AND POTASSIUM IN IGNEOUS ROCKS (4)

Rock	Thorium** (in ppm)	Uranium* (in ppm)	Potassium** (in $\%K_2O$)
Silicic Intrusives (Granites, Syenites)	1 - 25	1 - 6	1.5 - 6
Silicic Extrusives (Rhyolites, Trachytes)	9 - 25	2 - 7	
Basic Intrusives (Gabbros, Diabases)	0.5 - 5	0.3 - 2	0.4 - 3
Basic Extrusives (Basalts, Andesites)	0.5 - 10	0.2 - 4	
Ultrabasic Intrusives (Peridotites, Dunites)	low	0.001 - 0.03	0.1 - 1

* Adams, et al, 1959

** Daly, 1933

energy discrimination is used, these elements can be separated by their energy spectra. The potassium-40 spectrum shows a single peak at 1.46 mev; while thorium and its daughter products exhibit a spectrum of superimposed gamma with a major peak at 2.6 mev; and uranium, a superimposed spectrum with peaks at 1.76, 2.2, and 2.4 mev. The radioactivity of these three elements will also give evidence related to the process of nucleosynthesis of stars; that is, whether neutrons were captured at a rapid (r) rate or a slow (s) rate compared to intervening beta decays. Results based on meteoritic and earth radioactivities are not in agreement and lunar results are very much needed to resolve the problem.

Induced gamma-ray activity can be produced in a number of ways by solar and cosmic radiation. The cosmic-ray primaries themselves can produce gamma radiation by high-energy collisions with lunar-surface nuclei. Also, secondary products such as neutrons and pi mesons, generated in these collisions, can cause short- and long-lived activity through their interactions with the surface materials. Gamma spectral analysis will be helpful in determining how these processes modify the lunar surface.

Measurement Technique. Natural and spectral gamma measurements will be made using a scintillation detector, chosen over the Geiger-Mueller (G-M) counter for several reasons. The G-M counter is very rugged, reliable, and requires simple electronic circuitry. Stability characteristics are unusually good for specially designed tubes. However, detectors of the G-M type generally have a low efficiency for measuring gamma rays and, thus, longer counting times are required. The scintillation counter, which generally consists of a thallium-activated, sodium-iodide (or cesium-iodide) crystal with suitable photomultiplier, is much more sensitive and the output can be analyzed to ascertain the energy distribution or spectrum of the photons.

One major drawback, for the scintillation counter, has been the limited range of operating temperature and poor, temperature stability. This is the main reason they have only recently replaced G-M tubes in well-logging operations. Requirements for high-temperature operation have steadily increased as wells have gone deeper. It is not unusual for well temperatures to reach 150°C and sometimes even as high as 200°C. Accordingly, operating characteristics of scintillation detectors have improved. Certain companies have developed special photomultiplier tubes suitable for these temperatures (150°C). As is usually the case, compromises must be made and the resolution qualities for these tubes have not been as good as for standard models. Further development work along these lines is in process, however, and improvements are being made.

Scintillation detectors offer an additional advantage, in that, background effects due to charged particles can be reduced. This is done by enclosing the crystal in a plastic scintillator which is sensitive to charged particles but insensitive to gamma rays. This is the phoswich arrangement (phosphor sandwich). In this configuration charged particles interact with the plastic scintillator, and produce signals which are used to inhibit pulses, produced by the NaI or CsI crystal, from registering in the scaler or pulse-height analyzer. Gamma rays do not generate these inhibiting signals and thus are counted. This feature is difficult to achieve using G-M counters.

Figure 10, curves of efficiency and photofraction for a 1-3/4 x 2-in. NaI crystal, indicates that a subsurface system will have a reasonable efficiency for detecting gamma photons with energies out to 6 mev but will not provide very good energy conversion beyond about 3 mev. The photofraction decrease at high energy is due, of course, to the limited crystal size. This degradation of performance is not too serious, however, since resolution requirements are most severe from 0 to 2.2 mev.

Figure 11 is a block diagram of the circuitry required for the integrated natural gamma and spectral gamma measurements. It can be seen that the instrument response for natural gamma measurements can be handled in a number of ways:

- Displayed on a meter for astronaut observation and evaluation.
- Telemetered in real time back to earth.
- Stored in an on-board computer for future transmission.
- Any combination of the three.

Since the determination of the gamma spectrum will give much more information about the composition and relative amounts of the radioactive elements - especially K^{40}, U, and Th - this type of measurement will be much preferred for analysis of individual rocks, discrete surface formations, or borehole materials. This measurement technique will require, in addition to the scintillation detector described for gamma-ray measurements, use of a multi-channel, pulse-height analyzer for spectra determinations. The output from the analyzer would ordinarily be stored and transmitted to earth on command.

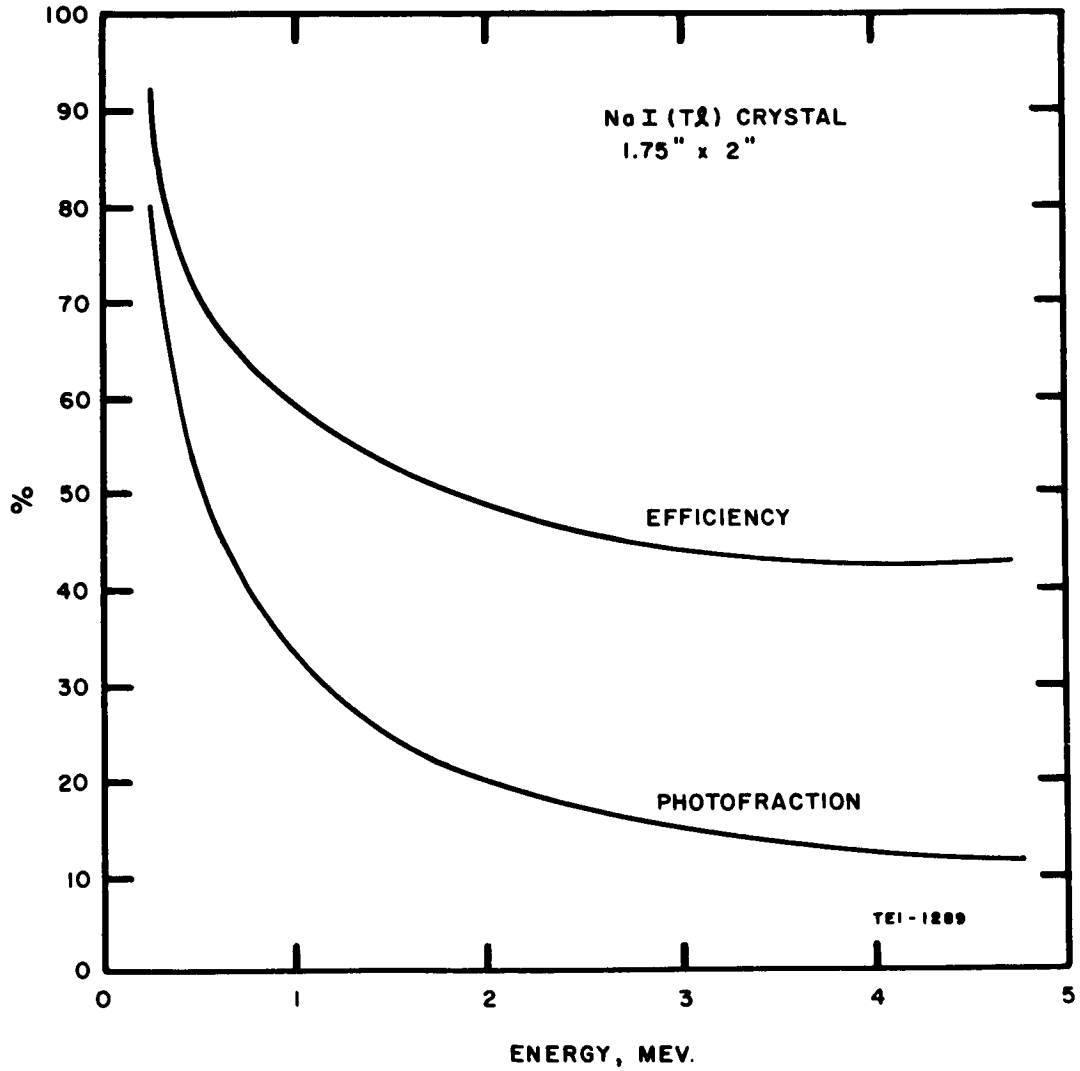

CURVES OBTAINED FROM LINEAR EXTRAPOLATION OF DATA BY MILLER, REYNOLDS, ET AL, REVIEW OF SCIENTIFIC INSTRUMENTS SEPT., 1957

Fig. 10 Efficiency and Photofraction of a Sodium-Iodide Crystal

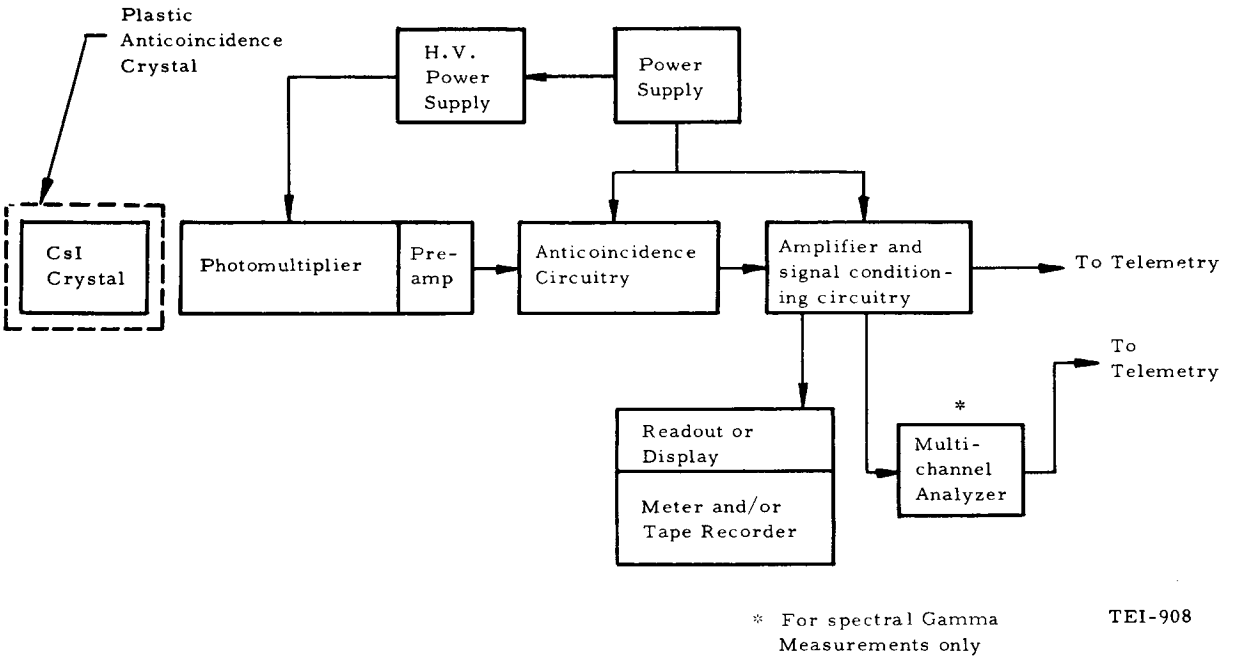

Fig. 11 Block Diagram - Natural- and Spectral-Gamma Systems

Probable Subsystem Elements.

Scintillation crystal: CsI (Tℓ) such as available from Henshaw Chemical Co. (chosen over NaI because of more suitable mechanical characteristics) surrounded by a Pilot B plastic scintillator.

Photomultiplier: Ascop Model 541N (chosen because of temperature range, efficiency, and ruggedness - certain RCA types under development may be substituted).

Supporting electronics: To be designed.

Pulse-height analyzer: 512-channel unit under development for JPL for generalized space use.

The detector subassembly to be used in the natural/spectral gamma measurements is shown in Fig. 12. The overall length of this probe section is about 7.0 in., the diameter is 1.75 in. and the weight about 1.20 lbs.

Operational Requirements. Operation of the natural-gamma experiment in borehole logging involves only the activation of the various electronic circuits (H.V. power supply, etc.) and occasional monitoring of the instrument output. If continuous logging is to be used, the astronaut should be able to vary the logging speed and system time constant to assure a counting rate high enough to be statistically meaningful. A logging speed of approximately 1 ft/min in the 10-ft holes and perhaps 5 ft/min in the 100-ft hole should be satisfactory. An additional recording and/or transmission channel should be available for instrument depth information. Caliper data will not be needed since it can be shown that response is not affected by hole size variations (5, 6). One or more small calibration sources should be included so that instrument response can be checked before and after measurement in each hole.

During surface traverses, the probe will be employed for measurement of the lunar-surface radioactivity. This can be done either by mounting the probe on the LSSM or by towing it behind the vehicle. In either scheme the astronaut may monitor instrument response for formation anomalies and thus be assisted in his sample selection task. Since a continuous record of vehicle position will be made, tie-in of instrument output with time signals will allow for radioactivity mapping. This will be helpful in analyzing data from orbiting vehicles and should provide the necessary "ground truth" information.

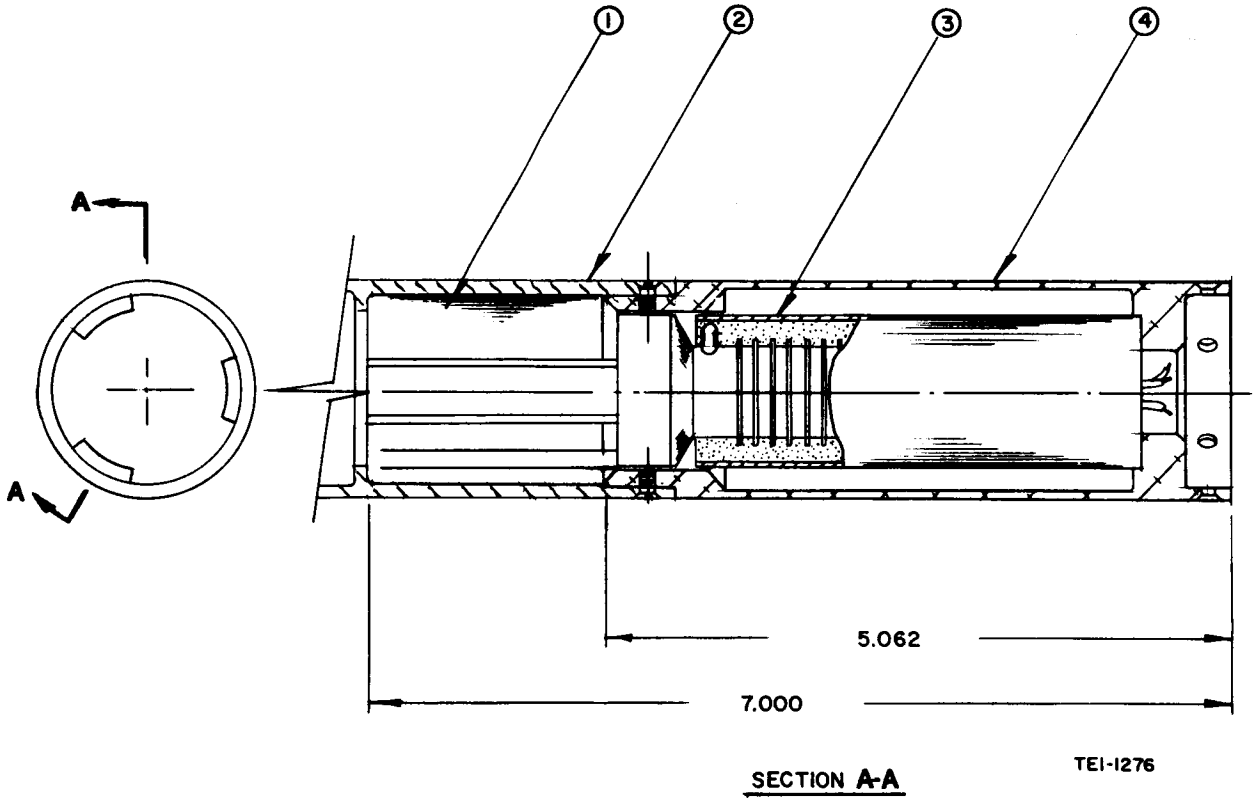

1 SCINTILLATION PHOSWICH
2 EPOXY-FIBERGLASS HOUSING
3 PHOTO MULTIPLIER PRE-AMP
4 PROBE SECTION

Fig. 12 Subassembly - Scintillation Detector (Phoswich Arrangement)

Operation of the spectral-gamma experiment is somewhat dependent on the level of activity of the formation. Estimates of the lunar, natural radioactivity range from much less than to greater than that of the earth. Results of the Russian soft lander indicate a level of about 30 mr/day, about 10 mr/day believed to be due to cosmic rays (7). In any event, the count rate will be low, thus requiring counting times for pulse-height analysis incompatible with continuous, borehole logging. Instead, it is recommended that measurements be made on a point-by-point basis with the probe stopped in the hole. Counting times could range up to several hours if the lower estimates are correct, but useful data could be obtained with measurement times on the order of 10 to 20 minutes. Astronaut duties will be similar to those for the natural-gamma measurement, including activation of the electronic circuits and occasional output monitoring. Periodic calibration, using small, capsule sources, will be necessary in order to correct for any system drift.

For surface surveys, particular attention should be accorded the area near the borehole so that effects due to induced radioactivity can be determined. These surface measurements can thus be compared with those obtained beneath the surface. A logical time for extensive counting might be during the borehole-drilling operation, but this assumes that sufficient power will be available. Other periods suitable for spectral analysis would include any time when the vehicle is stopped for some other operation, such as emplacement of seismic sources or detectors. The astronaut may choose to analyze by the gamma spectrometer certain areas shown to be of unusual activity by the integrated, gamma measurement.

Instrument Development Status. Most elements of the natural radioactivity subsystem have been or will have been used in space programs prior to the AAP. Similar scintillation detector equipment has been developed for Ranger and Surveyor. The pulse-height analyzer is currently under development for JPL for space use. Supporting electronic equipment must be designed. The major development effort will be the characterizing of the instrument in its particular mechanical configuration.

Instrument Characteristics. Table IX gives the characteristics of the natural radioactivity experiment.

TABLE IX

NATURAL RADIOACTIVITY EXPERIMENT CHARACTERISTICS

Subsystem Elements	Scintillation Phoswich, Photomultiplier-Preamp, High Voltage Supply, Anticoincidence Circuitry, Amplifier and Signal Conditioning Circuitry, Readout or Display, 512-Channel Analyzer.	
Dimensions	Downhole:	1.75-in. diameter, 7.0-in. length
	Surface:	Electronics - 4x4x2 in., Readout - 1.5-in. diameter, Pulse Height Analyzer - 6x6x6 in.
Weight	Downhole:	Scintillator - 0.6 lbs Phototube and Preamp - 0.35 lbs. Structure - 0.2 lbs
	Surface:	Electronics - 0.5 lbs, Readout - 0.1 lbs Analyzer - 5.0 lbs
Power	Peak:	N.A.
	Average:	2 watts, 5 watts with analyzer
	Power-time History:	Uniform
	Voltage:	28 VDC
Measurement Range	0.1 to 3.0 mev (a separate scale to be used for calibration)	
Accuracy or Resolution	Resolution of Detector - 7-10%	
	Accuracy a function of calibration technique	
Temperature Range	Operating:	Downhole - 218-373°K
		Surface - 250-350°K
	Storage:	Downhole & Surface - 120-400°K
Output Characteristics	Output form:	Integral counting - one pulse per a number of counts (scaled).

		Spectral analysis - a given word size per channel
	Voltage:	Fixed amplitude suitable to telemetry
	Number of Outputs:	Integral counting - 1 data, 1 depth, 1 temperature. Spectral analysis - 512 data, 1 depth, 2 temperature
	Frequency Range (Pulse Rate):	1 to 10,000 counts/sec
	Commutated or Continuous:	May be commutated.
	Impedance:	As required.
	Transmission Accuracy Req:	Standard
Logging Speed	Integral counting	- 10-ft holes - 1 ft/min 100-ft hole - 5 ft/min
	Spectral Analysis	- Fixed point - 10-20 min/point

b. Bulk Density (Gamma-Gamma Technique)

Background. One of the most informative measurements is the gamma-gamma technique which is widely used by oil companies to determine bulk density of borehole formations. The term "bulk density" is applied to the overall or gross density of a unit volume of rock and, in the case of porous rock, it includes the density of material in the pore spaces as well as the grain density of the rock. Bulk density is useful in determining formation material make-up, formation porosity, and in correlating measurements obtained from other experiments. Knowledge of the density of near-surface material is required for the reduction of data from gravity traverses. The density parameter also enters into many of the equations relating sensor output to the physical parameter in question (thermal

diffusivity, neutron-gamma, etc.) and is thus needed for measurement interpretation.

In situ measurements are especially important both on the surface and in the borehole because valid samples cannot be obtained if the material is of an unconsolidated nature. Density information of the near-surface layer will be extremely important in order to complement the various thermal analyses to be performed.

Measurement Technique. The gamma-gamma, density measurement will be made using an instrument consisting of a collimated, gamma-ray source and a gamma-ray detector.

When a collimated beam of gamma radiation of intensity I_o penetrates a thickness of matter, t, the interactions of the gamma radiation with the matter are such that after penetration and neglecting buildup, the flux is decreased to a value, I, where:

$$I = I_o e^{-\mu\rho t} \qquad (1)$$

and

I_o = initial gamma intensity

I = resultant gamma intensity

μ = total lunar absorption coefficient in cm^2/gm

ρ = density in gms/cm^3

t = thickness in cm

Taking the logarithms of both sides of equation (1) we have

$$\ln I - \ln I_o = \mu\rho t \qquad (2)$$

For a constant I_o, μ, and t, equation (2) reduces to

$$\ln I = A\rho + B \qquad (3)$$

From equation (3), it is seen that, under the conditions of constant I_o, μ, and t, by measuring I, and knowing the constants A and B, the density may be determined. The constants A and B are best determined experimentally for a given configuration. This empirical calibration can also take into account changes in μ, and t which occur.

The experimental arrangement used in most gamma-gamma density measuring devices employs a combination of scattering and direct transmission of gamma radiation. However, for most formations, equation (3) will hold.

It should be pointed out that the number of gamma rays reflected from a medium to the detector indicates an average density along the path traversed, not the density at the point from which they are scattered. Therefore, source collimation is used and the tool is pressed against the borehole wall in order to maximize the portion of the paths lying in the formation. In the lunar probe, however, other operational requirements indicate the desirability of having the instrument centralized in the hole. It seems feasible that proper combinations of source strength, collimation angle, detector location, etc., can be found to suit this positioning requirement. This is especially promising because of the small probe-to-hole-size ratio. In conventional earth surveys the tool may have a diameter only a third that of the hole.

The detector to be used can be of the Geiger-Mueller type since only integral counting is involved, but a scintillation detector is preferred for the reasons discussed in the section on natural-gamma measurements. Shielding is provided to minimize transmission of gamma rays directly from the source to the detector without penetrating the formation. Shielding materials will probably consist of tungsten alloys (Mallory 1000) which have high densities yet good mechanical properties. Depleted uranium may be employed in places where surface finishes are not important.

Commonly used sources in earth surveys are Co^{60} (1.25 mev) and Cs^{137} (0.661 mev) although both are too strong for optimum measurements with minimum shielding. If minimum shielding must be employed, a source such as Ir^{192} which has a broad energy spectrum with an average of about 0.42 mev, can be used. However, this isotope has a half-life of approximately 72 days which presents instrument calibration problems. Co^{60} amd Cs^{137} with relatively long half-lives (5.2 and 30 years respectively), do not suffer from this problem.

The desired measurement range for the AAP instrument is much greater than for conventional well-logging instruments because the lunar material can cover such a wide range of density. The material may be quite light (< 0.2 g/cc) such as solidified foam composed of volcanic overflow, or dust; or quite heavy (> 6.0 g/cc) if nickel-iron meteorites. Conventional instruments usually are designed to operate in the range from 2 to 3 g/cc. Accuracies for these instruments, when properly corrected using departure curves,

can be within ± 0.01 g/cc at 2.2 g/cc. Figure 13 shows the response curve obtained with a Surveyor-type instrument.

The elements of the system are shown in the block diagram, Figure 14. The detector and electronics portions are those used in the natural-gamma and spectral-gamma measurements.

Probable Subsystem Elements

Scintillation crystal: Same as natural/spectral-gamma experiment.

Photomultiplier: Same as natural/spectral-gamma experiment.

Supporting electronics: Same as natural/spectral-gamma experiment.

Gamma source holder: To be designed.

Gamma source: Probably Cs^{137}.

The probe subassembly to be used in the gamma-gamma density experiment is shown in Figure 15. The gamma source holder adds 3.5 in. to the probe length and about 3.65 lbs. to the probe weight. No additional power is required.

Operational Requirements. The gamma-gamma density measurement is one that can be readily made while pulling the tool from the hole. On earth, logging speeds of approximately 25 ft/min are used but should be reduced here since smaller sources will be used. A speed of 1 ft/min would be satisfactory for the 10-ft holes. A higher speed (5 to 10 ft/min) may be required in the 100-ft hole if measurement time becomes a limiting factor. This would result in only a minimum degrading of the measurement. Caliper data and depth marks should be recorded with the instrument output.

Since the experiment shares the scintillation detector with the natural-gamma experiment, they must be run independently. The gamma source holder is designed so that the source capsule can be removed except when the density measurement is to be made. This is necessary in order not to mask signals coming from the natural radioactivity of the formation with radiation coming from the capsule source. This insertion and removal of the source can be done by the astronaut without hazard.

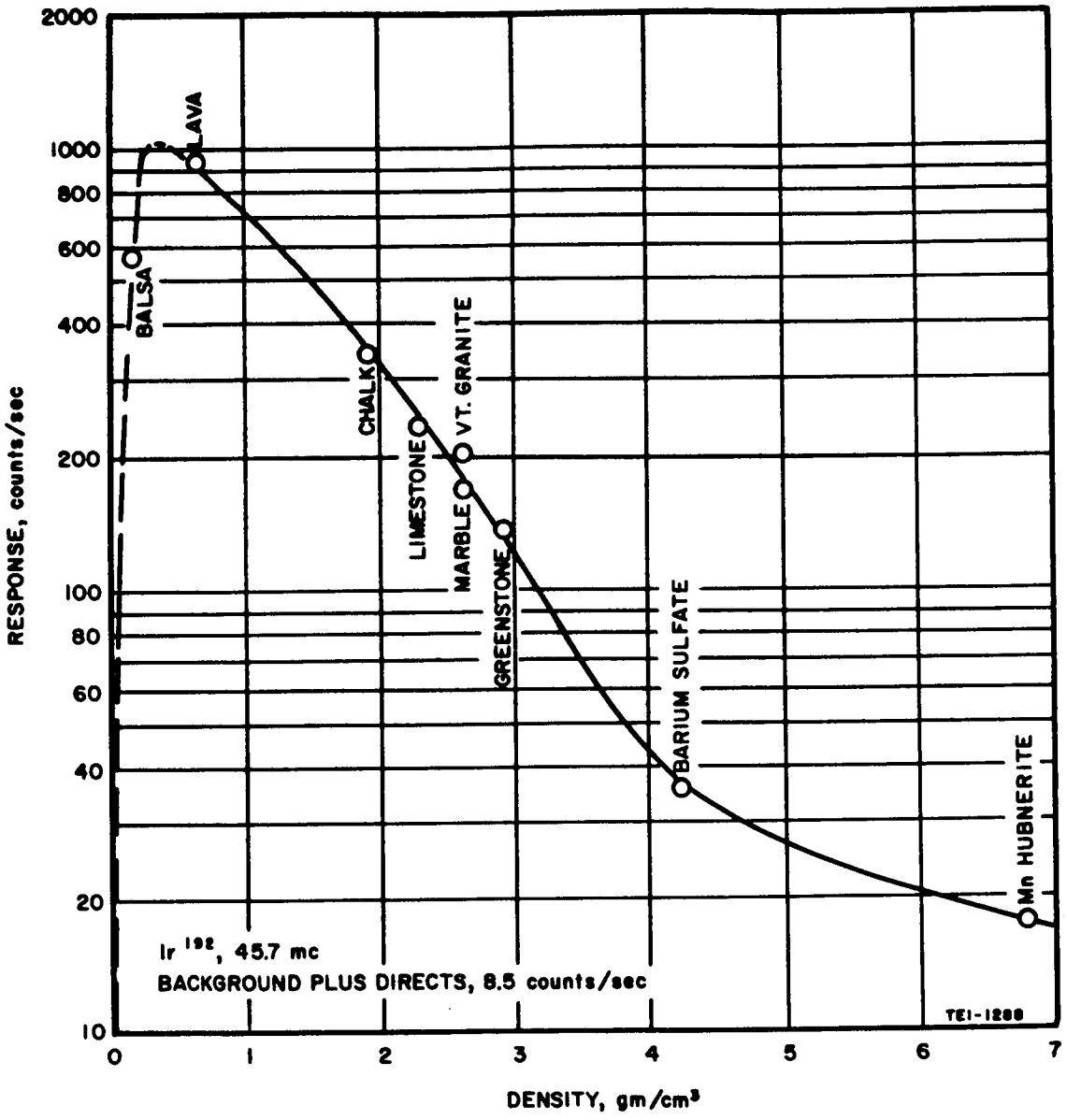

Fig. 13 Response Curve - Gamma-Gamma (Density) Instrument

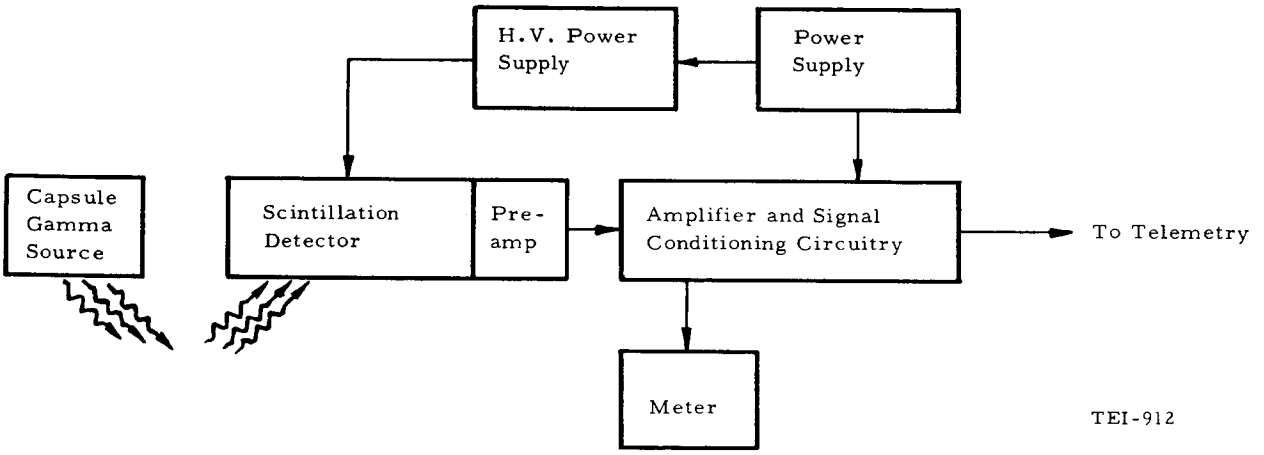

Fig. 14 Block Diagram - Gamma-Gamma (Density) System

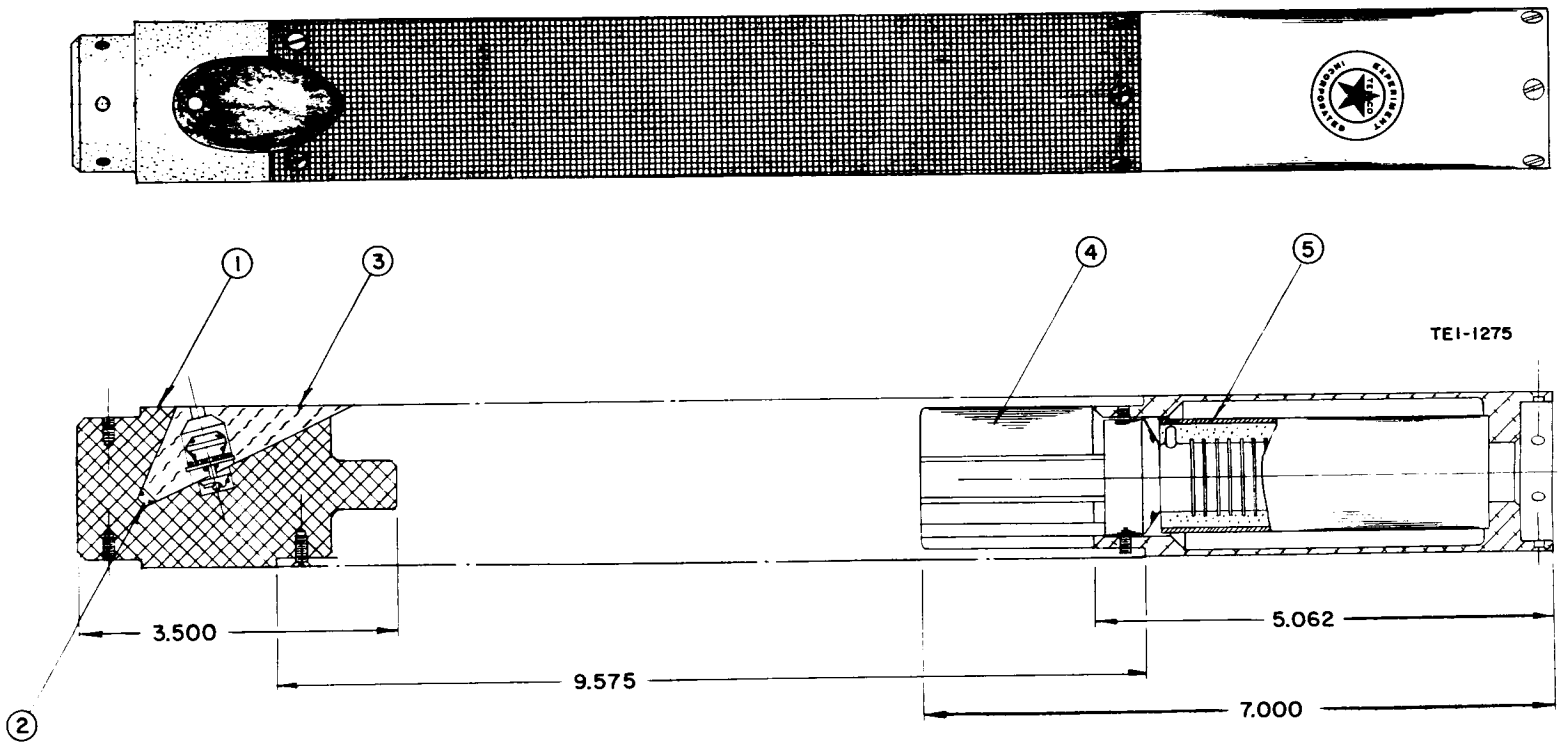

① SOURCE COLLIMATOR
② SOURCE CAPSULE
③ REMOVABLE PLUG
④ SCINTILLATION PHOSWICH
⑤ PHOTOMULTIPLIER

Fig. 15 Subassembly - Gamma-Gamma (Density) System

Count-rate (and thus density) data can be read on a meter so that the astronaut may direct additional measurements to regions of unusual response.

If properly adapted, surface measurements can be made with the instrument placed on the surface. These could possibly be performed continuously behind the LSSM if the terrain allows; otherwise the vehicle must be stopped. This measurement would be useful in locating near-surface anomalies.

Instrument Development Status. A subsurface gamma-gamma density instrument was developed for the Surveyor. This instrument was to work in a 1-in. diameter borehole and consisted of an Ir^{192} source and a G-M counter tube. Because of the limited space available for shielding, operation was only adequate. The AAP instrument should be greatly improved since its size will accommodate a scintillation detector, and more shielding can be used. The best combination of instrument parameters must be determined. The major subsystem elements will have been space-proven.

Instrument Characteristics. Table X gives the characteristics of the experiment.

TABLE X
BULK DENSITY EXPERIMENT CHARACTERISTICS

Subsystem Elements	Gamma Source and Collimator, Scintillation Crystal, Photomultiplier-Preamp, High Voltage Supply, Amplifier-Scaling-Signal Conditioning Circuitry, Readout or Display (All but gamma source same as that used in natural gamma experiment)	
Dimensions	Downhole:	Source Collimator - 1.75 in. diameter, 3.5 in. long Detector - included elsewhere
	Surface:	Included elsewhere
Weight	Downhole:	Source Collimator - 3.65 lbs.
	Surface:	Included elsewhere

Power	Peak:	N.A.
	Average:	2 watts (included elsewhere)
	Power-time History:	Uniform
	Voltage:	28 VDC
Measurement Range	0.15 to 7.0 g/cc	
Accuracy or Resolution	± 0.15 g/cc (0.15 to 2 g/cc) ± 7.5% (2 to 7 g/cc)	
Temperature Range	Operating:	Downhole - 218°-373°K Surface - 250°-350°K
	Storage:	Downhole & Surface - 120°-400°K
Output Characteristics	Output form:	Digital - may be scaled if needed
	Voltage:	Fixed amplitude, suitable to telemetry
	Number of Outputs:	1 data, 1 depth, 1 caliper, 1 temperature.
	Frequency Range (Pulse rate):	100 to 20,000 counts/sec
	Commutated or Continuous:	May be commutated if properly scaled and stored
	Impedance:	As required.
	Transmission Accuracy Required:	Standard
Logging Speed	10-ft holes - 1 ft/min 100-ft hole - 5 ft/min	

c. Neutron Irradiation Experiments (Neutron-Gamma)

Background. According to Urey (8) elemental abundance on the moon is in the following order: O, Si, Mg, Fe, S, Al, Ca, Na, Ni, and Cr. Interestingly, these elements also generally fall high on the list of elements having high neutron cross sections and thus submit to analysis by the neutron-gamma technique. See Table XI.

It is,therefore, important that analysis of the lunar surface and borehole material be accomplished in order to determine the presence and abundance of these materials. The neutron-gamma approach is attractive because of its ability to distinguish among a fairly wide group of elements otherwise not suitable to other analytical techniques, especially as relates to the lunar operation. It is recognized that neutron-activation and other neutron-gamma analyses will be performed on the returned samples, but in situ measurements are justified as a means of providing additional data points from many diverse locations. Results, if made available to the astronaut, could be used as an aid to sample selection.

Neutron-gamma analysis should be capable of determining the hydrogen content (water) if present in sufficient quantities.

Measurement Technique. The general technique of determining elemental presence or abundance by neutron irradiation methods is commonly referred to as neutron-gamma analysis. (The first word, neutron, referring to the type of irradiation used, and the second, gamma, referring to the resultant energy form used for analysis).

Several analytical techniques are possible because neutrons can interact with the formation materials in a number of ways. For example, if energetic neutrons are directed into a formation, several reactions can take place. These include (9):

- Elastic scattering; where the neutron collides with the atom and the kinetic energy is conserved with no nuclear radiation emitted.

- Inelastic scattering; in which the kinetic energy is not conserved and the atom is left in an excited state resulting in prompt emission of gamma radiation.

TABLE XI
NEUTRON CROSS SECTIONS OF LUNAR ELEMENTS[1]

Element	Thermal Capture Cross Section (Barns)
Oxygen	< 0.0002
Silicon	0.13
Magnesium	0.063
Iron	2.53
Sulphur	0.49
Aluminum	0.23
Calcium	0.43
Sodium	0.505
Nickel	4.6
Chromium	2.91
Hydrogen	0.33

[1]After BNL 325 Brookhaven National Laboratory, July 1955.

- Capture and subsequent decay. If the capture process results in an excited state of the nuclide, prompt gammas are emitted such as by inelastic scattering. After a relatively long period the nuclide may decay, emitting a beta particle, gamma ray, or both in the process. The latter gammas are known as activation gammas; the flux of which is characterized by its half-life.

The usual sequence of events in the bombardment process is for the neutron to make a number of elastic and inelastic collisions losing energy each time, until thermal energies are reached and capture takes place. Thus there are three analytical processes: (1) neutron-inelastic gamma analysis; (2) neutron-capture gamma analysis; and, (3) neutron activation analysis. The importance of any of the processes is that the emitted radiation is characteristic of the element participating in the reaction and, thus, the element can be defined if the proper detecting scheme is employed.

(1) Thermal Neutron-Gamma Technique

One technique which has proved useful in well-logging operation is the thermal neutron-gamma measurement. This involves irradiation of the formation with neutrons (usually from a capsule source such as Ra-Be or Po-Be) and detection of the activation gamma rays produced in the neutron-capture process.

A minimum system would require no pulse-height analyzer because half-life rather than energy would be the measured parameter. This approach is not well suited to the lunar mission, however, since only a few elements have half-lives compatible with overall system operation. Certain ambiguities can be resolved by using a multi-channel analyzer for determination of gamma energy.

In either case, two disadvantages are noted:

- Use of a capsule source with its attendant handling and crew safety problems.

- Many elements of major importance, such as oxygen, are not sensitive to thermal-neutron capture.

This approach is not recommended unless a miniature accelerator-neutron source discussed in the next section cannot be realized.

(2) Fast Neutron-Gamma Technique

This approach is related to that discussed above, except that high-energy neutrons from an accelerator-type source are used and prompt inelastic and/or capture gamma are detected and sorted by a multi-channel analyzer. The advantages of the accelerator source are:

- More energetic neutrons
- Higher flux
- Gamma free
- Can be switched on or off (no crew hazard problem).

The timing of the inelastic scattering, capture, and activation events which occur when using a pulsed-neutron source can be seen by referring to Figure 16.

At time "zero", the neutron pulse is initiated. Arrival of the gamma rays resulting from inelastic scattering begins after sufficient time has elapsed for the neutron to travel from the source to the formation and for the gammas to travel from the formation to the detector (the width of the peak, due to inelastic scattering, will be of the order of the neutron pulse width). After formation of the inelastic gammas, the neutrons continue to lose energy until thermal velocities are reached and capture occurs. This process normally requires 10 to 1000 μsec, and the resulting capture gammas appear as a broad peak extending over that period. Finally, arrival of activation gammas beings, the flux of which may vary in half-life from seconds to hours or longer.

It is clear then, that if we gate the detector to be responsive to different periods of the received radiation, we can effectively separate the gamma contributions of the different processes. This can be done by switching the detector or pulse-height analyzer on and off in step with the pulsed neutron source.

The elements which may be detected by this technique are shown in Table XII along with the probable minimum detectable abundance for each.

A block diagram of the equipment needed for the fast neutron-gamma measurement is shown in Figure 17. The accelerator neutron source would be similar to that developed by Lawrence Radiation Laboratory for Surveyor-type missions. The neutron generator itself, developed by Sandia Corp., was about 1.2 in. in diameter and was capable of producing neutron pulses 5-μsec long at a repetition rate of 1 KC and providing a total flux of 10^{-7} n/sec.

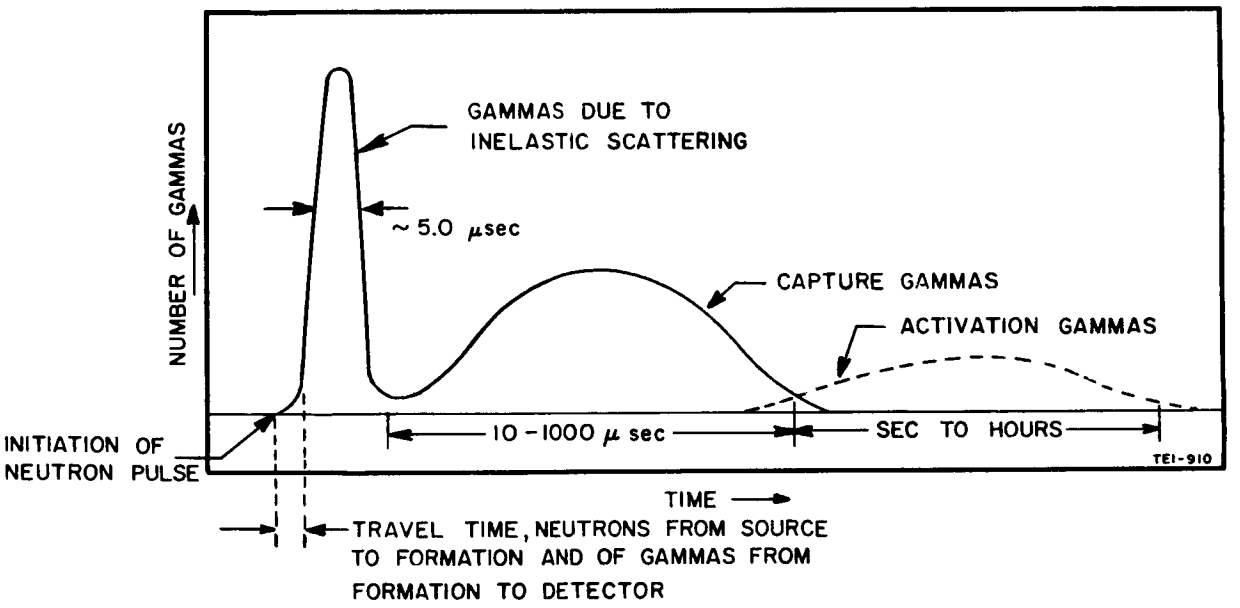

Fig. 16 Timing of Neutron Activation Events

TABLE XII
ELEMENTS DETECTABLE BY NEUTRON-GAMMA TECHNIQUES

Element	Minimum % Detectable
Iron	0.1
Silicon	0.5
Magnesium	0.3
Aluminum	2.0
Oxygen	3.7
Potassium	1.0
Calcium	1.2
Sodium	1.3
Nickel	1.0
Hydrogen	0.6
Sulfur	2.4

Data except Hydrogen and Sulfur from Stinner, 1961 (10).

Hydrogen and Sulfur from Green, 1960 (3).

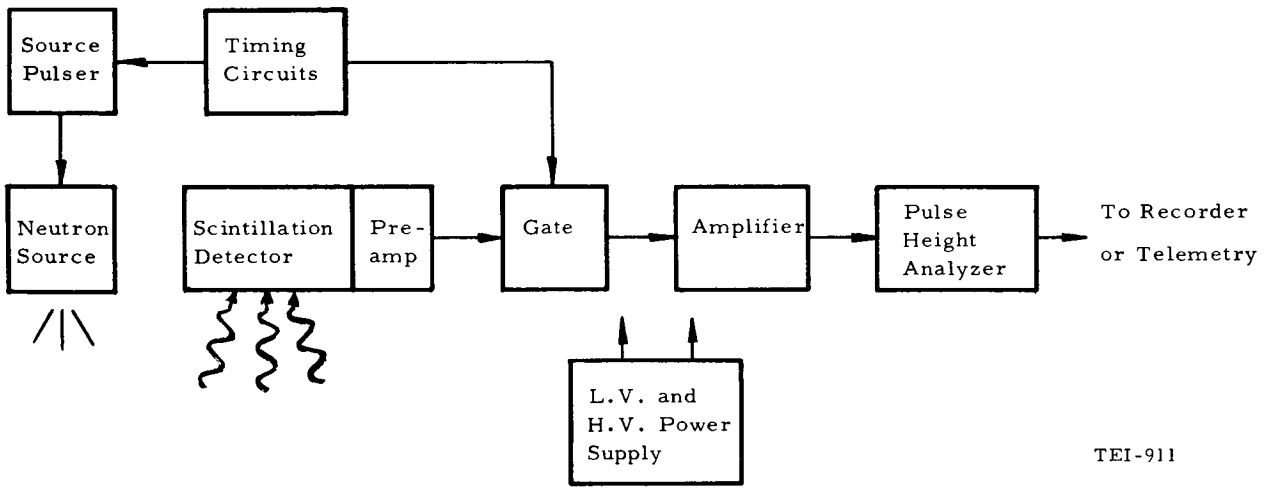

Fig. 17 Block Diagram - Fast-Neutron-Gamma System

A high voltage supply, pulsing, and control circuits are also required. In the LRL device the power supply had a diameter of 2.2 in. which is slightly too large for our probe. Dr. James Waggoner of LRL believes (personal correspondence) that the improvements made in components, particularly capacitors, since the Surveyor prototype was completed would allow for a smaller diameter compatible with this probe application. Other miniature accelerator sources have been developed for conventional well-logging operations and proposed for lunar missions. These were developed by such companies as High Voltage Engineering, Kamen Nuclear, Schlumberger, etc. They were in the 3- to 4-in. diameter size and some doubt exists as to the ability to fit these into a device of about 1-3/4 in. in diameter.

The timing and gating circuits shown in the diagram are those needed to pulse the neutron source and switch the detector-analyzer for separation of the different elements of the gamma flux. The scintillation detector would be the same type as that used in the natural/spectral gamma measurement and the pulse-height analyzer would be shared with that experiment. The detector should have sufficient capability to define the oxygen 6.14 mev triple peak.

Due to the overall lengths required for the instrumentation and the development aspects that exist, this experiment is being suggested as a separate probe. It could be used in the borehole while other surface operations are being carried out; or on the surface to analyze formations of interest, or core, or surface samples previously obtained, when borehole logging is underway. During the course of instrument development, the feasibility of using the neutron-gamma technique to determine formation bulk density should be evaluated. If successful, this experiment as well as the natural/spectral gamma experiment could be removed from the optimum probe to reduce its size or to make room for other experiments.

Probable Subsystem Elements.

Scintillation crystal: CsI (Tℓ) such as for natural gamma measurements. May not use plastic scintillator for charge particle discrimination.

Photomultiplier: Ascop Model 541N or RCA type under development.

Pulsed-neutron source: Basic system from LRL development.

Supporting electronics: To be designed.

Pulse-height analyzer: 512-channel unit under development for JPL for generalized space use.

The Subsurface Neutron-Gamma Probe was shown in Section II, pg. 24, as Figure 4.

The overall length is 40.9 in., the diameter is 1.75 in., and the weight 8.67 lbs.

Operational Requirements. Operation of the fast neutron-gamma experiment in borehole logging consists of the positioning of the tool in the hole and activation of the electronic circuitry. Since the pulse height analyzer is shared with the spectral-gamma experiment, the two measurements must be made independently. Obviously, any measurement of natural radioactivity should be made before measurements of artificially-induced radioactivity. The sequence for this experiment would be: (1) inelastic gamma analysis, (2) capture gamma analysis, and (3) activation analysis.

The probe, when equipped with the necessary auxiliary equipment such as a thermal shield, will also be used for surface measurements. Core and hand samples may be analyzed with a properly fitted-out probe.

Instrument Development Status. An instrument, very similar to the one described, has been developed by the Lawrence Radiation Laboratory for lunar use. This instrument was designed to be deployed on the lunar surface rather than for use in a borehole. As pointed out earlier, however, many of the essential elements are of a size suitable for use in a 2-in. borehole.

The power supply used with the LRL device had a diameter of 2.2 in. This must be redesigned to fit the probe constraint. The neutron generator tube is suitable in its present configuration. The scintillation detector would be the same as described for the other nuclear experiments. The major development effort will involve determining the overall capability of the instrument to distinguish among the various elements of interest in the face of all interferences which exist. The degree of difficulty, in detecting each element, will vary; depending upon such factors as interference from other elements within the formation, variation in cross section, and differences in activation energy levels required.

Instrument Characteristics. Table XIII gives the characteristics of the neutron-gamma experiment.

TABLE XIII
NEUTRON-GAMMA EXPERIMENT CHARACTERISTICS

Subsystem Elements	Neutron Generator Tube, High Voltage Supply, Pulsing, Control and Timing Circuitry, Photomultiplier-Preamp, Amplifier and Signal Conditioning Circuitry, 512 Channel Analyzer.	
Dimensions	Downhole:	1.75-in. diameter, 40.9-in. length.
	Surface:	4x4x4 in. (Pulse-height analyzer included elsewhere)
Weight	Downhole:	8.67 lbs.
	Surface:	2.0 lbs.
Power	Peak:	10 watts
	Average:	10 watts
	Power-Time History:	Uniform
	Voltage:	28 VDC
Measurement Range	400 kev to 7 mev	
Accuracy or resolution	± 5-7% of gamma energy	
Temperature Range	Operating:	Downhole - 218°-343°K Surface - 218°-343°K
	Storage:	Downhole & Surface - 73°-343°K
Output Characteristics	Output Form:	Digital, serial binary
	Voltage:	Arbitrary
	Number of Outputs:	512 data plus house-keeping
	Frequency Range (Pulse rate):	Arbitrary
	Commutated or Continuous:	Commutated
	Impedance:	As required
	Transmission Accuracy Req:	1 bit/10^3 bits
Logging Speed	Fixed point -	10-20 minutes/point.

2. Thermal Measurements

In situ thermal measurements of the moon will be among the most important to be made. This is true not only from the standpoint of determining basic information about the nature, structure, and origin of moon and planets but also to satisfy the need for data concerning properties of the lunar materials relevant to their practical use in setting up lunar bases.

The first area of interest, that of fundamental questions concerning the moon's nature and origin, is well represented in the literature by Urey's book on the planets (2) and by the recent conference on "Geological Problems in Lunar Research" (11). From these sources, it is clear that both thermal measurements and determinations of the composition of lunar material would do away with considerable controversy concerning the origin of the moon and the development of its surface features (e.g. lunar maria).

The problem of the heat balance of the moon, of course, requires thermal data. For example, consider the differential equation for the change in temperature due to surface cooling of a sphere heated uniformly by radioactive decay (ref. 2, pg. 52):

$$\frac{\partial T}{\partial t} = K \frac{\partial^2 T}{\partial r^2} + \frac{2}{r} \frac{\partial T}{\partial r} + \Sigma Q_i e^{-\alpha_i t}$$

Urey's solution of this equation for boundary conditions $T(x,o) = T_o$ for all values of r at t = o and T(a,t) = 0 for all times at the surface is:

$$T = \sum_{n=1}^{\infty} \frac{a}{r} \sum_i \frac{Q_i}{\alpha_i - \frac{Kn^2\pi^2}{a^2}} \frac{2(-1)^n}{n\pi} \sin n\pi \frac{r}{a} \left[e^{-\alpha_i t} - e^{-\frac{Kn^2\pi^2 t}{a^2}} \right] -$$

$$\sum_{n=1}^{\infty} \frac{a}{r} T_o \frac{2(-1)^n}{n\pi} \sin n\pi \frac{r}{a} e^{-\frac{Kn^2\pi^2 t}{a^2}}$$

Where:

K is the thermal diffusivity

$$K = \frac{k}{\rho c}$$

k = thermal conductivity

ρ = density

c = specific heat

a = radius of the planet

r = any radius

α_i = decay constant of the radioactive substance

Q_i = rate of increase of temperatures due to the ith radioactive substance at time equal to zero.

Thus it can be seen that a knowledge of thermal diffusivity (or thermal conductivity) and specific heat capacity of lunar material is essential for an understanding of the heat balance of the moon. This also requires a knowledge of the radioactive elements in the moon.

a. Temperature

Background. A temperature determination is considered of primary importance at both the surface and in the subsurface. These measurements should be obtained under day and night conditions. Measurement techniques utilizing radiation properties are probably to be preferred over those which depend upon thermal contact. Making good thermal contact is often difficult even under ideal laboratory conditions. When the material to be studied is a thermal insulator it becomes more difficult, and when that insulator is a dust, there are still further problems. Under such conditions, heat flow along connecting wire produces errors in temperature readings which can be of a large order. Methods of estimating errors in contact thermometry are given in Reference 12. Appendix VII gives an example of the range of error which might be expected. However, in view of the relative simplicity of contact- over radiation-temperature-measuring techniques, both types will be employed.

Subsurface measurements of temperature as a function of depth would yield additional valuable information about the temperature gradient and perhaps about heat flow from the interior of the moon. The proposed devices do not have the accuracy required for detailed heat flow measurements nor will they ordinarily be left in position long enough for the required equilibrium conditions to exist, but they will provide informative data concerning local variations in ambient temperature and drill heating effects. Accurate heat flow measurements are best made using the philosophy of the FSS.

The radiation technique may also furnish additional information in the form of possible water-vapor detection. The scan of this instrument is from 5 to 30 microns. There is a large absorption peak due to water vapor in the band from approximately 5 to 7 microns. Therefore, this instrument may yield valuable information pertaining to the presence of water. This should be determined under both day and night conditions since, if water is present, it may be frozen at night and evolve from the surface under solar radiation.

Measurement Technique. The lunar subsurface temperature will be determined by two separate methods: (1) non-contact by the use of an interferometer spectrometer (I.S.), and (2) a contact sensor.

(1) Non-Contact Temperature Experiment

The interferometer spectrometer, Figure 18, will be a modified Michelson interferometer which utilizes an electromechanical mirror-drive mechanism and a bolometer detector to convert incident infrared radiation into audio frequencies. The amplitude of the signals varies proportionally as the fourth power of the differential temperature between the object being viewed and the bolometer detector. The frequency of the resultant audio signal is a direct function of the velocity of the moving mirror and the wavelength of the incident radiation. With the mirror being swept at a constant rate, there exists a one-to-one relationship between incident wave length and audio frequency output. It is sufficient to say here that, by performing a Fourier analysis of the output wave form, the temperature of the viewed body can be determined (see Appendix II for a detailed theory of operation).

The instrument scans the 5-to-30 micron region. Since a strong, water-absorption peak lies in the 5-to-7 micron range, the same instrument can be used in determining the possible presence of water. This will not interfere with a temperature measurement since the full spectrum will be recorded and other portions of the instrument response can be used. It is anticipated that the I.S. will have a capability of approximately 1000 resolution elements, with only about 200 elements needed for a temperature measurement accurate to about 1 to 2 percent.

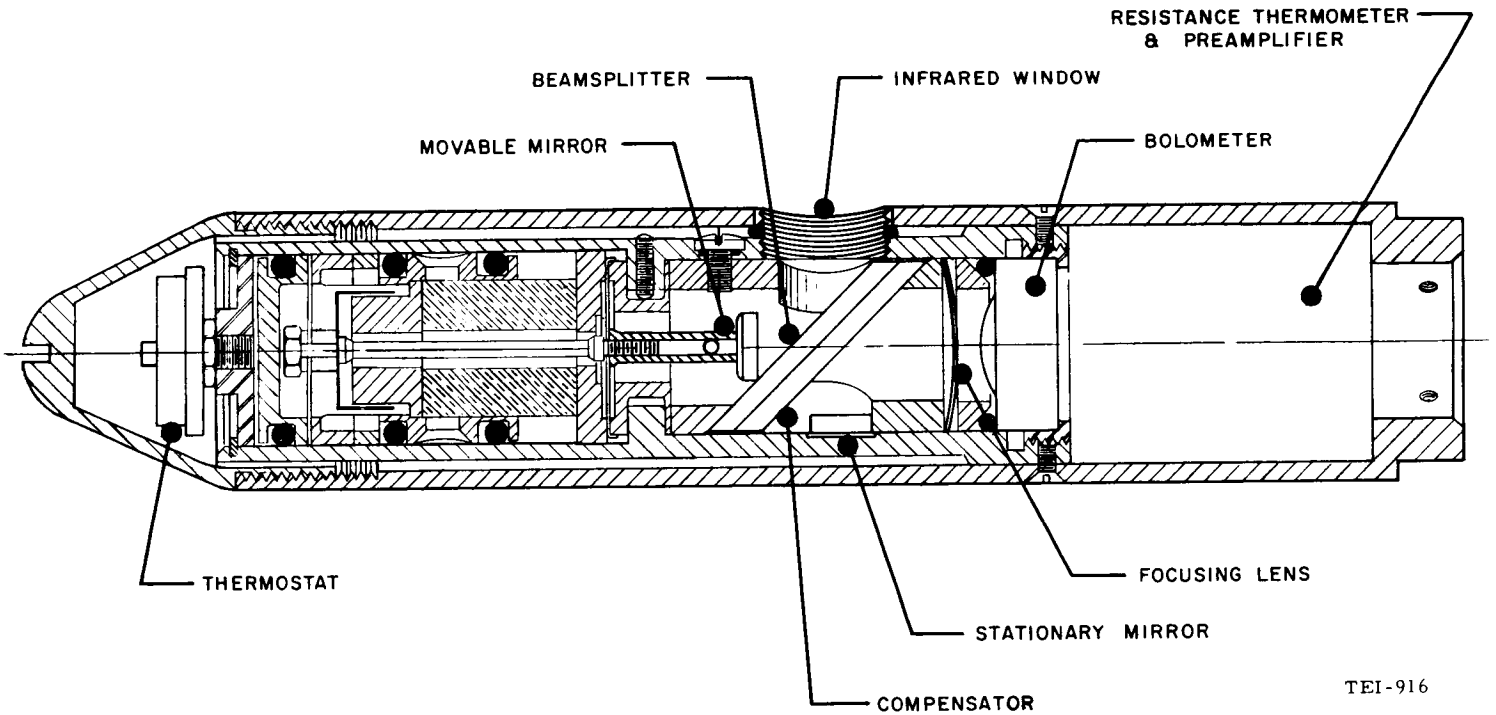

Fig. 18 Subassembly - Interferometer Spectrometer

A block diagram of the interferometer spectrometer is shown in Figure 19. The sensor and preamp are located in the probe whereas the other elements are contained in the surface electronics package.

Although calculations show that radiation-analysis techniques for temperature measurement are preferable for the possible range of lunar materials considered, simplicity and use of deployment warrant inclusion of contact-type thermal sensors. (See Appendix VII for detailed analysis of contact thermometry).

(2) Contact Temperature Experiment

Three, common, non-radiation type, electrical, temperature-sensing devices are available for remote, temperature measurement on the moon. These are the thermocouple, the resistance-temperature sensor and the thermistor.

Thermistors offer the advantage of small size and large temperature coefficients of resistivity. They can generally be of high resistance values to make lead-resistance errors negligible. They are, however, better suited to precise measurement of narrow spans of temperature rather than for use over wide ranges because of their non-linear response. Thermistors are also subject to changes in their response curve after temperature cycling and aging. They also suffer from problems of resistance changes due to self heating.

Thermocouples have the advantages of small, physical size and of requiring no excitation. Their main disadvantages are the low voltages they generate (for example, chromel/constantan generates 63 microvolts per degree in the range of 273°K to 373°K) and the need for a reference junction. Because accurate measurements must be made over a wide range of temperature, several reference junctions may have to be used, each maintained at a different temperature by its own temperature-control system.

The main advantages of resistive sensors are their ability to produce much larger outputs than obtainable from thermocouples, small drift due to aging or cycling, and the elimination of the need for a reference junction. For example, a typical platinum, resistance-sensor circuit with parameters compatible with the requirements of a number of lunar applications will yield about four millivolts per degree K. The main disadvantages of resistive sensing are the need for an accurately controlled, or accurately known, source of excitation, the relatively large size and mass of the sensors, and the need for thermal design of the structure relating the sensor to the point being sensed. This thermal

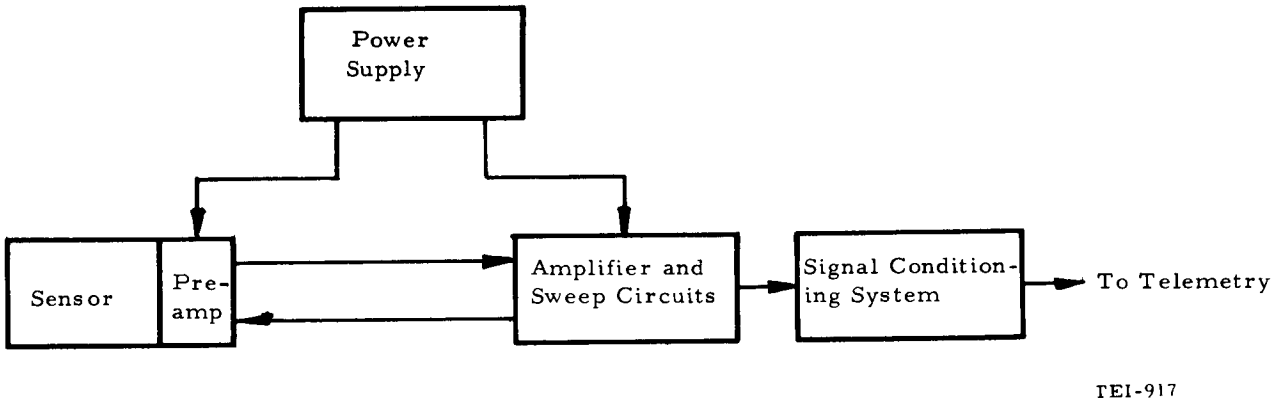

Fig. 19 Block Diagram - Interferometer Spectrometer

design encompasses the problem of self-heating by the excitation current, the problem of temperature changes in the point being sensed, because of the heat flow into or out of the sensor, and the problem of insuring a good thermal bond between the sensor and the point of measurement.

Both resistive sensors and thermocouples present problems with regard to their leads. Thermocouple leads must be very homogeneous because of the large temperature gradient which may exist along their length. The temperature at the junction of any dissimilar metals in the thermocouple circuit must also be controlled. Resistance variations in the leads from the resistive sensors will cause signal errors. This requires either a wire of sufficiently heavy gauge, or increased resistance of the sensor, or use of some compensating scheme. Thermal EMF's also have to be considered with resistance sensors. However, if the system can be designed to yield the higher outputs, these thermal EMF's will be a much less severe problem than in the thermocouple case.

After reviewing the different advantages and disadvantages of the three temperature-sensing devices, it is our opinion that the resistive sensor is best for lunar operation. The most outstanding feature of the resistive sensor that influenced this recommendation is their larger output. For instance, in the case where four millivolts per degree K is obtained, this signal can be fed without amplification into an analog-to-digital converter. This large output will also allow the use of solid-state commutation, in place of mechanical commutation, where more than one temperature is to be recorded through a common readout system. The combination of no amplification and solid-state commutation should increase the reliability of the temperature-measuring system. For the various reasons and recommendations as stated above, the remainder of this section will be devoted to a full examination into the use of resistive sensors.

The sensor that has been selected is a platinum, resistance, temperature transducer. The resistance of the unit is 1000 ohms ± 1% at 273°K. This value was chosen, along with an excitation current of 2.5 ma, to provide an output signal of from 0.97 to 3.73 volts over the temperature range from 120° to 400°K. As can be seen, the sensor output will still be in the required telemetry range (0-5V) for temperatures well outside these limits.

The size of the sensor is 0.062 in. in diameter and 0.125-in. long. It has two wires leading from the ceramic covered bulb. Its repeatability is within ± 0.3^{o}K at 273°K. The response of the basic sensor is less than 1 sec to reach 63% of a step change in temperature from room ambient air to boiling water.

Figure 20 indicates how the formation thermal conductivity influences the accuracy of the contact temperature sensor. The errors are those due to heat transfer between the formation and sensor and are in addition to any other errors which exist. These curves were obtained by solving the general surface-thermometry equations of Jakob (12). The difference in temperature is a transient affect and will steadily decrease with time from the instant the sensor and measured surface are brought into contact. It can be seen that, for measurements of high accuracy, the differential temperature must be low ($< 10^{o}K$) which could mean appreciable waiting time, especially for materials of very-low thermal conductivity. It is for this reason that the non-contact interferometer spectrometer is also being employed.

A block diagram of the contact temperature sensor is given in Figure 21. The commutator (discussed in Appendix VII) is used to switch the telemetry input among the various temperature sensors to be used.

The subsurface thermal-diffusivity instrument, described in a subsequent section, may also be used as a passive radiometer to make an independent temperature measurement. This instrument is included in the probe and needs only to have its sensing element energized for a subsurface temperature measurement. There are three outputs to be recorded. One is the instrument temperature obtained from a thermal sensor imbedded in the instrument body. The other two are the radiometer outputs which are a measure of the wall temperature. All are DC and of the order of $0.5^{o}K$ change in sensor temperature. The time required for this measurement is of the order of minutes. It is to be noted here that this is not an absolute measurement and interpretation of the data will depend on comparison of probe temperature and radiometer reading with curves of prior calibration. However, since this instrument will be present, and considering the ease of making the measurement, it is believed to be worthwhile. Details of this sensor are shown in Figure 23, page 93.

The lunar surface temperature will also be determined by both the interferometer spectrometer and contact-temperature-sensor methods.

Probable Subsystem Elements - Interferometer-Spectrometer

Sensor containing optics, mirror drive mechanism, bolometer detector and preamp: redesign of Block Engineering unit.

Power supply, amplifying and sweep circuits: Block Engineering.

Signal conditioning system: to be designed

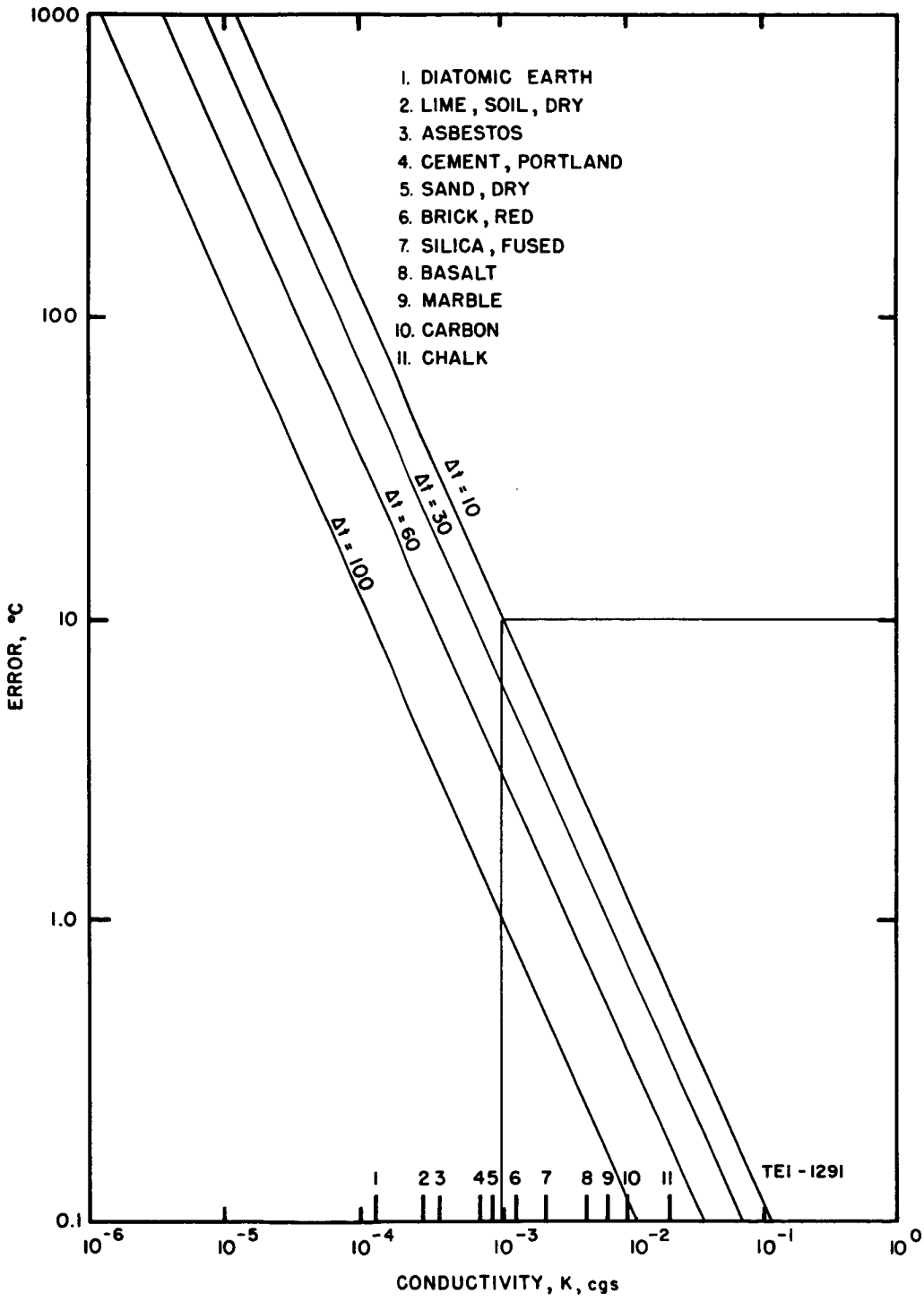

Fig. 20 Effects of Thermal Conductivity on Contact-Temperature Measurement Error

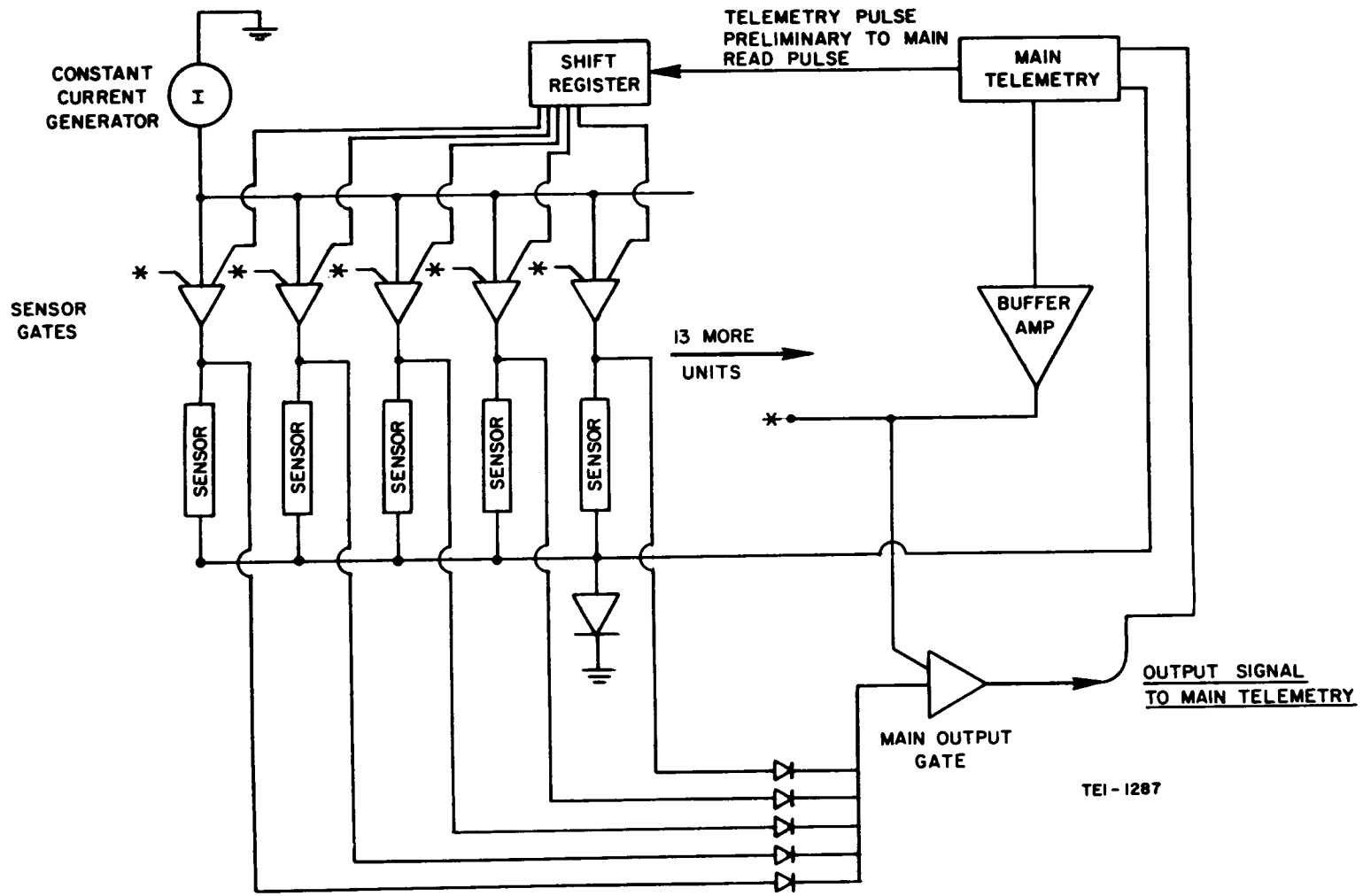

Fig. 21 Block Diagram - Contact Temperature System

Probable Subsystem Elements - Contact-Temperature Sensor

Sensor: Temtech Model 5129. This sensor used on Surveyor.

Constant current source and voltage divider: to be designed.

Commutator: to be designed.

The non-contact temperature sensor is shown in Figure 22.

Operational Requirements. All temperature measurements must be made with the probe stopped in the hole. In the case of the interferometer spectrometer, its electronic circuits will be energized and the two outputs of the instrument processed (co-added if deemed desirable - see Appendix II). One of the outputs is of a resistance thermometer, imbedded in the instrument body, to determine instrument temperature. The other is the audio output which is related to the temperature of the body viewed. The time required for the temperature determination is of the order of minutes. In the case of the contact sensor, the constant current supply will be energized and sensor output sampled. Time for this measurement will be dependent on formation thermal conductivity and must be determined from the rate-of-change of the output signal. Temperature measurements of the borehole formations should be made under both day and night conditions; to determine the effects of heat flow into, or out of, the hole via the probe.

The site for making the I.S. surface-temperature measurement must be selected and consideration should be given to the following in making this selection. For the measurements to be most meaningful, the site should be undisturbed and representative of the general lunar surface; that is, it should not contain gross departures from the characteristic lunar surface. The daytime measurement would be made preferably at local noon so that fringing effects of reflected solar radiation would be minimized. If the experiment is done when the sun is low in the sky, then the angle which the solar radiation makes with the local surface should be known. It is imperative that the instrument view a shadow-free area, and preferably an area which is removed as far as possible from shadowed areas.

For daytime measurements, after the instrument has been placed in position, the temperature determination should be made as quickly as possible to avoid the effects of local thermal currents, generated at the surface contact points by the instrument supports,

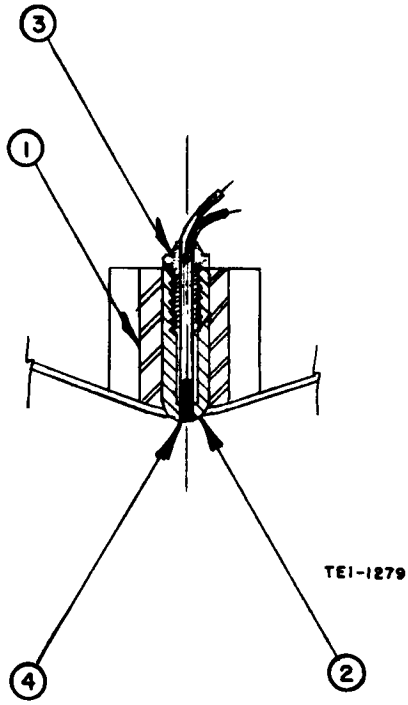

1. CALIPER SPRING GUIDE SUPPORT
2. CONTACT TEMP. SENSOR INSULATOR
3. CONTACT TEMP. SENSOR NUT
4. TEMP. SENSOR

Fig. 22 Subassembly - Contact Temperature Sensor

on the local surface temperature. The time for temperature determination is expected to be of the order of 1 or 2 minutes after the instrument is turned on.

The contact temperature measurements will be made at selected points on the lunar surface. Day and night readings will be included.

Instrument Development Status - Interferometer-Spectrometer

The instrument included in the Lunar Probe System will be a second generation instrument of the type developed for Surveyor. At that time certain thermal/mechanical problems had not been resolved but subsequent work has succeeded in correcting these. Several instruments of this type have flown on a number of satellite payloads as infrared analyzers and are space proven. The capabilities of the device as a temperature instrument have been reaffirmed by the manufacturer as a part of this study.

Instrument Development Status - Contact Temperature Instrument

The basic sensor is of the type proposed for contact temperature measurements for Surveyor. They were also used in a number of Surveyor instruments to monitor internal temperature. The major development effort will be in determining the housing design to provide the optimum heat transfer characteristics. Characterization of the device for a wide variety of samples will be time consuming.

Instrument Characteristics - Interferometer Spectrometer

Table XIV gives the characteristics of this device.

Instrument Characteristics - Contact Temperature Sensor

Table XV gives the characteristics of this instrument.

TABLE XIV

INTERFEROMETER SPECTROMETER CHARACTERISTICS

Subsystem Elements	Optics, Mirror Drive Mechanism, Bolometer Detector, Preamp, Amplifier and Sweep Circuits, Signal Conditioning System	
Dimensions	Downhole:	1.75-in. diameter, 4.5-in. long
	Surface Equipment:	Electronics - 8.5x4x1 in. Coadder - 6x6x6 in.
Weight	Downhole:	0.7 lbs
	Surface:	Electronics - 1.0 lbs Coadder - 4.0 lbs
Power	Peak:	N.A.
	Average:	Electronics - 2 watts Coadder - 8 watts
	Power Time History:	Uniform
	Voltage:	20-40 VDC
Measurement Range	120°-400°K	
Accuracy or Resolution	$<\pm 1^{\circ}$K (240°-400°K) $<\pm 5^{\circ}$K (120°-240°K)	
Temperature Range	Operating:	Downhole - 120°-400°K Surface - 250°-350°K
	Storage:	Downhole & Surface - 120°-400°K
Output Characteristics	Output form:	Interferometer - Analog Coadder - Digital (50x18 bits)
	Voltage:	0-5 volts
	Number of Outputs:	1 Data, 1 Instrument Temperature
	Frequency Range (pulse rate):	Interferometer - 0-200cps
	Commutated or continuous:	May be commutated
	Impedance:	As required
	Transmission Accuracy Req:	Standard
Logging Speed	Fixed point measurement, 1-2 min/point	

TABLE XV

CONTACT TEMPERATURE EXPERIMENT CHARACTERISTICS

Subsystem Elements	Resistance-Temperature Sensor, Sensor Housing, Constant-Current Power Supply, Voltage Divider, Commutator System	
Dimensions	Downhole:	0.315" x 0.468" x 0.730"
	Surface Equipment:	3" x 5" x 1/2"
Weight	Downhole:	0.1 lbs
	Surface:	0.5 lbs
Power	Peak:	150 mw
	Average:	2.5 mw
	Power-time History:	Input current switched between all sensors of the same type
Measurement Range	93° to $453^{o}K$ (wider range if necessary)	
Accuracy or Resolution	Basic accuracy, $\pm 1.5^{o}K$. Larger errors possible if material has low thermal conductivity and measure time is restricted.	
Output Characteristics	Data Form:	Analog
	Voltage:	0-5V
	Number of Outputs:	Approximately 18 sub-channels commutated to one main channel
	Frequency Range:	D.C.
	Commutated or Continuous:	Commutated
	Impedance:	1000 ohms, or as required
	Transmission Accuracy Req:	Standard
Logging Speed	Fixed point measurement - Time dependent on thermal conductivity of formation, several minutes for materials of interest.	

b. Thermal Diffusivity

Background. The thermal-measurements justification, previously expressed in the introductory section, applies to the measurements of both temperature and thermal diffusivity. In addition, this measurement should yield valuable information in terms of the change of diffusivity as a function of depth and the nature of the subsurface material, i.e., whether it is particulate or solid, degree of packing (if particulate), etc.

Thermal diffusivity experiments in situ, both surface and subsurface, are recommended. The surface measurement should result in thermal information concerning an undisturbed lunar sample area. The subsurface material will possibly be disturbed by the drilling operation, but still should be made in the borehole, rather than on a sample returned to earth, for the following reasons:

- If this measurement is made immediately upon termination of the drilling operation, valuable information may be gained from the time-temperature history.

- When a sample is returned to earth, it would be extremely difficult to ascertain whether occluded or chemisorbed gases were still present, or had been released by drill-generated heat.

- The effects of possible gas evolution from the lunar interior on the thermal characteristics could not be obtained.

Measurements on lunar samples returned to earth laboratories for diffusivity determinations will not necessarily provide accurate data. The material to be studied will certainly be disturbed in packaging and transporting which would result in a change in diffusivity. Simulation of the lunar conditions in an earth laboratory would be extremely difficult, and all handling and sample preparation would have to be carried out under lunar conditions. The lunar surface material has been subjected to extreme vacuum conditions for some 5×10^9 years, a condition that is extremely difficult to simulate in an earth laboratory. One must also consider the possibility of gas diffusion from the lunar interior through the surface layer which would affect the diffusivity measurement. In addition, the surface has been exposed to bombardment of the sun. This bombardment consists largely of hydrogen and some helium. This condition has existed for an extremely long time and it is possible that the surface has been thoroughly reduced by this action. The depth of this reduced layer is undetermined, but could be quite large if the surface is particulate and migration of surface particles has occurred. All of the foregoing conditions have an effect on the thermal diffusivity of a material and the measurement should be made on an undisturbed surface sample if it is to be meaningful.

In the determination of which of two measurements to make, thermal conductivity or thermal diffusivity, the below rationale was used:

$$K = \frac{k}{\rho C}$$

where:

K = thermal diffusivity in cm^2/sec

k = thermal conductivity in cal/cm sec ^oC

ρ = density in gm/cc

C = specific-heat capacity in cal/gm ^oC

Since density and specific-heat capacity will be measured in other experiments, one of the most important points to be considered is the number of different measurements involved. Thermal conductivity requires a knowledge of the rate input to the material and the temperature gradient across a given thickness of material (a measure of rate of heat input, difference in temperature, and distance). Thermal diffusivity, as proposed here, requires a knowledge of temperature rise of the material as a function of time. Time is a much more precise measurement than distance.

Thermal conductivity measurements require thermal contact with the material under investigation. In a material of very-low thermal conductivity, good thermal contact is extremely difficult to obtain. Then, too, the detector leads conduct heat away from the material, so that true temperature is difficult to determine. Again, this is especially true if the material has a low thermal conductivity. Ideally, temperature measurements by radiometer techniques, where no physical contact with the surface is necessary, should be used. Thermal diffusivity measurements lend themselves readily to this technique.

From the proposed method of downhole measurements, it may be possible to arrive at an independent value for the thermal conductivity of the lunar material; at least near the surface. Temperature will be measured at the surface and as a function of distance below the surface.

From a knowledge of incident radiation falling on the moon, and the reflectivity of the moon, the heat input at the surface of the moon can be determined. From these measurements a value for the thermal conductivity of the lunar material may be calculated. Since the radiometer measurement of temperatures represents the average temperature over a distance of several centimeters (2 to 5), thermal conductivity computed in this manner will not be precise. However, such a measurement should afford a rough independent check on the diffusivity measurement through the relation $K = k/\rho C$ without the use of additional equipment or of additional measurements.

Measurement Technique. Subsurface thermal-diffusivity measurements will be made using the instrument shown in Figure 23. This unit contains a radiant-heat source [1], a total radiation radiometer [6], suitable optics for radiation gain [2] and [5], and protective windows [3, 4, and 8]. A temperature sensing element [10] (resistance thermometer) is imbedded in the instrument body so that corrections for changes in instrument temperature may be made. Radiation from the heat source will be directed to a selected portion of the borehole wall, where a portion will be reflected and the rest absorbed. The absorbed energy is partly re-radiated from the borehole wall and the rest diffuses into the medium and raises its temperature. The radiometer responds to both reflection and radiation from the borehole wall. The effects that are detected by the radiometer are recorded and compared with curves of prior, empirical calibration (using selected standards) for the determination of thermal diffusivity. The heat source is scaled so that the differential temperatures obtained are suitable for analysis for the ranges of formation thermal conductivity and diffusivity expected. Figure 24 is a sample response curve obtained with a Surveyor-type instrument. It is expected that the response of the radiometer to the reflection of the borehole wall will yield knowledge of the gross reflectivity of the medium.

A second radiometer [7] is placed in the instrument facing 180°C away from the diffusivity radiometer. This second radiometer adds less than 1 ounce of weight and requires microwatts of power. From the response of this radiometer, we might gain added information pertaining to gross reflectivity and surface heat conduction at the borehole wall. This might well be expected to differ from conditions existing at the surface, if the material is particulate, due to packing of the material, or the presence of occluded gases and/or chemisorbed gases which might be released under the influence of wall heating.

A block diagram of this subsystem is shown in Figure 25.

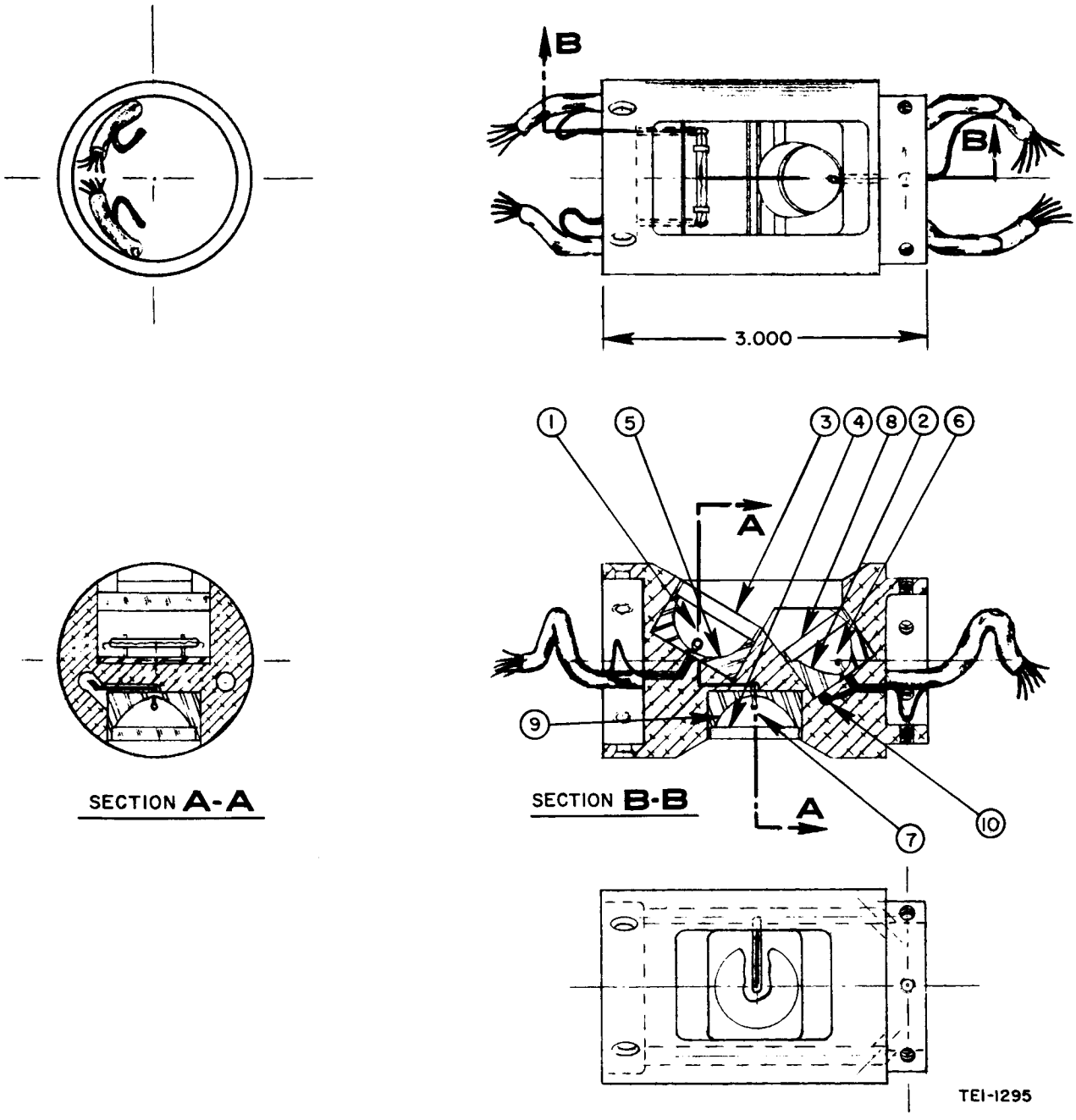

① RADIANT HEAT SOURCE
② OPTICS
③ PROTECTIVE WINDOWS
④ PROTECTIVE WINDOWS
⑤ OPTICS
⑥ TOTAL RADIATION RADIOMETER
⑦ SECOND RADIOMETER
⑧ PROTECTIVE WINDOWS
⑨ OPTICS
⑩ TEMPERATURE SENSING ELEMENT

Fig. 23 Subassembly - Thermal Diffusivity Instrument

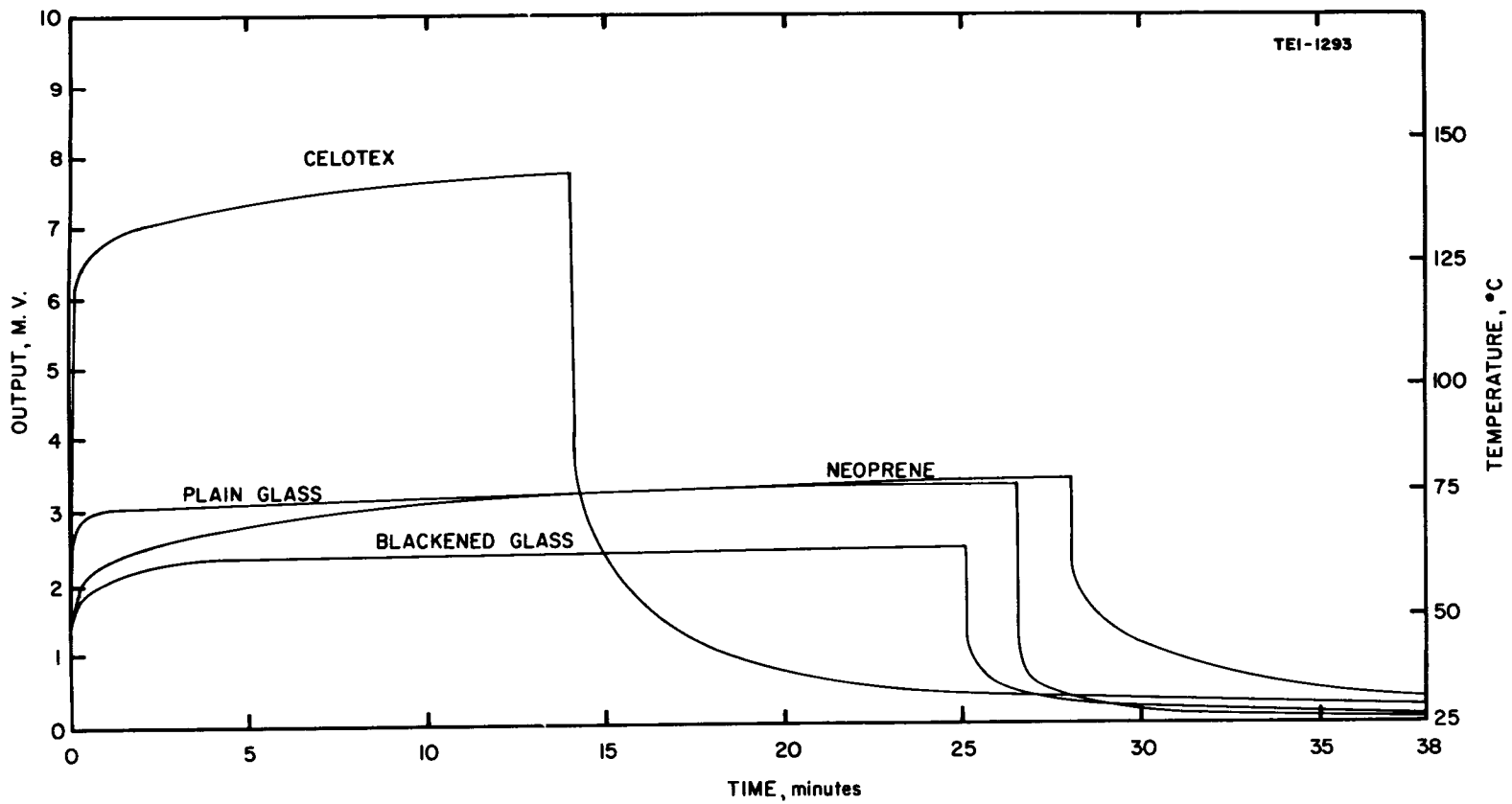

Fig. 24 Response Curve - Subsurface Thermal Diffusivity Instrument

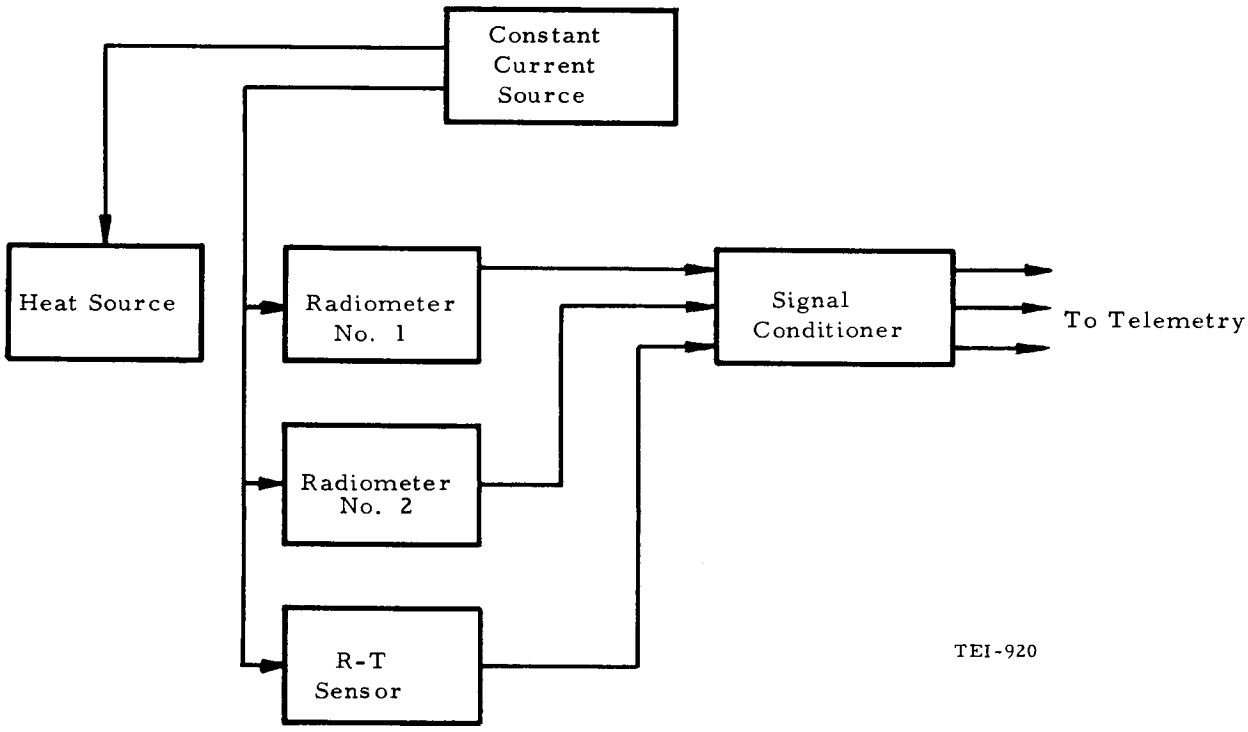

Fig. 25 Block Diagram - Subsurface Thermal Diffusivity Instrument

The surface thermal diffusivity instrument will utilize the interferometer spectrometer, described in a previous section, for the determination of the temperature-time history of a selected portion of the lunar surface when the heat input to this surface is abruptly altered. A solar shield with skirt, having the interferometer spectrometer centrally mounted, will be used to cast a shadow on the lunar surface for daytime measurements. The shield and skirt assembly is provided with an electrically-heated, thermostatically-controlled heater plate to provide radiant energy to the lunar surface for nighttime diffusivity determinations. This instrument is an integral part of the Integrated Surface Probe shown in Figure 6, page 28.

The advantages of using the I.S. for this measurement are that the same instrument may be used for the surface-temperature determination, since it will read absolute temperature. Further, the I.S. has an infrared range which includes the 5-to-7-micron region where water absorption occurs, and useful information relating to the presence of water may be obtained. The disadvantages pertain to increased size, weight, and instrument complexity. The choice has been made in favor of the I.S.

The block diagram of the surface thermal diffusivity instrument is shown in Figure 26.

Probable Subsystem Elements - Subsurface Instrument

Radiometer: A gallium-arsenide sensor of the type used with the Surveyor instrument

Heat Source: An incandescent lamp or miniature line heater (See Appendix IX for a large-scale line heater)

Current Source: To be designed

Signal Conditioning System: To be designed

Probable Subsystem Elements - Surface Instrument

Temperature Sensor: An interferometer spectrometer of the type previously discussed

Heat Source: Spiral-etched heater plate similar to Surveyor instrument type

Thermal Shield: To be designed

Electronics and Signal Conditioning Circuits: To be designed

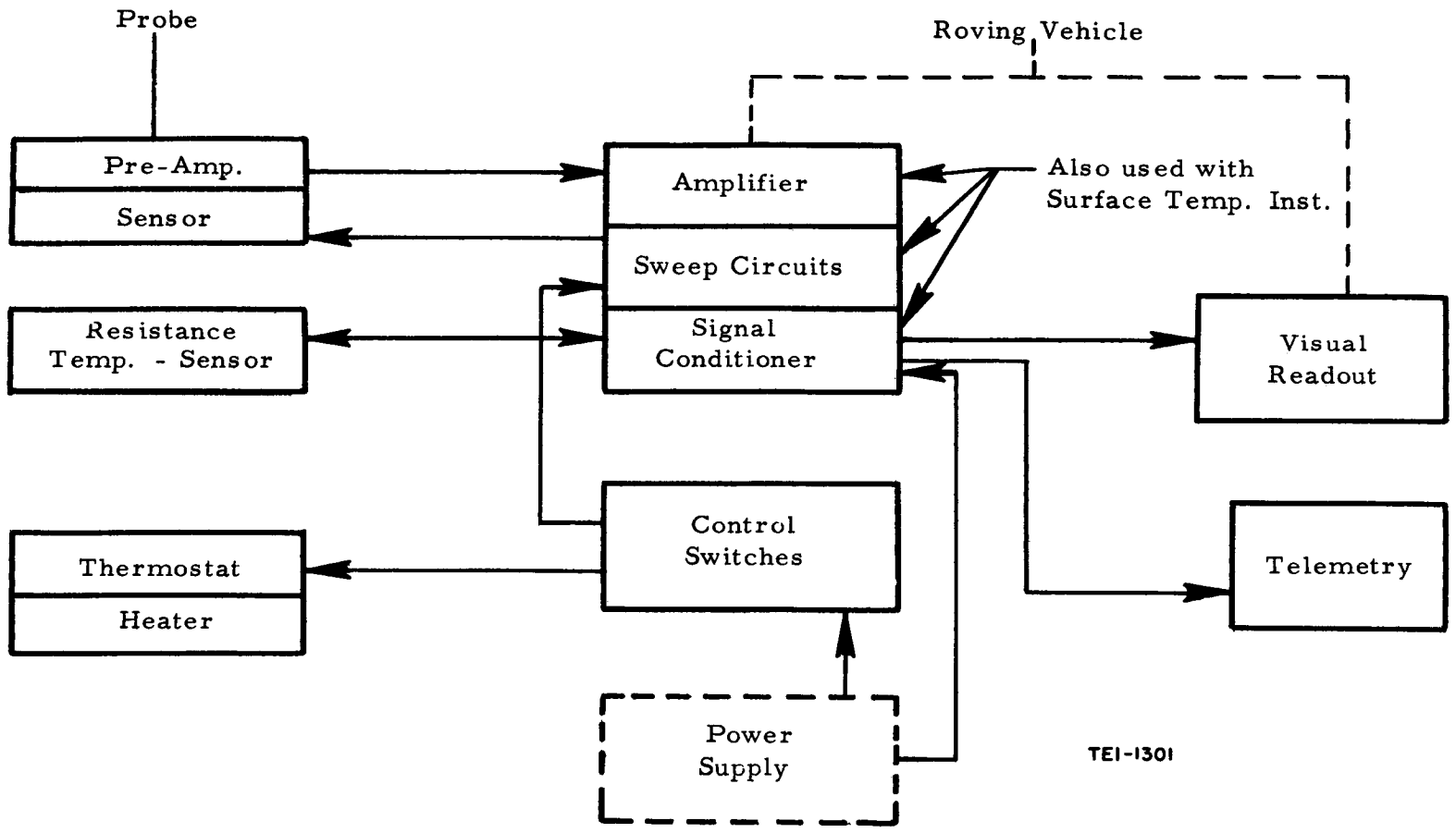

Fig. 26 Block Diagram - Surface Thermal Diffusivity Instrument

Operational Requirements. In operating the thermal diffusivity instrument, the probe will be positioned in the hole and the radiometer and body sensors allowed to come to thermal equilibrium. The thermal diffusivity experiment should be performed under both lunar day and night conditions, to determine the effect of the thermal conductivity of the probe and deployment boom upon the measurement, unless it is concluded from the temperature measurements that this effect is either negligible or sufficiently identified. The diffusivity instrument will be energized (both sensors and radiant-energy source). The energy source will radiate the wall and the radiometer will respond to effects at the wall. From the initial response of the radiometer it is expected that information related to the gross reflectivity will be obtained. The output of the radiometer should, therefore, be monitored continuously, or sampled frequently until the rate of rise of temperature had dropped to 1/e times the initial rate. The sampling rate may then be reduced, and upon attaining thermal equilibrium at the wall, the radiant energy source may be turned off. The rate of cooling of the wall is monitored and the same monitoring and sampling times observed as for the heating part of the cycle. Upon attaining thermal equilibrium at the wall, the experiment is terminated. Total time for this experiment is expected to be not more than one hour for both heating and cooling, and could be appreciably less, depending upon lunar subsurface thermal characteristics. For some materials having certain thermal characteristics, it may take a long time to reach thermal equilibrium when heating the wall. From prior experiments it would be determined when the heating cycle can be terminated under these conditions, with this time being related to the rate-of-change of measured temperature compared to the initial rate.

Site selection criteria used in the surface temperature measurement are applicable to the surface diffusivity instrument also. In fact the two experiments may be combined to the extent that, when in position, the initial measurement yields the surface temperature and the time-temperature history gives the thermal diffusivity data.

The instrument is to be turned on as for the daytime temperature measurement and the solar shield and skirt are quickly lowered into position so that a shadow of known geometry is cast on the lunar surface immediately around the area to be viewed. The instrument will record the time-temperature history of the area being viewed as this area radiates and cools. The instrument should be allowed to continue operation until the area being observed comes to temperature equilibrium, or until the rate of change of temperature as a function of time has decreased below an experimentally pre-determined value. The rate of change of

temperature as a function of time should be monitored continuously, or sampled frequently, until the rate of change has decreased to 1/e times the initial value. The sampling rate can then be reduced.

This experiment should be conducted only after the lunar surface has been exposed to solar radiation for a minimum of one hour. Preferably, the experiment should be performed around local noon to reduce fringing effects of solar radiation to a minimum. If performed when the sun is low in the sky, the angle made by the solar radiation with the local lunar surface should be known.

For nighttime thermal diffusivity measurements, the instrument should be placed with solar shield, skirt and heater plate in position to allow the local surface to reach temperature equilibrium. The instruments should be turned on as for nighttime temperature measurements. The heater plate will be energized and the local lunar surface radiated with radiant energy. The instrument responds to the rate of change of temperature as a function of time and produces an output indicative of the surface-time history. After temperature equilibrium has been attained, or after the rate of change of temperature has been decreased below an experimentally predetermined value, the heater is to be turned off and the cooling curve monitored. The same sampling conditions apply to this cooling part of the experiment as to the heating part. One should experimentally determine the effect of the presence of the cooling heater plate on the data so that this may be accounted for. The heater plate must reach operating temperature in 1/2 hour or less, and maintain this temperature for periods up to one hour. Total time for this measurement (both heating and cooling) is expected to be less than three hours. The actual time required depends on the thermal characteristics of the lunar surface material.

Instrument Development Status - Subsurface Instrument

The device employed in the subsurface probe is of the same basic design as the unit developed for Surveyor. The heater and sensor characteristics have been reasonably well defined but experiment capability for a wide range of materials and environmental conditions has not been determined. Some re-selection of components may be desirable to fit the larger instrument volume provided.

Instrument Development Status - Surface Instrument

The same conditions apply here as for the subsurface instrument. Characterization of the device for a wide variety of sample materials will be required.

Instrument Characteristics - Subsurface Instrument

Table XVI gives the characteristics of this device.

Instrument Characteristics - Surface Instrument

Table XVII gives the characteristics of this instrument.

TABLE XVI

SUBSURFACE THERMAL DIFFUSIVITY CHARACTERISTICS

Subsystem Elements	Radiometers, Heat Source, Protective Windows, Constant Current Source, Signal Conditioning System	
Dimensions	Downhole:	1.75-in. diameter, 2.5-in. long
	Surface Equipment:	4x2x2 in.
Weight	Downhole:	0.35 lbs
	Surface:	0.2 lbs
Power	Peak:	1.5 watts (1.0 watts for heater)
	Average:	0.5 watts
	Power-Time History:	1.5 watts heating, 0.5 watts other
	Voltage:	50% heating, 50% cooling (heating period about 30 min)
Measurement Range	$1x10^{-6}$ cm^2/sec to $2x10^{-2}$ cm^2/sec	
Accuracy or Resolution	Determined by calibration technique	
Temperature Range	Operating:	Downhole - 120°-400^oK
		Surface - 250°-350^oK
	Storage:	Downhole and surface - 120°-400^oK
Output Characteristics	Output form:	Analog
	Voltage:	0-5 volts
	Number of Outputs:	2 data, 1 body temperature
	Frequency Range:	DC
	Commutated or Continuous:	Commutated
	Impedance:	As required
	Transmission Accuracy Req:	Standard
Logging Speed	Fixed Point Measurements - 20-60 min/point	

TABLE XVII

SURFACE THERMAL DIFFUSIVITY INSTRUMENT CHARACTERISTICS

Subsystem Elements	Temperature Sensor - Interferometer Spectrometer, Heat Source, Current Source, Signal Conditioning System (coadder included elsewhere)	
Dimensions	Probe:	Heater plate and shield 8 in. dia x 0.25 in., sensor - included elsewhere)
	Supporting Equipment:	Included elsewhere
Weight	Probe:	Heater plate and shield - 0.71 lbs
Power	Peak:	N.A.
	Average:	100 watts (heater plate)
	Power-time History:	When turned on
	Voltage:	28 VDC
Measurement Range	1×10^{-6} cm^2/sec to 2×10^{-2} cm^2/sec	
Accuracy or Resolution	Depends on calibration technique	
Temperature Range	Operating:	Probe - 120°-$400^{\circ}K$ Supporting equipment - 250°-$350^{\circ}K$
	Storage:	120°-$400^{\circ}K$
Output Characteristics	Same as interferometer spectrometer	
Measurement Time	1-3 hr/point	

3. Seismic Measurements

Of all the instruments developed for geophysical exploration, the seismic devices are relied on for the majority of subsurface stratigraphic determinations by the oil companies in their search for oil reservoirs. Other instruments, such as gravimeters and magnetometers, are employed for large-scale surveys to determine gross anomalies; and, following these surveys, the promising areas are further delineated using seismic techniques on which the decision to drill or not is based. It follows, therefore, that seismic survey instruments are the most highly developed of the various geophysical tools, and interpretation of these records has progressed from an art to almost a science through the use of computer techniques.

On this basis alone, seismic investigations should have a high priority on lunar exploration programs in that, if this tool is our most successful device for investigations on earth, it behooves us to take advantage of this knowledge and adapt it for lunar use. Many problems obviously will be encountered in using this tool on the moon, but this will be true of most instruments used in such a hostile environment.

If the lunar craters are of impact origin, as is generally postulated, and since erosion processes as we know them are non-existent on the moon, the lunar subsurface is quite possibly in an extremely-fractured state to a considerable depth (considering the size of many of these lunar craters). If such is the case, this presents a serious obstacle to the interpretation of lunar seismic records, as any reflections from subsurface layering contacts will most probably be completely obscured by the multiple reflections from the fracture surfaces. Below the fracture zone, however, good reflections should be obtainable, provided sufficient seismic energy can be coupled to the lunar body, and, of course, provided layering or some form of stratigraphy forming a density interface is present (intrusions, etc.). This would seem to indicate that better information might be obtained using refraction techniques, even though it is generally more difficult to obtain good refraction records and normally these would require more seismic energy input.

A geophone, included as part of the downhole probe, can be a valuable asset in determining subsurface lithology and stratigraphy. The velocity profile obtained, when used in correlation with the results from other probe instruments such as the densitometer, magnetic susceptibility, neutron-gamma log and natural radioactivity logs, can be used to define the rock materials and types encountered, based on knowledge obtained in studies here on earth. Careful

interpretation of the seismic data can provide a good delineation of interfaces between different rock types.

a. Acoustic Velocity

Background. The two major classifications of seismic experiments are the natural (passive) and the induced (active) measurement. Since natural measurements depend on the seismicity of the moon, and it cannot be expected that a natural seismic event will occur during a probe measurement, this group does not appear to fit the concept established for the probe.

The primary application, for downhole seismic instrumention, is the determination of acoustic velocity as a function of depth. A secondary application which, used in conjunction with data obtained from the cores, would provide some knowledge of the subsurface structure, is short-range refraction and reflection shooting; with the geophone at various levels within the drill hole for the refraction records.

Determination of the acoustic velocity is important to the interpretation of surface reflection and/or refraction shooting, and will aid in the interpretation of the passive seismic records.

The selection of a seismic energy charge represents considerable tradeoffs in desired range vs. weight, power, and capability. If the experiment is restricted to a limited range of less than 100 feet, it may be possible to accomplish the measurements using one or more electric squibs. These could be fired together in a holder similar to that previously designed for Surveyor by TEI. Beyond these distances, it will be necessary to use higher-energy explosives such as dynamite or its equivalent.

In order to provide effective energy transfer to the lunar body for large scale measurements, it will be necessary to restrict the energy dissipation in some manner, such as by placing the explosive in a drill hole and back-loading with surface material. This will be especially important in the reduced-lunar-gravity field. In a 10-ft hole, five pounds of 1 1/2-in. dynamite should extend the useful range to at least 1000 feet.

Two methods are primarily used in acoustic velocity measurements on earth; the average-velocity method and the incremental velocity method. Figure 27 is a pictorial representation of the two methods. In the average-velocity method, the geophone is placed sequentially at increasing depths within the borehole, and the seismic source, located near the mouth of the borehole, is energized at each position of the geophone. The travel-time of

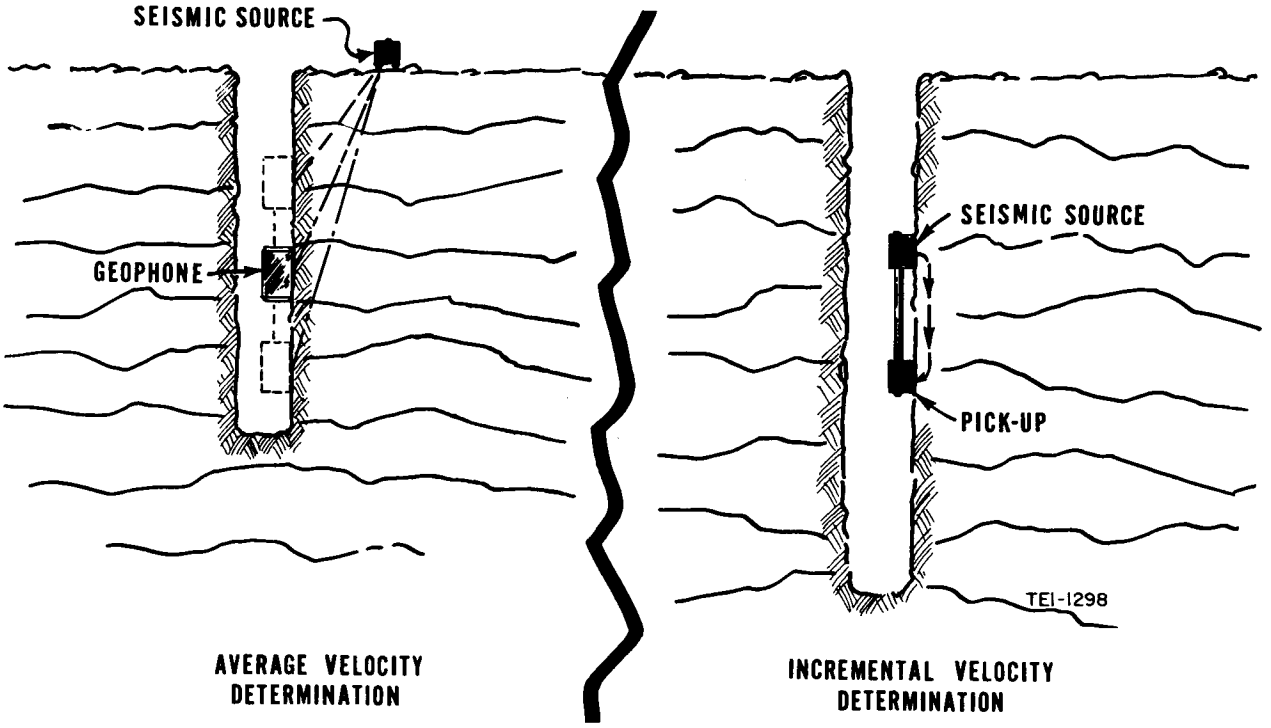

Fig. 27 Subsurface Acoustic Velocity Techniques

the seismic energy from source to geophone is determined, and knowing the depth to the geophone, an average velocity to that depth can be determined. From these measurements an average velocity profile for the entire borehole can be generated, from which it is possible to deduce the formation velocities at specific depths.

An alternate means of performing the average-velocity measurement is to locate the geophone at the surface, and energize the seismic energy source at specific depths within the borehole. The obvious disadvantage here is that if explosives are used, the hole in the vicinity of the charge is generally destroyed. This procedure is commonly employed at shot holes in conventional seismic work to obtain information on velocities in the weathered layer, which are important to the interpretation procedure.

The other method, incremental-velocity measurement, is usually used in deeper holes, wherein the energy source requirements become excessive to propagate sufficient energy down the borehole wall by the average-velocity method. In this approach, both the energy source and the pickup are contained in the probe a fixed distance apart, and both must contact the borehole wall if fluid coupling is not present in the borehole. The energy source for this device is generally a magneto-strictive or piezo-electric transducer operating at 10KC or above, and the pickup can be an accelerometer or piezo-electric pickup.

In operation, the energy pulse travels into the borehole wall, down through the formation and back into the pickup; where the travel-time is measured, and from which the formation velocity is calculated. When there is fluid in the hole, the energy pulse will also travel through the fluid to the pickup; but the velocity through the liquid is usually much lower than through the formation, and the formation wave, therefore, arrives first.

Since the spacing of the source and detector is usually about 4 to 6 feet, the timing on this measurement becomes quite critical, and one of the more difficult factors to determine is the exact instant of time when the energy pulse is initiated (i.e., the exact phase shift, between when the electrical energy is applied to the transducer and when it actually responds physically to this stimulus, must be determined).

Additionally, adequate decoupling in the probe body must be provided to prevent the energy pulse from traveling down the probe itself to the pickup.

The "average velocity" technique, described above, will be used for the probe application because coupling of the geophone with the formation is considered a less severe problem than coupling both source and detector as is required in the incremental velocity measurement.

Measurement Technique. In this experiment artificial seismic waves, created by explosives, are reflected and refracted by near-surface density interfaces and picked up by geophones, where they are translated into electrical signals. These signals are then analyzed to determine the acoustic velocity of the material from the "first arrivals", and other transmission characteristics from the amplitudes and arrival times of other portions of the waves. The geophones, commonly called moving-coil sensors, have high sensitivities, considering their size. They differ from seismometers in that they are velocity-type rather than displacement-type pickups. Actually, the term "moving coil" is misleading since the coil represents the seismic mass, and, as such, normally remains stationary with the geophone body moving in respect to it. Standard geophone sensitivity is approximately one volt per inch per second of ground velocity.

In conventional surveys, the geophone is connected to a seismic amplifier having a high gain (approx.100 db) and variable a.g.c., which can be adjusted for fast or slow response. Suppression is normally provided to prevent swamping the amplifier with the high-level, first arrivals. Suppression decay may also be varied. Generally provided, too, are high and low cutoff-frequency filter sections to permit optimizing the seismic record. For lunar use, operation will probably be broadband without filtering, and recorded earthside on magnetic tape where it can be played back through selective filters to achieve the best records. One channel will be required for each geophone used, with an additional channel for time-break and other timing signals. Alternately, it may prove desirable to record on tape at the test site and either telemeter (perhaps at a different speed) back to earth when convenient, or to return the tape for analysis. The use of a tape recorder may be the only solution to accurate measurement of velocity for very short spacing. A travel-time resolution of 20 micro-seconds is required for an accuracy of 20% in the velocity measurement when the source to geophone distance is one (1) foot and the velocity is 10,000 ft/second. For the same conditions, the accuracy improves to about 3% when the source to geophone distance increases to six (6) feet. This time-resolution requirement does not seem consistent with real-time telemetry transmission.

One problem often encountered on earth, and which will be magnified by the much-lower lunar gravity, is the coupling of the seismic energy into the lunar subsurface. Normal earth procedure is to drill a shot hole up to 100-ft deep, place the charge on the bottom and fill the hole with water to prevent the energy from being dissipated in the air. On these missions such procedures obviously cannot be employed, so the optimum method must be determined. Several methods have been suggested, such as mortars, blanket or sheet explosives, shaped charges, etc., all of which have certain inherent defects. This problem, however, is more pertinent to larger seismic surveys; for a source holder, of the type developed by TEI for Surveyor, should be adequate for the short shot spacings that are proposed.

A second problem will involve providing a satisfactory mounting and deployment configuration for the geophone in the probe, to insure good seismic contact with the surrounding formation. In the proposed design, the geophone will be housed so that it can be moved out and pressed against the formation whenever a test is to be made. It is necessary that the geophone not be restrained to any appreciable degree in the vertical direction, but should have a firm contact with the formation in the horizontal direction.

A block diagram of circuitry required for the acoustic velocity experiment is shown in Figure 28.

Probable Subsystem Elements.

Acoustic Sensor:	A Hall-Sears geophone, type HSJ-L (Same as proposed for Surveyor)
Geophone Actuator:	To be designed. This unit to employ a Ledex size 1E rotary actuator.
Timing and Time-Break Circuits:	To be designed.
Amplifier and Conditioning Circuits:	To be designed.
Source Initiation Circuits:	To be designed.
Seismic Charge:	Bowl-type source holder (similar to Surveyor-type)

The downhole detector subassembly used in the acoustic velocity experiment is shown in Figure 29. This section of the probe

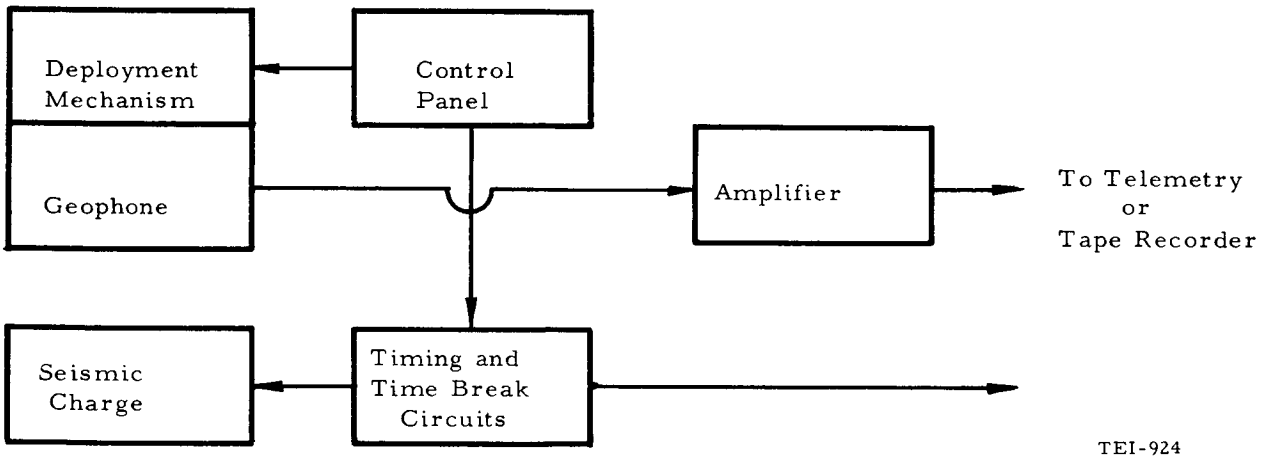

Fig. 28 Block Diagram - Acoustic Velocity Experiment

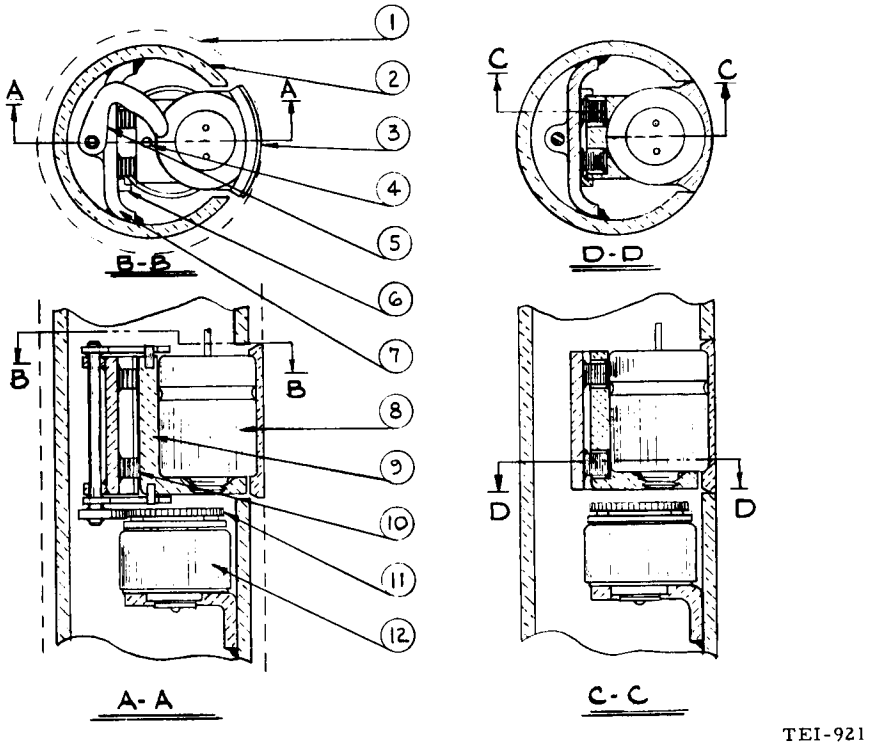

1	BOREHOLE	7	SPRING MOUNTING PLATE
2	PROBE OUTER WALL	8	ACOUSTIC SENSOR
3	RECEIVING PLATE	9	SENSOR BRACKET
4	LATCHING PIN	10	SUSPENSION SPRING
5	LATCH	11	DRIVE GEAR
6	REAR GUIDE AND STOP	12	ROTARY ACTUATOR

Fig. 29 Subassembly - Subsurface Geophone and Actuator

has a length of about 3.0 in., the diameter is 1.75 in. and the weight about 0.40 lbs. The seismic source holder is shown in Figure 30. It has a maximum diameter of 3.95 in., a height of 3.09 in. and weighs about 0.63 lbs with six squibs installed.

Operational Requirements. Since the geophone cannot operate while in motion up or down the hole, this measurement must, of necessity, be a step-type operation. The interval will be determined by the depth of the hole and the resolution required in definitizing the velocity profile and any lunar subsurface layering. Operation will involve placing the seismic source on the surface in a position near the hole (see Figure 31), stopping the probe in the hole and deploying the geophone against the borehole wall. Geophone deployment will be accomplished by the actuator on signal from the surface control panel. After sufficient delay to allow vibration of the sensor to be damped out, a second button will activate the recorder or telemetry and, a short time later, the seismic energy charge. The data channels will remain open for a specific interval after which they will automatically shut off. Activation of the retraction button on the control panel will retract the geophone and the probe will be ready to be moved to the next position. At certain of these stops it is proposed that a series of shots be made in a radial distribution around the hole, at varying distances from the hole, in order to develop additional knowledge about the local subsurface structural features. Figure 31 shows the type of shot pattern envisioned. The distances will depend on the energy contained in the shot and the coupling efficiency to the surface.

In addition to the subsurface detector just discussed, a second geophone of the same type is to be included with the Integrated Surface Probe for surface deployment. This unit will allow correlation and comparison of signals obtained through the different acoustic paths. This should be particularly helpful in defining any subsurface layering condition.

The seismic source will be so arranged that either single or multiple charges may be initiated for any measurement. This will allow for optimum signal conditions for a variety of formation materials and states.

Instrument Development Status. The acoustic sensor (geophone) to be employed in the subsurface probe is of the type used for Surveyor as a surface detector. The Surveyor subsurface detector was an accelerometer, chosen because of the limited available space. The characteristics of the detector and actuator mechanism must

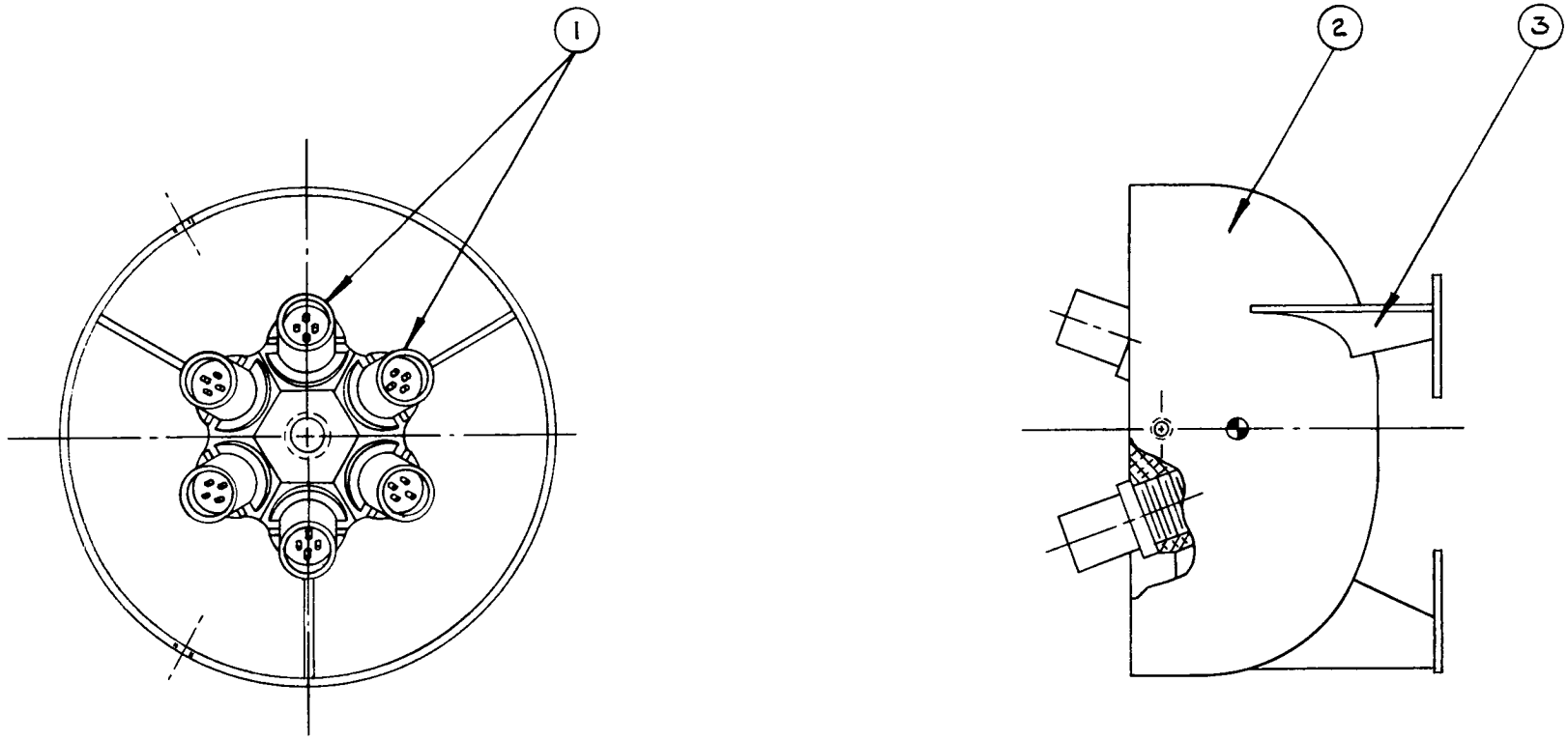

1 SOURCE EXPLOSIVE

2 STABILIZER BOWL

3 SUPPORT LEGS

TEI-922

Fig. 30 Seismic Source Holder

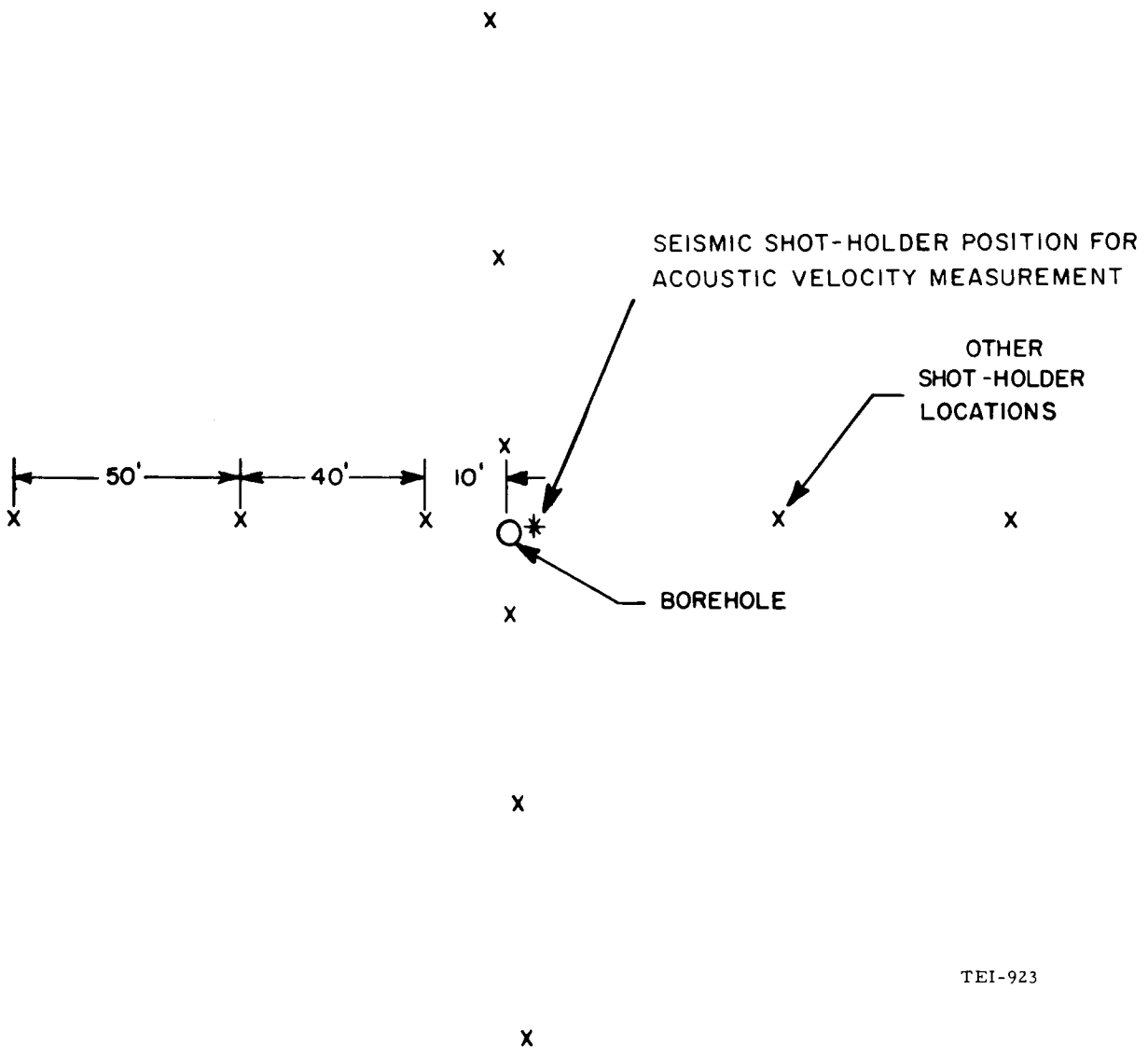

Fig. 31 Shot Pattern for Seismic Experiments

be determined. The seismic source will be of similar design to that of the Surveyor instrument. Total system characterization for a wide variety of materials must be determined.

Instrument Characteristics.

Table XVIII gives the characteristics of this device.

TABLE XVIII
ACOUSTIC VELOCITY EXPERIMENT CHARACTERISTICS

Subsystem Elements	Acoustic Sensor, Sensor Actuator, Timing and Time-Break Circuits, Source Initiation Circuits, Amplifier and Signal Conditioning Circuits, Acoustic Source.	
Dimensions	Downhole:	1.75-in. diameter, 3-in. length
	Surface Equipment:	Electronics - 5x7x1¼ in., Seismic Source - 4-in. diameter x 3-in.high
Weight	Downhole:	0.45 lbs.
	Surface:	Electronics - 1 lb., Seismic Source (with 6 charges)- 0.63 lbs.
Power	Peak:	7 watts
	Average:	150 milliwatts
	Power Time History:	150 milliwatts for circuit operation, 7 watts for geophone positioning.
	Voltage:	28 Volts D.C.
Measurement Range	300 to 25,000 ft/sec	
Accuracy or Resolution	To be determined	
Temperature Range	Operating:	Sensor - 120° to 400°K, Electronics- 250°-350°K
	Storage:	Surface and Subsurface - 120° to 400°K
Output Characteristics	Output form:	Analog
	Voltage:	Conventionally 0 to 1 volt A.C.; could be 0 to 5 volts A.C.
	Number of Outputs:	2 signal, 1 timing and time-break
	Frequency Range:	10 - 1000 CPS
	Commutated or Continuous:	Continuous
	Impedance:	As required
	Transmission Accuracy Needed:	Best possible
Logging Speed	Fixed Point Measurements - 2 minutes per point.	

4. Electrical Measurements

In general, in situ, geophysical, electrical measurements are used to determine an electrical parameter of the formation which has been shown to be related to some geological property. Electrical measurements are used to determine:

- The electrical conductivity of the formations (resistivity).
- The dielectric constant of the formations (capacity).
- The polarization of the formations.
- The ability of the formations to generate an electrical potential (battery).
- The magnetic susceptibility of the formation (permeability).

Most of these measurements can be made by either direct or alternating currents or by a combination of both. If direct-current measurements are made, a current path must be provided to the formation by the use of electrodes. The properties of these electrodes are extremely important to the success of the measurement. If alternating current is used, direct contact to the formations may not be required as the energy from the source can be coupled inductively or capacitively to the formations.

a. Background

Induction Log. The primary utilization of induction log experiments, on earth, is in the location of conductive-fluid-containing zones. For example, these are used quite commonly to locate the level or depth of the water table. This method is also useful for detecting the presence of other elements, such as chlorine and sulphur. Chlorine, in the form of a chloride in solution, greatly lowers the resistivity, whereas sulphur has a very high resistivity.

As mentioned above, however, the primary application, of induction log measurements on the moon, will be to determine the presence or absence of sufficient water in the lunar subsurface to effectively alter the water-free resistivity of the lunar material. This factor obviously is extremely important in determining the history and evolution of the moon and indirectly that of the earth.

Magnetic Susceptibility. Determination of magnetic susceptibility is one of the more important measurements to be made on the lunar surface and subsurface materials.

Not only is it necessary to the proper interpretation of magnetic-intensity measurements, but magnetic-susceptibility measurements will assist greatly in establishing or discrediting the validity of theories relating to meteorite impacts as the source of most lunar surface features. As most meteorites contain iron to some degree, the average magnetic susceptibility should be high if there is any appreciable accretion of meteorites on the lunar surface. Subsurface measurements should give an indication of the depth of any such accretion.

Magnetic-susceptibility measurements can also be an important lithologic tool to aid in the identification of lunar rock material. This is especially important in the subsurface domain, as it may not always be possible to recover the core material from the drilling process, or it may lose its integrity in the recovery process. These measurements would be helpful to the astronaut in his sample selection task; both on surface and borehole samples.

b. Measurement Technique

A combination instrument will be used to measure both the magnetic susceptibility and conductivity of the lunar formations. This combination magnetic-susceptibility/induction-log measurement is performed with a pair of coils, a transmitting coil and a receiving coil, wound on a cylindrical form and separated longitudinally by several inches. An AC signal, generally in the range from 1,000 to 10,000 cycles per second, is connected to the transmitting coil. Due to mutual coupling, a voltage is induced in the receiving coil dependent upon the coil geometry and the magnetic and resistive properties of the material surrounding the coils. A second set of coils (nulling coils) are connected in series-opposition to the measuring coils; such that in air or vacuum, the vector sum of the two receiving coil voltages is zero. The nulling coils are shielded from the influence of outside disturbing media, and remotely located from the sensing coils.

The sensing coils are then placed in the hole, in the case of the probe; or near the surface to be measured, in the case of the surface instruments. Two factors can now influence the receiving coil output, magnetic susceptibility and electrical conductivity of the measured medium. Magnetic susceptibility is related to permeability as follows:

$$\mu = 1 + \chi$$

where μ = permeability

χ = volume susceptibility in cgs units

Changes in permeability due to changes in magnetic susceptibility will affect the mutual coupling between the transmitting and receiving coil by providing a different reluctance path for the magnetic flux lines. If the medium has any appreciable conductivity, the magnetic field created by the transmitting coil will set up eddy currents in the medium which will, in turn, induce a voltage in the receiver coil. The voltage generated by the eddy currents will be 180° out of phase with the current in the transmitting coil, while the voltage generated by the change in magnetic susceptibility will be 90° out of phase with the current in the transmitting coil. The output voltage, then, will be the vector sum of these two voltages which are 90° apart.

By using phase-sensitive detector, the output signal can be separated into its two components corresponding to conductivity and magnetic susceptibility. Calibration of the instrument is performed empirically by introducing the device successively into material of known susceptibility and conductivity and then preparing a calibration curve from this data. Figure 32 shows a calibration curve for a Surveyor-type surface magnetic susceptibility instrument.

A second technique has been used in a field-type magnetic-susceptibility instrument. With this approach, the change of inductance of a coil is measured as the coil is moved through the borehole. These changes in inductance are due to the changes in formation permeability due to changes in magnetic susceptibility (see equation above). The test inductor is located in a bridge circuit so that small changes in inductance can be determined. This technique does not have the same sensitivity as the one proposed because changes in inductance are not greatly sensitive to susceptibility changes. In the null-balance method proposed, the "1" in the above equation is bucked out so that a direct relationship exists between susceptibility changes and output voltage changes. The change-of-inductance device was also very sensitive to changes in temperature and was never too successfully used.

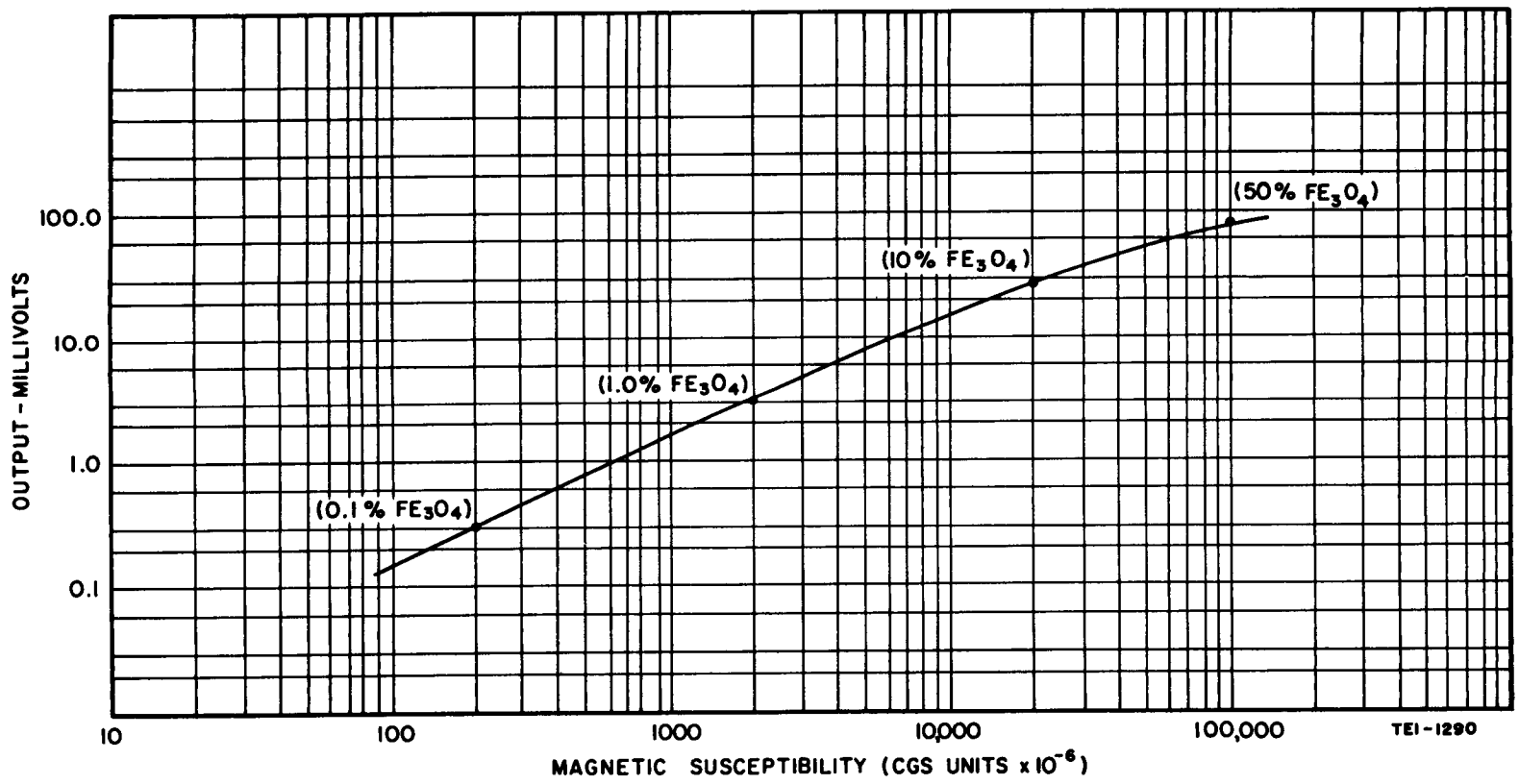

Fig. 32 Calibration Curve - Surveyor-Type Magnetic Susceptibility Instrument

A block diagram of the recommended system is shown in Figure 33. This diagram holds for both the surface and subsurface instruments.

c. Probable Subsystem Elements

Transmitter and Receiver Coils: Low impedance transmitter coil wound with high-temperature-type wire; receiver coil wound with low-coefficient-of-temperature wire such as Advance. Design to be modified from Surveyor.

Null Coils: To be designed.

Oscillator and Power Amplifier: To be designed.

Signal and Reference Amplifiers: To be designed.

Phase Detectors and Signal Conditioners: To be designed.

The transmitter-receiver coil section of the subsurface probe is shown in Figure 34. This section has a diameter of 1.75 in., a length of 6 in., and weighs 1.5 lbs. The coil system for the surface probe is shown in the Integrated Surface Probe, Figure 6, pg. 29 .

d. Operational Requirements.

A continuous log can be run for subsurface surveys, since movement does not present a restriction to the measurement operation. To make the survey, the instrument is energized and allowed to stabilize. A reading is made with the probe suspended above the lunar surface, so that the null or "zero" value can be determined. The probe is then lowered into the hole and the output monitored or sampled as the probe is moved through the hole. A logging speed of approximately 5 ft/min should be used in the 10-ft. hole for best results. This speed can be increased to about 10 ft/min in the 100-ft. hole if necessary to conserve measurement time. A null reading should be repeated after the operations in the hole have been completed. Borehole caliper information should also be read out as well as instrument temperature.

For surface measurements, the device would simply be placed on the lunar surface, the output monitored, and then the instrument moved to another location. Null readings should be made from time to time to allow for measurement corrections due to changes in instrument temperature. Although continuous surface surveying is possible (the measurement is essentially instantaneous), the sensor-to-surface distance must be kept relatively constant; and for an irregular surface, point-to-point surveying is recommended.

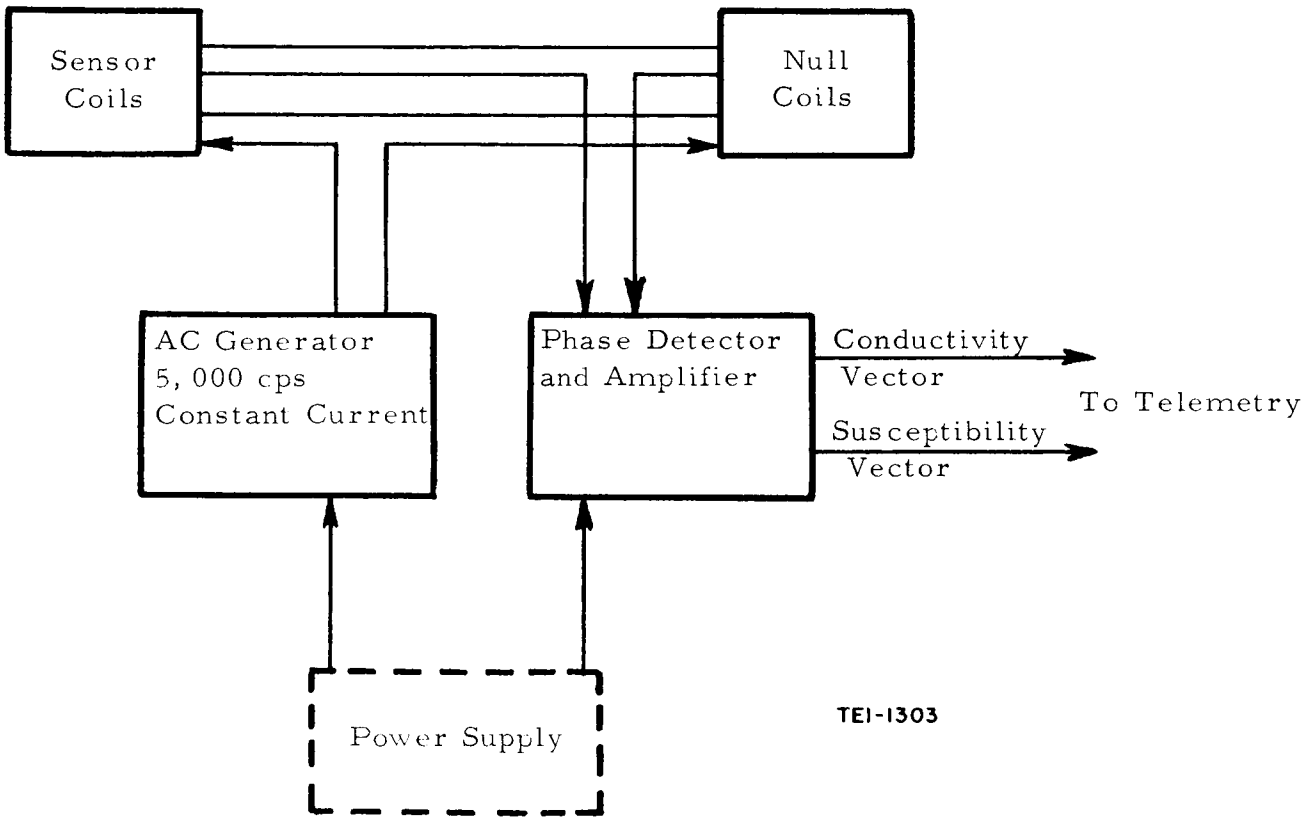

Fig. 33 Block Diagram - Magnetic Susceptibility/Induction Log Experiment

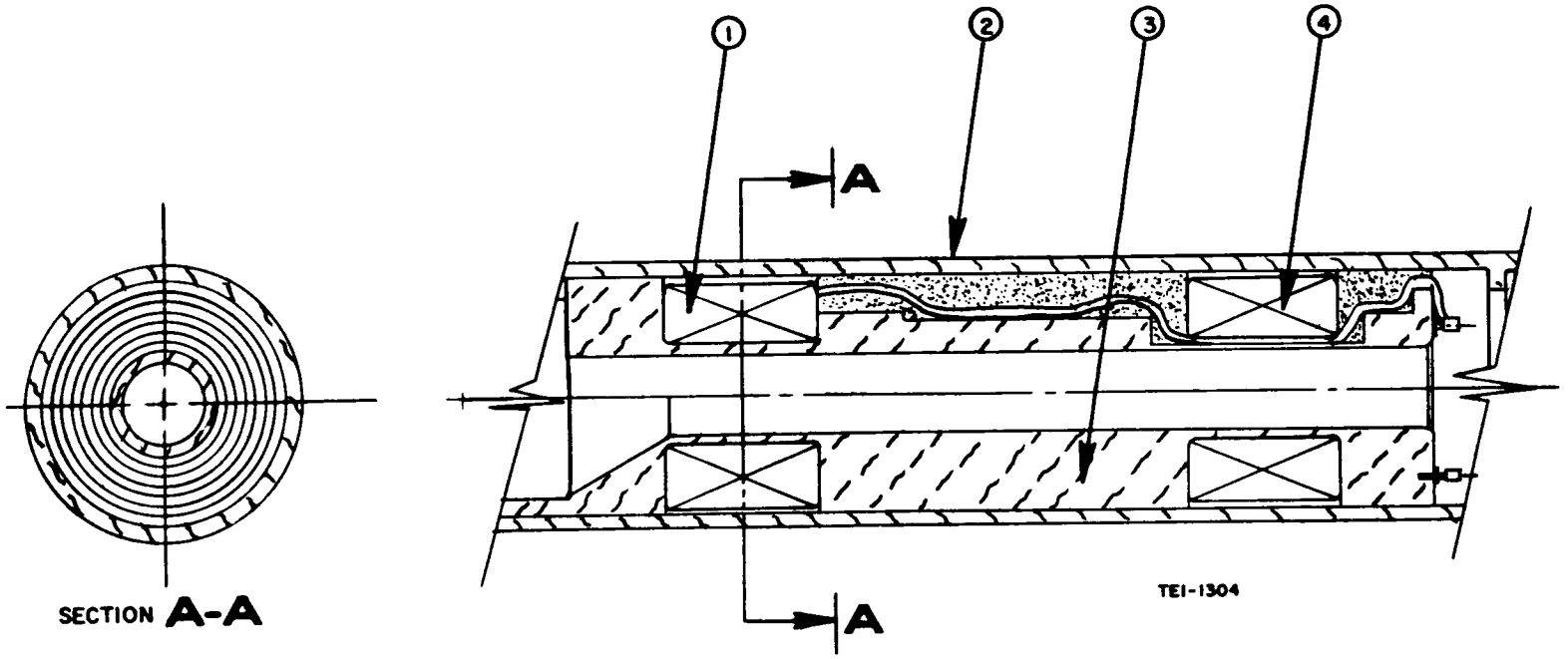

① TRANSMITTING COIL
② EPOXY-FIBERGLASS TUBE
③ EPOXY-FIBERGLASS BODY
④ RECEIVING COIL

Fig. 34 Subassembly - Magnetic Susceptibility/Induction Log Instrument

e. Instrument Development Status

Surface and subsurface magnetic susceptibility instruments were under development for Surveyor. The surface unit successfully met the design specifications and operated properly. The AAP device would be a modification of this instrument.

The subsurface instrument was never fully developed. The major problems associated with this instrument were the proper design and location of remote null coils, and temperature stability. Work is currently underway at TEI to develop a subsurface magnetic-susceptibility instrument for use in the Mohole Project. Solutions to the above problems are expected to result from this effort.

The electronic circuits to be used will be based on the Mohole development work.

f. Instrument Characteristics - Subsurface Instrument

The characteristics of this instrument are given in Table XIX.

g. Instrument Characteristics - Surface Instrument

The characteristics of this instrument are given in Table XX.

TABLE XIX

SUBSURFACE MAGNETIC SUSCEPTIBILITY/INDUCTION LOG CHARACTERISTICS

Subsystem Elements	Transmitter and Receiver Coils, Oscillator and Power Amplifier, Signal and Reference Amplifier, Phase Detectors, Signal Conditioning Equipment
Dimensions	Downhole: 1.75-in. diameter, 6-in. length Surface Equipment: 6x6x2 in.
Weight	Downhole: 1.5 lbs Surface: 2.0 lbs
Power	Peak: N.A. Average: 10 watts Power-Time History: Uniform Voltage: 28 VDC
Measurement Range	50 to 50,000 μcgs units (magnetic susceptibility - wider range possible with scale switching) 10^{-4} to 10^{0} ohm-cm (resistivity)
Accuracy or Resolution	Absolute accuracy ±15%, relative accuracy ±5%, resolution ±5% (magnetic susceptibility), accuracy ±25% (resistivity)
Temperature Range	Operating: Downhole - 120°-400°K Surface - 248°-373°K Storage: Downhole and Surface - 120°-400°K
Output Characteristics	Output Form: Analog Voltage: 0-5 V Number of outputs: 1 susceptibility, 1 resistivity, 1 temperature Frequency: 5000 cps Commutated or Continuous: May be commutated Impedance: As required Transmission accuracy required: Standard
Logging Speed	5-10 ft/min

TABLE XX

SURFACE MAGNETIC SUSCEPTIBILITY/INDUCTION LOG CHARACTERISTICS

Subsystem Elements	Sensor-Null-Coil Assembly, Oscillator and Power Amplifier, Signal and Reference Amplifier, Phase Detectors, Signal Conditioning Equipment (the majority of the electronics equipment will be shared with the subsurface unit - only impedance-matching changes required)
Dimensions	Sensor: 12.5-in. diameter, 1.5-in. high Electronics: Shared with subsurface unit
Weight	Sensor: 3.8 lbs. Electronics: Shared with subsurface unit
Power	Included with subsurface unit
Measurement Range	50 to 50,000 μcgs units (magnetic susceptibility - wider range possible with scale switching) 10^{-4} to 10^{0} ohm-cm (resistivity)
Accuracy or Resolution	Absolute accuracy ±15%, relative accuracy ±5%, resolution ±5% (magnetic susceptibility), accuracy ± 25% (resistivity)
Temperature Range	Operating: Probe - 120°-400°K Supporting Electronics - 248°-373°K Storage: 120°-400°K
Output Characteristics	Output Form: Analog Voltage: 0-5 V Number of Outputs: 1 susceptibility, 1 resistivity, 1 temperature Frequency: 5000 cps Commutated or Continuous: May be commutated Impedance: As required Transmission accuracy required: Standard
Measurement Time	<1 min/point

5. Atmospheric Pressure and Compositional Analysis

The existence of a possible lunar atmosphere can be explored by two approaches: (a) the interpretation of experimental measurements carried out on the lunar disc, or (b) theoretical calculations concerning the retentive ability of the moon in regard to gaseous molecular matter (13).

Experimental observations rely on interpretation of measurements aimed at the determination of other variables, since no direct indication of a lunar atmosphere has ever been obtained. These methods lead to estimates of the upper limits of the lunar atmospheric density.

For example, polarimetric measurements have yielded an upper limit of 10^{-6} torr. A less sensitive measurement, the analysis of the lack of observable optical effects near the moon's cusps, placed an upper limit of 10^{-3} torr at the lunar surface. Measurement of the occultation of a radio star by the lunar disc and the absence of refraction due to the presence of an atmosphere yields an upper limit of 10^{-10} torr for the lunar surface pressure.

It is seen that all experimental techniques predict the presence of, at most, an exceedingly thin lunar atmosphere. If firmer estimates are required, it becomes necessary to resort to theoretical calculations.

One theoretical approach concerns the escape velocity and the probable mean residence time of an atom of gas in the lunar gravitational field.

One can immediately dispense with the lighter gases, particularly those with a mean free velocity greater than the lunar escape velocity. Considering heavier gases such as zenon and krypton, calculations indicate a lifetime of about 3000 years in the lunar atmosphere. In view of the lunar age, even these cannot be expected to contribute significantly to a lunar atmosphere.

One is forced to the conclusion that the lunar atmosphere consists of:

- Gases which may be liberated under solar bombardment from the surface layers (both U.V. and proton bombardment).
- Particles accumulated by the lunar body as it sweeps through space and retained for a short period at the surface. This considers the interplanetary gas as an extension of the solar coronal flux (solar wind).

Calculations of this accreted lunar atmosphere using representative values for the solar wind, both during quiescent periods and periods of high solar activity, lead to estimates of the lunar surface atmospheric density of 10^{-14} to 10^{-15} torr during quiescent periods and 10^{-10} to 10^{-11} torr during periods of high solar activity.

Using the above estimates together, one might expect the lunar surface atmospheric pressure to vary over a rather large range from 10^{-15} torr at lunar night and periods of low solar activity to perhaps 10^{-9} torr with high solar activity and daytime conditions; when added liberation of gases might be expected from heat, radiation, and bombardment considerations. In addition, evolvement of gases from the interior might be expected to raise this pressure in a very thin layer at the surface, and the subsurface pressure might be expected to be still higher. Experimental data are, therefore, needed and in situ measurements should be made.

a. Mass Spectrometer Experiment

Background. Gas analysis at the lunar surface could give valuable information pertaining to the atmospheric constituents. This experiment should be performed under both day and night conditions so that gases evolved under solar radiation might be detected. Subsurface gas analysis would be expected to yield information of changes in pressure and gas constituents as a function of depth. The instrument might be lowered into the borehole immediately upon completion of drilling to detect any evolution of gases from the material caused by the generated heat of drilling or opening of gas-filled pores. This might give information as to the nature of the subsurface material. Total normal ion concentration might be evaluated by operating the mass spectrometer with the ionizer off. Total ion current, with the ionizer on, would provide information pertaining to the ambient atmospheric pressure.

Use of the mass spectrograph is one of the standard analysis techniques used in geology and is useful in obtaining both qualitative and quantitative analysis of materials. However, the analysis of solids presents some problems since the solid has to be ionized. This indicates sample preparation and operator time. Analysis of solids or particulate materials would best be deferred and performed on samples returned to earth unless a device such as a solar furnace could be designed to be attached to the subsurface probe assembly when this experiment is to be used on the surface.

It is to be noted that the total pressure determination and the normal ion current measured by this experiment would be added information which could be checked against the separate measurements to be made of these parameters by other instruments.

Types of mass spectrometers considered as applicable to the lunar probe are time-of-flight, quadrupole, and the Bennett RF type. None of these require bulky and heavy magnets, but the electronics are quite complex. Both the quadrupole and time-of-flight types have been flown in upper atmosphere studies and the state-of-the-art is such that either of these could probably be reduced in size and geometry to conform with the probe requirements. It is visualized that only the ionizer, mass separator, and electron multiplier would be placed in the probe. The electronics package would be contained in the roving vehicle or elsewhere.

It must be emphasized that miniaturized, off-the-shelf apparatus is not available for this experiment and a very carefully thought out, well-engineered approach must be adopted if success is to be expected.

Measurement Technique. If certain conditions related to geometry, power requirements and instrument sensitivity can be met, a mass spectrometer of the quadrupole type will be included in the probe. The instrument will be in two sections. The analyzer will be included in the probe and the electronics package will be located on the surface. The instrument will be used for determining:

(1) Local atmospheric pressure

(2) Total normal density, and

(3) Identification of lunar atmospheric constituent gases.

A brief description of the RF spectrometer and the quadrupole spectrometer follows, with advantages and disadvantages of each included.

In the RF spectrometer, ions are accelerated through a potential gradient and then sent through a series of grids which have an RF voltage applied to them (see Fig. 35a). If the transit time of the ions in going through the grid structure is in proper phase with the frequency of the applied RF voltage, they will gain maximum energy. A repelling potential, placed on a grid between the RF structure and the detector (multiplier), prevents all but those ions which have gained maximum energy from getting through to the detector. The advantage of this instrument is that it does not require a magnetic field and is fairly simple in construction. The disadvantage is that it requires a fair amount of circuitry and tends to produce ghost signals which can be confusing. Scanning is accomplished by varying the voltage or the frequency. The equation relating to the operation is:

$$m/e = 0.266\ V/S^2F^2$$

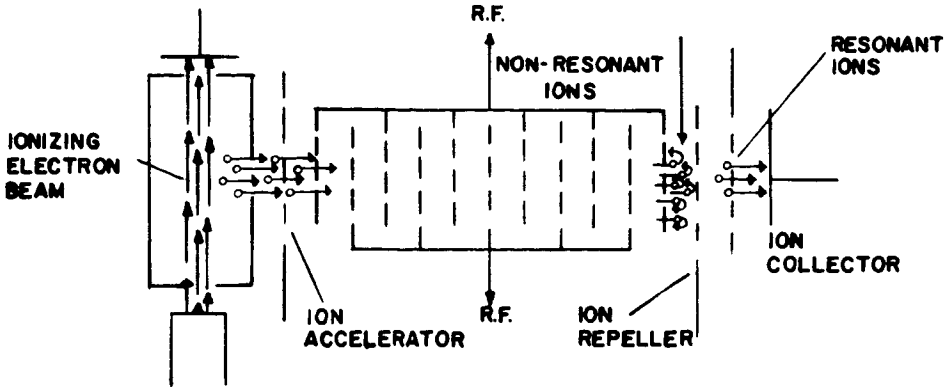

a. R.F. MASS SPECTROMETER

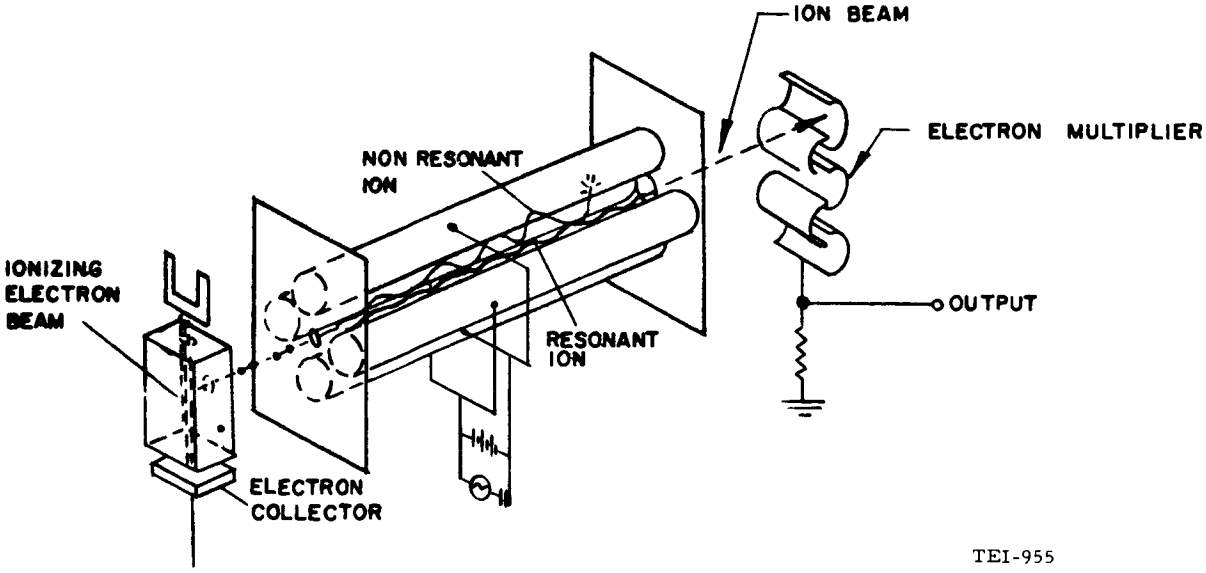

b. QUADRUPOLE MASS FILTER

Fig. 35 Operational Schematic - RF and Quadrupole Mass Spectrometer

where m/e is in atomic mass units (amu) per electronic charge, V is in volts, S is grid spacing in cm, and F is frequency in MC.

In the quadrupole spectrometer, ions are injected into a quadrupole field produced by four rods which have both a DC and RF voltage applied to them. (See Fig. 35b.) Most ions will undergo unstable oscillations and be collected by the rod surfaces. Only ions with certain values of m/e will have stable oscillations and travel the length of the separating region and be collected.

Advantages of this instrument are as follows: it does not require a magnetic field, it can accept a larger spread of ion energies entering the analyzing region without loss of resolution, and, since it is a wide-open system (no grid transmission losses), it is capable of very high ultimate sensitivity. For those reasons it is preferred for the probes. Its disadvantage is its somewhat complex circuitry.

Under the assumption that the ions are singly charged, the mass of the ion which reaches the detector (multiplier) is given by:

$$m = 0.136\ V_o / (r_o^2 F^2)$$

where m is in amu, V_o is in volts, r_o is radius in cm and F is in MC.

A block diagram of the quadrupole mass spectrometer is shown in Fig. 36.

In view of the extremely rare atmosphere present at the surface, it must be noted that all measurements will be near the limit of present state-of-the-art sensitivities, and at total pressures which are not attained in space simulators. Therefore, a carefully thought out, calibration test procedure will be required.

Probable Subsystem Elements

Ionizer-Mass Separator (consisting of an ionizing, electron-beam, quadrupole resonator and electron multiplier): This unit to be similar to the residual gas analyzer Series 210 developed by Electronic Associates, Inc. (See Appendix IX)

Electronics System (consisting of power supplies, an RF and DC generator, RF regulator, sawtooth generator and signal conditioning circuitry): to be developed from basic Series 210 units.

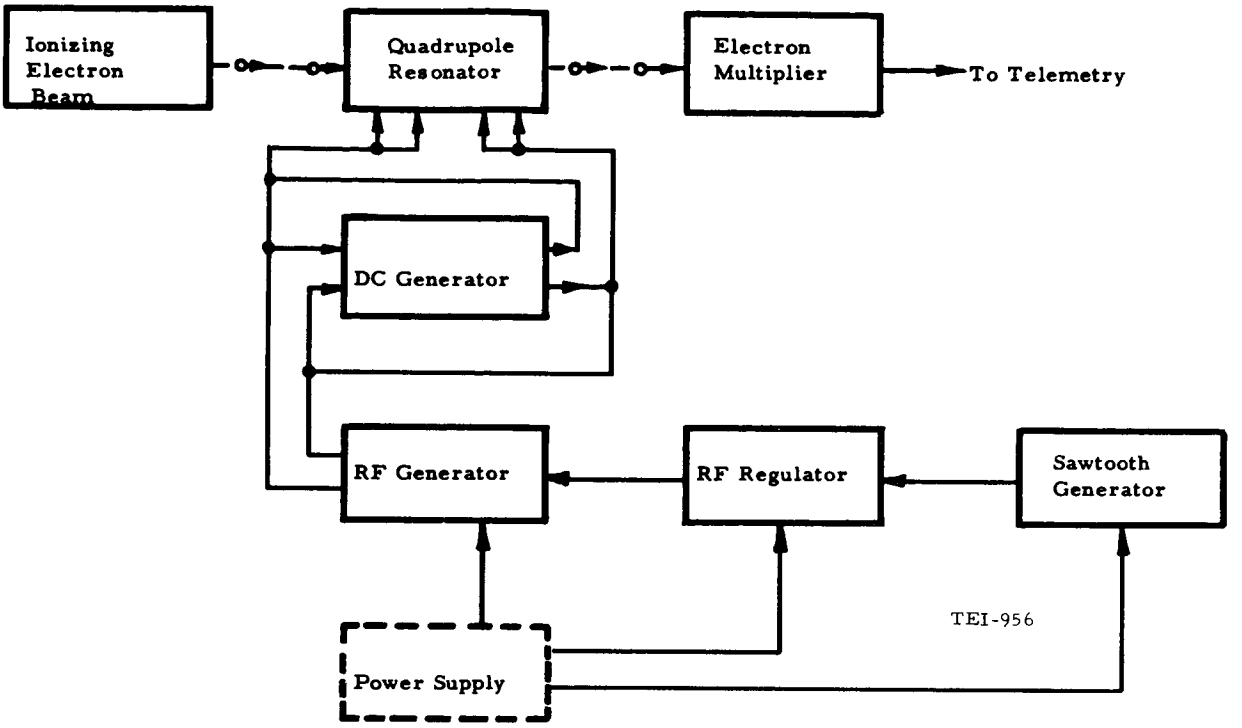

Fig. 36 Block Diagram - Quadrupole Mass Spectrometer

The sensor analyzer subassembly to be used in the subsurface probe is shown in Figure 37. The overall length of this probe section is about 9.80 in., the diameter is 1.75 in., and the weight is about 1.50 lbs.

Operational Requirements. In operation the probe will be positioned in the borehole and the instrument turned on and allowed to reach operating equilibrium. First the ionizer and mass filter will be left unenergized and a total, normal ion-density determination will be made. Secondly, the ionizer will be turned on and a total ion-density determination will be made. This measurement can be related to the lunar ambient pressure. Thirdly the mass filter will be turned on and spectra will be obtained. The spectra would identify constituents of the lunar atmosphere, if present at partial pressures above the sensitivity level of the instrument.

A measurement as described above, made immediately upon termination of drilling operations, might be very valuable. The heat, generated by the drilling operation, might release occluded gases from the lunar material and these might be detected, giving insight into the composition of the subsurface material.

With the probe positioned flat on the surface it might also be possible to obtain measurements as outlined above at various surface locations (crevasses, etc.) where one might expect an issuance of gasses from the lunar interior. Solar shield and solar furnace devices could also be attached and selected samples analyzed.

The time required to scan a spectrum is of the order of 50 milliseconds, so the total experiment time is expected to be of the order of minutes.

Instrument Development Status. The sensor portion of the Series 210 mass spectrometer, is presently of a size compatible with the subsurface probe dimension. This unit can be modified to suit AAP mission requirements. The supporting surface electronics is presently of hard tube design and must be modified to reduce power and weight requirements. The problem of operating the sensor separated from the electronics unit by as much as 100 ft or more must be solved.

Instrument Characteristics. Table XXI gives the characteristics of the quadrupole mass spectrometer.

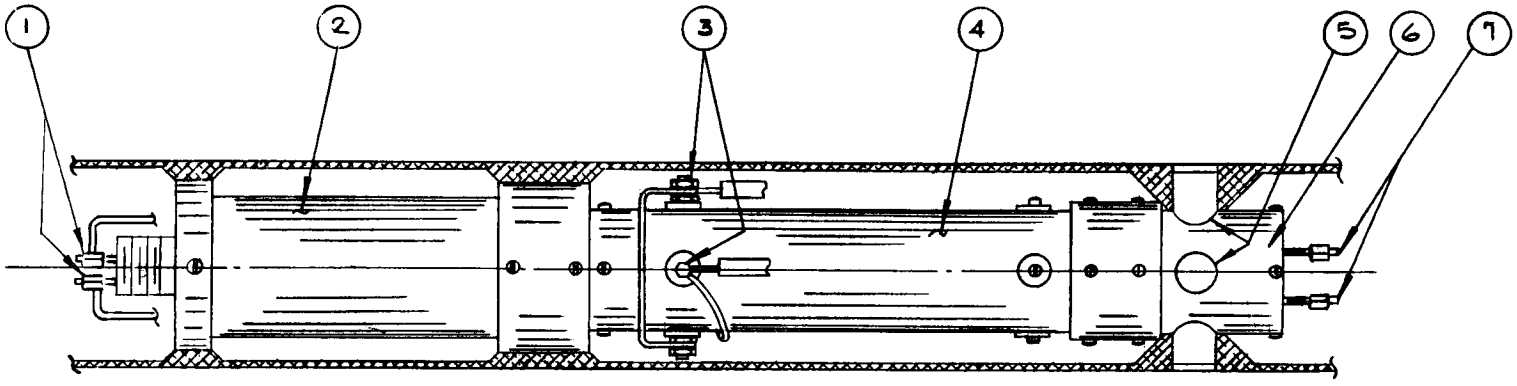

1. ELECTRON MULTIPLIER CONNECTIONS
2. ELECTRON MULTIPLIER
3. DC & RF POLE CONNECTIONS
4. QUADRUPOLE HOUSING
5. GAS INLETS
6. IONIZATION SECTION
7. FILAMENT CONNECTIONS

TEI-957

Fig. 37 Subassembly - Quadrupole Mass Spectrometer Sensor

TABLE XXI

QUADRUPOLE MASS SPECTROMETER CHARACTERISTICS

Subsystem Elements	Ionizer-Mass Separator (consisting of an ionizing electron beam, quadrupole resonator and electron multiplier) Electronics System (consisting of power supplies, an RF & DC generator, RF regulator, sawtooth generator and signal conditioning circuitry)
Dimensions	Downhole: 1.75-in. diameter 9.80-in. length Surface: 1 ft^3
Weight	Downhole: 1.50 lbs Surface: 10 lbs
Power	Peak: 100 watts Average: 1.5 watts Power time history: 150 ms sweep/10 sec.
Measurement Range	1-150 amu; partial pressure sensitivity 1×10^{-14} torr
Accuracy or Resolution	Unit resolution (Resolution is defined as two mass peaks 1 amu apart and of equal height with a valley between them 90% the height of either peak) 1-150 amu
Temperature Range	Operating: 218°-373°K Storage: 208°-448°K
Other Environment Control Required	<10% humidity for storage. Pressure range $<10^{-4}$ torr
Interference Problems	RF: Quad generates 3.3 mc Magnetic: 500 Gauss (constant)
Output Characteristics	Data form: Analog Voltage: 0.05-5 volts Number of Outputs: 1 data, 1 temperature Frequency Range: 1 amu per millisecond (entire mass range in 150 millisecond) Commutated or Continuous: Commutated (1 mass sweep every 10 seconds) Impedance: As required Transmission accuracy needed: ±1%
Logging Speed	Fixed point: Approximately 1 min/point

6. Borehole Television System*

a. Background.

Surface geological-geophysical surveys rely heavily upon visual aids. It is, therefore, important to consider extending this capability into the investigation of the subsurface. Visual observations such as continuity of strata, color, grain size, pore size, and the general appearance of hand specimens are primary study techniques of the surface geologist. For subsurface surveys the geologist must work indirectly in studying underlying strata or other formations. And then the data is not always meaningful, since subterranean structure is not necessarily uniform. Layering in the presence of fissures and faults is not easily detected with ordinary logging techniques.

To obtain data pertaining to the age, origin, and history of the moon, core samples will be taken. These are expected to give profiles of the rock formations at the drill site. If complicated tectonic structures or weak strata are encountered, core samples will be unreliable in a number of ways. The strike and dip of structures are not obtained from cores since drilling will disturb the orientation of a core with respect to its surroundings.

A complementary probe is therefore recommended which will carry an imaging system into the borehole to provide a picture of the cross-section of the crust as a function of depth and to provide a visual correlation with the measurements made by the other geophysical probes. A timely presentation of a panoramic view of the wall sections of the borehole will enable the team of experimenters to examine and interpret the pictures in time to request additional views of interesting wall vesicles or boundaries between a sequence of flows. This capability suggests a television system for the imaging application. The limited time for picture taking, by the astronaut on the lunar surface, also suggests a television system.

The performance characteristics of the Apollo-TV camera were investigated to determine the modifications which would be required to adapt that design to the subsurface probe application.

b. Measurement Technique.

The preliminary study performed for this design has been for a television camera which is contained in a subsurface probe. The camera is only one portion of the total television subsystem which,

* This material prepared and furnished by RCA, Astro-Electronics Division, Princeton, N. J.

in addition, consists of the video channel, provided by the unified S-band link, and television monitor at Mission Control Center (MCC), where hard copy storage of the television imagery is made possible by photographing the kinescope with a film camera. The total delay in viewing a hard copy print of the television image will be primarily governed by the time required to process and print the kine-recorder film at MCC. In concept, this process can be performed while the borehole survey is in progress. All the elements of the system are shown in Figure 38.

The principal constraints to be satisfied in the preliminary design are as follows:

1) That the video data be contained within the 500 kHz video bandwidth allocated for that purpose in the Apollo-LEM, S-Band Channel.

2) That the camera be configured to an outside diameter of 1.75 inches and an overall length of about 21 inches. Efforts should be made to minimize weight and power.

3) That the camera should take high-resolution, high-quality television pictures of the side walls of the two-inch diameter borehole.

4) That the camera should utilize a simple thermal control feature for operation and survival in the borehole environment.

5) That the camera should be a complete, self-contained unit with a simple mechanical attachment to the remainder of the probe; or if a separate probe, to the deployment mechanism.

6) That it should be equipped with an electrical connector to attach to the cable for the primary power input and telemetry signals and video output. The cable length to be as much as 130-ft long to permit the photographic survey of a borehole 100-ft deep.

7) That the first flight-model probe to be available at least a year before the earliest scheduled AAP, Apollo-LEM landing.

To meet the communication channel restrictions of the Apollo system, the initial approach taken in the conceptual design is to use, to the greatest extent possible, the present Apollo TV camera. The Apollo

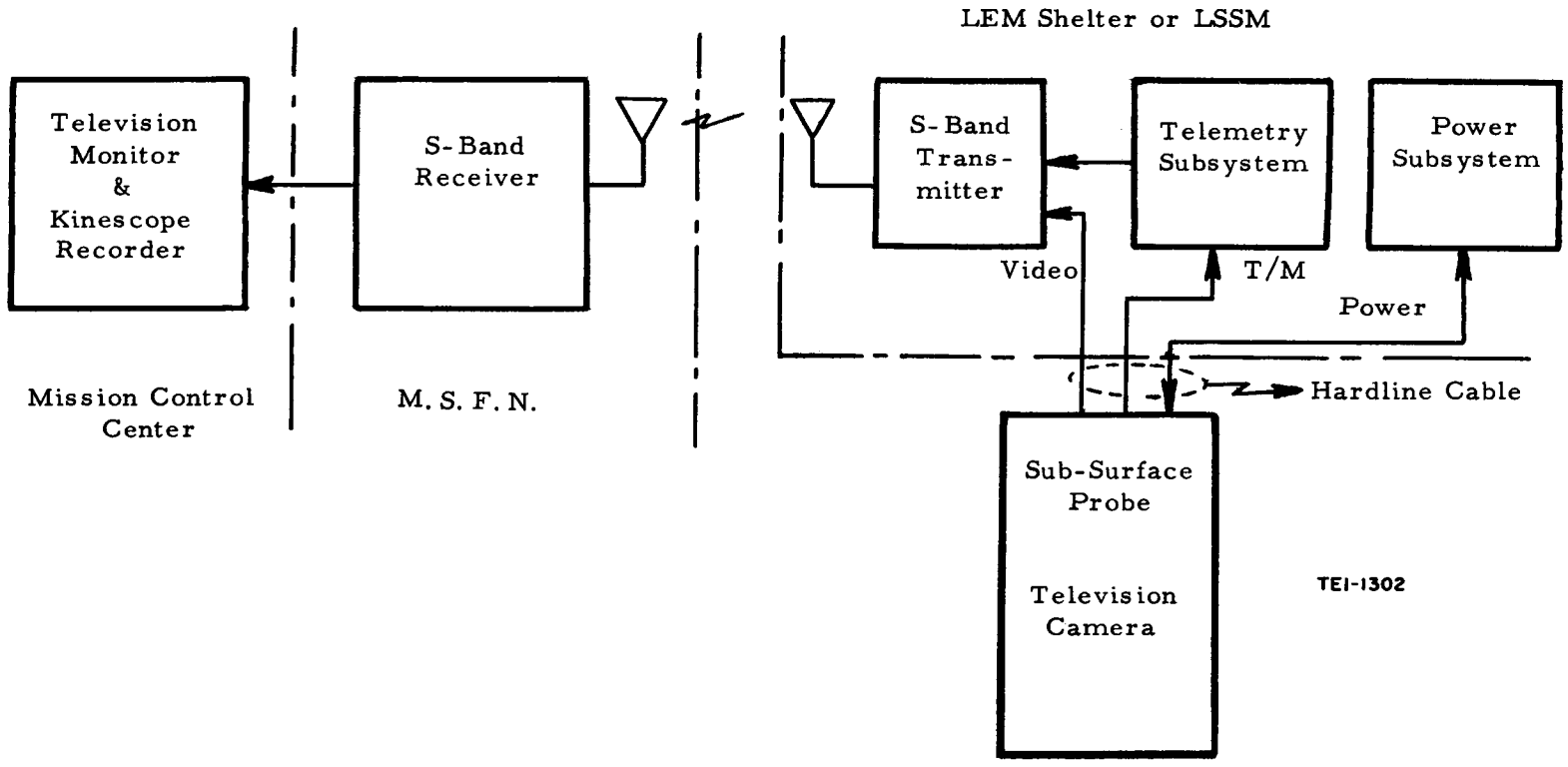

Fig. 38 Subsurface Television Probe System Link

TV camera utilizes a one-inch "hybrid" vidicon sensor that can be repackaged to fit within the probe's dimensional constraints. This vidicon, when operated at a reduced scan rate of about one frame per second, will yield 700 TV lines of resolution. This mode of operation is desirable to achieve the high quality images for interpretation by the geologists. Two alternative approaches which would provide equal performance, with some saving in weight and power, are the use of an all electrostatic one-inch vidicon, or the use of a high resolution 1/2-inch vidicon. These two camera systems would require additional development time and are presented here to indicate the trade-offs to be considered in selecting the final design approach.

Within the bandwidth constraints of the 500 kHz video channel, the Apollo vidicon can be operated to achieve a 700 TV line, horizontal resolution on a 4:3 image aspect ratio by operating the vidicon with 600 volts on the Mesh electrode. The operation is based on a Kell factor of 0.7 and a 5% horizontal blanking time with 1040 scan lines generated to fill the vertical frame. The result is a readout time for the complete frame of 1.015 seconds. This is an indication of the trade-offs which can be made between horizontal resolution and picture repetition rate. The selection, of the final scan parameters, will be based on maximizing resolution and picture repetition rate, and on the capability to operate into the presently planned TV monitor and kinescope recorders for the MCC. It is clear, however, that an adequate, high-resolution TV camera can be designed to meet the video bandwidth constraints.

There is some uncertainty as to the resolution required to perform useful geological interpretations of the side walls of a two-inch diameter borehole. The proximity of the probe TV camera to the side wall, however, makes low-power microscopic imaging possible. It is to this mode of operation that the preliminary optical considerations have been aimed. This will permit the interpreter to see vesicles, in certain kinds of basalt, of a fraction of a millimeter in extent.

The initial condition for imaging of the rather deep hole, is the absence of light and the requirement for an auxiliary source of light in the probe. The lens aperture or F-number can then be selected to provide adequate depth of field with the intensity of the lamps selected to provide a video output from the vidicon with the high signal to noise ratio inherent in a high quality image. With a high signal to noise ratio the camera can perform at a resolution of 700 TV lines, or better than 30 optical line pairs per millimeter in the image plane.

Other aspects of the quality of the image are attributable to the amount of contrast or shades of relief, present in the scene. Such parameters of the wall material as its topographic relief, its

albedo, and its photometric function will all contribute to the amount of detail which will be present. A search of the scientific literature and discussions with the experimenters, will permit expected values for these characteristics to be selected; and the angles of incidence for the illumination to be specified to provide a maximum degree of shade relief at a high signal to noise ratio. For the microscopic views planned, single images will be made of a one-inch section of the wall. For this small area, it might reasonably be expected that the wall will be fairly homogeneous in the above characteristics. As the probe scans out an annular section of the wall, by repetitive images provided as a mirror is stepped in azimuth, the wall photometric characteristics may change. As the probe is permitted to descend into the hole, without any azimuthal movement, a vertical slice of the wall will be imaged in repetitive one-inch images. The vertical image strip may also indicate a change in photometric properties. The images, formed from either one or a combination of these two modes of operation, can be formed into a mosaic at the MCC. With the changes of photometric properties, visible in the mosaic, the geologist can interpret the bore hole geology.

The salient points of the conceptual design of the TV Camera Probe which will permit lunar subsurface imaging are discussed in further detail in paragraphs that follow. Four design areas: packaging, electronic circuit, thermal control, and optical considerations have been considered. The result of this study is a high degree of confidence that an adaptation of the Apollo TV Camera can be designed to fit a 1.75-in. diameter probe and which will provide a high quality image.

c. System Summary

The subsurface television camera probe is completely self-contained, within a tube 28-in. long and 1.75 in. in diameter. The 28-in. length includes 4 in. for the flexure-joint-centralizer unit. It is connected with either the LEM Shelter or the LSSM by cable. The total electrical interface for the camera is at the cable connector, from which it receives primary power, a simple on/off command, and to which it delivers composite video and four telemetry signals. Contained within the subsurface camera is a vidicon sensor, a scanning mirror, illumination lamps, and optics consisting of an F-22 lens. It also contains a complete set of camera electronics which generates its own synchronizing and deflection wave forms, produces the range of voltages required for vidicon operation, and processes the video signals derived from the vidicon. A 1.75-in. long, cylindrical glass window for the viewing port is also included. A block diagram showing these subsystem elements is shown in Figure 39. The total assembly of parts was shown as the Subsurface Television Probe in Figure 5, page 27.

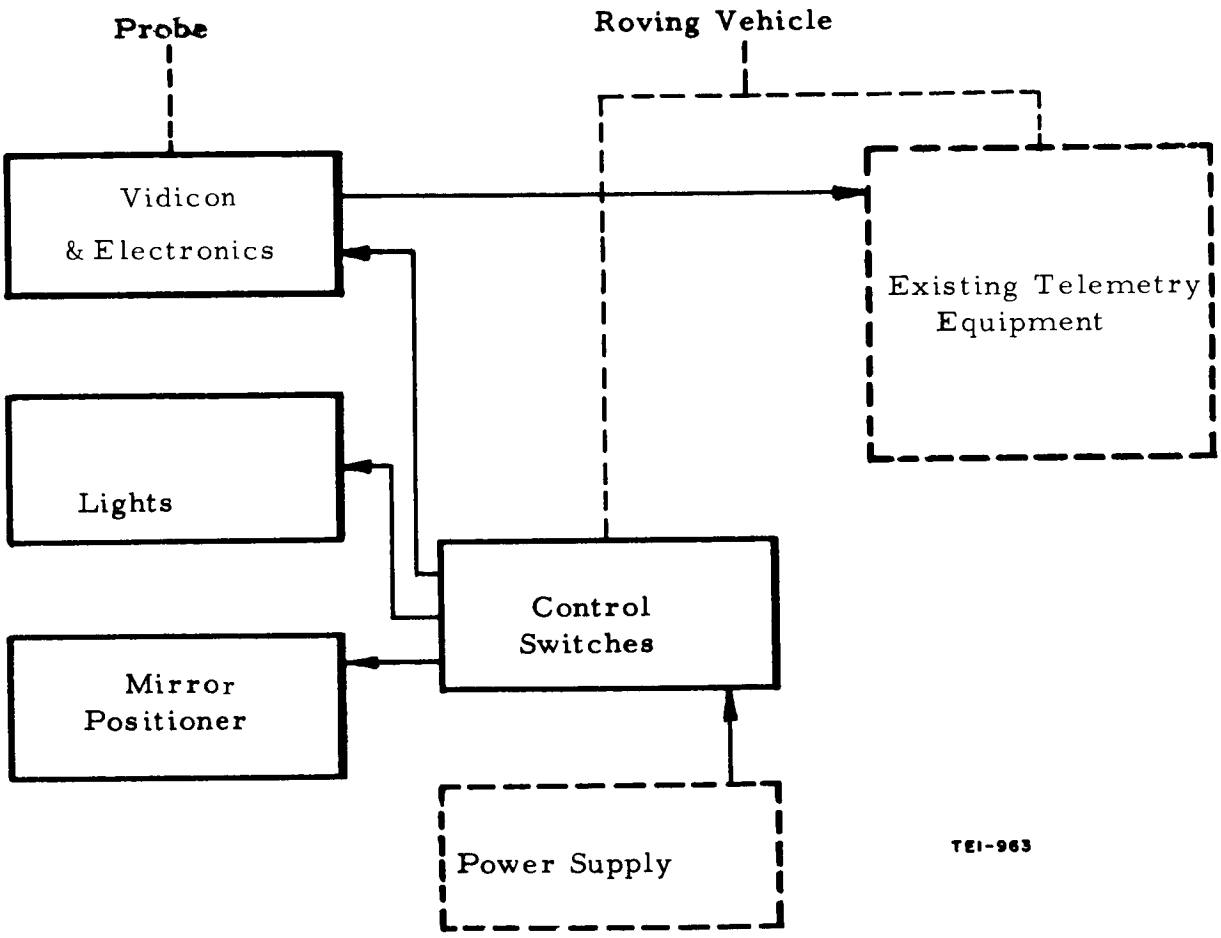

Fig. 39 Block Diagram - Subsurface Television System

Thermal control of the camera is realized passively with a white paint on the outer surface of the probe jacket. A search of the literature shows the subsurface temperature of the moon to be in the range of 211°K to 264°K. Preliminary calculations indicate that at the high end of the band, no additional heat would be required to maintain the probe at its proper operating temperature of 0 to 40°C. At the low end, however, some additional heat would be required. These preliminary considerations also indicate that, for the case where the subsurface material behaves as an infinite heat sink, the probe can be operated continuously if the subsurface temperature is below 280°K. If the subsurface material does not function as an infinite heat sink, the operational time is limited and is a function of initial temperature, thermal conductivity, and heat capacitance of the subsurface material. A preliminary calculation indicates that, for starting temperatures of 20°C, a perfectly insulated camera will operate continuously for 100 minutes before reaching its upper operating temperature of 40°C.

A baseline optical system was considered which would image a 1-in.x 0.75-in. section of the wall on the 12 x 9 mm, 4:3 aspect of the vidicon. A lens with an aperture ratio of F/22 will provide a depth of field of ± 2 millimeters which is sufficient to accommodate the deviation from flatness for the inside wall of a 2-in. diameter cylinder and for small camera decentering. The wall darkness and the small lens aperture will require an illumination level of 260 lumens on the 1-in. high, 360° cylindrical section. Partial illumination of this sector can be accommodated at the expense of about 2 watts average power to drive the illumination lamps.

d. Operational Requirements

The camera would be put into operation by the astronaut, by connecting the probe to the cable and the cable to the LEM shelter or the LSSM. The camera is designed for unattended operation and will only require the astronaut to turn on the power. Depending on the camera's starting temperature, it may be necessary to wait until the camera temperature reaches 0°C before initiating picture taking. With the camera at its proper operating temperature (0 to 40°C) the sequence of operation is as follows: the lamps are lit and the vidicon is exposed forming an image of the sidewall of the borehole through its optics and front surface mirror. The vidicon is then scanned, with the 1040 lines reading out the total frame of video in 1 second. This video is gated through to the S-band transmitter. The mirror is then stepped to the next position and three frames are allocated to erasing thoroughly the residual image. During this period of operation the video output is gated off. The sequence of operation of illumination

for vidicon exposure and vidicon readout is repeated. The picture repetition rate, then, is readout in one second and a rate of 15 pictures per minute. The sector of wall, imaged with each readout, is a sector 1-in. high and 0.75-in. wide. With modest overlap, it is possible to scan and photograph the complete wall surface at a rate of more than a foot of wall for each 15 minutes of operation.

e. Alternate Vidicon Considerations

One-Half-Inch Vidicon System. A camera system has been developed at RCA, as part of a classified program, which employs an improved version of the vidicon and vidicon components used in the TIROS, 1/2-inch vidicon camera. This new vidicon, in conjunction with integrated circuit electronics, offers a lower volume density and a lower power consumption than the Apollo camera for an equivalent performance. The decrease in volume results simply because the 1/2-inch vidicon displaces only half the volume of the one-inch vidicon. In addition, new integrated circuit technology permits synthesizing a larger portion of the camera functions with these compact circuits. The lower power consumption is possible because there is no longer any need to use discrete components to interface with the integrated circuits. An additional power savings results from the fact that less deflection power is required for the 1/2-inch vidicon. A switching-type pre-regulator will be used instead of a series regulator resulting in additional power economy. All of these power savings are offset slightly by the requirement to supply focus current for this high performance 1/2-inch vidicon. This version of the vidicon is all magnetic and there is a need for a focus coil and hence the addition of a focus current regulator circuit. This current can be most economically derived by connecting the focus coil and the vidicon filaments in series permitting them to share the same current from the same regulator.

One-Inch Electrostatic Vidicon System. Another approach to the probe camera to meet the size, weight and power constraints is the use of the RCA-C74078, one-inch electrostatic-focus, electrostatic-deflection vidicon. It is possible that by the elimination of the requirement for the deflection yoke, considerable savings could be made in power consumption, weight and size by employing this vidicon in a new camera design. The present Apollo camera circuits would require radical modifications in the deflection amplifier and power supply in order to accommodate this tube. The deflection circuits would be changed from a low-voltage current-drive used in the Apollo camera to a high-voltage voltage-drive for this camera design. The power supply modifications would provide for the higher vidicon grid voltages required for the

electrostatic tube to achieve equal resolution. The resolution performance of this tube is not quite as good as the Apollo tube. This slightly-relaxed performance could be traded in favor of the weight, volume and power savings.

Operation of the high-performance 1/2-inch vidicon, or all electrostatic one-inch vidicon, camera would be similar to that described for the modified Apollo camera.

f. Instrument Characteristics

A brief summary of the camera characteristics are shown in Table XXII.

TABLE XXII
SUBSURFACE TELEVISION CHARACTERISTICS
(MODIFIED APOLLO CAMERA APPROACH)

Subsystem	Vidicon, Optics, Electronic Circuits, Lamps, Movable Mirror, Mirror Drive Mechanism
Dimensions	Downhole: 1.75-in. diameter, 28-in. length Surface: N.A.
Weight	Downhole: 7.04 lbs
Power	Peak: 16 watts Average: 8.5 watts Power-Time History: 16 watt peak for 1 out of every 4 seconds, with a 6 watt steady state power drain.
Measurement Range	0 - 100 ft depth
Resolution	700 TV lines per picture
Temperature Range	Operating: 273°-313°K Storage: 233°-338°K
Other Environmental Control Required	Additional thermal control for lunar surface storage may be required.
Interference Problems	RF: Shielding built-in Magnetic: Shielding built-in
Output Characteristics	Data Format: Analog Video; Analog Telemetry Voltage: Video 0-1 volt; telemetry 0-5 volts Number of Channels: Video-1; Telemetry-4 Frequency: Video - 500 kHz Telemetry - 1 sample per 4 seconds
Commutated or Continuous	Video: Continuous for 1 second out of every 4 seconds Telemetry: Data available continuously - commutated at telemetry subsystem
Impedance	Video: <100 Ω Telemetry: <1000 Ω
Transmission Accuracy Needed	Video: ≈± 1db from 10 Hz to 400 kHz ± 3db at 500 kHz Telemetry: 5% linearity

7. Centralizer - Caliper Experiment

Background. The accuracy of most experiments, included in the Optimum Subsurface Probe, depends upon the geometry of the individual measurements. For proper interpretation of the measurement data, the borehole size must be known. The position of an instrument (for example, TV probe), relative to the borehole wall, will also affect the results.

Most measurements, proposed for the Optimum Subsurface Probe, are aided by placing the probe in the center of the borehole. These include, for example, the non-contact temperature, thermal diffusivity, and the acoustic velocity measurement. In some cases, such as radioactivity surveying, the position in the hole is immaterial. The density instrument, however, normally requires that the probe be pressed against the formation in order to maximize the scattering path in the formation.

In the Phase I period of this study, a preliminary design of a device, which would allow for both centralizing and decentralizing of the probe, was developed. This device employed motor driven contact pads. Operation involved energizing a motor drive mechanism and a solenoid actuator to force either two or three contact pads against the borehole wall. A decentralized position was provided when two pads were in contact with the formation, and a centralized position provided when all three pads were in contact with the formation. These operations resulted in rather high demands of astronaut time on complex switching arrangements. The reliability of this device would also be harder to assure. Because of these penalties, the desirability of limiting probe positioning to just centralizing was considered. It appears that this will be possible using passive spring members only. As previously mentioned, the most critical experiment is the bulk density measurement. It seems feasible that the proper combination of source strength, collimation angle, detector location, etc., can be found to meet this positioning requirement. This is especially promising because of the near probe-to-hole size. In conventional earth surveys, the tool may have a diameter only a third that of the hole.

In any case a system is needed to position the probe in the borehole and to measure the borehole diameter.

Measurement Technique. The centralizer-caliper instrument consists of a beryllium-copper, spacing assembly located at the upper end of the probe, a three-component, spacing mechanism located approximately 10.5 in. from the lower end of the probe, and a caliper linkage combined with this lower assembly. Figure 40 shows the

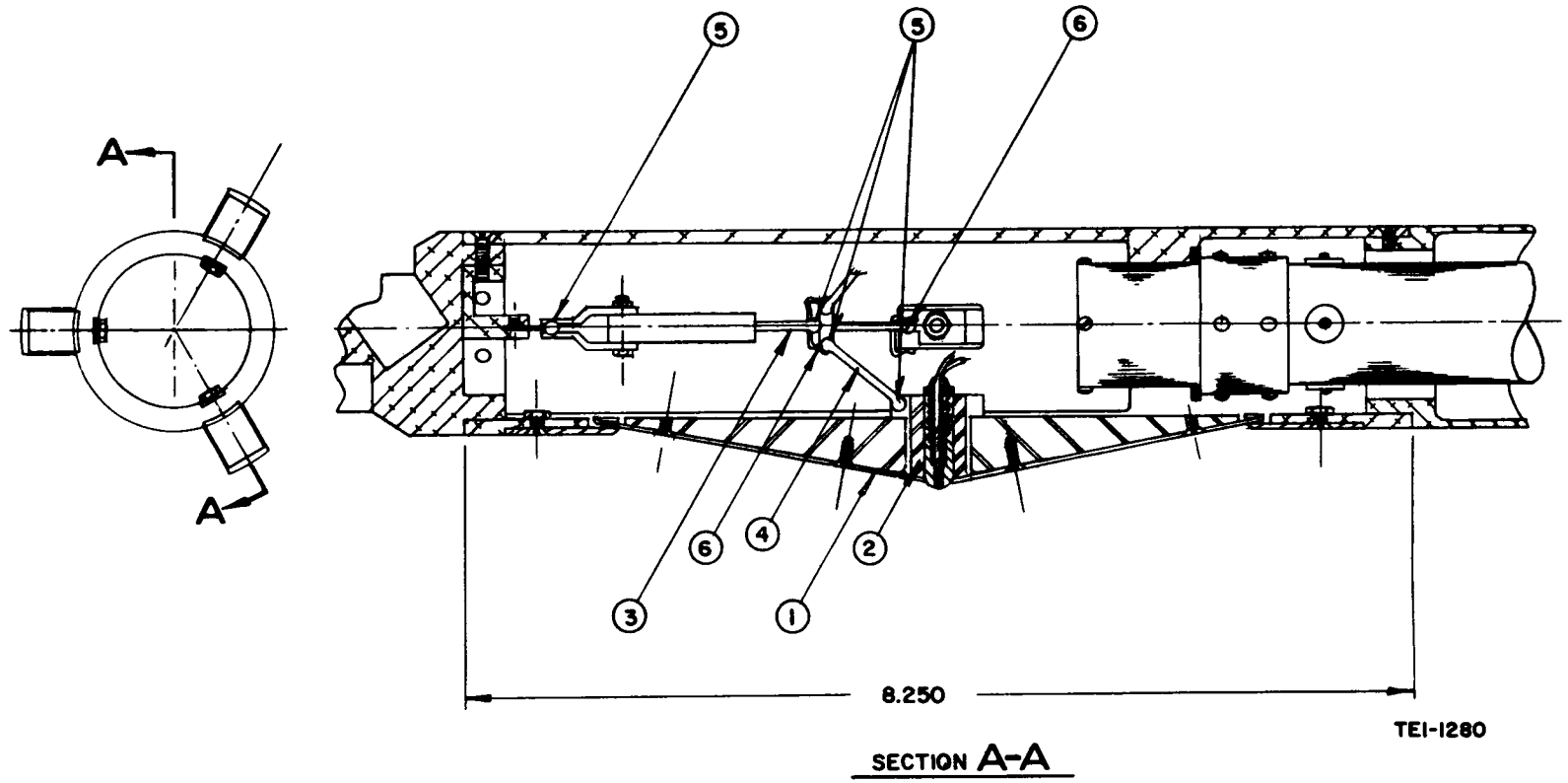

1. SPRING
2. SPRING GUIDE SUPPORT
3. PUSH ROD
4. CONNECTING ARM
5. BALL AND SOCKET
6. SPRING CLIP

Fig. 40 Subassembly - Centralizer-Caliper

construction of this lower assembly. The upper unit serves to provide centering of this end of the probe. Being located outside the probe body, it does not add to its functional length. That is, the distance from probe tip to any experiment is not changed. The lower assembly employs three spring members [1], each located 120° from the other. Contact with the formation is made by three translating slides [2]. Each slide is connected to the transducer push rod [3] by a connecting arm[4]. In the relaxed position each arm is at an angle of approximately 45° with center line of the probe. As the slides move inward each of the angles between the arms and the probe center line decreases and the push rod travels into the transducer. Articulation is provided at the end of each arm, and at each end of the transducer, by ball and socket joints[5] that are retained by spring clips[6]. A system block diagram is shown in Figure 41.

Probable Subsystem Elements

Upper Spring Assembly: To be designed.

Lower Spring Assembly: To be designed.

Caliper Linkage: To be designed.

The Linear Displacement Transducer (potentiometer) will be of a type qualified for space use.

Constant Current Source and Signal Conditioning Circuit: To be designed. (May utilize portion of temperature sensor equipment thus minimizing circuitry).

Operational Requirements. Operation of the instrument is limited to energizing the constant current supply for the caliper potentiometer. The output can be visually read out, recorded or telemetered along with data from the other experiments. The measurement may be made during continuous logging or on a point-by-point basis.

Instrument Development Studies. Development of this supporting device should be straightforward. Technology pertaining to conventional well logging positioners can be used, as well as the special material requirement determined for Surveyor. Major design considerations will involve avoiding cold-welding of contacting or sliding metal members, and sealing the device to prevent clogging by dust or chips.

Instrument Characteristics. Table XXIII gives the characteristics of the experiment.

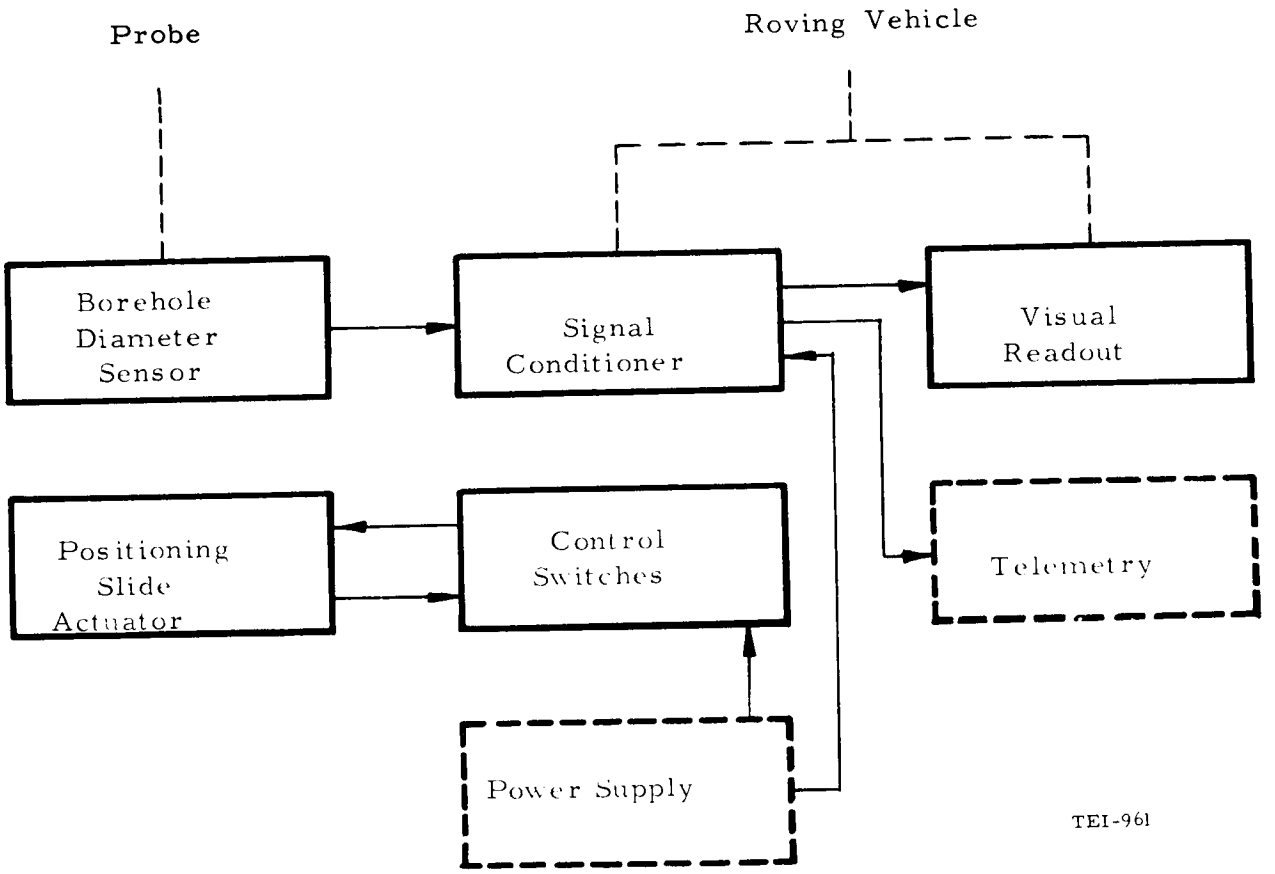

Fig. 41 Block Diagram - Centralizer-Caliper

TABLE XXIII
CENTRALIZER - CALIPER EXPERIMENT CHARACTERISTICS

Subsystem Elements	Upper Spring Assembly, Lower Spring Assembly, Caliper Linkage, Constant Current Source and Signal Conditioning Circuitry.	
Dimensions	Downhole:	1.75-in. diameter (slides compressed) 2.50-in. diameter (slides extended), 4.7-in. length
	Surface Equipment:	3x2x2 in.
Weight	Downhole:	0.80 lbs.
	Surface:	0.3 lbs.
Power	Peak:	N. A.
	Average:	0.3 watts
	Power-Time History:	Uniform during measurement
	Voltage:	28 VDC
Measurement Range	1.75 - 2.50 in.	
Accuracy or Resolution	± 1% accuracy, 0.01 inch resolution (transducer)	
Temperature Range	Operating:	Downhole - 120°-400°K Surface - 250°-350°K
	Storage:	Downhole and Surface - 120°-400°K
Output Characteristics	Output Form:	Analog
	Voltage:	0-5 V
	Number of Outputs:	1
	Frequency Range:	DC
	Impedance:	As required
	Transmission Accuracy Req:	Standard
Logging Speed	Fixed point or up to 10 ft/min	

B. OTHER POSSIBLE EXPERIMENTS

1. Neutron-Neutron (Hydrogen Log)

Background. A commonly used tool in well surveying is the neutron-neutron instrument. It has been shown that it is possible to determine the presence of hydrogenous material (hydrocarbons or water) by irradiating the formation with fast neutrons and then measuring the moderated (slowed down) neutrons by a BF_3 or other neutron detector, arranged to measure epithermal or thermal neutrons. Very light elements, especially hydrogen, are more effective in slowing down neutrons than are heavy elements, and this can be used to indicate the presence of water on the moon if it is there in any form. Although the probability of free water (ice) or permafrost may be low, water of hydration in various minerals is a good possibility.

Green (3) shows that most igneous rock types have water content in the 0.5 to 1 percent water-by-weight category which is within the measurement capability of the neutron-neutron technique. The advantage of this technique is that it is not sensitive to effects of natural or induced gamma.

The neutron-neutron measurement is not strongly recommended for the probes if the neutron-gamma measurement is to be included. This is mainly because the detector required is not compatible with the other nuclear experiments being considered. In addition, the sensitivity of the neutron-gamma instrument to hydrogen is about the same as for the neutron-neutron approach. If the neutron-gamma experiment is not included then consideration should be given to a simple capsule-source experiment since determining the possible presence of water will be so important. This experiment would support the mass spectrometer and interferometer spectrometer experiments.

System Summary. The neutron-neutron system is made up of a capsule or accelerator-type neutron source and a neutron detector. The detector could be of the semi-conductor type with a converter foil, or a BF_3 counter. The semi-conductor detectors are smaller and require lower operating voltages but are also less efficient. BF_3 counters are rugged, as well-proven in terrestrial surveys, and are chosen here.

The measurement involves determining the degree of thermalization taking place and, therefore, no pulse-height analyzer is needed (no energy discrimination required).

Figure 42 is the system block diagram.

The physical arrangement includes a capsule neutron source [2] a source collimator [3] and a detector [1] shown in Figure 43. The collimator section is 2.75-in. long while the BF_3 detector requires 5 in. The total weight would be about 2.5 lbs. Power requirements are 3 watts.

Operation of the instrument is similar to that of the gamma-gamma measurement. It will involve activation of the detector, and the surface electronics. The capsule source would require no power. The experiment can be conducted as the probe is being pulled from the hole. One channel should be provided for depth-mark signals. Another would be needed for caliper data. Surface measurements would be carried out in a manner similar to that for the gamma-gamma density instrument.

2. Resistivity

Background. Several methods of measuring resistivity, in addition to the induction log previously recommended, were analyzed with two additional methods having sufficient merit to warrant further consideration as possible probe experiments. These are designated the change-of-Ω method and the scratcher-electrode method.

System Summary. The scratcher-electrode method, as used in subsurface measurements, would be more or less as the name implies. A metallic finger would extend from the probe and scratch into the formation under test. The return electrode can be either a second scratcher arm for sampling between discreet portions of the formation, or it can be a solid electrode firmly driven into the formation at the surface. The two electrodes are then connected to a bridge circuit wherein the apparent resistance of the formation is measured. Either AC or DC power may be used for the bridge power.

Direct-current methods are preferred due to the greater simplicity of application and, in general, greater sensitivity. A serious problem exists in earth formations, however, when fluids are present which can cause polarization at the electrodes. A second problem is that of naturally occurring earth potentials (spontaneous potentials) which can influence the measurement.

Alternating-current methods are hampered by phase-shift and eddy-current effects, unless the frequency is very low. The generally accepted practice is to utilize a direct-current source which is commutated at a frequency of 15 to 30 cps. This method alleviates

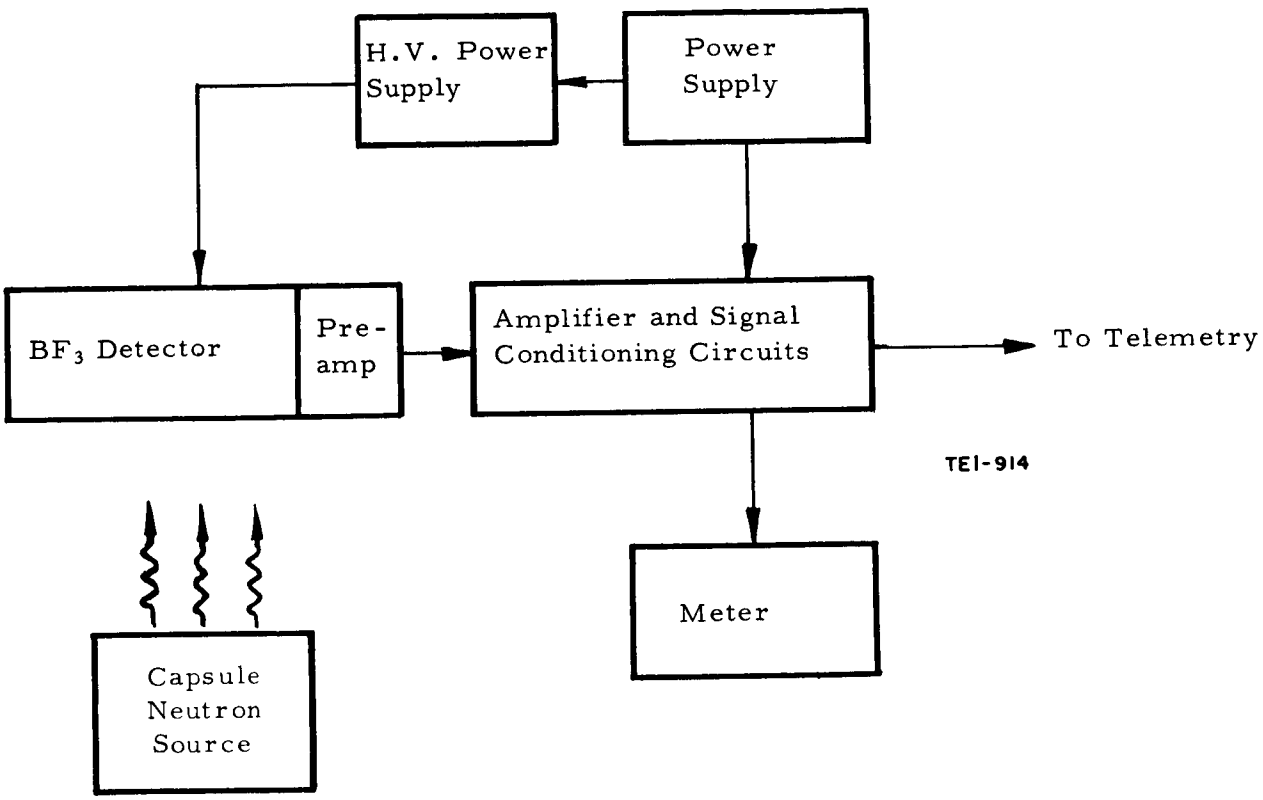

Fig. 42 Block Diagram - Neutron-Neutron System

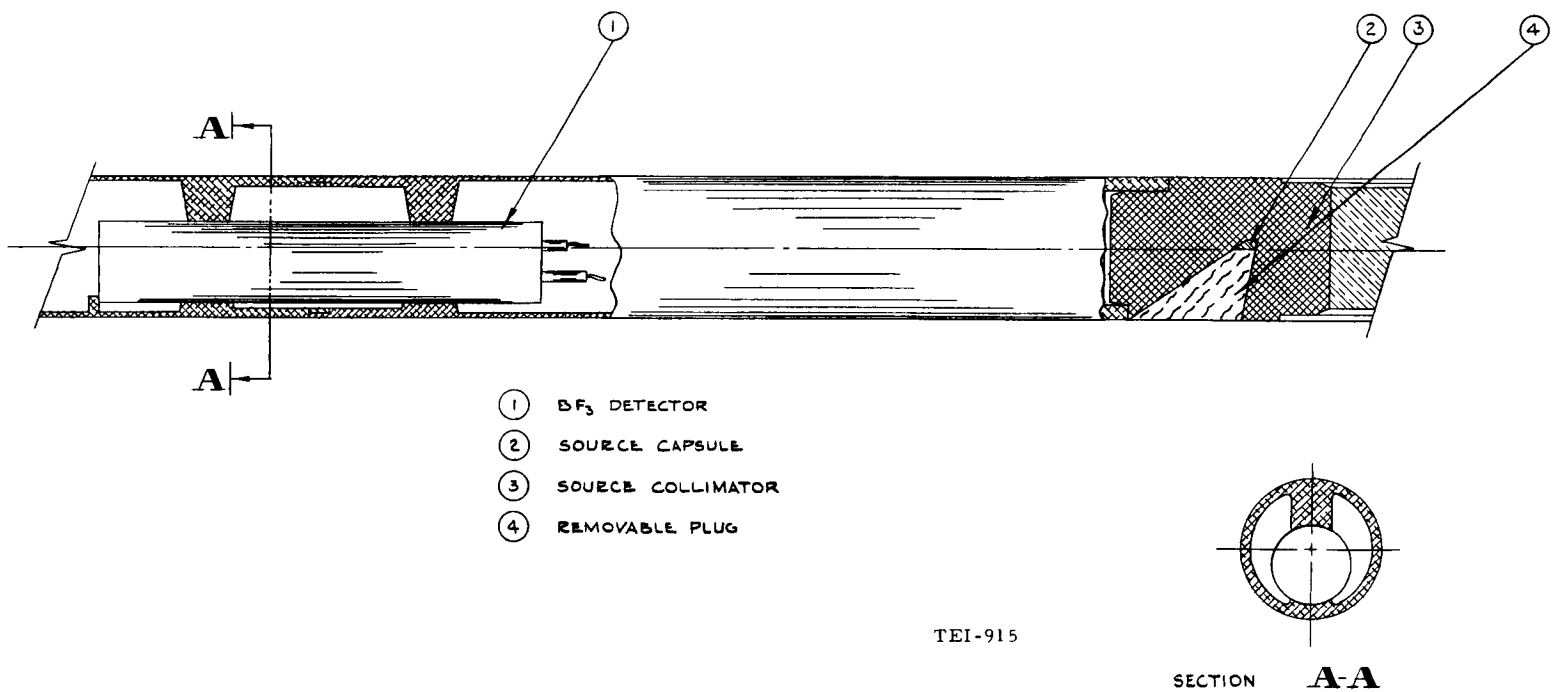

Fig. 43 Subassembly - Neutron-Neutron System

the electrode polarization problem while retaining the preferred aspects of the direct-current method, since the primary current is essentially an alternating, polarized, direct current.

The direct-current approach in lunar measurements would not suffer from the polarization effects due to the low probability of free water in the formations.

Figure 44 is the block diagram of this resistivity measurement.

A technique for providing good electrode-to-formation contact must be developed before this can be incorporated into a probe device. Small sensor size and a limited electronic requirement make this an attractive experiment if formation resistivities below about 10^{-1} ohm-centimeter are suspected.

Resistivity measurements by the change-of-Q method has a particular appeal where the inherent resistivity is high, as is anticipated for the lunar material. The basis of the device is the definition of the Q of an inductance which is the ratio of the inductive reactance to the equivalent series resistance. This includes both I^2R losses and eddy-current losses as well as other minor effects such as dielectric losses and skin effects. In order to measure eddy-current losses where the resistivity is high, the Q of the circuit must also be high. To accomplish this, the inductive reactance of the circuit must be high, which is most readily achieved by using a very-high operating frequency - on the order of 10 megacycles per second.

The method selected for measuring the Q is known as the elapsed-time method wherein the time interval between two preselected voltage points on the decay curve is measured. In use, the inductor is pulsed with radio frequency energy and allowed to decay, during which time the measurement mentioned above is made. The Q can now be calculated using the equation:

$$Q = \frac{\omega \Delta t}{2 \ln(e_1/e_2}$$

where $\omega = 2\pi f$, Δt is the time between the two selected voltage points e_1 and e_2 on the decay curve. Resistivity information is then obtained by reference to empirical calibration curves relating Q to R. A block diagram of the instrumentation is shown in Fig. 45.

The probe section required for the change-of-Q coil is shown in Fig. 46. It is 1-in. long and weighs 0.3 lbs. Total power required is 3 watts.

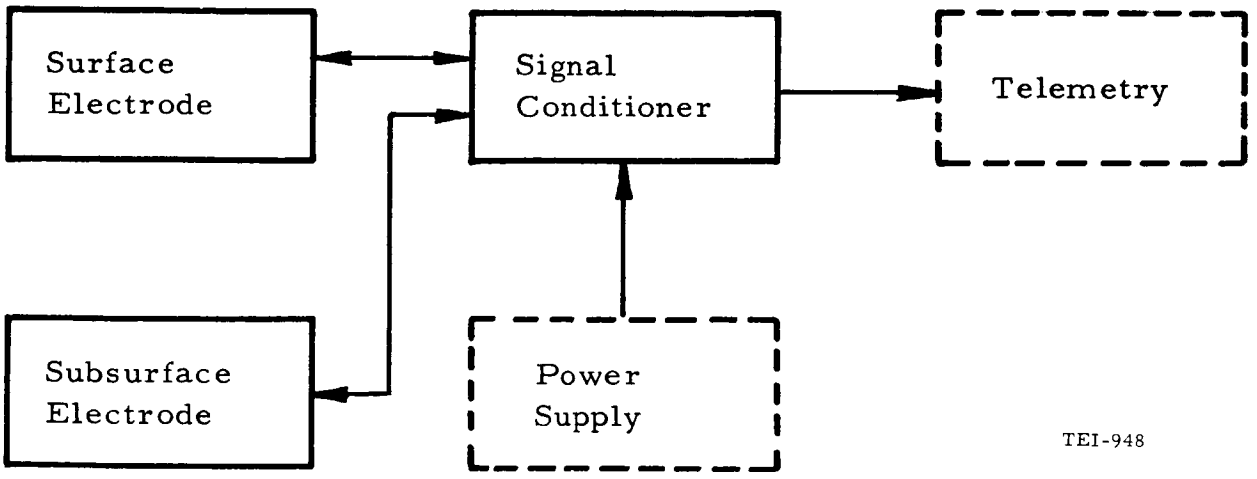

Fig. 44 Block Diagram - Scratcher-Electrode Resistivity Experiment

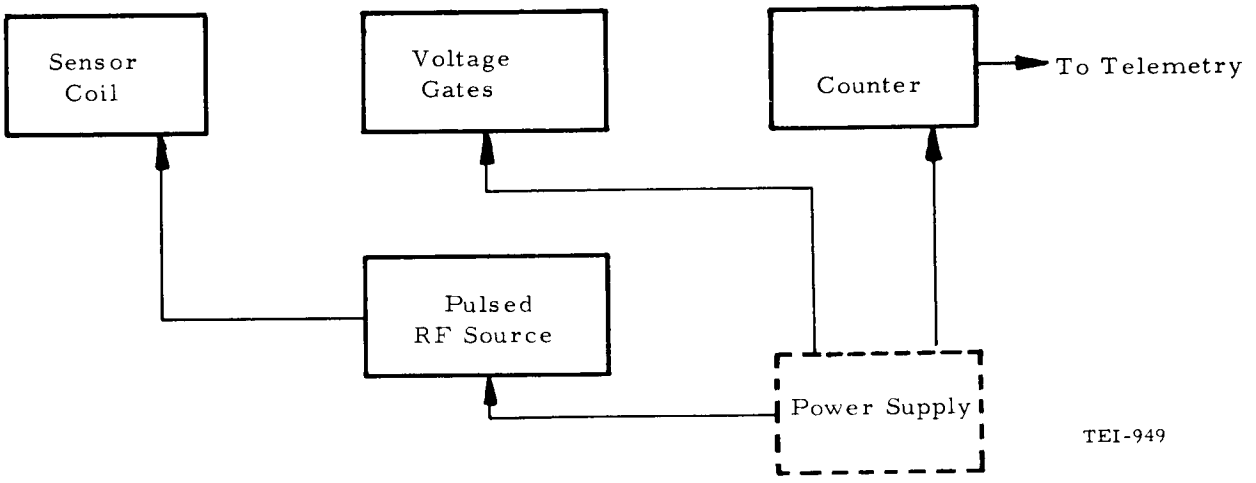

Fig. 45 Block Diagram - Q Resistivity Experiment

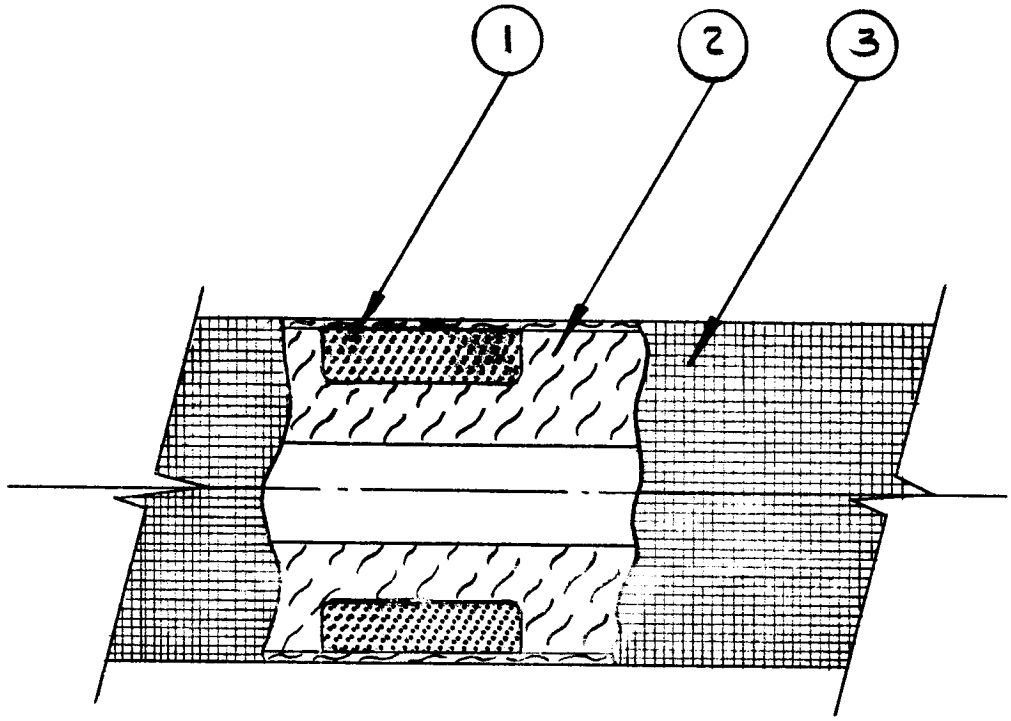

TEI-950

1 Q RESISTIVITY COIL

2 EPOXY-FIBERGLASS BODY

3 EPOXY-FIBERGLASS TUBE

Fig. 46 Subassembly - Change-of-Q Coil Section

This experiment, although recommended in the Phase I report, is not included in the Optimum Probe Configuration because the state of development is not at a level which would guarantee a workable lunar device. The desirability of determining resistivity values within the range of this instrument is significant and a separate development program is recommended.

3. Formation Tester

Background. A formation-tester instrument is proposed which will perform as follows:

- Provide dead-tight sealing of a section of the sidewall of a borehole by inflating an elastic bladder. The sealing action might be improved by the application of a semi-plastic material, which is caused to flow into the formation by pressure exerted by the bladder.
- Inject a given volume of gas into the cavity which has been sealed off.
- Monitor the history of the decaying gas pressure with a transducer such as a CEC type 4-325 (an unbonded, strain-gage-type instrument).
- Deflate the bladder so that the instrument can be positioned and another measurement made.

Figure 47 shows two configurations which might be used. In Figure 47 a, the probe seals off an annular chamber to be pressurized while in Figure 47 b, the probe seals off a smaller, disk-shaped chamber. It is believed that the "b" configuration will be capable of more-meaningful measurements. However, the "a" type will be better able to detect fractures or faults and have more of an averaging effect.

Experiment Summary. The proposed instrument will measure the rate at which a certain gas is absorbed by the media being investigated and can provide information related to permeability. No attempt will be made to measure permeability, per se, for the following reasons:

> Exact measurements of permeability are usually made under carefully controlled laboratory conditions. Either gas or liquid is forced through a sample being tested. Close control of the pressure across the sample is needed to give a steady-state flow. Measurement of the flow rate, pressure gradient,

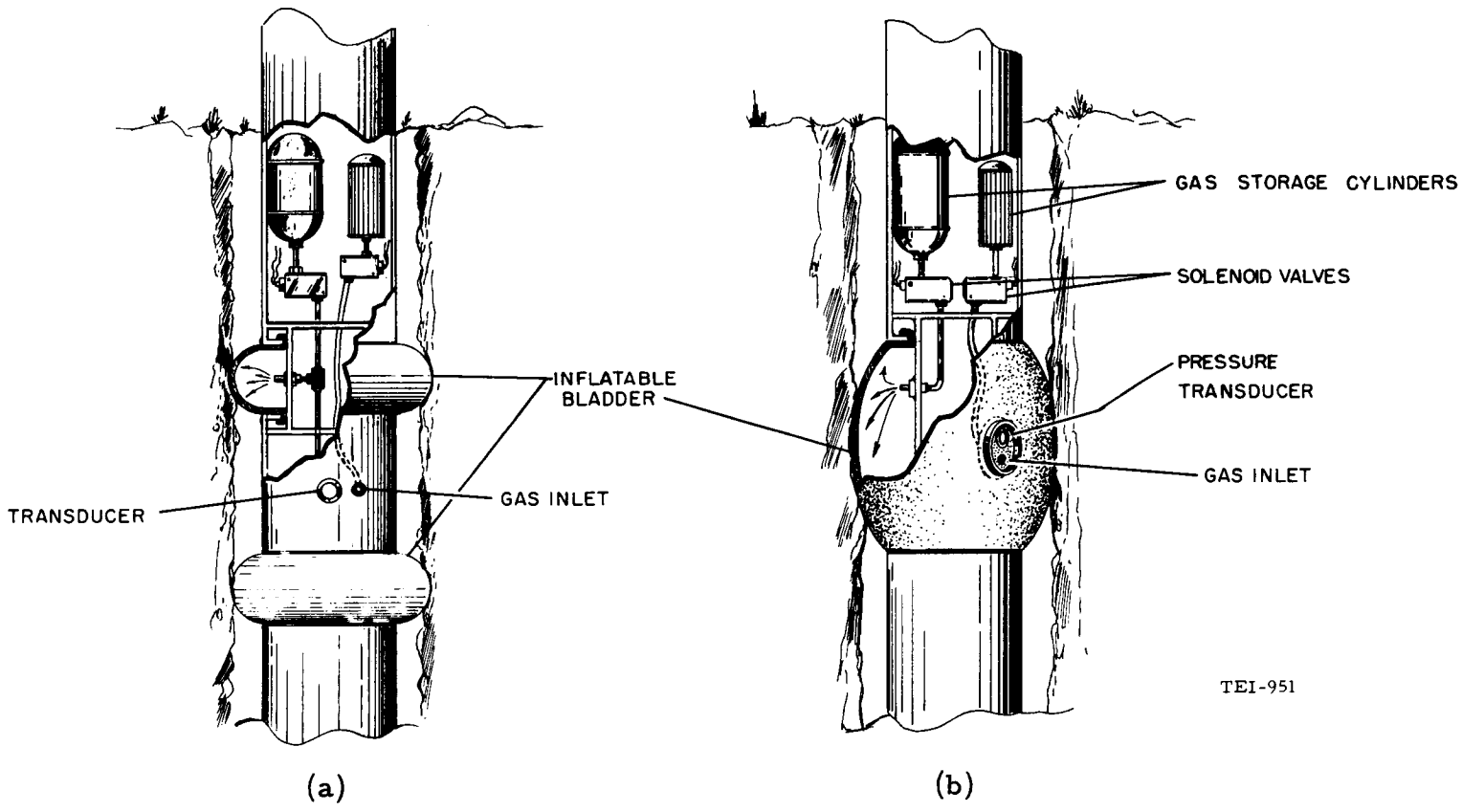

Fig. 47 Formation Tester Configurations

viscosity of the fluid, sample cross-sectional area, and length will define the permeability of the sample. Measurements of this type would best be made when samples are brought back to earth on return missions. In formations where the permeability is appreciable, very large fluid reservoirs are needed to produce steady-state flows for in situ measurements. Thus, steady-state, in situ measurements would not be practical on the moon.

A dynamic gas-flow measurement provided by a limited gas supply would be affected by the initial absorption of porous media. Under steady-state conditions the measurement is made after sufficient time has elapsed for the pores to completely fill.

The indicated permeability of a porous material will change with a change in the mean pressure of gas flow.

Nevertheless, the information to be gained from the experiment warrants further consideration of the measurement as proposed.

If the last two reasons are neglected, an established equation for gas flow through porous media can be used to approximate the pressure-time curves which are expected for different values of permeability. The equation is:

$$Q_m = \frac{2k\pi \, (P_w - P_e) \, r_w}{\mu \left(1 - \frac{r_w}{r_e}\right)} \qquad \text{Ref. (14)}$$

where Q_m = rate of gas flow - cc/sec.
k = permeability - darcies
P_w = pressure applied - atmosphere
P_e = pressure at the outer edge - atmospheres
r_w = radius of applied pressure - cm
r_e = radius of outer edge - cm
μ = viscosity - centipoise

If the b configuration in Figure 47, which exposes a small part of the borehole to the pressurizing gas, is considered, Figure 48 represents the geometry which delineates the above equation. The following assumptions are made. The volume of the pressure source is 10 cc and the gas used has a viscosity of 0.01 centipoise. P_e approaches zero and r_e approaches infinity. Since $Q_m = V/t$, values of P_w are plotted as a function of t. Figure 49 shows a family of curves representing the equation when different values of k are used. Calculations to determine these curves were made assuming that the full 10 cc volume is available immediately and does not flow through an appreciable restriction.

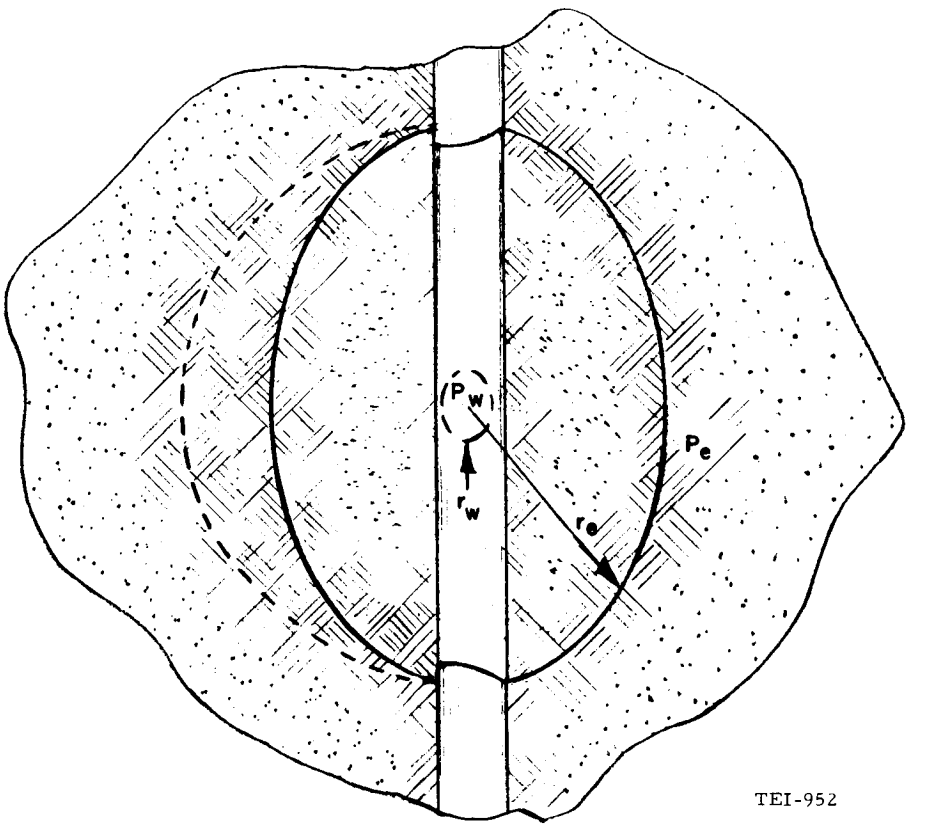

Fig. 48 Experiment Geometry - Formation Tester

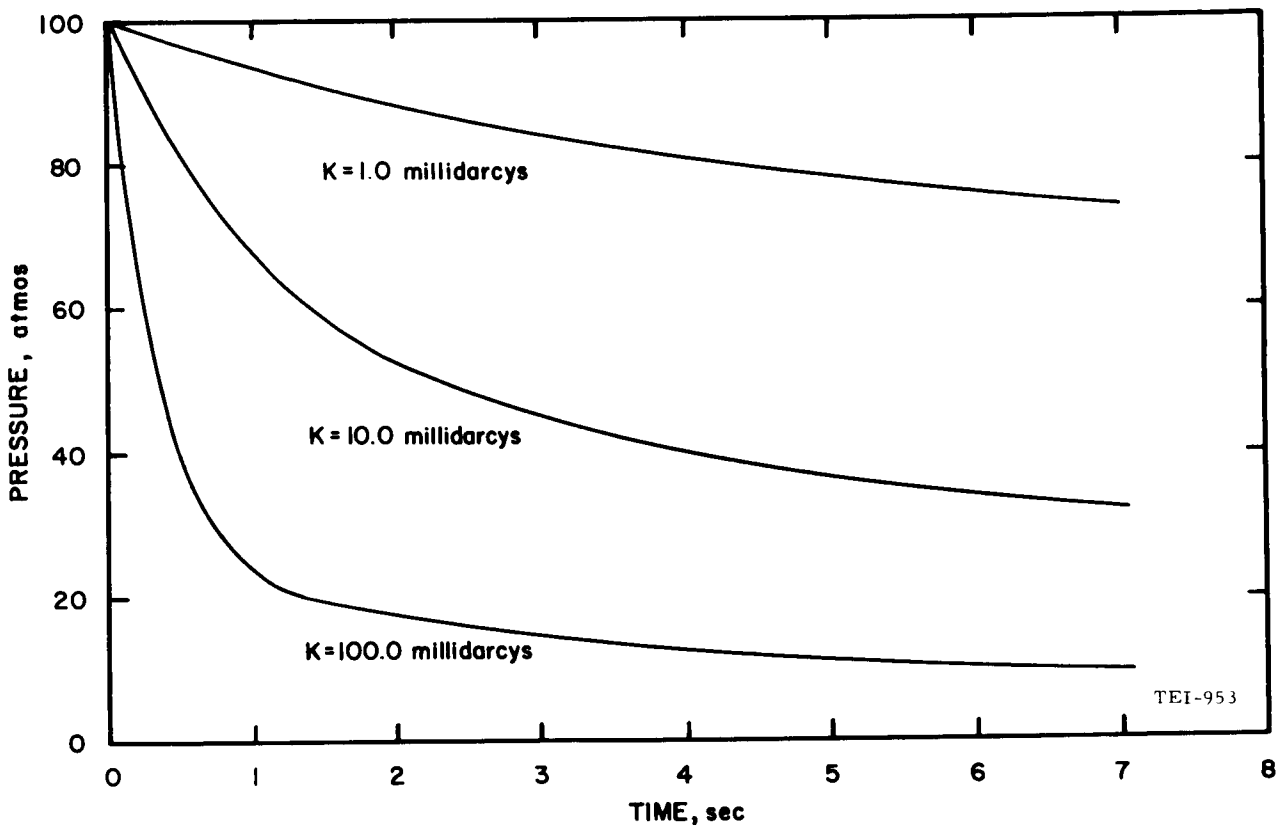

Fig. 49 Response Curves - Formation Tester

The equation is also useful in determining the length of the sealing surface. If r_e is altered appreciably by allowing the escape of gas into the borehole, there will be an error in the measured absorption. An error of less than 10 percent will exist if $r_e = 10r_w$.

In another approach, a close analysis of the initial slope of the pressure-time curve, obtained when gas is being discharged into a formation, will provide data related to porosity. When drilled into a porous material, the borehole wall will cut through and expose pores directly to the gas pressure. The passages leading into the pores, adjacent to the borehole, will be larger and offer less restriction to gas flow that the interconnecting passages between pores. As the gas moves into the formation it will encounter less resistance at first, and then, as the pores fill, it will find more resistance to flow. This will show as a point of inflection on the pressure-time history. The data will not be as meaningful where the porosity is very low or the permeability is very high.

Variations in the discharge orifice area can be used to broaden the operating range of the instrument. Also, if two gases with different physical characteristics, such as viscosity, are used the range might also be extended. The gases might be oxygen with a viscosity of 0.025 centipoise at 400°K and hydrogen with a viscosity of 0.011 centipoise at 400°K. When referring to the equation it can be seen that the flow rates of the two gases will be different by a factor of two.

Before measuring the gas absorption of a particular formation, it would be desirable that the probe be located to measure absorption near the center of the bed. This assumes that layering is first detected by continuous logging or other means.

In operation, the following steps are performed:

a. Sealing of a section of the borehole wall is done by pressing a button that energizes a solenoid. The energized solenoid allows pressurizing gas to flow from a storage cylinder to an inflatable elastic bladder.

b. An indicator light shows when the bladder force against the borehole wall is sufficient for sealing. If the bladder is fully expanded and does not make contact with the wall, gas flow is stopped automatically.

c. A pushbutton switch energizes a solenoid, which releases a charge of gas into the formation. A time-delay stops the flow of gas after a pre-selected period of time.

d. The astronaut monitors a meter which is calibrated to display output pressure. If the formation is permeable, the meter will deflect for a very short period of time. If it is impervious, the meter will deflect for a long period. In either case, the measurement is complete when the meter shows zero pressure.

After a period of one minute, the signal is changed from being sampled continuously to being sampled once each minute. When all other measurements are complete for a particular probe position, the bladder is deflated by pressing a button.

The system block diagram for this experiment is given in Figure 50. The length of the device is estimated at 5 in. and the weight at less than 1 lb. Total power required is 6.5 watts during bladder actuation, falling to 0.5 watts during pressure measurement.

This experiment is recommended for further study. If a feasible engineering model can be developed, suitable for the AAP, then it should be considered for inclusion in the probe.

4. Total Pressure Gage

If the subsurface, quadrupole mass spectrometer cannot be satisfactorily developed to fit the probe, an atmospheric pressure measurement should be substituted. Although not providing information concerning constituent gases, it will indicate differences in pressure at different locations.

Background. Atmospheric pressure measurements, of the lunar surface and subsurface, will be useful in the interpretation of data obtained from other instruments used to determine the age, origin, and history of the moon. Also, it will be instructive to measure changes in pressure as a function of time and place, or changes resulting from the difference in conditions between the lunar day and night.

The contribution to the lunar atmospheric pressure by the exhaust gases, of the LEM, descent-stage rockets, must be measured. The detection of out-gassing, as a result of volcanic activity, or the volatilization of chemical compounds (minerals) is important.

Pressure measurements will enhance gas analysis as made by the mass spectrometer. The knowledge of atmospheric conditions where samples are taken will be important to good lab analysis.

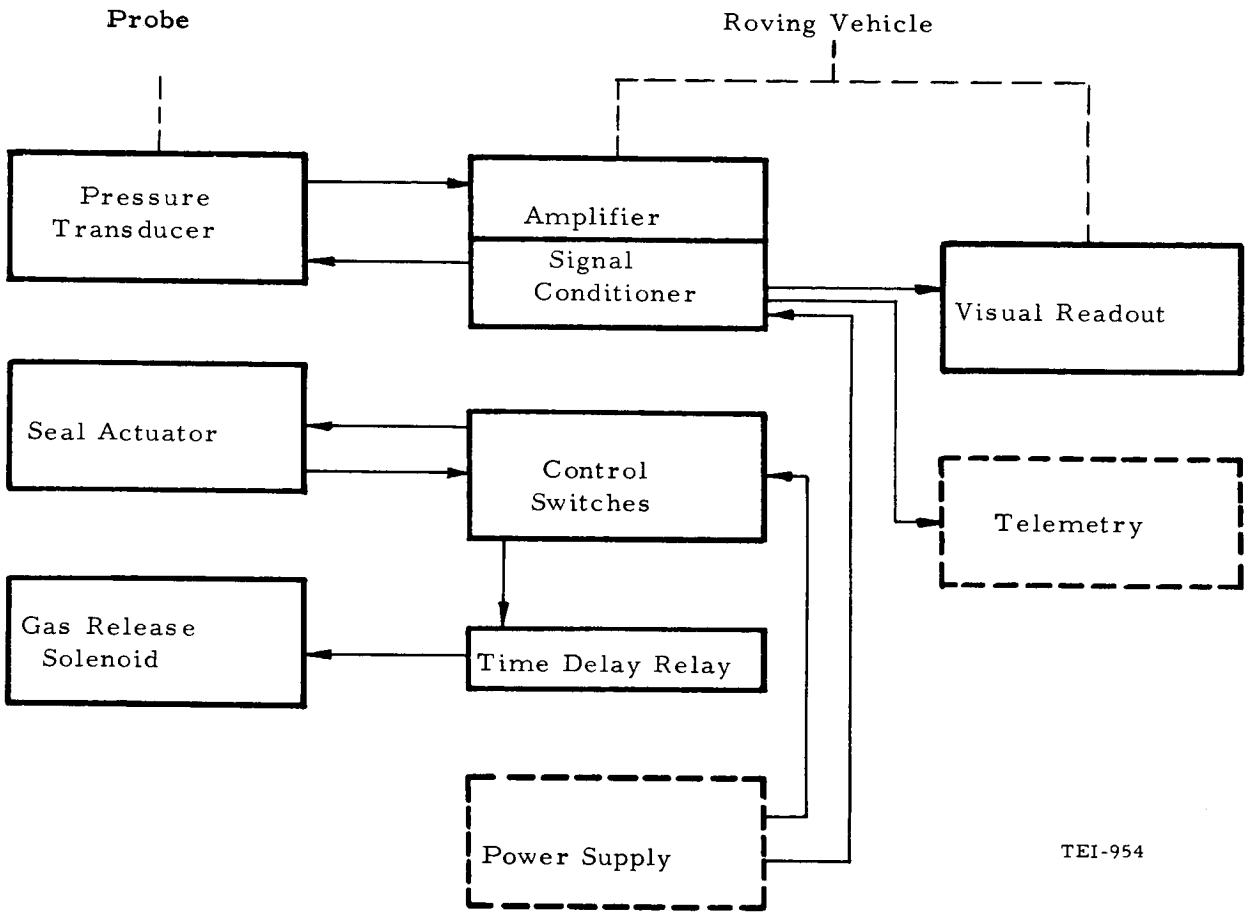

Fig. 50 Block Diagram - Formation Tester

Subsurface measurements will be important in determining the presence of cracks or fissures and the effects on the formation due to the drill operation. The measurements in deep holes will be particularly important, as the decay time for escaping gases will be longer at the greater depths.

Experiment Summary. Pressures of extreme vacuums can be measured by a number of instruments. Thermal conductivity and ionization vacuum gages do not have ranges which are capable of measuring the expected lunar atmospheric pressure (10^{-6} to 10^{-16} torr). The lowest pressure measurement made by ionization gages is 10^{-8} torr and the thermal conductivity type is much higher. Even the Bayard and Alpert, modified, ionization gage is not useful much below 10^{-10} torr. A "Magnetron Gage" known as the "Redhead" is much too large for use in a subsurface sonde. It is a cold-cathode device capable of measuring pressures as low as 10^{-13} torr and below.

Because of the light weight and small volume of the G. E., Model 22, GT 210 gage, it is adaptable for use in the subsurface sonde. It is a triggered gage which utilizes a cold-cathode discharge in a magnetic field. A stable pressure measurement is made from 10^{-4} to 10^{-14} torr. Gas molecules that enter the gage tube are ionized by collisions with electrons. An efficient ring magnet, with a uniform field, greatly increases the electron path length and also the possibility of collision. A measure of the positive ion current which flows between 2000-volt electrodes can be correlated as a pressure measurement.

Instant starting, no matter how low the pressure, is accomplished by momentarily heating a filament. Electrons from the hot filament are injected into the ionization region through a small hole in one of the cathodes. These electrons trigger the discharge.

The following measurements can be made with the G. E. trigger gage:

a. The neutral particle pressure can be measured as described above provided that -

- There are no ionized particles present or an ion trap or shield is attached to the gage tube. (The gage will measure current that results from ions diffusing onto the electrodes. Whether the ions are those already present or those produced by collisons will not be discernible.)

- There are only two or three major components of the lunar atmosphere. As gas molecules are ionized by colliding with electrons, the degree of ionization is dependent upon not only the molecular concentration but upon the electron-binding energy level of the gases present. If more than two or three major gases are present, it will be difficult to determine whether the ions result from a particular neutral-particle concentration or whether they result from the ability of certain gas molecules to be ionized. As the number of components increase the complexity also increases.

- The major components are identified.

- The gage is calibrated with gases having ionization properties similar to those in the lunar atmosphere.

b. The total ion concentration can be measured by observing the difference between ion current with and without the electrostatic shield.

c. A measurement of the directed ion flux can be made by physically manipulating the gage (probe). If the open-ended tube is directed toward oncoming ions, they will be received and recorded. Here again the measurement is made with and without the electrostatic shield. Ions, which do not have direction and velocity such that they enter the 1-in. diameter aperture, will not be measured. This measurement will have little significance in a borehole unless a baffle is added to deflect a radial ion flux that enters the borehole from the sidewall. If a baffle is not used, the gage will sense only flux that is directed straight up the borehole.

d. The total gas-pressure measurement is made without the electrostatic shield. Both the neutral-particle pressure and the molecular ions will be represented by a total current flow. Here again the components must be identified and the gage calibrated to measure these components.

A preliminary design of this instrument is given in Figure 51. The device is 5.5-in. long, weighs 1.25 lbs and requires 12 watts of power (est.). Figure 52 is the system block diagram.

Operation of this instrument involves actuation of three switches and monitoring of a meter for output readout. The switches are:

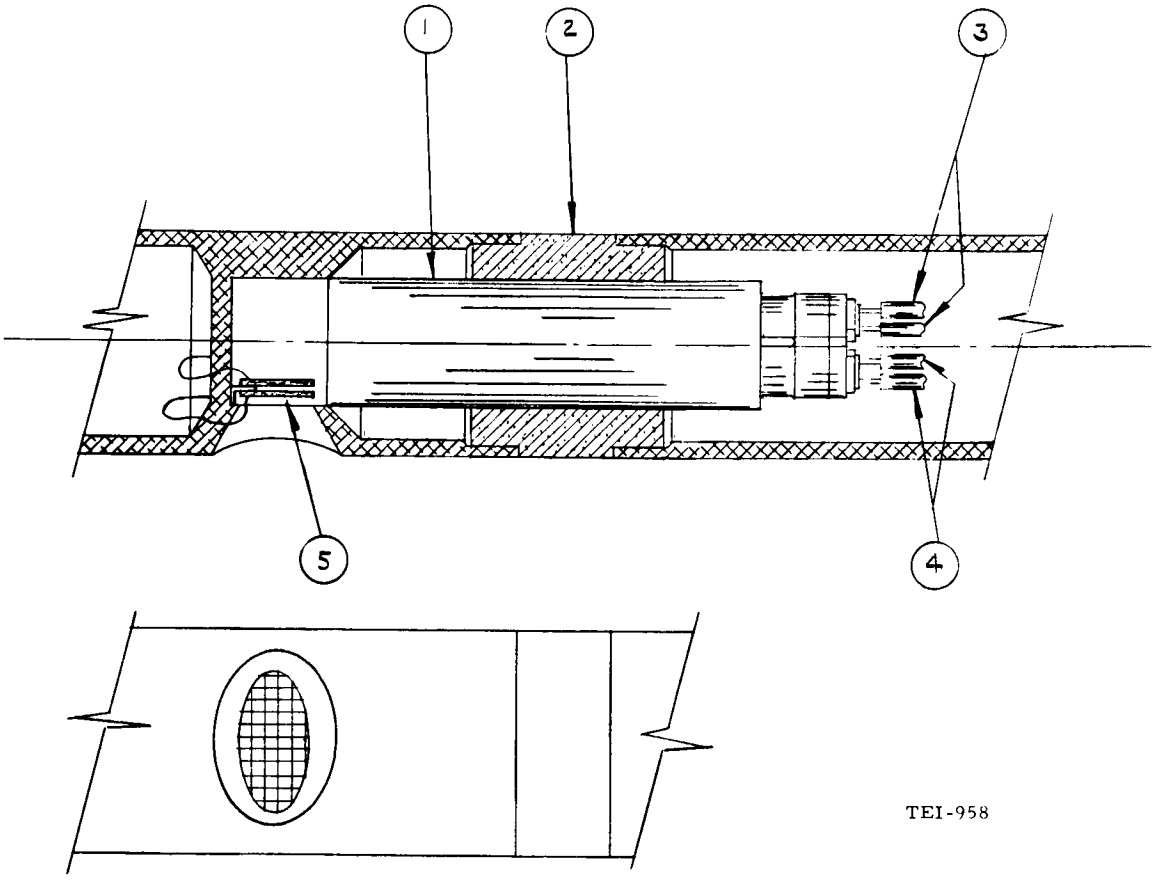

1 TUBE

2 RING MAGNET

3 HIGH VOLTAGE CONNECTIONS

4 FILAMENT CONNECTIONS

5 ION SHIELD

Fig. 51 Subassembly - Atmospheric Pressure Gage

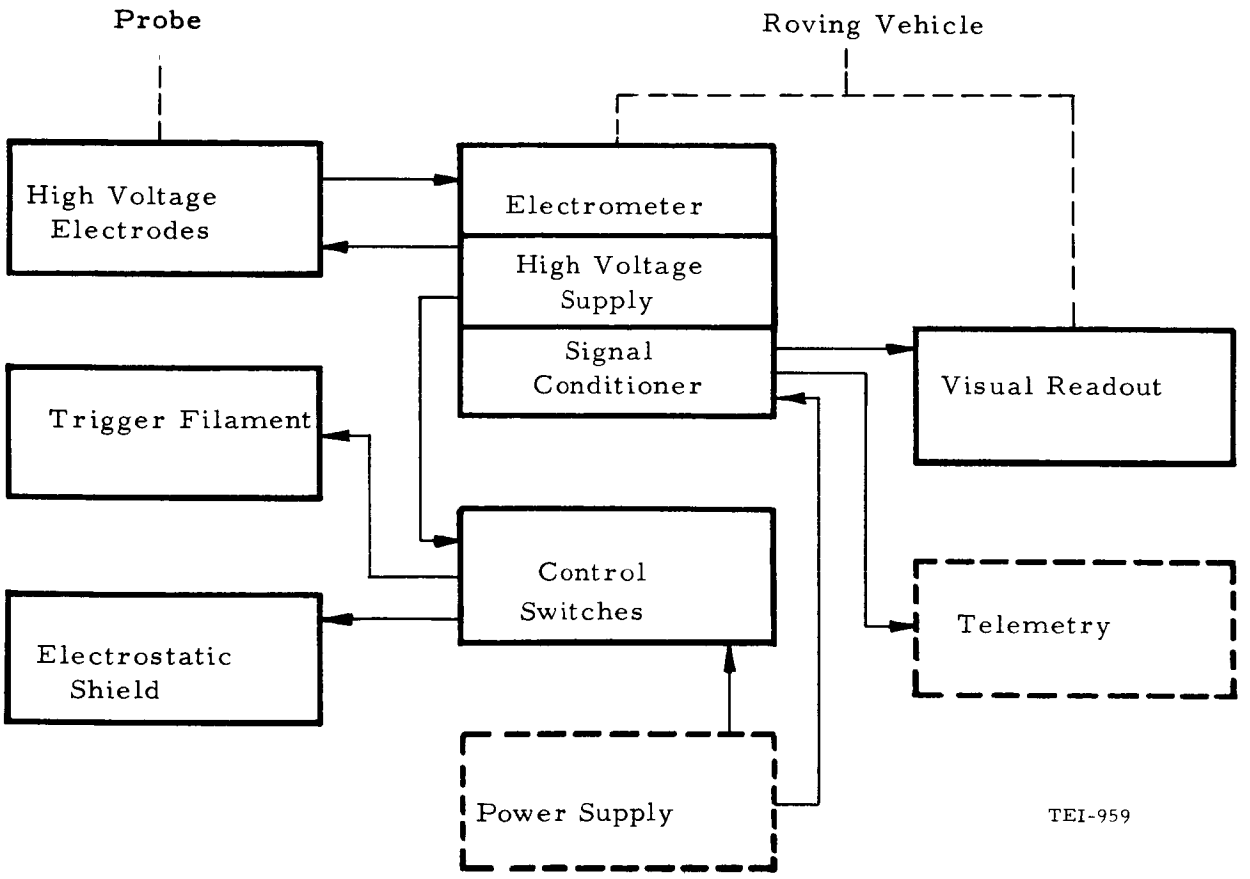

Fig. 52 Block Diagram - Atmospheric Pressure Gage

(1) "On-Off" for power supplies, (2) "Trigger" for heating and starting filament, and (3) "Shield" for energizing the electrostatic shield.

After actuating the "On" switch and then the "Trigger" switch, the output is monitored on readout equipment within one second. Continuous operation of the gage is permissible provided that power consumption is not objectionable. The sampling rate may be selected for compatibility with other experiments.

Measurements of directed ion flux require that the astronaut manipulate the probe while monitoring a readout meter or have the probe manipulation automated.

C. REJECTED EXPERIMENTS

1. Nuclear Experiments

a. Alpha and Beta Detection

These measurements can be used to augment knowledge of natural radioactivity. The beta measurement, in particular, has been used in the discrimination between Th, U, and K^{40} radiation in formations because of ambiguities which sometimes exist. Alpha measurements are not as useful since they are easily absorbed and, thus, only thin, surface layers are sampled.

These measurements are not deemed justified in view of the instrumentation required.

b. Neutron Phoswich Detector

This experiment measures the neutron radiation incident on the lunar surface and the lunar neutron albedo. Measurements of both "fast" and "slow" neutron flux is generally made using scintillation detectors. The "fast" and "slow" neutron detectors are the same except that the detector for fast neutrons has a moderator plug placed in front to slow down the neutrons. Since scintillation detectors are sensitive to charged particle flux, a phoswich system (phosphor sandwich) is used to distinguish between neutrons and charged particles. One scintillation material is sensitive only to charged particles while the other is sensitive to both charged particles and neutrons. Thus, by using anticoincidence circuitry, the contribution of each to the total count can be determined.

A simple "slow" neutron system could be designed for use in a 2-in. hole but a "fast" detector with necessary moderator could not. There is no particular advantage to making the measurement below the surface except for determining neutron-shielding properties and detecting local concentrations of hydrogen (possibly water) which can be measured by other experiments such as neutron-gamma. Therefore, this experiment is better suited for Emplaced Scientific Station type deployment.

c. Radioactive Dating

Many schemes have been developed for determining the age of materials using radiation measuring techniques. This will be a very important measurement for obvious reasons but, because of the elaborate procedure and complex instrumentation required, it is not suited to the probe concept. These measurements will have high priority on returned samples and should also be considered for a "lunar laboratory".

d. Charged-Particle Spectrometer

This experiment measures energy vs. flux spectrum for charged particles (protons and electrons) incident on lunar surface. The proposed experiment contains sensors for simultaneously viewing the sun and viewing in a direction perpendicular to the sun-instrument line. Thus, the experiment is best suited to ESS. No advantage exists in making measurements below the surface.

e. Alpha-Particle Mass Spectrometer

This instrument is designed to measure the lunar material for elements up to mass 40 (except hydrogen). The use of alpha particles for bombardment limits depth of investigation to a maximum of about 100 microns. The sensor equipment is too large to fit into a 2-in. hole, therefore, this measurement is not suited to probe concept. Equipment could be stored on LSSM or at LEM/Shelter and measurements made of surface materials and on core samples.

f. X-Ray Diffractometer

This instrument is used to identify the types of minerals of the lunar assemblage, to determine the relative quantities of the mineral types, and to ascertain, as far as possible, the precise composition of the complex minerals. The detector assembly is much too large for use in a 2-in. hole. The experiment should be considered for use with the LEM/Shelter or LSSM.

g. X-Ray Fluorescence Spectrometer

This experiment is used to determine the composition of lunar surface materials. In conventional operations, electromagnetic radiation from an x-ray tube falls on a sample and the resulting fluorescent x-rays (which have energies characteristic of the elements in the sample) are analyzed with a crystal spectrometer and detected with a suitable G-M, scintillation, or proportional-counter detector. It is impractical for the probe application to incorporate an x-ray tube source and suitable detector in the envelope available. However, one can use a capsule source of x-ray radiation in simpler applications and where longer count rate times are possible. Even in this case the measurement appears useful only as a means of determining borehole wall contamination due to the core drill since the maximum depth of measurement is generally in the 10^{-3}-in. range. This measurement might better be coupled with a surface x-ray diffractometer.

h. Alpha and Deuteron Activation

Both techniques are used, in a way similar to neutron activation, to perform chemical analysis of materials. The disadvantage, when compared with neutron activation, is that both alpha particles and deuterons have very limited penetrating power and thus provide readings of a thin, surface layer only.

i. Solar and Cosmic Radiation

None of the solar and cosmic radiation measurements given in the Lunar Experiment List is considered applicable to probes, since they are measuring radiation incident upon the lunar surface. These measurements should be considered for inclusion with the Emplaced Scientific Station.

j. Radiological Equipment

To be included as part of hazards-monitoring equipment and, therefore, not considered here.

k. Nuclear Magnetism Logging (NML)

The nuclear-magnetism type of logging is a comparatively new system which is primarily used in geophysical work to detect hydrogen. This is the only common nuclei species found in formations to be logged that is favorable for detection by NML methods. The hydrogen nuclei must be in matter in the fluid state for measurements with the normal NML system.

In operation, current is sent through a coil which is part of the sonde, producing a magnetic field in the borehole formations. This field is called the "polarization field" and serves to align protons in water, oil, and gas. After the polarization current has been applied long enough to build up polarization, the current is rapidly removed, leaving the polarized protons to precess in the earth's magnetic field and, in so doing, to induce a damped sinusoidal signal in the same coil originally used to induce the polarization. The induced-signal amplitude at the instant the precession begins is directly proportional to the total number of protons per unit rock volume in the vicinity of the borehole. This type of logging was considered for use in the lunar probe since it would be a means by which free water could be detected. However, since the moon apparently has no magnetic field, a second field would have to be applied to cause the protons to precess. While such a system could be developed, the power requirements, temperature sensitivity, difficulty in achieving a tool to work in a 2-in. borehole (most conventional logging tools have approximately 5-in. diameter) and low

probability of free water being present has led to elimination of this fairly complex logging device for the probes. If free water is present in the subsurface formations, it can be detected by use of simpler measurement techniques.

2. Thermal Experiments

a. Mercury in Glass Thermometers

Mercury in glass thermometers are rejected mainly on the basis that lunar-surface temperatures are expected to vary from approximately 120°K at nighttime to 400°K in the day. Since Hg solidifies at 233°K, it cannot be used as a temperature-determining device. Even if the temperature range is restricted to temperatures above 233°K, there still exists the following features which are undesirable: 1) The glass apparatus will be fragile and make transport, handling, and placement difficult. 2) The mass and heat capacity of the Hg in glass thermometer is gross when compared with present-day thermocouples and resistance thermometers. 3) The thermal conductivity of the glass is low when compared with metals. These characteristics would inevitably lead to a large time lag which would rule out the use of this device where transients exist.

b. Nuclear Resonance

Apparatus for elemental determination by the use of nuclear resonance is quite complex and bulky. Radio-frequency and magnetic fields are required. Some temperature information is available in the course of operation since the nuclear relaxation time is temperature dependent and results in spectrum line broadening. This would be considered as a bonus from an experiment designed for other purposes, but in view of the simplicity, small size, and ruggedness of thermocouples and resistance thermometers, use of nuclear resonance is not considered practical solely for temperature measurement.

c. Quartz Crystal

Quartz-crystal temperature-sensing devices have been designed and have recently been used with considerable success. Development efforts are underway to reduce sensor size and extend operating temperature range. Present state-of-the-art devices suffer disadvantages, when compared with the thermocouple and resistance thermometer, for probe use as follows:

- The mass is greater (the quartz sensor is mounted in a TO-5 case which contains helium), thus increasing response time.
- Deployment of the sensor would be difficult as it is fragile and easily fractured if not protected by a case.

- The measurement range is limited on the low end to around 200°K.

- Supporting circuitry is more complex.

This sensor does not seem suitable for probe use at its present state of development. The device does appear attractive as an emplaced sensor or probe and its development should be followed.

d. I. R. Absorption and Reflectance Surveys

These surveys would be useful in obtaining information concerning the surface emissivity and the identification of compositional materials at the surface. The interferometer spectrometer is expected to yield some information with respect to the presence of water since it scans the range 5 to 30 microns. The thermal diffusivity instrument is expected to yield gross reflectivity information which will be useful in determining the emissivity. Extending the surveys to greater coverage, in view of the added complexity of equipment and sample preparation involved, is not considered to be advantageous.

e. Thermal Conductivity, Surface and Subsurface

To obtain in situ thermal-conductivity data is not feasible within the present state-of-the-art. The thermal-diffusivity experiment, together with the density experiment and the specific heat (which will be measured on returned samples), will yield the data required to calculate thermal conductivity from the following relation:

$$K = \frac{k}{\rho C}$$

where K is thermal diffusivity, k is thermal conductivity, ρ is density, and C is specific heat. Therefore, the thermal-conductivity experiment is rejected.

f. Heat-Flux or Heat-Flow Measurements, Surface and Subsurface

The surface and subsurface experiments of temperature and thermal diffusivity should yield heat-flux information. Further instrumentation is not justified.

g. Differential Thermal Analysis

Differential thermal analysis is a procedure used to determine transformations in materials in which heat is taken up or given off. The technique, which is neither very accurate nor definitive, involves a block of metal containing a set of symmetrically arranged

holes. Into one hole is placed a control sample, a material which is inert and has similar thermal characteristics to the reactive sample. Thermocouples are imbedded in each sample at the same geometrical location. The block is then subjected to a controlled temperature rise. If reactions involving absorption or liberation of heat occur in the test sample the resulting changes in temperature will be recorded.

Although some qualitative information results from this technique, it is believed that other methods will yield thermal data which is more accurate. For example, the proposed thermal diffusivity, temperature and heat-capacity experiments. In addition, the differential thermal analysis requires sample preparation and operator time. The sample preparation would disturb the lunar material and invalidate an in situ experiment. If desired, this experiment would best be done on samples returned to earth laboratories.

h. Single-Crystal Probe, IR, (Water Detector)

The interferometer spectrometer should yield information relating to the presence of water in vapor form. If liquid or solid, perhaps visual observation would give the required information. The single-crystal probe indicates sample preparation in powder form and, for the added information to be expected, is not considered to be expedient.

i. Visible, IR, U.V. Spectrometer

An IR spectrometer, covering the 5 to 30 micron range, is to be used in the thermal experiments. Extension of coverage into the visible and U.V. is not deemed practical. Spectrometric studies are considered best done on samples returned to earth in view of the complexity of the experiments and equipment, and the demands on operator time.

j. Specific Heat Capacity

Measurements of specific heat capacity of lunar materials are essential in calculations involving the internal temperature as well as in calculating thermal conductivity from thermal diffusivity measurements. In general, such measurements require sample preparation and so are not readily adaptable to downhole measurements. Rather, the measurements would, of necessity, be performed on core samples extracted from the hole. Since many of these core samples will be returned to earth for complete analysis, it is believed that measurements of specific heat capacity should be delayed until

they can be performed by scientists on earth. Much more accurate measurements would be obtained in this manner, and there is no obvious reason for making such a measurement on the moon (under lunar conditions). By returning core samples to earth and then making the measurements, the astronaut is left free to perform other, more vital, measurements which must be done on the moon.

k. Melting Points

Melting points of lunar materials are also of considerable interest in determining the nature of the interior of the moon (i.e., is the interior of the moon molten or solid?). Knowledge of melting points of lunar materials is required. Again, rather than send necessary equipment to the moon and use astronaut time, these measurements could be done on samples returned to earth-based laboratories.

l. Thermal Expansion Coefficients

The same is true concerning thermal expansion coefficients of lunar material. Although this information is most desirable in attempting to understand the nature of the moon's surface (source of rubble and/or dust), the measurements could best be made after core samples have been returned to earth. In situ measurements are not necessary and would require astronaut time plus added weight of measuring devices.

3. Gravity and Magnetic Experiments

a. Gravity Measurements

Measurement of lunar tidal effects by gravimetric observations would be of importance in determining the elasticity of the moon and, perforce, would present information relative to the possible internal construction of the moon.

Measurement of regional variations in gravity can be used to help determine the shape of the moon, while measurement of the absolute mean value of lunar gravity will permit verification of the mean lunar density (calculated to be 3.34 gm/cc.), which would provide a rough measure of the segregation of the lunar body, if any exists, when compared with average surface material density. It has also been postulated that measurement of inter-spatial gravitational waves, if they exist, would add considerably to our understanding of the history and evolution of our planetary system.

However, there is no advantage to downhole gravity measurements rather than surface measurements for the shallow holes contemplated on the moon. Further, no commercial instrument is available which is adaptable to a 2-in. hole.

The gravimeter produced by LaCoste-Romberg (Model G), adapted for use by the astronauts, represents a logical instrument choice for gross anomaly measurements on the lunar surface. The instrument is small (approx. 6 in. by 7 in. by 9 in. exclusive of thermal carrying case), lightweight (7 lbs) and quite portable. The major difficulties in using this instrument by the astronauts would be in leveling the device, in manipulating the nulling controls, and in sighting through the telescope.

The leveling problem can probably be handled by use of motors; pop-up extension handles on the nulling dials can reduce the difficulty of setting these dials; and possibly the telescopic eyepiece could be replaced with a ground-glass screen on which an image was projected, to eliminate the problem of sighting through the telescope.

b. Magnetic Measurements

Determination of the lunar, magnetic-field intensity is important to the study of the history, evolution, and internal construction of the moon. At the same time, when correlated with other information expected to be obtained (e.g., the presence or absence of a lunar molten core), this information will be of considerable aid in proving or refuting theories presently held for the presence of the earth's magnetic field, and should be of assistance in establishing the earth's past history.

Studies of the effect of solar flares and prominences on the lunar magnetic field will provide a better understanding of the effects on our own magnetic field on earth. They may also permit the development of improved theories as to the primal source of planetary magnetic fields.

If a sufficiently coherent magnetic field exists on the moon, to the extent that it could be used for navigational purposes, this would be a great assist for future lunar explorers. A concerted effort would be required to specifically define and delineate the lunar magnetic field.

Magnetic measurements on the earth's surface are used for navigation, exploration for mineral deposits, and to obtain a better understanding of the creation of the earth and the workings of the solar

system. Conceivably, they could be used for locating strategic materials at or near the lunar surface. Magnetic measurements have also been of assistance in delineating subsurface structures such as igneous intrusives which may be rich or poor in magnetic material compared to the intruded country rock. The natural magnetic field of the earth is not constant but varies considerably over any given period of time. The understanding of the cause of these variations, as well as the basic cause of the primary magnetic field, is a problem still unanswered completely.

Certain formations have a remanent magnetism which seems to have been frozen into the materials as they passed from a temperature above the Curie point to a lower temperature. The direction and magnitude of this remanence is thought to be a function of the magnitude and direction of the external field present when they were formed.

Iron and a few other minerals have a magnetic permeability that is high compared to free space. Thus, these materials offer a lower reluctance path to the magnetic field, causing a concentration of the magnetic lines of flux within the material. This flux concentration will warp the external magnetic field, thus making possible the detection of these minerals.

In addition to warping the magnetic field, the concentration of flux within the materials polarizes the mineral. This polarization of the magnetic dipoles within the minerals, plus the remanent magnetic movement of the mineral if present, add vectorially to set up a secondary magnetic field. Thus, before a knowledge of the surface external magnetic field at any point can be determined accurately, knowledge of the magnetic susceptibility and the remanent magnetism of the materials below the surface must be known.

In situ magnetic measurements of the moon will add greatly to our understanding of the moon's formation. Since the moon has no apparent significant magnetic field of its own, these may be large, local anomalies due to iron meteorites which may or may not have a remanent magnetism from being formed in a magnetic field.

Thus, magnetic-susceptibility and magnetic-intensity measurements, and remanent-magnetic measurements made in the low intensity field of the moon on drill cores or rock samples, will contribute greatly to our understanding of the formation of the moon.

However, no advantage exists for magnetic-intensity measurements in shallow holes over surface measurements. Such measurements may have some application in deeper holes for locating ore bodies, but

would not be applicable to the concepts of these early missions. For this reason the experiment is listed as rejected but this applies only to its inclusion in the subsurface probe.

Surface measurements will be very important and should be made at each drill site for correlation with magnetic-susceptibility measurements.

Magnetic-susceptibility measurements should be made in the borehole. Because of the proposed measurement technique, this experiment is discussed in another section.

4. Electrical Experiments

a. Telluric Currents

While determination of telluric currents would be desirable in the study of the lunar interior body, measurement of these currents is primarily a surface-survey function requiring rather large electrode spreads and good electrical contact with the lunar surface. Since the lunar surface is quite probably extremely arid, the chances of obtaining valid information are not particularly good and, for this reason, this experiment was rejected.

b. Self Potential

Self-potential measurements would be helpful in determining the presence and relative abundance of conductive fluids in the lunar formations since their generation is a function of electrolytic action in the entrapped fluids. However, measurement of these potentials requires a good electrical contact with the medium and, as is the case with telluric-current measurements, chances of making sufficiently good electrical contact with the formation to produce valid data are rather poor. On earth, these measurements are usually made only in boreholes wherein a conductive fluid such as salt water or mud is present. Therefore, this experiment was omitted from further consideration.

c. Dielectric Constant or Permittivity

Determination of the dielectric constant of the lunar near-surface material is desirable to ascertain the feasibility of extended-range lunar communications. This parameter could be measured in a laboratory with a fair degree of accuracy on uncontaminated samples returned to earth. Instrumentation to perform this measurement in the field is not very well developed. It is believed that these factors preclude its use in the proposed group of instruments.

d. Induced Polarization

This experiment would provide a measure of the presence of electrolytes (and presumably water) in the lunar subsurface formations since the phenomenon depends upon the polarization potential generated in an electrolyte when an electric field is applied. In practice, electrodes are introduced into the formation and a D.C. source connected for a short time, then removed. The decay rate on two other electrodes, located between the power electrodes, provides a measure of the diffusion constant of the electrolyte.

As with most other such measurements, electrode-formation contact resistance is critical to the interpretation of the results. Since this appears to be an indefinite quantity at this time, this experiment was eliminated.

5. Soil Mechanics and Soil Properties Experiments

The soil-mechanics and soil-properties experiments were expressly deleted from this study by NASA.

6. Compositional Experiments

a. Gas Chromatograph

This instrument, although yielding valuable information, requires sample preparation, column packing, and large amounts of operator time. However, if compatible, this technique might be combined with a soil-permeability test to yield additional information. It is believed that chromatographic work should be performed on samples returned to earth laboratories.

b. Wet Chemical Analysis

The laboratory equipment required and the pressurization of the laboratory makes this a very unattractive venture. Unless considerable power-consuming automation is used, the operator time required is large. Wet-chemical analysis is best deferred to earth laboratories and returned samples.

c. Chemical Reactivity Detector

This consists of placing reactive and inert temperature sensing elements in contact with the surface and measuring the temperature which would result from the reaction. The selection of suitable

reacting agents would be a problem when considering the pressure at which the test will take place and the initial temperature of the surface.

d. Atomic Absorption

In atomic absorption experiments an electrical discharge is passed through a selected gas sample and the light emitted from this gas is passed through the unknown which must be vaporized. If the light has the proper frequency, the vapor from the unknown will absorb energy from the light and lower the light transmission. This decrease in transmission is detected and the sample may be identified. Atomic absorption lines are quite narrow and well defined and, in order to make this experiment feasible, one would have to have a fair knowledge of the unknowns to be expected and carry a suitable sample cell for each unknown. This means a lot of operator time and, considering the uncertainties of the lunar materials and the need for a furnace or other means of vaporizing the sample, the experiment was deleted.

e. Spectrophotometer

In the spectrophotometer, a sample of the lunar material would be arranged between two electrodes. An electrical spark would then be passed through the electrode gap and the sample. The spark must contain enough energy to volatilize some of the sample, giving rise to the spectral-emission characteristic of the sample material. This spectral emission is focused on a photographic plate (or suitable device) and a record obtained which is then compared with the spectra of a known material. In this way the lunar material can be identified. This apparatus will require sample preparation, whether automated or by a human operator. It is also necessary to carry known sample materials for calibration purposes and the alignment of the optical system presents formidable problems. When considering these factors and the amount of information gained, the experiment was deleted.

IV. ENVIRONMENTAL CONSIDERATIONS

Analyses have been performed to determine the requirements for environmental protection for the various probes when exposed to the lunar surface environment. Additional studies have been concerned with the environmental conditions (especially temperature) which may exist in the boreholes to be surveyed, and how the probes may be affected by heat transfer between the probe and the formations. In the latter, the concern was for (1) how the probe temperature would vary, (2) what thermal control would be needed to maintain proper operating temperature and, (3) how the formation temperature, and thus the several temperature measurements, would vary. The following sections include the results of these studies.

A. THERMAL/METEOROID SHIELD DESIGN

In general, the requirements for environmental protection are limited to providing thermal control and meteoroid protection for the various instruments. Meteoroid protection will normally be provided by the instrument case or skin but in some cases special precautions must be taken. Passive thermal control - the use of special surface coatings and finishes - will be employed to the maximum degree possible, with resistance heaters used to maintain satisfactory minimum temperatures for critical components during the lunar night.

Since the subsurface probes are required to operate both in the borehole and on the lunar surface, and since the ambient temperature ranges can vary appreciably, thermal shield adapters are recommended. These adapters can be fitted to the probe while being used on the surface and could form the attachment device for mounting the probe to the LSSM when the device is not in use or when measurements are to be made with the vehicle underway.

A design example for a thermal/meteoroid shield, to be used with the Optimum Subsurface Probe, may be found below (see Appendix III for detailed analysis). The primary constraint on the shield design was that the upper temperature of the probe not exceed 360°K during the lunar day. The shield must also have the capability to dissipate the internal power generated while in use.

1. Meteoroid Analysis

There have been many studies made on the effects of meteoroid shielding design. The main conclusions from these studies are*:

---

* Data extracted from Brown Engineering Report SIB-TR-8

a. The meteoroid particle is defined as the Apollo particle whose density is 0.44 g/cm^3, mean velocity is 30.4 km/sec, and diameter is 1.02 mm.

b. An outer shield, called a bumper, is desirable as a particle break-up sheet, and energy absorber.

c. Optimum thickness of the bumper with respect to penetration damage is one-half the projectile diameter.

d. Bumpers which are too thick, lead to other problems such as spallation.

e. Aluminum appears to be the best bumper material.

f. A space of one inch between the bumper and shield increases the shielding efficiency 100 percent. A glass wool filler in the same space increases the efficiency 440 percent.

g. High density fillers can cause disasterous failures due to pressure or shock waves causing spallation of low velocity projectiles. Several materials are listed below, in the order of their effectiveness:

   (1) Fiberglass with preceding space.
   (2) Fiberglass without preceding space.
   (3) Open cell foams.
   (4) Closed cell foams.
   (5) Low density cork.
   (6) Superinsulations (foil layers).

h. Optimum shield thickness decreases with increasing velocity.

i. A shield thickness of 1.25 times the particle diameter is suitable.

Using the above conclusions, a meteoroid protection device having a bumper thickness of 0.02 in. of aluminum and an inner shield thickness of 0.05 in. with one inch of glass wool filler would be practical.

2. Thermal Analysis

The thermal control problem is one of providing minimum temperature excursion of the probe during the lunar day/night cycle. That is, a shield is needed which will limit the upper temperature of the probe during the lunar day, yet minimize heat loss from the probe during the lunar night. The upper temperature can be controlled

by choosing an outer skin coating with a minimum α/ε ratio. Protection against low temperatures can be provided by the use of insulation between the probe and any heat sink. A problem exists with the use of insulation, however, because the shield must be able to dissipate any excess internal heat generated under use. Thus it can be seen that an anomaly exists. Insulation is needed to keep the probe warm at night but not so much that the probe will get too hot during the day due to its own heat generation. Obviously, a compromise is required. Figure 53 represents a cross-section drawing of the final shield design. The shield consists of an outer bumper, an inner shield, and a clamp assembly. The bumper and inner shield are constructed of aluminum. The bumper outer surface is anodized and exhibits a α/ε ratio of 0.3, thus causing the probe to absorb a minimum of external energy. Both surfaces of the inner shield as well as the inner surface of the bumper are coated with flat black lacquer to allow maximum dissipation of internal heat. Curves of probe temperature variations with time are shown in Figure 54. Included are the cases where zero, mean, and maximum power are being dissipated. As seen, it may be desirable to alter the surface finishes slightly in order to raise the minimum temperature when the probe is totally inoperative.

3. Design Summary

The shield (Figure 53) can be attached to the probe by two spring clips as shown. In each clip there are three teflon buttons to hold the probe away from the shield and contact the probe at 120° spacing. The probe and shield can be fastened to the lunar roving vehicle by two similar clips permanently attached to the vehicle. Both the shield and vehicle clips are teflon coated to prevent cold-welding and to prevent damage to the surface of the probe. All clips are designed to facilitate the removal and attachment of both the shield to the probe and the assembly to the lunar vehicle.

The overall length of the shield is three inches longer than the probe and may be adapted at one end to allow a power/signal cable to pass through.

The bearing surface of the shield is formed by bending the inner shield outward at 90° and affixing it to the bumper. This bridge gives about 90 square inches of bearing surface which should be sufficient to prevent sinking of the total probe/shield assembly by more than one inch into the lunar surface. A nominal spacing from probe to lunar surface of 1/8 inch is provided to allow for optimum optical coupling of several experiments. Pertinent characteristics of the shield assembly are given in Tables XXIV and XXV. The total estimated weight of the shield assembly is 3.5 lb, including clips and spacers.

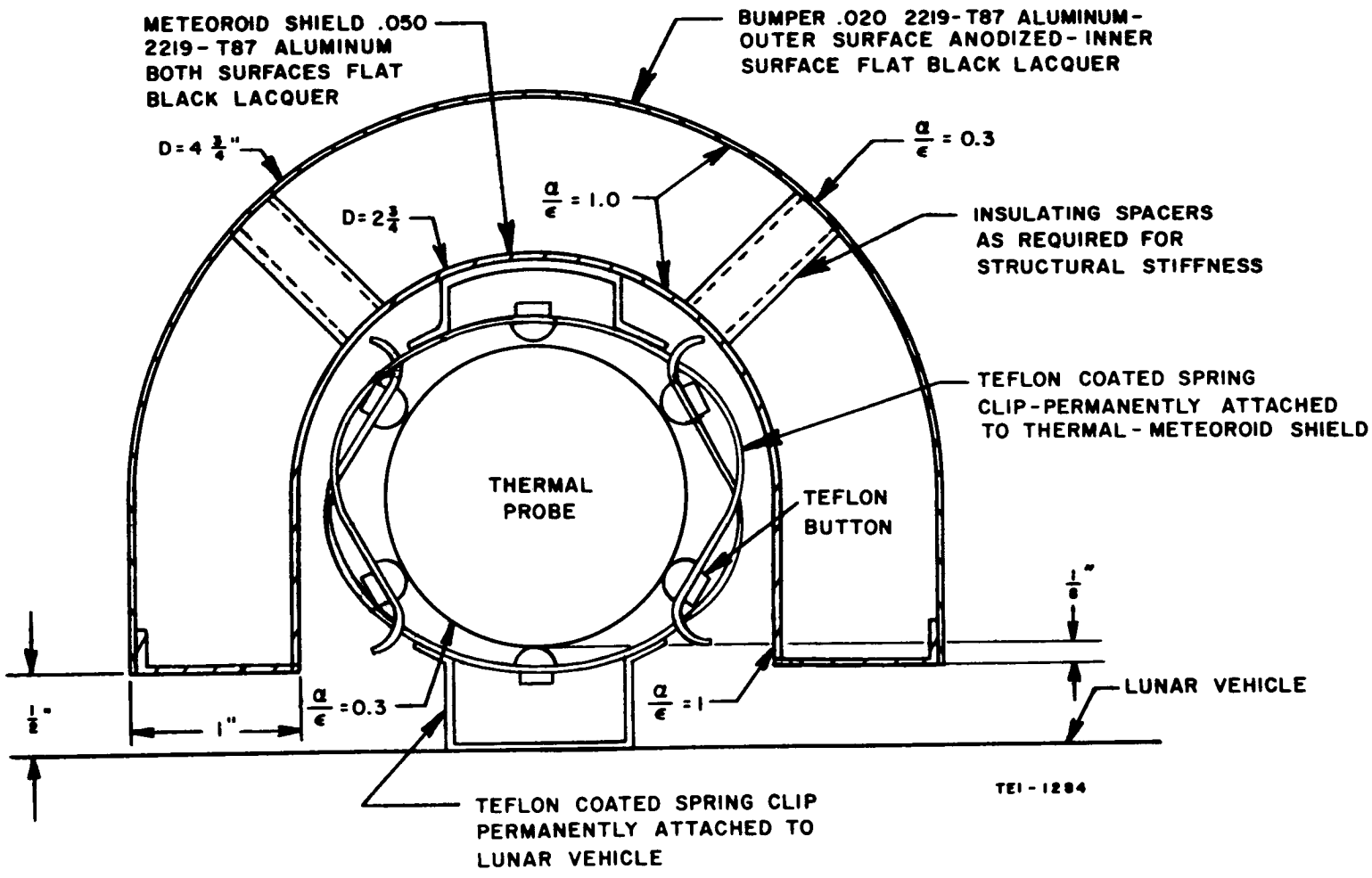

Fig. 53 Thermal/Meteoroid Shield Design

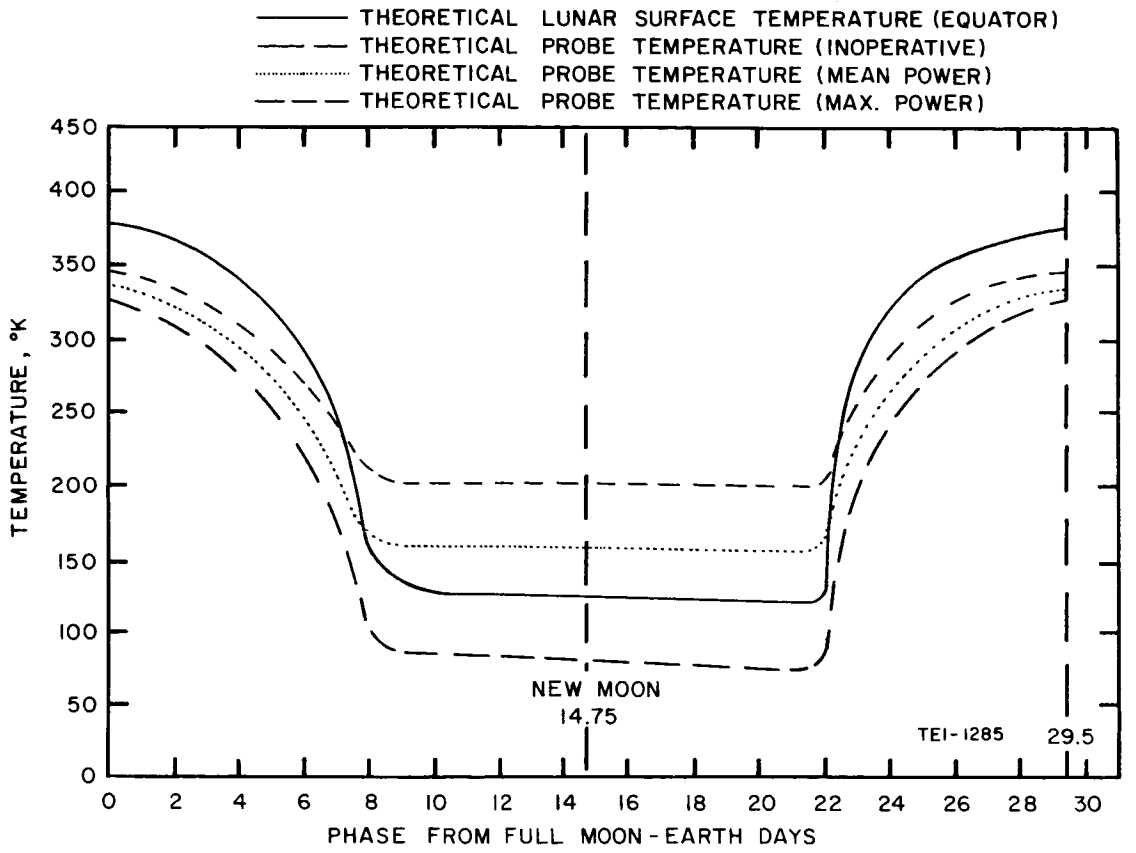

Fig. 54 Theoretical Temperature Variations - Shielded Probe

Table XXIV

PROBE TEMPERATURE LIMITS

Heating Condition	Maximum Temperature	Minimum Temperature
Probe inoperative	327°K	73°K
Maximum power	344°K	201°K
Mean power	335°K	157°K

Table XXV

METEOROID PUNCTURE PROBABILITY

Condition	Confidence Level	No Puncture Probability	Earth Days
Lunar Primary	50%	.999	1,750
		.990	18,400
		.900	193,000
	75%	.999	613
		.990	6,570
		.900	65,700
Lunar Secondary	50%	.999	2.28×10^{11}
		.990	2.37×10^{12}
		.900	2.45×10^{13}

B. THERMAL ANALYSIS - PROBE IN BOREHOLE

Preliminary analyses were performed to determine the heat transfer characteristics between a subsurface probe and the subsurface borehole wall. The objectives were: to determine how the probe temperature would vary with time as a function of borehole depth and temperature; and, how the borehole wall temperature would vary due to the influence of the probe. The detailed analysis and results can be found in Appendix IV.

For the purposes of these calculations, it was assumed that the probe would have attained the equilibrium temperature determined by its thermal shield (See Table XXIV). Three values of probe power dissipation were used; maximum - 13 watts, mean - 5 watts, and zero. A lunar surface model was employed in which arithmetic average temperatures existed in the first 100 cm of depth and a uniform temperature below 100 cm. Three values of borehole wall emissivity were also considered; 0.25, 0.70, and 0.90.

Figures 55 and 56 summarize the findings of this analysis. They show the temperature-time relationship for a borehole wall emissivity of 0.90 which is the most probable. It can be seen from the curves that very favorable probe temperature will exist during the lunar day situation for all degrees of probe use (maximum, mean and zero power dissipation). The same is not true for lunar night operation, however. With zero power dissipation, the probe temperature will range from 73°K (-200°C) to 170°K (-103°C) which is too low for most instruments. With 13 watts being dissipated the probe temperature range becomes 200°K (-73°C) to 263°K (-10°C). This suggests that resistive heaters will probably be required at strategic locations to raise the temperatures of critical elements to an acceptable level. Additional power required should be less than 10 watts since only the critical elements must be heated, not the entire probe.

Figure 57 indicates that formation temperatures will be changed by less than 3°K during daytime operations and by less than 1°K during nighttime operations. Thus, the probe does not seriously influence the formation ambient temperature, allowing these and other thermal properties measurements to be made when desired.

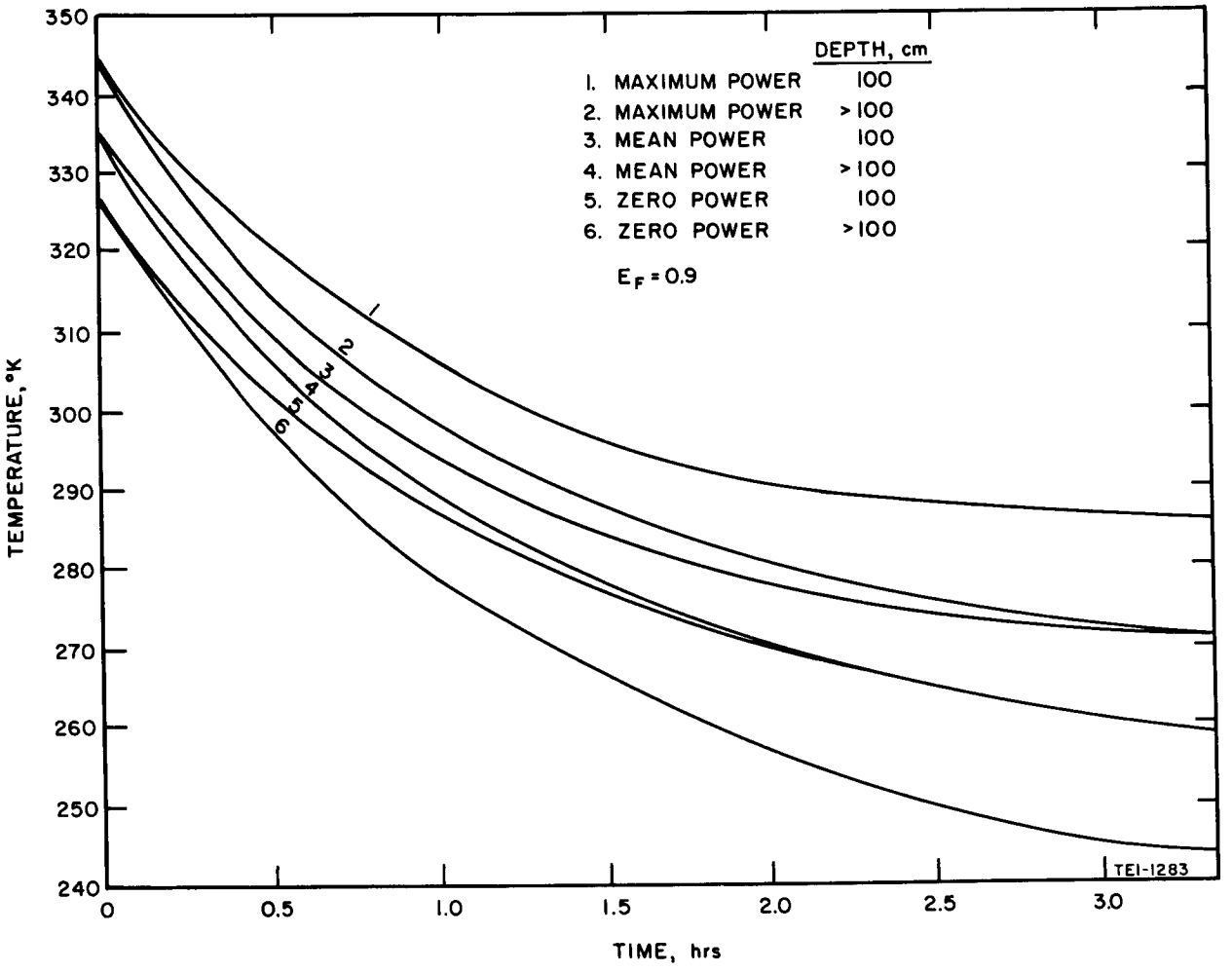

Fig. 55 Probe Temperature vs. Time - Lunar Noon

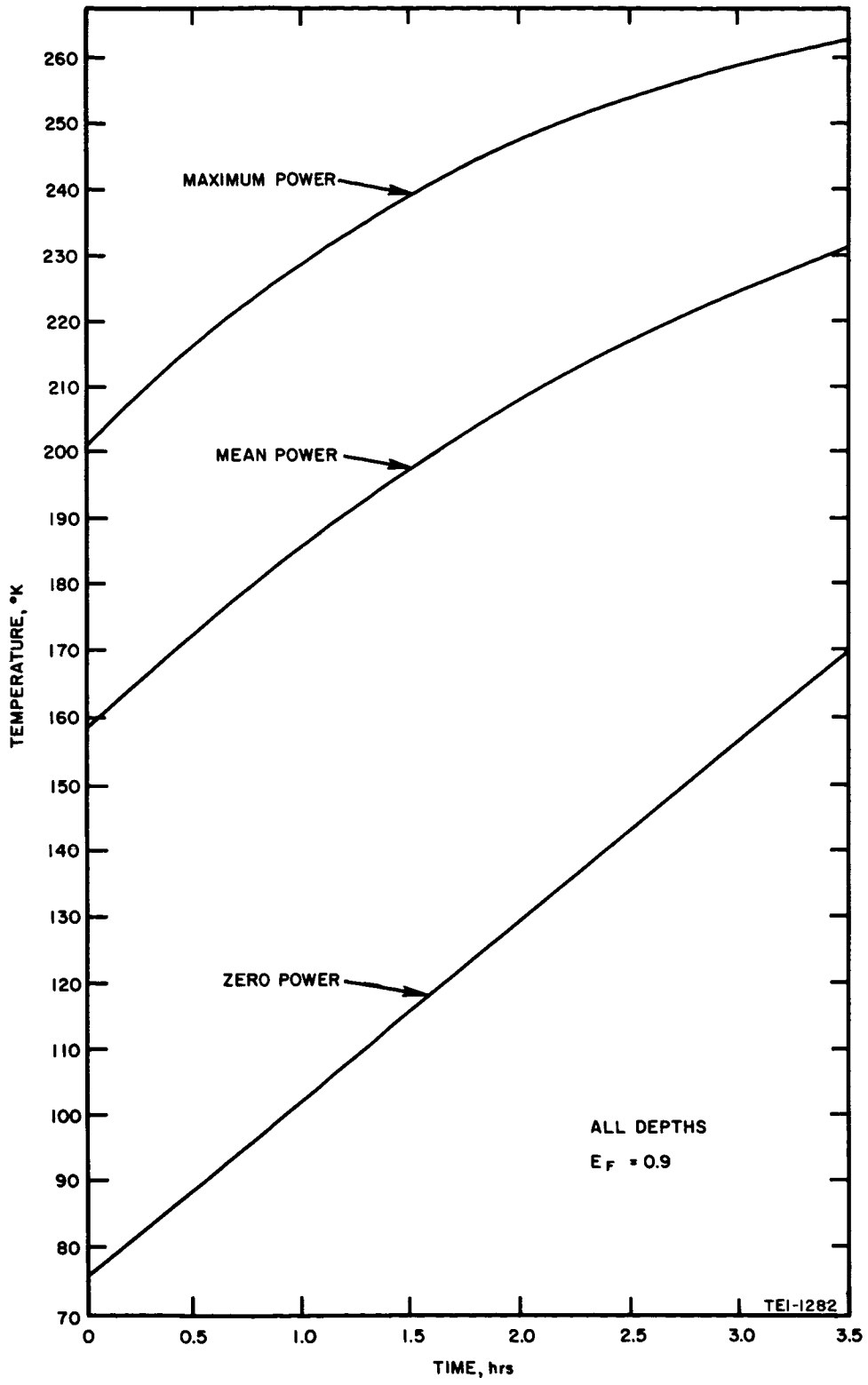

Fig. 56 Probe Temperature vs. Time - Lunar Night

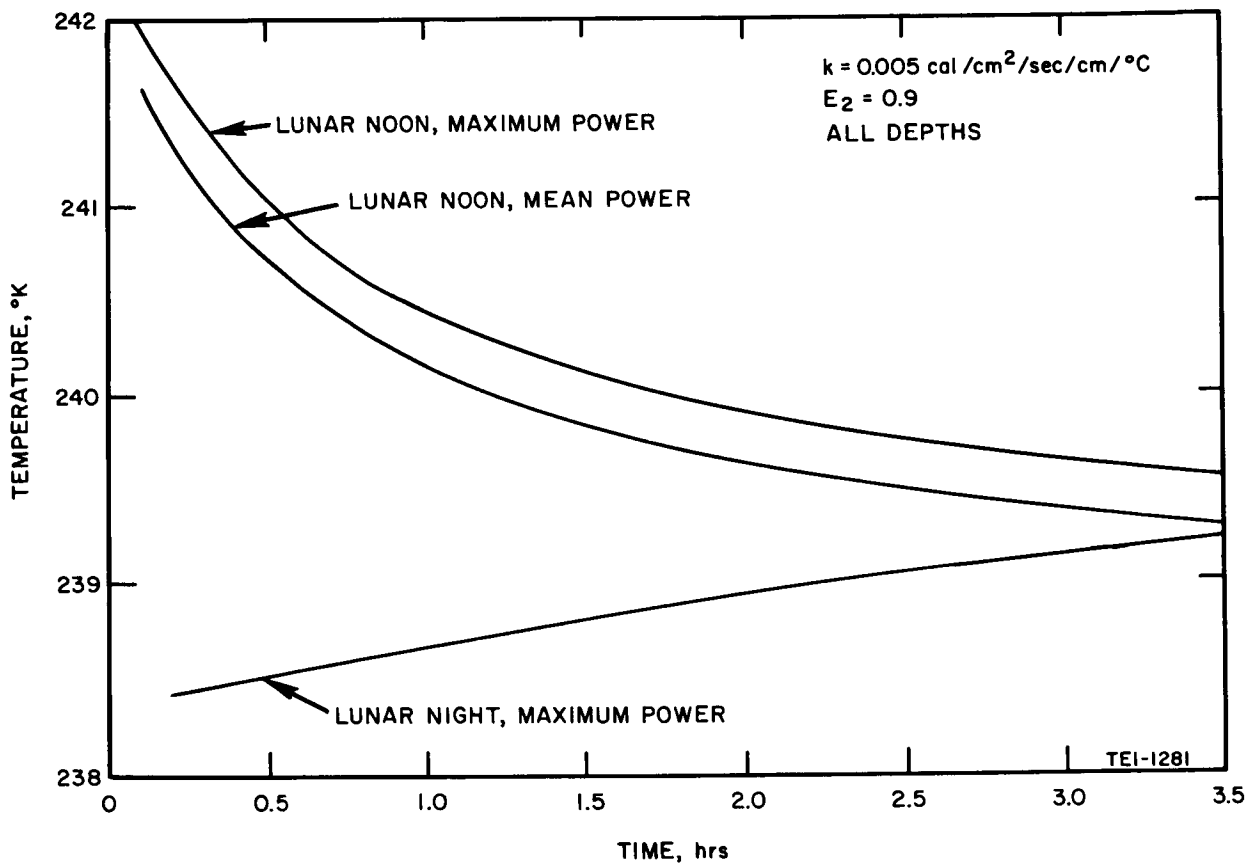

Fig. 57 Probe Effects on Borehole Wall Temperature

V. EXPERIMENT RATING TECHNIQUE

Choosing the best combination of objects from a set having different qualities is always a difficult task, and, when this effort applies to lunar measurements selection, it represents a most arduous undertaking. Some of the difficulty stems from having to compare experiments having strongly desirable characteristics in dissimilar categories. Are two apples better than three oranges? Is a basically simple and reliable experiment that tells a limited amount about the moon more justified than a complex one that tells a great deal?

One technique which is often used in the selection process is to have a group of knowledgeable people examine the various qualities of the experiments being considered and then rate them on a subjective basis. The success of this approach depends on the ability of the selection panel to individually weigh the various measurement and instrument factors in a uniform manner and to avoid letting bias influence their rating. Often this results in the experiment losing its identity in the mechanics of the weighing system and intuitive reason is excluded. Another approach is to judge them strictly from an objective viewpoint.

The technique used in this study employs a compromise between the objective and subjective aspects of the selection problem.

The rating scheme requires that each candidate experiment be subjected to an "examination" during which it is asked a number of questions (most of which can be answered "yes" or "no") to determine overall worth as related to factors such as:

- Scientific and engineering justification.
- Constraining operational aspects.
- Instrument development status.
- Reliability considerations.
- Other constraints (such as weight, power, telemetry requirements, measurement time, etc.).

Each of these questions is assigned a different point value depending on its importance as related to the other questions. The point totals obtained are then used, along with other factors, in comparing the various experiments.

When considering candidate experiments for inclusion in the subsurface probe, primary consideration is given the criteria of measurement worth as determined from the first four listed factors above, and instrument length. This is possible because the other constraints such as weight, power, etc., are closely related to length. Thus, a figure of merit would be the experiment's W/L ratio (worth-to-length ratio).

For surface experiments, the choice is predicated primarily on experiment worth.

It must be emphasized that, although the selection procedure makes use of arithmetic to some extent, it is not an attempt to substitute numbers for judgment; but rather to provide an unbiased framework for incorporating the various judgments.

The value of this system is that it allows for comparisons between experiments having a high importance rating in a number of diverse categories. It is also clear that the technique is a "dynamic" one, since the weighting of the various questions can be changed to suit changes in mission emphasis, etc., and individual experiment values can be changed with advancement in the state-of-the-art, etc.

The following pages include the questions used in arriving at the selected optimum probes.

EXPERIMENT RATING QUESTIONS

I. EXPERIMENT JUSTIFICATION

A. Scientific Justification (will measurements contribute to a better understanding of the moon's composition or of the age, origin, or history of the earth-moon system?)

1. Will it define a physical or environmental parameter?

2. Will it help validate or refute a commonly accepted theorem?

3. Is the measurement needed to define another parameter?

4. Will it indicate the presence of life or materials basic to the existence of life?

5. Will it help define rock type?

6. Will it help define the moon's thermal history and/or characteristics?

7. Will it help distinguish between primary and accreted lunar material?

8. Will it detect layering?

9. Will it indicate important elements present?

10. Will it indicate important molecular species present?

11. Will it assist in determining tectonic history of moon?

12. Does measurement detect fracturing?

13. Will it identify external forces working to modify the moon?

14. Will it identify physical state of lunar material (solid, particulate, blocks, homogeneity)?

B. Engineering Justification

1. Will the measurement assist the astronaut in selecting lunar surface and/or subsurface samples?

2. Engineering aspects of lunar basing. Measurement will provide data concerning:

   a. Rock type,

   b. Grading and tunneling characteristics,

   c. Foundation stability,

   d. Thickness of bedding, if present,

   e. Presence of natural shelter or storage areas,

   f. Thermal properties,

   g. Possible crew hazards,

   h. Tectonic activity and history,

   i. Shielding and insulating properties of material.

3. Exploitation of lunar resources. Measurement will:

   a. Indicate present of water or its constituents,

b. Indicate present of useful minerals,

c. Indicate presence of radioactivity,

d. Provide information necessary to the recovery of resources.

II. INSTRUMENT PARTICULARS

A. Operational Aspects

1. Could the process of performing the measurement preclude making another measurement, or could it jeopardize the validity of another measurement?

2. Are consumables involved in the measurement technique which limit when and/or how often the measurement can be made?

3. Does the proposed measurement process require on-the-spot judgment or interpretation by the astronaut?

4. Are special setup or handling requirements imposed on the astronaut?

5. Can measurement or instrumentation in any way jeopardize the integrity of accumulated samples?

6. Is measured parameter likely to vary from in situ to returned sample?

7. Experiment will: (only one)

   a. Provide direct measure of parameter in question,

   b. Sort and/or identify by class,

   c. Provide general (correlative) information only.

B. Instrument Development Status

1. Is the proposed technique a proven and accepted one?

2. Is the proposed technique suitable for the full range of values and conditions postulated for the moon?

3. What is the instrumentation status (only one)?

   a. Lunarized, flown, and tested,

   b. Lunarized - not flown,

   c. Used in field on earth,

   d. Lab model only,

   e. Concept only.

C. <u>Reliability Aspects</u>

1. Degree of instrument simplicity (only one).

   a. Simple - few or no moving parts, minimum electronics needed,

   b. Moderate,

   c. Complex - many intricate moving parts, and/or complex electronics required.

2. Can failure of one unit affect a second contained in the same probe?

3. What is the probability that failure of one unit will jeopardize operation of the entire probe (ex. probe stuck in hole)?

   a. Some,

   b. Minor,

   c. None.

4. Estimated reliability factor (a x b).

   a. Reliability of earth model (only one).

      1) Very high (technique well developed, considerable operational experience).

      2) High (technique well understood, some improvements needed).

3) Medium (technique just reaching favor, development problems remain).

4) Low (new technique, little operational history).

5) Unknown

b. Conversion of earth model to lunar model (only one).

1) Straightforward - little or no modification required.

2) Only minor changes required to adapt to environment.

3) Changes of some major component or subsystem required.

4) Redesign essentially the complete device.

III. SUBJECTIVE APPRAISAL

1. What is the probability that the experiment, as suggested, will be successful in making its intended measurement (excluding reliability aspects)?

EXPERIMENT RATINGS

The final point ratings and W/L ratios for the recommended experiments and certain additional experiments are given in Table XXVI.

Table XXVI

FINAL EXPERIMENT RATINGS

Experiment	W/L Ratio	Point Rating
Contact Temperature	236.	118
Thermal Diffusivity	66.9	167
Natural Gamma	48.0	168
Acoustic Velocity	46.4	139
Spectral Gamma	44.7	156
Nm-contact Temperature	36.5	146
Magnetic Susceptibility/Ind. Log	33.0	181
Bulk Density	20.4	143
Centralizer-Caliper	18.2	85.5
Mass Spectrometer	16.4	161
Borehole TV	7.4	200
Neutron-Gamma	7.4	133
Change of Q Resistivity	29.9	82.1
Scratcher-Electrode Resistivity	17.0	8.5
Atmospheric Pressure	15.0	75.0
Neutron-Neutron	8.9	75.2
Formation Tester	1.4	7.1

REFERENCES

1. Materials for Missiles and Spacecraft, McGraw-Hill, 1963, p. 16.

2. Urey, H. C., The Planets Their Origin and Development, Yale University Press, 1952.

3. Green, J., Geophysics as Applied to Lunar Exploration, Final Report Contract AF 19(604)-5886, 1960.

4. Survey of Lunar Surface Measurements, Experiments and Geologic Studies, Final Report Contract NAS9-2115, Texas Instruments Incorporated, Aug. 1964.

5. McCullough Nuclear Logging, Bulletin 901, McCullough Tool Co.

6. Blanchard, A. and Dewan, J. T., The Calibration of Gamma Ray Logs, The Petroleum Engineer, August, 1953.

7. Metzger, Albert, Jet Propulsion Laboratory, Personal Correspondence.

8. Urey, H. C., Z Physik Chem., Vol. 16, 1958, p. 346.

9. Muench, N. L., and Osoba, J. S., Identification of Earth Materials by Induced Gamma-Ray Spectral Analysis, J. Pet. Techn., March 1957, pp. 89 to 92.

10. Stinner, R. J., A Feasibility Study of a Method to Analyze The Moon's Surface Using Nuclear Inelastic Scattering, Thesis U. of Calif., May 1961.

11. Annals of The New York Academy of Sciences, Vol. 123, 1965, pp. 367 to 1257.

12. Jakob, Max, Heat Transfer Vols I and II, John Wiley and Sons, Inc., New York, 1957.

13. Weil, N. A., Lunar and Planetary Surface Conditions, Academic Press, 1965.

14. Calhoun, J. C., Jr., Fundamentals of Reservoir Engineering, Univ. of Okla. Press 1947, p. 82.

BIBLIOGRAPHY

1. Arnold, James R. - Gamma-Ray Spectroscopy of the Moon's Surface - Lunar and Planetary Exploration Colloq. Proc. Vol. 1, No. 3 - 1958.

2. Baker, P. E. - Density Logging with Gamma Rays, AIME Petroleum Transactions, Vol. 210, 1957.

3. Baker, P. E. - Neutron Capture Gamma-Ray Spectra of Earth Formations - Journal of Petroleum Technology, Vol. 9, No. 3, Mar. 1957.

4. Baldwin, J. E. - Thermal Radiation from the Moon and the Heat Flow Through the Lunar Surface, Astronomical Society, Vol. 122, 1961.

5. Barringer, A. R. - Radio Frequency Reflectivity Experiments Proposed for AES Lunar Orbital Flights, Barringer Research Limited, Contract AF 19(628)-2998.

6. Beattie, Donald A. -Apollo Extension System (AES) Lunar Surface Missions, Symposium on Post Apollo Space Exploration, AAS Meeting, May, 1965.

7. Bollin, Edgar M. - Lunar Surface and Subsurface Magnetic Susceptibility Instrumentation, IRE Transactions on Instrumentation Vol I, 1962.

8. Brannon, H. R., et al. - Spectral Gamma-Ray Logging, AIME Petroleum Transactions Vol 207, 1956.

9. Brannon, H. R., et al. - Spectral Gamma-Ray Logging Journal of Petroleum Technology, Vol. 8, No. 2, Feb. 1956.

10. Broner, M. A. - Instrumentation Requirements for Lunar Exploration - Instrument Society of America, Vol 19, Part II, 1965.

11. Caldwell, R. L., Mills, W. R. Jr., et al. - Combination Neutron Experiment for Remote Analysis - Science Vol. 152, 22 April 1966.

12. Caldwell, R. L., et al. - Gamma-Ray Spectroscopy in Well Logging, Geophysics Vol. XXVIII, No. 4 August 1963.

13. Caldwell, R. L., et al. - New Developments in Radioactive Well-Logging Research - Bulletin of the American Association of Petroleum Geologists, Vol 42 No. 1 - Jan. 1958.

14. Canup, R. E., Clinard, R. H., et al. - Surveyor Geophysical Instrument - Interim Report - Contract 950155, May 1962.

15. Carr, J. H., Romano, S. R. - A Mobile Lunar Laboratory System - Symposium on Post Apollo Space Exploration, AAS Meeting, May 1965.

16. Causse, J. P. - New Rugged High-Temperature Photo-Multipliers, Proceedings of the Seventh Scintillation Counter Symposium, February, 1960.

17. Clewell, D. H., et al. - Instrumentation for Geophysical Exploration, Review of Scientific Instruments, Vol 24, No. 4, April 1963.

18. Chaney, Lucien W., et al. - An Infrared Interference Spectrometer - Its Evaluation, Test, and Calibration, NASA Contractor Report No. CR-61, June, 1964.

19. Dobrin, Milton B. - Introduction to Geophysical Prospecting, McGraw-Hill, 1960.

20. Doll, H. G. - Introduction to Induction Logging and Application to Logging of Wells with Oil Base Mud, Journal of Petroleum Technology, June 1949.

21. Doll, H. G. - The S. P. log: Theoretical Analysis and Principles of Interpretation, AIMME Tech. Pub. #2463, Sept., 1948.

22. Doelling, Ralph P. - Space Instrument Handbook - Texaco Experiment Incorporated, Nov. 1962.

23. Duesterhoeft, W. C. - Propagation Effects in Induction Logging, Geophysics, Vol XXVI, No. 2, April 1961.

24. Duesterhoeft, W. C., et al. - The Effect of Coil Design on the Performance of the Induction Log., Journal of Petroleum Technology, November, 1961.

25. Duffin, R. J. - Measurement of Magnetic Susceptibility with the Hughes Induction Balance., Terrestrial Magnetism and Atmospheric Electricity, Vol. 51, No. 3, 1946.

26. Eichholz, G. G., et al, - The Determination of Uranium & Thorium in Ores, Canadian Journal of Physics Vol. 31.

27. Eimer, M. - Measurement of Properties of the Moon from a Soft-Landed Vehicle, National IAS-ARS Joint Meeting, Low Angeles, California, June 1961.

28. Foster, W. B., et al. - Scientific Missions for Extended Lunar Space Exploration, Symposium on Post Apollo Space Exploration, AAS Meeting, May, 1965.

29. Glasstone, Sanuel - Sourcebook on the Space Sciences, D. Van Nostrand Co. - 1965.

30. Grant, F. S. & West, G. F. - Interpretation Theory in Applied Geophysics, McGraw-Hill, 1965.

31. Green, W. W., et al. - Well Logging by Radioactivity, Geophysics, Vol. 5, No. 3, July 1940.

32. Greenfield, S. M. - On Lunar and Planetary Experiments - The Rand Corporation P-1535, October 1958.

33. Guinn, V. P. - Instrumental Neutron Activation for Rapid, Economical Analysis - Nucleonics Vol 19, No. 8 August, 1961.

34. Happe, Ralph A. - Materials in Space - JPL Oct. 1960.

35. Hauck, A. M. III - Deep Structure Resistivity Measurements in Massachusetts - Masters Thesis, MIT, September 1960.

36. Hibbs, A. R. - Exploration of the Moon, the Planets, and Interplanetary Space - JPL Report 30-1, April 30, 1959.

37. Hoste, J., et al. - Minor-Constituent Analysis with Neutron Activation, Nucleonics, March 1961.

38. Hyman, Seymour C., et al. - How Drill-Hole Diameter Affects Gamma-Ray Intensity, Nucleonics, February, 1955.

39. Jaeger, J. C. - The Surface Temperature of the Moon, Australian Journal of Physics, Vol. 6, 1953.

40. Kokesh, F. P., - The Development of a New Method of Science Velocity Determination - Geophysics Vol 17, July 1952.

41. Kopal, Zdenek - Thermal History of the Moon and of the Terrestrial Planets, J.P.L. Technical Report #32-108 May, 1961.

42. Kopal, Zdenek - Thermal History of the Moon and of the Terrestrial Planets: Convection in Planetary Interiors, J.P.L. Technical Report No. 32-276, April, 1962.

43. Kopal, Zdenek - Water on the Moon? Discovery Vol 27, No. 4, 1961.

44. Kovach, R. L., et al. - Seismic Exploration of the Moon, AIAA Summer Meeting, June, 1963.

45. Lehner, F. E., et al. - A Seismometer for Ranger Lunar Landing, Final Report, NASA Contract NASw-81, May 1962.

46. Levine, N. - Cost Estimation for Aerospace Projects - NASA TM X-53316, 13 July 1965.

47. Lingenfelter, R. E., et. al. - The Lunar Neutron Flux Journal of Geophysical Research, Vol. 66, No. 9, Sept., 1961.

48. Loomis, A. A. - Interpretation of Results from Surveyor Alpha-Scattering Experiment, J.P.L. Technical Report No. 32-606, April 1964.

49. Lowman, P.D. Jr. - The Relation of Tektites to Lunar Igneous Activity - Icarus, Vol 2, June 1963.

50. Lowman, Paul & Beattie, Donald - Manned Lunar Scientific Operations - Annual Meeting American Astronautical Society, May 1964.

51. Lynn, Ralph D. - A Low-Frequency Geophone for Borehole Use, Geophysics, Vol XXVIII, No. 1, Feb., 1963.

52. Marshak, Robert E. - Theory of the Slowing Down of Neutrons by Elastic Collision with Atomic Nuclei, Reviews of Modern Physics, Vol 19, No. 3, July 1947.

53. Martina, E. F., et al. - Analysis of the Moon's Surface by Nuclear Reactions, S.T.L. Report STL/TR-60-0000-0078, April 1960.

54. Meidav, T. - An Electrical Resistivity Survey for Ground Water - Geophysics Vol. XXV, October 1960.

55. Mero, John L. - Uses of the Gamma-Ray Spectrometer in Mineral Exploration, Geophysics, Vol XXV, No. 5 Oct. 1960.

56. Metzger, A. E., et al. - Ranger Gamma-Ray Spectrometer Nucleonics, October 1962.

57. Meyers, W. R. - An Electrodeless Method for the Measurement of Electrolytic Conductivity and Magnetic Susceptibility Journal of Scientific Instruments, Vol. 35, No. 5, May, 1958.

58. Miller, David C., et al. - X-Ray Analysis of the Lunar Surface, Joint Meeting IAS & AES, June 1961.

59. Miller, W. F., Reynolds, J., et al. - Efficiencies and Photofractions for Sodium - Iodide Crystals, The Review of Scientific Instruments, Vol 28, September 1957.

60. Mooney, Harold M. - Magnetic Susceptibility Measurements in Minnesota, Geophysics, Vol. 17, No. 3, July, 1952.

61. Moran, J. H., et al. - Basic Theory of Induction Logging and Application to Study of Two-Coil Sondes, Geophysics, Vol. XXVII, No. 6, December 1962.

62. Mott, W. E., et al. - Evaluation of Borehole and Formation Effects in Spectral Gamma-Ray Logging - Annual Meeting Society of Professional Well-Logging Analysts, May 1961.

63. Muench, N. L., et al. - Identification of Earth Materials by Induced Gamma-Ray Spectral Analysis, Transactions AIME, Vol 210, 1957.

64. Nogata, Tokesi - Some Physical Properties of the Lavas of Volcanoes Asama and Mihara II - Magnetic Susceptibility Bulletin of Earthquake Research Institute Vol. 18, 1940.

65. Norton, K. A. - The Calculation of Ground-wave Field Intensity over a Finitely Conducting Spherical Earth, Proceedings of the I.R.E., Dec. 1941.

66. Palm, A., Strom, R. G. - Elemental Abundances of the Lunar Crust According to Recent Hypothesis - Research Report, Space Science Laboratory, University of California, January 1962.

67. Paterson, R. G. - Determination of Magnetic Susceptibilities of Rocks in Situ, Transactions, AIME, Vol. 164, 1945.

68. Pickell, J. J., et al. - Density Logging, Geophysics, Vol XXV; No. 4, August, 1960.

69. Press, F., et al. - A Lunar Seismic Experiment, Journal of Geophysical Research, Vol 65, No. 10, Oct., 1960.

70. Rogers, J. R., Vaughan, O. H. Jr. - Lunar Environment: An Interpretation of the Surface of the Moon and its Atmosphere - NASA TM X-53124, September 1964.

71. Salisbury, J. W. - Lunar Natural Resources, Nature, Aug. 4, 1962.

72. Schaefer, E. J., Nichols, M. H. - Mass Spectrometer for Upper Air Measurements - ARS Journal, December, 1961.

73. Schrader, C. D., Waggoner, J. A., et al. - Neutron-Gamma Ray Instrumentation for Lunar Surface Composition Analysis - ARS Journal April 1962.

74. Segesman, F., et al. - Well Logging - The Exploration of Subsurface Geology, Proceedings of the IRE, November, 1962.

75. Speed, R. C. - Water in Lunar Materials JPL Seminar Proceeding Sept. 25-26, 1962.

76. Speed, Robert C., et al. - A Lunar X-Ray Diffraction Experiment, Advances in X-Ray Analysis Vol. 8, 1965.

77. Tiffany, O. L., et al. - Scientific Exploration of the Moon using a Roving Vehicle, Symposium on Post Apollo Space Exploration, AAS Meeting, May, 1965.

78. Tittle, C. W. - Theory of Neutron Logging, Geophysics, Vol. XXVI, No. 1, February 1961.

79. Tixier, M. P., et al. - New Developments in Induction and Sonic Logging - Petroleum Transactions, AIME Vol. 219, 1960.

80. Vogler, L. E. - A Study of Lunar Surface Radio Communication, National Bureau of Standards Monograph 85, Sept. 1964.

81. Waggoner, J. A., Knox, R. J. - Elemental Analysis Using Neutron Inelastic Scattering - UCRL - 14654-T, Lawrence Radiation Laboratory, Livermore, California.

82. Wait, I. R. - Radiation Resistance of a Small Circular Loop in the Presence of a Conducting Ground, Journal of Applied Physics, Vol. 24, No. 5, May 1953.

83. Watson, K., Murray, B. et al. - On the Possible Presence of Ice on the Moon - Journal of Geophysical Research, Vol. 66, May 1961.

84. Weatherred, C. J., et al. - System Approach to Lunar Surface Exploration, Symposium on Post Apollo Space Exploration, AAS Chicago Illinois, May 1965.

85. Wesselink, A. F. - Heat Conductivity and Nature of the Lunar Surface Material, Bulletin of the Astronomical Institutes of the Netherlands, Vol X, No. 390, April, 1948.

86. Wheeler, H. A. - Radio Wave Propagation in the Earth's Crust, Journal of Research, Vol. 65, No. 2, Mar-April 1961.

87. Wheeler, H. A. Useful Radiation from an Underground Antenna, Journal of Research, Vol 65D, No. 1. Jan-Feb. 1961.

88. Wolf, R. & Canup, R. - A Theoretical Study of the Propagation and Attenuation of Acoustic Waves in the Lunar Surface, Texaco Experiment Incorporated, TM-1325, Feb., 1962.

89. Young, Niels O., et al. - Research and Development of A Laboratory Model Infrared Interferometer Spectrometer for Use in a Mars Probe - Phase I Technical Report, J.P.L. Contract #950037, August 1961.

90. Zaitzeff, E. M. & Tiffany, O. L. - Scientific Mission Support Study (AES) First Interim Report, Contract NAS 8-20199 - The Bendix Corporation, July 1965.

91. ALSS Scientific Mission Support Study, Final Report Contract NASW-1064 - The Bendix Corporation, March 1965.

92. ALSS Scientific Mission Support Study, Interim Report Contract NASW-1064 - The Bendix Corporation, Dec. 1964.

93. Apollo Configuration Management Manual - NASA NPC 500-1, 18 May 1964.

94. Apollo Experiment Guide, NASA, NPC 500-9, 15 June 1965.

95. Apollo Extension Systems (AES) Capabilities for Earth Orbited and Lunar Experiments - Directorate of Special Manned Space Flight Studies, NASA, July 1965.

96. Apollo Program - Natural Environment and Physical Standards for the Apollo Program, NASA, April, 1965.

97. Apollo Program Specification - NASA, May 1965.

98. Apollo Test Requirements - NASA NPC 500-10, May 20, 1964.

99. Bioengineering Aspects - Astronaut Limitations Study - From Bendix Final Report BSR 1112 March 1965.

100. Compilation of Working Papers and Discussion Briefs, Conference on Lunar Technology, Washington, D. C., May 14, 1964.

101. Conference on Lunar Exploration - Part A, Virginia Polytechnic Institute, August 1962.

102. Conference on Lunar Exploration - Part B Virginia Polytechnic Institute, August 1962.

103. Conference on Lunar Exploration - Part C Virginia Polytechnic Institute, August 1962.

104. Conference on Lunar Exploration - Supplement Virginia Polytechnic Institute, August 1962.

105. Design and Construction of a Lunar Seismograph Prototype Model, Final Report, Lamont Geological Observatory, June, 1962.

106. Engineering and Fabrication of Prototype and Production Models of Interferometer Spectrometer Temperature Instruments for the Surveyor Program - A proposal. Block Associates Proposal #60-July 1962.

107. Environmental Effects on AFS Scientific Instruments, January 1966, SSD 60014R, Hughes Aircraft Company.

108. Environmental Specifications for Apollo Scientific Equipment - NASA, 15 July 1964.

109. Final Report of the Geochemistry-Petrology Working Group (Woodshole - First Draft).

110. Gamma-Ray Spectrometer - J.P.L. Technical Report No. 32-199.

111. IEEE Transactions on Antennas and Propagation, Vol. AP-11, May, 1963.

112. Initial Concept of Lunar Exploration Systems for Apollo - Vol I - Summary - NASA CR-35 by the Boeing Company, March 1964.

113. Lunar Seismograph, J.P.L. Technical Report No. 32-199.

114. NASA 1965 Summer Conference on Lunar Exploration and Science, July 19-31, 1965, NASA SP-88.

115. Natural Environment and Physical Standards for the Apollo Program - NASA, April 1965.

116. Report of Geophysics Working Group, NASA Lunar Exploration Summer Conference, July 1965 (Woodshole).

117. Texaco Geophysical Instruments, A Capabilities Survey - March, 1963.

118. Thermal Diffusivity Measurement on Metals and Ceramics at High Temperatures, Technical Documentary Report No. ASK-TDR-62-24, Part II, June, 1963.

Design Features

MECHANICAL

A wide variety of types of metal strip may be used to form the element. The choice of metal depends upon the STEM application. Stainless steel, beryllium copper and titanium have all been used with success. The strength and rigidity of the extended tube can be increased by wrapping a number of tubes inside the main tube. For space applications, antennas have already been manufactured varying in length from 15 inches to 850 feet. The photograph shows the compact size of the 850 ft. antenna unit; Type A21.

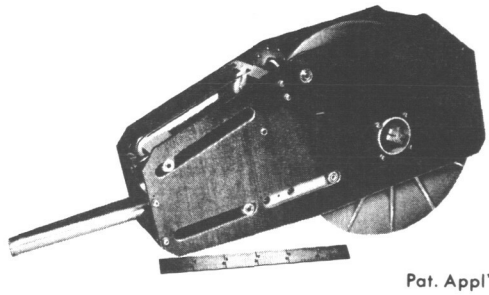

Pat. Appl'd. for

Type A 21 Unit (850 ft Antenna; Weight 16 lbs.)

STRENGTH OF UNFURLED TUBULAR STRUCTURES

Some of the mechanical design parameters involved are discussed in the following paragraphs and will give an indication of the strength of a STEM tube when unfurled.

The tubular element itself must be strong enough to withstand the calculated loads with an adequate margin of safety. In the case of the overlapped tube, the bending and torsional strengths are of prime interest.

It has been proven that when adequate element restraints are provided at the root and tip, the overlapped tube exhibits buckling characteristics similar to that of a thin walled seamless tube and that the critical bending moment may be expressed as:

$$BM_{CR} = \cdot 042 \frac{K_b E d t^2 n}{F_b (1-\nu^2)} \quad (1)$$

K_b = EXPERIMENTAL CONSTANT (0.75) Based on Zero Torsional Stress.
E = MODULUS OF ELASTICITY (30×10^6 lbs/in^2)
n = NUMBER OF ELEMENTS
d = ELEMENT DIAMETER (in.)
ν = POISSON'S RATIO
t = ELEMENT THICKNESS (in.)
F_b = SAFETY FACTOR (1.3)

$$BM_{CR} = \cdot 042 \frac{K_b E d t^2 n}{F_b (1-\nu^2)} \quad (1)$$

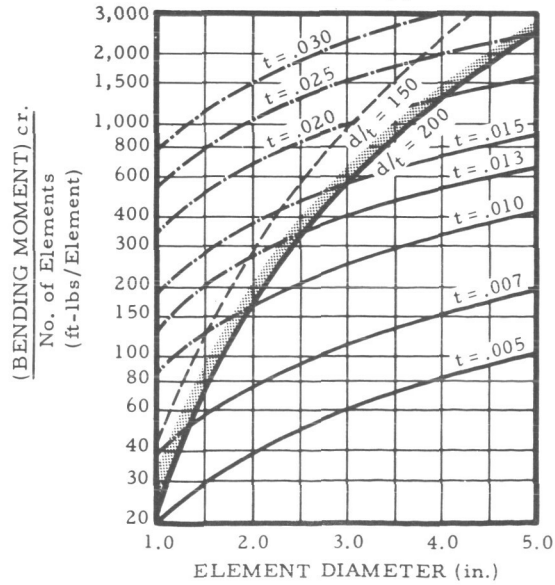

Critical Bending Moments in Tubular Elements

The torsional strength, however, is similar to that of an open tube, the critical buckling torque being described by:

$$T_{CR} = \cdot 083 \frac{K_t E t^3 n}{F_t (1-\nu^2)^{3/4}} \sqrt{\frac{t}{d}} \quad (2)$$

These equations are plotted in the diagrams below and reveal that while bending strength is high, torsional strength is much lower and could present design problems unless carefully examined during preliminary engineering investigations.

Torsional and bending strength may be improved by several techniques. One very attractive solution is to depart from a circular cross-section to either an ellip-

K_t = EXPERIMENTAL CONSTANT (0.75) Based on Zero Bending Stress.
E = MODULUS OF ELASTICITY (30×10^6 lbs/in^2)
n = NUMBER OF ELEMENTS
d = ELEMENT DIAMETER (in.)
ν = POISSON'S RATIO (0.3)
t = ELEMENT THICKNESS (in.)
F_t = SAFETY FACTOR (1.3)

$$T_{CR} = \cdot 083 \frac{K_t E t^3 n}{F_t (1-\nu^2)^{3/4}} \sqrt{\frac{t}{d}} \quad (2)$$

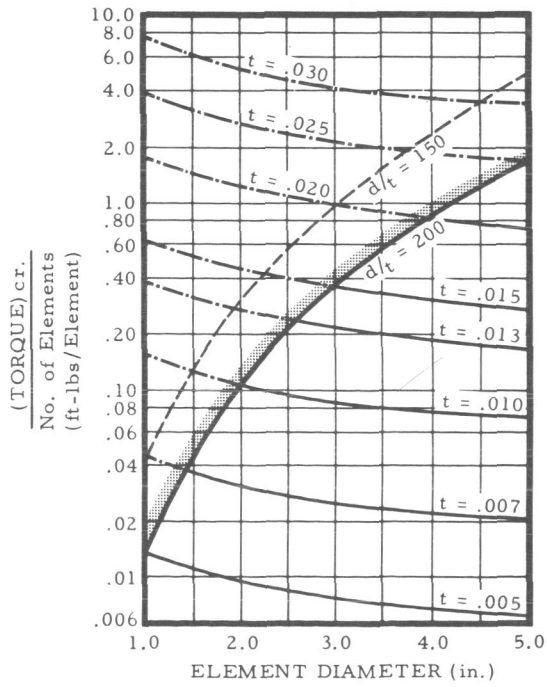

Critical Torque in Tubular Elements

Strength of Unfurled Tubular Structures (cont'd)

tical or triangular shape, ensuring of course, that the minimum radius of curvature does not introduce stresses exceeding the allowable limit when the element is flattened during storage. These and other methods for improving strength-to-weight ratios are currently under development. Results to date indicate that it is quite practical to consider unfurlable metal elements as torque bearing structures.

In some applications the inherent strength of the STEM element in tension and compression may be important. The element is extremely strong in tension, its load carrying ability being expressed by:

$$L_T = 0{\cdot}005\,\pi\,\gamma\,\mathcal{S}\,d^2 \qquad (3)$$

Since 'd' and 't' are proportionally related, the load capacity of the STEM in tension is proportional to the second power of the tube diameter. This equation is presented in the diagram below for a typical steel element.

On the other hand, the element is relatively weak in compression. Its behaviour is similar to that of a thin walled seamless tube. The theory governing thin walled seamless tube in compression is well developed only for a perfectly straight tube. Based on this criterion the load carrying capacity of the STEM in compression can be expressed as:

$$L_C = 0{\cdot}158 \times 10^{-4}\,\frac{K_C\,E\,\pi\,\gamma\,d^2}{(1-\nu^2)} \qquad (4)$$

It should be noted that this equation implies that the buckling load is independent of element length (Euler's theory applying only to solid struts). Practical experience shows that length is a degrading factor and is related to tube straightness. Equation (4) is also presented in the diagram below for a typical steel element.

γ = OVERLAP FACTOR
$\mathcal{S}$ = 0.1% PROOF STRESS = 200,000 (lbs/in²)
d = ELEMENT DIAMETER (in.)
t = ELEMENT THICKNESS (in.)
d/t = 200
K_C = EXPERIMENTAL CONSTANT = 0.7
E = MODULUS OF ELASTICITY = 30×10^6 (lbs/in²)

$$L_T = 0{\cdot}005\,\pi\,\gamma\,\mathcal{S}\,d^2 \qquad (3)$$

$$L_C = 0{\cdot}158 \times 10^{-4}\,\frac{K_C\,E\,\pi\,\gamma\,d^2}{(1-\nu^2)} \qquad (4)$$

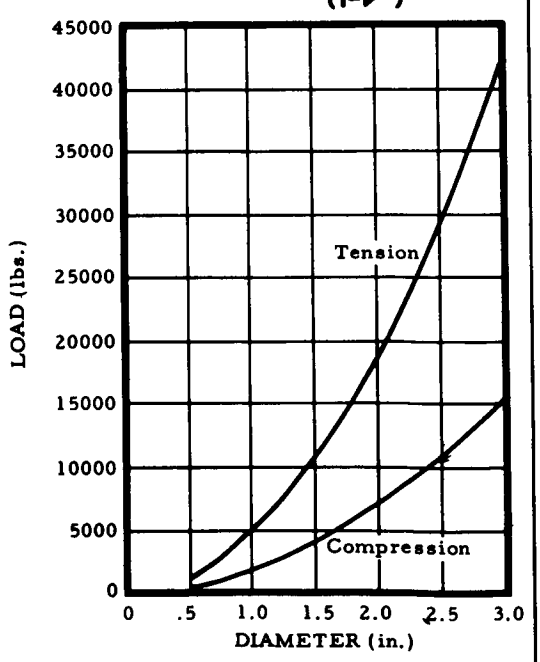

Tensile and Compressive Strengths of Typical Tubular Elements

SYSTEM POWER REQUIREMENTS

The power required to drive the electric motor is dependent on a number of factors including, rate of element retraction; antenna element diameter and thickness; number of tubular elements; and electrical and mechanical efficiency. The maximum power required to operate the boom may be expressed as follows:

$$p = \frac{\gamma\,\pi\,E t^3\,n V_m}{6 Z d\,(1-\nu^2)}\left[1-\frac{d^2}{d_o^2}\right] \qquad (5)$$

This equation is plotted in the diagram below for a typical element configuration. Overall mechanical and electrical efficiencies between 30% and 50% are currently obtainable.

p = POWER-WATTS
γ = OVERLAP FACTOR
E = MODULUS OF ELASTICITY = 30×10^6. (lbs/in.²)
Z = EFFICIENCY = 50%.
d/t = 200
ν = POISSON'S RATIO = .3
d_o = OUTSIDE DRUM DIAMETER.
V_m = RETRACTION VELOCITY ft/sec.
d = ELEMENT DIAMETER (in.)
t = ELEMENT THICKNESS (in.)
n = NUMBER OF ELEMENTS.

$$p = \frac{\gamma\,\pi\,E t^3\,n V_m}{6 Z d\,(1-\nu^2)}\left[1-\frac{d^2}{d_o^2}\right] \qquad (5)$$

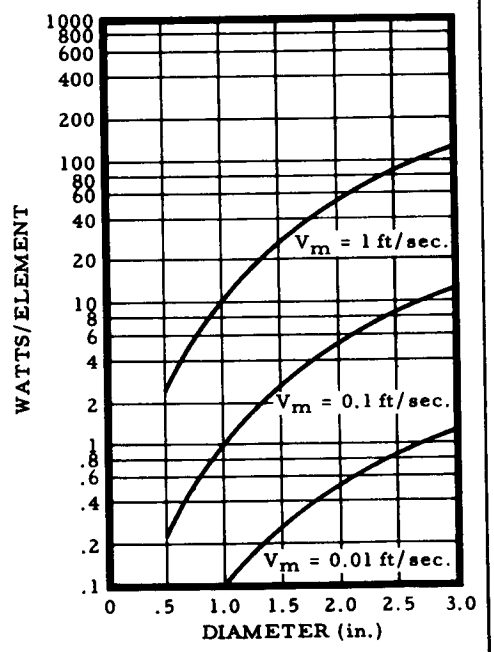

Power Requirements for Typical 'STEM' Elements

CONCLUSION

The STEM unit operates on an operationally proven principle and when used to form an antenna or boom, in space or on land, the simple electro-mechanical device has neither the leakage nor contamination problems of a hydraulic system. The STEM has an ease of extension/retraction cycling that cannot be approached by inflatable or explosively actuated devices.

STEM units have been manufactured for many applications in both space and ground environments. A vigorous development program is expanding the market for these devices into such diverse areas as exotic, high gain, deep space antennas and simple, inexpensive hand operated mobile ground communications masts.

You are invited to explore the possibility of the de Havilland Special Products & Applied Research Division designing a STEM device to suit your particular requirement.

STEM DEVICES

Storable Tubular Extendible Member

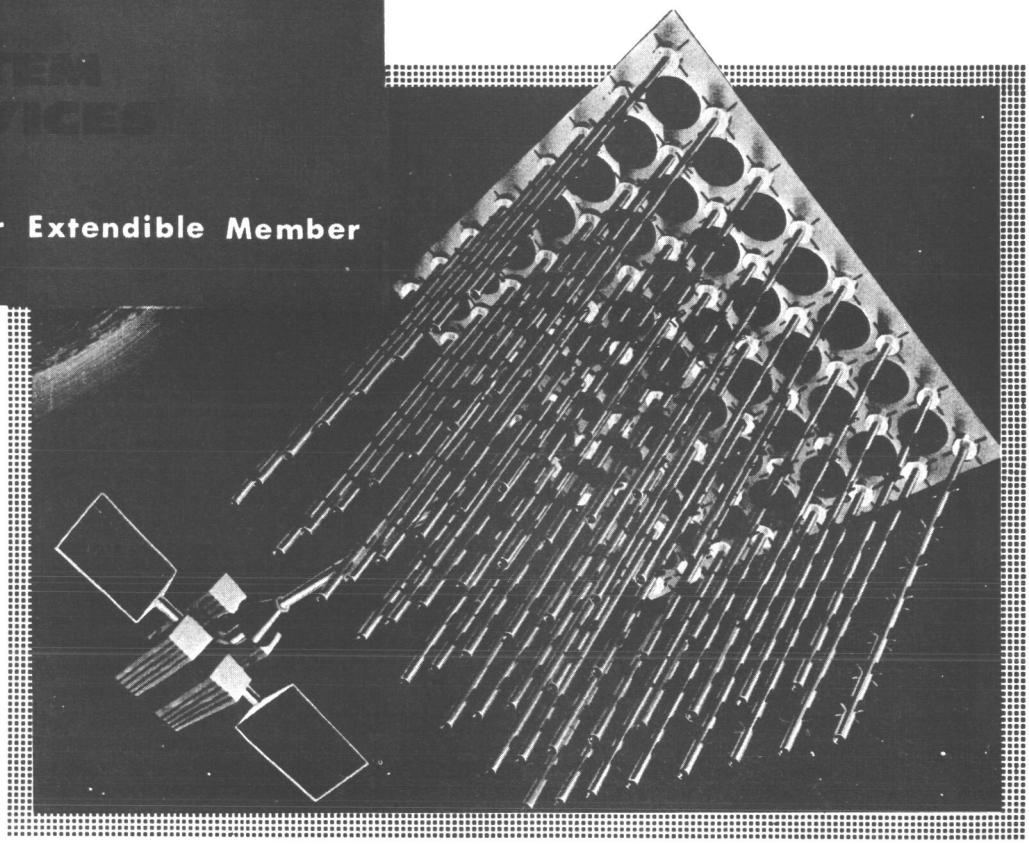

INTRODUCTION

There has been a long acknowledged need for antennas that can be stored in a minimum of space, that can easily be extended and retracted and yet have a high reliability and require minimum maintenance. The advent of space communication systems placed even more stringent limitations upon the parameters of low weight, small volume and high reliability.

Early in 1960, the Special Products & Applied Research Division undertook a design program to manufacture an antenna unit that would satisfy these requirements for a satellite system yet extend an antenna element for the length required. The program was a success and produced the first of a whole series of units that have become widely known as Storable Tubular Extendible Member (STEM) devices. Initially, the units were designed for space applications as either antennas or instrumentation booms but a vigorous development program has produced a range of STEM units that can be used in the ground environment as either antennas or mechanical booms.

APPLICATIONS

IN SPACE

- ★ **Spacecraft Antennas**
- ★ **Satellite Gravity Gradient Stabilization Rods**
- ★ **Instrumentation Booms**
- ★ **Space Station Docking Booms**

ON GROUND

- ★ **Land Based Antennas**
- ★ **Vehicular Mounted Masts**
- ★ **'One-Shot' Robot Weather Station Antennas**
- ★ **Hand Operated, Inexpensive Antennas for Exploration Party Communication**

The "STEM" Principle

Since many unfurlable metal structures are based on STEM techniques, a short description of this principle is presented below. The illustration shows the STEM principle in its basic form. The tubular elements are formed out of strip metal, heat-treated into a circular section in such a manner that the edges of the material overlap by approximately 180°. This provides the tubular element with a bending strength almost equivalent to that of a seamless tube of the same diameter and wall thickness. The elements, when retracted, are stored in a strained, flattened condition by winding them onto or into a drum. As the circular element is retracted, it is smoothly transformed into the flattened condition by passing it through a suitable guidance system. The element may be extended or retracted by rotating the drum in the appropriate direction. Retracting the element involves supplying strain energy to the element material as it flattens, thus the stored elements have a natural tendency to self-extend, and hence provide low power extension. Conversely, positive power must be supplied for element retraction. The bending and torsional strength of an element may be increased for a given formed diameter, by nesting several elements together.

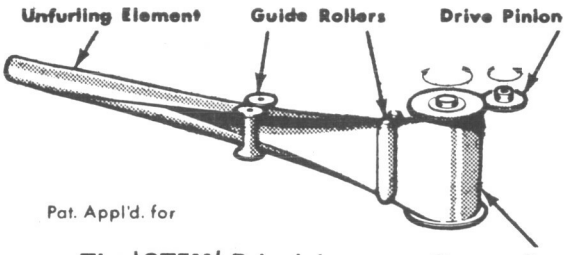

Pat. Appl'd. for

The 'STEM' Principle

Types of "STEM" Devices

Unfurlable metal structures employing the STEM principle fall into two main categories; those which require both extension and retraction, and those requiring extension only. The first type is usually powered by an electric motor and the latter is released by a pyrotechnic or solenoid actuated latch, extension taking place by controlled release of the strain energy stored in the coiled and flattened element.

MOTORIZED UNITS

The Type A18 unit is a good example of a motorized STEM unit that can extend or retract the element many times. Developments of this model have been used in many space programs. The unit can easily hold a 30 ft. long element.

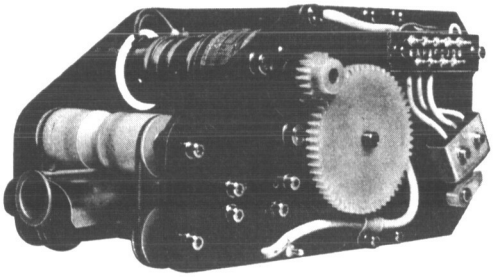

Pat. Appl'd. for

Type A18 Motorized 'STEM' Unit

SELF-EXTENDING UNITS

Where "one-shot" operation is desired, with no retraction, the inherent spring energy of the unreeling element may be used as its sole source of extension force. The unit shown below is provided with this capability, the free end of the element being tethered, the spool unreeling the material and travelling along the produced element until it finally flies off the end. Units have also been developed employing two of these spool arrangements back-to-back with a centrifugal brake acting differentially between them, such that the rate of ejection is within the allowable limits of the system with which the elements are being used. This automatic self-ejecting feature is useful in applications where weight and power are at a premium and retraction is unnecessary.

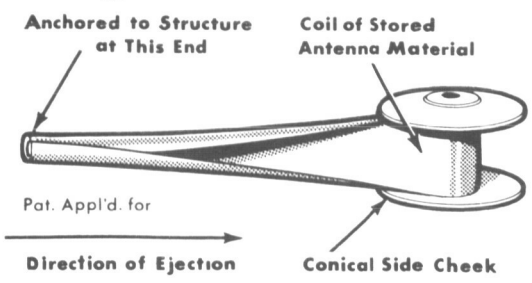

Pat. Appl'd. for

Design Employing Conical Drum Cheeks to Provide Constraint for Unwinding Strip

Pat. Appl'd. for

An operational example of this type of STEM unit is the type A45. Two of these 16 ft antenna units were successfully used on the Mercury spacecraft.

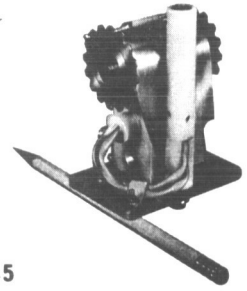

Type A45

A further type of self-ejecting automatic unit has also been developed, known as the "jack-in-the-box". In this arrangement, the element is ejected sideways in the form of an expanding spiral.

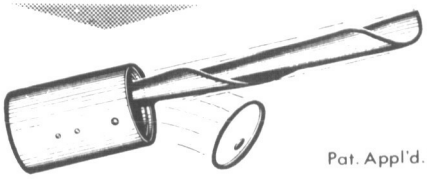

Pat. Appl'd. for

"Jack-in-the-box"

A production model using this method of ejection is the Type A35 unit, a 15 inch long element that will form the UHF antennas on the GEMINI spacecraft.

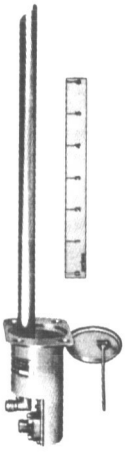

Type A35

SERIES 210 QUADRUPOLE RESIDUAL GAS ANALYZER

PRINCIPLES OF DESIGN AND OPERATION

THEORY

The purpose of this section is to describe the EAI Quadrupole Residual Gas Analyzer (QUAD 210), derive the theoretical principles of its operation, discuss the equipment which is required to properly operate the instrument, and present experimental data pertaining to its operation.

1-A. DESCRIPTION: The EAI Quadrupole Residual Gas Analyzer is shown schematically in Figure 1. The primary components are the ionizer, the quadrupole section and the ion detector. The substance which is to be analyzed is introduced into the ionizer as a gas at low pressure. A small percentage of the atoms or molecules which make up this substance is ionized by electron bombardment. These ions are then accelerated and focused into the quadrupole section. The ion beam is filtered by permitting only those ions within a specific range of charge-to-mass ratios to pass through the quadrupole. (The mechanism of this filtering action is discussed in a later section of this report.) Those ions which are able to pass through the filter are collected by the ion detector. The detector is an electron multiplier or a Faraday cup.

The output current of the detector is a measure of the number of atoms or molecules in the substance which, when ionized, have a particular charge-to-mass ratio. The charge-to-mass ratio detected is determined from the values of a D.C. voltage and an R.F. voltage which are applied to the poles of the quadrupole section. The majority of the ions which are produced in the ionizer are singly charged; therefore, the mass of the atoms or molecules may be directly determined. A display of quantitative abundance as a function of atomic mass weight can be conveniently presented on many types of instruments, such as oscilloscopes, x-y recorders, and strip chart recorder.

1-B. THEORY OF OPERATION: The heart of the RF Quadrupole RGA is the quadrupole section. This assembly is composed of four stainless steel rods which are approximately five inches long and one-quarter inch in diameter. These rods are precisely located in a rectangular array by alumina insulators. A D.C. voltage and a superimposed R.F. voltage are applied to the rods as shown in Figure 2. An electrostatic field is thereby generated in the region between the rods. If the rods were hyperbolic cylinders (Figure 3) rather than circular cylinders, the potential of this electrostatic field would be,

$$\phi = (V_1 + V_o \cos \omega t)\ (x^2 - y^2)/r_o^2 \qquad (1)$$

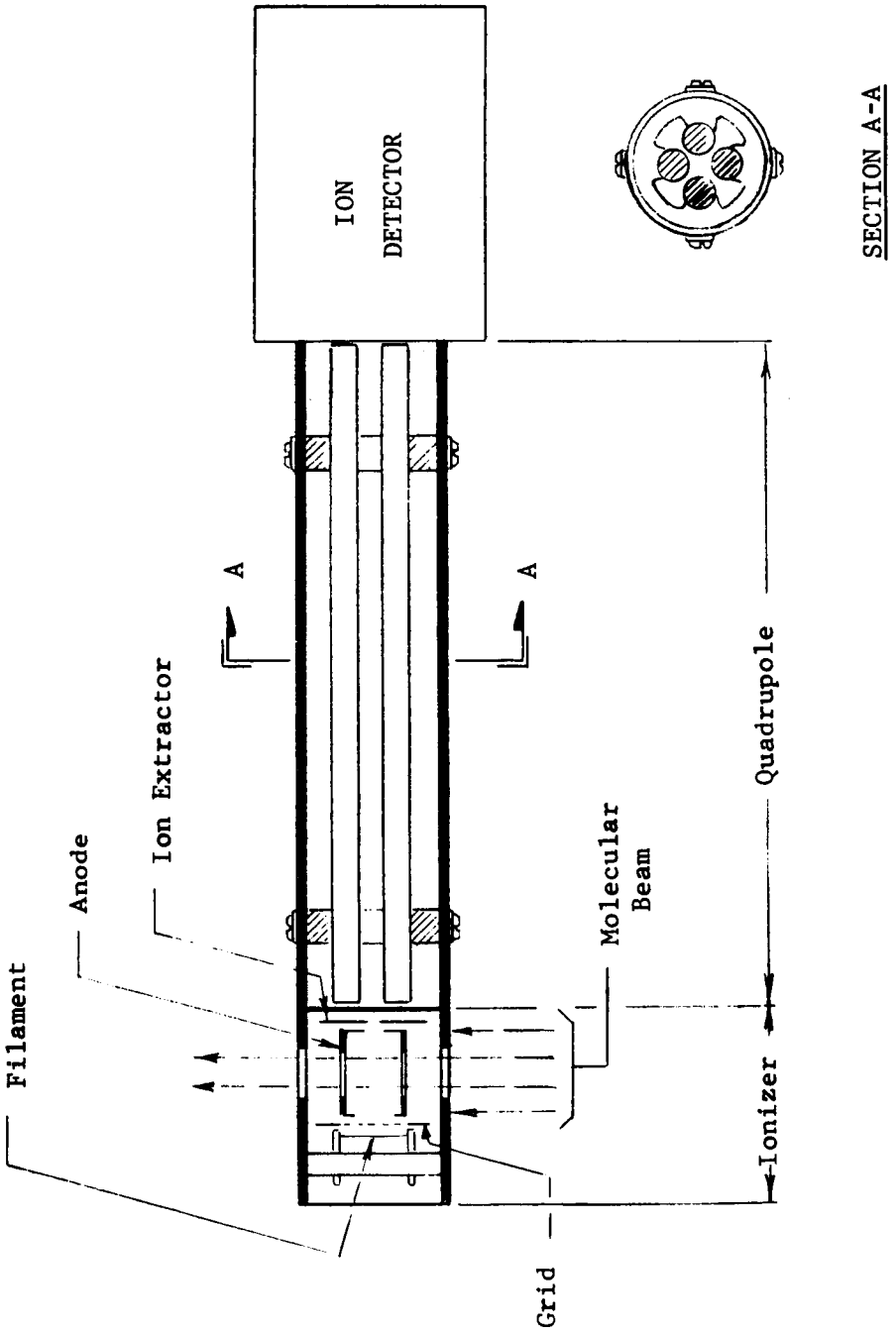

FIG. I
EAI QUADRUPOLE RESIDUAL GAS ANALYZER

This potential is approximately that which is generated in the actual geometry.

When a singly charged ion enters the filter, it is accelerated by the electrostatic field. The cartesian force components are:

$$F_x = -e \frac{d\phi}{dx} = -e \ (V_1 + V_o \cos \omega t) \ (2x/r_o^2) \tag{2}$$

$$F_y = -e \frac{d\phi}{dy} = +e \ (V_1 + V_o \cos \omega t) \ (2y/r_o^2) \tag{3}$$

$$F_z = -e \frac{d\phi}{dz} = 0 \tag{4}$$

where e is the electronic charge.

Therefore, the equations of motion of a singly charged ion of mass, m, are,

$$m \ddot{x} + (2e/r_o^2) \ (V_1 + V_o \cos \omega t) \ x = 0 \tag{5}$$

$$m \ddot{y} - (2e/r_o^2) \ (V_1 + V_o \cos \omega t) \ y = 0 \tag{6}$$

$$m \ddot{z} = 0 \tag{7}$$

Equation (7) may be immediately integrated to determine the axial motion of the ion,

$$\dot{z} = \dot{z}_o = \text{constant} \tag{8}$$

Therefore, the axial velocity of any ion is constant and is not affected by the voltages applied to the poles of the filter. The magnitude of the axial velocity is its value at the entrance to the filter. The ionizer system thereby governs the time required for an ion to pass through the filter.

The filtering action of the quadrupole results from the trajectory characteristics of Equations (5) and (6). Under certain conditions the amplitude of the trajectory increases without bound; the ion then collides with one of the poles and is removed from the ion beam. The characteristics of these Mathieu equations have been analyzed by many investigators (1), and for the particular case of the RF Quadrupole Mass Spectrometer, stability diagrams have been developed by Paul (2), Stanford Research Institute (3), and Electronics Associates, Inc.

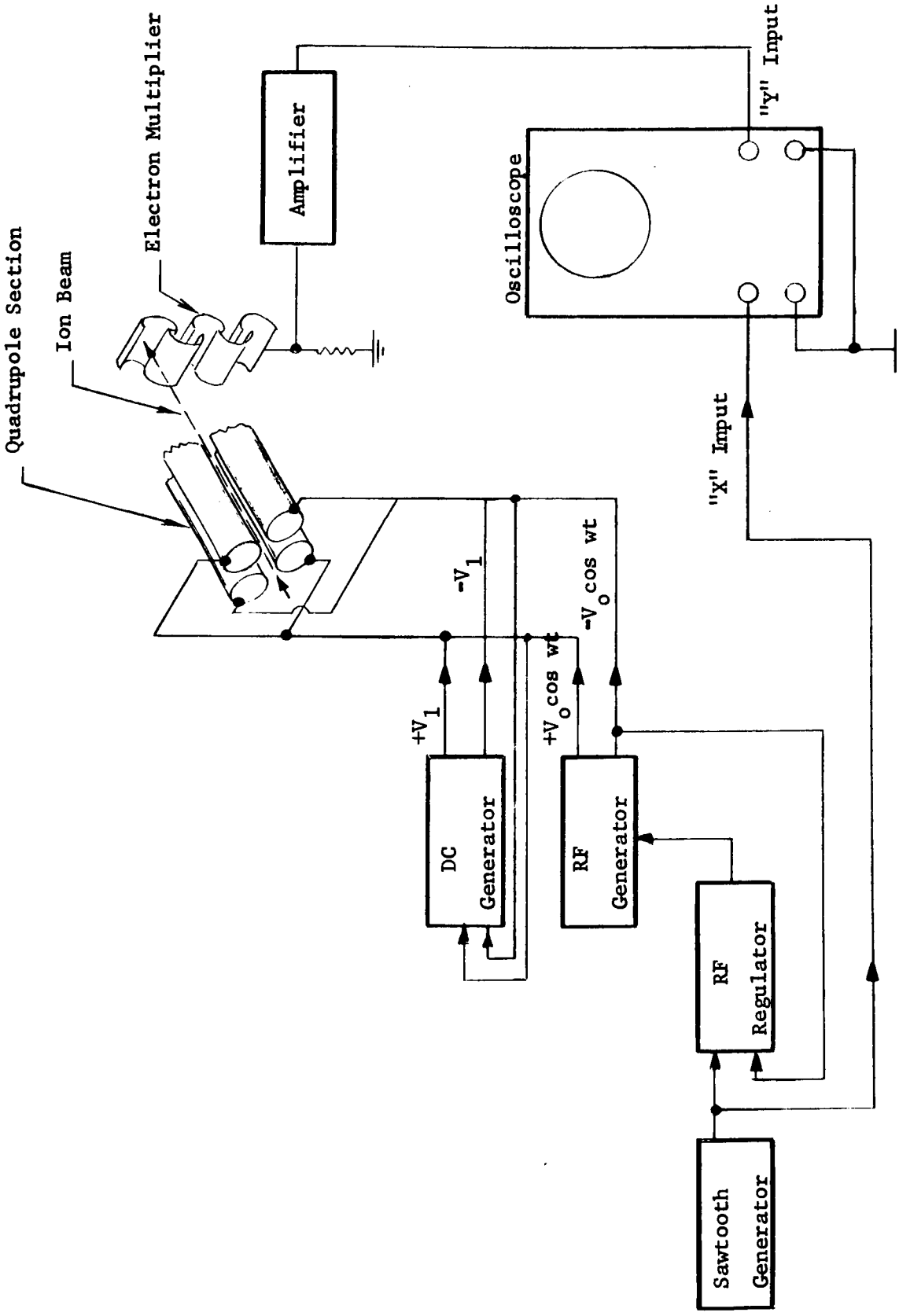

Figure 2

Quadrupole Voltages

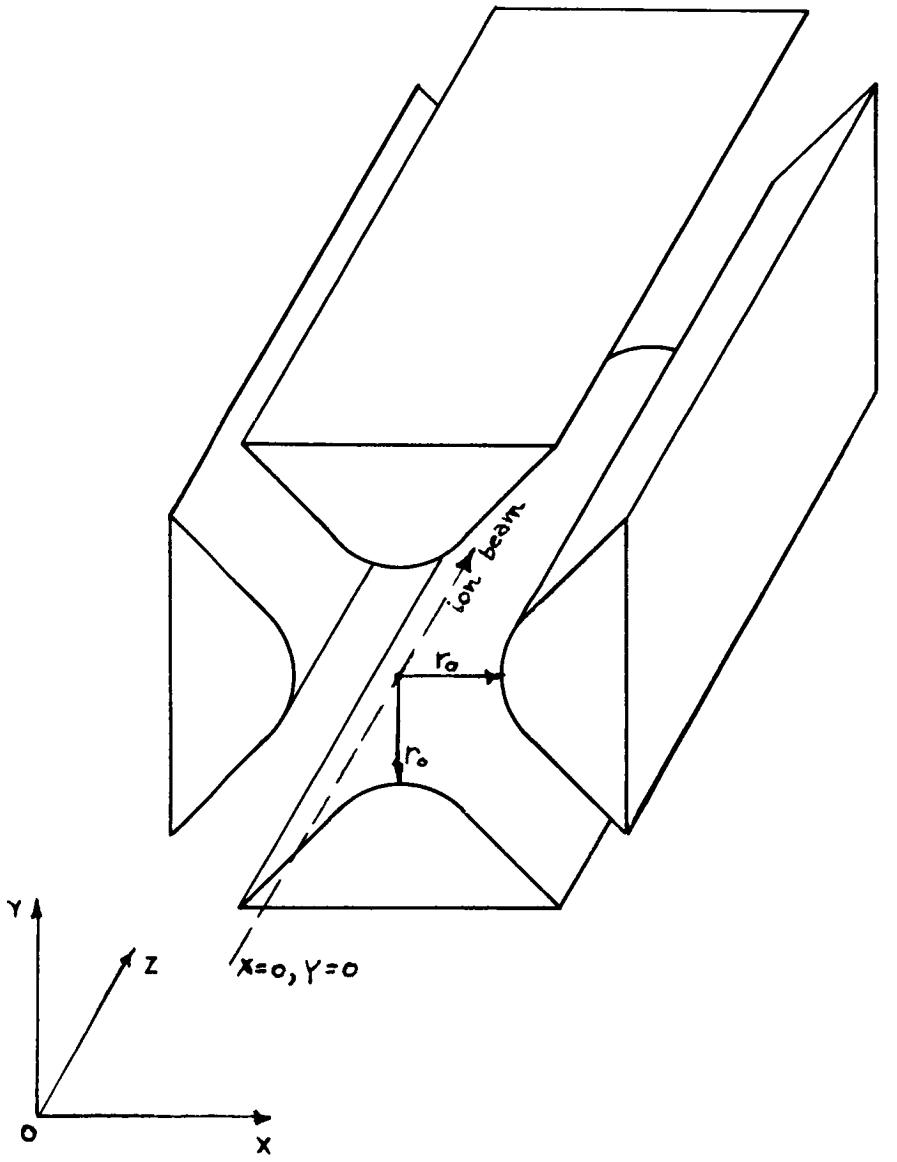

Figure 3

Hyperbolic Quadrupole Rods

Typical stable and unstable trajectories of an ion are shown in Figure 4. (A PACE analog computer was used to obtain these solutions of the equations of motion.)

The Paul and SRI stability diagrams are given in Figure 5. In this, and in Figure 6, certain non-dimensional groupings have been introduced into the equations of motion. These parameters are,

$$\theta = \omega t \tag{9}$$

$$\alpha = (2eV_o)/(mr_o^2\,\omega^2) \tag{10}$$

$$\beta = V_1/V_o \tag{11}$$

The transformed equations of motion are,

$$\ddot{x} + \alpha\,(\beta + \cos\theta)\,x = 0 \tag{12}$$

$$\ddot{y} - \alpha\,(\beta + \cos\theta)\,y = 0 \tag{13}$$

For a given value of the parameter, α, there exists a value of the parameter, β, which divides a region of stability from a region of instability. The locus of points which form this division are plotted in Figure 5 for Equations (12) and (13). It may be seen that of all possible values these parameters may take, only a small portion will result in the stability of both equations. An alternate form of the stability diagram has been developed at EAI and is given in Figure 6. Notice that if the parameter, $\beta = V_1/V_o$, is constant at a value of approximately 0.168, there is a very small range of values of the parameter, α, which will result in stable solutions. Physically, this implies that only ions within a very small range of charge-to-mass ratios will have trajectories which will allow them to traverse the quadrupole structure. Ions having charge-to-mass outside this range will have trajectories which result in collisions with the poles.

Furthermore, if either the voltage, V_o, or the frequency, ω, (or both) are varied in such a manner that the ratio of voltages, V_1/V_o, remains constant at about the 0.168 level, the value of the transmitted and detected charge-to-mass ratios will vary in a known manner. That is, the charge-to-mass ratios of the ions which reach the detector will be that value necessary for α to have the value 0.354. Therefore, this ratio may be determined from the relation,

$$e/m = 0.354\,(r_o^2\,\omega^2)/(2V_o) \tag{14}$$

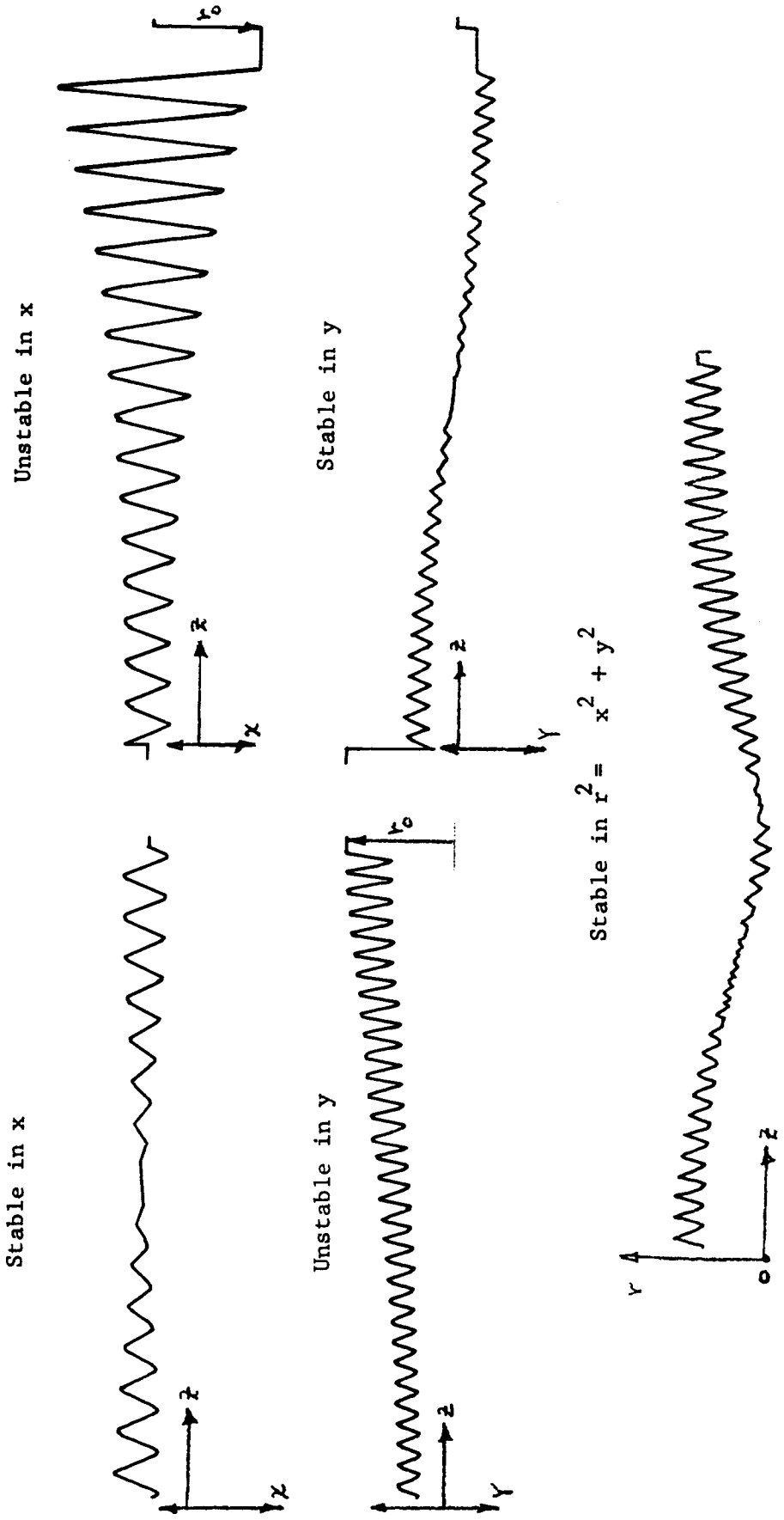

Figure 4

Typical Ion Trajectories

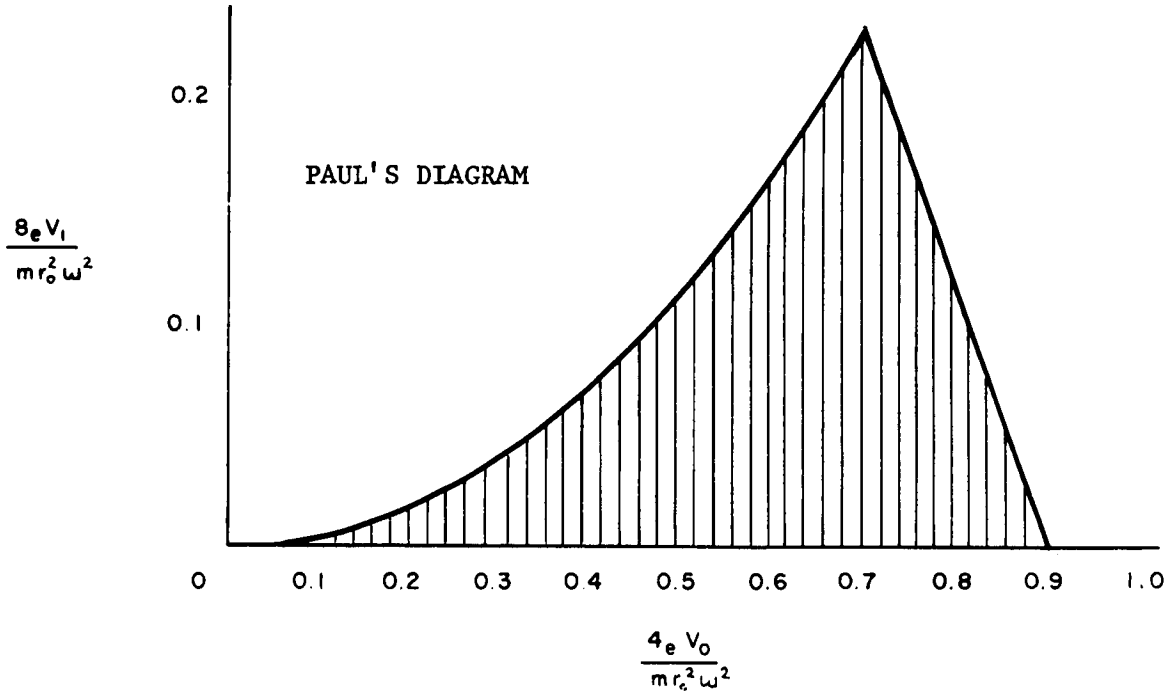

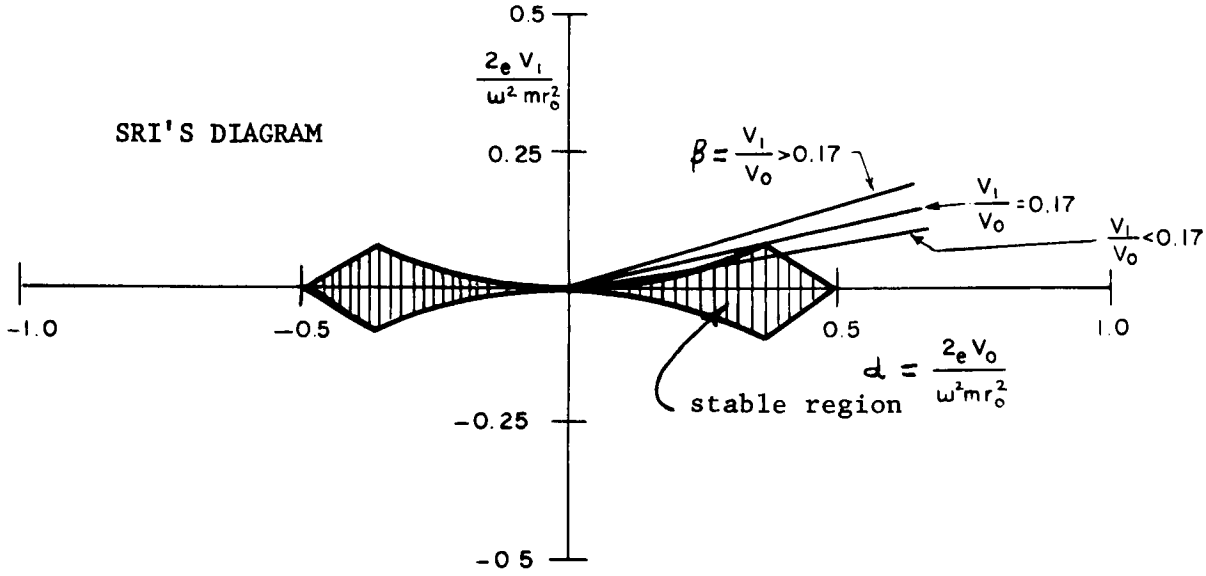

Figure 5

Stability Diagrams

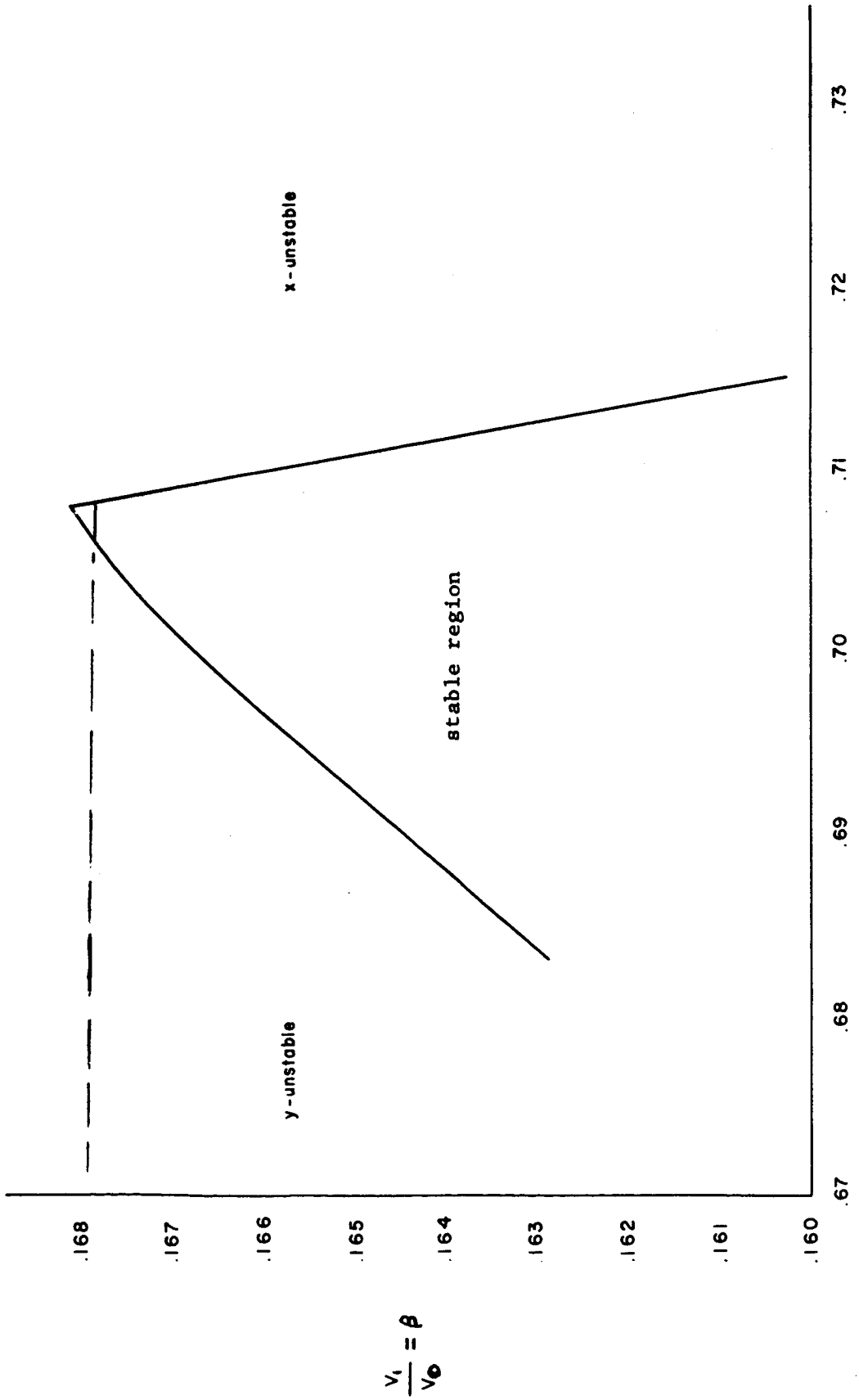

Figure 6

EAI Stability Diagram

Under the assumption that the ions are singly charged, the mass of the ion which reaches the detector is,

$$m = 0.136\ V_o/(r_o^2\ f^2)\ \text{amu} \qquad (15)$$

Where V_o is in volts, r_o is in cm., and f is in mc.

1-C. EQUIPMENT: The gaseous sample enters the ionizer which produces positive ions by electron bombardment. Ions pass through an electrostatic focusing system into the quadrupole structure. The ions are then separated with the "unstable" ions being collected at the poles and the "stable" ions being collected by the detector. The signal from the detector is amplified by a D.C. amplifier and the spectrum is displayed on an oscilloscope, x-y plotter or strip chart recorder.

Ionizer: The ionizing section of the EAI spectrometer consists of a filament, grid, ionizing chamber (Figure 7) and three electrodes, all of which are enclosed. Atoms and molecules enter the ionizing chamber via holes in the tube and are ionized by low energy electrons emitted by the filament.

Electrons produced at the filament are accelerated by a controllable voltage between the filament and the grid. Those electrons passing through the grid and into the ionizing chamber encounter neutral atoms and molecules. If the resulting transfer of energy through electron interaction is adequate, a positive ion is produced. In this manner one electron may produce several ions before it loses its energy and is collected.*

The ions are drawn from the ionizing chamber by a starting electrode which is operated at a positive potential (Figure 7) slightly less than the potential of the chamber itself. After passing through the starting aperture, the ions are accelerated by a focusing aperture which is set at a negative potential V_f. The approximate energy of the ions then becomes $(eV_c - eV_s) + (eV_s - eV_f)$. Finally, in going from the focusing aperture to the grounded exit aperture, the ions lose energy eV_f. The net ion energy is then computed as follows:

$$\text{ion energy} = (eV_c - eV_s) + (eV_s - eV_f) + eV_f = eV_c \qquad (16)$$

---

*The average primary ionization potential of most atoms is in the neighborhood of 10 eV, varying in extremes between Cesium (3.87 eV) and He (24.5 eV). The first ionization potential of most organic molecules is in the order of 10 eV.

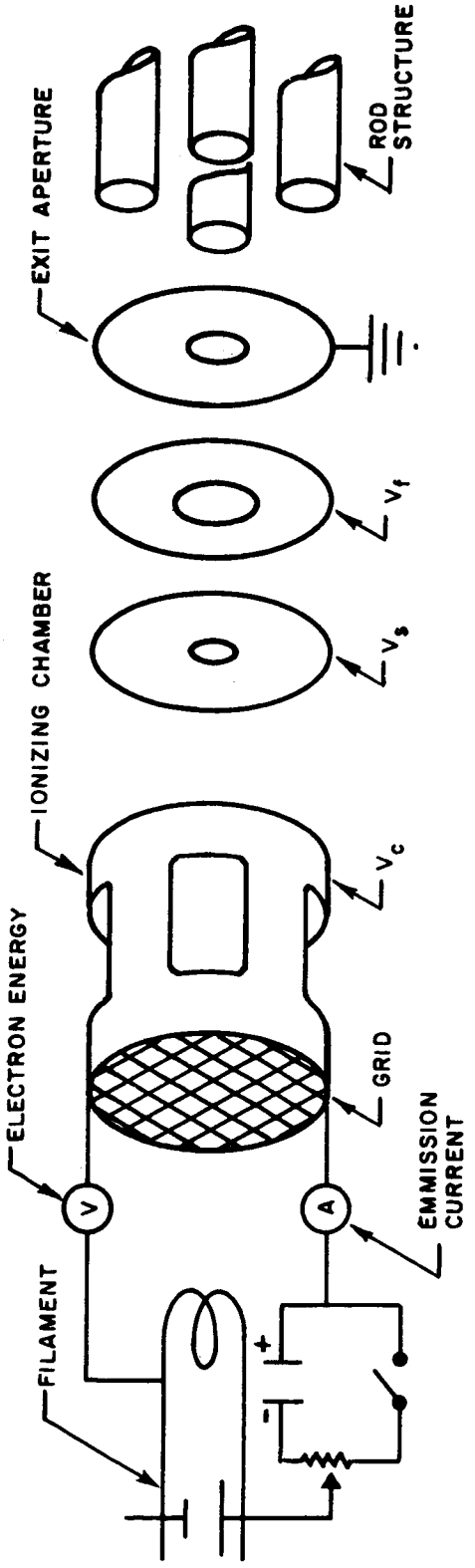
EXIT APERTURE
ROD STRUCTURE
IONIZING CHAMBER
V_f
V_s
ELECTRON ENERGY
V_c
GRID
EMMISSION CURRENT
FILAMENT
V
A
+
-

Figure 7

Therefore, the energy with which the ion enters the quadrupole structure is determined by the potential on the ionizing chamber. The lens system serves the dual purpose of extracting the ions from the chamber and giving them optimum entrance conditions with respect to velocity and position when entering the quadrupole structure.

The ionizer and lens system is constructed of tungsten, alumina and type 304 stainless steel. It is well suited to applications in the high to ultra-high vacuum range (10^{-5} - 10^{-15} torr).* Variations of this ionizer may be used to suit the particular user's needs.

Quadrupole Section: The quadrupole section is composed of four stainless steel rods which are attached to alumina insulators. This structure is enclosed in a stainless steel cylinder. The ionizer attaches to one end and the ion detector the other. The critical parts are machined to a tolerance of better than 0.0002 inches. If reasonable care is taken, the assembly can be disassembled, cleaned and reassembled without difficulty. The filter is designed for 400°C. baking and has actually withstood a 900°C. bakeout; however, the latter resulted in a deterioration of resolution.

D.C./R.F. Generator: The D.C./R.F. Generator supplies the D.C. and R.F. voltages to the poles and regulates the ratio of the voltages to the desired level. Three RF frequencies are employed to provide a mass range of 1 to 500 amu. These frequencies correspond to 1-50 amu, 10-150 amu and 50-500 amu for the EAI Quadrupole RGA. The fine selection of the mass unit measurement is accomplished by varying the R.F. and D.C. voltages. This operation may be either manual or automatic. During automatic operation, the full range of mass units for the given frequency are scanned in times as short as 10 milliseconds. This is accomplished by sweeping the voltage amplitudes in the form of a sawtooth while holding the voltage amplitude-ratio constant. A resolution control is provided to change the amplitude-ratio manually.

The maximum R.F. voltage is about 1000 volts. As required by the stability diagram, the maximum D.C. voltage is about 170 volts. The D.C./R.F. Generator is designed so that its frequency is stabilized to better than one part in 5000. Through use of feedback techniques, the R.F. and D.C. amplitudes are stabilized to better than one part in 100,000. These stability levels are required for satisfactory operation of the analyzer. This is implicitly shown by the stability diagrams (Figures 5 and 6).

Detectors: Collection of the ions at the output end of the spectrometer is accomplished by the use of a Faraday cup or an electron multiplier.

The Faraday cup detects singly charged particles on a one-to-one input to output ratio regardless of their energy, mass or cross section. Unfortunately, it lacks the sensitivity required for measuring low partial pressures at reasonable scan rates.

---

*torr = mm Hg

The EAI electron multiplier is a bakeable (400°C.) multiplier with internal vacuum-sealed resistors, beryllium-copper dynodes, and a current gain when new of about 5×10^6. Positive ions strike the first dynode and produce secondary electrons which in turn strike the second dynode, starting an electron cascade. The secondary emission ratio for properly activated Be-Cu dynodes varies from 2.3 at 100 volts per stage to 5.5 at 400 volts per stage (4). While this ratio is considerably lower than the ratio of several other common dynode materials, (i.e., silver-magnesium has a secondary emission ratio of 9.5 at 400 volts per stage (4)) it appears to give the best long-term gain stability.

The electron multiplier allows sweep times as low as 10 milliseconds to be used. It is also used to make ion current measurements in the quadrupole system corresponding to a partial pressure of 10^{-14} torr and lower. Its limitations are its susceptability to contamination and its response non-linearity over the mass spectrum.

Normally, the output of the electron multiplier is amplified by a D.C. amplifier and displayed on an oscilloscope or recorder. An electrometer amplifier may also be used. The quadrupole analyzer is supplied with or without a vacuum enclosure.

1-D. Experimental Data:

Resolution: Two peaks of equal height are said to be resolved when the valley between them is 10 percent of the height of either peak. For example, the spectrometer would be said to have a resolution of 100 if the valley between two peaks corresponding to isotopic masses 100 and 101 was 10 percent of the peak height of either.

Based on this definition, resolutions of approximately 200 have been obtained as shown in Figure (8). For a R.F. Quadrupole Mass Spectrometer, resolution is highly dependent upon the stability of the D.C./R.F. Generator, the alignment of the filter rods, the length of the Quadrupole structure, the frequency of the D.C./R.F. Generator and the injection energy of the ion.

Sensitivity and Linearity: The sensitivity of a clean spectrometer system using a freshly activated electron multiplier is at least 10^{-14} torr. A partial pressure measurement of 4×10^{-13} torr is presented in Figure (9).

Sensitivity can be enhanced by increasing scan time and noise filtering. With a scan time of 50 milliseconds, partial pressures of 10^{-11} torr are readily observed on an oscilloscope.

Two general types of system non-linearities are possible. The first type is a non-linearity in the mass number dispersion observed at the beginning of the sweep where the R.F. voltage is not able to track the D.C. voltage. Throughout each quoted mass range, the dispersion is virtually constant, however.

The second type of non-linearity is a quantitative non-linearity resulting in abundance ratio errors.* This non-linearity is primarily produced by a combination of effects in the ionizer and the electron multiplier.

As an extreme example of ionizer non-linearity, consider the case where equal molar amounts of helium (ionization potential 24.5 eV) and cesium (ionization potential 3.9 eV) are present. Since more cesium is ionized than helium, the number ratio of cesium ions to helium ions captured by the multiplier cannot be one-to-one. Therefore, in making abundance ratio measurements of this type it is necessary to have known standards available for calibration.

The response of the electron multiplier is not only dependent upon the ion's charge, but also its mass and cross-section. That is, equal currents of He and Ce ions reaching the multiplier will not produce signals of equal magnitudes. Also, ions of the same mass and charge (i.e., halfnium and anthacene) may produce different numbers of secondary electrons in striking the first dynode.

The quantitative non-linearity of the multiplier is caused primarily by ion velocity differences. Ploch and Walcher (5) have shown that the number of secondary electrons produced by isotopes of a given atom depends only upon ion velocity. This effect has been observed by EAI and SRI and is corrected for by the relation,

$$\frac{I_1}{I_2} = \sqrt{\frac{m_2}{m_1}} \qquad (17)$$

where I_1 and I_2 are the amplitudes of the signals produced by isotopes of massed m_1 and m_2. Isotopic abundance ratios for Xenon and Krypton are shown in Figures (10) and (11).

In general, if it is necessary to accurately analyze material composition more diverse than the isotopes of a particular element, it becomes necessary to calibrate the spectrometer system with a standard known mixture.

Speed of Response: One of the assets of the EAI Quadrupole Mass Spectrometer is its ability to scan one mass range of the spectrum in 10 milliseconds or less. Beyond a certain minimum sweep rate, both intensity and resolution decrease. This is caused by ion "flight-times" becoming relatively short with respect to sweep time. In general, it is not recommended that sweep times less than 50 milliseconds be used for precision analyses.

---

*The density ratios of substances in the ionizing volume are commonly called abundance ratios.

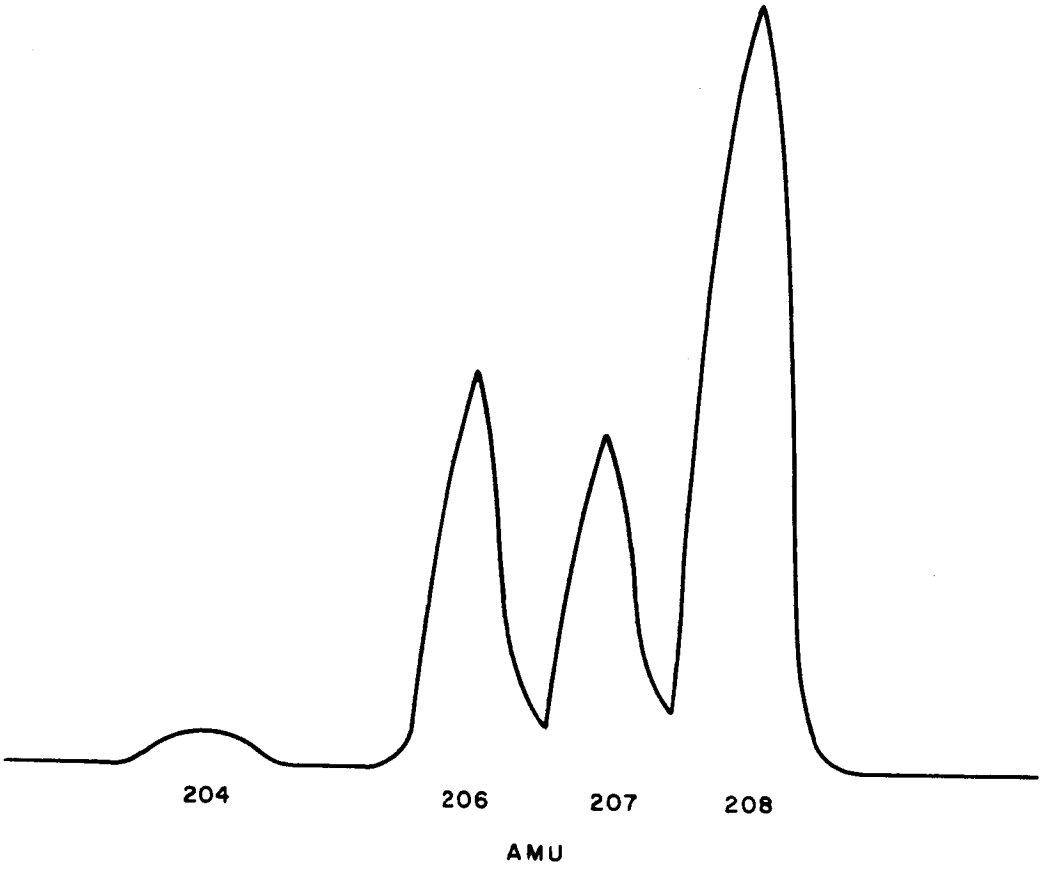

Isotope	Measured Isotopic Fraction (Percent)	Actual Isotopic Fraction (Percent)
204	1.40	1.37
206	25.50	26.26
207	21.20	20.82
208	51.80	51.55

Figure 8

Lead Spectrum

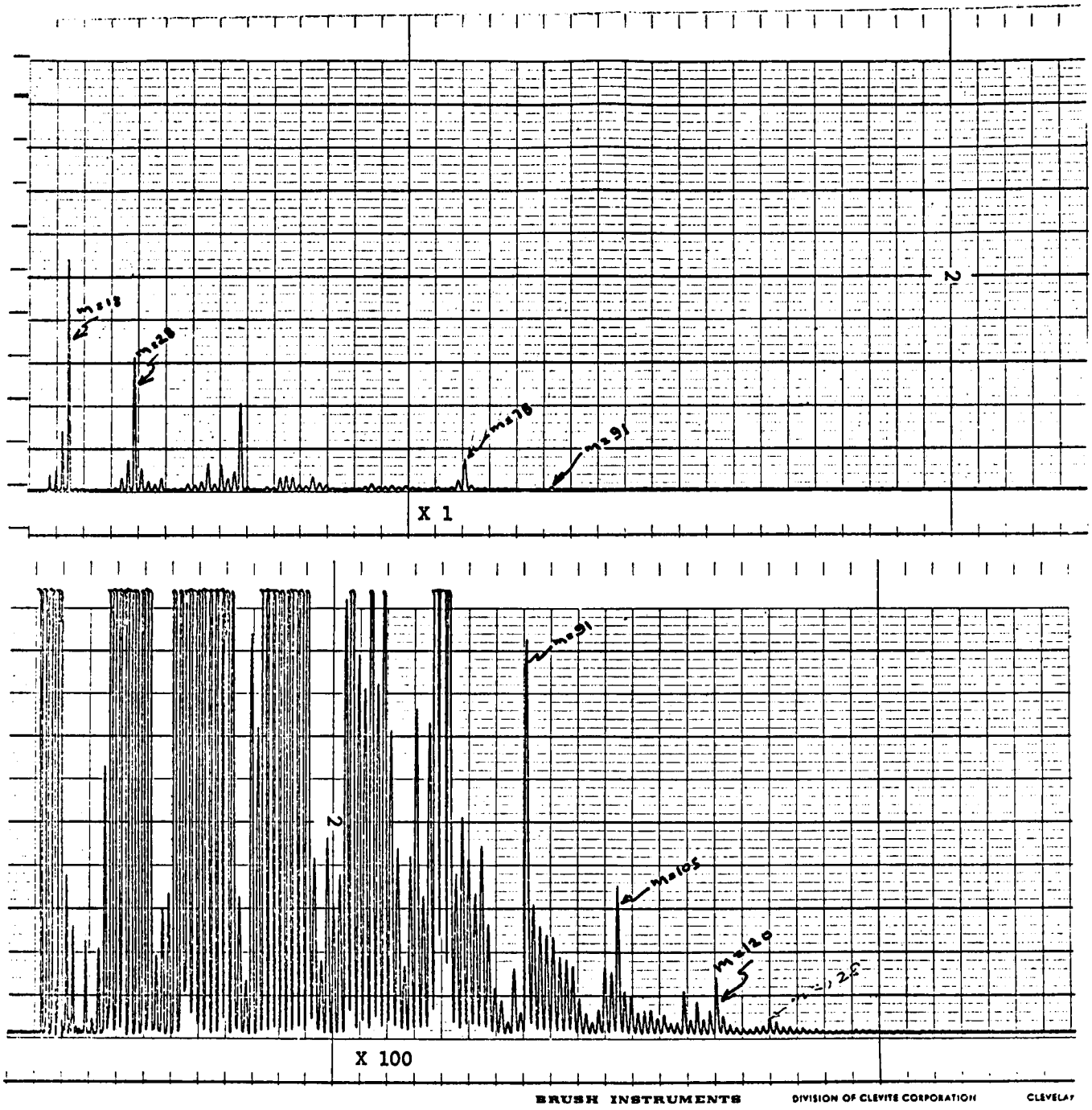

FIGURE 9

Partial Pressure Sensitivity

Total Pressure = 7×10^{-8} Torr.

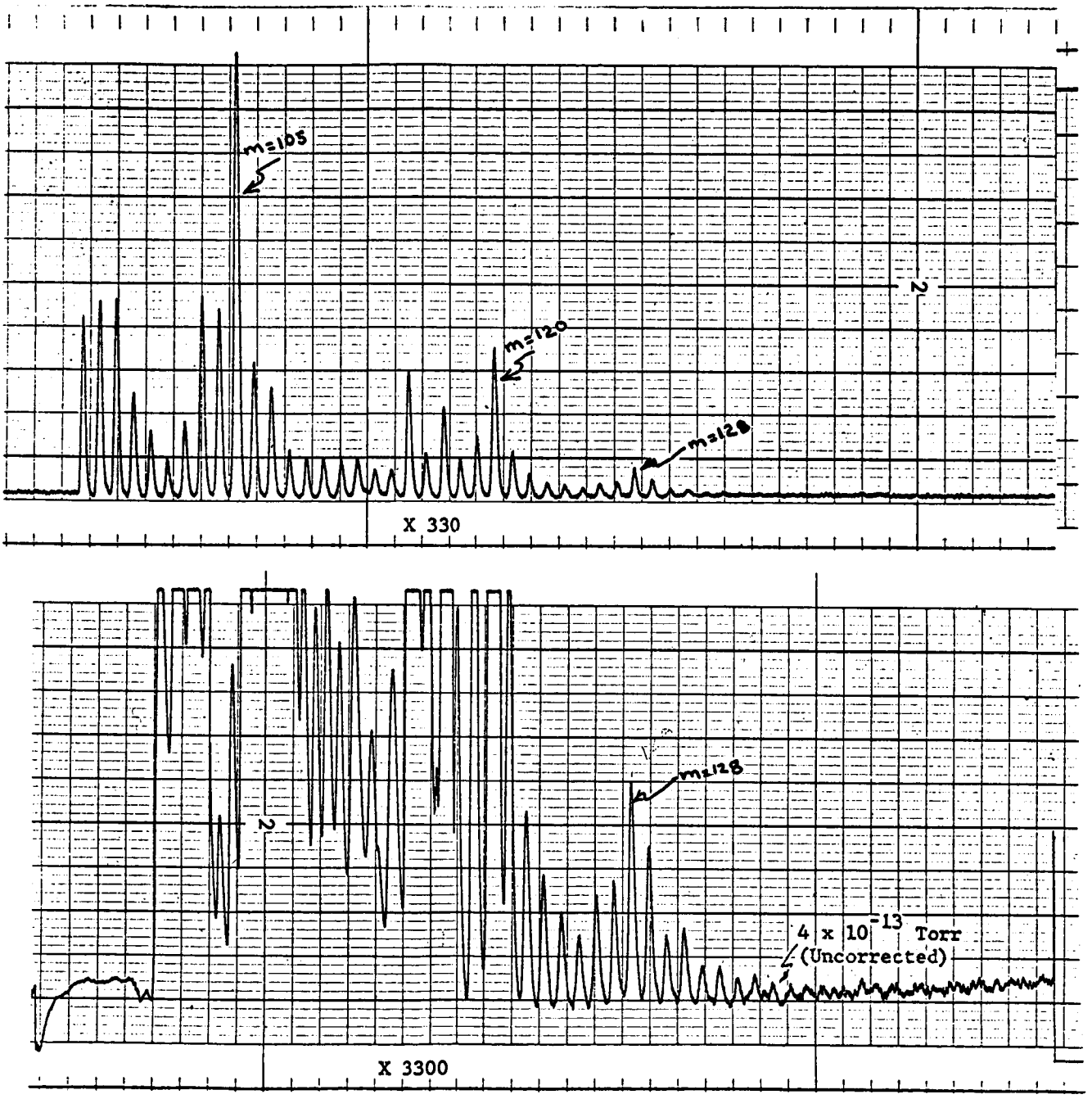

FIGURE 9a

AMU	MEASURED & CORRECTED ISOTOPIC FRACTIONS (PERCENT)	LITERATURE VALUE ISOTOPIC FRACTIONS (PERCENT)
128	1.6	1.92
129	26.1	26.23
130	4.4	4.05
131	21.0	21.24
132	26.9	26.93
134	9.6	10.52
136	7.7	8.93
124, 126 AMU not measured Total Pressure $\simeq 7 \times 10^{-7}$ Torr		

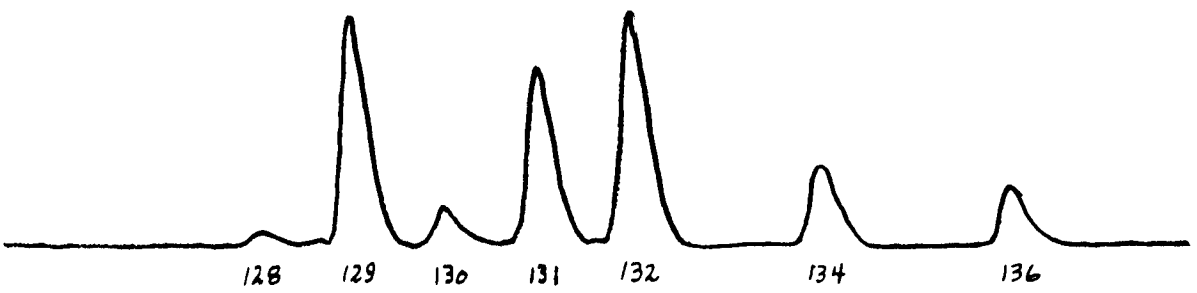

Figure 10

Xenon Spectrum

Total Pressure = 5×10^{-7} torr.

Typical Krypton Spectrum

Mass	Actual Abundance Ratio	Observed Ratio	% Deviation
82	11.56	12.1	+ 5.3%
83	11.55	12.1	+ 5.3%
84	56.90	56.90	None
86	17.37	16.8	- 3.0%

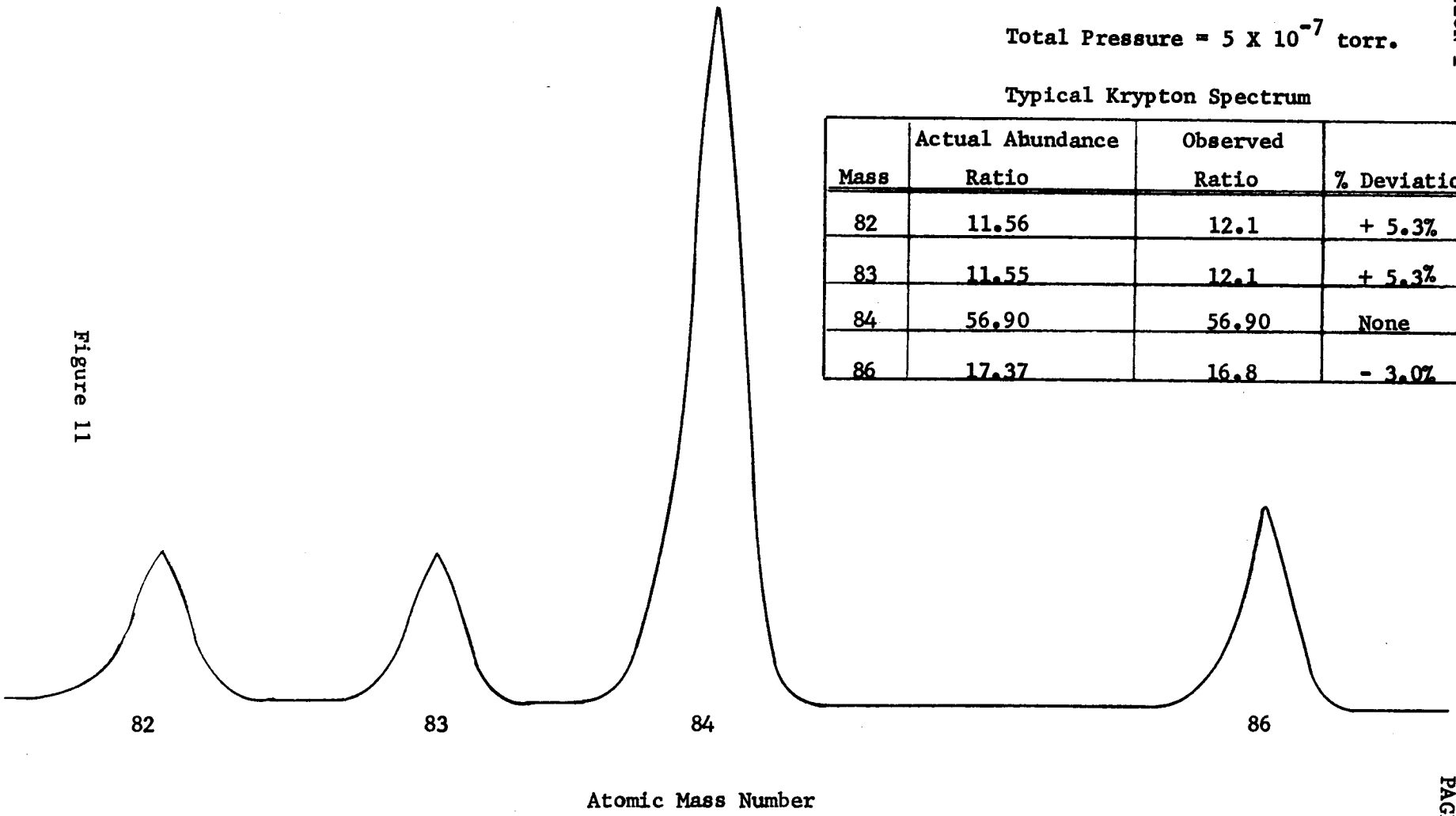

Figure 11

Long-Term Stability of the System: Long-term instabilities are caused primarily by electron multiplier gain changes and focusing system contamination when operated for extended periods at pressures greater than 10^{-6} torr. The gain of an EAI multiplier deteriorates after several days of use from 5×10^6 to about 10^5. Upon reaching a gain of about 10^5, the multiplier appears to restabilize itself. The gain loss of 50 is due to a combination of hydrocarbon contamination and activated surface deterioration.

The second source of instability is caused by focusing system and analyzer rod contamination. This occurs when the spectrometer is operated for an extended time in a high hydrocarbon background. The polymerized hydrocarbons form a dielectric coating on the surfaces which makes sensitivity and resolution adjustments extremely critical. In addition, spectra peaks will begin to take on a "ragged" appearance.

Contamination is minimized by operating the quadrupole at the lowest pressures available.

Conclusions: A highly stable D.C./R.F. Generator combined with four accurately aligned filter rods makes possible a compact mass spectrometer with a sensitivity of 10^{-14} torr and a resolution of twice unity. It is significant that this performance can be obtained with sweep times as low as 50 milliseconds.

For optimum performance, the spectrometer system should be cleaned by baking at 400°C. and should be operated within a vacuum in which the hydrocarbon background pressure is 10^{-7} torr or less.

When precise abundance ratio measurements are to be made on samples of varying atomic numbers, it is necessary to calibrate the system using mixtures of known composition which approximate the sample's composition. An abundance ratio measurement of the isotopes of one atom does not require use of standards but should be corrected by the inverse-square-root relation because of the non-linear response of the electron multiplier.

19 February 1965

REFERENCES

1. McLachlan, N., Theory and Applications of Mathieu Functions, (Oxford Press, 1947).

2. Paul, W., H. Reinhard and V. Von Zahn, Z Physik, 152, No. 2, Page 143, (1958).

3. Rice, P., Quadrupole Mass Spectrometers, Interim Report No. 2, (Stanford Research Institute, 1962).

4. _____, DuMont Multiplier Phototubes, (DuMont Laboratories, 1963).

5. Baynon, J., Mass Spectrometry and Its Applications to Organic Chemistry, (Elsevier Publishing Co., 1960).

EAI Series 210
Residual Gas Analyzer

ULTEK

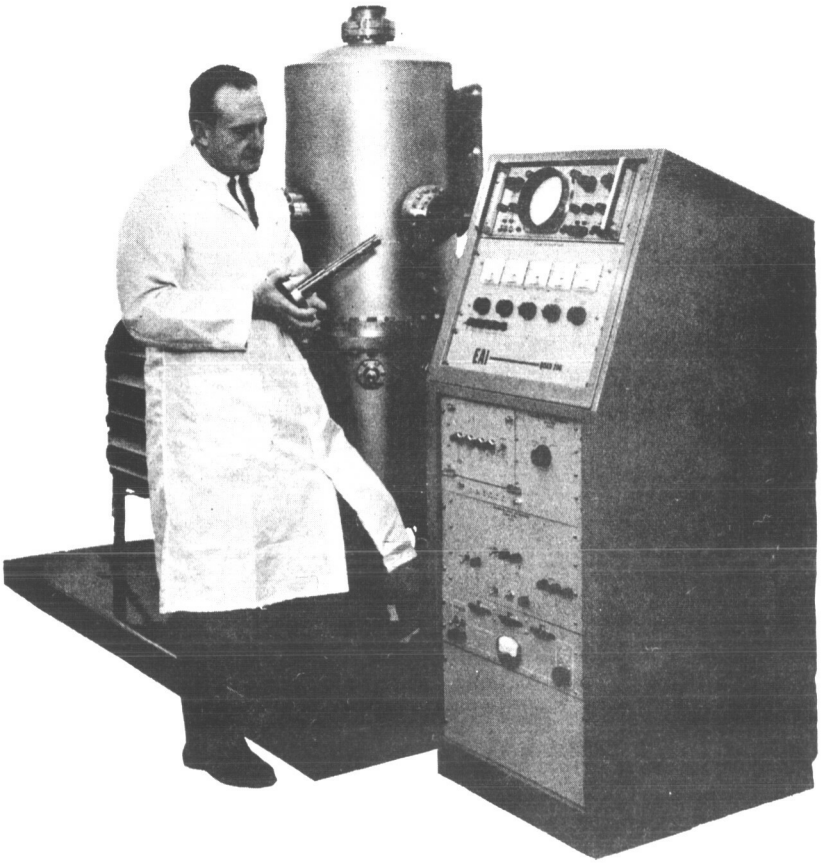

RESIDUAL GAS ANALYZER

PRINCIPLES OF DESIGN & OPERATION

SECTION	CONTENTS	PAGE
1-A	DESCRIPTION	1
1-B	THEORY OF OPERATION	1 Through 10
1-C	EQUIPMENT	10 Through 14
1-D	EXPERIMENTAL DATA	14 Through 18

Distributed By: ULTEK CORP.
Manufactured By: ELECTRONIC ASSOCIATES, INC.

19 February 1965
B-1320-3/65

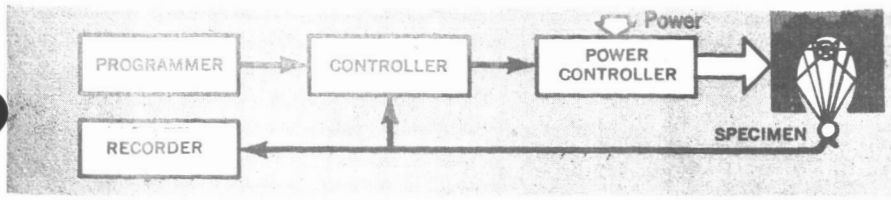

INFRARED HEATING SYSTEMS

INFRARED LINE HEATER MODEL 5215

HIGH-INTENSITY INFRARED ELLIPTICAL-REFLECTOR

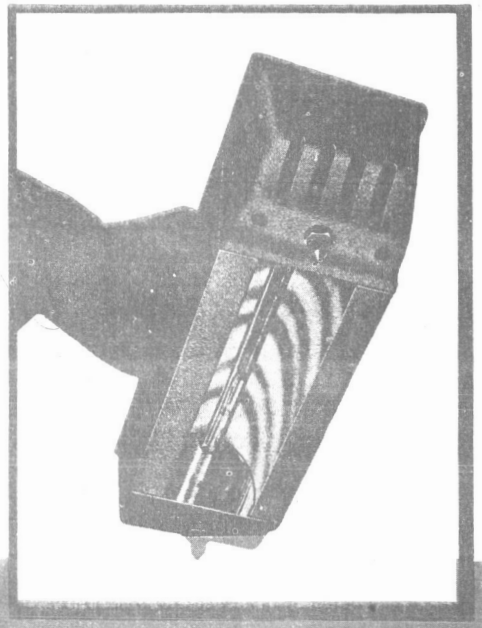

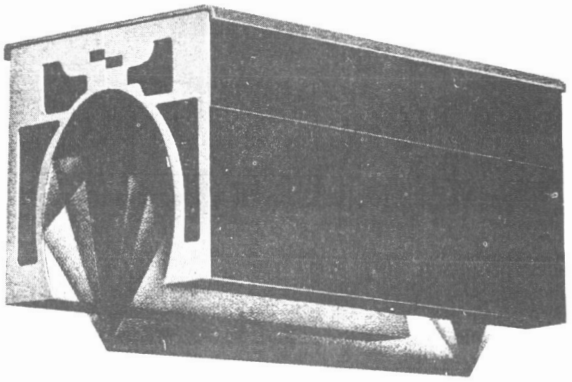

LINE HEATER

Compact Model 5215 Infrared Line Heater generates highly-concentrated radiant heat flux density along a thin line at the external focal axis of an elliptical reflector. The radiant energy emitted from a high-temperature (4000-5400°F) tungsten filament enclosed in a clean quartz envelope is direct-imaged on an external focal line by a highly polished aluminum elliptical reflector.

The Line Heater produces rapid heating rates and high workpiece temperatures dependent upon geometry and heat loss characteristics of the material to be heated. Typical heating rate performance curves are shown in the chart at left. Note table of standard Line Heater lengths and other specifications on reverse side.

IMPORTANT LINE HEATER FEATURES

CONCENTRATED HEAT FLUX DENSITY — High density radiant heat energy concentrated on a focal line produces rapid heating to high temperatures on material objects located on this line.

RAPID RADIANT ENERGY OUTPUT — Rapid emitter response provides efficient heating within seconds after power applied. The lamp filament emitter reaches 90% of its full operating temperature within 3 to 4 seconds, due to its relatively low thermal mass.

RAPID COOL-DOWN — Radiant energy dissipates to only 10% within 5 seconds after power is cut, due to the rapid cooling rate of the low-thermal-mass emitter — an important factor in plastics work.

VARIABLE HEAT DENSITY — Variations in radiant heat flux density at the focal line can be attained by varying the lamp voltage.

ADJUSTABLE FOCAL LINE — Pins are provided on the reflector end covers to aid the user in narrowing or broadening the focal line and to accommodate various specimen thicknesses. Additional threaded holes are also provided for adding four stabilized-support pins or caster accessories.

STANDARD SIZES — Available with 5- to 25-inch lighted lengths (see Specifications on reverse side).

MODULAR UNITS — Ideal components for a wide variety of systems or radiant heating arrays.

WATER COOLING within the reflector is provided for applications where high heat flux density or long-term operation is required. Also permits operators to work closely with equipment for extended periods without discomfort.

GAS PURGING — Purging port for applications where the specimen is to be heated in a non-oxidizing atmosphere. This purging system also provides a means for cooling the quartz envelope of the lamp if desired.

EASY SERVICING — The Line Heater is designed for easy servicing. All major elements are assembled to the main frame of the unit. Lamp quickly replaced by removing 4 cover screws.

EXAMPLES OF HEATING RATES

Heating rates are dependent on (1) voltage applied to the heater, (2) specimen or workpiece characteristics and (3) specimen heat loss characteristics. Below are examples of two typical metal rod specimens (stainless steel with surfaces blackened to increase absorption) indicating the heating rate on each specimen with the Line Heater operating on each of four voltages.

NOTE: An anti-radiation loss reflector shield or thermal insulator will permit more rapid heating rates and higher workpiece temperatures. Note curve "T" with Line Heater operated at double rate voltage.

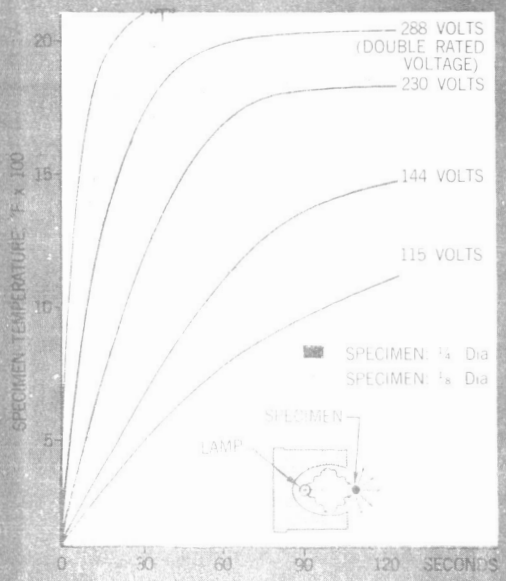

TYPICAL SPECIMEN HEATING RATES FOR MODEL 5215-5 LINE HEATER WITH 1200T3/CL/HT LAMP

APPLICATIONS

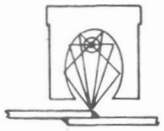

LINE SEAM BRAZING
Braze joints with aluminum, copper, stainless steel, etc., by rapid localized concentrated line heating. Automate your brazing operations with line heaters at various stations.

MATERIALS TESTING
Generate high radiant heat flux densities on linear specimens to produce high heating rates.

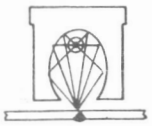

WELD JOINT HEATING
Maintain weld joint at elevated temperatures during welding according to metallurgists specifications as is required for many exotic alloy steels.
Post weld anneal weld joint with same line heater unit.

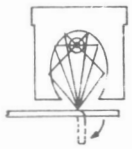

PRE-BEND HEATING
Locally anneal hardened metals or soften plastic prior to sharp bending to prevent bend fatigue.

STRIP HEATING
Continuously heat or heat indexed portions of moving strip material.

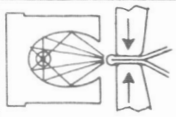

PLASTIC JOINING AND SEALING
Join and seal thermal setting plastics with short term high intensity radiant energy.

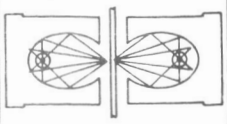

DOUBLE POWER
Increase heat flux by adding another unit on opposite side.

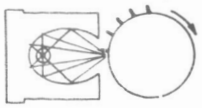

CYLINDER HEATING AND BRAZING
Braze parts (such as cooling fins) to indexed portions of rotating cylinder.

OPTIONAL ACCESSORIES*

The following optional accessories can be attached to standard Line Heater units to facilitate their use for certain applications:

OPTION H — Carrying Handle
For easy portability. Length varies with Heater model. See Specifications for ordering details.

OPTION C — Caster Assembly
Used to convey the Heater over an area to be scanned or index-heated. Set of four.

OPTION S — Support Pins
Provides four-point adjustable Heater support for fixed heating and brazing applications. Set of four.

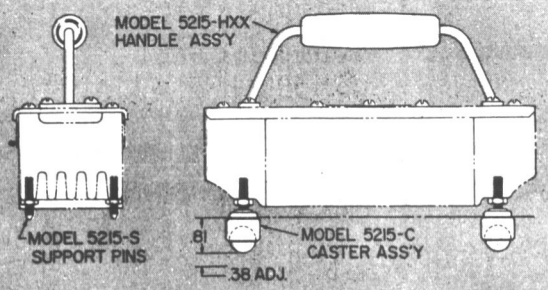

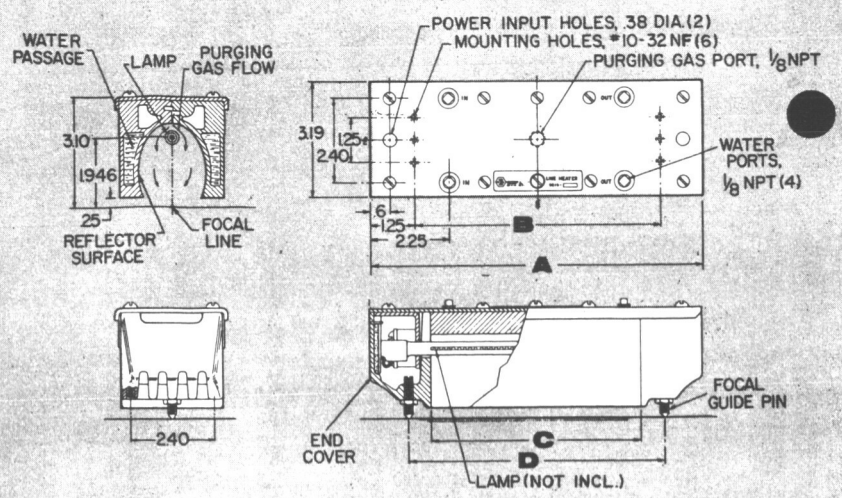

PERFORMANCE DATA

HEAT FLUX DENSITY	High density radiant heat flux up to 453 watts per linear inch (based on calorimeter tests) on a narrow (.06 to .09 inch) focal line can be generated.
POWER RATINGS ▲ ●	See table. Units may be operated at up to double rated voltage for short duty cycles provided the lamp envelope and reflector are not permitted to overheat. When operating Model 5215-25 at twice rated voltage, special electrical insulator considerations must be made.
EMITTER CHARACTERISTICS	Emitter is a tungsten filament in Argon atmosphere enclosed in a 3/8 inch (O.D.) clear quartz tube. Operates at approximately 4000°F at rated and 5400°F at 2X rated voltage, with .83 and .64 micron spectral energy peak, respectively.
REFLECTOR	The reflector used to focus the energy radiated from the linear emitter filament is a two-dimensional ellipse of specular aluminum with provisions for water cooling and lamp envelope gas cooling.
MODULAR CONSTRUCTION	Line Heater construction consists of an electro-polished stainless steel backbone to which aluminum end covers and reflector are attached.
MOUNTING PROVISION	Six #10-32NF threaded holes are provided on the main frame for mounting and for attaching various accessories such as a handle.
SERVICES ■	Power is applied to lamp through 3/8" dia. holes at each end of main frame. Clean water at 70°F or less for reflector cooling should be supplied to the reflector through four #1/8-27 NPT ports provided. Gas for purging the work-piece heated area or for cooling lamp envelope can be introduced through the #1/8-27 NPT port centered on the main frame.

SPECIFICATIONS

MODEL NUMBER	5215-5		5215-10		5215-16	5215-25	
(From Dimensional Dwg. Above) A Overall Length, Inches	9.50		14.50		20.50	29.50	
B Mounting Hole Location, Inches	7.000		12.000		18.000	27.000	
C Chamber Length, Inches	6.00		11.00		17.00	26.00	
D Guide Pin Distance, Inches	7.38		12.38		18.38	27.38	
Weight, Pounds	4.0		6.0		8.3	11.9	
HANDLE (Optional)	-H5		-H10		-H16	-H25	
LAMP (one required, not incl.) Type	500T3/CL/HT	1200T3/CL/HT	1000/T3/2CL/HT	2000/T3/CL/HT	1600T3/CL	2500T3/CL CL/HT	5000T3/1CL/HT
Lighted Length, Inches	5.0	6.0	10.0	10.0	16.0	25.0	25.0
Rated Voltage	120	144†	240	240	240	480	600
Current, Amps	4.17	8.34	4.35	8.70	6.96	5.32	8.33
Rated Power, KW ▲	.5	1.2†	1.0	2.0	1.6	2.5	5.0
Power at 2x Rated ▲ Voltage, KW	1.4	3.4	2.8	5.7	4.5	7.1	14.2●
Water Coolant Flow, GPM■	.05	.12	.10	.20	.16	.25	.50
Heat Flux at Focus, Watts/Lin. Inch. At Rated Voltage	66	143	72	145	75	76	153
At Double Rated Voltage	186	453	203	414	211	128	437

†At 240 Volts 1200 T3/CL/HT dissipates 2.6 KW, produces 346 Watts/lin. inch @ focus
■ At Rated Voltage, steady state conditions

▲ Lamp Lighted Length ▲ "H" Carrying Handle ▲ "C" Caster Assembly (Order Lamp Separately from Table by Part Number)

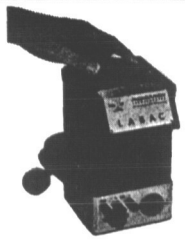

LABAC Solid-State
Proportional Power Controller

CLOSED-LOOP TEMPERATURE CONTROL

Standard R-I Controls THERMAC Temperature/Power Controllers and DATA-TRAK Curve-following Programmers offer practical high-performance closed-loop temperature control for both static (i.e., set point) or dynamic (i.e., programmable) heating conditions.

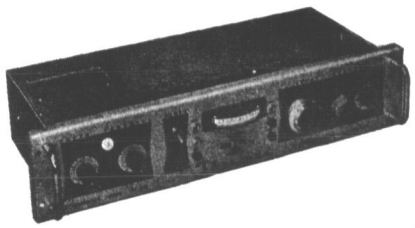

THERMAC Solid-State
Proportional Temperature Controller

R I CONTROLS DIVISION
RESEARCH, INCORPORATED
P.O. BOX 6164 MINNEAPOLIS, MINN. 55424

REPRESENTED BY

Model L . . . offered in 7.5, 10, 14 and 20 cps, is recommended for use in applications where external damping is desirable. This model is characterized by high intrinsic voltage sensitivity.

HS-J MODEL-L SPECIFICATIONS

Standard Frequencies: Model L-1: 7.5, 10, 14 cps
Model L-2: 10, 14, 20 cps

Standard Impedances: Model L-1: 28, 72, 300 ohms
Model L-2: 27, 69, 280 ohms
(Other impedances available)

Basic Unit Height: 1″
Diameter: .875″
Weight: 1.8 oz.

FREQUENCY RESPONSE CURVES

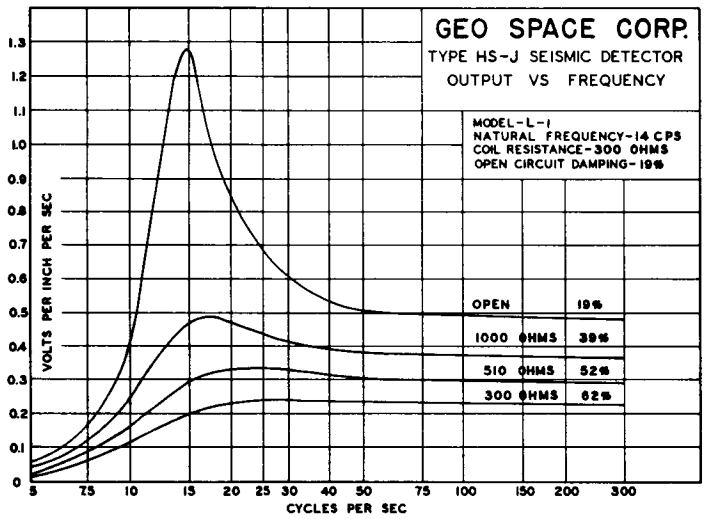

MODEL L-1
NATURAL FREQUENCY—14 cps

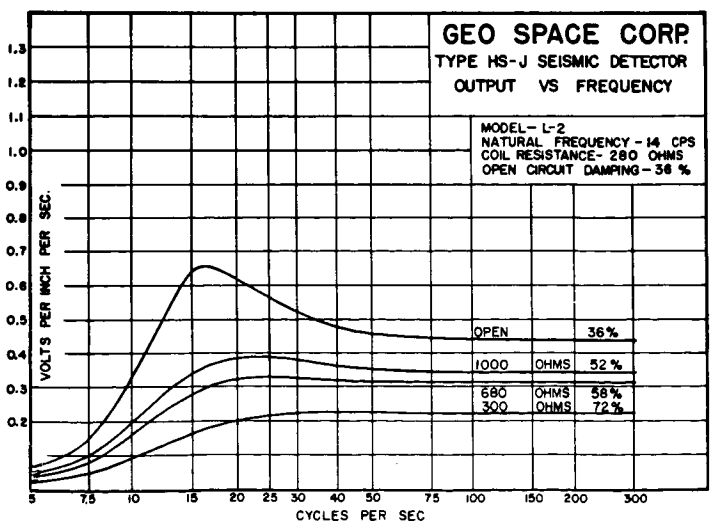

MODEL L-2
NATURAL FREQUENCY—14 cps

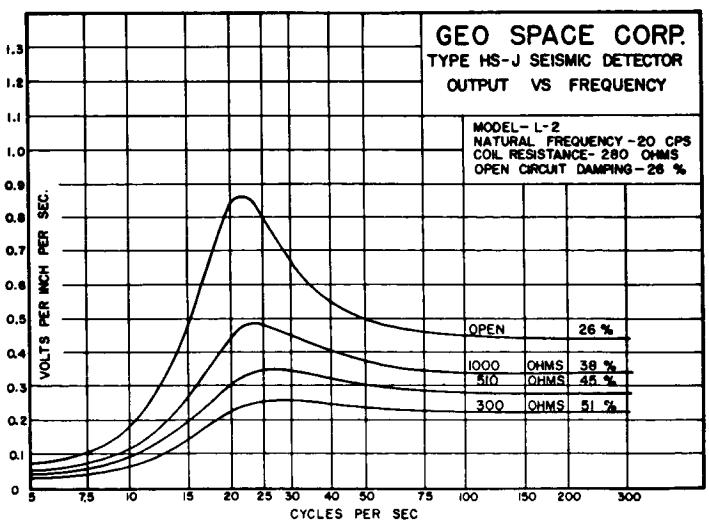

MODEL L-2
NATURAL FREQUENCY—20 cps

Model K . . . has output comparable to that of larger geophones, achieved through the use of thick section aluminum coil form for damping. This model is recommended for all applications utilizing high input impedances.

HS-J MODEL K SPECIFICATIONS

Standard Frequencies: 14, 18, 20, 28, 30 cps
Standard Impedances: 20, 50, 215 ohms
(Other impedances available)
Basic Unit Height: 1″
Diameter: .875″
Weight: 1.8 oz.

FREQUENCY RESPONSE CURVES

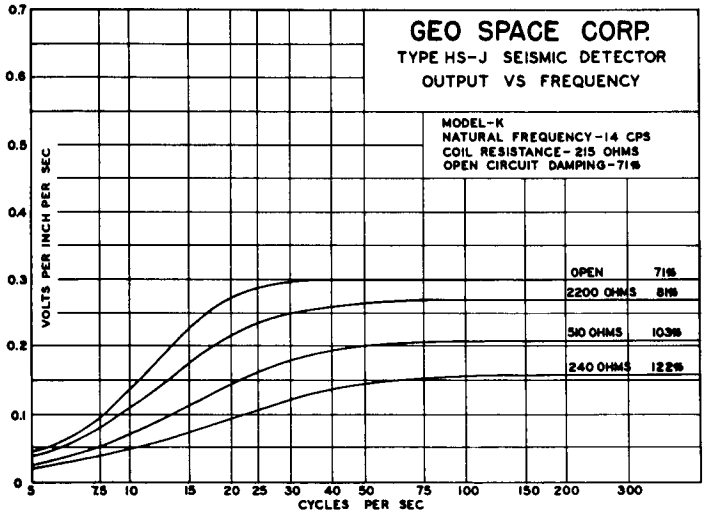

MODEL-K
NATURAL FREQUENCY—14 cps

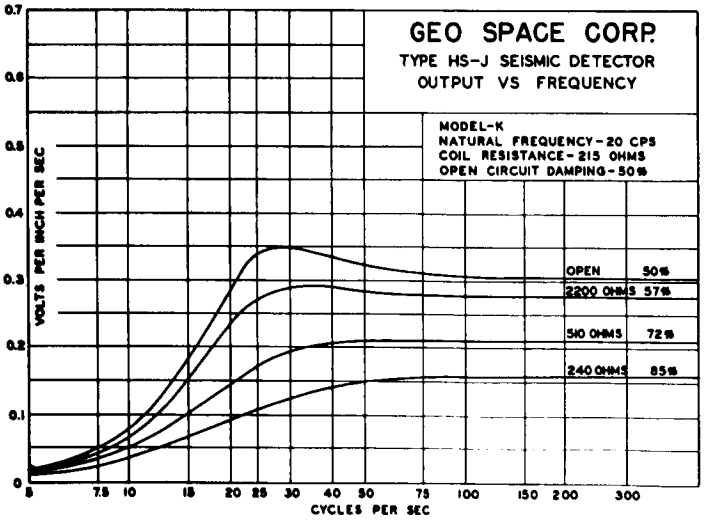

MODEL-K
NATURAL FREQUENCY—20 cps

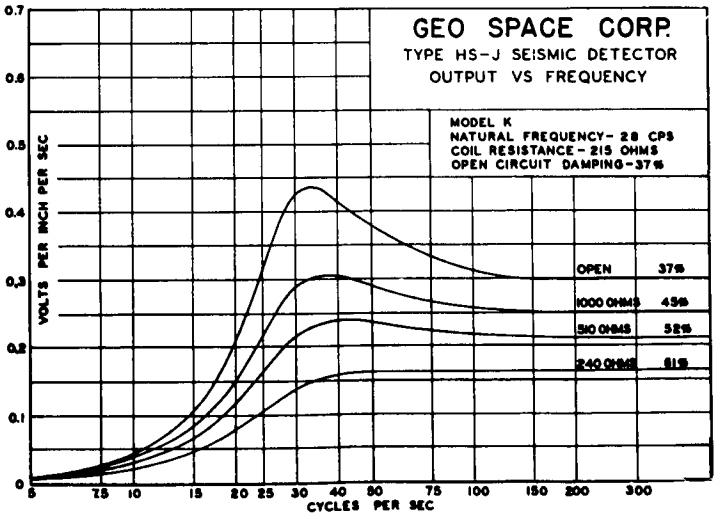

MODEL-K
NATURAL FREQUENCY—28 cps

Hall-Sears Geophone

The PC-7 plastic cases add to HS-J sub-miniature geophone a new dimension of field durability and ease of handling. These new cases, available in the style shown below, are made of practically indestructible Kralastic. They employ a new cable anchoring system that makes the takeout as strong as the cable itself, and reduces the cable wear at the case entry.

NEW CASE DESIGNS INCREASE DURABILITY AND HANDLING EFFICIENCY OF HS-J GEOPHONES

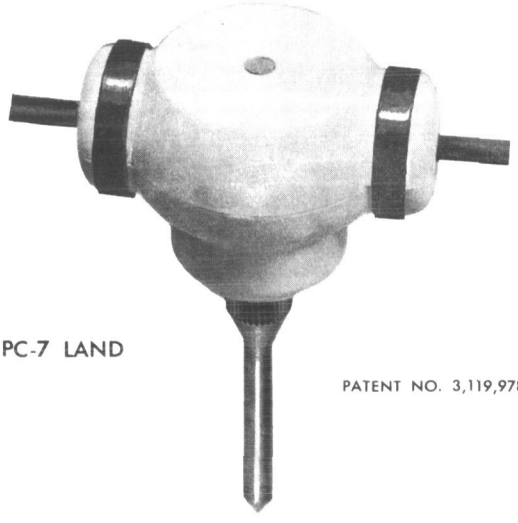

PC-7 LAND

PATENT NO. 3,119,978

DESIGN FEATURES

1. Knot anchoring—makes takeout as strong as the cable itself.
2. Virtually indestructible Kralastic case—light in weight, bright easy-to-see permanent color.
3. Dependable watertight seal by injection of silicone rubber into closed case.
4. Radius at cable entries give longer flexing arc—adds to cable life.
5. Plastic case provides complete insulation from ground—reduces extraneous pick-up.
6. Easy field cabling with knot anchoring and replaceable silicone rubber sealing compound.

HS·J SUB-MINIATURE LAND DETECTOR

ALL HS-J GEOPHONES HAVE DUAL SPRINGS.

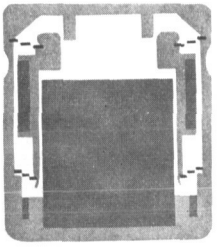

Balanced coil minimizes horizontal sensitivity and spurious resonances. No other geophone with possible exception of the HS-1 has less horizontal sensitivity.

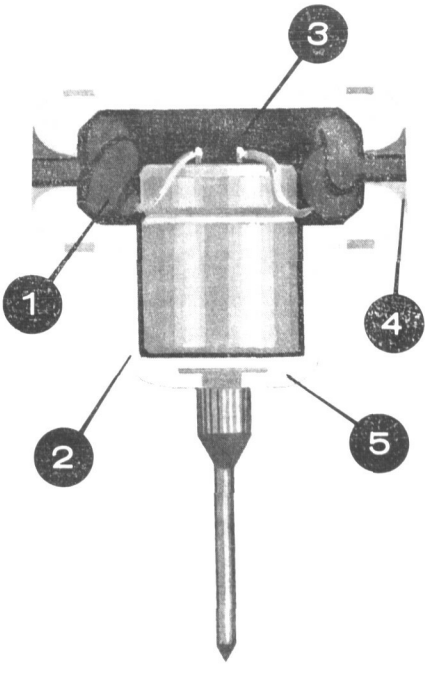

Appendix IX

SPECIFICATION SHEETS

Hall-Sears Geophone
Line Heater
EAI Series 210 Residual Gas Analyzer
STEM Device

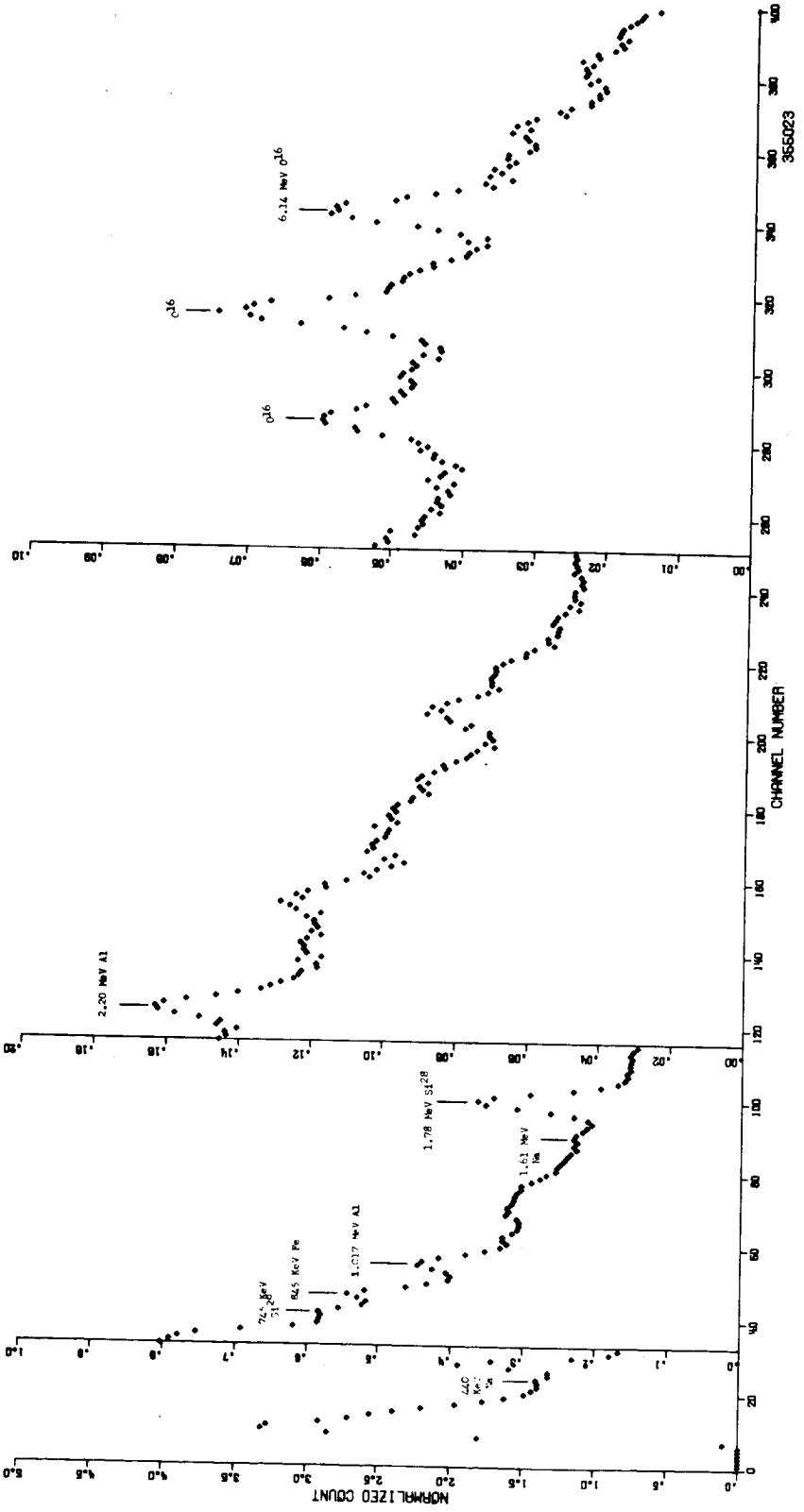
NORMALIZED COUNT
CHANNEL NUMBER
355023
2.20 MeV Al
1.78 MeV Si28
1.61 MeV Na
1.017 MeV Al
845 KeV Fe
745 KeV Si28
440 KeV Na
6.14 MeV O16
O16
O16

Fig. 1

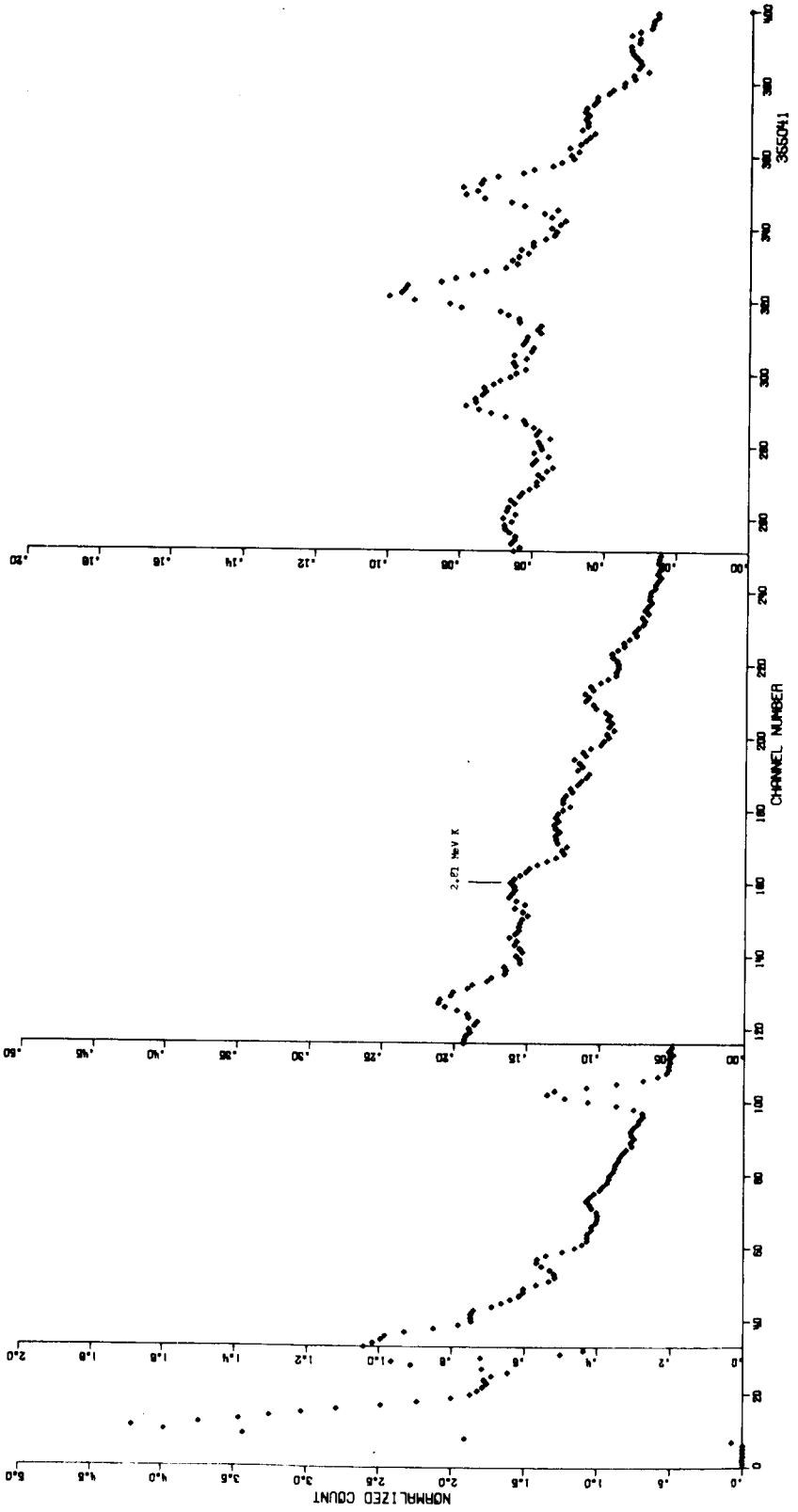

Fig. 2

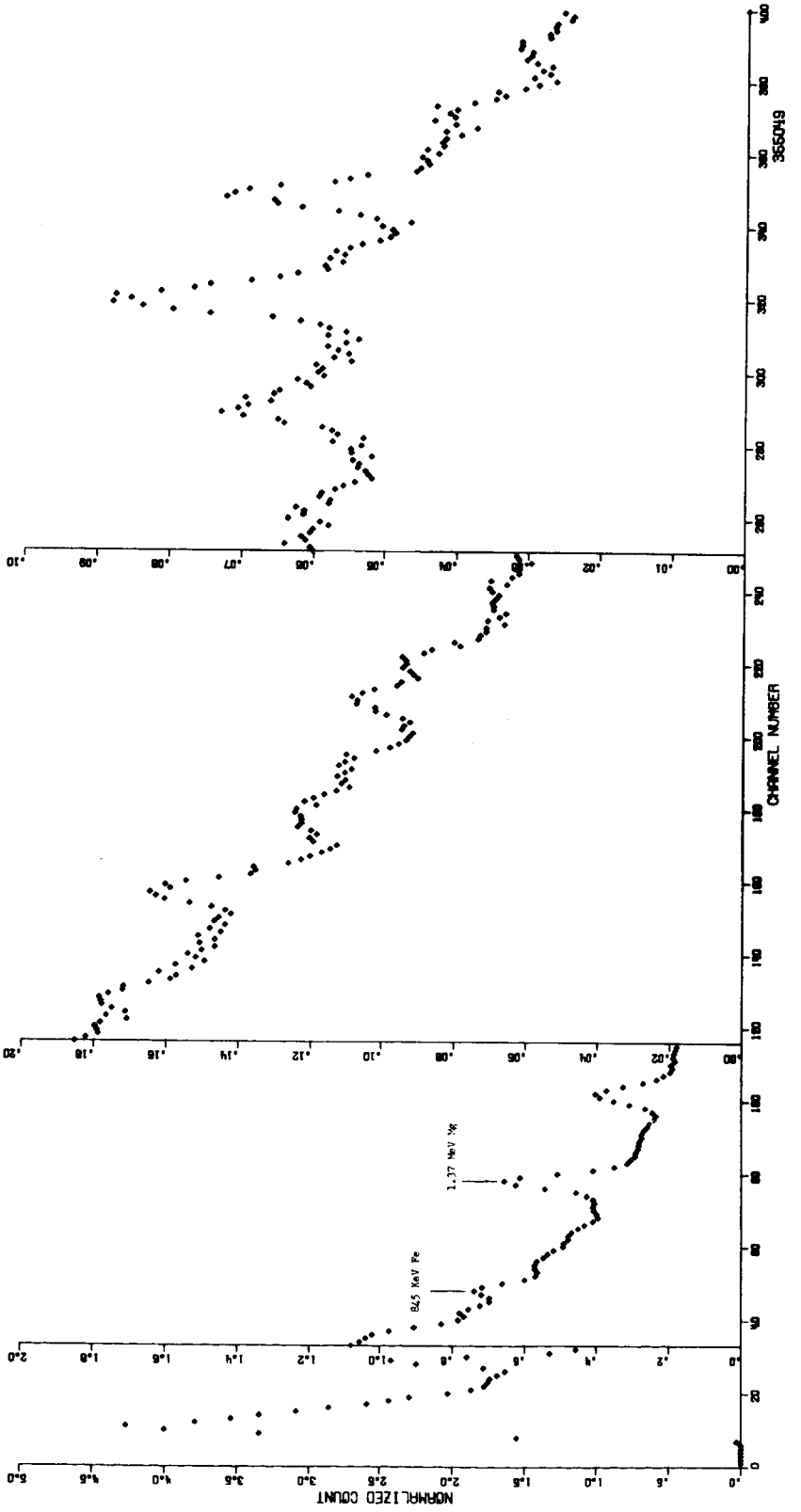
NORMALIZED COUNT
CHANNEL NUMBER
845 KeV Fe
1.37 MeV Ni
365049

Fig. 3

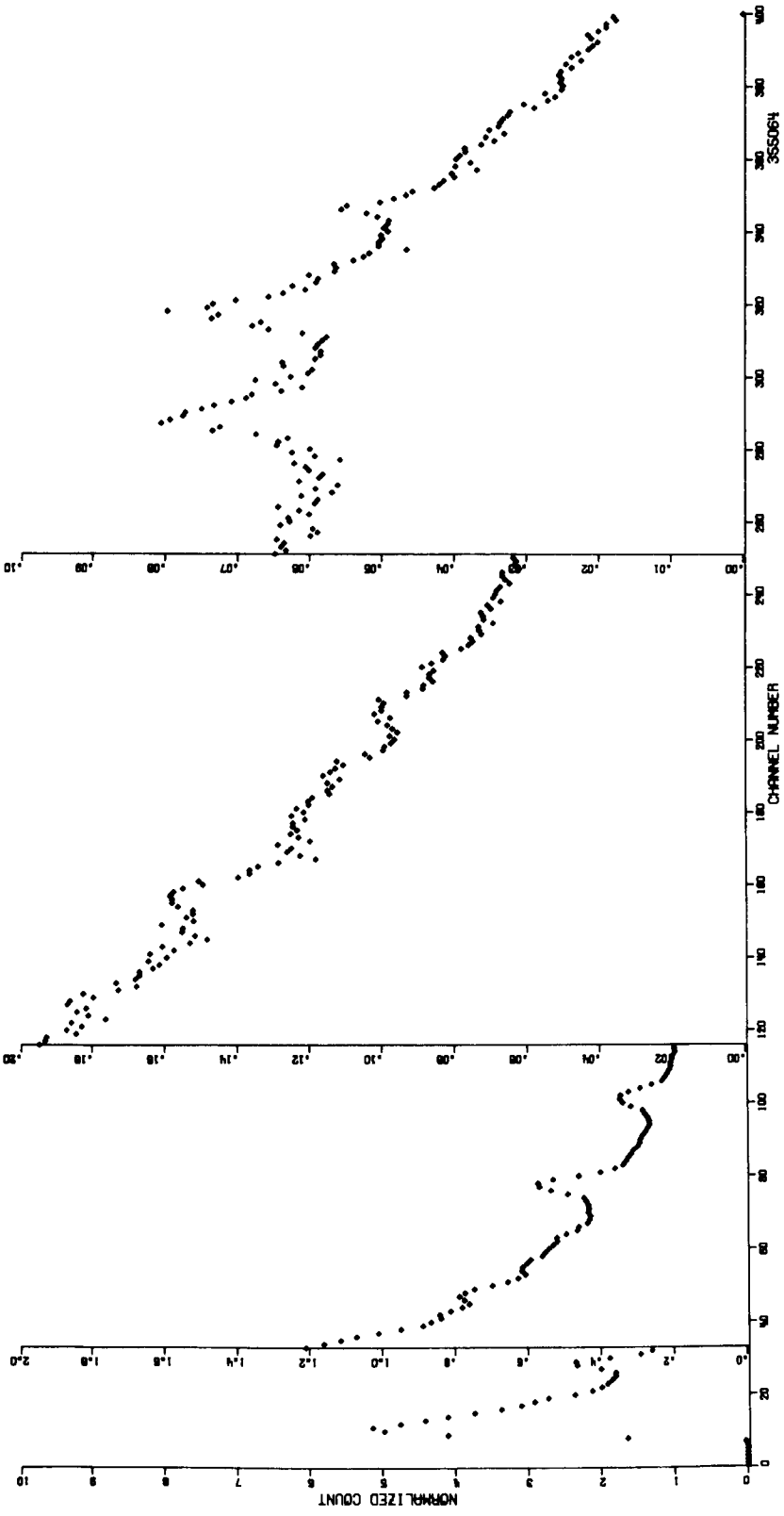

Fig. 4

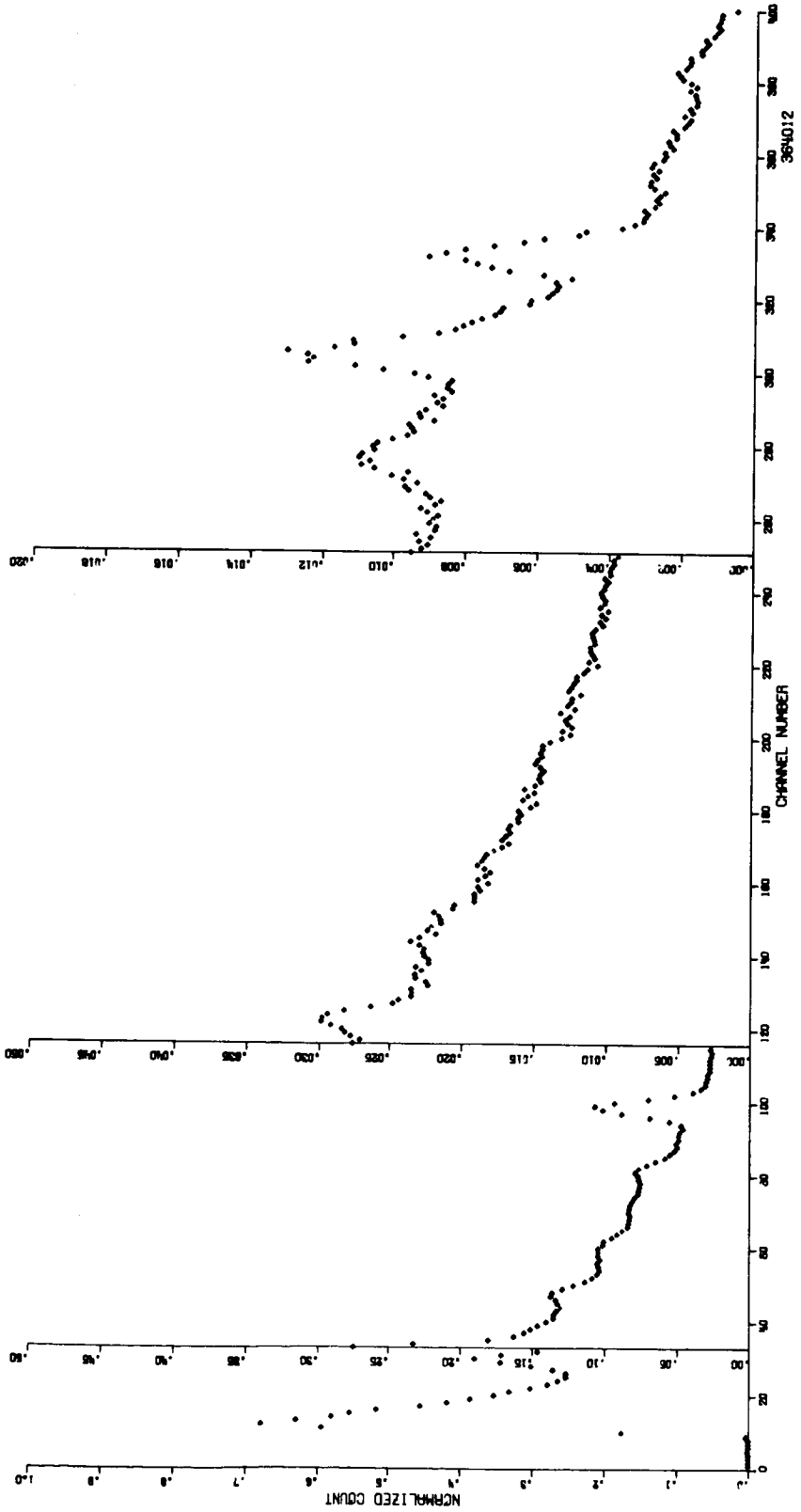

Fig. 5

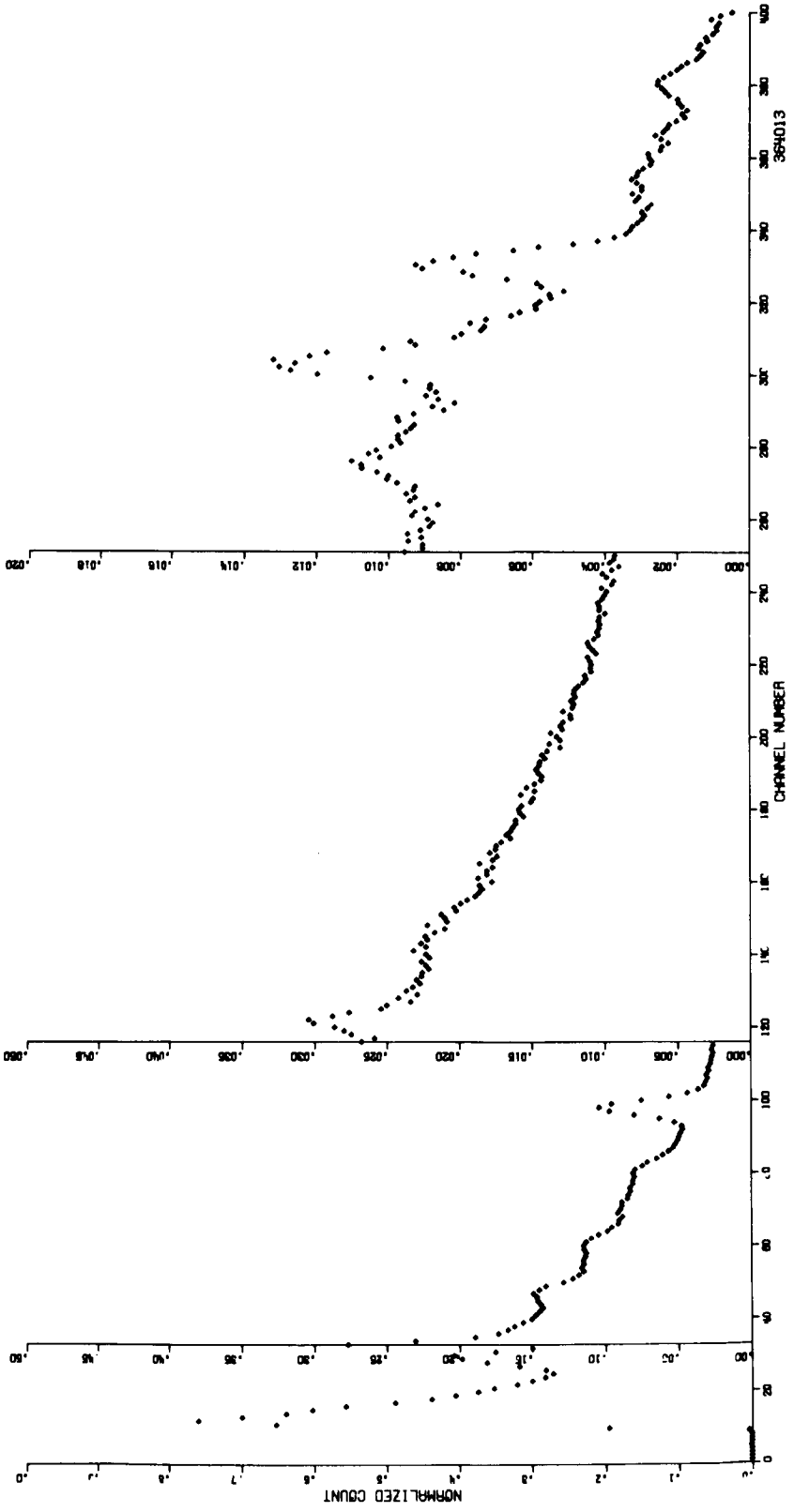

Fig. 6

NEUTRON-GAMMA EXPERIMENT RESULTS

Experiments have been performed by Lawrence Radiation Laboratory (Stinner and Schrader, 1, 2) to determine the feasibility of using neutron inelastic scattering for compositional analysis and a prototype instrument has been developed for JPL for Surveyor. Additional experiments have been done by Waggoner and Know (3) of LRL to determine the sensitivity of the inelastic scattering technique for the analysis of rocks.

The Figures 1 through 6 attached, are taken from an LRL document UCRL-14654-T and indicate the results obtained with the experimental equipment.

FIGURE CAPTIONS

1. Prompt Gamma Rays From Basalt 3" x 3" NaI (Tl) detector
2. Prompt Gamma Rays From Granite 3" x 3" NaI (Tl) detector
3. Prompt Gamma Rays From Dunite 3" x 3" NaI (Tl) detector
4. Prompt Gamma Rays From Dunite 2" x 2" NaI (Tl) detector
5. Delayed Gamma Rays From Trachyte 3" x 3" NaI (Tl) detector
6. Delayed Gamma Rays From Achrondrite 3" x 3" NaI (Tl) detector

REFERENCES

1. C. D. Schrader and R. J. Stinner, "Remote Analysis of Surfaces by Neutron-Gamma Ray Inelastic Scattering Technique," Journal of Geophysical Research, Vol. 66, No. 6 (1961)

2. R. J. Stinner, "A Feasibility Study of a Method to Analyze the Moon's Surface Nuclear Inelastic Scattering," UCRL-6487 (1961)

3. J. A. Waggoner and R. J. Know, "Elemental Analysis Using Neutron Inelastic Scattering," UCRL-14654-T (1966)

Line Heater

Appendix VIII

NEUTRON-GAMMA EXPERIMENT RESULTS

Stem Device

A. TYPES OF SENSORS

Three common non-radiation type electrical temperature sensing devices are available for remote temperature measurement on the moon. These are the thermocouple, the resistance temperature sensor and the thermistor.

Thermistors offer the advantage of small size and large temperature coefficients of resistivity. They can generally be of high resistance values to make lead-resistance errors negligible. They are, however, better suited to precise measurement of narrow spans of temperature rather than wide ranges because of their non-linear response. Thermistors are also subject to changes in their response curve after temperature cycling and after aging. They also suffer from problems of resistance changes due to self heating.

Thermocouples have the advantages of small physical size and of requiring no excitation. Their main disadvantages are the low voltages they generate (for example, chromel/constantan generates 63 microvolts per degree in the range of 273°K to 373°K) and the need for a reference junction. Because accurate measurements must be made over a wide range of temperatures, several reference junctions may have to be used, each maintained at a different temperature by its own temperature control system.

The main advantages of resistive sensors are their ability to produce much larger outputs than obtainable from thermocouples, small drift due to aging or cycling, and the elimination of the need for a reference junction. For example, a typical platinum resistance sensor circuit with parameters compatible with the requirements of a number of lunar applications will yield about 4 millivolts per degree K. The main disadvantages of resistive sensing are the need for an accurately controlled or accurately known source of excitation, the relatively large size and mass of the sensors, and the need for thermal design of the structure relating the sensor to the point being sensed. This thermal design includes the problem of self-heating by the exciting current, the problem of temperature changes in the point being sensed because of the heat flow into or out of the sensor, and the problem of insuring a good thermal bond between the sensor and the point being sensed.

Both the resistive sensors and thermocouples present problems with regard to their leads. The thermocouple leads must be very homogeneous because of the large temperature gradient along their length. The temperature at the junction of any dissimilar metals in the thermocouple circuit must also be controlled. Resistance

variations in the leads from the resistive sensors will cause signal errors. This requires either a wire of sufficiently heavy gauge, or increased resistance of the sensor, or use of some compensating scheme. Thermal EMF's also have to be considered with resistance sensors. However, if the system can be designed to yield the higher outputs, these thermal EMF's will be a much less severe problem than in the thermocouple case.

After reviewing the different advantages and disadvantages of the three temperature sensing devices, it is our opinion that the resistive sensor is the best sensor for lunar operation. The most outstanding feature of the resistive sensor that influenced this recommendation is their larger output. For instance, in the case where 4 millivolts per degree K can be obtained, this signal can be fed without amplification into an analog-to-digital converter. This large output will also allow the use of solid-state commutation in place of mechanical commutation where more than one temperature is to be recorded through a common readout system. The combination of no amplification and solid-state commutation should increase the reliability of the temperature measuring system. For the various reasons and recommendations as stated above, the remainder of this section will be devoted to the full examination into the use of resistive sensors.

B. CHOICE OF SENSOR

It is planned that the output of the sensors be fed directly into the analog-to-digital converter without amplification. The converter accepts input voltages of between 0 and +5 volts. Therefore, by choosing the resistance of the sensor at a known temperature and the excitation current to be employed, the maximum temperature at which that sensor can be used can be determined. This temperature is that at which the resistance is equal to 5/I, where I is the constant current into the sensor.

Due to a number of considerations, a constant current of 2.5 ma has been chosen. Based on this value of current, the maximum value of resistance that produces a readable output voltage is 5/0.0025 = 2000 ohms. This means that a sensor with a resistance of 2000 ohms at 0°C would be useful solely for measuring temperatures below 0°C. Likewise, for any value of sensor resistance that is chosen, there is a maximum useful temperature for that sensor.

After considering the temperature range that must be monitored during lunar operations (-153°C to +127°C), a sensor with a resistance value of 1000 ohms has been chosen. This sensor will

give an output voltage of 2.5 volts at 0°C, and has a range from there of ± 260°C, before the signal into the converter goes off scale. The element in this sensor is platinum and the following equations give the resistance of platinum as a f function of temperature:

Above 0°C,

$$t = \left[\frac{R_t - R_o}{R_{100} - R_o}\right] + \delta\left[\frac{t}{100} - 1\right]\frac{t}{100} \qquad (1)$$

Below 0°C and above - 185°C,

$$t = 100\left[\frac{R_t - R_o}{R_{100} - R_o}\right] + \delta\left[\frac{t}{100} - 1\right]\frac{t}{100} + \beta\left[\frac{t}{100} - 1\right]\frac{t^3}{10^6} \qquad (2)$$

where t = temperature in °C

R_t = resistance of platinum at temperature t

R_o = resistance at 0°C

R_{100} = resistance at 100°C

δ = constant, nominally 1.493

β = constant, nominally 0.111

solving for $\frac{R_t}{R_o}$, and using the value

$$\frac{R_{100} - R_o}{100} = 0.00389\ R_o \text{ (for platinum)}$$

equation (1) becomes:

$$\frac{R_t}{R_o} = 1 + 0.00389\left[t - \delta\left(\frac{t}{100} - 1\right)\frac{t}{100}\right] \qquad (3)$$

and equation (2) becomes:

$$\frac{R_t}{R_o} = 1 + 0.000389 \left[t - \delta\left(\frac{t}{100} - 1\right)\frac{t}{100} - \beta\left(\frac{t}{100} - 1\right)\frac{t^3}{10^6} \right] \quad (4)$$

The ratios shown above have been computed for temperatures from -180°C to +180°C, and are shown in Table I.

Also shown in Table I in normalized form is the slope of the sensor output voltage at each temperature, i.e., its sensitivity. This quantity is tabulated as follows:

$$\frac{S}{IR_o} = \left[\frac{I}{IR_o} \cdot \frac{d\,E_R}{dt} \right] \quad (5)$$

where S = sensitivity (volts per degree C)

I = constant current through sensor

E_R = sensor output voltage

To obtain the sensitivity in volts per degree, multiply the quantity given in Table I by IR_o.

The sensor that has b-en selected is a platinum resistance temperature transducer. The resistance of the unit is 1000 ohms ± 1% at 0°C. The size of the sensor is 0.062 in. in diameter and 0.125 in. long. It has two wires leading from the ceramic covered bulb. Its repeatability is within ± 0.3°C at 0°C. The response of the unit is less than 1.0 second to reach 63% of a step change in temperature from ambient air to boiling water. The insulation resistance of the sensor is greater than 10 megohms at 50 VDC and ambient temperature. The unit has been vibration tested at 40 g. to 5000 cps with the lead wires cemented in place. It will withstand a steady acceleration of 40 g. and a 50 g. shock up to 11 milliseconds duration. Each sensor has been calibrated by the vendor and will have its own calibration sheet furnished.

TABLE I
NORMALIZED RESISTANCE OF PLATINUM AND NORMALIZED SENSITIVITY, AS A FUNCTION OF TEMPERATURE

Above 0°C			Below 0°C		
t °C	R_t/R_o	S/IR_o	T °C	R_t/R_o	S/IR_o
180	1.692	0.00374	0	1.000	0.00395
160	1.617	0.00376	-20	0.021	0.00397
150	1.579	0.00377	-40	0.841	0.00400
140	1.541	0.00379	-60	0.761	0.00403
127	1.492	0.00380	-80	0.680	0.00406
120	1.465	0.00381	-100	0.599	0.00409
110	1.421	0.00382	-120	0.516	0.00414
100	1.389	0.00383	-140	0.433	0.00418
80	1.312	0.00386	-160	0.346	0.00424
60	1.235	0.00388	-180	0.263	0.00430
40	1.157	0.00390			
20	1.079	0.00392			
0	1.000	0.00395			

C. TEMPERATURE MEASUREMENT ERRORS DUE TO THERMAL CONDUCTIVITY

The nature and composition of the moon is unknown and is probably variable from place to place on its surface. The resistive sensor elements to be used in the various instruments will have to be placed in contact with a surface which could be a dust layer, a fiarly soft rock, or a hard glassy rock. Placement of the sensor with the wires necessary for measurement involves the transfer of heat between the measuring sensor and the measured surface which produces an uncertainty in temperature measurement, particularly when the measured surface is a material of low heat capacity and low thermal conductivity.

Methods of estimating errors in surface thermometry are given by Jakob (1). Assume an infinitely extended body of thermal conductivity k and uniform temperature t bounded by a plane surface, which is perfectly insulated against heat losses except at one small circle of diameter 2r, from which a wire of thermal conductivity k_w of length l and radius r, perfectly insulated except at the ends, extends to a body of constant temperature t_e. Allow the contact between wire and surfaces to each end to be without resistance to heat flow. The temperature t_o of the interface between infinite body and wire is to be determined. For the amount of heat per unit time transferred between wire and infinite body Jakob gives the equation:

$$q_o = 4\ r\ k\ (t - t_o) \tag{6}$$

For the amount of heat transferred per unit time along the wire:

$$q_o = \frac{kw}{l}\ \pi r^2\ (t_o - t_e) \tag{7}$$

The quantity $(t_o - t_e)$ is the measured difference between reference point and the resistive thermometer sensor, while the quantity $(t - t_o)$ can be considered the error in measurement. Equating (6) and (7) gives:

$$(t - t_o) = \frac{kw}{k}\ \frac{\pi}{4}\ \frac{r}{l}\ (t_o - t_e) \tag{8}$$

---

(1) Heat Transfer, by Max Jakob - Chapter 33, section 33-4, pp. 153-154.

The sensor that has been chosen for use has platinum wire leads 0.018 cm in diameter, 10 cm long, and a thermal conductivity of 0.1733 (cal cm^{-2} sec^{-1} C^{-1}). Substituting these values in (8) gives:

$$\text{error} = \frac{0.000122\ (t_o - t_e)}{k} \qquad (9)$$

It will be noticed in (9) that there are two variables which can affect the error, the conductivity of the surface and the difference in temperature between the surface and the sensor. The difference in temperature is a transient effect and will steadily decrease with time from the instant the sensor and surface are in contact. Therefore, the error as calculated and shown in graphs 1 and 2 is the maximum error that will be encountered due to the thermal conductivity of the surface. Figure 1 shows a log-log plot of error vs. thermal conductivity for four temperature ranges. Since the sensor that will be used is very small compared to the surface being measured, the temperature difference should fall to within 10°C within a reasonable period of time. Therefore, to assure that the 1% accuracy is met, the sensor should be operated within the dotted lines shown on Figure 1. Table II shows the errors possible for a range of materials and Δt's.

D. COMMUTATION

The idea of commutating the circuitry among the various sensors has been mentioned several times. The main advantages of doing this are:

1. Reduce the average power dissipated in each sensor. This allows a much larger excitation current for the same self-heating. This will in turn increase the sensitivity.

2. Reduce a large portion of processing equipment necessary if each sensor was in a separate system. With as many as 18 sensors being used, the unnecessary equipment is quite significant, even after accounting for the commutating circuitry.

The main disadvantage of commutation is reduced reliability because one failure can throw out all the measurements that are being commutated. For most of the temperature measurements this is of no serious consequence since most of the measurements are either not associated with the scientific experiments, or even

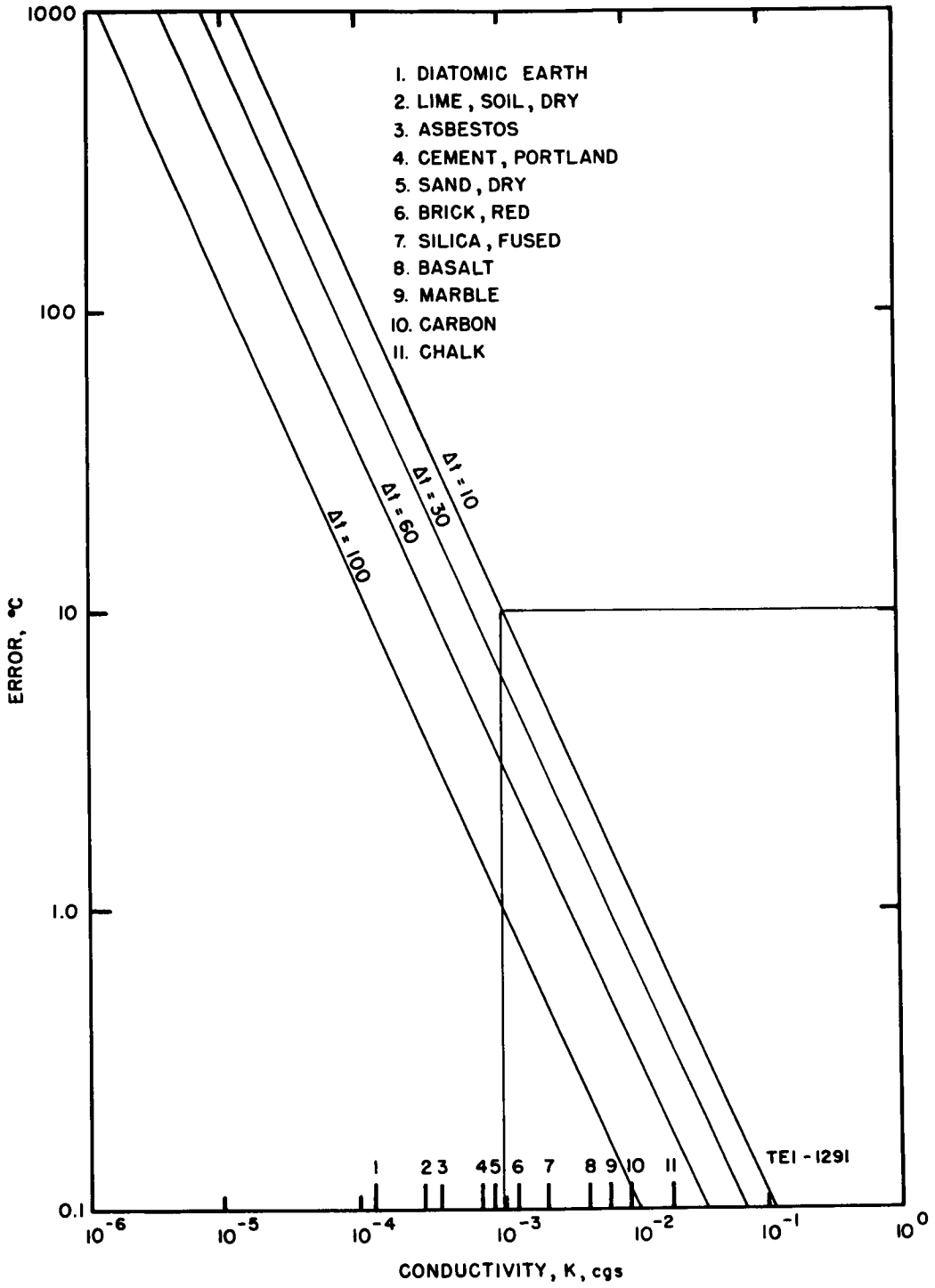

Fig. 1 Effects of Thermal Conductivity on Contact-Temperature Measurement Error

TABLE II

Material	k	Error Δt = 100	60	30	10
Asbestos	0.0004	31.0	18.3	9.15	3.10
Basalt	0.0052	2.35	1.41	0.70	0.235
Brick, red	0.0015	8.13	4.88	2.44	0.81
Carbon	0.0100	1.22	0.73	0.37	0.12
Carborundum	0.0005	24.4	14.64	7.32	2.44
Cement, Portland	0.00071	17.2	10.3	5.15	1.72
Chalk	0.0020	6.10	3.66	1.83	0.61
Concrete, stone	.0022	5.55	3.33	1.66	0.56
Diatomic earth	0.00013	93.85	56.3	28.15	9.38
Earth's Crust, Ave.	0.0040	3.05	1.83	0.92	0.31
Ebonite	0.00042	29.05	17.43	8.71	2.91
Glass, flint	0.0020	6.10	3.66	1.83	0.61
Granite	0.0047	2.60	1.56	0.78	0.26
Graphite	0.0120	1.02	0.61	0.31	0.10
Gypsum	0.0031	3.94	2.36	1.18	0.39
Ice	0.0050	2.44	1.46	0.73	0.244
Line	0.00029	42.07	25.24	12.62	4.21
Magnesia, MgO	0.00031	39.35	23.61	11.81	3.94
Marble	0.0071	1.72	1.03	0.52	0.17
Mica	0.0018	6.78	4.07	2.03	0.68
Plaster of Paris	0.0007	17.43	10.46	5.23	1.74
Porcelain	0.0025	4.88	2.93	1.46	0.49
Quartz, parallel to Axis	0.0300	0.41	0.24	0.12	0.04
perpendicular " "	0.0160	0.76	0.46	0.23	0.08
Sand, dry	0.00093	13.12	7.87	3.94	1.3.
Sandstone	0.0055	2.22	1.33	0.67	0.22
Silica, fused	0.0024	5.08	3.05	1.53	0.51
Slate	0.0047	2.60	1.56	0.78	0.26'
Soil, dry	0.00033	36.97	22.18	11.09	3.70

where associated with the experiments are not essential to the interpretation of data from these experiments. For the remaining measurements, without which the data from the associated experiments is meaningless, the question of reliability in connection with commutation is of prime importance. A case could be made for not commutating these temperature measurements in line with the philosophy of keeping each experiment separated, from a failure standpoint, from the others. However, after considering the advantages and disadvantages above, it was decided that commutation was the best method for temperature readout.

In order to allow each sensor to be connected during a full 11-bit ward, and to provide time for switching, a total time of two words per reading should be allocated. At the standard bit rate of the analog-to-digital converter of 540 bits per second, the time allocated will be $2 \times 11/540 = 0.04074$ seconds. While temperature measurements are being taken, this would allow each sensor to be read every $0.04074 \times 64 = 2.607$ seconds.

The time lag in the data due to wiring capacity can be computed. With DC excitation, an impedance of 1000 ohms, a one-way wire length of 30 feet, a capacity to ground of 100 picofarads/foot, the time constant is $1000 \times 30 \times 100 \times 10^{-12} = 3 \times 10^{-6}$ second which, compared to the 1.85×10^{-3} second per bit, is small enough to be neglected.

The commutating system that will be used is shown in Figure 2. A constant current generator will feed a bank of 18 sensor gates which will be controlled by pulses from a shift register and from the main telemetry. The output temperature signal is sent to the main telemetry through a single output gate. The main read pulse being fed from the main telemetry will pass through a buffer amplifier.

E. CONSTANT CURRENT VS. CONSTANT VOLTAGE SOURCE

In considering the circuitry to be used for the temperature measurements to be taken, it was not known which type of power supply would result in the smallest error in the measurements. Below is the computation made for the two systems:

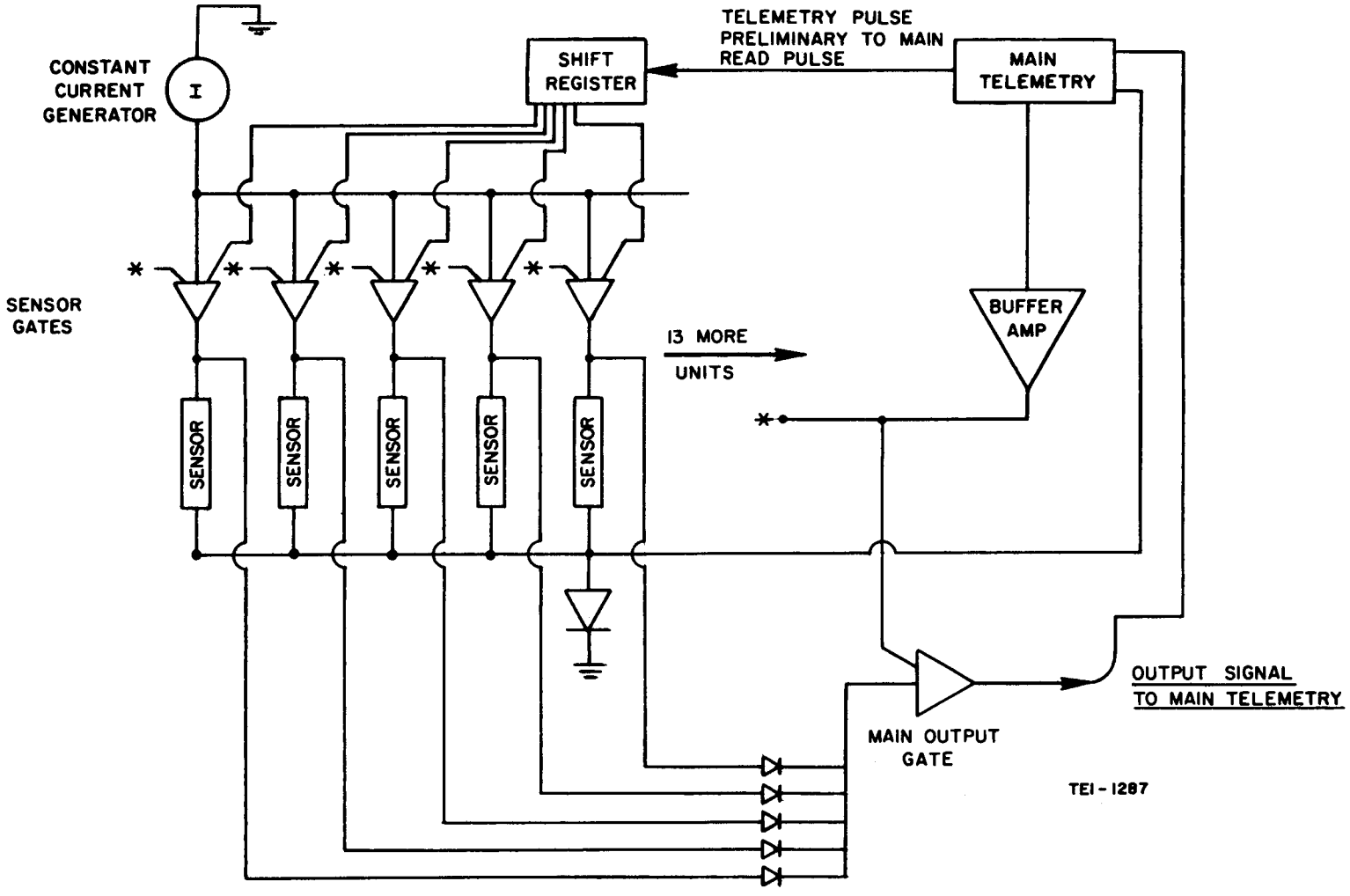

Fig. 2 Block Diagram - Contact Temperature System

Constant Current Supply

Conditions:

1. $\pm$ 5 mv random error always present in telemetering circuitry.

2. Resistance thermometer of 1000 ohms at 0°C.

3. Constant current source of 2.5 ma $\pm$0.1%.

4. Definition of Error:

   Error will be the deviation from what is called "true temperature", which is the temperature computed using the following equations:

   (a) $$t = 100 \frac{R_t - R_o}{R_{100} - R_o} + \delta\left(\frac{t}{100} - 1\right)\frac{t}{100}$$ For temperature > 0°C

   (b) $$t = 100 \frac{R_t - R_o}{R_{100} - R_o} + \delta\left(\frac{t}{100} - 1\right)\frac{t}{100} + \beta\left(\frac{t}{100} - 1\right)\frac{t}{100}^{3}$$

   For temperature < 0°C only

where t = temperature in °C

δ = 1.492

β = 0.11

R_o = resistance of thermometer at 0°C

$$\frac{R_{100} - R_o}{100\ R_o} = 0.003926 \quad (\therefore R_{100} = 1392.6)$$

R_t = resistance calculated at temperature t

t = temperature in degrees K

R_t' and t' - calculated with $\pm$ .1% constant current change.

5. Definition of Accuracy.

   Accuracy will be prescribed as the actual deviation of calculated temperature (calculated after inclusion of the $\pm$ 0.1% constant current change) from "ture temperature as described in (4).

Computations and Results:

1. The procedure used in making the following computations is:

   (a) Select the temperature (t)

   (b) Using the appropriate equation solve for R_t at the selected temperature.

   (c) Determine next the new value of R_t due to the $\pm$ 0.1% current change.

$$R_t' = \frac{Ic'}{Ic} R_t$$

where $Ic' = Ic + 0.001\ Ic$ and $Ic = 2.5$ ma

   (d) Now, again using the appropriate formula, insert R_t' and solve for t', which is the new value of t due to the current change.

   (e) The difference between t and t' will describe the accuracy achieved.

2. Effects of current change on temperature accuracy were determined at the extreme temperatures of the following temperature ranges:

   (a) Temperature range of 89°K to 400°K

   (1) 400°K (127°C)

$$R_{127} = R_o + \frac{R_{100} - R_o}{100}\left[-t + \delta\left(\frac{t}{100} - 1\right)\frac{t}{100}\right]$$

$$R_{127} = 1000 - 3.926\ [-127 + 1.492\ (0.27)(1.27)]$$

$$R_{127} = 1496.59342$$

Then

$$R'_{127} = \frac{Ic'}{Ic} R_{127}$$

$$R'_{127} = 1498.090013$$

Then

$$t'_{127} = 100\,\frac{R'_{127} - R_o}{R_{100} - R_o} + \delta\left(\frac{t'_{127}}{100} - 1\right)\frac{t'_{127}}{100}$$

Simplifying

$$0 = (t'_{127})^2 - \frac{(R_{100} - R_o) \times 10^4}{(R_{100} - R_o)}\,(t'_{127}) - \frac{\left(\frac{R_{100} - R_o}{100}\right)\delta \times 10^4}{(R_{100} - R_o)}\,t_{127}$$

$$+ \frac{100\,(R'_{127} - R_o)}{(R_{100} - R_o)\,\delta \times 10^{-4}}$$

$$(t'_{127})^2 - 6802.4\,(t'_{127}) + 850330 = 0$$

$$t'_{127} = 125.004°C$$

$$\underline{t'_{400}} = t'_{127} + 273 = \underline{398.004°K}$$

<u>(2) 89°K (-184°C)</u>

$$R_{-184} = Ro - \frac{(R_{100} - R_o)}{100}\,t - \frac{\delta}{100}\left(\frac{t}{100} - 1\right)\frac{t}{100} - \frac{\beta}{100}\left(\frac{t-1}{100}\right)\frac{t}{100}^3$$

$$R_{-184} = 1000 - 3.926\left[-1.01492(-184) + 1.492 \times 10^{-4}(-184)^2 - 0.11 \times 10^6\,(-184)^3 + 0.11 \times 10^{-8}\,(-184)^4\right]$$

$$R_{-184} = 277.6389$$

Then

$$R'_{-184} = \frac{Ic'}{Ic}\,(277.\cancel{9165}\,6389)$$

$$R'_{-184} = 277.9165$$

Then

$$t'_{-184} = 100\,\frac{R'_{-184} - R_o}{R_{100} - R_o} + \delta\left(\frac{t'_{-184} - 1}{100}\right)\left(\frac{t_{-184}}{100}\right) + \beta\left(\frac{t'_{-184} - 1}{100}\right)\left(\frac{t'_{-184}}{100}\right)^3$$

Simplifying

$$0 = 183.92344 - 1.01492\ (t'_{-184}) + \frac{1.492}{10^4}\ (t'_{-184})^2 - \frac{0.11}{10^6}\ (t'_{-184})^3$$

$$+ \frac{0.11}{10^8}\ (t'_{-184})^4$$

From computer calculations:

$t'_{-184} = -\ 185.6937°C$

$t'_{89} = t'_{-184} + 273 = \underline{87.31°K}$

2. Effects of current change on temperature accuracy were determined at the extreme temperatures of the following temperature ranges:

(a) Temperature range of 89°K to 400°K

<u>(1) 400°K (127°C)</u>

$$R_{127} = R_o + \frac{R_{100} - R_0}{100} \left[-t + \delta\left(\frac{t}{100} - 1\right) \frac{t}{100} \right]$$

$$R_{127} = 1000 - 3.926\ [-127 + 1.492\ (0.27)\ (1.27)$$

$$R_{127} = 1496.59342$$

Then $R'_{127} = \frac{Ic'}{Ic}\ R_{127}$

$$R'_{127} = \frac{2.5025}{2.5}\ (1496.59342)$$

$$R'_{127} = 1498.090013$$

Then

$$t'_{127} = 100 \left[\frac{R'_{127} - R_o}{R_{100} - R_o} + \delta\left(\frac{t'_{127}}{100} - 1\right) \frac{t'_{127}}{100} \right]$$

Simplifying

$$O = (t'_{127})^2 - \frac{(R_{100} - R_o) \times 10^4}{(R_{100} - R_o)}\ (t'_{127}) - \frac{\left(\frac{R_{100} - R_o}{100}\right) \delta \times 10^4}{(R_{100} - R_o)}\ t_{127}$$

$$+ \frac{100(R'_{127} - R_o)}{(R_{100} - R_o)\ \delta \times 10^{-4}}$$

(b) For a temperature range of 120°K to 400°K

(1) $t'_{400} = 398.004°K$

(2) $t'_{120} = 119.09°K$

(c) For a temperature range of 150°K to 400°K

(1) $t'_{400} = 398.004°K$

(2) $t'_{150} = 149.76°K$

(d) Determination of accuracy for the three temperature ranges involved will be as follows:

(1) accuracy = $t_{true} - t_{calculated}$

accuracy @ 400°K = 400 - 398.004 = + 1.99°K

accuracy @ 150°K = 150 - 149.76 = + 0.24°K

accuracy @ 120°K = 120 - 119.09 = + 0.91°K

accuracy @ 89°K = 89 - 87.31 = + 1.69°K

(2) Since the change in resistance of the resistance thermometer is linear over whatever temperature range we choose, it appears that the accuracy would improve as 273°K (0°C) is approached from either temperature extreme. To aid in this assumption, temperature calculations for 200°k, 250°K, 300°K, and 350°K are shown below:

accuracy @ 200°K = -0.47°K

accuracy @ 250°K = -0.50°K

accuracy @ 300°K = -0.17°K

accuracy @ 350°K = + 0.54°K

The above calculations show that the greatest accuracy that can be achieved from a constant current source is ± 0.5°K over the temperature range of 150°K to 350°K.

Constant Voltage Supply

Conditions:

1. ± 5 mv random error always present in telemetering circuitry.

2. Voltage range of output: 0.5 V DC

3. Definition of Accuracy: "Accuracy" will be the accuracy of the temperature determinination (°K) over the temperature range used.

$$\text{Acc.} = \frac{\text{Error due to monitoring supply voltages and output voltage}}{\text{Voltage Gradient of Output (mv/°K)}}$$

4. Definition of Error:

   "Error" will be the change in monitored supply voltage (mv) due to 5 mv telemetering error, plus the ± 5 mv random error due to output voltage monitoring.

5. The + 12 v and -12 v power supplies of this system are both monitored producing at the instrument output monitor point a millivolt error, due to the error within the monitoring system itself. The millivolt error produced by a 5 mv random error, either plus or minus, will be the maximum error and will not be exceeded over the temperature range chosen. The 4 volt monitor level was chosen in order to give the maximum system accuracy in the 0-5 volt output range.

Computations and Results:

1. Assuming 5 mv random error, determine maximum possible output voltage deviation caused by the monitoring system.

   (a) Assume 4 v is true voltage at (a) Figure 3.

   (b) Due to 5 mv random error, this reading could be 4.005 v.

   (c) The current in the circuit is:

$$\frac{12^V - 4^V}{R_1} = I$$

(Fig. 3)

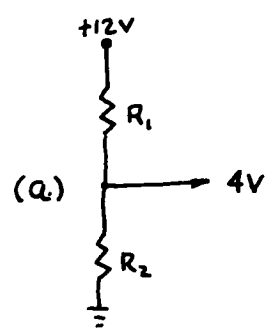

(d) The voltage across R_2 would then be:

$$V_{R_2} = IR_2 = \frac{(12 - 4)}{R_1} R_2 = 4V$$

$$8 R_2 = 4R_1 + R_1 = 2R_2$$

(e) $E_{+12} = IR_1 + IR_2$

or $E_{+12} = I(2R_2) + IR_2 = 3 IR_2 = 3 V_{R_2}$

but $V_{R_2} = 4.005$ V

$E_{12} - 3(4.005) - 12.015$ volts

2. With the + 12 volt supply known, the - 12 volt supply must be found.

(a) Assume that point (a) of Fig. 4 is at 4 v.

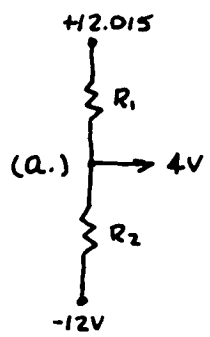

Fig. 4

(b) Due to $\pm$ 5 mv random error, reading at (a) is 3.995 v.

(c) Actual current is: $\frac{12-4}{R_1} = I$

(d) Voltage across R_2 would be:

$$V_{R_2} = IR_2 = \left(\frac{12-4}{R_1}\right) R_2 = 4 - (-12) = 16 \text{ volts}$$

$$8 R_2 = 16 R_1 + R_2 = 2R_1$$

(e) From (1-e) above:

$V_{R_1} = 12.015 - 3.995 = 8.020$ volts

then $E_{-12} = 3.995 - 2 V_{R_1} = 3.995 - 2(8.020)$

$E_{-12} = -12.045$ volts

3. Having determined the values of the +12 and -12 volt power supplies as stated by the monitors, now the effect this has on temperature accuracy is as follows:

(a) Let monitor read 0.0 v at (a) Fig. 5.

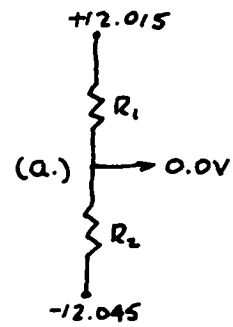

Fig. 5.

(b) However, due to our calculated values for E +12 and E -12, the monitor actually sees 30 mv.

(c) Now, to see what effect this 30 mv error has on temperature accuracy, various temperature ranges will be chosen, the voltage gradient determined, and from the definition in step 3 of the conditions, accuracy will be expressed.

(1) for the maximum temperature range of 89°K to 400°K: the voltage gradient is

$$V.G. = \frac{5000 \text{ mv}}{(400-89)\ ^\circ K} = 16 \text{ mv}/^\circ K$$

$$\text{accuracy} = \frac{\text{supply monitor error} + \text{random error}}{V.G.}$$

$$\text{accuracy} = \frac{30 + 5}{16} = + \underline{2.18^\circ K}$$

(2) temperature range 120°K to 400°K

$$V.G. = \frac{5000}{400-120} = 18 \text{ mv}/^\circ K$$

$$\text{accuracy} = \frac{30 + 5}{18} = \pm 1.75^\circ K$$

(3) temperature range 150°K to 400°K

$$V.G. = \frac{5000}{400-150} = 20 \text{ mv/°K}$$

$$\text{accuracy} = \frac{30 + 5}{20} = \pm 1.75°K$$

(4) temperature range 150°K to 350°K

$$V.G. = \frac{5000}{350-150} = 25 \text{ mv/°K}$$

$$\text{accuracy} = \frac{30 + 5}{25} = \pm 1.20°K$$

It is again seen that the greatest accuracy is in the 150°K to 350°K range. However, in comparing the accuracy of measurements between the constant current system and constant voltage system, it is seen that constant current system is more accurate by approximately 240%. Therefore, it is planned to use the constant current system in connection with the contact temperature experiment.

F. LEAD RESISTANCE EFFECTS ON ACCURACY

The resistance of the leads that transfer the measured signal from the sensor to the telemetry will cause some error. One of the standard methods for reducing this error is to use two wires to supply the sensor with current and two additional wires to carry the signal to the recorder. Following is a comparison of the two wire and four wire systems in regard to measurement accuracy.

From previous calculations, section E, disregarding lead resistance, the error due only to variations in Ic through the sensor is 0.54°K at 350°K. It can be shown through standard equations that the apparent change in sensor temperature resulting from the change in lead resistance is as follows:

$$\Delta_{tp} = \frac{R_e}{R_o} \Delta T_1$$

Now assuming a 26 gauge wire, with a round trip length of 30 feet, a sensor resistance of 1000 ohms, and a temperature of 350°K, then the following is calculated:

The resistance of 26 gauge wire is 40.81 ohms per 1000 feet. Therefore, the resistance of 30 feet would be

$$R_e = (40.81) \left(\frac{30}{1000} \right) = 1.2224 \text{ ohms}$$

350°K = 77°C

$$\Delta_{tp} = \frac{(1.224)\ (77)}{1000}$$

Δ_{tp} = 0.049°K = lead resistance error

Total error = error due to Ic + Δ_{tp} = 0.54 + 0.094

Total error = 0.634°K

In a four wire system, two wires carry the constant current of 2.5 ma to the sensor and two wires carry the signal from the sensor to the telemetry. Now, assuming that the internal impedance of the telemetry is 200K ohms and that there is a maximum signal of 5 volts across the sensor, the current in the two signal wires are:

$$I_s = \frac{5}{200{,}000} = 25 \times 10^{-6} \text{ amps}$$

Comparing the current in the two systems,

$$I_s \ \frac{25 \times 10^{-6}}{2.5 \times 10^{-3}} \times 100 = 1\%$$

This means that the error in the four wire system is only 1% of the error that was in the two wire system,

or (0.094)(0.01) = 0.00094°K error

or Total error = 0.54 + 0.00094
Total error = 0.54094°K

From the above computations, the four-wire system is definitely the best method for eliminating the error due to lead resistance. However, its decrease in total error from 0.634" to 0.541°K hardly justifies the complexity of adding the extra two wires. Therefore, a two wire system will be employed in the thermal measurements.

Appendix VII

CONTACT TEMPERATURE MEASUREMENTS

Control Element	Experiment Group
e_5	e_5, e_7, e_{10}
e_{12}	e_6, e_{10}, e_{12}
e_{11}	e_1, e_2, e_4, e_{11}
e_8	e_1, e_2, e_4, e_{11}, e_8
e_3	e_3, e_8, e_9

The control element switch activates the entire experiment group and, as indicated in Assumption (1), all switches, excluding the control switches, are wired to act independently to provide maximum reliability. Since e_8 is located in another experiment grouping in a non-control element position, it also has individual capability.

Each switching block diagram presented gives the actual switching sequence indicating the experiment group to be activated or deactivated. The minimum number of switching movements indicated in Table 2 is based on control element activation rather than individual activation.

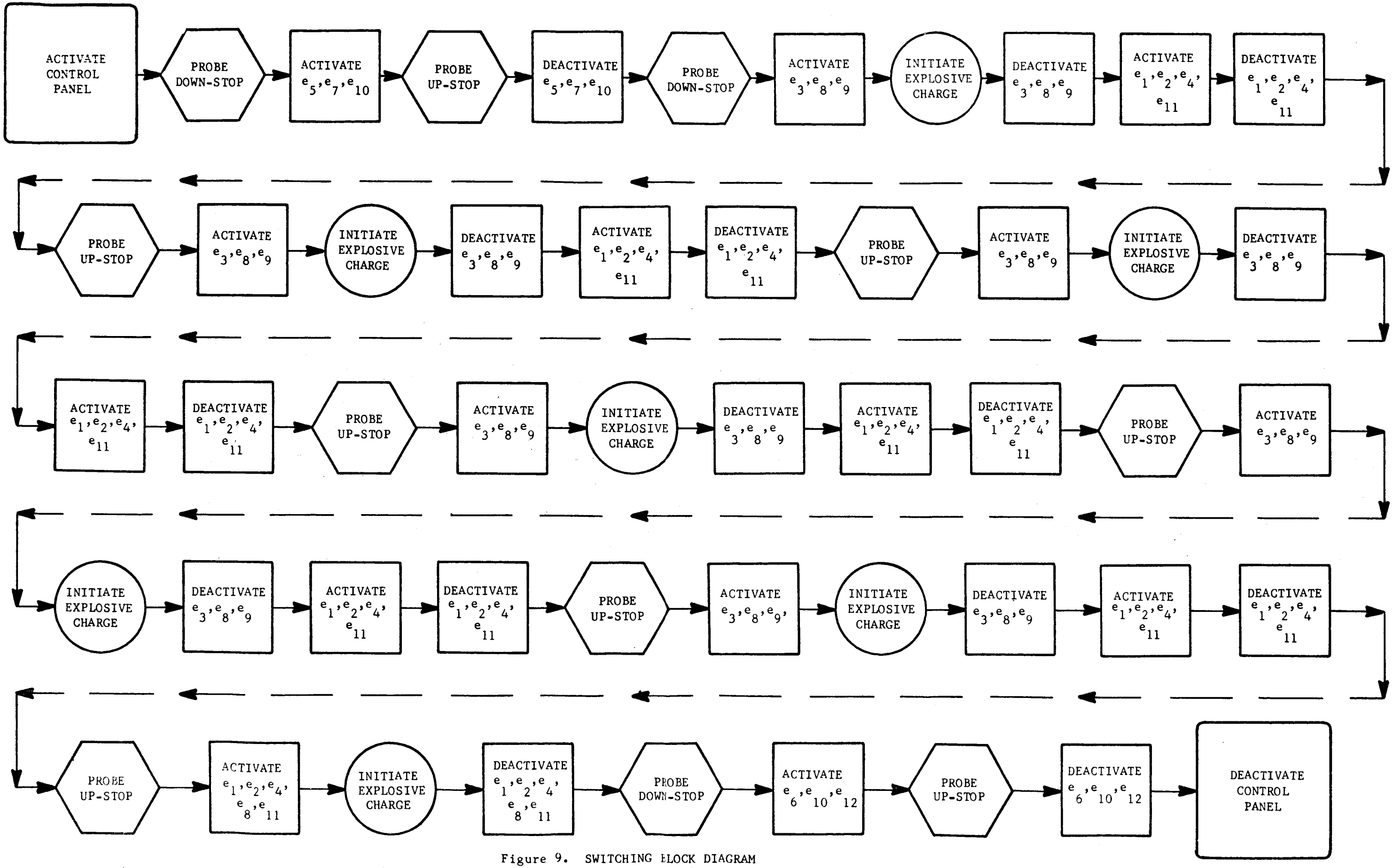

Figure 9. SWITCHING BLOCK DIAGRAM
OPTIMUM PLAN NO. 2 (100-FT. HOLE)

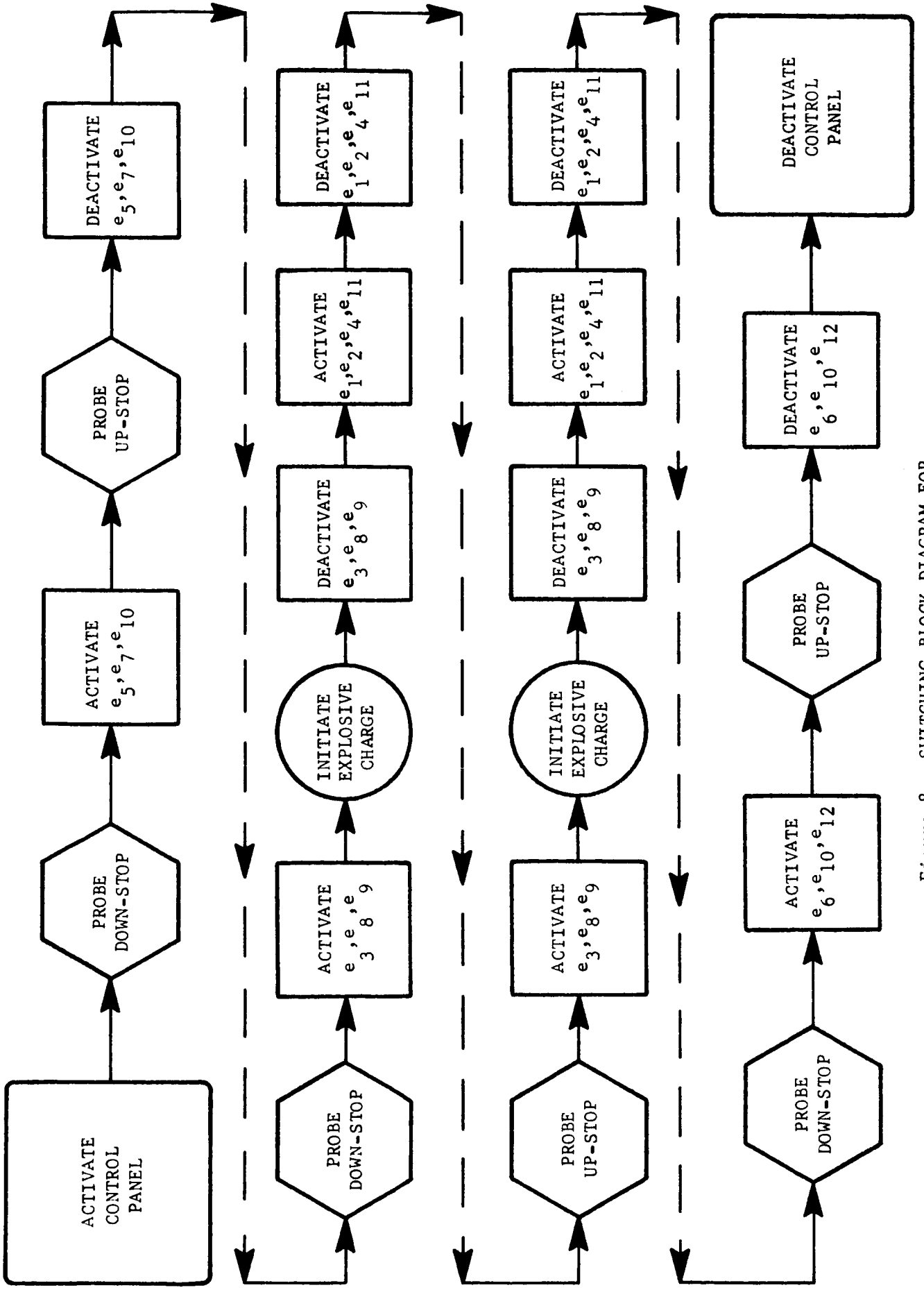

Figure 8. SWITCHING BLOCK DIAGRAM FOR OPTIMUM PLAN NO. 2(10-FT. HOLE)

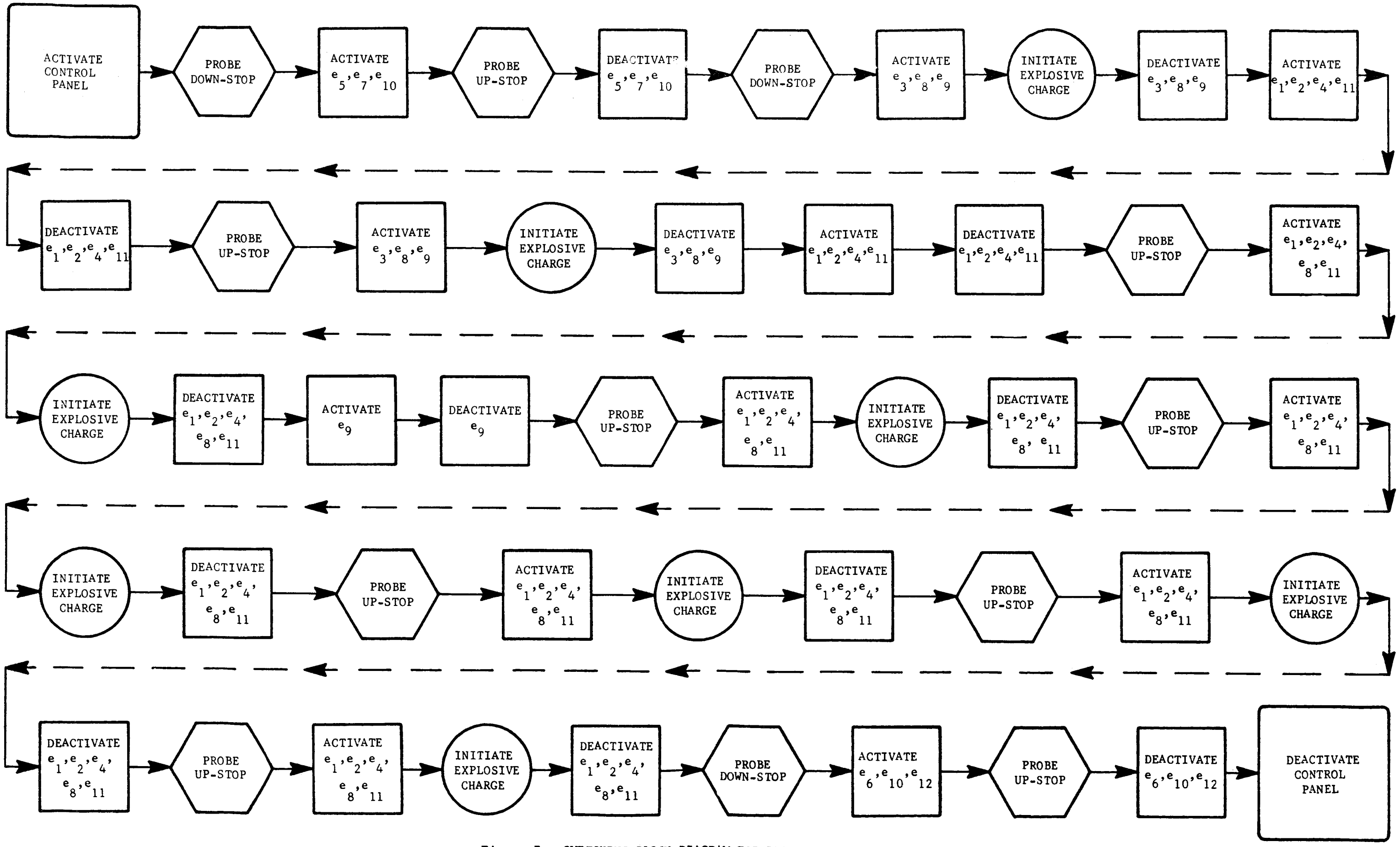

Figure 7. SWITCHING BLOCK DIAGRAM FOR EXPERIMENT SCHEDULING: PLAN NO. 3 (100-FT. HOLE)

Appendix IV

ANALYSIS OF HEAT TRANSFER BETWEEN SUBSURFACE PROBE AND BOREHOLE WALL

PREFACE

This informal report was prepared by the Systems Section of Northrop Space Laboratories, Huntsville, Alabama, for Texaco Experiment Incorporated. Efforts were performed under Task Order NSL No. 3, Purchase Order No. 40510-3, March 23, 1966. The TEI Project Engineer was Mr. Ralph H. Clinard, Jr.

TABLE OF CONTENTS

Paragraph		Page
	PREFACE	i
1.	INTRODUCTION	1
2.	DISCUSSION	1
3.	ASSUMPTIONS	1
4.	ANALYSIS	5
5.	CONCEPTUAL DESIGN	11

LIST OF TABLES

Table		
1	Experiment Characteristics	4
2	Required Switching Movements	11

LIST OF FIGURES

Figure		
1	Optimum Plan No. 2 (10-Ft. Hole)	2
2	Optimum Plan No. 2 (100-Ft. Hole)	3
3	Experiment Scheduling for 10-foot Holes: Plan No. 1	6
4	Conceptual Panel Design	8
5	Experiment Scheduling for 100-foot Holes: Plan No. 3	9
6	Switching Block Diagram for Experiment Scheduling: Plan No. 1	12
7	Switching Block Diagram for Experiment Scheduling: Plan No. 3	13
8	Switching Block Diagram for Optimum Plan No. 2(10-ft Hole)	14
9	Switching Block Diagram for Optimum Plan No. 2(100-ft Hole)	15

1. INTRODUCTION

This report contains the result of investigations conducted by Northrop Space Laboratories to determine optimum switching requirements for operation of the lunar subsurface probe and the conceptual design of a subsurface probe control panel. Investigation and design efforts were performed under Task Order No. 3 which required:

(1) Determining which sequencing plan in NSL Task Order Report No. 2 requires a minimum of switching for:

(a) Logging both holes

(b) Logging ten-foot hole only

(c) Logging hundred-foot hole only

(2) Preparing a switching block diagram in accordance with optimum Plan No. 2, 10-ft hole (Figure 1) which will result in the optimum utilization of the astronaut's time during measurement period and prepare a preliminary design of the control panel necessary to carry out the switching required.

(3) Preparing a switching block diagram and preliminary design of the control panel as in (2) above for Optimum Plan No. 2, 100-ft hole (Figure 2).

(4) Preparing a switching block diagram for each of the minimum situations and a preliminary design of the control panel to carry out the necessary switching.

2. DISCUSSION

Experiment scheduling and sequencing plans, as presented in NSL Task Order Report No. 2, and the activation and control operations required for these experiments as presented in Table 1, have been used in this analysis to determine optimum panel design. The above mentioned report defines specific experiment groups and sequences which dictate to an extent the switching to be used to meet the design goals. This analysis has utilized optimum grouping theory and basic design logic to arrive at minimum switching requirements for each situation requested.

3. ASSUMPTIONS

Since certain experiments are always grouped together (for example: e_5, e_7, e_{10}; e_3, e_8, e_9), the following assumptions have been made to aid in the design of a minimum switching situation:

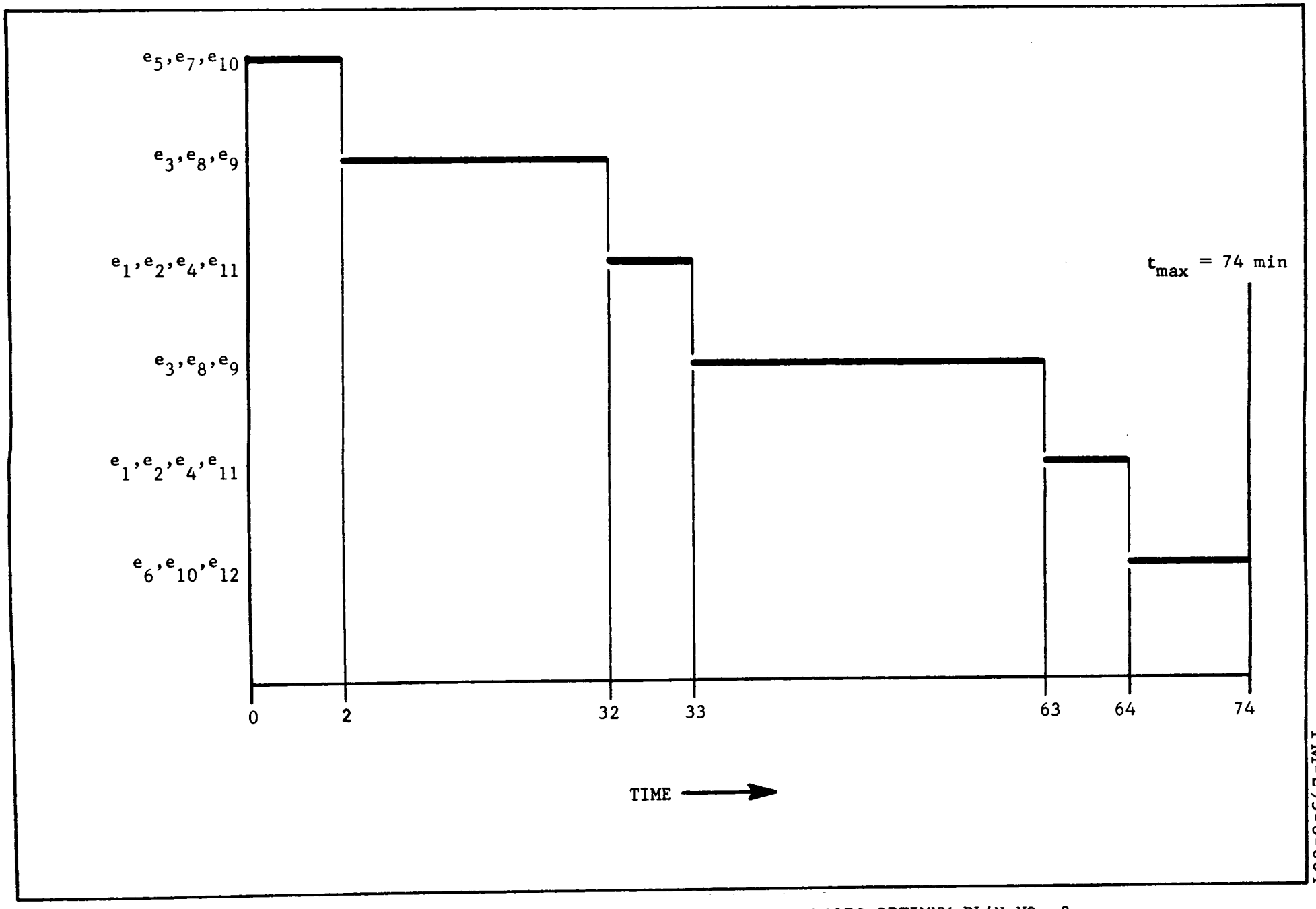

Figure 1. EXPERIMENT SCHEDULING FOR 10 FOOT HOLES OPTIMUM PLAN NO. 2
(Abstracted from NSL Task Order No. 2)

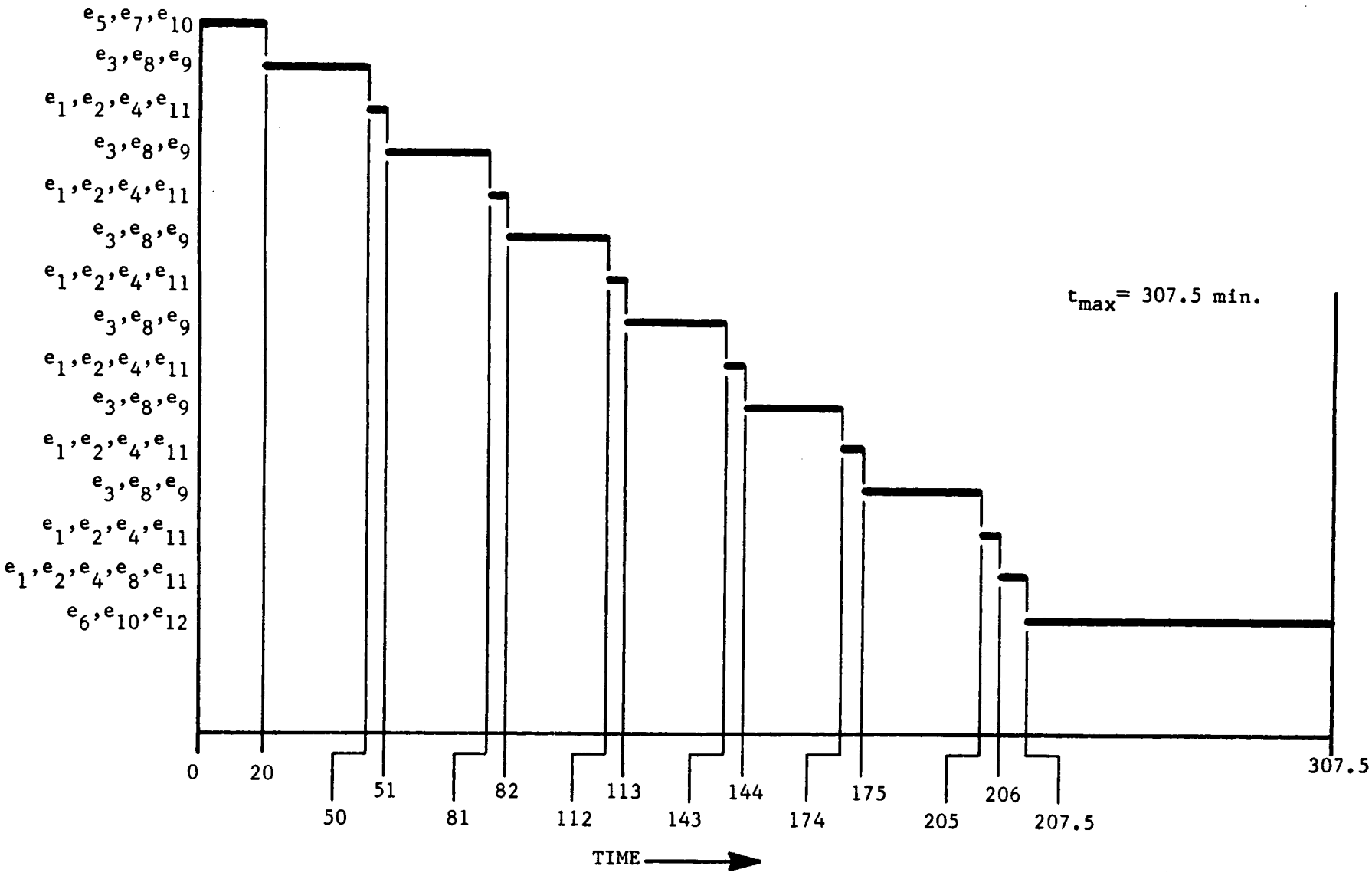

Figure 2. EXPERIMENT SCHEDULING FOR 100 FOOT HOLES OPTIMUM PLAN NO. 2
(Abstracted from NSL Task Order No. 2)

Table 1 EXPERIMENT CHARACTERISTICS

Experiment	Operations	Notes
1. Non-Contact Temperature	Experiment On-Off	
2. Contact Temperature	Experiment On-Off Meter Readout	
3. Thermal Diffusivity	Experiment On-Off Heater On-Off Meter Readout	
4. Mass Spectrometer	Experiment On-Off Ionizer On Mass Filter On	Total Ion Density, total Ion neutral pressure, mass spectra
5. Natural Gamma	Experiment On-Off Meter Readout	
6. Gamma-Gamma Density	Experiment On-Off Meter Readout	
7. Magnetic Susceptibility	Experiment On-Off Meter Readout	
8. Acoustic Velocity	Experiment On-Off Geophone positioning out and in (momentary switch closure) Explosive charge initiation	For each measurement point
9. Spectral Gamma	Energize pulse height analyzer	In addition to other circuits as in (5); no meter readout
10. Caliper	Experiment On-Off Meter Readout	
11. Electrode Resistivity	Experiment On-Off	
12. Change of Q Resistivity	Experiment On-Off	
13. Probe Vertical Positioning	Up-Down Control speed control position readout	

(1) Experiments in a grouping can be operated simultaneously or independently. For example, in the group (e_3,e_8,e_9), control switch e_3 will activate e_8 and e_9; e_8 and e_9 can be operated separately to leave only e_3 activated, or deactivated, as desired.

(2) Individual elements can be electrically locked in (or out) to minimize the number of switches required.

(3) Experiment equipment (such as the heater, mass filter, ionizer, geophone, and pulse height analyzer) can be incorporated in the experiment ON-OFF switch with indicator lights to present equipment status.

(4) An automatic-reset clock will indicate the termination point for each experiment group and reset itself when each group is deactivated.

(5) Miniature lighted pushbutton switches with multiple screen color combinations will be used for optimum efficiency. (Size 1.3" x .99" x .81").

(6) Readout meters are located at a minimum distance from the control switch and utilize colored screens corresponding to its control switch for maximum association.

(7) A pushbutton switch incorporation a sequencing mechanism will be used to initiate explosive charges.

(8) The subsurface probe can be positioned at any desired level (as indicated by probe position indicator) consistent with depth of hole; i.e. a series of stationary readings can be made without moving the probe to the bottom of the hole between each reading.

4. ANALYSIS

The control panel design should afford optimum use of the astronaut's time and require a minimum of manual switching. All sequence plans were analyzed to establish all possible switching arrangements which would result in a control panel design requiring minimum switching, yet consistent with good design and acceptable reliability.

The minimum switching arrangement for each plan would be one which permits the maximum occurrence of experiment groupings. All possible groupings for each plan would then be represented in a manner that all elements of the group could be activated by one movement. Although panel size would not permit such an inclusive arrangement, this approach would permit rapid determination of the minimum switching plan. For example, Experiment Scheduling For 10-foot Hole; Plan No. 1 (Figure 3) requires the following experiment grouping: (e_5,e_7,e_{10}), (e_3,e_8,e_9), (e_1,e_2,e_4,e_8,e_{11}), (e_1,e_2,e_4,e_{11}),

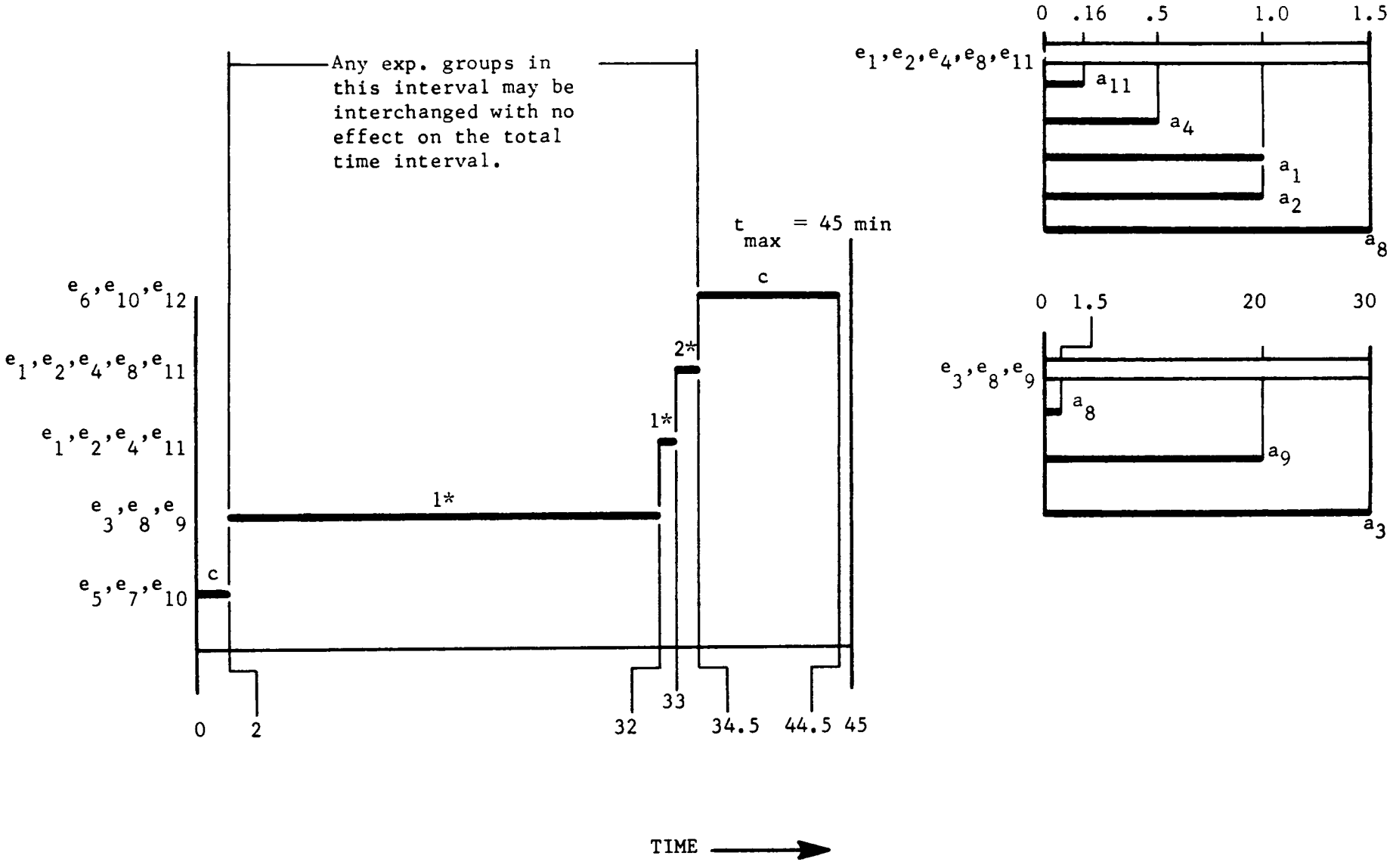

*THE NUMBERS REPRESENT THE PROBE POSITION WHILE "C" DESIGNATES A CONTINUOUS RUN.

Figure 3. EXPERIMENT FOR 10 FOOT HOLES. PLAN NO. 1
(Abstracted from NSL Task Order No. 2)

and (e_6, e_{10}, e_{12}). It can be seen that group activation, rather than multiple switch activation, would result in minimum switching movements. For instance, it would require two movements (on-off) to complete the (e_5, e_7, e_{10}) group if they were electrically locked; whereas, it would require $2\sum e_k$ movements if they had to be activated individually. In addition, maximum reliability is maintained by designing switches to be activated individually or as a group. The optimum arrangement of switches for Plan No. 1: 10-ft hole proved to be:

e_5	e_7	e_{10}	e_6	e_{12}
e_8	e_2	e_4	e_1	e_{11}
	e_3	e_8	e_9	

Figure 4 presents the preliminary panel design indicating the switch groupings by distinct screen patterns. Some groups have common elements and are presented in the same horizontal row; i.e., groups (e_5, e_7, e_{10}) and (e_6, e_{10}, e_{12}) have the common element e_{10}; groups (e_1, e_2, e_4, e_8, e_{11}) and (e_1, e_2, e_4, e_{11}) have the common elements (e_1,e_2,e_4,e_{11}).

Each of the experiment groups can be activated by one movement, using the control element philosophy. Consider the following:

Control Element	Experiment Group Activated				
e_5	e_5	e_7	e_{10}		
e_{12}	e_{10}	e_6	e_{12}		
e_8	e_8	e_2	e_4	e_1	e_{11}
e_{11}	e_2	e_4	e_1	e_{11}	
e_3	e_3	e_8	e_9		

Each element of the group, excluding the control element, could be activated individually to provide maximum reliability.

Experiment Scheduling For 100-Foot Hole (Figure 5) would require a maximum of five grouping arrangements; i.e., (e_5, e_7, e_{10}), (e_3, e_8, e_9), (e_1,e_2,e_4,e_8,e_{11}), and (e_1,e_2,e_4,e_{11}). If each group of experiments could

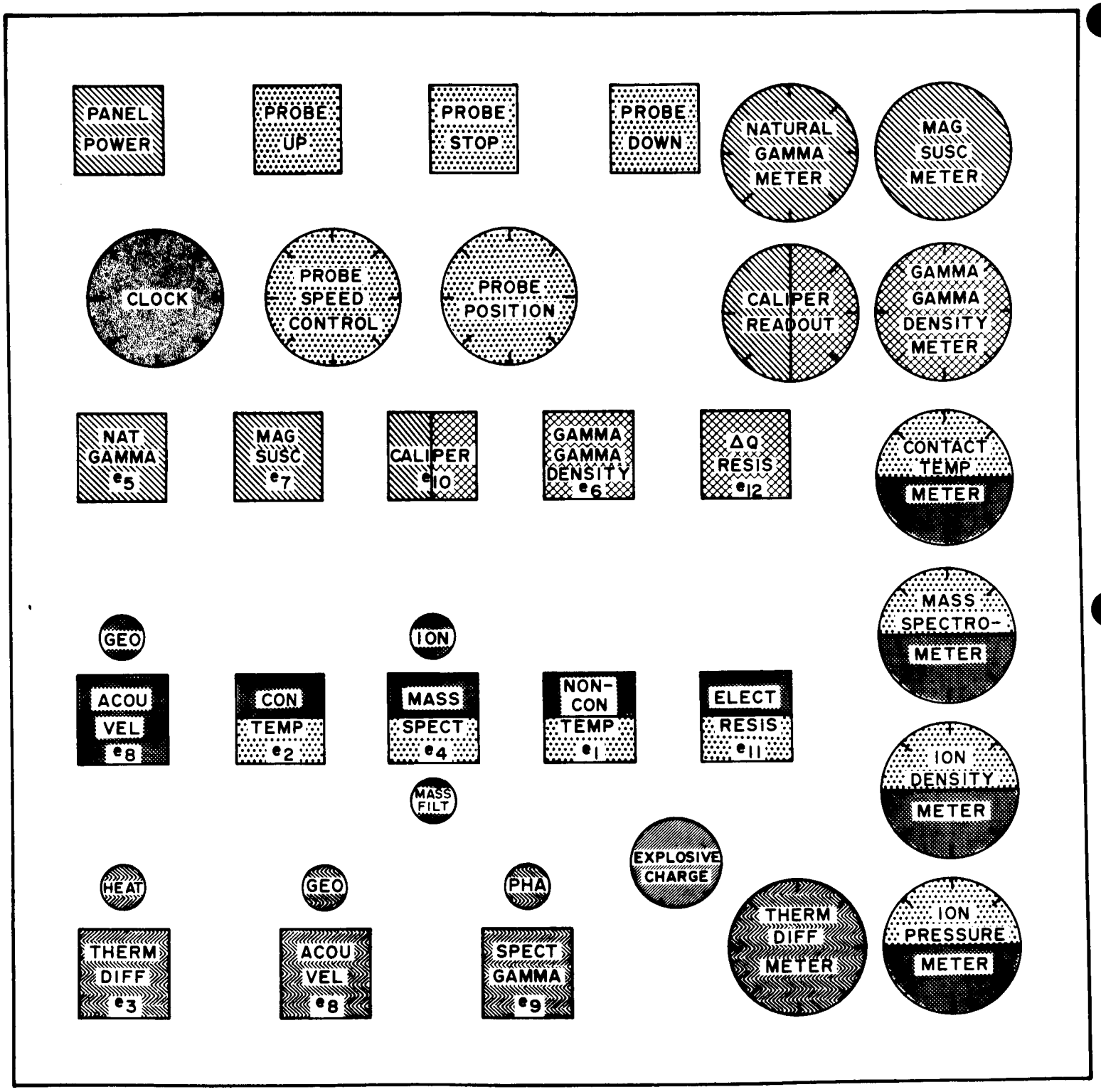

Figure 4. CONCEPTUAL PANEL DESIGN FOR LUNAR SUBSURFACE PROBE

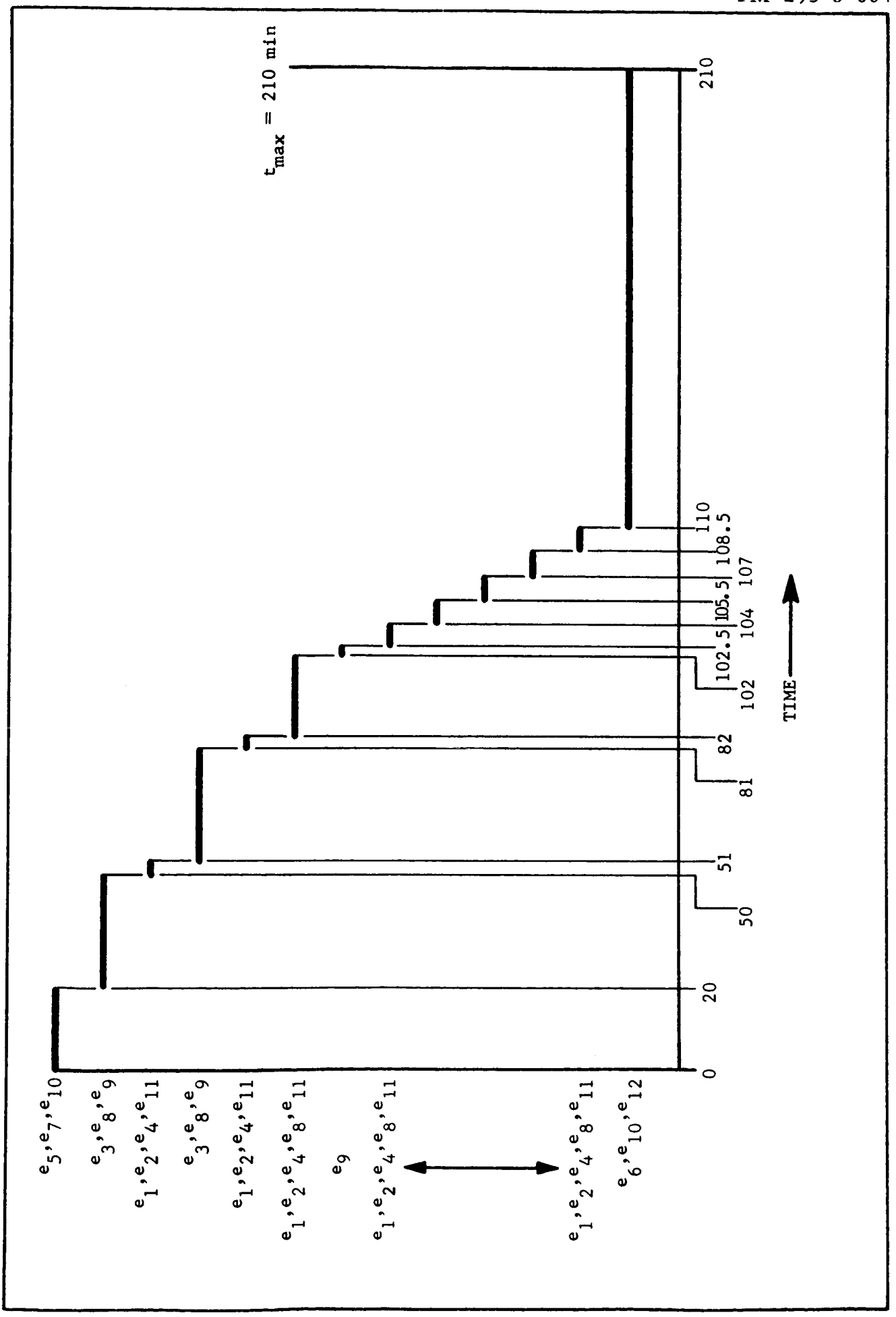

Figure 5. EXPERIMENT SCHEDULING FOR 100 FOOT HOLES PLAN NO. 3
(Abstracted from NSL Task Order No. 2)

be activated by one switching movement, the result would be an optimum switching arrangement for each plan.

The frequency of each experiment group (Plan No. 3, for instance), will establish a priority for panel space; that is, the group occurring most frequently would be considered first for minimum switching arrangements. Consider the following:

Experiment Group	Frequency
1. (e_5, e_7, e_{10})	1
2. (e_3, e_8, e_9)	2
3. (e_1, e_2, e_4, e_{11})	2
4. (e_9)	1
5. $(e_1, e_2, e_4, e_8, e_{11})$	5
6. (e_6, e_{10}, e_{12})	1

Since experiment group 5 occurs most frequently, it was considered as the basic group. The next step would be to analyze other groups which have elements common to the basic group in an effort to establish optimum arrangement for minimum switching.

Basic Group	e_1	e_2	e_4	e_8	e_{11}

The resulting arrangement (100-ft hole) offered minimum switching as presented in Table 2.

e_5	e_7	e_{10}	e_6	e_{12}
e_8	e_2	e_4	e_1	e_{11}
	e_3	e_8	e_9	

This panel is identical to that required for the 10-foot hole and would incorporate the same control element theory.

Elementary logic and optimum grouping techniques resulted in a minimum switching situation for each plan as listed in Table 2. Only those plans which included all experiments were considered.

TABLE 2

REQUIRED SWITCHING MOVEMENTS		
Plan No.	10-Ft. Hole	100-Ft. Hole
1	26	*
3	32	62
4	66	71
5	*	105
6	76	95
7	41	*

*Plan does not include all experiments and was excluded from study.

5. CONCEPTUAL DESIGN

Comparison of the switching arrangements for the 10-foot hole and the 100-foot hole reveal that the latter could serve for the 10-foot hole as well. The logging for both the 10-foot hole and the 100-foot hole would be the sum of the minimum values of each. Switching block diagrams (see figures 6 and 7) present the minimum sequencing plans (Plan No. 1, 10-ft hole and Plan No. 3, 100-ft hole), respectively. A switching block diagram for the logging of both holes is not presented since it would merely be an addition of the two. The preliminary panel design as presented in figure 4 meets the requirements of paragraph (4) of Task Order No. 3.

Similar techniques were utilized in the determination of minimum switching for the two Optimum Plans for the 10-ft hole and 100-ft hole. Figures 8 and 9 present the switching block diagrams for the optimum cases. An optimum control panel common to all minimum switching plans is presented in Figure 4 which satisfies the five separate panel designs requested in paragraph (4) of Task Order No. 3. Assumptions (3), (5), and (7) explain in general the physical nature of the control panel but for specific application, the following operational procedure is presented:

Each experiment group contains one control element, usually the extreme right or left hand switch of a horizontal row.

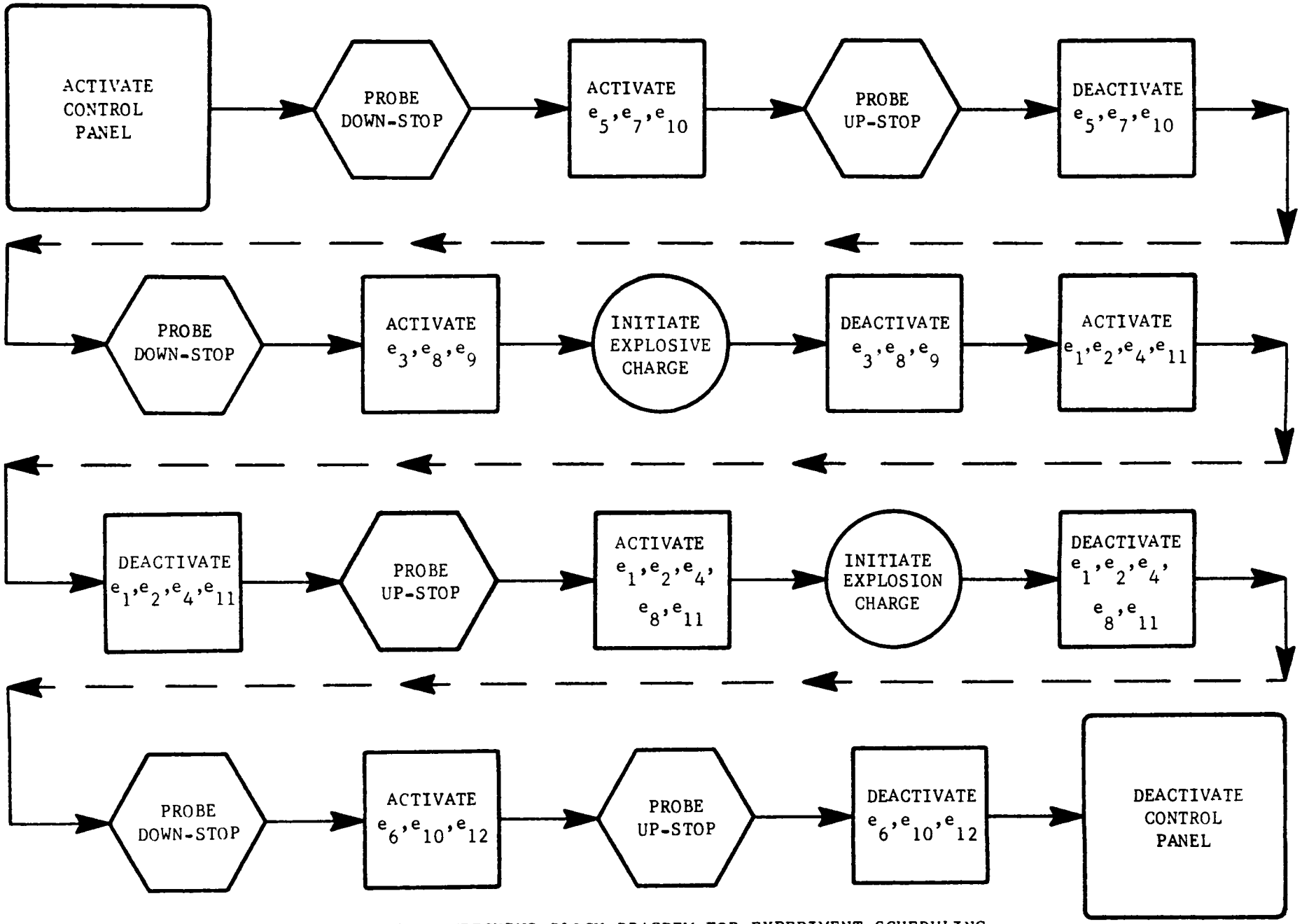

Figure 6. SWITCHING BLOCK DIAGREM FOR EXPERIMENT SCHEDULING PLAN NO. 1 (10-FT. HOLE)

Appendix VI

CONTROL SYSTEM OPTIMIZATION

AND PRELIMINARY PANEL DESIGN FOR SUBSURFACE PROBE

TM-293-6-004

CONTROL SYSTEM OPTIMIZATION

AND PRELIMINARY PANEL DESIGN FOR SUBSURFACE PROBE

BY

JOHN T. BLAIR, JR.

Prepared For:

TEXACO EXPERIMENT INCORPORATED

Richmond, Virginia

Reviewed:

J. E. Ligocki

Approved:

J. A. Barclay
Acting Director,
Systems Section

Prepared Under:

NSL TASK ORDER NO. 3

PURCHASE ORDER NO. 40510-3

SYSTEMS SECTION
NORTHROP SPACE LABORATORIES
HUNTSVILLE, ALABAMA

INTRODUCTION

The problem, as viewed by NSL, consists of three parts.

1. Adapt or develop a sequencing methodology which minimizes the time requirement while scheduling experiments.

2. Determine the maximum number of replications possible for all experiments given the three time intervals, and schedule these experiments.

3. Determine alternate scheduling plans for each level of resource and recommend an optimal time interval.

The approach taken in this study accomplishes the task. The method is general enough that any changes or additions to the experiment interrelations will be reflected in the sequencing and scheduling plans.

Elementary set theory and logic are employed as the sequencing methodology. A brief discussion of the approach follows.

Minimization of Time

Consider a set of experiments, E. If all $e_k \in E$ can be conducted simultaneously, the required time interval to execute the entire set E is equal to the time requirement of that e_k in E whose execution time is the largest (i. e., a_k/max). If all $e_k \in E$ cannot be conducted simultaneously, the set E will have to be partitioned. Each partition will cost us time, since a partition means that the execution times for the partitioned sets cannot overlap. The total execution time for the set E will be the sum of the execution times of all the partitioned sets. It is clear that in order to minimize the total execution time for the set E, the number of partitions must be minimized. Also, the partitions must be defined in such a way, that the sum of their execution times is minimum.

The procedure of partitioning begins with the identification of that $e_k \in E$ whose execution time a_k is maximum ($a_{k/max}$). Define a set X where $X \subseteq E$. The elements of X are all e_k which can be executed in conjunction with that e_k whose requirement is $a_{k/max}$. Each element of X must be

executable with every other element of X. Once the set X has been defined, examine the complement set (E-X). Identify all elements of (E-X) which may, individually, be executed in conjunction with the $e_k \in X$. Identify that $e_j \in (E-X)$ which can, by itself, be executed with the $e_k \in X$ and whose requirement is $a_{j/max}$. Include this e_j in X. Repeat this examination of (E-X) until all such elements e_j have been included in X. If all the elements of (E-X) can be simultaneously executed, the minimal partition has been made. If not, the procedure continues exactly as before. That is, identify that $e_i \in (E-X)$ whose execution time a_i is maximum ($a_{i/max}$). Define a set Y where $Y \subseteq (E-X)$. The elements of Y are all e_i which can be executed in conjunction with that e_i whose requirement is $a_{i/max}$. etc. Continue partitioning until each element of the remaining set can be executed in conjunction with every other element of the remaining set.

As an example, consider the set, E where

$$E = (e_1, e_2, e_3, e_4, e_8, e_9, e_{11})$$

and the corresponding set of execution times, A is

$$A = (a_1, a_2, a_3, a_4, a_8, a_9, a_{11})$$

Some of the e_k interfere with the execution of others as shown in Table I. The execution times are also listed opposite the corresponding e_k. By use of the partitioning procedure, we find $a_{k/max} = 30$ minutes where $k = 3$. Of those elements of E, e_8 and e_{11} can be simultaneously conducted with e_3 and with each other without interference. The elements, e_4 and e_9, can also be conducted with e_3, e_8, and e_{11} but e_4 and e_9 interfere with each other. Hence e_4 and e_9 belong to (E-X). The sets X and (E-X) are

$$X = (e_3, e_8, e_{11})$$

$$(E-X) = (e_1 \ e_2 \ e_4 \ e_9)$$

Upon examining (E-X) we find that individually, either e_4 or e_9 can be conducted simultaneously with the set X and not interfere. Since a_9 is the maximum of the two (a_9 or a_4) we include e_9 in X. Our new sets X and (E-X) are

$$X = (e_3, e_8, e_9, e_{11})$$

$$(E-X) = (e_1, e_2, e_4)$$

Table I EXAMPLE PROBLEM EXPERIMENT RELATIONS

k	Experiments (e_k)	Execution time (a_k)	Interference
1	e_1	1 min/pt	e_3
2	e_2	1 "	e_3
3	e_3	30 "	e_1, e_2
4	e_4	< 1 "	e_9
8	e_8	1.5 "	
9	e_9	20 "	e_4
11	e_{11}	.166 "	

The new set (E-X) consists only of elements which can be simultaneously executed with each other. Hence the minimal partition has been identified.

The total time interval required for the execution of the entire set E is the sum of the individual set requirements. The individual set requirements are equal to $a_{k/max}$ and $a_{i/max}$ for X and (E-X) respectively. The calculation is shown.

k = 3	a_3 = 30 minutes
i = 1 or 2	a_1 = 1 minute
Total	= 31 minutes

The minimal time requirement of 31 minutes can be determined by calculating the requirements for all combinations of the elements of E, and selecting the one whose requirement is minimum. The procedure can be shown to give the minimal partition by simple reasoning, however. Consider the resulting set X immediately after partitioning E into X and (E-X). The requirement of X is $a_{k/max}$. This value is the smallest possible value that can be assigned to X and yet provide a long enough interval to execute all elements of X. Thus the allocation of time to X is minimum. The requirement of (E-X) may not be a minimum. The set (E-X) has a requirement equal to the largest requirement of any of its elements e_j. Now, the total requirement for E is $a_{k/max} + a_{j/max}$. Note that $a_{k/max}$ equals or exceeds $a_{j/max}$. If that e_j corresponding to $a_{j/max}$ can be included in X, its requirement will easily fit within the time interval for X. The effect has been to reduce the requirement for (E-X). The requirement for X is unchanged and remains at a minimum, while the requirement for (E-X) has been reduced. Certainly the total requirement for E has been reduced. Since in the example only the necessary partitions were made, both sets (after redefinition) have minimum requirements. The sum is, therefore, minimum.

Scheduling

The foregoing discussion demonstrates the optimal sequencing methodology, where the criterion for optimization is minimum time. Consider the scheduling of the experiments. Given the partial priority order of the experiments and the three levels of resource requirements (the resource being time), it is possible to write a linear constraint expressing the

experiment requirements, and define a method of optimization. The criterion for optimization is the maximization of the number of experiment replications. The number of replications is constrained by the upper limit of time.

The method is to initially schedule all experiments once. If any time is left for replication, as many of the top priority experiments as there is time for, are scheduled for replication. As the resource of time is used, the group of experiments which fit within the given time frame diminishes. When the set of all twelve experiments, E, require more time for execution than there is available, the lowest priority experiment is removed from E. If the requirement is still too great the next to the lowest priority experiment is removed from the set. The process continues until the remaining set fits within the remaining time frame. This set is scheduled for replication.

Since a complete priority order is not given, more than one schedule will usually result from such a procedure. However, in correspondence with the optimization criterion of minimum time and maximum replications, those experiments of a particular priority group whose requirements were greatest, are forced out of E first. This allows more replications of the top priority experiments.

Note that when any element of E is forced out due to the contraint of time, the sets X and its complement set can be redefined. This will sometimes allow the simultaneous execution of more experiments if that e_k which is being forced out, interferred with any of remaining experiments. This again saves resources.

Optimum Resources

Considering the optimization criteria of minimum time and maximum replication, it is impossible to define the optimum time interval per se. The difficulty is that without a limit on the time interval, the two criterion are contradictory. The necessary measure of effectiveness such as the unit cost of time and unit value of an experiment replication is not available. It is recognized that such a measure of effectiveness does not appear realistic in this study, for these measures are not available before the time has been expended and the data collected.

One alternative to the measure, is to subjectively evaluate the use of the probe by selecting a reasonable number of replications of each experiment,

and letting the time fall where it must. This is the method employed here. The recommendations for both the 10 foot and 100 foot holes are listed in Table V.

Problem Formulation

For convenience, the subscripts of the experiments have been changed to reflect the partial priority order (one for first, two for second, etc.) and are listed in Table II. It is recognized that a complete priority order is not given, but the assignment has no adverse effect on the scheduling since the execution times are the primary consideration for scheduling.

Upon examination of the twelve experiments it was deemed most desirable to class the continuous experiments separate from the stationary experiments. It was further noted that of the continuous experiments the Gamma-Gamma Density experiment (e_6) interferes with other continuous experiments. Thus it appears most advantageous to make three runs of the probe in each hole. The three runs (designated r_1, r_2 and r_3) constitute a minimal partition as defined in a previous section of this report. Our Geologists have indicated that r_1, which consists of continuous experiments, is most valuable if conducted as the first run in the sequence. The reason is that the logging records will indicate those depths of special interest to be further investigated by the stationary experiments. The run r_2, which consists of all stationary experiments, will follow. The run r_3, which includes the Gamma-Gamma Density experiment is appropriately last, since it interferes with experiments of both r_1 and r_2, and may render the hole temporarily unusable.

Only the stationary experiments were considered for replication. The continuous experiments yield data at every point within the hole and do not require replication.

Table II EXPERIMENT PRIORITY ORDER

	Experiment	Priority Group
1.	Non-Contact Temp.	I
2.	Contact Temp.	I
3.	Thermal Diffusivity	I
4.	Mass Spectrometer	I
5.	Natural Gamma	I
6.	Gamma-Gamma Density	I
7.	Magnetic Susceptibility	I
8.	Acoustic Velocity	I
9.	Spectral Gamma	II
10.	Caliper	II
11.	Electrode Resistivity	III
12.	Change of Q Resistivity	III

$r_1 = (e_5, e_7, e_{10})$

$r_2 = (e_1, e_2, e_3, e_4, e_8, e_9, e_{11})$

$r_3 = (e_6, e_{12})$

Table IIIa NO. OF MEASUREMENTS OF e_k FOR 10 FOOT HOLES

Resources in Minutes	45	45	75	75	75	90	90	90
Experiments								
e_1	2	10	3	10	4	13	6	13
e_2	2	10	3	10	4	13	6	13
e_3	1	0	2	1	0	2	1	0
e_4	2	9	3	9	4	13	6	13
e_5*	1	1	1	1	1	1	1	1
e_6*	1	1	1	1	1	1	1	1
e_7*	1	1	1	1	1	1	1	1
e_8	2	9	2	10	4	12	6	13
e_9	1	1	2	2	3	2	3	3
e_{10}**	2	2	2	2	2	2	2	2
e_{11}	2	10	3	10	4	13	6	13
e_{12}*	1	1	1	1	1	1	1	1
Plan No.	1	2	3	4	5	6	7	8

*These experiments are continuous. Hence the optimum number of measurements is 1.

**This experiment is the caliper log which may be made with either r_1 or r_3 or both, with no additional cost in time.

Table IIIb NO. OF MEASUREMENTS OF e_k FOR 100 FOOT HOLE

Resources in Minutes	120	120	210	300	300	300
e_1	8	1	8	9	16	17
e_2	8	1	8	9	16	17
e_3	3	0	2	5	4	3
e_4	8	0	8	9	16	17
e_5*	1	0	1	1	1	1
e_6*	0	1	1	1	1	1
e_7*	1	0	1	1	1	1
e_8	7	1	8	9	16	17
e_9	3	1	3	6	6	7
e_{10}**	1	1	2	2	2	2
e_{11}	8	1	8	9	16	17
e_{12}*	0	1	1	1	1	1
Plan No.	1	2	3	4	5	6

Table IV SCHEDULING PLANS FOR GIVEN TIME INTERVALS

Note: The scheduling plans correspond to the plan numbers at the bottom of Table III.

Plan No. 1 for the 10 foot holes contains a detailed explanation of how to interpret the entire set of plans, hence, these details do not appear on other than Plan No. 1. The interpretation is, however, the same for all plans.

EXPERIMENT SCHEDULING FOR 10 FOOT HOLES. PLAN NO. 1

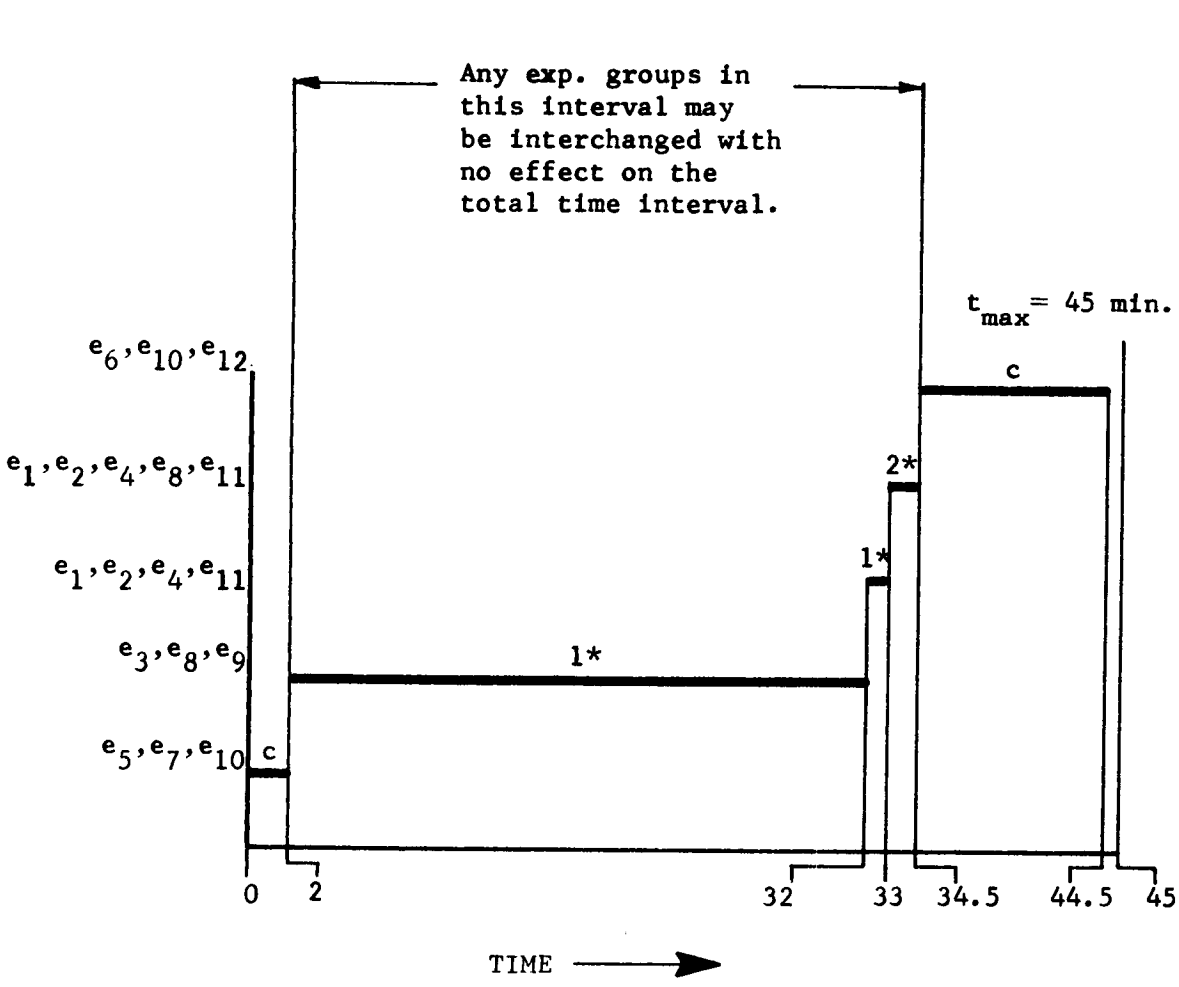

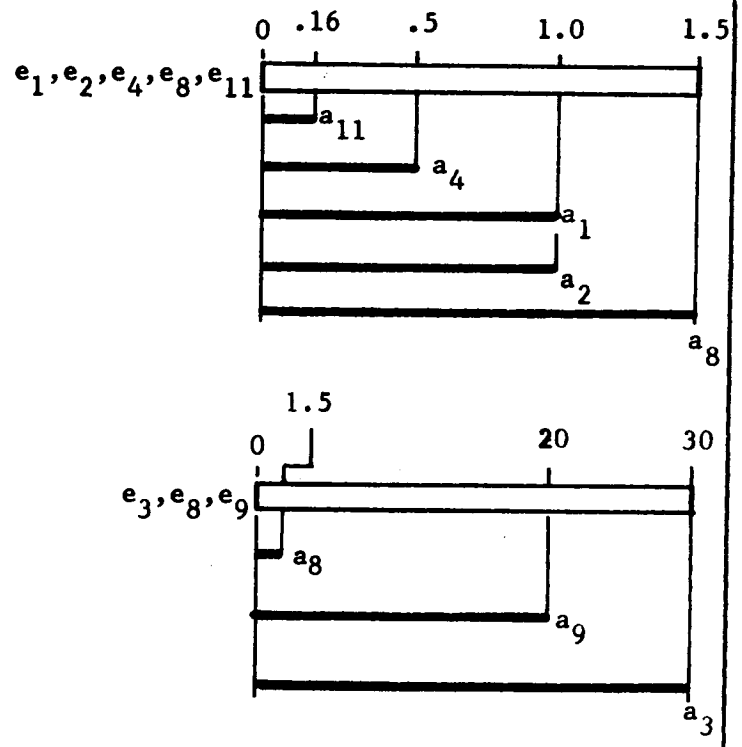

*THE NUMBERS REPRESENT THE PROBE POSITION WHILE "C" DESIGNATES A CONTINUOUS RUN.

EXPERIMENT SCHEDULING FOR 10 FOOT HOLES PLAN NO. 2

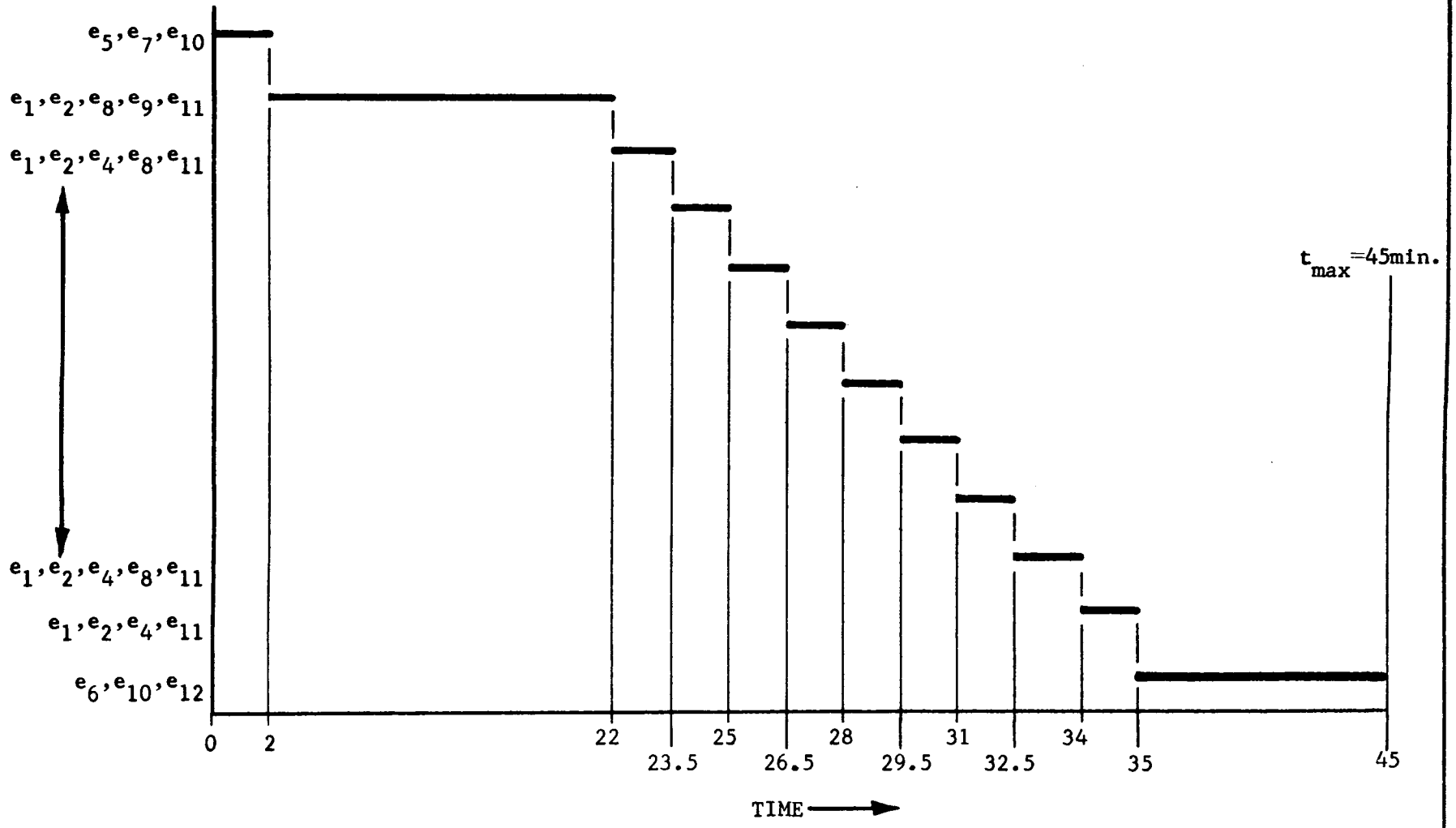

EXPERIMENT SCHEDULING FOR 10 FOOT HOLES PLAN NO. 3

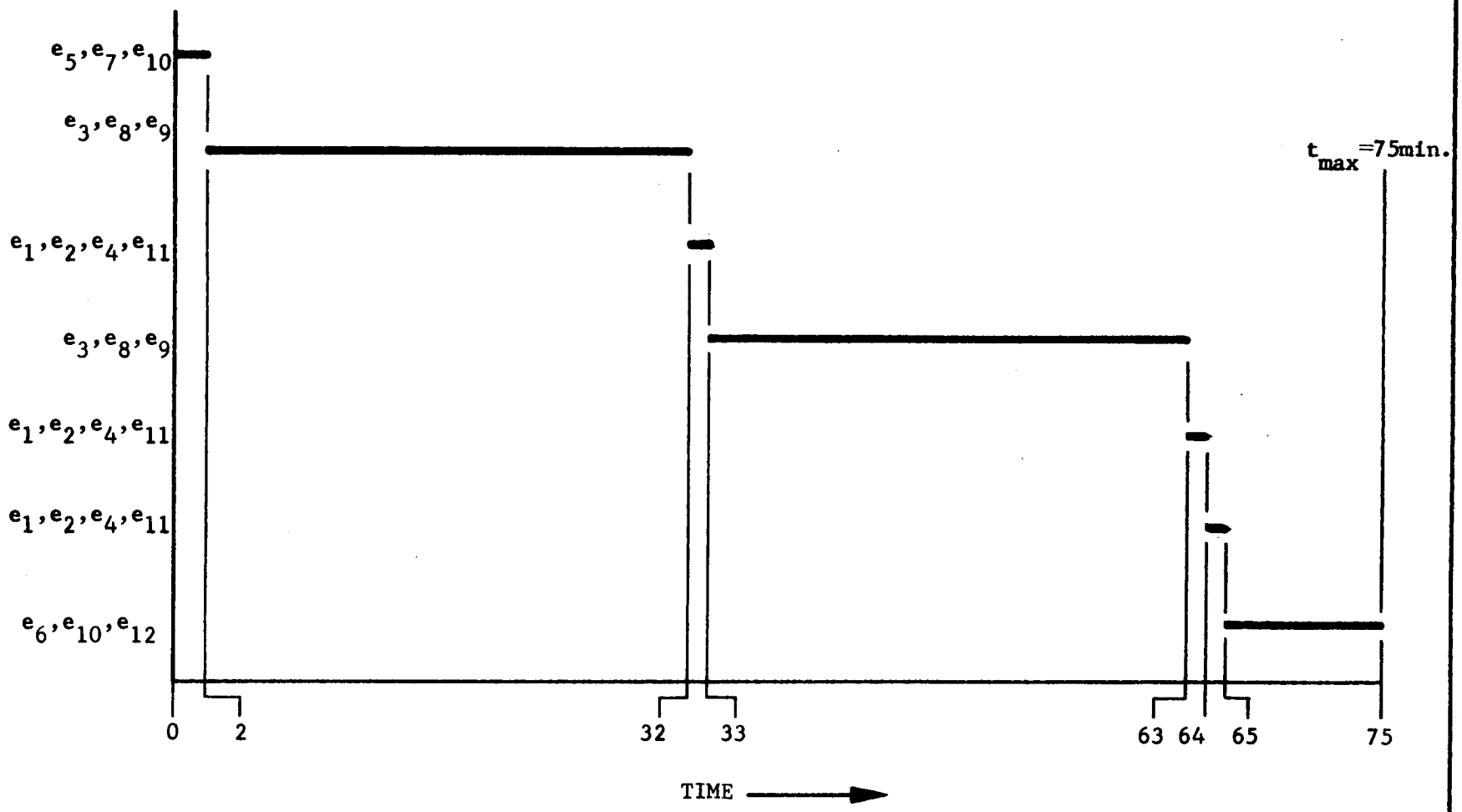

EXPERIMENT SCHEDULING FOR 10 FOOT HOLES PLAN NO. 4

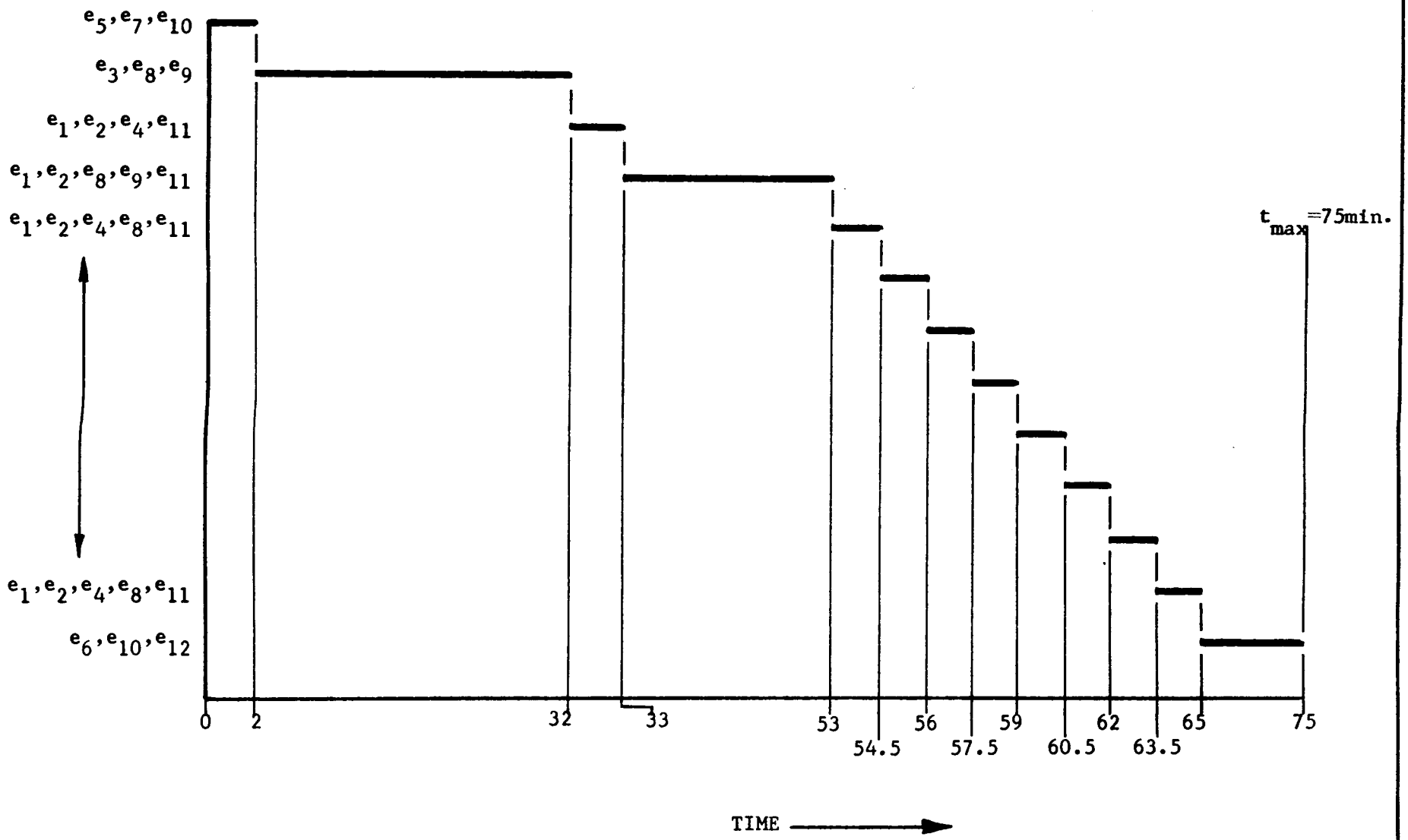

EXPERIMENT SCHEDULING FOR 10 FOOT HOLES PLAN NO. 5

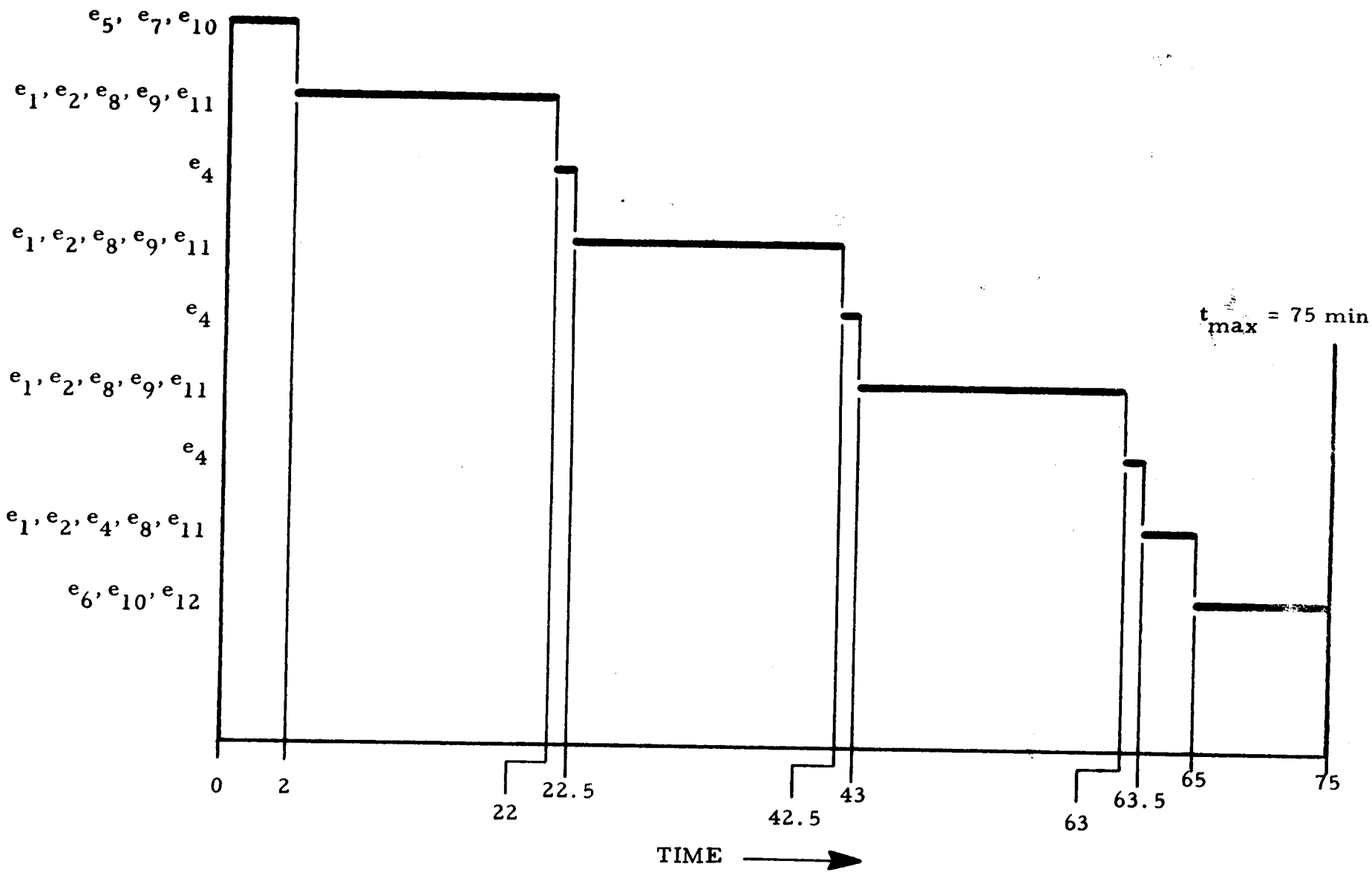

EXPERIMENT SCHEDULING FOR 10 FOOT HOLES PLAN NO. 6

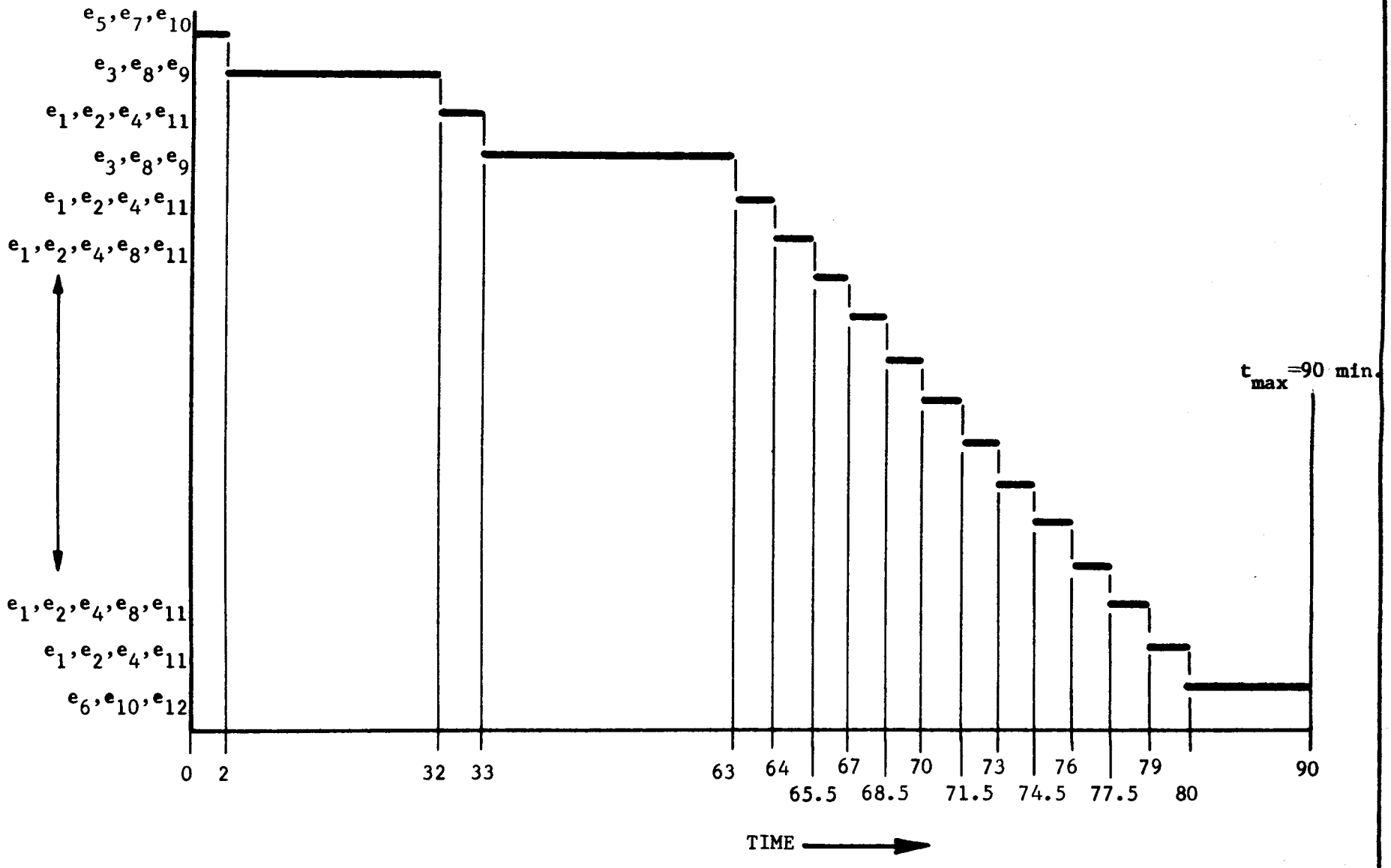

EXPERIMENT SCHEDULING FOR 10 FOOT HOLES PLAN NO. 7

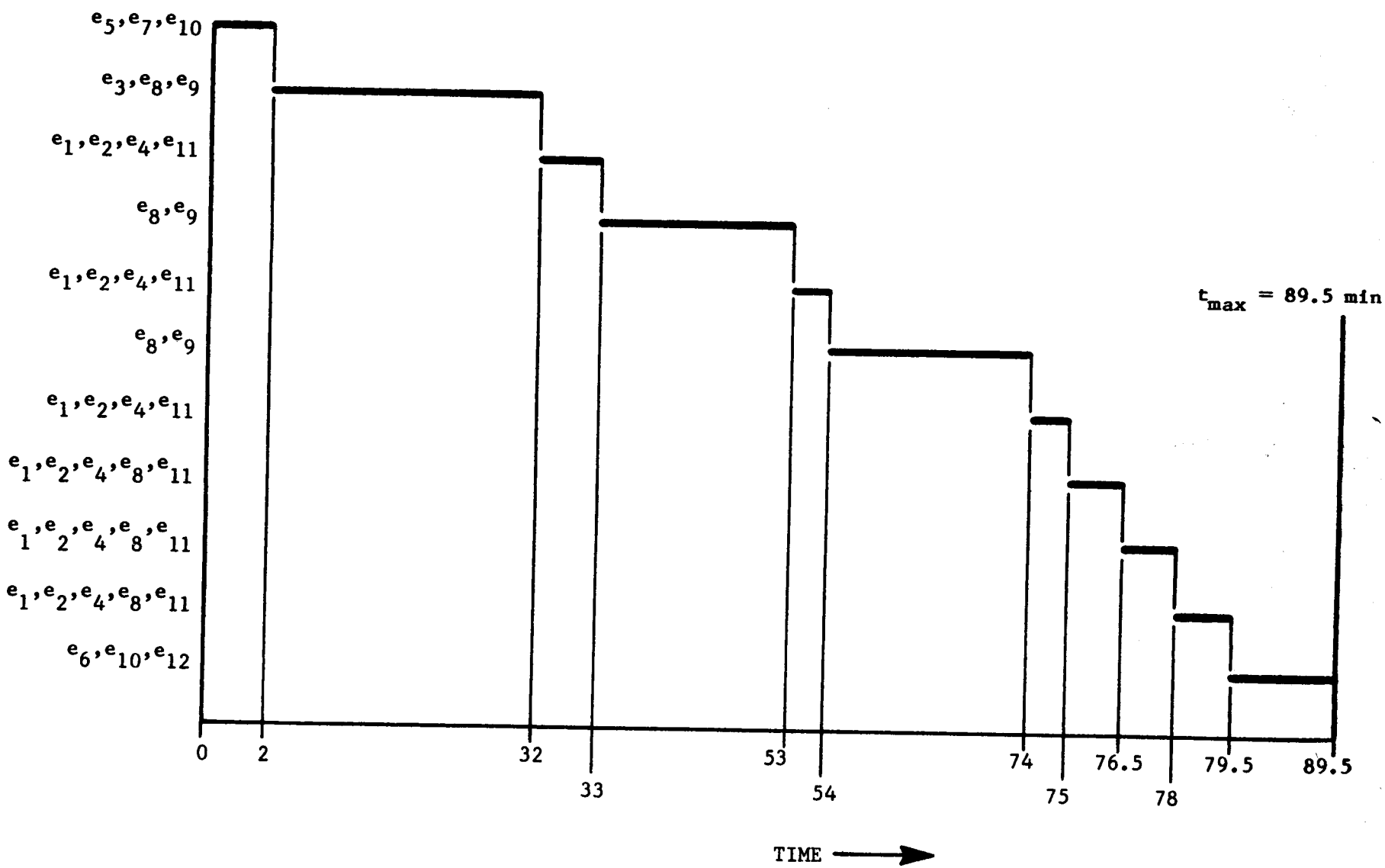

EXPERIMENT SCHEDULING FOR 10 FOOT HOLES PLAN NO. 8

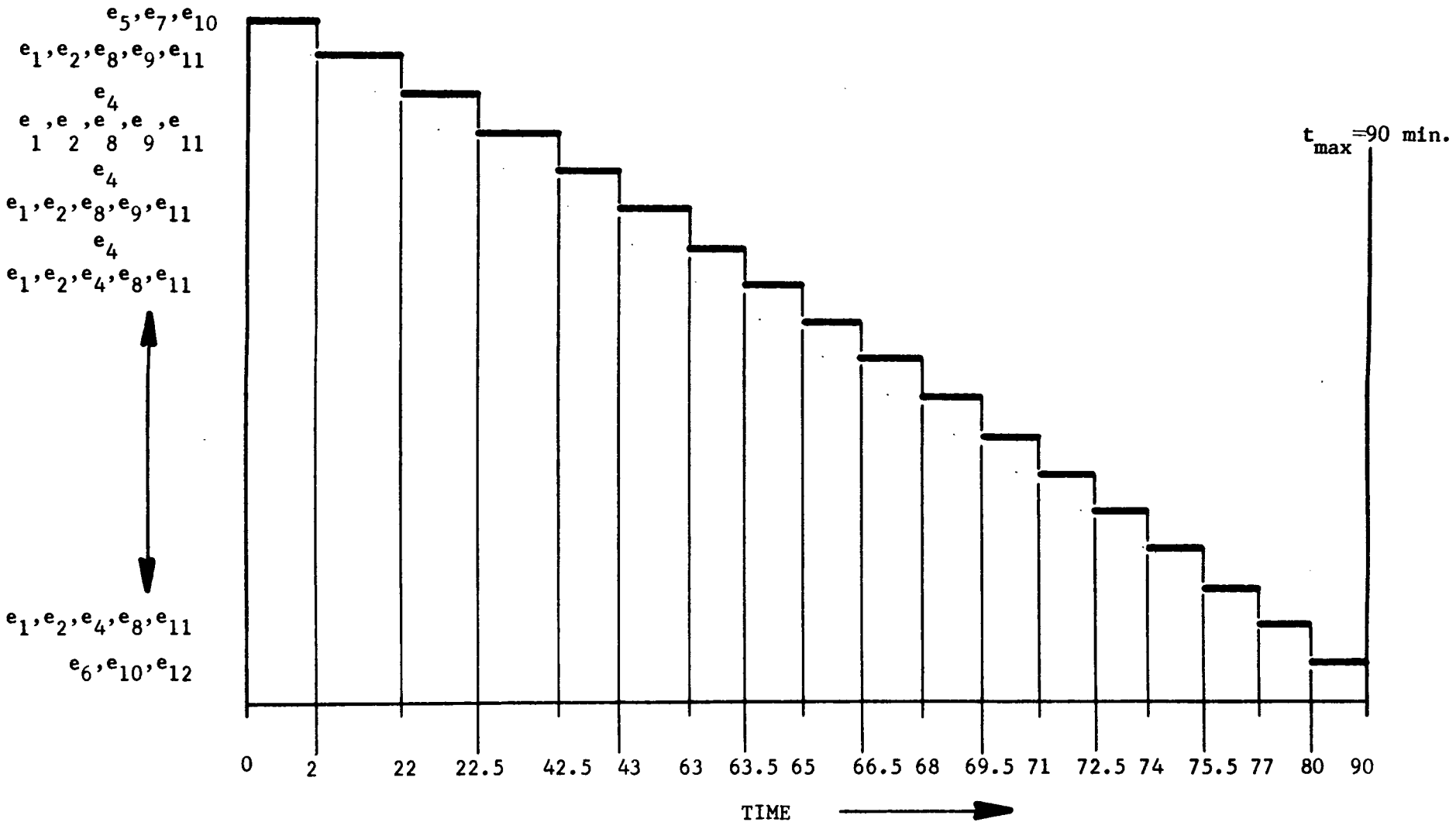

EXPERIMENT SCHEDULING FOR 100 FOOT HOLES PLAN NO. 1

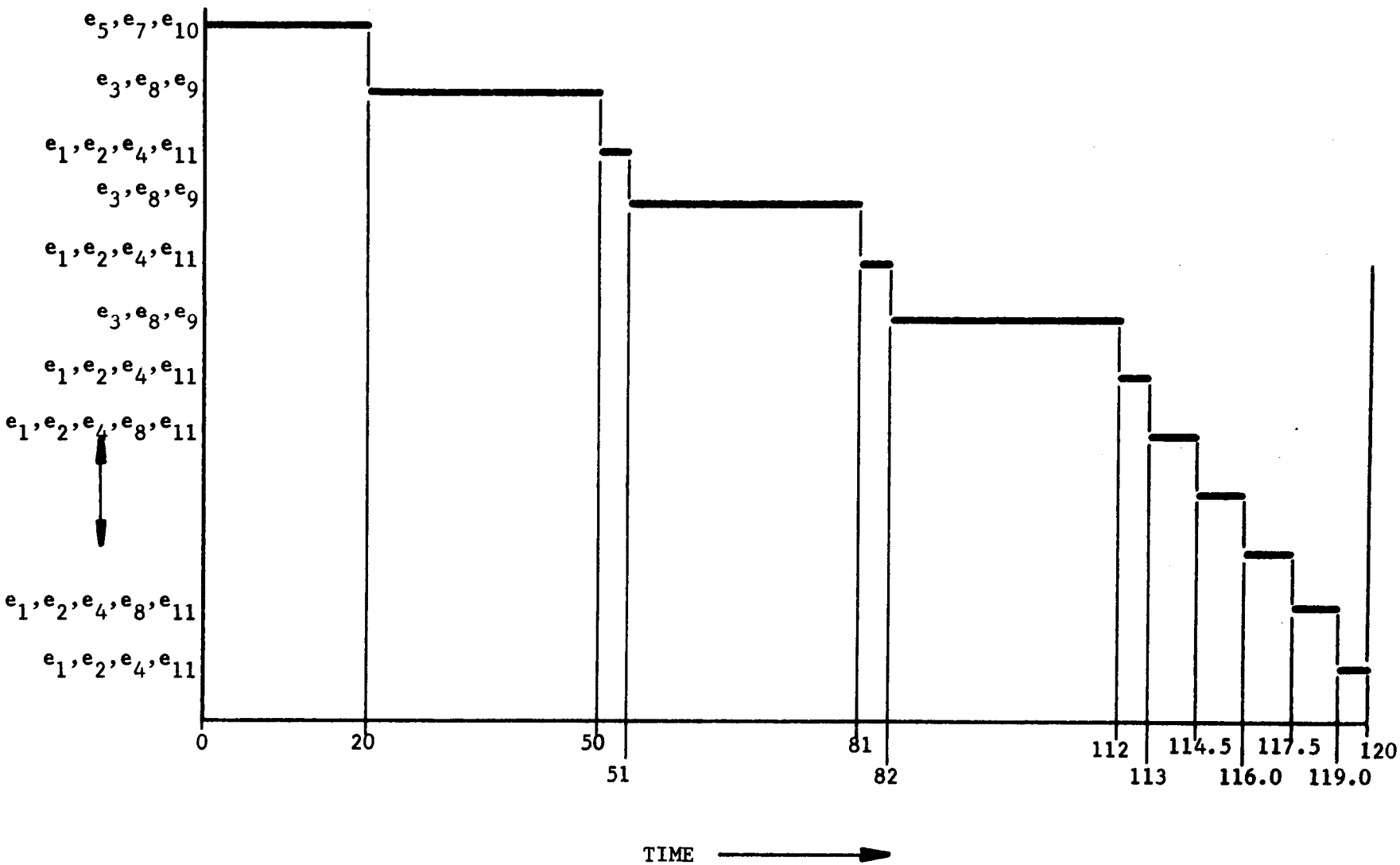

EXPERIMENT SCHEDULING FOR 100 FOOT HOLES PLAN NO. 2

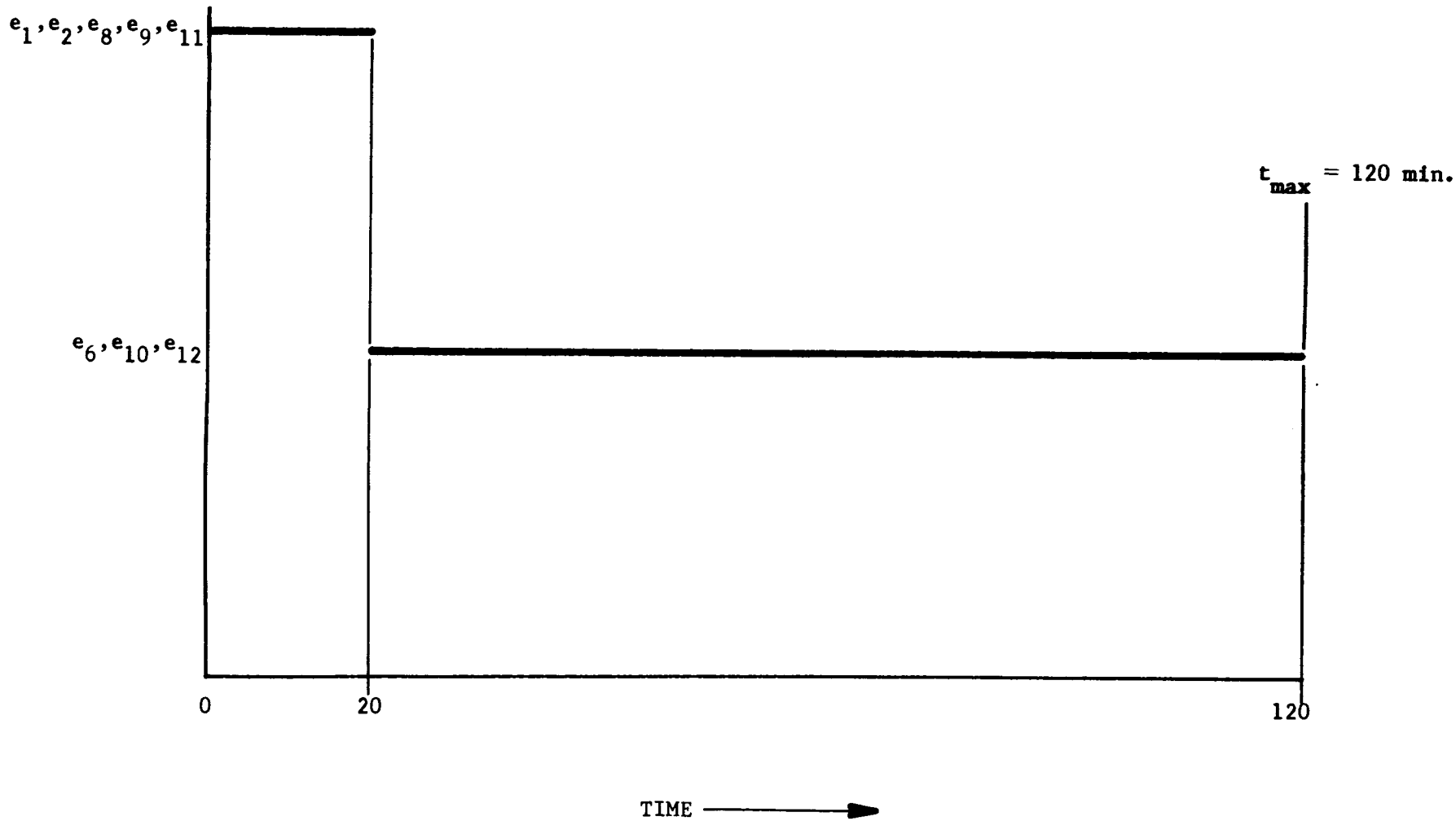

EXPERIMENT SCHEDULING FOR 100 FOOT HOLES PLAN NO. 3

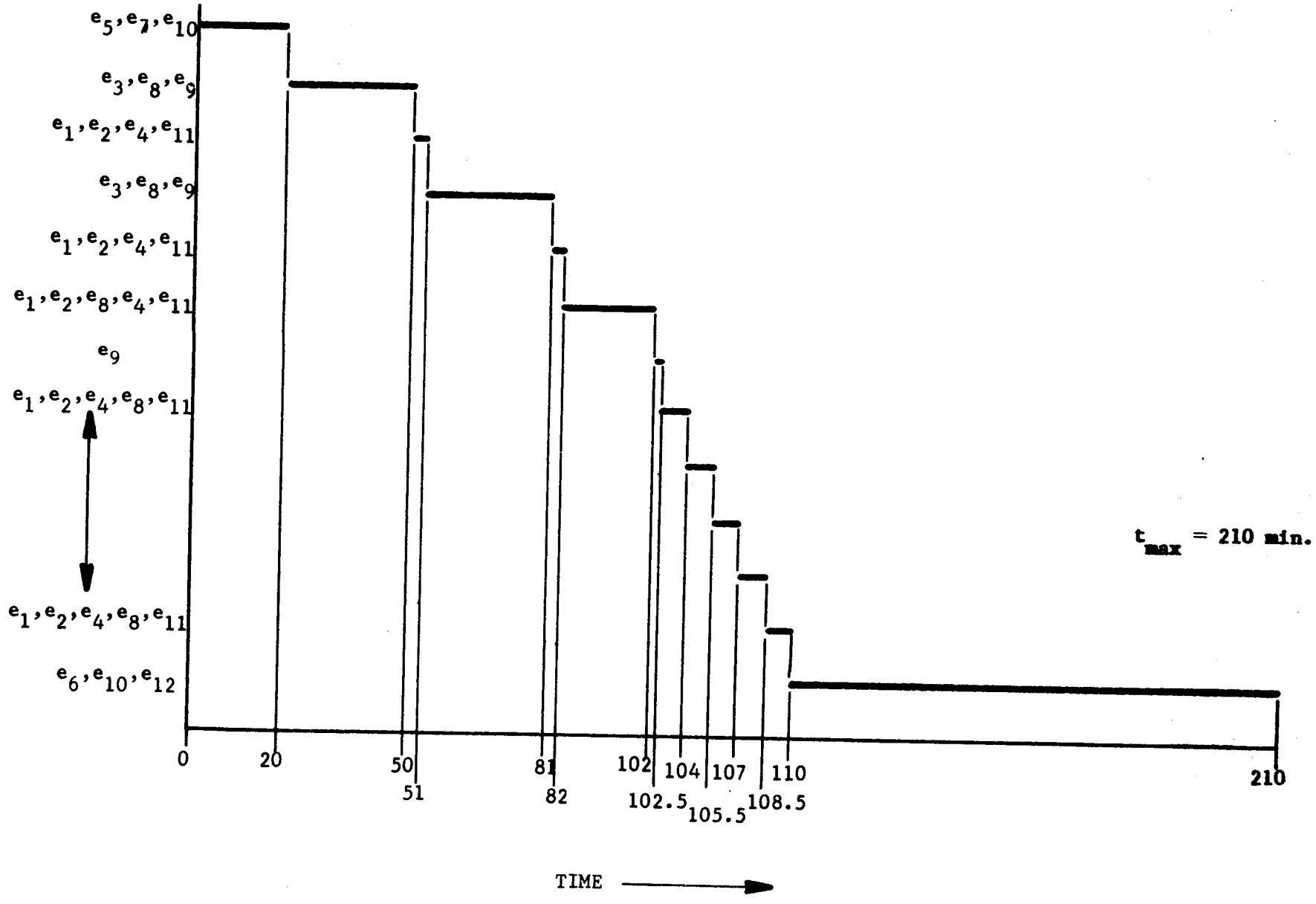

EXPERIMENT SCHEDULING FOR 100 FOOT HOLES PLAN NO. 4

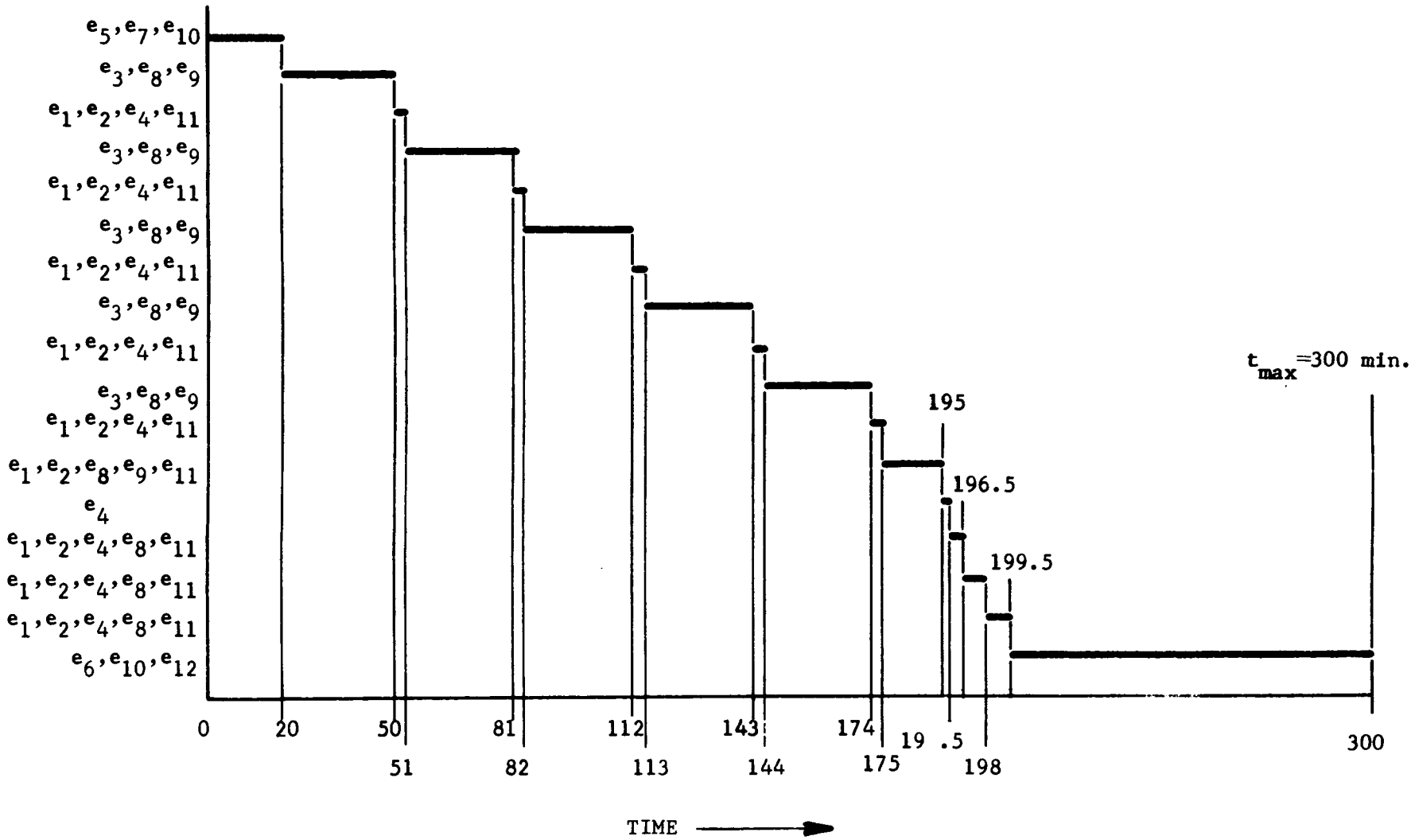

EXPERIMENT SCHEDULING FOR 100 FOOT HOLES PLAN NO. 5

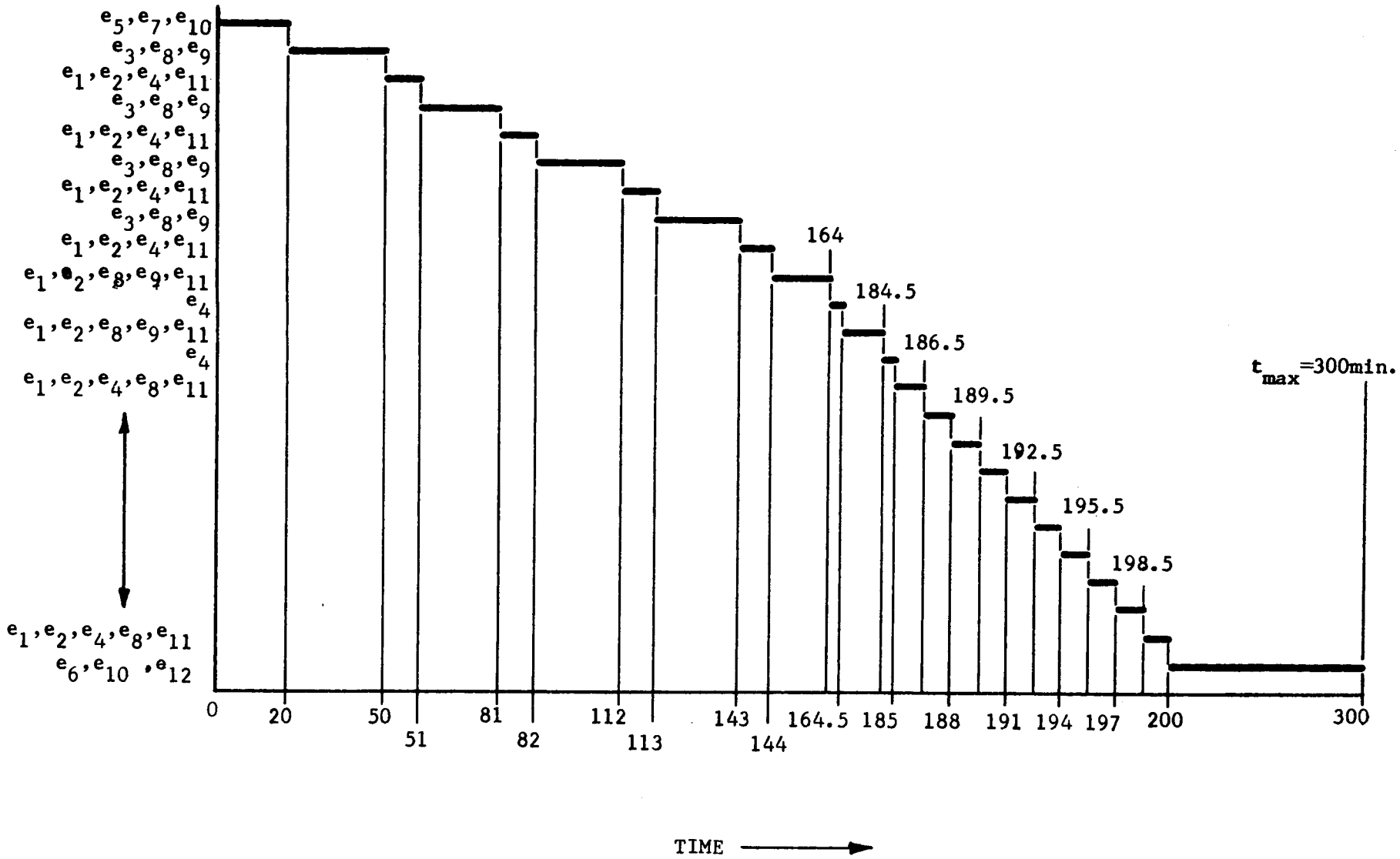

EXPERIMENT SCHEDULING FOR 100 FOOT HOLES PLAN NO. 6

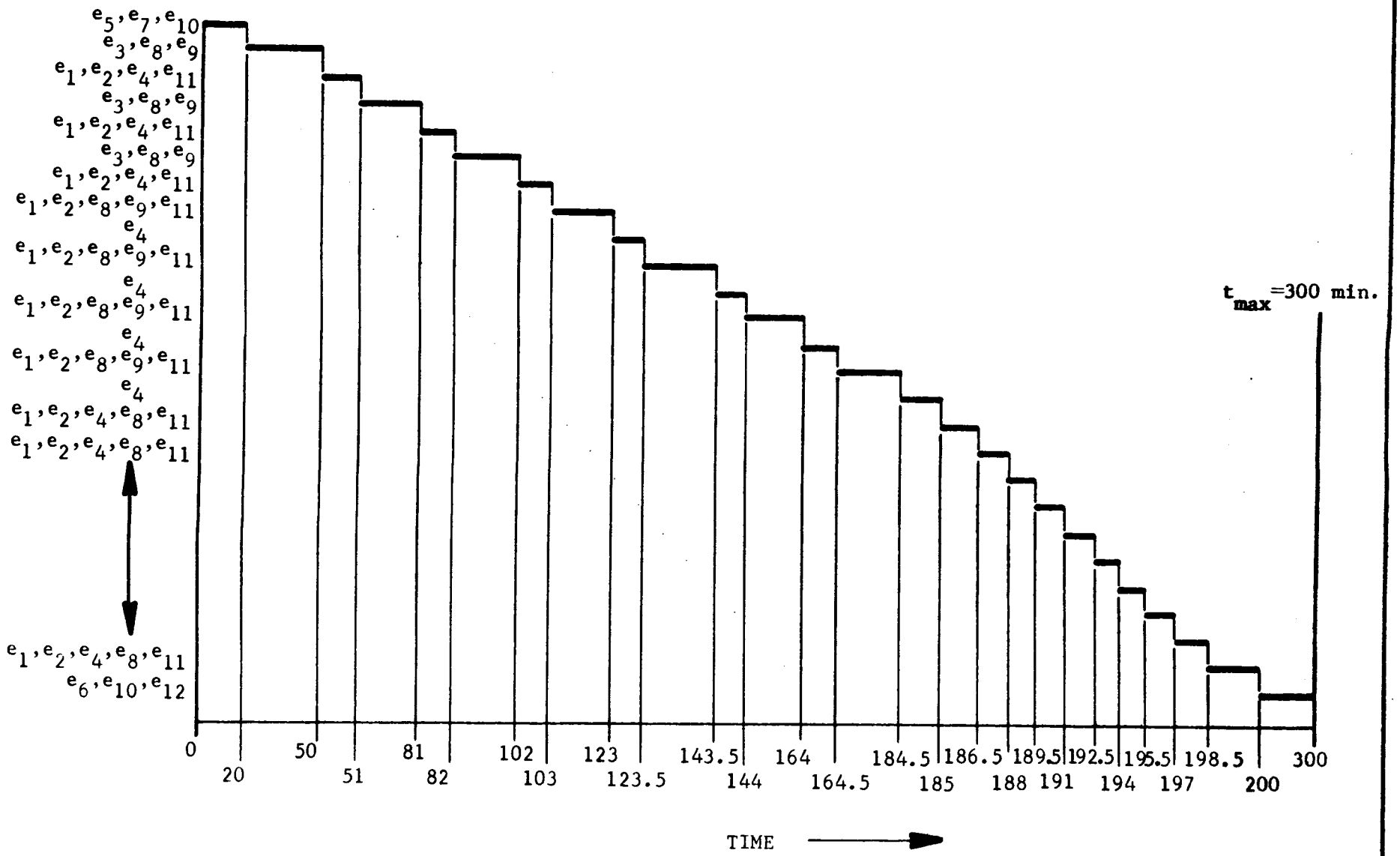

Table V OPTIMUM TIME FOR THE GIVEN NO. OF MEASUREMENTS OF e_k

Experiments	10 Foot Holes		100 Foot Holes		
e_1	4	2	7	7	7
e_2	4	2	7	7	7
e_3	0	2	5	6	7
e_4	4	2	7	7	7
e_5*	1	1	1	1	1
e_6*	1	1	1	1	1
e_7*	1	1	1	1	1
e_8	4	2	7	7	7
e_9	4	2	5	6	7
e_{10}**	2	2	2	2	2
e_{11}	4	2	7	7	7
e_{12}*	1	1	1	1	1
Total Requirements in Minutes	93	74	278	307.5	337
Optimum Plan No.	1	2	1	2	3

Table VI OPTIMUM SCHEDULING PLANS

Note: The scheduling plans correspond to the plan numbers at the bottom of Table V.

EXPERIMENT SCHEDULING FOR 10 FOOT HOLES OPTIMUM PLAN NO. 1

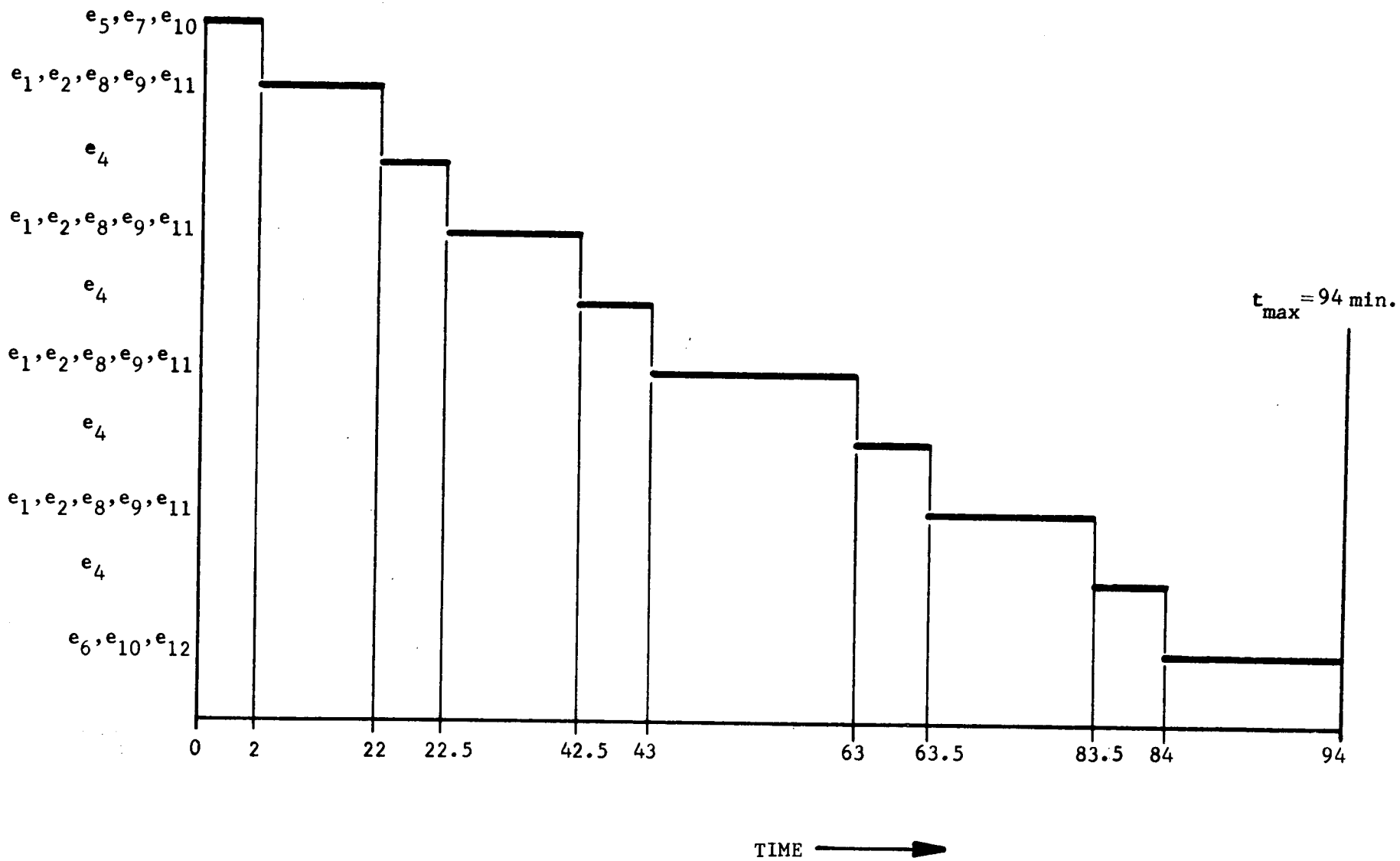

EXPERIMENT SCHEDULING FOR 10 FOOT HOLES OPTIMUM PLAN NO. 2

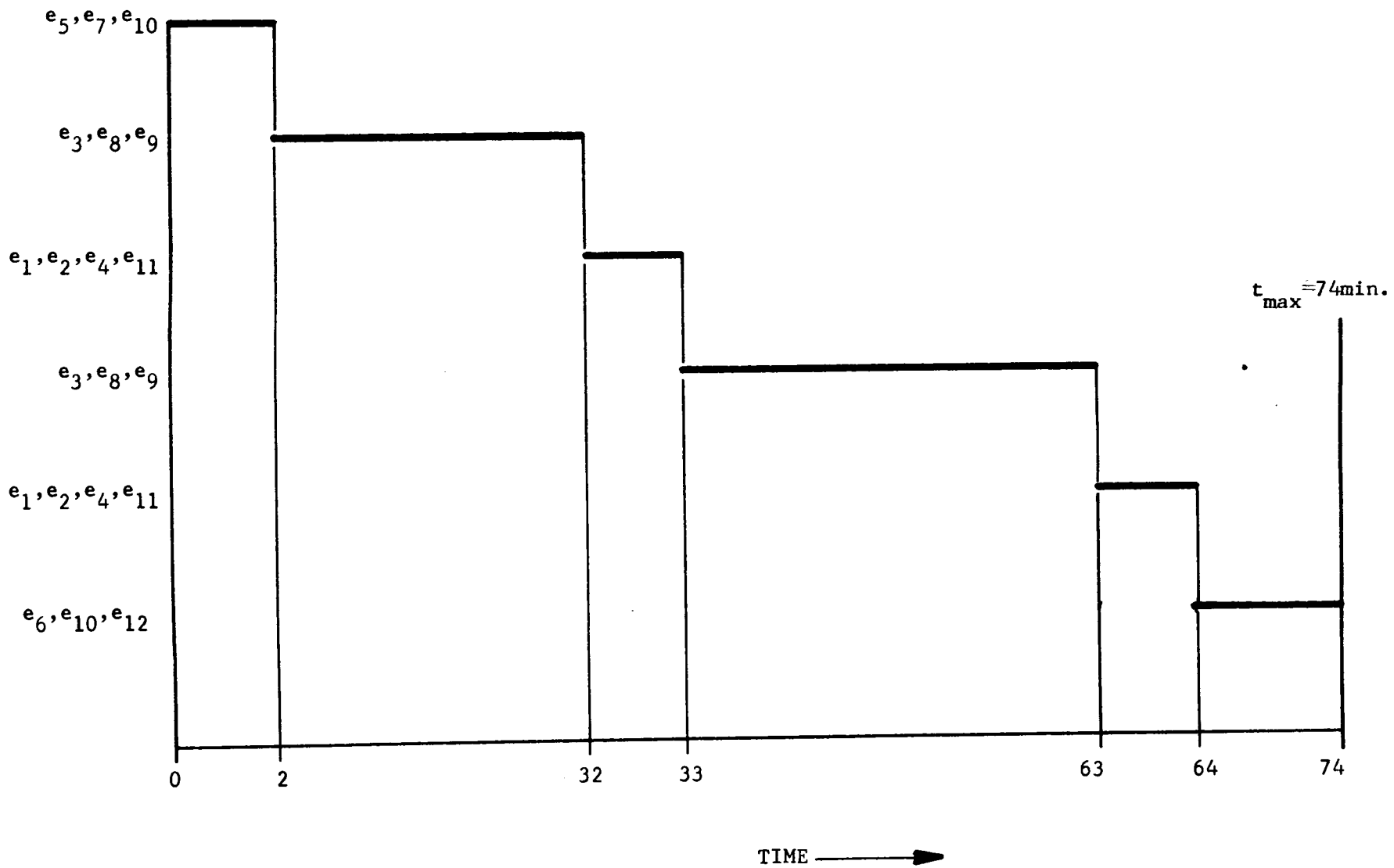

EXPERIMENT SCHEDULING FOR 100 FOOT HOLES OPTIMUM PLAN NO. 1

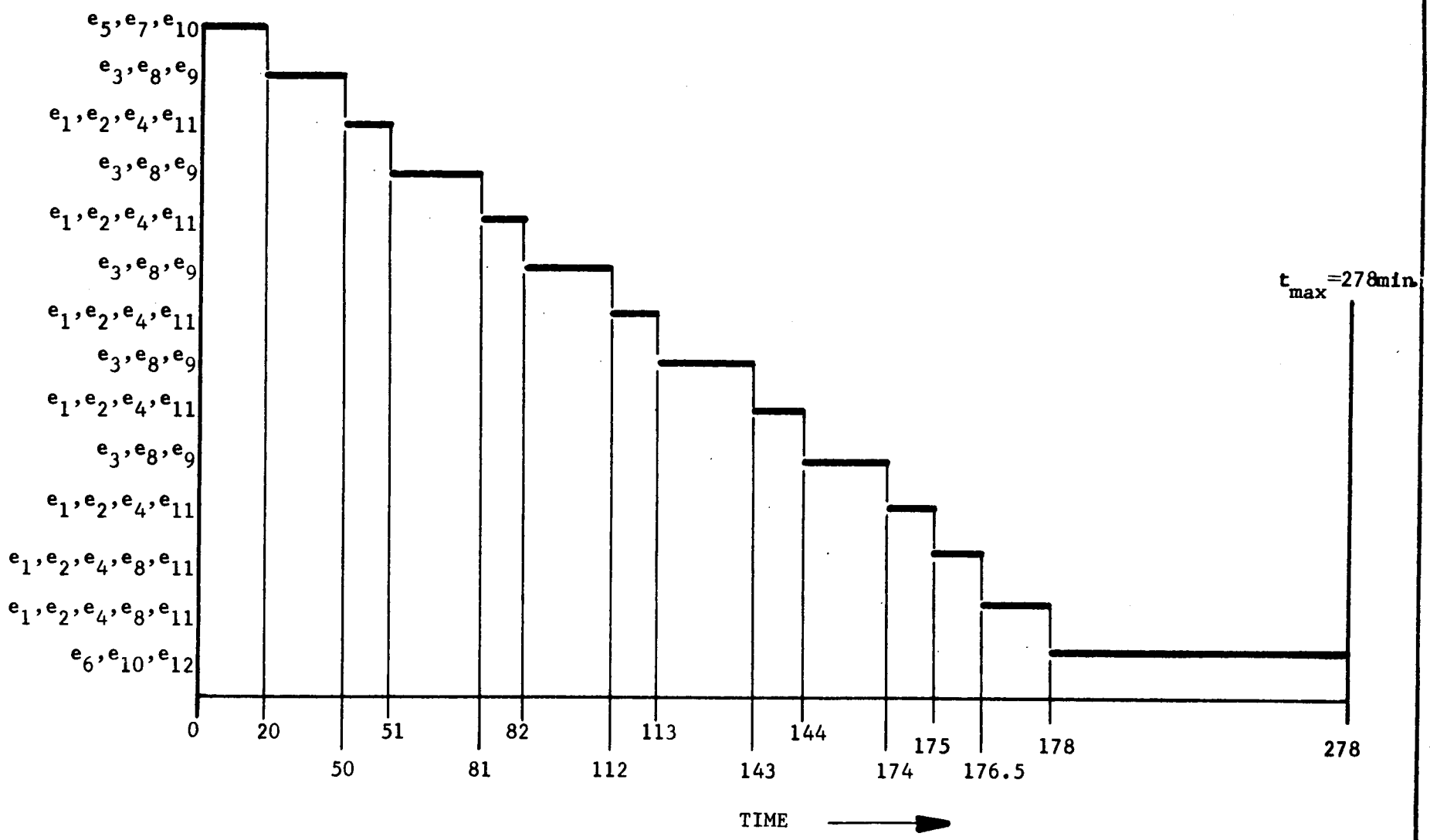

EXPERIMENT SCHEDULING FOR 100 FOOT HOLES OPTIMUM PLAN NO. 2

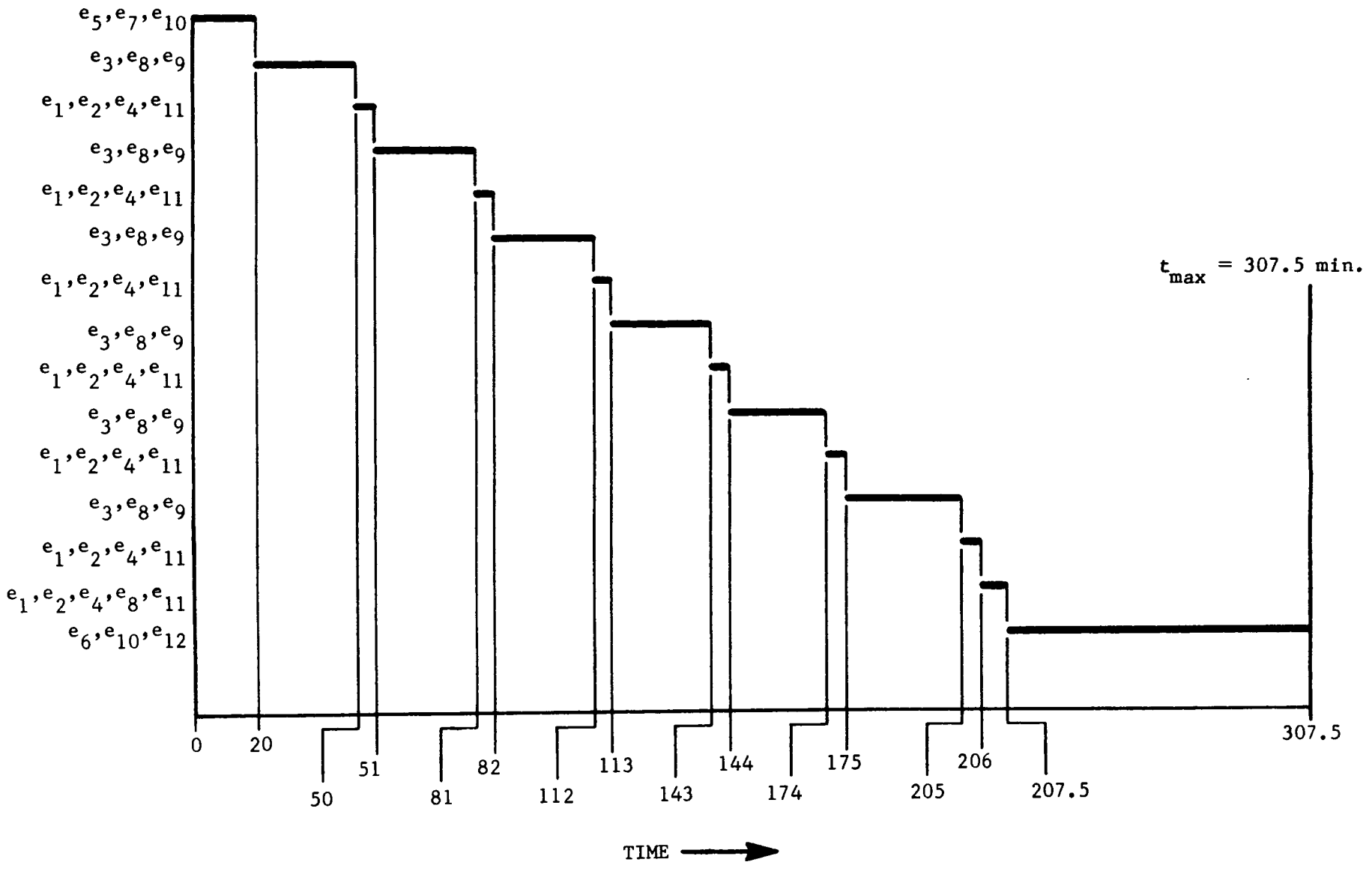

EXPERIMENT SCHEDULING FOR 100 FOOT HOLES OPTIMUM PLAN NO. 3

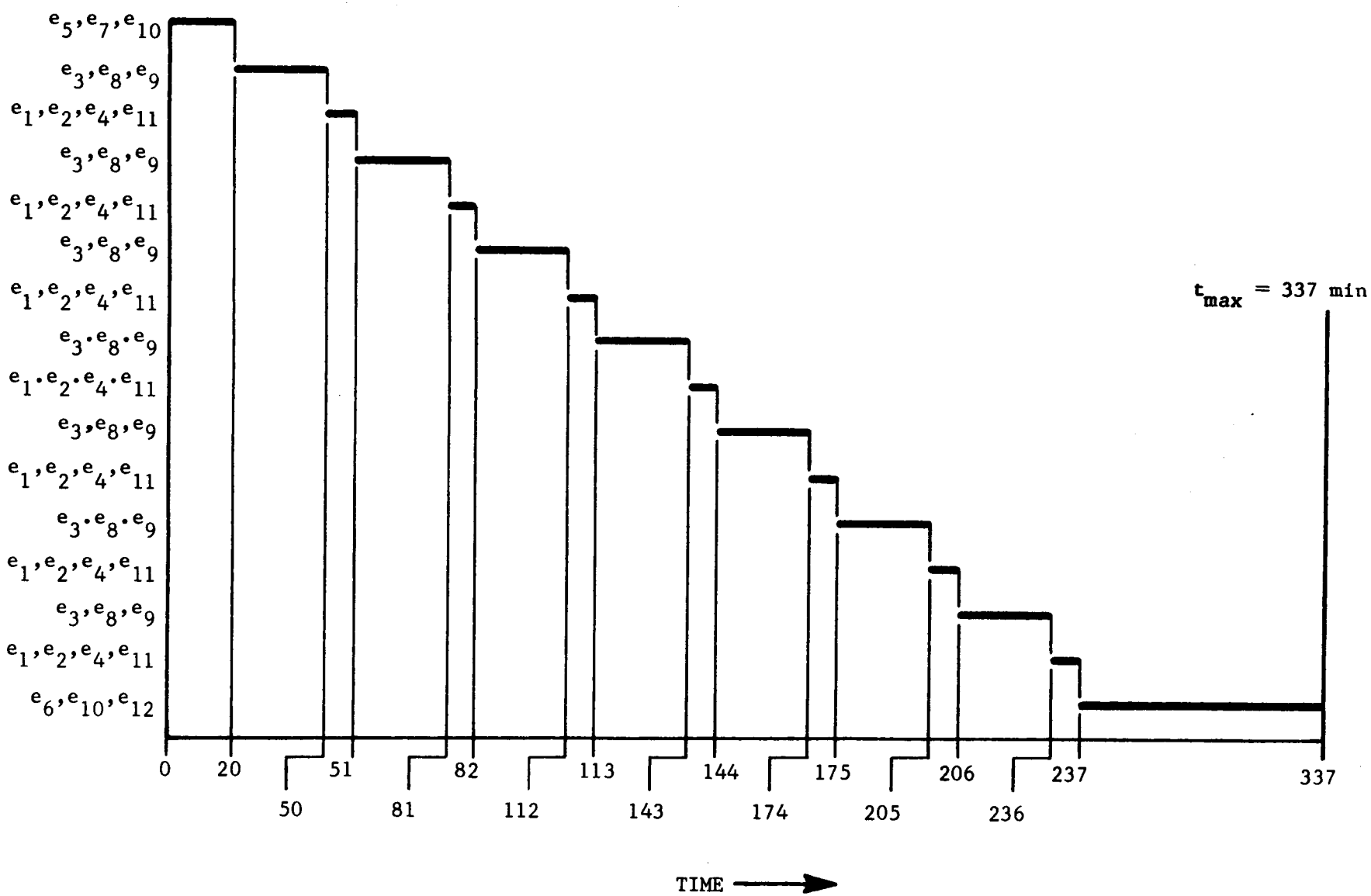

Appendix V

EXPERIMENT SCHEDULING AND SEQUENCING PLANS AND METHODOLOGY

FOR

TEXACO EXPERIMENT INCORPORATED SUBSURFACE PROBE

NORTHROP SPACE LABORATORIES

E30-87
Revision A
April 1966

EXPERIMENT SCHEDULING AND SEQUENCING PLANS AND METHODOLOGY

FOR

TEXACO EXPERIMENT INCORPORATED SUBSURFACE PROBE

By

Joseph A. Svestka

NSL Task Order No. 2
Purchase Order No. 40510-3
Dated 16 December 1965

Systems Section
Northrop Space Laboratories
Huntsville, Alabama

APPROVED:

Milton Beilock
Director-Systems Section

TM-293-6-007
April 1966

ANALYSIS OF HEAT TRANSFER BETWEEN SUBSURFACE PROBE AND BOREHOLE WALL

By

M. C. Thadani
C. M. Mackenzie

PREPARED FOR
TEXACO EXPERIMENT INCORPORATED
RICHMOND, VIRGINIA

PREPARED UNDER:
NSL TASK ORDER NO. 4
PURCHASE ORDER NO. 40510-3

Reviewed by:

J. E. Ligocki
Supervisor Design Branch

Approved By:

J. A. Barclay
Acting Director-Systems Section

SYSTEMS SECTION
NORTHROP SPACE LABORATORIES
6025 TECHNOLOGY DRIVE
HUNTSVILLE, ALABAMA

TABLE OF CONTENTS

Paragraph		Page
	PREFACE	ii
	LIST OF SYMBOLS	iii
1	INTRODUCTION	1
2	DISCUSSION	1
3	ASSUMPTIONS	2
4	DATA FOR CALCULATIONS	3
5	CALCULATIONS AND RESULTS	4

LIST OF TABLES

Table No.	Title	Page
1	Initial Probe Surface and Borewall Temperatures	3

LIST OF ILLUSTRATIONS

Figure No.	Title	Page
1	Probe Temp. vs. Time (Max. Power - Lunar Noon)	6
2	Probe Temp. vs. Time (Max. Power - Lunar Noon)	7
3	Probe Temp. vs. Time (Max. Power - Lunar Night)	8
4	Probe Temp. vs. Time (Mean Power - Lunar Noon)	9
5	Probe Temp. vs. Time (Mean Power - Lunar Noon)	10
6	Probe Temp. vs. Time (Mean Power - Lunar Night)	11
7	Probe Temp. vs. Time (Zero Power - Lunar Noon)	12
8	Probe Temp. vs. Time (Zero Power - Lunar Noon)	13
9	Probe Temp. vs. Time (Zero Power - Lunar Night)	14
10	Borehole Wall Temp. vs. Time (Max. Power - Lunar Noon)	15
11	Borehole Wall Temp. vs. Time (Mean Power - Lunar Noon)	16
12	Borehole Wall Temp. vs. Time (Max. Power - Lunar Night)	17
13	Borehole Wall Temp. vs. Time (Mean Power - Lunar Night)	18

PREFACE

This informal report was prepared by the Systems Section of Northrop Space Laboratories, Huntsville, Alabama, for Texaco Experiment Incorporated. The work was performed under NSL Task Order No. 4, Purchase Order No. 40510-3, March 24, 1966. The TEI Project Engineer was Ralph H. Clinard, Jr.

LIST OF SYMBOLS

T = temperature

T_p = probe temperature

T_w = borehole wall temperature

T_∞ = lunar subsurface temperature at large distance from heat source

D = thermal diffusivity

r = local radial position coordinate

q_r = heat transferred by radiation

F_{12} = view factor

A = cylindrical surface area

E = emissivity

q_E = heat generated by power dissipation

Greek symbols

σ = Stefan - Boltzman Constant

θ = coordinate angle

Subscripts

1. refers to probe material

2. refers to lunar subsurface

1 INTRODUCTION

This report describes the heat transfer analysis between a subsurface probe and the lunar subsurface borehole wall. The probe is expected to be positioned in a two-inch diameter borehole to a depth of up to 100 feet, and is held co-axially by six centralizing members. Calculations are performed to establish the variation of the probe temperature with time due to the internal heat generation for zero, mean, and maximum power, and heat loss or gain by radiation to the wall. Further calculations are performed to establish the borehole wall temperature variation with time for maximum and mean power dissipation.

2 DISCUSSION

For the purposes of these calculations, it is assumed that in each case the thermal probe will initially be at the equilibrium temperature attained on the lunar surface during lunar noon or midnight and for zero, mean, and maximum power dissipation. The values of equilibrium temperatures have been computed in NSL Report E30-76, Revision A, dated 18 February 1966. The radial distribution of the lunar temperature has been calculated for 0° Longitude and 0° Latitude as a function of lunar time. The lunar subsurface temperature is almost constant beyond the first 100 cm, both during lunar noon and during lunar midnight. The results are presented in NSL Report E20-175. The appropriate data are presented in Table 1.

The differential equations governing the conduction of heat in cylindrical coordinates are:

$$\frac{\partial T_1}{\partial t} = D_1 \left[\frac{\partial^2 T_1}{\partial r^2} + \frac{1}{r} \frac{\partial T_1}{\partial r} + \frac{1}{r^2} \frac{\partial^2 T_1}{\partial \theta^2} + \frac{\partial^2 T_1}{\partial z^2} \right]$$

$$\frac{\partial T_2}{\partial t} = D_2 \left[\frac{\partial^2 T_2}{\partial r^2} + \frac{1}{r} \frac{\partial T_2}{\partial r} + \frac{1}{r^2} \frac{\partial^2 T_2}{\partial \theta^2} + \frac{\partial^2 T_2}{\partial z^2} \right]$$

The subscript "1" refers to conduction in probe and subscript "2" refers to conduction in lunar subsurface hole. The radiant interchange between the probe and the lunar wall is given by:

$$q_r = \sigma \left[\frac{1}{\frac{1}{E_1} + \frac{1}{E_2} - 1} \right] F_{12} A \left(T_p^4 - T_w^4 \right)$$

when:

T	= temperature
T_p	= probe surface temperature
T_w	= hole wall temperature
D	= thermal diffusivity
r	= local radial coordinate
θ	= coordinate angle
q_r	= heat transfered by radiation
F_{12}	= view factor
A	= cylindrical surface area of the probe
E_1	= emissivity of probe
E_2	= emissivity of borehole wall
σ	= Stefan Boltzman Constant

The solution of the two partial differential equations, coupled with each other through the radiation heat transfer equation, is complicated and an exact solution was not considered feasible within the time frame available for the present task. It was therefore decided to make an engineering approximation to the partial differential equations, with several simplifying assumptions, in order to get some information regarding the transient behavior of the thermal probe and borehole wall temperatures.

3 ASSUMPTIONS

- The probe is initially assumed to be at the equilibrium temperature under the appropriate lunar environments and for the power dissipation rate being considered.
- The probe temperature is uniform and the internal power generation is uniform.
- The radiant heat interchange is two dimensional and end effects can be ignored.
- Arithmetic average temperature of the moon is assumed for the first 100 cm depth. The temperature beyond 100 cm is assumed uniform.
- The lunar wall temperature is held constant during radiation. (for probe temperature calculations)
- The overall specific heat of the probe is 0.126 BTU/lb.
- The probe radiates to the lunar wall at constant temperature.
- The radiation to the lunar wall above the probe location is very small and can be neglected.

- All conduction to the wall through centralizing members stipulated in NSL Task No. 4 is not considered significant. and therefore neglected.
- The probe and wall temperatures are constant during small but discrete intervals of time of radiant interchange.
- The lunar subsurface temperature does not change beyond six borehole radii.

4 DATA FOR CALCULATIONS

Calculations were performed for the variation of probe temperature with time for the initial probe temperature in equilibrium with lunar surface noon, and midnight. In each case the internal probe power dissipation of zero, five and thirteen watts was assumed for the thermal balance. For each power dissipation, emissivities of 0.25, 0.7, and 0.9 were considered.

Table 1 INITIAL PROBE SURFACE AND BORE WALL TEMPERATURES

	LUNAR TIME					
	Noon			Midnight		
	Power Dissipation			Power Dissipation		
	Zero	5 Watts	13 Watts	Zero	5 Watts	13 Watts
Initial Probe Temp. °K	327	344	335	173	201	157
Lunar Hole Wall mean temp. °K (first 100 cm)	256	256	256	239	239	239
Lunar Hole Wall mean temp. °K (deeper than 100 cm)	239	239	239	239	239	239

5 CALCULATIONS AND RESULTS

The procedure for calculations consisted of:

5.1 Calculations for variation of probe temperature with time.

(1) Calculation of radiant heat transfer between the probe and hole wall at constant probe and wall temperatures from the equation.

$$q_r = F_{12} \cdot A \cdot \left[\frac{1}{\frac{1}{E_1} + \frac{1}{E_2} - 1} \right] (T_p^4 - T_w^4)$$

(2) Assume a discrete but small interval of time Δt during which Q_r heat is transferred.

$$Q_r = q_r \cdot \Delta t.$$

(3) Calculate the heat generated due to internal power dissipation during the discrete time interval Δt.

$$Q_e = q_E \cdot \Delta t$$

(4) Make the heat balance on the probe to calculate the heat left in the probe after time interval Δt. Sensible heat of the probe + heat generated due to power dissipation - heat lost by radiation = heat left in the probe.

$$Q_s + Q_e - Q_r = Q_s^1$$

(5) The new probe temperature T_p^1 is then calculated;

$$T_p^1 = \frac{Q_s^1}{w \cdot C_p}$$

5.2 Calculations for the variation of bore wall temperature with time.

The equation of heat conduction in a cylinder has the solution of the form

$$q = 2\pi k \left[\frac{(T_w - T_\infty)}{\ln \frac{r}{r_i}} \right]$$

which gives $$T_w = \left[\frac{q(\ln \frac{r}{r_1})}{2 \pi k}\right] + T_\infty$$

The calculations for wall temperature are carried out by using the values of q (based on emissivity of 0.9) computed for the probe heat transfer as a function of time, and by assuming that the temperature T_∞ is reached at 6 borehole radii. The equation for the wall temperature as function of heat transfer reduces to:

$$T_w = 0.236\ q + 430.$$

The wall temperatures are calculated using this equation and the values of q at different times for maximum and mean powers, and for lunar noon and midnight.

Figures 1 through 9 show the variation of mean probe temperature with time for different values of emissivity. Figures 10 through 13 show the variation of borehole wall temperature with time.

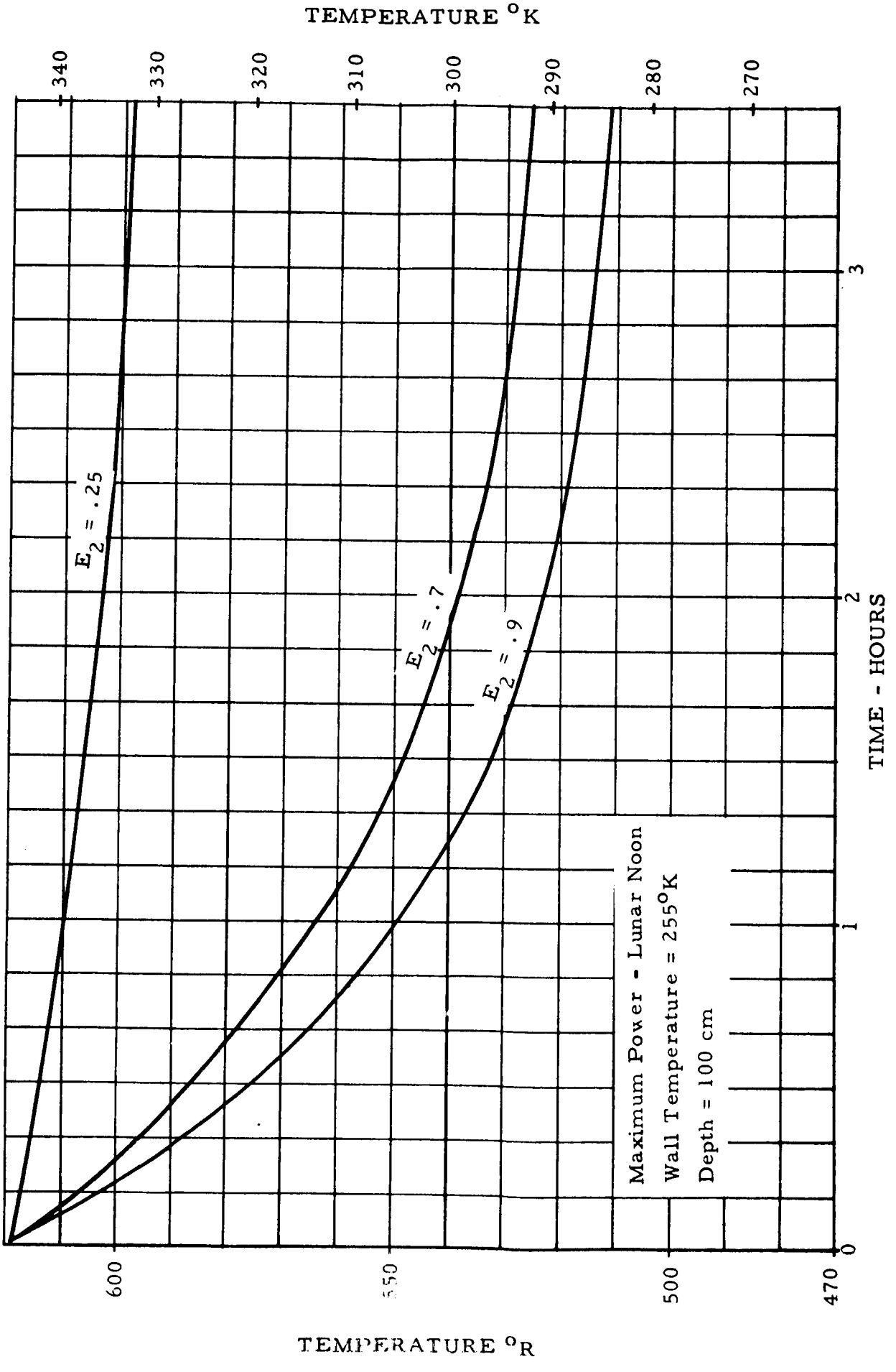

Figure 1 PROBE TEMPERATURE VS. TIME

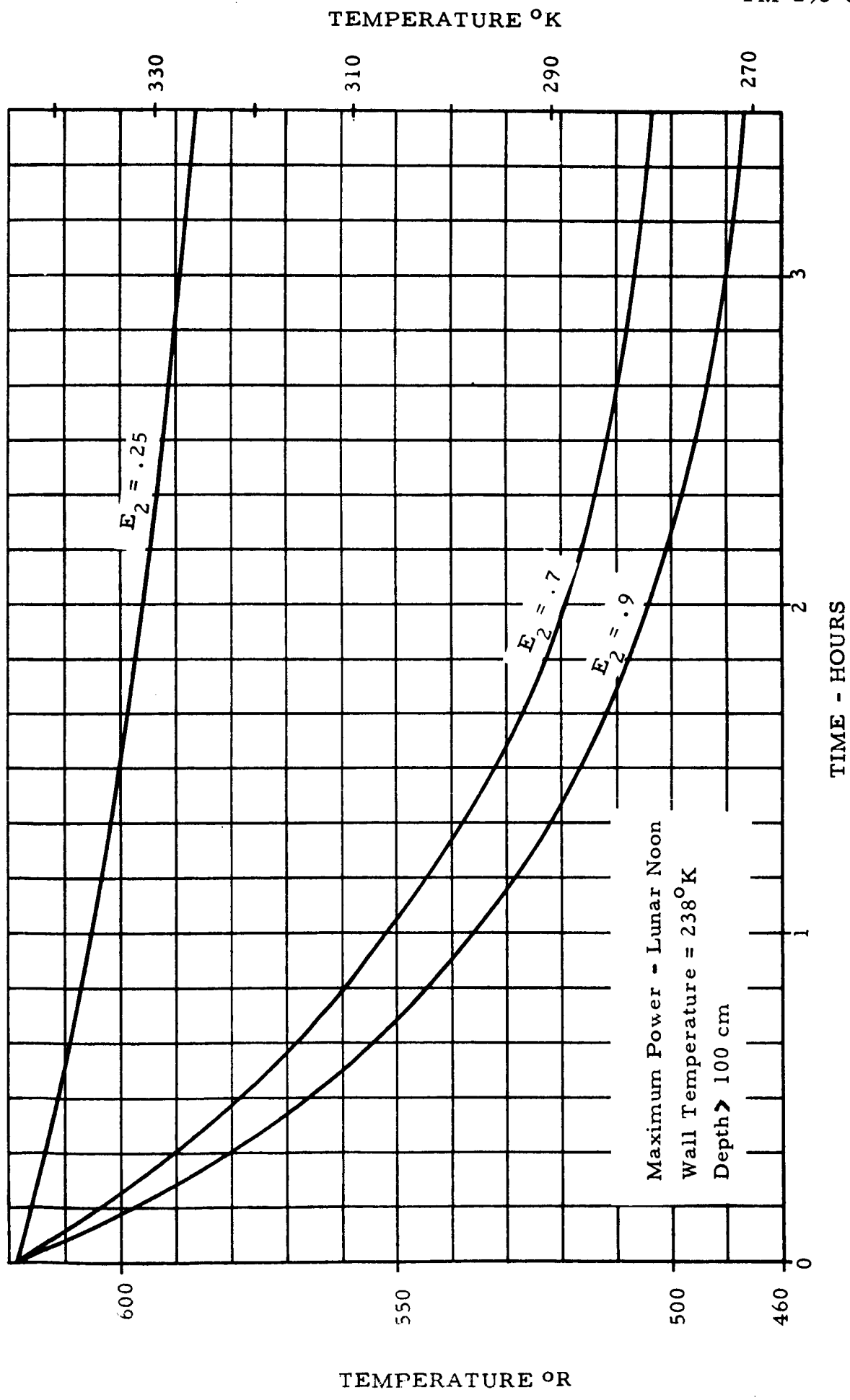

Figure 2 PROBE TEMPERATURE VS. TIME

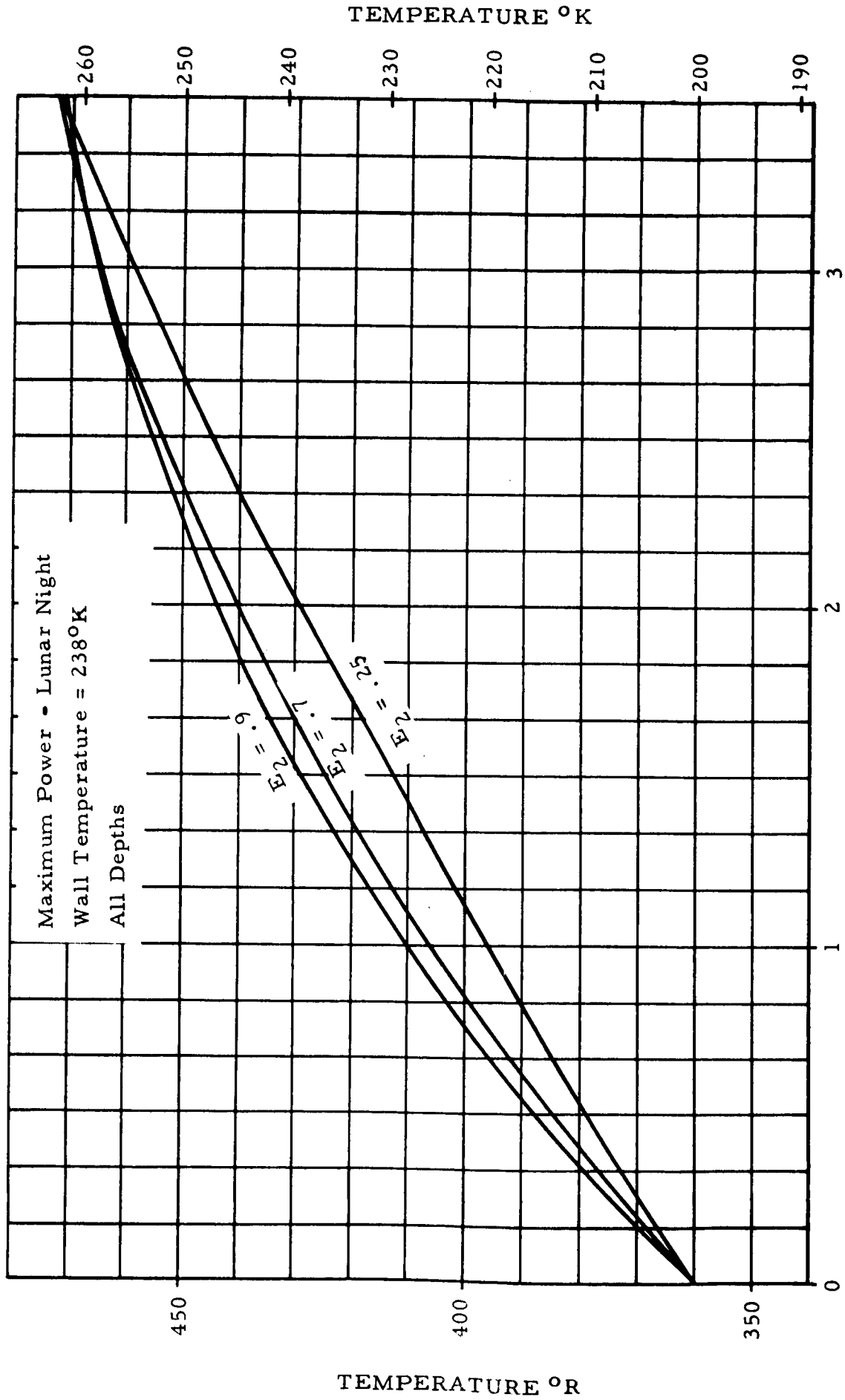

Figure 3 PROBE TEMPERATURE VS. TIME

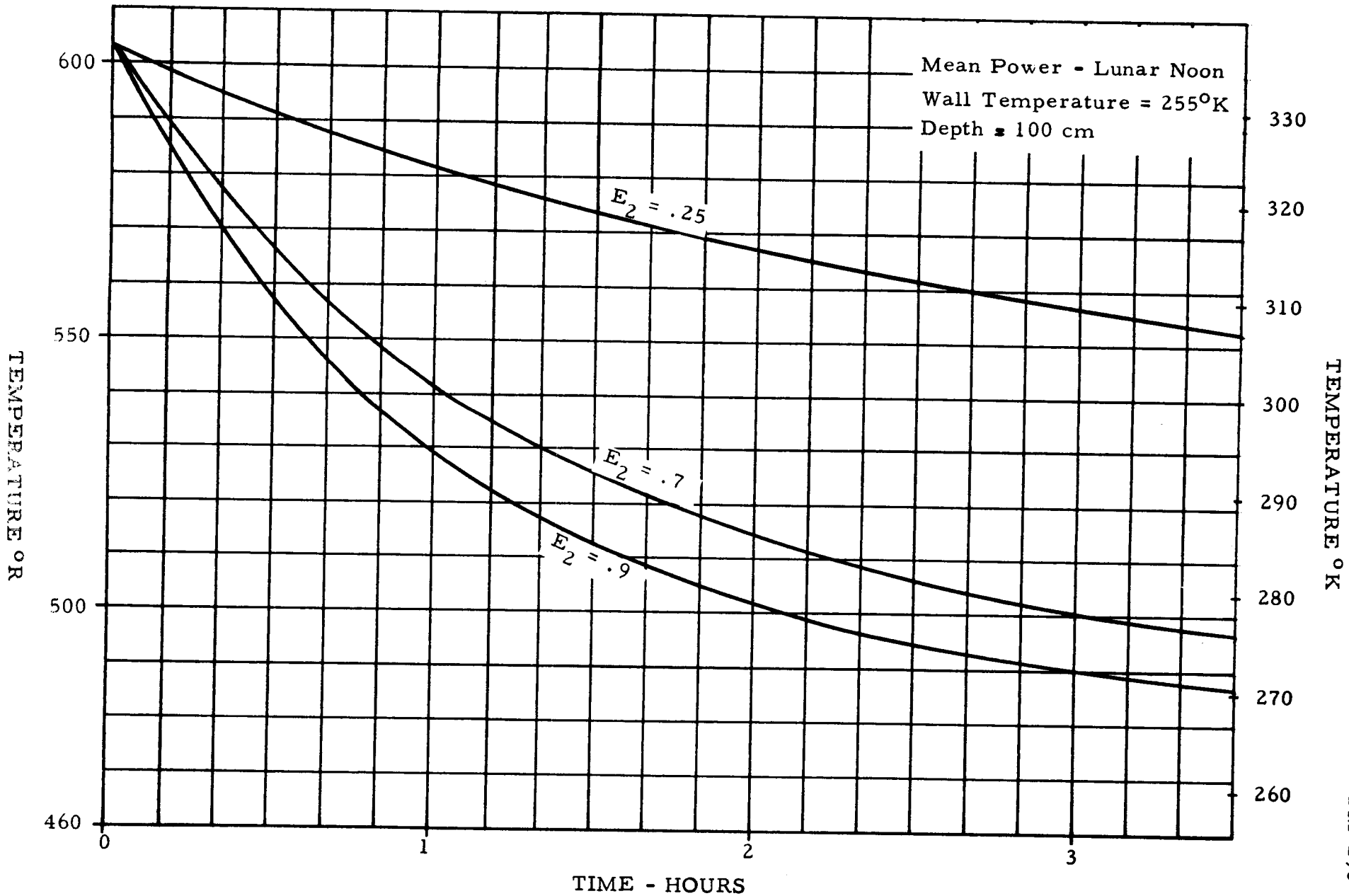

Figure 4 PROBE TEMPERATURE VS. TIME

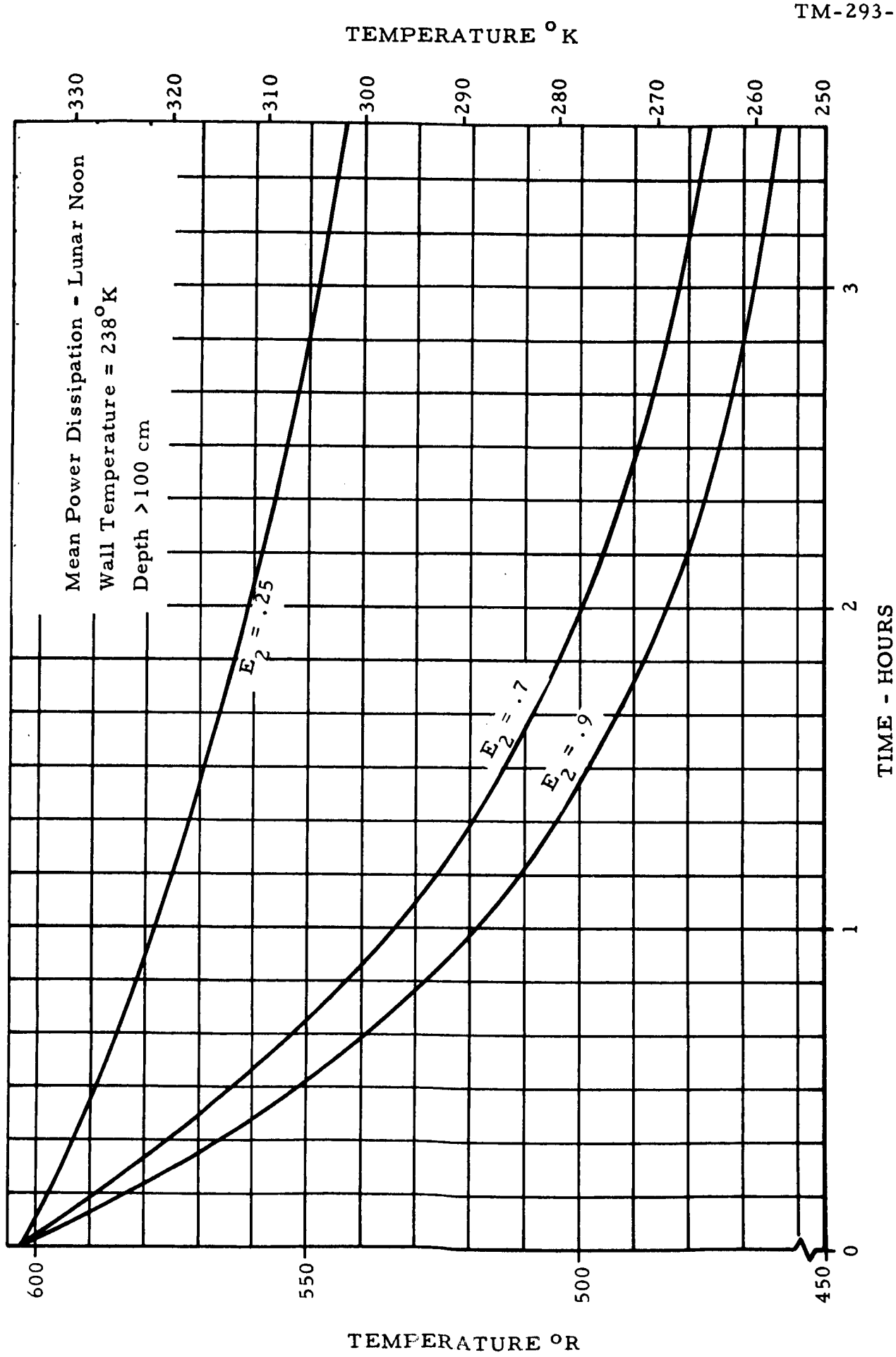

Figure 5 PROBE TEMPERATURE VS. TIME

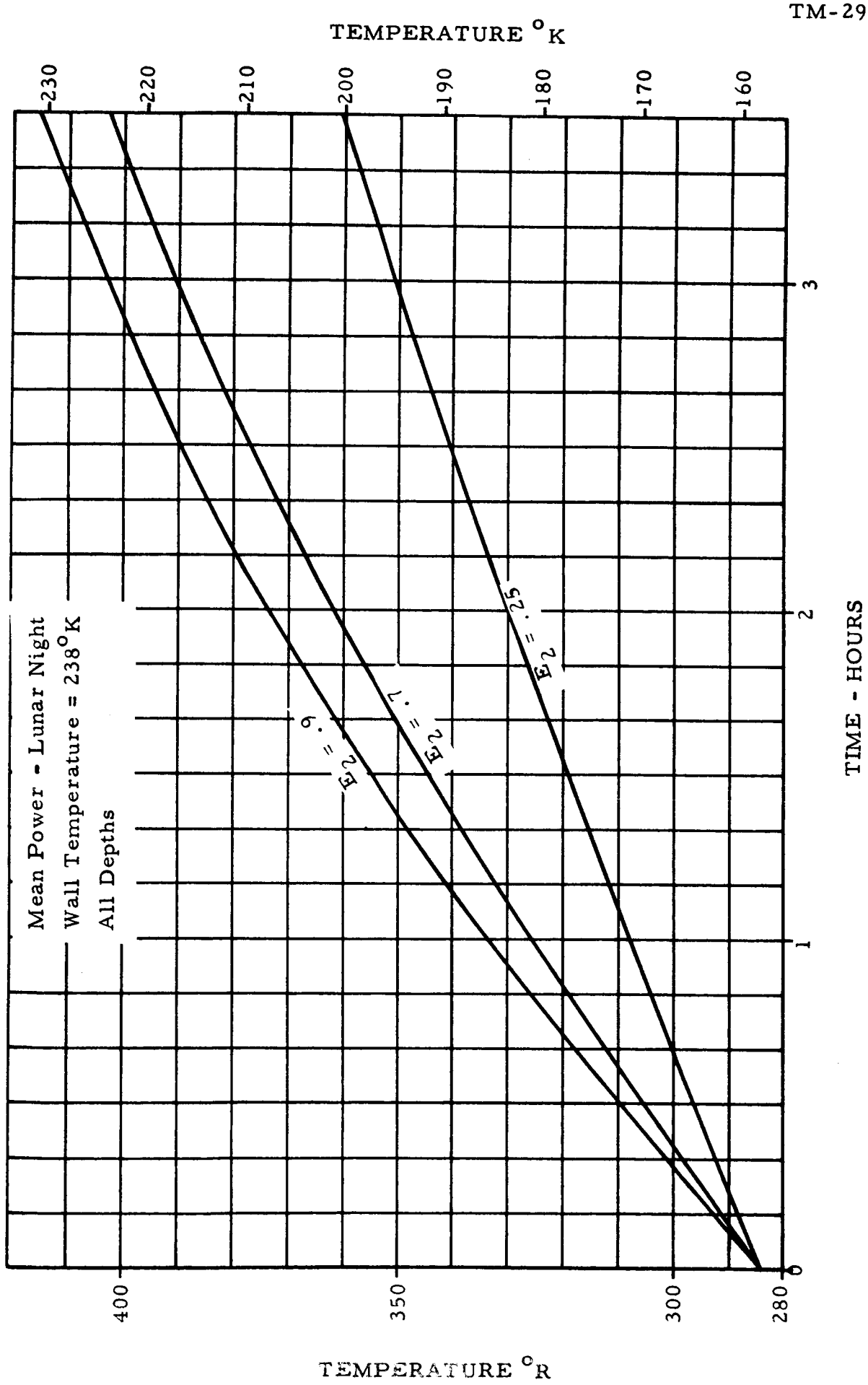

Figure 6 PROBE TEMPERATURE VS. TIME

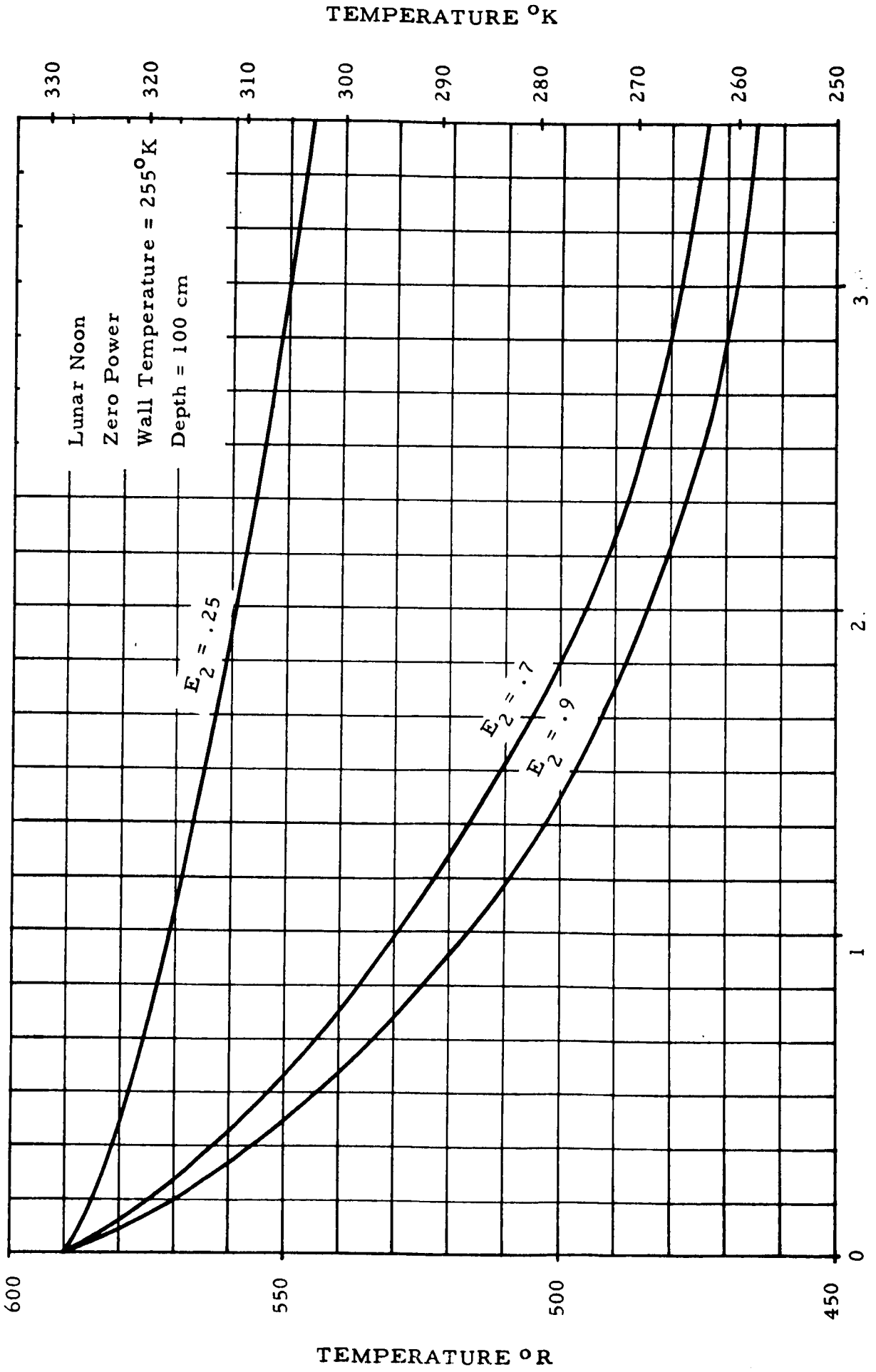

Figure 7 PROBE TEMPERATURE VS. TIME

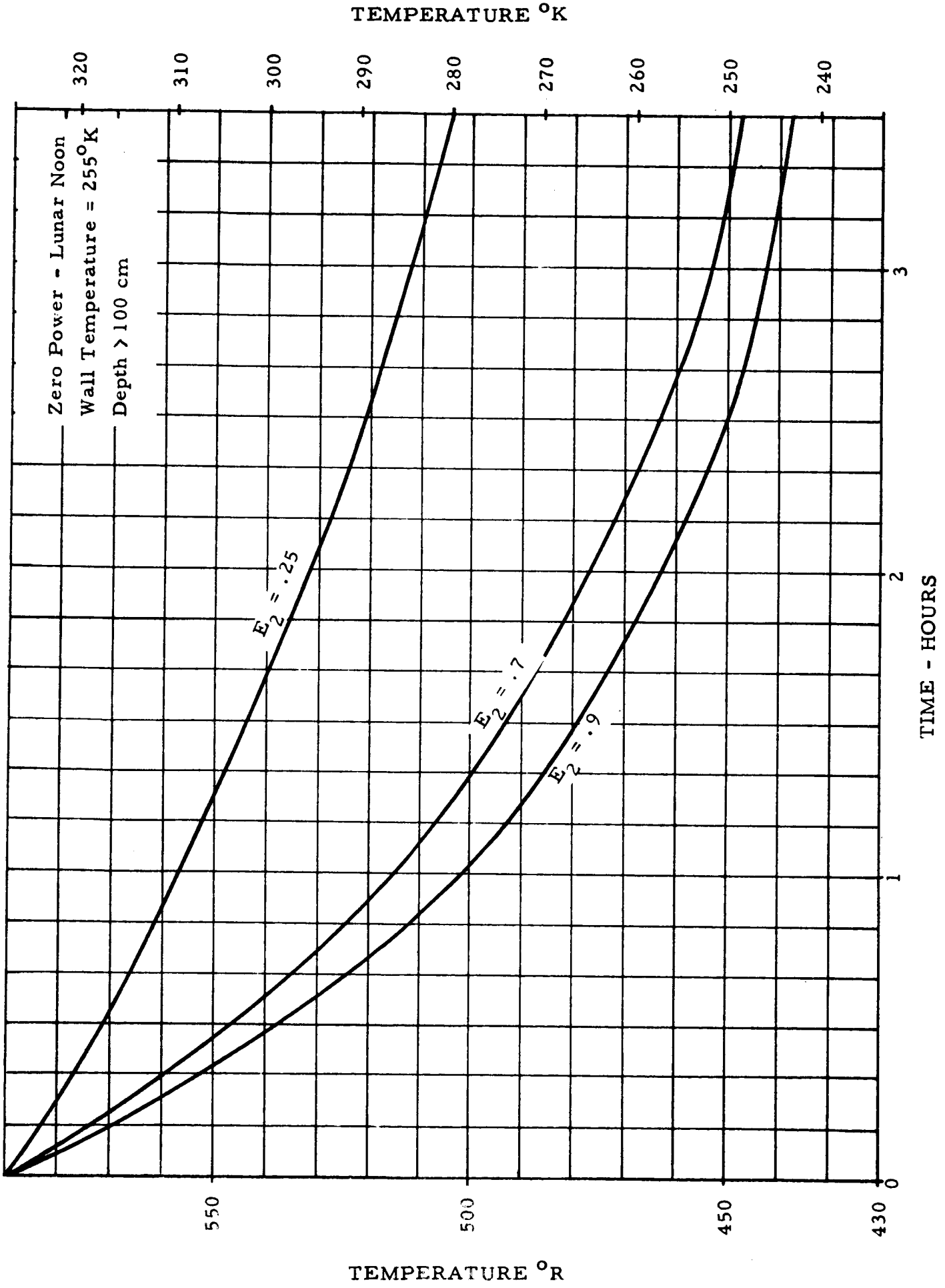

Figure 8 PROBE TEMPERATURE VS. TIME

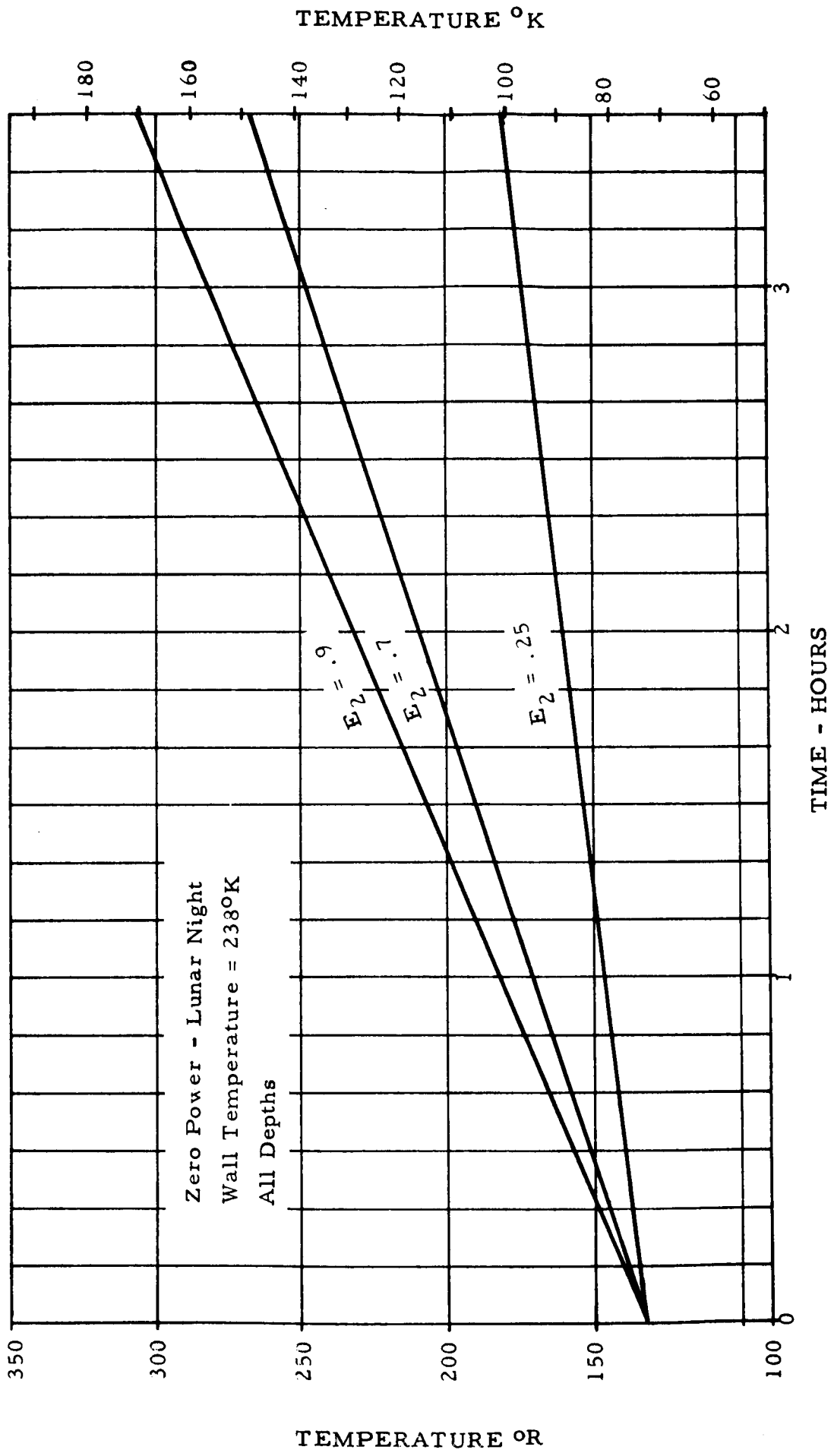

Figure 9 PROBE TEMPERATURE VS. TIME

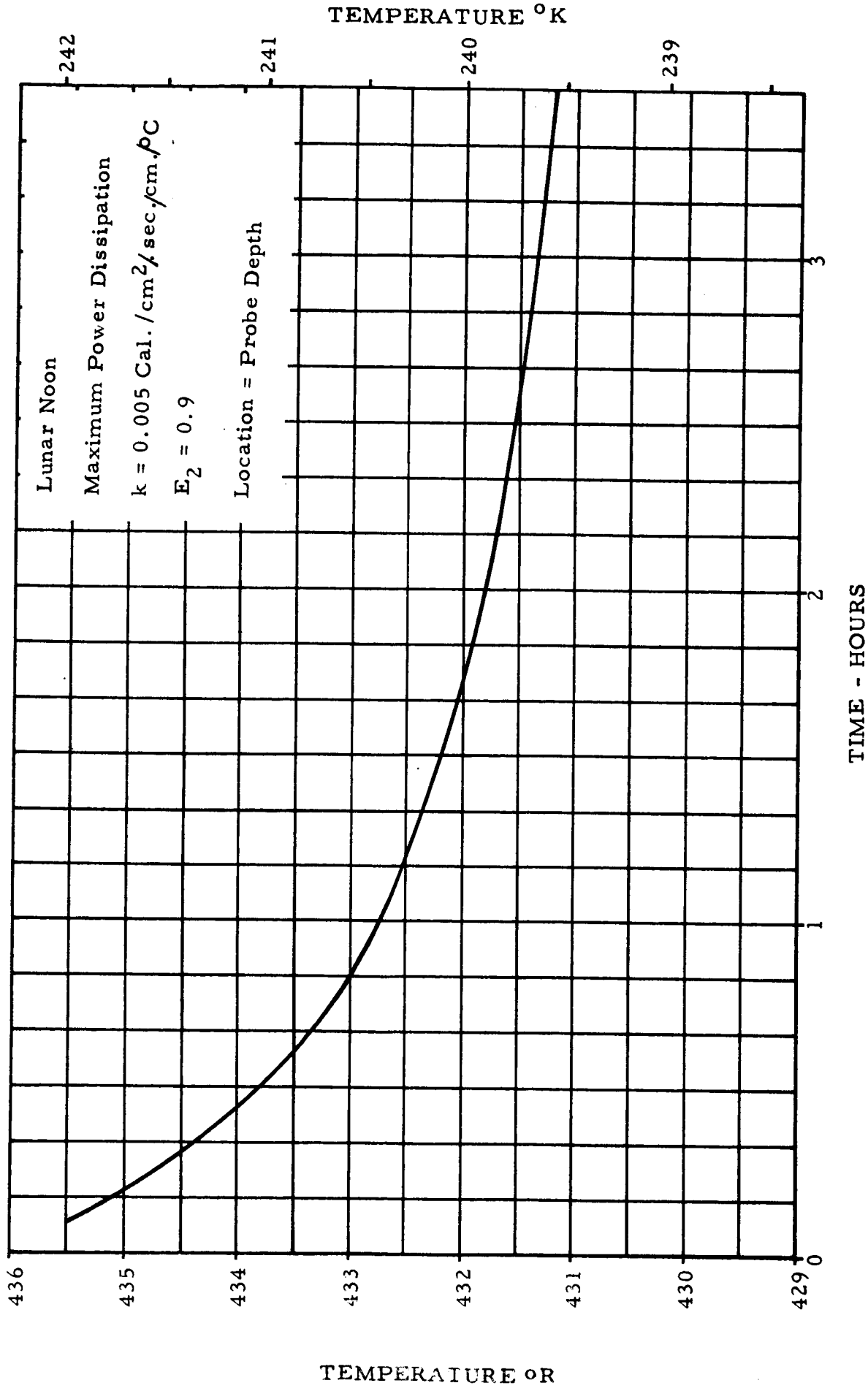

Figure 10 BOREHOLE WALL TEMPERATURE VS. TIME

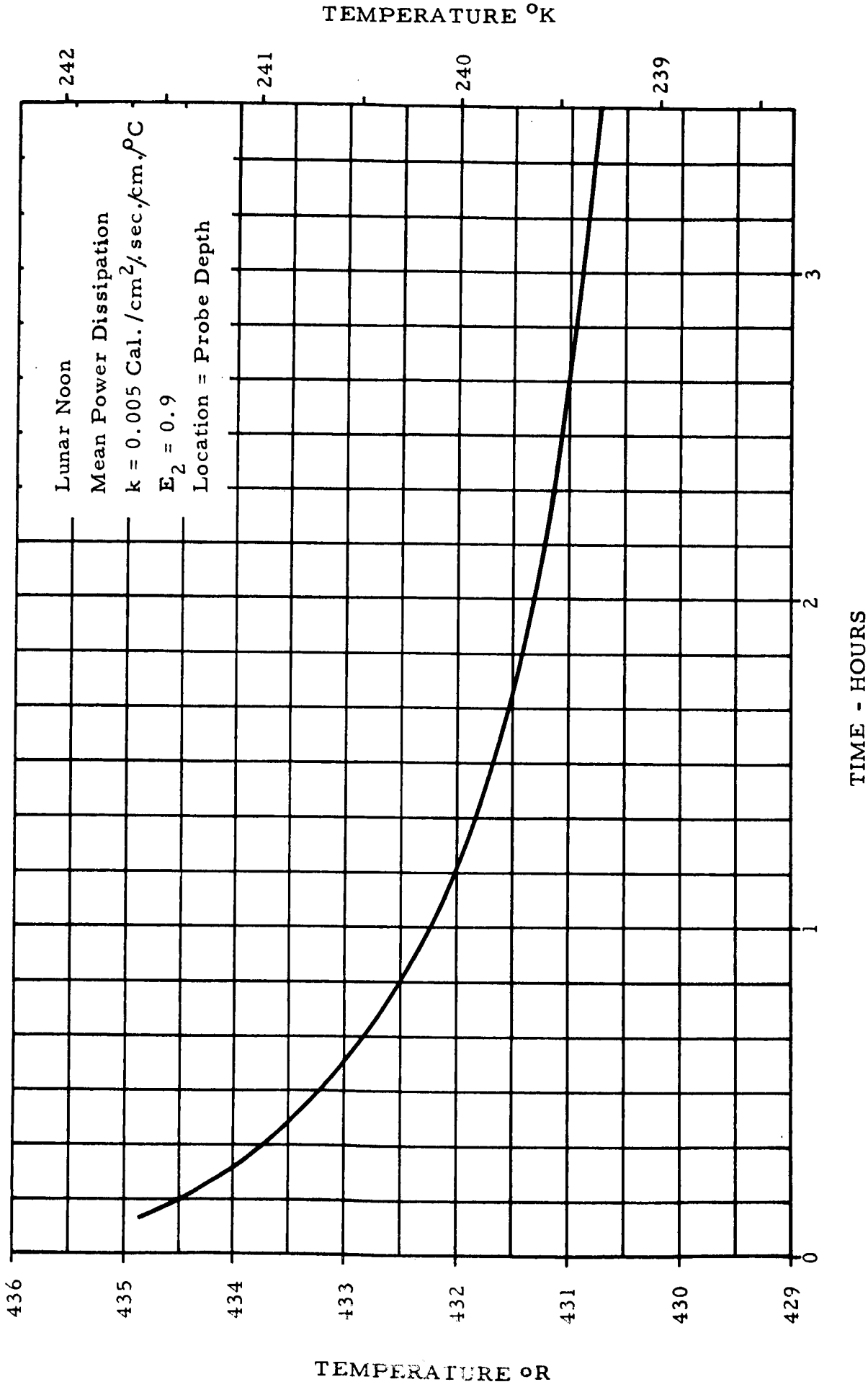

Figure 11 BOREHOLE WALL TEMPERATURE VS. TIME

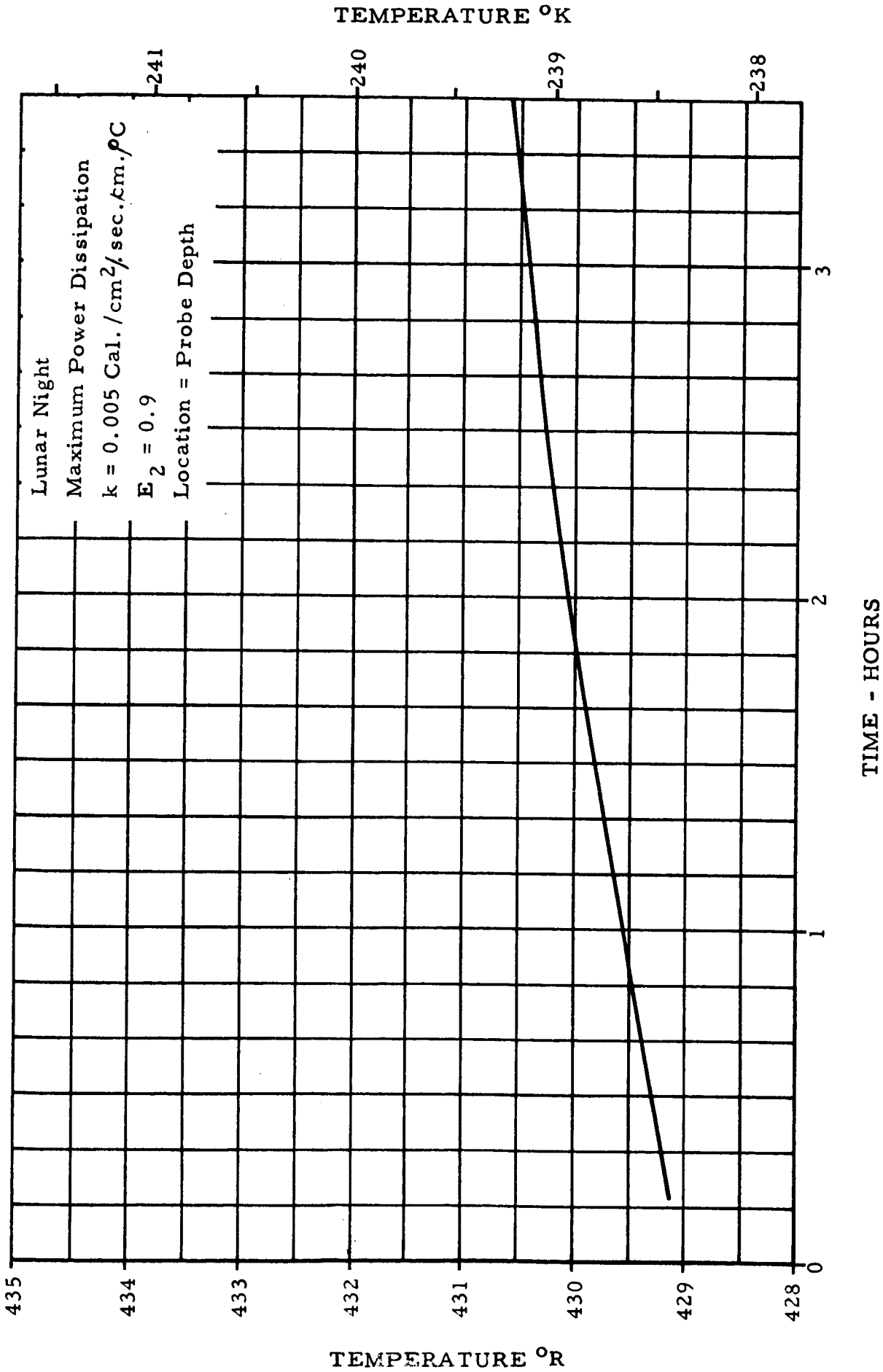

Figure 12 BOREHOLE WALL TEMPERATURE VS. TIME

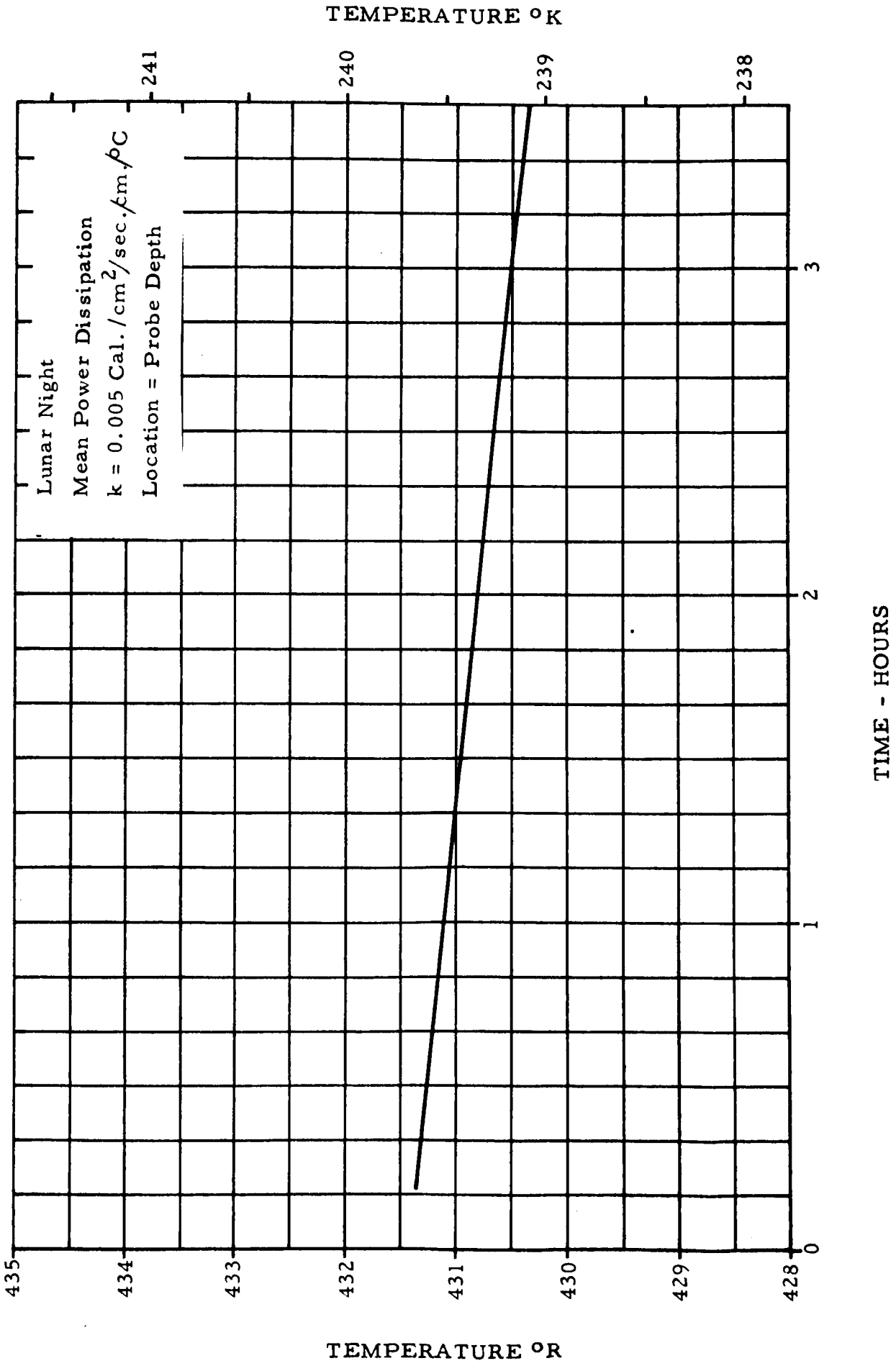

Figure 13 BOREHOLE WALL TEMPERATURE VS. TIME

Appendix III

A THERMAL-METEOROID SHIELD DESIGN STUDY FOR THE LUNAR THERMAL PROBE

NORTHROP SPACE LABORATORIES

E30-76
Revision A
18 February 1966

A THERMAL-METEOROID SHIELD DESIGN STUDY FOR THE LUNAR THERMAL PROBE

By

C. M. Mackenzie

PREFACE

This informal report was prepared by the Systems Section of Northrop Space Laboratories, Huntsville, Alabama, for Texaco Experiment Incorporated. Efforts were performed under Task Order NSL No. 1, Purchase Order No. 40510-3, December 16, 1965.

TABLE OF CONTENTS

	PAGE
INTRODUCTION	1
DISCUSSION	1
CONCLUSIONS	4
APPENDIX A - METEOROID ANALYSIS	5
APPENDIX B - THERMAL ANALYSIS	7
APPENDIX C - DESIGN ANALYSIS	16

LIST OF TABLES

TABLE		
I	PROBE TEMPERATURE	2
II	METEOROID PUNCTURE PROBABILITY	2

LIST OF FIGURES

FIGURE		
1	CROSS SECTION OF THERMAL - METEOROID SHIELD - STOWED POSITION	3
2	HEAT SOURCES	7
3	BUMPER AND SHIELD	10
4	THEORETICAL TEMPERATURE VARIATIONS OF PROBE	14
5	PROBE TEMPERATURE VS. MAXIMUM CONTINUOUS TOTAL POWER	15

INTRODUCTION

The thermal-meteoroid shield study, described and analyzed in this report, provides preliminary data necessary for future detailed analyses. This preliminary analysis shows the feasibility and practicality of the selected design. The latest state-of-the-art values for meteoroid protection along with the latest data on the lunar environment are used to produce a workable design.

DISCUSSION

The primary constraint on the shield design was that of limiting the upper temperature to 648°R (360°K). This can be done by selecting an outer skin coating with a minimum α / ϵ ratio. The shield must also have the capability to dissipate the internal heat generated under use. There is a trade-off between the insulating factor of radiation shielding and the necessity of removing internal heat, in order that the probe will not exceed the desired temperature. Limiting the amount of insulation in turn limits the amount of protection against the lunar night. Thus it can be seen that there is an anomaly in that the probe should stay cool in daytime and warm at night and yet be relatively uninsulated.

There is no rapid hand method for solving the differential equations encountered in transient radiation problems. Therefore,

computer programs are usually written using numerical methods to solve these equations. The analytical results presented herein were achieved only after making assumptions and simplifications. The overall effect was to sacrifice a small amount of accuracy to gain time.

The final design selected is shown in Figure 1. The data, analysis, and reasoning are presented in the appendices.

The analyses yield the temperature ranges indicated below in Table I.

TABLE I

PROBE TEMPERATURE

Heating Condition	Maximum Temperature		Minimum Temperature	
Probe inoperative	590°R	(327°K)	131°R	(73°K)
Maximum power	619°R	(344°K)	362°R	(201°K)
Mean power	603°R	(335°K)	284°R	(157°K)

The meteoroid puncture probability is given below in Table II.

TABLE II

METEOROID PUNCTURE PROBABILITY

Condition	Confidence Level	No Puncture Probability	Earth Days
Lunar Primary	50%	.999	1,750
		.990	18,400
		.900	193,000
	75%	.999	613
		.990	6,570
		.900	65,700
Lunar Secondary	50%	.999	2.28×10^{11}
		.990	2.37×10^{12}
		.900	2.45×10^{13}

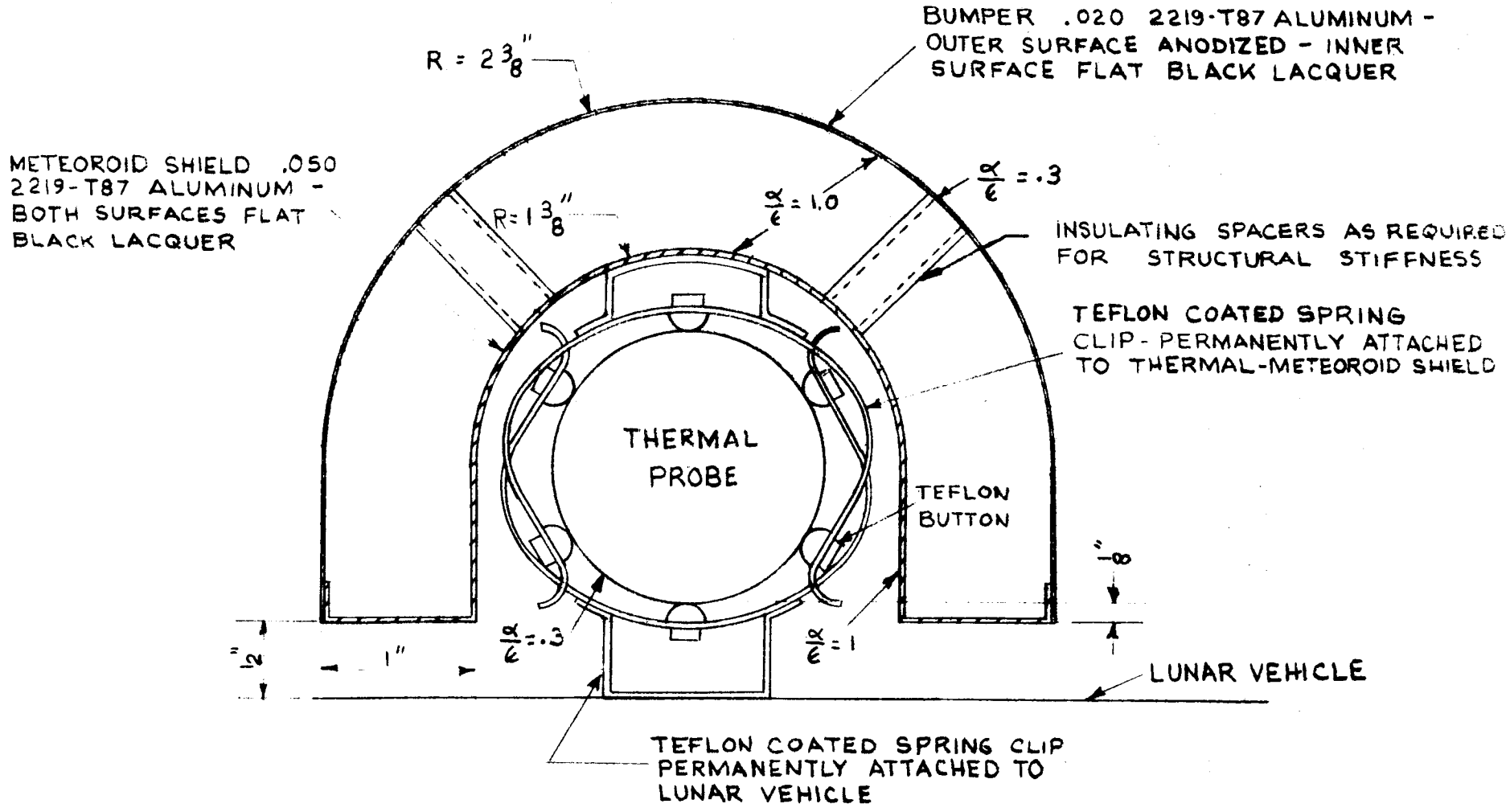

FIG. 1 CROSS SECTION OF THERMAL - METEOROID SHIELD - STOWED POSITION

CONCLUSIONS

The temperature maximums have been shown to be within the guidelines. Minimum temperatures can be quite low without the probe being operative and additional power may be required because of thermal limitations of the probe . The area of the meteoroid shield is so small that the puncture probability is practically zero.

Information has been requested concerning a material manufactured by Goodyear Aerospace, Akron, Ohio. The material is a flexible foam with very good meteoroid protective and insulative qualities. Unfortunately, this information has not been received. When it becomes available it will be passed on for consideration.

APPENDIX A

METEOROID ANALYSIS

There have been many studies made on the effects of meteoroid shielding design. A complete discussion of all the results is too extensive to report here. The complete findings will be utilized for this analysis with the main conclusions presented.

(1) The meteoroid particle is defined as the Apollo particle whose density is .44 g/cm^3, mean velocity is 30.4 km/sec, and diameter is 1.02 mm.

(2) An outer shield, called a bumper, is desirable as a particle break-up sheet, and energy absorber.

(3) Optimum thickness of the bumper with respect to penetration damage is one-half the projectile diameter.

(4) Bumpers which are too thick present other problems such as spallation.

(5) Aluminum appears to be the best bumper material.

(6) A space of one inch between the bumper and shield increases the shielding efficiency 100 percent. A glass wool filler in the same space increases the efficiency 440 percent.

(7) High density fillers can cause disasterous failures due to pressure or shock waves causing spallation of low velocity

projectiles. Several materials are listed below in order of their effectiveness:

(a) Fiberglass with preceding space

(b) Fiberglass without preceding space.

(c) Open cell foams

(d) Closed cell foams

(e) Low density cork

(f) Superinsulations (foil layers)

(8) Optimum shield thickness decreases with increasing velocity.

(9) A shield thickness of 1.25 times the particle diameter is suitable.

Using the above conclusions, a meteoroid protection device having a bumper thickness of .02 in. aluminum and an inner shield thickness of .05 in. with one inch of glass wool filler would be practical.

Meteoroid data extracted from Meteoroid Design Data For Apollo Applications, Brownie R. Johnson, Brown Engineering Report SIB-TR-8.

APPENDIX B

THERMAL ANALYSIS

There are two principal constraints for the thermal analysis. The first is the upper limiting temperature of the probe of 648°R. The second is the ability to conduct and/or radiate a minimum of 44.1 BTU/hr. These two constraints dictate the surface coating requirements and the maximum amount of insulation which may be used. Figure 2 shows the heat inputs from various sources to an object on the lunar surface.

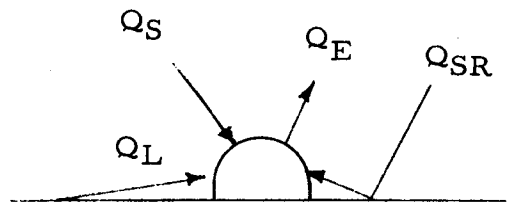

Figure 2 HEAT SOURCES

Q_S = Heat input from the sun

Q_{SR} = Reflected heat (Albedo)

Q_L = Heat input from the lunar surface

Q_E = Heat emitted to surroundings and space

For steady-state conditions

$$\Sigma Q = 0 \tag{1}$$

$$Q_E = Q_S + Q_{SR} + Q_L \tag{1a}$$

By definition

$$Q_S = 443\alpha_E \text{ BTU/hr ft}^2$$

$$Q_{SR} = 45\alpha_E \text{ BTU/hr ft}^2 \text{ (Average maximum)}$$

$$Q_L = \alpha_E \epsilon_L \sigma \mathcal{F}_L A_L (T_L^4 - T_E)^4$$

$$Q_E = \epsilon_E \sigma \mathcal{F}_{ES} A_E T_E^4$$

Where ϵ = Emissivity

σ = Stefan Boltzmann constant $.174 \times 10^{-8}$ BTU/hr ft^2 $^oR^4$

$\mathcal{F}$ = View Factor

T = Temperature

α = Absorbtivity

Therefore $\epsilon_E \sigma \mathcal{F}_{ES} A_E T_E^4 = \mathcal{F}_{ES} A_E 488 \alpha_E + \epsilon_L \alpha_E \sigma \mathcal{F}_{LE} A_L (T_L^4 - T_E^4)$ (1b)

For a half cylinder on an infinite flat surface

$$\mathcal{F}_{LE} A_L = \mathcal{F}_{EL} A_E = .83$$

$$\mathcal{F}_{LE} = .364$$

$$\mathcal{F}_{ES} = 1 - \mathcal{F}_{EL} = .636$$

For anodized aluminum $\alpha_E / \epsilon_E = .3$*

Substituting into Equation 1b

$$.228 \left(\frac{T_E}{100}\right)^4 = 192.0 + .035 \left[\left(\frac{T_L}{100}\right)^4 - \left(\frac{T_E}{100}\right)^4\right] \qquad (1c)$$

Under maximum conditions of lunar noon and where the temperature of the lunar surface is nearly that of the shield, the last term becomes

*Passive Temperature Control in the Space Environment, R.M. Van Vliet, Macmillan Company, N. Y., 1965

insignificant. Equation 1c solved for T_E, the outer shield temperature, gives

$$T_E = 538^oR = 299^oK$$

When the probe is generating its maximum power of 44.1 BTU/hr, the outer shield temperature increases to

$$.228\left(\frac{T_E}{100}\right)^4 = 192 + (44.1)$$

$$T_E = 567^oR = 315^oK$$

At the mean power dissipation of 17.1 BTU/hr

$$T_E = 551^oR = 306^oK$$

When the probe is dissipating its maximum power consumption of 44.1 BTU/hr, the minimum thermal conductivity allowable between the temperature extremes of 648^oR (360^oK) and 567^oR (315^oK) is expressed by Equation 2

$$44.1 = \frac{\pi K\,(648 - 567)}{\ln\,(4.75/1.75)}\left(\frac{44}{12}\right) \qquad (2)$$

$$K = \frac{(44.1)(.434)}{\pi\,(81)}\left(\frac{12}{44}\right) = .0153 \text{ BTU/hr ft}^2\ {}^oR$$

Any configuration where the equivalent thermal conductivity is greater than .0153 BTU/hr $ft^2\,^oR$ may be used. For periods of the lunar night where excessive heat loss is to be avoided, a configuration whose equivalent thermal conductivity is as close as possible to .0153 BTU/hr $ft^2\ ^oR$, is desirable.

As mentioned in the shield discussion, a bumper provides better protection than does a single sheet. The bumper arrangement of the final design is simplified and is shown in Figure 3. Each piece of metal acts as a radiation shield. Under the condition of maximum power dissipation and where the external skin or bumper is at the maximum temperature of 567°R (315°K), the inner shield has a temperature expressed by Equation 3.

$$q_{12} = \sigma A_1 (T_1^4 - T_2^4) \frac{1}{1/\epsilon_1 + 1/\alpha_2 - 1} \qquad (3)$$

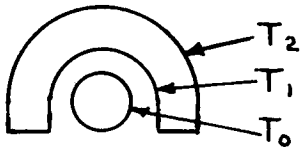

Figure 3 BUMPER AND SHIELD

Solving for T_1

$$T_1 = 588^oR\ (327^oK)$$

The maximum temperature of the probe is determined from Equation 3a.

$$q_{01} = \sigma A_o (T_o^4 - T_1^4) \frac{1}{1/\epsilon_o + 1/\alpha_1 - 1} \qquad (3a)$$

Solving for T_o

$$T_o = 619^oR\ (344^oK)$$

If the space between the shields were filled with an insulating material the minimum thermal conductivity can be determined to be .0053 BTU/hr ft^2 °R.

This value is for maximum allowable probe temperature and maximum bumper temperature.

From Equation 3a $\left(\frac{T_{1max}}{100}\right)^4 = 1765 - 272$

$$T_{1max} = 612^oR \ (344^oK)$$

The quantity of heat conducted through a cylinder is given by Equation 4

$$q = \frac{KA\ (\Delta T)}{\ln r_2/r_1} \qquad (4)$$

Solving for K

$$K = .0065 \text{ BTU/hr ft}^2\,^oR$$

Although there are many materials whose conductivity is greater than .0065, for best meteorite protection, as explained in the previous section, the material should be loosely packed. (Values for loosely packed fillers under vacuum conditions are still not known to the author.)

The previous calculations were based upon maximum probe temperature at lunar noon. It was shown that at this time the temperature effect of lunar surface is insignificant. As the sun sets the temperature of the probe drops rapidly. This is because the total heat content of the probe at maximum temperature is only 1200 BTU. The initial rate of heat loss is 448 BTU/hr. With no power input the temperature of the probe will be approximately .65 times that of the lunar surface. The minimum expected temperature of the lunar surface is 216°R (120°K). Therefore the minimum temperature of the

probe, under a no power condition, is 131°R (73°K). Under a peak power dissipation of 44.1 BTU/hr (13 watts), the probe temperature follows Equation 5. The minimum temperature now increases to 362°R (201°K).

$$\left(\frac{T_E}{100}\right)^4 = .133\left(\frac{T_L}{100}\right)^4 + 168 \qquad (5)$$

Under the mean power dissipation of 17.1 BTU/hr (5 watts), the probe temperature follows the equation

$$\left(\frac{T_E}{100}\right)^4 = .133\left(\frac{T_L}{100}\right)^4 + 65 \qquad (6)$$

The probe temperature for this condition is 284°R (157°K). Equations 5 and 6, along with the no power temperature relationship, are presented as a function of the lunar temperature in Figure 4.

Under periods of lunar sunset and night it may be desirable to furnish additional power to the temperature probe to maintain a higher temperature than that during normal operating conditions. The simplest way to obtain such temperature control is with a thermostatic switch with constant value power addition. Continuous high power input is unacceptable since the upper temperature of the probe could be exceeded. Using equations 1 and 3, the maximum amount of continuous total power input, without exceeding the upper temperature limit of the probe, is determined to be 66 BTU/hr. The minimum temperature under this condition would be 398°F, and the maximum temperature be 648°F. Any value of power input higher than 66 BTU/hr would have to be intermittent.

If the desired minimum temperature is higher than 398°F a thermostat is required. The lower limit of the thermostat would be the lowest desired temperature. As the probe temperature dropped during sunset and lunar night,the thermostat would allow additional power to be applied to the probe to increase its temperature. Reaching an established upper limit the thermostat would shut off. An on-off cycle would be established during the period of sunset and sunrise while a relatively continuous power supply would occur during night-time conditions. The maximum continuous amount of total power as a function of minimum temperature is presented in Figure 5. This temperature-power curve is based on the theoretical minimum lunar surface temperature of 216°R.

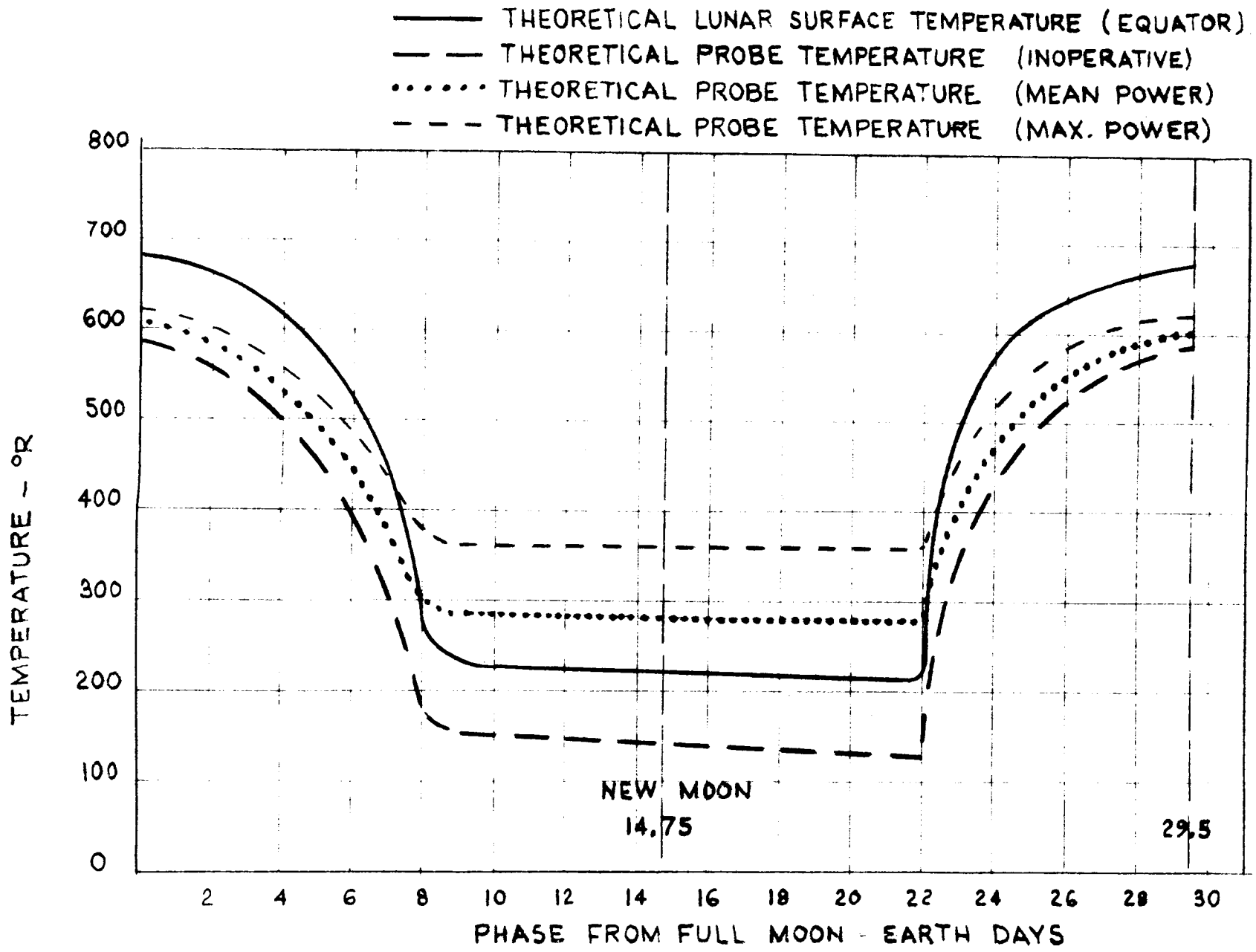

FIG. 4. THEORETICAL TEMPERATURE VARIATIONS OF PROBE

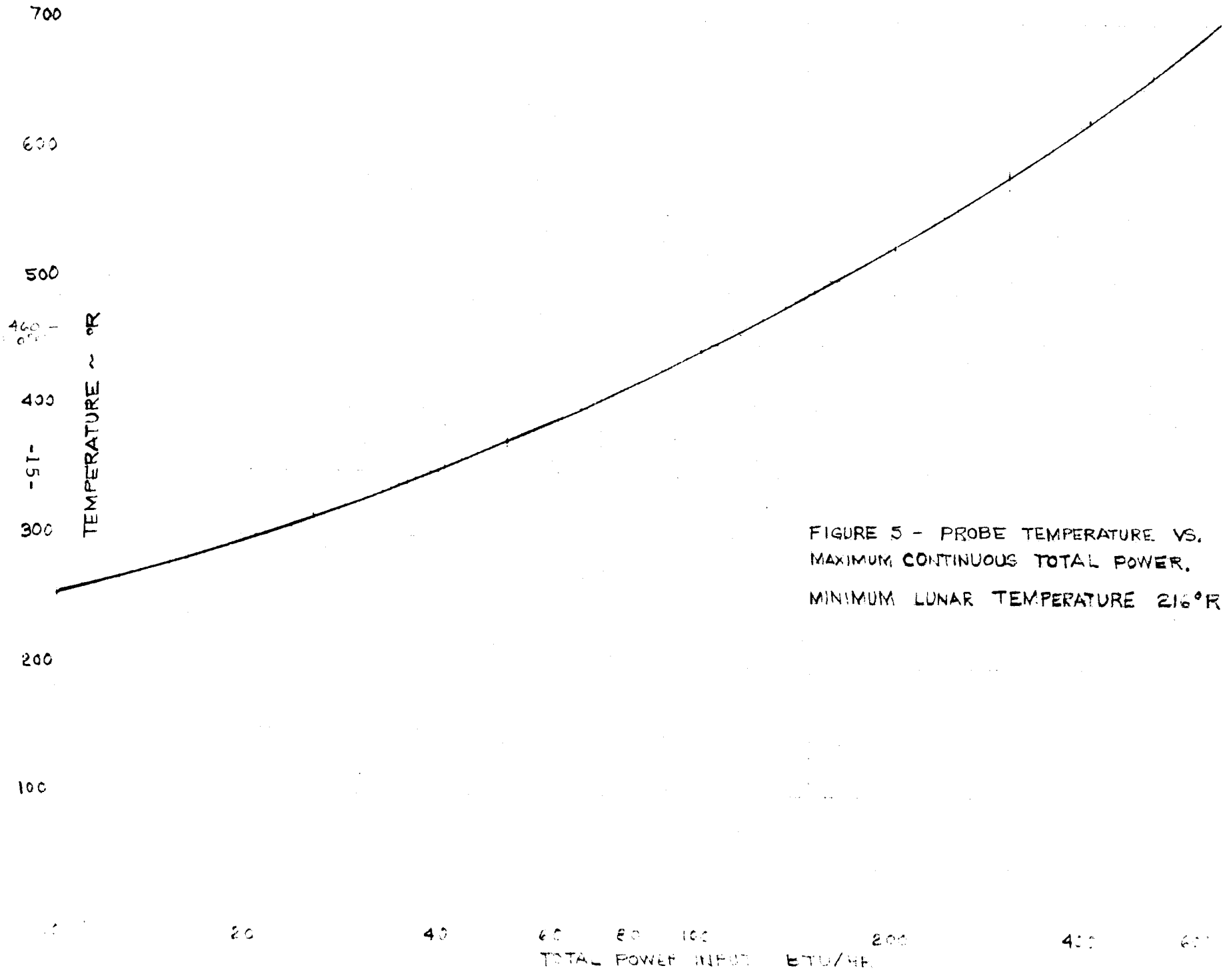

FIGURE 5 - PROBE TEMPERATURE VS. MAXIMUM CONTINUOUS TOTAL POWER.

MINIMUM LUNAR TEMPERATURE 216°R

APPENDIX C

DESIGN ANALYSIS

Figure 1 is a full size cross section of the thermal-meteoroid shield selected from the preceding analysis. It consists of a bumper and a shield. The bumper is 2219-T87 aluminum .02 inches thick, anodized on the outer surface to give an α/ϵ ratio of 0.30. The inside surface of the bumper is painted with flat black lacquer, to give both a high adsorbtivity and a high emissivity. The inner shield is also 2219-T87 aluminum coated both sides with flat black lacquer. There is a one inch space between the bumper and the inner shield. This space is void or may be filled with loose material having a thermal conductivity, in vacuum conditions, greater than .0065 BTU/hr ft^2 ^oR. The shield can be attached to the probe by two spring clips as shown. In each clip there are three teflon buttons to hold the probe away from the shield and contacting the probe at 120° spacing. The probe and shield can be fastened to the lunar vehicle by two similar clips permanently attached to the lunar vehicle. Both the shield and lunar vehicle clips are teflon coated to prevent damage to the surface of the probe. All clips are designed to facilitate the removal and attachment of both the shield to the probe and the assembly to the lunar vehicle.

The overall length of the shield is three inches longer than the probe and may be adapted at one end to allow a power cord to pass through. The cord may also be brought out from underneath. The ends of the shield can

be of any practical configuration but are assumed to be square and allow 1/2 inch clearance between the inner shield and the probe. There should also be the one inch space between the inner shield and the bumper.

The bearing surface of the shield is formed by bending the inner shield outward at 90° and affixing it to the bumper. This bridge gives 90 square inches of bearing surface. This is sufficient to prevent sinking more than one inch into the lunar surface. Since the shield extends 1/8 inch below the probe the maximum height of the probe above the lunar surface is 1/8 inch. Any sinking into the surface would reduce this clearance.

For structural rigidity, spacers are used between the bumper and the inner shield. These spacers are insulators to prevent excessive heat loss from the probe.

The total estimated weight of the shield assembly is 3.5 lb, including clips and spacers but no filler material.

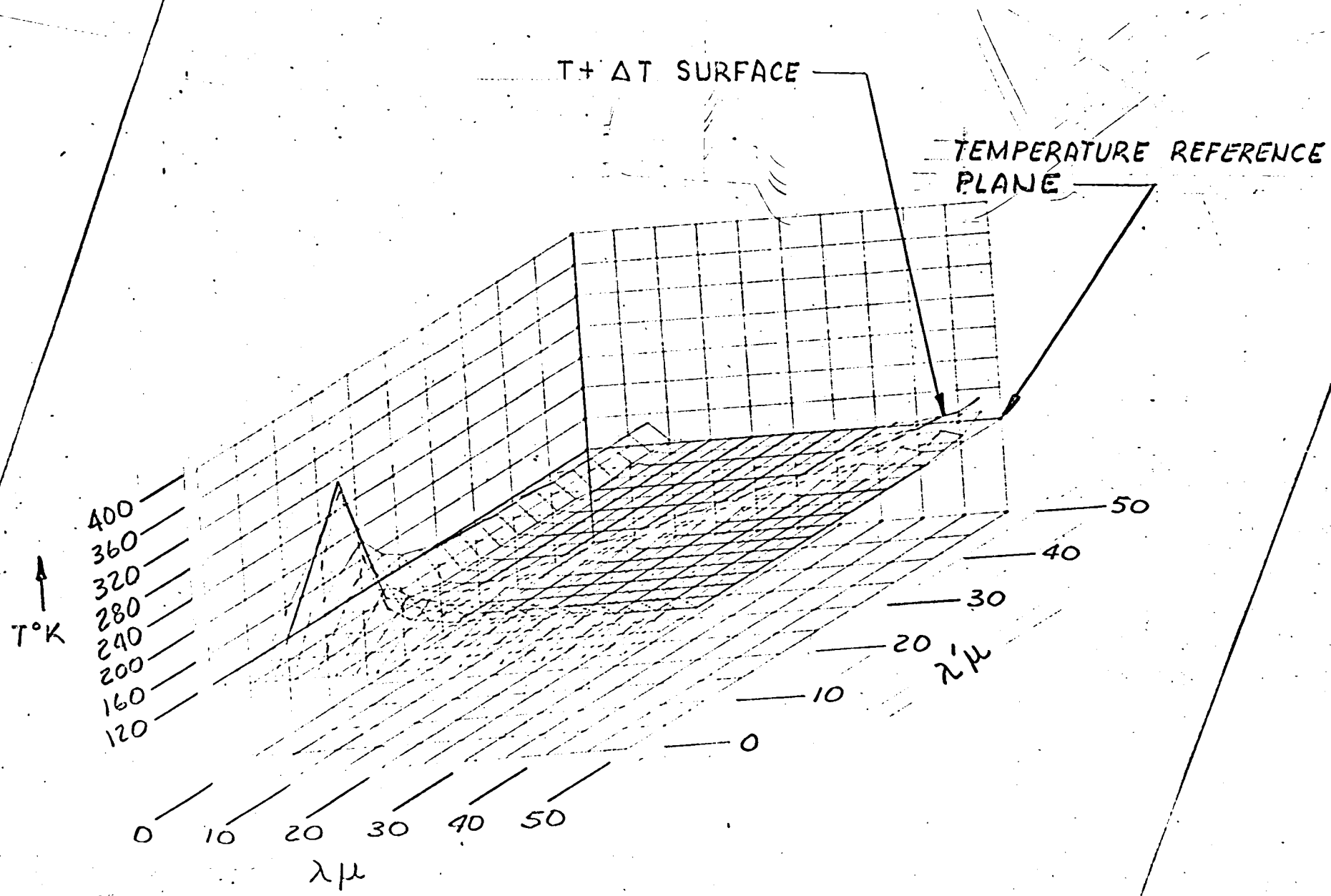
T+ ΔT SURFACE
TEMPERATURE REFERENCE PLANE
T°K
400
360
320
280
240
200
160
120
0
10
20
30
40
50
λμ
λ'μ

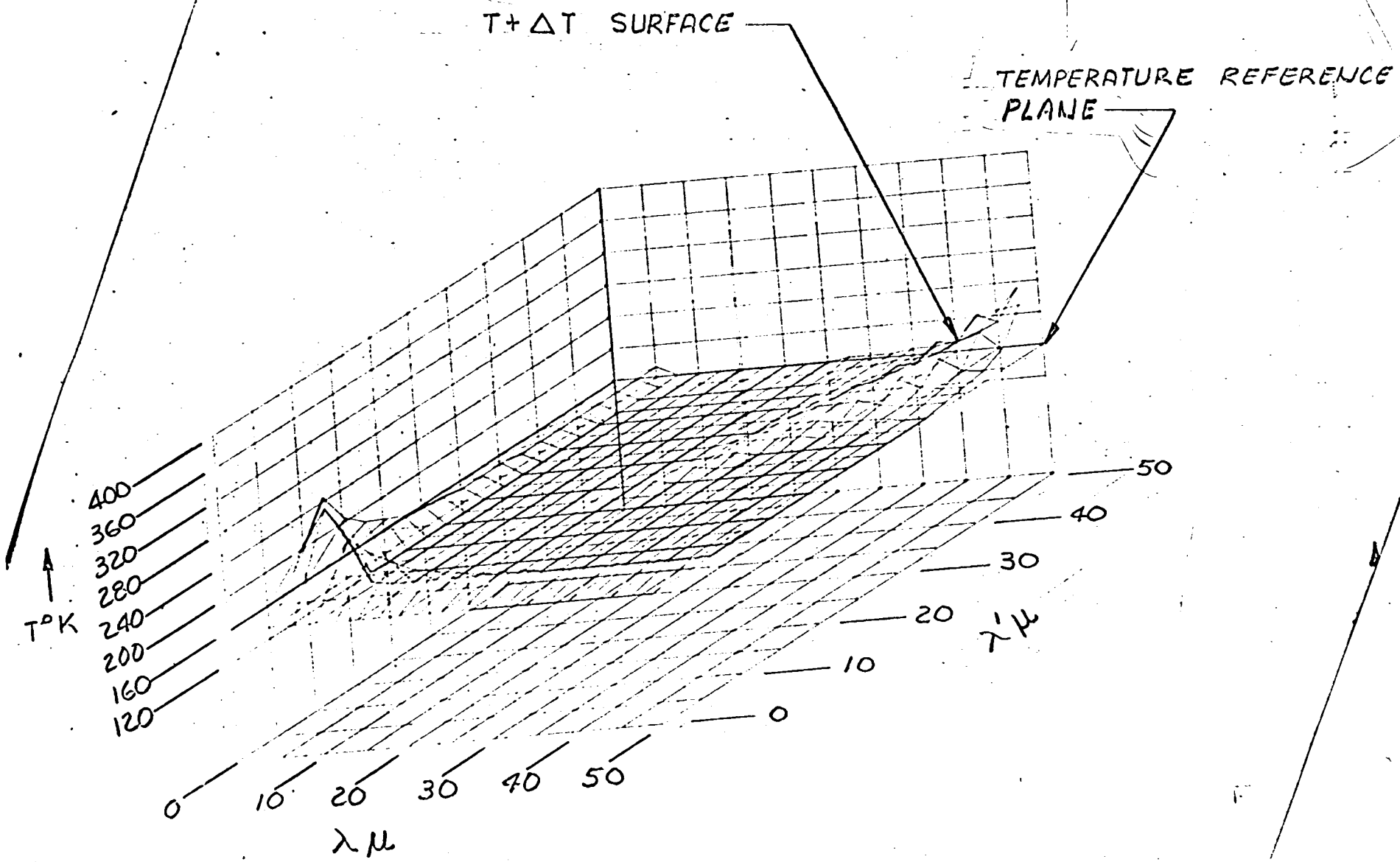
T + ΔT SURFACE
TEMPERATURE REFERENCE PLANE
400
360
320
280
240
200
160
120
T°K
0
10
20
30
40
50
λ μ
0
10
20
30
40
50
λ' μ

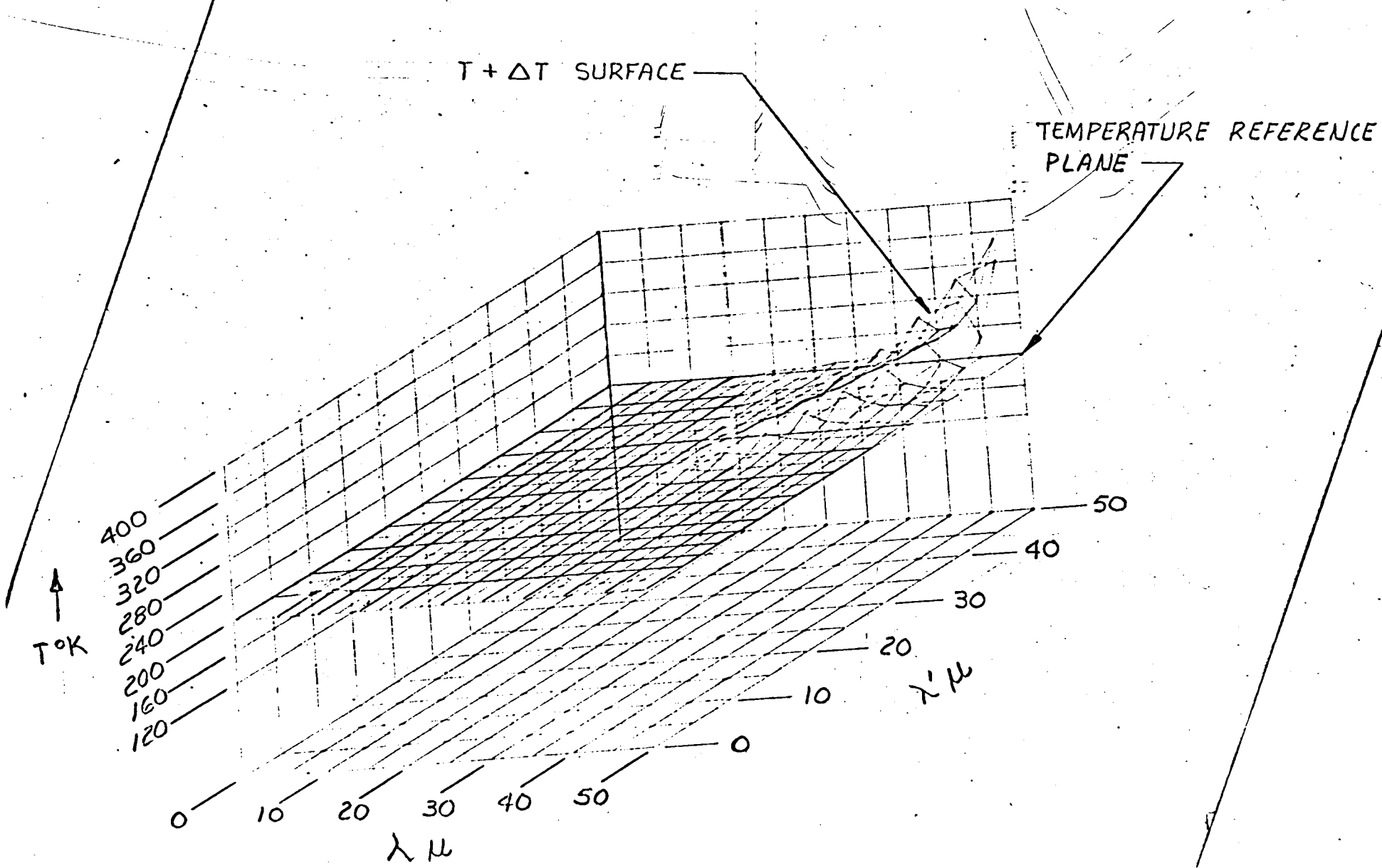
T + ΔT SURFACE
TEMPERATURE REFERENCE PLANE
T°K
400
360
320
280
240
200
160
120
0
10
20
30
40
50
λ μ
0
10
20
30
40
50
λ' μ

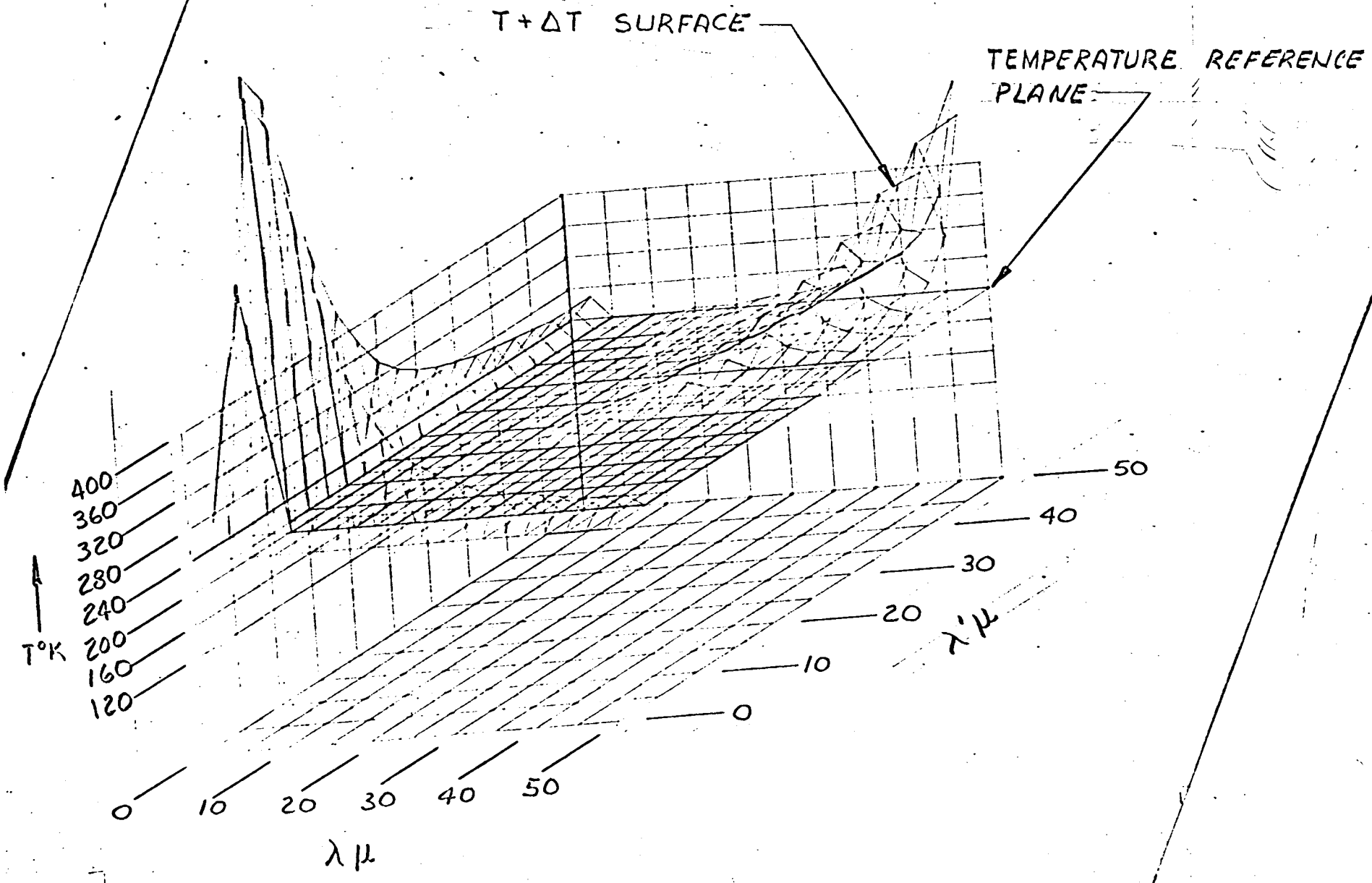
T + ΔT SURFACE
TEMPERATURE REFERENCE PLANE
400
360
320
280
240
200
160
120
T°K
0
10
20
30
40
50
λ μ
0
10
20
30
40
50
λ' μ

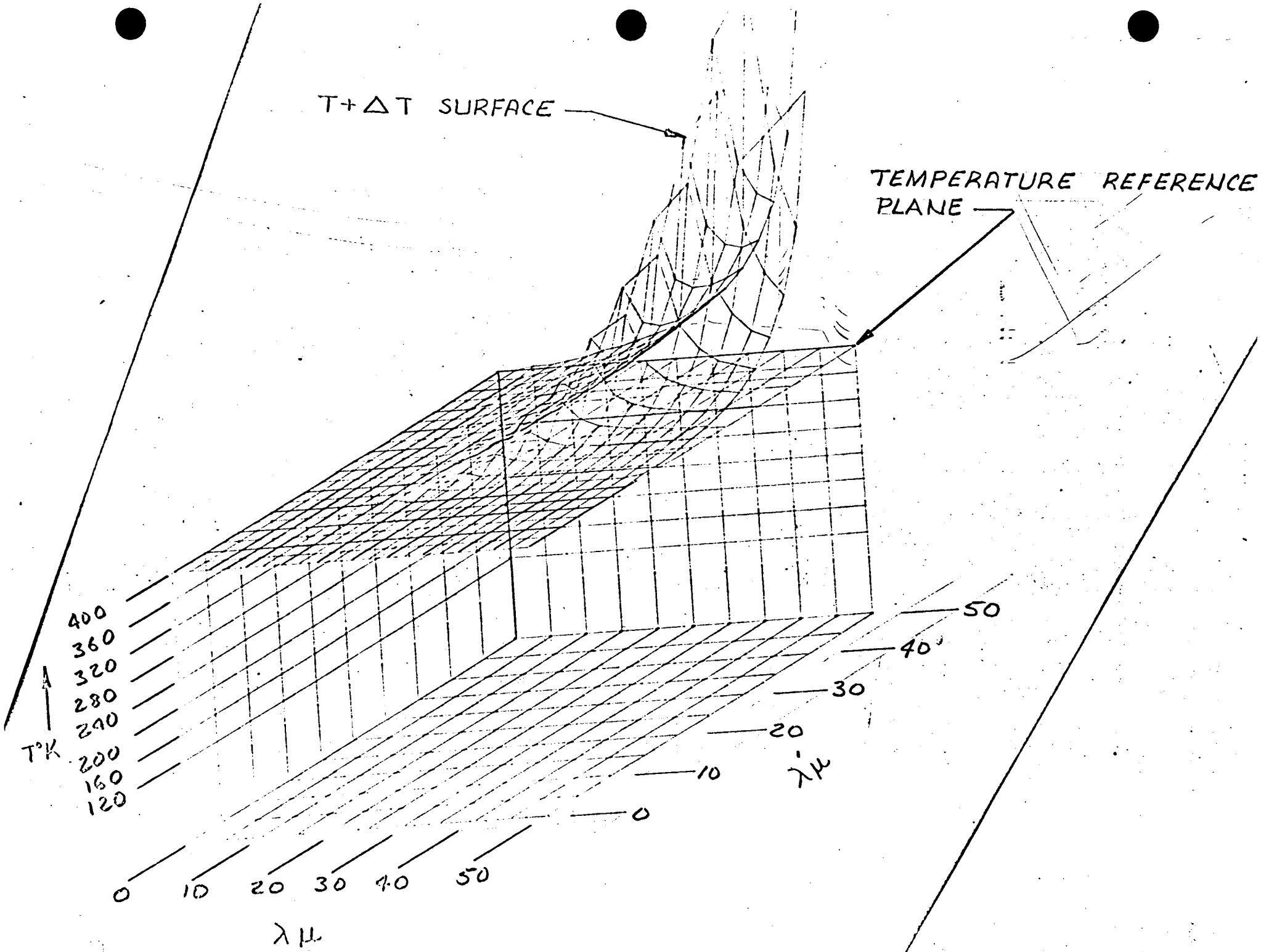
T+ΔT SURFACE
TEMPERATURE REFERENCE PLANE
400
360
320
280
240
200
160
120
T°K
0
10
20
30
40
50
λμ
0
10
20
30
40
50
λμ

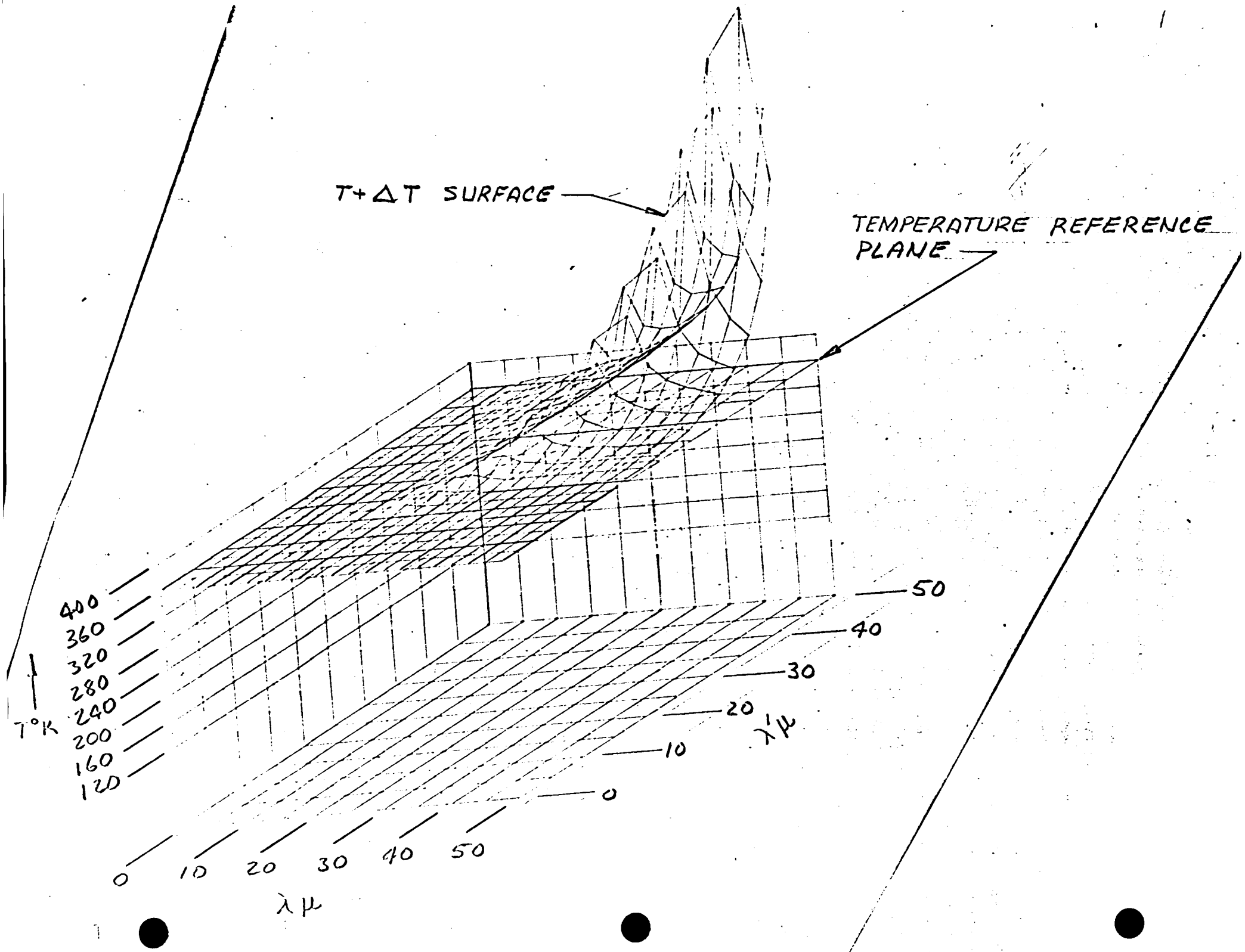
T+ΔT SURFACE
TEMPERATURE REFERENCE PLANE
400
360
320
280
240
200
160
120
T°K
0
10
20
30
40
50
λμ
0
10
20
30
40
50
λ'μ

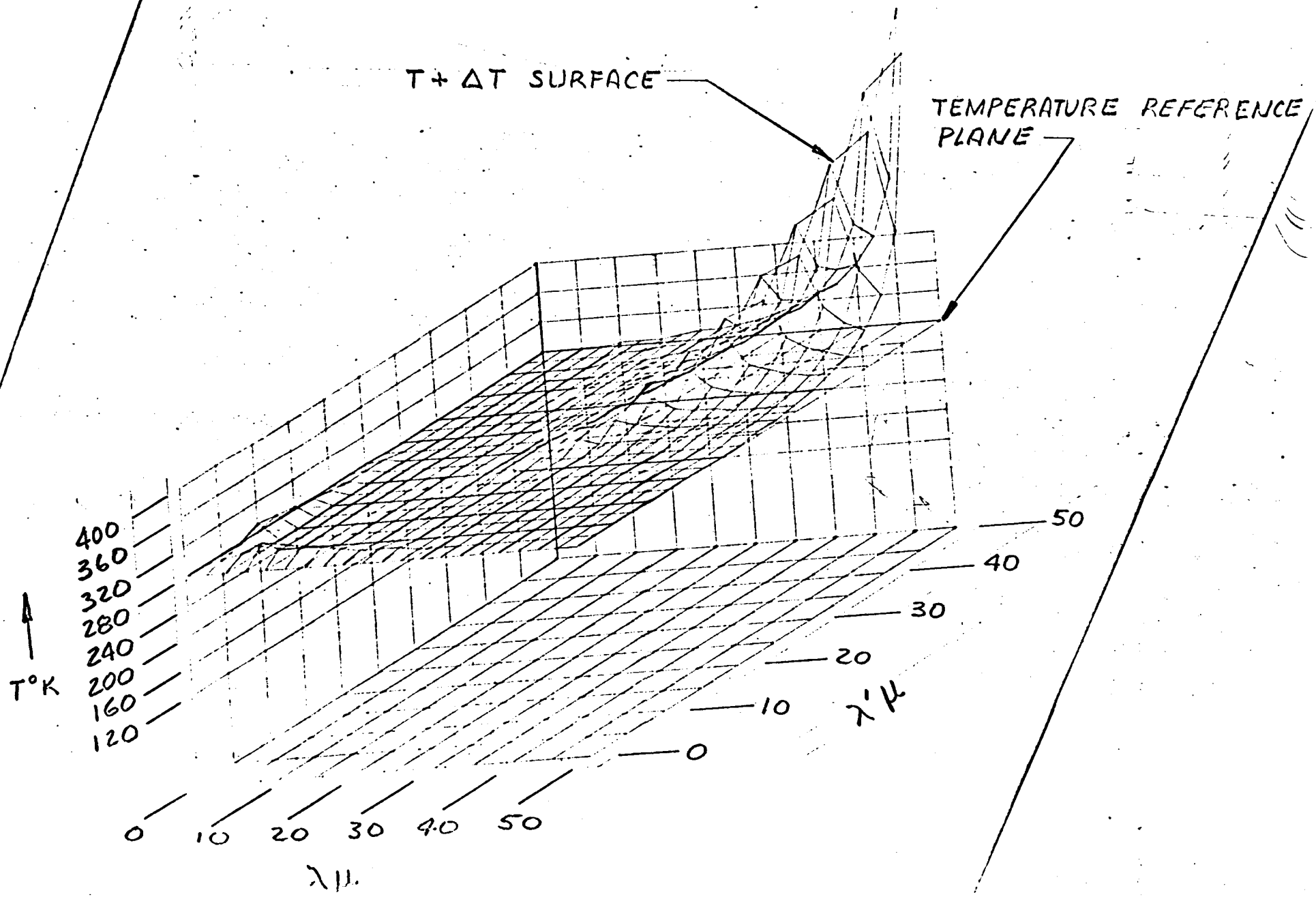
T + ΔT SURFACE
TEMPERATURE REFERENCE PLANE
400
360
320
280
240
200
160
120
T°K
0
10
20
30
40
50
λ μ.
0
10
20
30
40
50
λ' μ

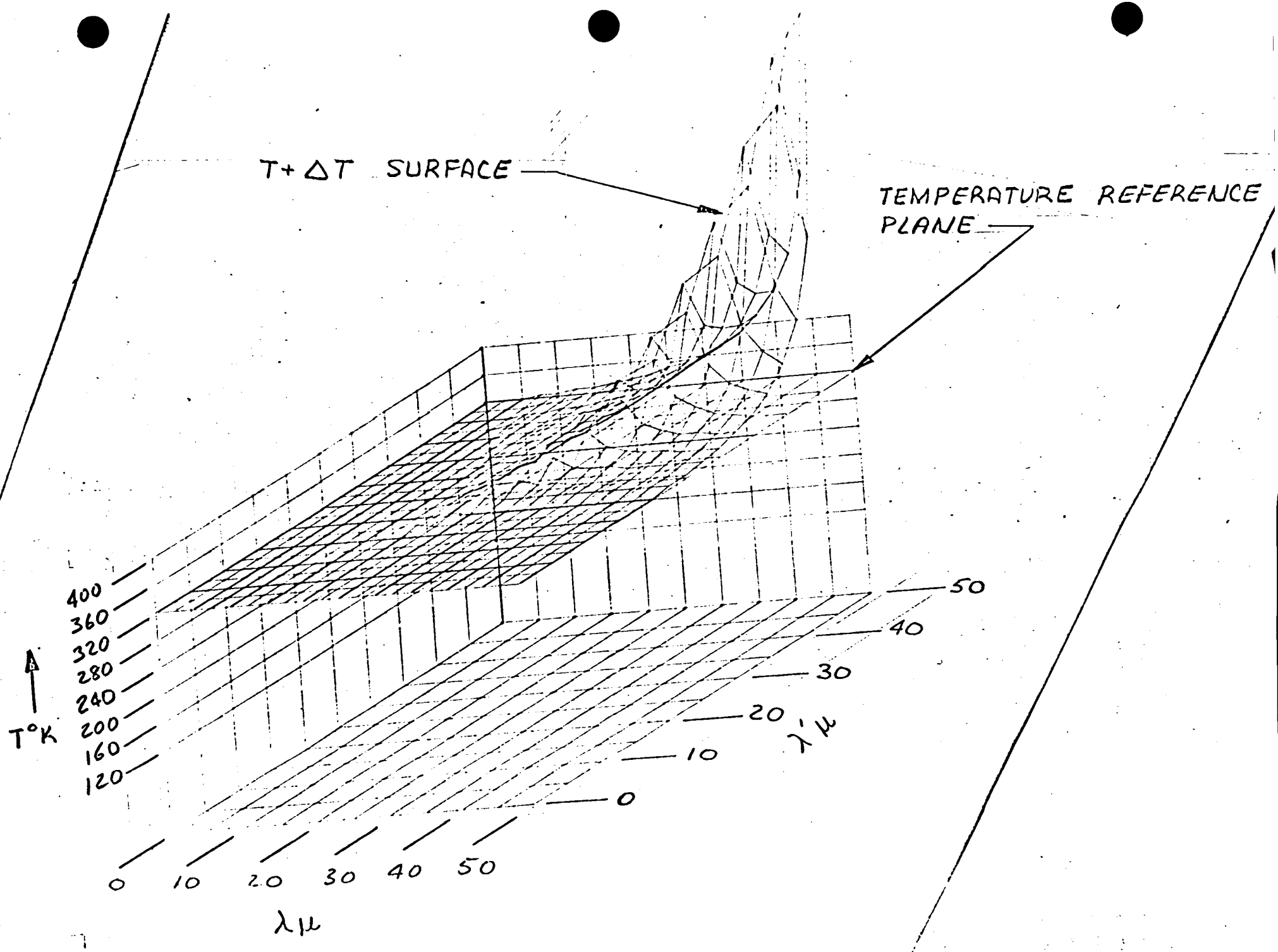
T+ΔT SURFACE
TEMPERATURE REFERENCE PLANE
400
360
320
280
240
200
160
120
T°K
0
10
20
30
40
50
λ μ
0
10
20
30
40
50
λ' μ

APPENDIX 4

GRAPHS

Graphs for the Ratio Method

A scheme has also been devised to graph data in three dimensions. The large amount of data to be presented and the complex relations involved made this desirable. The wavelength scales going from 0 - 50μ are the x and y coordinates. Temperatures are on the z coordinate. In each graph, a reference plane is drawn at the temperature of interest. A surface of $T(\lambda, \lambda') = T + \Delta T$ where ΔT is computed from the appropriate partials and the error weights for a representative instrument. The absolute value of the maximum theoretical error is the distance between the T reference plane and the $T + \Delta T$ surface. Of course, temperatures vary both above and below the reference temperature but only one surface is drawn in the interest of clarity. The ΔT used making these plots was also used in the weighting function so we can see immediately how the data will be emphasized.

```
      C2 = 14388
      C1 = 37403
      ZONK = LOGF(2.)
      EYEMAX = .008
      ZAP = 45
      DO 125 KAY= 6, 14, 2
      QUE = KAY
      WRITE OUTPUT TAPE 6, 991,  QUE
      DO 125 I = 1,8
      T = I
      T = 80. + T*40.
      WRITE OUTPUT TAPE 6,  994, T
      DO 125 J = 1, 10
      WRITE OUTPUT TAPE 6, 992
      E = J
      E = E*5.
      EE = EXPF(C2/(E*T))
      BEE = (EE - 1.)
      W =  C1/(E**5*BEE)
      DTDW = C1*C2/(E**6*W**2*(LOGF(C1/(E**5*W) + 1.))**2*(C1/(E**5*W) + .
     1 1.))
      DTDL = 5.*C1*C2/(W*E**7*(LOGF(C1/(E**5*W) + 1.))**2*(C1/(E**5*W) + .
     1 1.)) -C2/(E**2*LOGF(C1/(E**5*W) + 1.))
      EN = QUE/4.
      X = DTDW
      Y = DTDL
      DTDL = ABSF(DTDL)
      DTDL = ABSF(DTDL)
      DO 8 K = 1, 6
      EM = EN - QUE
      WONK = 2.**EM
      WUNK = 1./2.**EN
      DELT = DTDW*EYEMAX*WONK + DTDL*ZAP*WUNK
      F    = DTDW*EYEMAX*WONK      - DTDL*ZAP*WUNK
    8 EN = EN - F/(DELT*ZONK)
      DELT = DTDW*EYEMAX*WONK + DTDL*ZAP*WUNK
      SNR = 1./WONK
      RES = ZAP*WUNK
      DTDW = X
      DTDL = Y
      WRITE OUTPUT TAPE 6, 995, E, DTDL, RES, W, DTDW, SNR, EN, DELT
      EN = QUE/4.
      EM = EN - QUE
      WUNK = 1./2.**EN
      WONK = 2.**EM
      DTDW = ABSF(DTDW)
      DTDW = ABSF(DTDW)
      DELT = DTDW*EYEMAX*WONK + DTDL*ZAP*WUNK
      SNR = 1./WONK
      RES = ZAP*WUNK
      WRITE OUTPUT TAPE 6, 996, RES, SNR, EN, DELT
      DO 125 K = 1,20
      IF(2*J-K) 10, 9, 10
    9 WRITE OUTPUT TAPE 6, 993
      GO TO 125
   10 EP = K
```

```
      C2 = 14388

      EP = EP*2.5
      RE = (EP/E)**5
      EEP = EXPF(C2/(EP*T))
      BEEP = (EEP - 1.)
      DHDT = RE*BEEP*EE*C2/(E*T**2*BEE**2) - RE*EEP*C2/(EP*T**2*BEE)
      DHDR = -1.
      DHDL =-5.*RE*BEEP/(E*BEE) + RE*BEEP*EE*C2/(BEE**2*E**2*T)
      DHDLP =  5.*RE*BEEP/(EP*BEE) - RE*EEP*C2/(EP**2*T*BEE)
      DTDR = DHDR/DHDT
      DTDL = DHDL/DHDT
      DTDLP = DHDLP/DHDT
      X = DTDR
      Y = DTDL
      Z = DTDLP
      DTDR = ABSF(DTDR)
      DTDL = ABSF(DTDL)
      DTDLP = ABSF(DTDLP)
      WP=  C1/(EP**5*BEEP)
      RI = W/WP
      XKLOOG = DTDR*RI*EYEMAX*(1./W + 1./WP)
      YKLOOG = ZAP*ZONK*(DTDL + DTDLP)
      DO 110 M = 1,6
      EM = EN - QUE
      WONK = 2.**EM
      WUNK = 1./2.**EN
      F  = WONK*XKLOOG - WUNK*YKLOOG
      DT  = WONK*XKLOOG + WUNK*YKLOOG
  110 EN = EN - F/(DT*ZONK)
      DT  = WONK*XKLOOG + WUNK*YKLOOG
      SNR = 1./WONK
      RES = ZAP*WUNK
      DTDR = X
      DTDL = Y
      DTDLP = Z
      WRITE OUTPUT TAPE 6, 997, E, DTDL, EP, DTDLP, RES, RI, DTDR, SNR,
     1EN, DT
      EN = QUE/4.
      EM = EN - QUE
      WUNK = 1./2.**EN
      WONK = 2.**EM
      DT  = WONK*XKLOOG + WUNK*YKLOOG
      SNR = 1./WONK
      RES = ZAP*WUNK
      WRITE OUTPUT TAPE 6, 998, RES, SNR, EN, DT
  125 CONTINUE
  991 FORMAT( 1H1 4H K = F4.0)
  992 FORMAT(1H07H LAMBDA 4X 6H DT/DL 6X 6H LAMBDA'4X 7H DT/DL' 5X 11H R
     1ESOLUTION 1X  5H I/I' 7X 6H DT/DR  6X 4H SNR  8X  2H N 10X  8H DEL.
     2TA T)
  993 FORMAT(22H LAMBDA = LAMBDA PRIME/)
  994 FORMAT(/// F12.4, 4H T K)
  995 FORMAT(// 2(1X E11.3) 24X 6(1X E11.3))
  996 FORMAT(48X 1X E11.3, 24X 3(1X E11.3)////)
  997 FORMAT(10(1X E11.3))
  998 FORMAT(48X 1X E11.3, 24X 3(1X E11.3)//)
      CALL EXIT
```

APPENDIX 3

This appendix presents the system used to evaluate all the partials derived in this report. It also contains the schemes used to optimize an instrument for temperature measurement purposes. The partials were subsequently used in weighting the temperatures calculated at each wavelength for taking a weighted average.

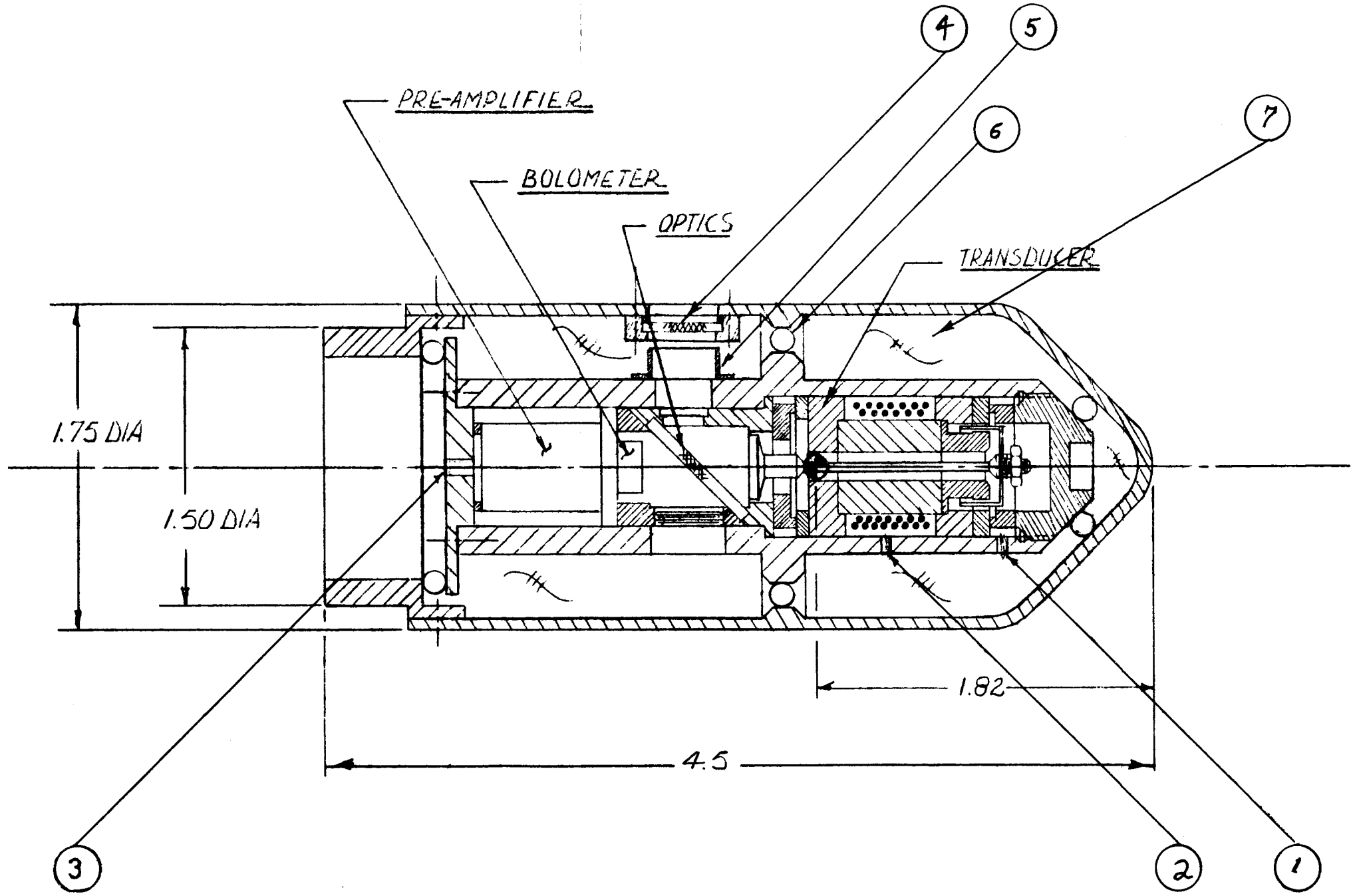

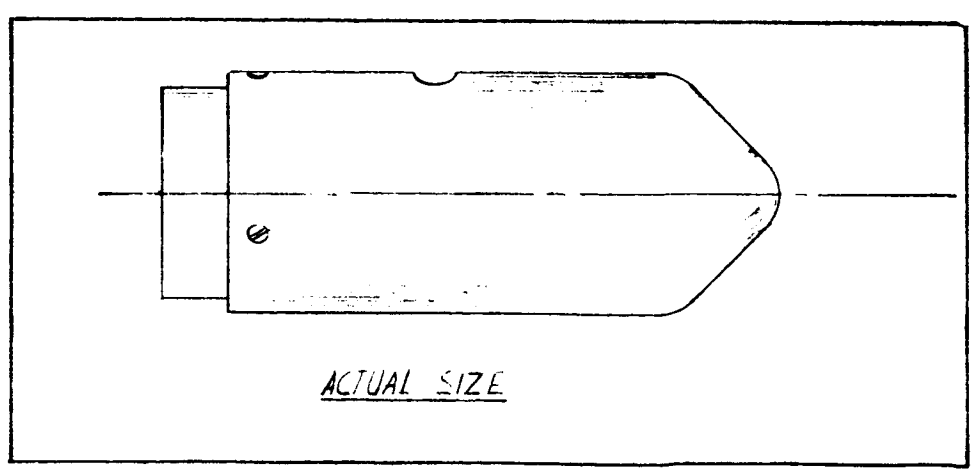

Block Engineering, Inc.
CAMBRIDGE, MASSACHUSETTS 02138

INTERFEROMETER
SPECTROMETER SENSOR
ASSEMBLY

SIZE	CODE IDENT NO.	DRAWING NO.	
C			
SCALE 2 ×		Weight. Est = .4#	SHEET

APPENDIX 2

Down Hole Probe Assembly

The down hole probe must be designed with overall experimental requirements in mind. The appended drawing shows the preliminary design.

Standard dewar techniques are used to thermally isolate the inner shell from the outer. This will provide a more stable bolometer temperature necessitate less power for heating and will help to minimize energy exchange between the probe and the walls of the hole.

The following notes apply to the drawing.

1. Transducer drive lead exit. 2 leads
2. Heater lead exit. 2 leads
3. Preamp bolometer high voltage and temperature monitor lead exit. 6 leads
4. Window IRTRAN 6
5. Glass tube
6. Glass bead
7. Super insulation

The leads from the preamp can be dressed into two bundles of three wires each for convenient transit through subsequent sections. The heater and transducer leads will run between the two shells after leaving their respective units and can therefore easily leave the end of the probe at any point.

As voltages will be relatively high and impedances sufficiently low, the probability that the leads will pick up stray radiation in subsequent sections, is minimal; therefore, shielded cables will not be necessary.

G. AUTH

```
      DIBLP = ADBL(M)
      DT = XKLOOG*(DDELI + DIBL + DIBLP) + DTDL*RESOL*E**2 + DTDLP*RESOL*
     1*EP**2
C
C     TAKE RATIO OF IRRADIANCE AND ITERATE FOR TEMP.
C
      W = DW(N)
      WP = DW(M)
      IF(W) 71, 71, 70
   70 IF(WP) 71, 71, 72
   71 AT(N,M) = 0.
      GO TO 125
   72 RI = W/WP
      T = TX - 50.
      L = 0
      ENOISE = RESOL*RANDR(3.1415)*E**2
      E = E + ENOISE
      ENOISE = RESOL*RANDR(3.1415)*EP**2
      EP = EP + ENOISE
   81 EE = EXPF(C2/(E*T))
      EEP = EXPF(C2/(EP*T))
      BEE = (EE - 1.)
      BEEP = (EEP - 1.)
      IF(EE - 10.**16) 82, 82, 90
   82 IF(EEP - 10.**16) 83, 83, 90
   83 H = RI - RE*BEEP/BEE
      DHDT = RE/T**2*C2*(BEEP/BEE*EE/BEE*1./E - EEP/BEE*1./EP)
   85 T = T + H/DHDT
      L = L + 1
      IF(T - TX - 500.) 86, 86, 90
   86 IF(T - 25.) 90, 88, 88
   88 IF(L - 20) 89, 89, 90
   89 IF(ABSF(H) - .0005)   117, 117, 81
   90 AT(N,M) = 0.
      GO TO 125
  117 CONTINUE
      AT(N,M) = T
      TNAV = TNAV + T
      RSLMNS = RSLMNS + 1.
  120 SUMDT = SUMDT + 1./DT
      TN = TN + T/DT
  125 CONTINUE
  127 CONTINUE
      TN = TN/SUMDT
      TNAV = TNAV/RSLMNS
      WRITE OUTPUT TAPE 6, 778, ((AT(I,J), J = 1, 10), I = 1,20)
      WRITE OUTPUT TAPE 6, 778, ((AT(I,J), J = 11,20), I = 1,20)
      ST = TN - TX
      SNT = TNAV - TX
      WRITE OUTPUT TAPE 6, 779, RSLMNS, TN, TNAV, ST, SNT
  130 CONTINUE
  777 FORMAT(1H1 4(F20.6))
  778 FORMAT(1H1 10(E12.4))
  995 FORMAT(-/  5X F8.3, 8X 3(10X E16.7))
  985 FORMAT(     5X F8.3, 8X 3(10X E16.7))
  779 FORMAT(F4.0 4(16.4))
```

G. AUTH

```
      AEBL(J) = EEBL
      ABEBL(J) = BEEBL
      AWB(J) = WBL
      ADBL(J) = DIBL
      WRITE OUTPUT TAPE 6, 995,  E,  W, WBL, DELTAW
C
C     ADD NOISE TO IRRADIANCE
C
      WNOISE = (DELEMS*WBL + DDELI)*RANDR(3.1415)
      DELTAW = DELTAW + WNOISE
      TNOISE = DBLT*RANDR(3.141)
      BLT = BLT + TNOISE
      EEBL = EXPF(C2/(E*BLT))
      BEEBL = EEBL - 1.
      WBL = C1/(E**5*BEEBL)
      W = DELTAW + WBL
      WRITE OUTPUT TAPE 6, 985,  E,  W, WBL, DELTAW
      DWB(J) = WBL
      DW(J) = W
   50 DDW(J) = DELTAW
C
C     CALCULATE PARTIALS FOR WEIGHTING FUNCTION
C
      DO 127 N = 1, 20
      DO 125 M = 1, 20
      IF(N - M ) 69, 125, 69
   69 E = AE(N)
      EP = AE(M)
      RE = (EP/E)**5
      T = TX
      BLT = BLTX
      EE = AEE(N)
      EEP = AEE(M)
      BEEP = (EEP - 1.)
      BEE = (EE - 1.)
      W = AW(N)
      WP = AW(M)
      RI = W/WP
      DHDT = RE/T**2*C2*(BEEP/BEE*EE/BEE*1./E - EEP/BEE*1./EP)
      DHDR = -1.
      DHDLP = 5.*RE/EP*BEEP/BEE - RE/EP**2*EEP/BEE*C2/T
      DHDL = -5.*RE/E*BEEP/BEE + RE/E*BEEP/BEE*EE/BEE*C2/EE*1./T
      DTDR = DHDR/DHDT
      DTDL = DHDL/DHDT
      DTDLP = DHDLP/DHDT
      DTDR = ABSF(DTDR)
      DTDL = ABSF(DTDL)
      DTDLP = ABSF(DTDLP)
      XKLOOG = DTDR*RI*        (1./W + 1./WP)
      EEBL = AEBL(N)
      EEBLP = AEBL(M)
      BEEBL = EEBL - 1.
      BEEBLP = EEBLP - 1.
      WBL = AWB(N)
      WBLP = AWB(M)
      DIBL = ADBL(N)
```

G. AUTH 12/27/

```
C     PROGRAM TO SIMULATE AN INTERFEROMETER  AS ATEMPERATURE SENSING DEVICE
      DIMENSION AE(20), AEE(20), AB(20), AW(20), AEBL(20), ABEBL(20),
     1AWB(20), ADBL(20), ADW(20), DDW(20), DW(20), DWB(20), AT(20,20)
C
C     SET INSTRUMENT PARAMETERS
C
      C1 = 37403
      C2 = 14388
      PI = 3.1416
      RESOL = .008
      SEMS = .5
      THRP = .123
      DSTR = .5*10.**10
      DBLT = .5
      RTA = 1.
      RTF = 17
      EF = .03
      EMS = .95
      DELEMS = .01
      DDELT = PI/THRP*RTA/DSTR*RTF/EF
      BLTX = 300.
C
C     CHOOSE SOURCE TEMPERATURE AND RESET TEMPERATURE PARAMETERS
C
      DO 130 I = 1, 8
      T = I
      T = 80. + T*40.
      TN = 0
      SUMDT = 0
      TNAV = 0
      RSLMNS = 0
      TX = T
      BLT = BLTX
      WRITE OUTPUT TAPE 6, 777, T, BLT, DDELT, DBLT
C
C     CHOOSE LAMBDA CALCULATE SPECTRAL IRRADIANCE AND RESET PARAMETERS
C
      DO 50  J = 1, 20
      E = J
      E = E*2.5
      AE(J) = E
      BLT = BLTX
      T = TX
      EE = EXPF(C2/(E*T))
      BEE = (EE - 1.)
      W =  C1/(E**5*BEE)*SEMS
      AEE(J) = EE
      AB(J) = BEE
      AW(J) = W
      EEBL = EXPF(C2/(E*BLT))
      BEEBL = EEBL - 1.
      WBL = C1/(E**5*BEEBL)
      DIBL =          WBL*(DELEMS + EMS*EEBL/BEEBL*C2/E*DBLT/BLT**2)
      DELTAW = W - WBL
      ADW(J) = DELTAW
```

```
      C2 = 14388                                                        11/29/65

      C2 = 14388
      C1 = 37403
      PI = 3.1416
      THRP = .C3
      RTA = .05
      DSTR = .5*10.**8
      RTF = 3
      EF = .03
      EMS = .95
      DELEMS = .05
      EN = 10
      DBLT = .1
      DDELI = PI/THRP*RTA/DSTR*RTF/EF
      DO 130 I = 1, 8
      SUMDT = 0
      TNAV = 0
      RSLMNS = 0
      TN = 0
      T = I
      T = 80. + T*40.
      WRITE OUTPUT TAPE 6, 994, T
      DO 125 J = 1, 10
      BLT = 300
      E = J
      E = E*5.
      EE = EXPF(C2/(E*T))
      BEE = (EE - 1.)
      W =  C1/(E**5*BEE)
      DTDW = C1*C2/(E**6*W**2*(LOGF(C1/(E**5*W) + 1.))**2*(C1/(E**5*W) +
     1 1.))
      X = DTDW
      DTDW = ABSF(DTDW)
      EEBL = EXPF(C2/(E*BLT))
      BEEBL = EEBL - 1.
      WBL = C1/(E**5*BEEBL)
      DELTAW = W - WBL
      WNOISE = (DELEMS*WBL + DDELI)*RANDR(3.1415)
      DELTAW = DELTAW + WNOISE
      TNOISE = DBLT*RANDR(3.141)
      BLT = BLT + TNOISE
      EEBL = EXPF(C2/(E*BLT))
      BEEBL = EEBL - 1.
      WBL = C1/(E**5*BEEBL)
      W = DELTAW + WBL
      DIBL = WBL*(DELEMS + EMS*EEBL/BEEBL*C2/E*DBLT/BLT**2)
      DELT = DTDW*(DDELI + DIBL)
      IF(W) 110, 110, 115
  110 WRITE OUTPUT TAPE 6, 993
      GO TO 125
  115 TEE = C2/(E*LOGF(C1/(W*E**5) + 1.))
      RSLMNS = RSLMNS + 1.
      TNAV = TNAV + TEE
      TN = TN + TEE/DELT
      SUMDT = SUMDT + 1./DELT
      WRITE OUTPUT TAPE 6, 995, TEE, TNOISE, WNOISE, DELTAW
  125 CONTINUE
```

from the geometry

$$D_1 = D_2 = S/2$$

so that

$$\begin{aligned}
\theta &= \frac{\pi^2}{8} D^2 \left[18 - \sqrt{(18)^2 - 4}\right] \\
&= \frac{\pi^2}{8} D^2 \left[18 - \sqrt{320}\right] \\
&= \frac{\pi^2}{8} D^2 \left[18 - 8\sqrt{5}\right] \\
&= \pi^2 D^2 \left[9/4 - \sqrt{5}\right] \\
&= \pi^2 D^2 \left[2.25 - 2.236\right] \\
&\approx \pi^2 D^2 \left[.014\right] \\
&\approx D^2 \left[.14\right]
\end{aligned}$$

$\sqrt{A_d}$ = the square root of the detector's area

D^* = Jones' specific detectivity

$\sqrt{\Delta f}$ = detective bandwidth

EFF = the total efficiency of the optics

ϵ_s = emissivity of the source

$\sqrt{N/2}$ = factor by which signal to noise is increased by coadding N times of equivalently $\sqrt{2/N}$ is the factor by which the noise is reduced.

To simulate noise, ten times the NESPD was multiplied by a pseudo-random number, range -1. to 1., distribution roughly Gaussian, and added to the irradiance calculated from Planck's function.

Other errors considered were the uncertainties in the bolometer's temperature and emissivity. Since we only measure the

differential irradiance between the bolometer and source, errors in the measurement of the bolometer temperature effect the calculated irradiance of the bolometer hence the source irradiance. Similarly, the bolometers emissivity.

From these considerations the following scheme was derived: a ΔT for the bolometer was multiplied by a pseudo-random number. The spectral irradiance for the resulting temperature was computed and the difference between this and the true irradiance was added to the source irradiance as noise.

The following program was used to simulate the blackbody case.

The noise scale factor is calculated rather than measured. It can be called noise equivalent spectral power density; NESPD for short. It is a convenient basis of comparison for full field of view sources, assuming the source is a Lambertian radiator. For calculation purposes, it is:

$$\text{NESPD} = \frac{\pi}{\theta} \frac{\sqrt{A}}{D^*} \frac{\sqrt{\Delta f}}{EF} \epsilon \text{ source } \frac{2}{N}$$

where θ, the throughput of the optics, is a geometrical figure relating the fraction of the available energy which the system will pass. (see the JOSA ad on the following page)

We consider the geometry of an interferometer

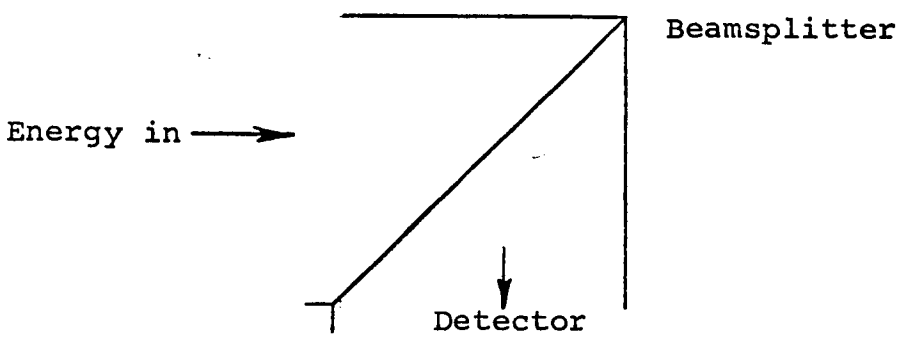

(A)

or its equivalent optical diagram

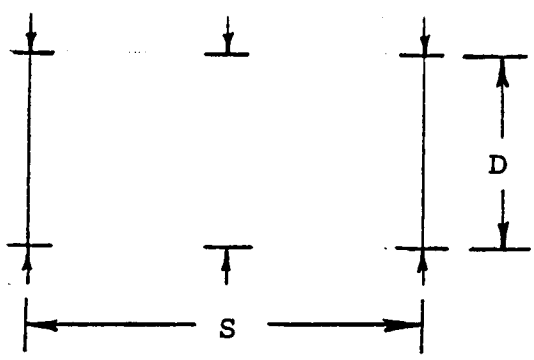

(B)

From the JOSA ad we have

$$\theta = \frac{\pi^2}{8} \left[D_1^{\,2} + D_2^{\,2} + 4S^2 - \sqrt{(D_1^{\,2} + D_2^{\,2} + 4S^2)^2 - 4D_1^{\,2}D_2^{\,2}} \right]$$

Reprinted from JOURNAL OF THE OPTICAL SOCIETY OF AMERICA, Vol. 54, No. 1, January 1964

AN ADVERTISEMENT

THROUGHPUT: A FIGURE OF MERIT FOR OPTICAL SYSTEMS

The spectral power P_ν intercepted (or collected) by any system of apertures, lenses, mirrors, etc., under illumination by a diffuse source may be expressed by an equation of the form $P_\nu = FB_\nu$, where F is a geometrical factor that is determined by the size, shape and relative orientation of the radiating and collecting elements, and B_ν is the spectral radiant sterance* of the radiation field, defined by

$$B_\nu(\nu,T) = \lim \left| \frac{dP_\nu(\nu,T)}{d\omega dA \cos\theta} \right|_{d\nu,\, d\omega,\, dA \to 0}; \qquad P_\nu = dP/d\nu$$

In this equation dP is the radiative power per unit spectral interval $d\nu$ per unit solid angle $d\omega$ that is transmitted across (or emitted by) an area dA in the direction θ, where θ is the angle between the radiation and the normal to dA. The area dA is located anywhere in the radiation field, and may be taken as a unit area of the source or a unit area of the collector. The spectral sterance B_ν is independent of the direction of P (and of the position at which dP is measured) since $dP/d\nu d\omega dA$ varies as $\cos\theta$ in the case of diffuse radiation. If the source is a blackbody, $B_\nu(\nu,T)$ is given by Planck's function evaluated for the frequency ν and for the temperature T of the source.

Note that if the source is infinite in extent, or if it fills the field of view of the system, the collected spectral power P_ν is independent of the distance of the source; i.e., the factor F is then determined by the optical system alone. Since F, in this special case, is a measure of the radiant power accepted by the system under the most favorable conditions of illumination, it represents the maximum light gathering power, or the "throughput" of the system. For this reason, the throughput is a useful concept for comparing different optical systems.

From the equation defining B_ν, the throughput is given by

$$\Theta = F_{max} = \int\int \cos\theta d\omega dA$$

where $d\omega$ is a unit solid angle through which an element dA of the collecting aperture receives radiation from the source. The integration with respect to ω extends over the field of view of the optical system. If there are no absorption or reflection losses, the throughput may also be calculated at any point "inside" the optical system, since the power collected at the aperture is conserved.

The throughput equations are given below for three simple configurations:

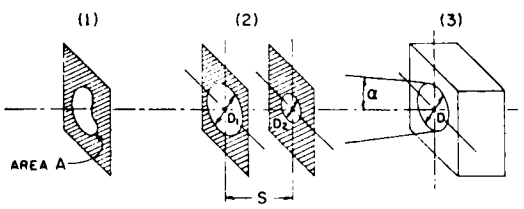

$$\Theta_1 = \pi A \qquad \Theta_3 = \pi^2 \frac{D^2}{4} \sin^2\alpha$$

$$\Theta_2 = \frac{\pi^2}{8}\left[D_1^2 + D_2^2 + 4S^2 - \sqrt{(D_1^2 + D_2^2 + 4S^2)^2 - 4D_1^2 D_2^2}\right]$$

The expression for Θ_1 corresponds to the well-known blackbody relation $B = \int_0^\infty B_\nu d\nu = (\sigma T^4)/\pi$. The throughput Θ_2 is related to the "view factor" derived by Hottel[1] for parallel radiating discs. Finally, Θ_3 gives the throughput of an optical system with a circular entrance aperture (dia. D) and circular field of view (half-angle α). In a future JOSA advertisement, we will give a nomograph for evaluating $\Theta_3(D,\alpha)$.

A. Zachor

* Using the nomenclature adopted this year by the IRIS Specialty Group on Radiometric Units.

[1] Hottel, H. C., Mech. Eng., 52, 699–704 (1930).

BLOCK ENGINEERING, INC.

385 Putnam Avenue Cambridge 39, Mass.

AN ADVERTISEMENT

APPENDIX 1

The contents of Appendix 1 give mathematical justification for the magnitude of the random noise added to the I_{λ_i}'s calculated from Planck's function. Also included is the computer program in which data from a blackbody curve was generated and made noisy and analyzed by the blackbody method, and in the second program included by the ratio method.

Conclusion

A miniaturized state of the art interferometer spectrometer, with a noise equivalent spectral power density of 100 to 200 μwatts cm^{-2} μ^{-1}, in the region from 5 to 40μ, resolution better than 80 cm^{-1} would yield spectra of sufficient accuracy to calculate temperatures from 240 to 400°K with an expected accuracy of better than 10°K, using blackbody single color methods. Using greybody ratio methods it would give an expected accuracy of 50°K in the range 120 to 400°K. Coadding 100 times in order to improve the S/N would reduce the ΔT in either case by an order to magnitude.

The necessary instrument can be fabricated by modifying previous space-worthy designs for this use. The data analysis schemes to calculate temperatures from the spectra have been written and debugged as part of this feasibility study.

the maximum frequency present in the signal. The samples are sequentially digitized and stored in the core memory. Each series of samples is initiated by a triggering pulse supplied by the interferometer at the beginning of each interferogram. Therefore, the samples from successive interferograms correspon d precisely in time and their levels are digitally added in the memory, so that the coherent signal increases linearly in amplitude with the number of interferograms accumulated. On the other hand, the noise present at the input accumulates, due to its random character, in such a way that the noise power increases RMS i.e. with the square root of the number of scans. The resultant gain in signal to noise is thus $\sqrt{n}$, where n is the number of times the same signal is sampled. For example, if the Coadder accumulates as few as 16 interferograms, the S/N will be increased by a factor of four.

The Coadder also lends flexibility to the system since its input rate is tailored to the interferometer. Yet its output rate can be tailored to fit telemetry optimization requirements. Also, interferograms can be stored at the convenience of the astronaut and transmitted when a data channel is open.

Recommended System

The recommended design for a Michelson interferometer system suitable for lunar use will conform to the following parameters.

SUBSYSTEM	WEIGHT	SIZE	POWER
Sensing Head	300 gms.	1.75"D x 4.5"L	
Surface Electronics without Coadder	450 gms	1 liter*	2 watts+
Coadder	2 Kg.	1.6 liter*	8 watts+

*Can be tailored to fit any reasonable shape.

+Stable supply voltage in the range 20 - 40 volts.

Output

The output from the interferometer will have a maximum audio frequency of 200 cps. Signal to noise requirements of storage and transmission systems should be 100 in order not to significantly degrade the signal. The rate will be 3 interferograms per second with an 85% duty cycle, i.e. 15% for mirror flyback.

The Coadder output will be digital 50 x 18 bits neglecting housekeeping. The word length and readout rate can be tailored to the telemetry systems used. The contents of the Coadder can be transmitted whenever a data link is free. The readout need not be destructive allowing retransmission in case of necessity. The output impedance and level of either the interferometer or Coadder can be matched to input requirements of storage and transmission devices.

An additional word of at least 8 bits must be transmitted for bolometer temperature monitoring.

Accuracy and Resolution

The instrument as proposed with Coadder will have a spectral resolution of 60 - 80 cm^{-4} and yield temperature data from 240 to 400°K with an error less than one degree Kelvin; using ratio methods tempeatures from 120 - 400°K can be calculated with a standard deviation of less than 5°K.

The system without the Coadder would have respective errors of approximately one order of magnitude higher.

Appendix I

LUNAR EXPERIMENT LIST

```
      C2 = 14388

      TN = TN/SUMDT
      TNAV = TNAV/RSLMNS
      WRITE OUTPUT TAPE 6, 992, TN, TNAV
  130 CONTINUE
  992 FORMAT(2(E14.6, 2X))
  993 FORMAT(20H NEGATIVE IRRADIANCE)
  994 FORMAT(/// F12.4, 4H T K)
  995 FORMAT(4(4X E11.3))
      CALL EXIT
      END(1,C,0,0,0,1,1,0,0,1,0,0,0,0,0)
```

A B S T R A C T

An investigation of the accuracy with which temperature can be measured using radiation sensing devices was performed. A miniaturized state of the art Michelson interferometer was found adequate for an accuracy of approximately 10-20 degrees over the range of temperatures 120°K to 400°K. Coadding 100 times yielded an accuracy of 2-3 degrees. Physical requirements of the instrument and two schemes for data interpretation were investigated. Finally, recommendations for a proposed temperature measuring system were made.

TABLE OF CONTENTS

TITLE	PAGE
TASK 1	1
TASK 2	1
Part 1 - Theoretical Derivation of Mathematical Techniques	2
Error Analysis	2
Case 1 - The Blackbody Method	3
Case II - Greybody - Two Color Method	4
Part 2 - Experimental Results	8
Simulation	8
Typical Results of Simulation	9
Non-Constant ϵ Computation	13
Discussion of Necessary Instrument	14
Theory of Operation of an Interferometer	14
Recommended System	21
Output	22
Accuracy and Resolution	22
Conclusion	23
Table 1 - Blackbody Method	10
Table 2 - Ratio Method	11
Figure 1 - Optical Equivalent to Show Ray Paths	15

APPENDIX 1

APPENDIX 2

APPENDIX 3

APPENDIX 4

TASK 1

The extremely low thermal mass of the object to be measured, plus the low probability of making good contact rules out making precise, accurate temperature measurements by contacting methods. Having thus eliminated methods other than radiometric, attention was turned to investigation of the possible portions of the spectrum from which temperature could be accurately measured. The use of portions of the spectrum $\lambda < 5\mu$ was not considered feasible due to variation in surface reflectivity and scattering that are not functions of temperature and involve the variation of solar aspect angle. This use of the IR spectrum for measuring temperature becomes the only method that warrants further consideration.

TASK 2

Contact means having already been eliminated in Task 1, an analysis of the methods of single color and/or two color monitoring vs. the method of scanning was made.

The technique for choice would be scanning because of several factors. Filtering out most of the signal, as one or two color methods would require, significantly degrades the final signal to noise ratio, making accurate temperature measurements that much more difficult. Further, with little prior knowledge of the nature of the spectrum radiated, any measurements would be meaningless as far as temperature calculations are concerned. Our lack of knowledge as to the emissivity of the soil of the moon makes any value we might assign to ϵ suspect. In the equations from which we would have to calculate temperature from data gathered in a single color system, the presence of ϵ as a major factor would make suspect all final results.

Unless the emissivity is one, or a constant for the arbitrarily chosen wavelengths, the data would not admit to a valid interpretation.

In a two color system, the ratio method of calculating temperature would make temperature calculations more correct since assumptions made about ϵ in this method would involve its behavior as a function of wavelength rather than its absolute value. Still, however, all information at wavelengths other than the two chosen would be lost. In scanning, we can ratio not just two wavelengths,all or as many as we desire.Block Engineering's recommended instrument ratios twenty resolution elements, making even the function of ϵ with λ less necessary to be known, for a given temperature accuracy.

For these reasons as well as the accuracy considerations which follow, anything other than a scanning spectrometer would be inadequate for an unknown source.

Part 1 Theoretical Derivation of Mathematical Techniques

Error Analysis

The following is a rather general error analysis applicable to any instrument measuring temperature via radiation measurements. Various precision requirements may be deduced from it.

The analysis is based on the fact that all temperature calculations for remote, unknown sources will be made using Planck's equations. Also, assumptions are made as to the nature of the emissivity. In the first case treated below, the emissivity, ϵ, is taken to be equal to one and error effects are analyzed for computations based on single color methods. In the second, more realistic case, ϵ is taken to be a constant less than one and an error analysis is made for ratio methods.

Case 1 - The Blackbody Method

In this section is derived the equation from which T can be calculated from λ and I_λ, equation (2). Then the effects of errors in the measurement of λ and I_λ on the accuracy of T are measured.

Since $\epsilon \approx 1$ within each emission band, the case of blackbody and band spectra can be treated together by computing the temperature at each resolution element λ_i using Planck's equation. The two cases will then differ only in the number of usable elements at which the temperature can be computed.

Taking Planck's equations in the form:

$$I_{\lambda_i} = \frac{C_1}{\lambda_i^5} \epsilon_\lambda \frac{1}{e^{\left(\frac{C_2}{\lambda_i T}\right)} - 1} \qquad (1)$$

we invert to get:

$$T = \frac{C_2}{\lambda_i} \frac{1}{\ln\left[\frac{C_1}{I_{\lambda_i} \frac{\lambda_i^5}{\epsilon_\lambda}} + 1\right]} \qquad (2)$$

Since ϵ_λ is assumed equal to 1 for all λ, the temperature calculated from this equation is a function of λ_i and I_{λ_i}. To calculate the effects in I_{λ_i} and λ_i on the accuracy of T, we use the equation:

$$\Delta T_{\lambda_i} = \frac{\partial T}{\partial I_{\lambda_i}} \Delta I_{\lambda_i} + \frac{\partial T}{\partial \lambda_i} \Delta \lambda_i \qquad (3)$$

where: ΔT_{λ_i} is the error in the calculated temperature caused by

errors ΔI_{λ_i} in I_{λ_i} and $\Delta\lambda_i$ in λ_i. It is clear that the relative effect of errors in measurement of irradiance and wavelength on the accuracy of temperature measurements is dependent on the relative magnitudes of the partials $\frac{T}{I_{\lambda_i}}$ and $\frac{T}{\lambda_i}$. Their values are the following:

$$\frac{\partial T}{\Delta I_{\lambda_i}} = \frac{5\ C_1\ C_2}{\lambda_i^6\ I_{\lambda_i}^2 \left[\ln\left(\frac{C_1}{\lambda_i^5\ I_{\lambda_i}} + 1\right)\right]^2 \left(\frac{C_1}{\lambda_i^5\ I_{\lambda_i}} + 1\right)} \tag{4}$$

$$\frac{\partial T}{\partial_{\lambda_i}} = \frac{5\ C_1\ C_2}{\lambda_i^7\ I_{\lambda_i} \left[\ln\left(\frac{C_1}{\lambda_i^5\ I_{\lambda_i}} + 1\right)\right]^2 \left(\frac{C_1}{\lambda_i^5\ I_{\lambda_i}} + 1\right)}$$

$$= \frac{C_2}{\lambda_i^2\ \ln\left(\frac{C_2}{\lambda_i^5\ I_{\lambda_i}} + 1\right)} \tag{5}$$

<u>Case II</u>

<u>Greybody - Two-color Method</u>

Taking equation (1) for two values of λ and dividing we get:

$$\frac{I_\lambda}{I_{\lambda'}} = \frac{\dfrac{C_1\ \epsilon_\lambda}{\lambda^5\left(e^{\frac{C_2}{\lambda T}} - 1\right)}}{\dfrac{C_1\ \epsilon_{\lambda'}}{\lambda'^5\left(e^{\frac{C_2}{\lambda' T}} - 1\right)}} \tag{6}$$

If $\epsilon_\lambda = \epsilon_{\lambda'}$,

$$\frac{I_\lambda}{I_{\lambda'}} = \frac{+\lambda'^5 \left(e^{\frac{C_2}{\lambda' T}} - 1\right)}{\lambda^5 \left(e^{\frac{C_2}{\lambda T}} - 1\right)} \tag{7}$$

To evaluate T from this equation, we subtract one side from the other.

$$f(t) = \frac{I_\lambda}{I_{\lambda'}} - \frac{\lambda'^5 \left(e^{\frac{C_2}{\lambda' T}} - 1\right)}{\lambda^5 \left(e^{\frac{C_2}{\lambda T}} - 1\right)} \tag{8}$$

If at some T, f(t) = 0, then that value of T will be the correct value. In order to find the roots of equation (8) both Newton's method and Bolzano's bisection theorem were programmed. The bisection method proved the slower of the two and therefore Newton's method was subsequently used.

To obtain error estimates for temperatures computed using this scheme, we rewrite f(T) in the form:

$$H(T, \lambda, \lambda', RI) = RI - \frac{\lambda'^5 \left(e^{\frac{C2}{\lambda' T}} - 1\right)}{\lambda^5 \left(e^{\frac{C2}{\lambda T}} - 1\right)} \tag{9}$$

$$RI = \frac{I_\lambda}{I_{\lambda'}}$$

take the partials

$$\frac{\partial H}{\partial T}, \frac{\partial H}{\partial \lambda}, \frac{\partial H}{\partial \lambda'} : \frac{\partial H}{\partial RI}$$

and set

$$\frac{\partial T}{\partial \lambda} = \frac{\frac{\partial H}{\partial \lambda}}{\frac{\partial H}{\partial T}}$$

$$\frac{\partial T}{\partial \lambda'} = \frac{\frac{\partial H}{\partial \lambda'}}{\frac{\partial H}{\partial T}} \qquad (10)$$

$$\frac{\partial T}{\partial R} = \frac{\frac{\partial H}{\partial R}}{\frac{\partial H}{\partial T}}$$

the necessary partials are:

$$\frac{\partial H}{\partial T} = \frac{\lambda'^4 \, c_2 \, e^{\frac{c_2}{\lambda' T}}}{\lambda^5 T^2 \left(e^{\frac{c_2}{\lambda T}} - 1\right)} - \frac{\lambda'^5 \, c_2 \, e^{\frac{c_2}{\lambda T}} \left(e^{\frac{c_2}{\lambda T}} - 1\right)}{\lambda^6 T^2 \left(e^{\frac{c_2}{\lambda T}} - 1\right)^2} \qquad (11)$$

$$\frac{\partial H}{\partial \lambda} = 5 \frac{\lambda'^5}{\lambda^6} \frac{\left(e^{\frac{c_2}{\lambda' T}} - 1\right)}{\left(e^{\frac{c_2}{\lambda T}} - 1\right)} - \frac{\lambda'^5}{\lambda^5} \frac{\left(e^{\frac{c_2}{\lambda' T}} - 1\right)}{\left(e^{\frac{c_2}{\lambda T}} - 1\right)} \cdot \frac{c_2 \, e^{\frac{c_2}{\lambda T}}}{\lambda^2 T} \qquad (12)$$

$$\frac{\partial H}{\partial \lambda'} = -5 \frac{\lambda'^4}{\lambda^5} \frac{\left(e^{\frac{c_2}{\lambda' T}} - 1\right)}{\left(e^{\frac{c_2}{\lambda T}} - 1\right)} - \frac{\lambda'^5}{\lambda^5} \frac{c_2 \left(e^{\frac{c_2}{\lambda' T}}\right)}{\lambda^2 T \left(e^{\frac{c_2}{\lambda T}} - 1\right)} \qquad (13)$$

$$\frac{\partial H}{\partial R} = 1 \qquad (14)$$

A program was written to evaluate these derivatives in the region of interest. The results indicated that precise irradiance measurements were more important than high resolution. Typically at each wavelength a commercial Block instrument with spectral irradiance noise of 100 to 200 μwatts/cm$^2\mu$ sterad and a resolution of 60 - 80 cm^{-1} would give temperatures around 160°K with expected errors of 20 - 40°K caused by irradiance noise and errors of less than 1°K caused by resolution effects.

As a check, a scheme was incorporated to find the optimum error distribution for the minimum temperature error. In all cases, the resolution we can easily achieve was better than the optimization scheme required.

Part 2 - Experimental Results

Simulation

Having determined that irradiance precision should be our main area of interest in developing our instrument, we felt that a better estimate of the accuracy of present or future instruments could be obtained through simulation. By approaching the problem through a different conceptual route we also obtain an independent check on the validity of previous results. Consequently, a program was written to generate spectral irradiance from Planck's function, add appropriately scaled random noise, and store. All combinations of the two values of irradiance where chosen, ratioed, and temperatures computed through the use of equation (8). These temperatures were then averaged. Alternatively, our irradiance value, with noise was used with Equation (2). With this scheme various instruments can be simulated by varying the scale factors for the noise. These programs are presented in Appendix 3.

In debugging the program, it was found necessary to use a bit of a priori knowledge to insure convergence. We know that the spectral irradiance is never negative so any values noisy enough to be negative were discarded; also, if during the course of iteration, T became less than 10°K or greater than 900°K the scheme was interrupted and another pair chosen. The iteration scheme proceeds nicely however once these limits are placed on T. In only a few cases was it necessary to interrupt because of slow convergence. Generally, 4 - 5 iterations were adequate to achieve the desired precision.

In the process of debugging and checkout under extremely noisy conditions an interesting difference between the two schemes became apparent. Though the blackbody methods gave better results

for high temperatures, below 250° the accuracy degenerated completely. On the other hand, while the accuracy was not good, it was uniform throughout the range of temperatures for the greybody methods.

In simulating the instrument, we are given the chance to observe the efficacy of taking a weighted average as opposed to an unweighted average. To obtain a weight function for a given instrument, we multiply the appropriate partials by the noise scale factors for that instrument and add. For all the successful runs, weighting produced an average deviation which was about half as large as that produced without weighting.

The ratio method was run at low noise levels with and without adding noise to the wavelength to account for resolution effects. The difference was not noticeable. Likewise, knowing the bolometer temperature to .1°K,as opposed to .5°K, does not improve accuracy appreciably.

Typical Results of Simulation

These data are typical of all data gathered both in trends and relative magnitudes. Characteristically, the ratio method yielded better results for temperatures below 240°K while the blackbody methods were more accurate for the higher temperatures. The two noise levels used 200μwatt/cm$^2\mu$ or 20μwatts/cm$^2\mu$ are slightly pessimistic for what can be achieved with a single scan or by coadding 100 times.

		BLACKBODY METHOD			
		HIGH NOISE LEVEL 200 $\mu W/cm^2 \mu$		COADDING 100 TIMES LOW NOISE LEVEL 20 $\mu W/cm^2 \mu$	
N.E.S.P.D.					
TRUE TEMPERATURE		WEIGHTED AVERAGE	UNWEIGHTED AVERAGE	WEIGHTED AVERAGE	UNWEIGHTED AVERAGE
120°K	T	231	251	117.2	123.4
	ΔT	111	131	2.8	3.9
160°K	T	192	251	160.5	168.2
	ΔT	32	91	.5	8.2
200°K	T	216	328	197.0	199.0
	ΔT	16	128	3.0	1.0
240°K	T	242	275	239.9	244.9
	ΔT	2	85	.1	4.9
280°K	T	280	340	282.0	284.7
	ΔT	0	60	2.0	4.7
320°K	T	318	369	318.3	318.0
	ΔT	2	49	1.7	2.0
360°K	T	359	392	360.1	358.9
	ΔT	1	32	.1	1.1
400°K	T	398	388	399.9	395.3
	ΔT	2	12	.1	5.3
	Average ΔT	21°	67°	1.35°	3.9°

TABLE 1

TRUE TEMPERATURE	N.E.S.P.D.	RATIO METHOD: HIGH NOISE LEVEL 200 $\mu W/cm^2 \mu$ WEIGHTED AVERAGE	HIGH NOISE LEVEL UNWEIGHTED AVERAGE	COADDING 100 TIMES LOW NOISE LEVEL 20 $\mu W/cm^2 \mu$ WEIGHTED AVERAGE	COADDING 100 TIMES LOW NOISE LEVEL UNWEIGHTED AVERAGE
120°K	T	132	141	129.0	138.0
	ΔT	12	21	9.0	18.0
160°K	T	164	185	162.1	166.8
	ΔT	4	25	2.1	6.8
200°K	T	237	210	207.9	207.0
	ΔT	37	10	7.9	7.0
240°K	T	240	247	245.9	262.1
	ΔT	0	7	5.9	22.1
280°K	T	264	263	279.9	284.7
	ΔT	4	3	.1	4.7
320°K	T	335	316	323.1	326.5
	ΔT	15	4	3.1	6.5
360°K	T	361	331	361.5	365.2
	ΔT	1	29	1.5	5.2
400°K	T	409	400	400.4	403.8
	ΔT	9	0	.4	3.8
	Average ΔT	10.2°	12.3°	3.7°	9.2°

TABLE 2

This section on simulation graphically demonstrates the improvements one can expect by using ratioed results compared with straight forward blackbody calculations. In addition, weighted data as a function of anticipated or actual S/N per resolution element is also seen to significantly improve the results. Also of significance is that the technique of calculation actually represents a noisy synthesized signal reduced to yield the temperature information it contains.

Non-Constant ϵ Computations

Some thought has been given to the most general class of spectra, those with non-constant ϵ. We may limit the investigation to smoothly, and most likely, monotonically varying ϵ. If we calculate the temperature using the ratio method with two wavelengths which are fairly close together; or better, using all the available wavelengths in a small interval to get an average, we might then use Planck's equation in the form:

$$I_{measured} = \frac{c_1 \epsilon}{\lambda^5 \left(e^{\frac{c2}{\lambda T}} - 1\right)} \tag{15}$$

to obtain estimates for ϵ.

We invert to get

$$\epsilon = \frac{I_{meas} \lambda^5 \left(e^{\frac{c2}{\lambda T}} - 1\right)}{c_1} \tag{16}$$

If we can do this for a range of wavelength intervals, we might then obtain ϵ as a function λ. A check on the results of such calculations would be a plot of T vs. λ' for each fixed λ both before and after use of the estimate for ϵ. If the T's calculated, taking variations in ϵ into account lie closer to the line through the temperatures calculated for λ' within a small interval around λ for a significant range of λ, then we have reason to trust our estimate of ϵ.

However, we can see from the graphs included in Appendix 4 that the fixed λ used should lie in an area of good signal to noise since there is a ridge of poor temperature accuracy along the $\lambda = \lambda'$ line.

Discussion of Necessary Instrument

The sensitivity of temperature calculations to noise in radiance measurements and the small available volume for the instrument dictate the use of an interferometer spectrometer. The analysis of a suitable Michelson interferometer below explains the signal to noise advantage of an interferometer over dispersion instruments.

Theory of Operation of an Interferometer

The interferometer spectrometers built by Block Associates, Inc. utilize the Michelson optical system. (Optical ray traces are shown in Figure 1). S is a semi-reflective mirror (called a beamsplitter) which reflects 50% of the light which strikes it and permits the other 50% to pass. M_1 and M_2 are mirrors which reflect all the light which reaches them; they are identical except that M_1 can be displaced a distance Δx.

If a light beam enters as shown, 50% of it will pass through the beamsplitter and continue toward M_1 while the other 50% will be reflected toward M_2. Upon reaching mirrors M_1 and M_2, each fractional half of the original energy will be completely reflected back toward the beamsplitter. Upon striking the beamsplitter the portion of the light transmitted to the detector and the portion of the light lost from the interferometer depend on the relative phases of the recombined rays in the exit and detector legs of the interferometer. For example, let us determine these phases for the case where the optical distances in legs M_1 and M_2 are equal and the splitter is an ideal metal film. When the input radiation beam encounters the metal splitter, the reflected ray to leg M_2 is phase shifted by an increment of π and the transmitted beam to leg M_1 by $\pi/2$. When the beams return to

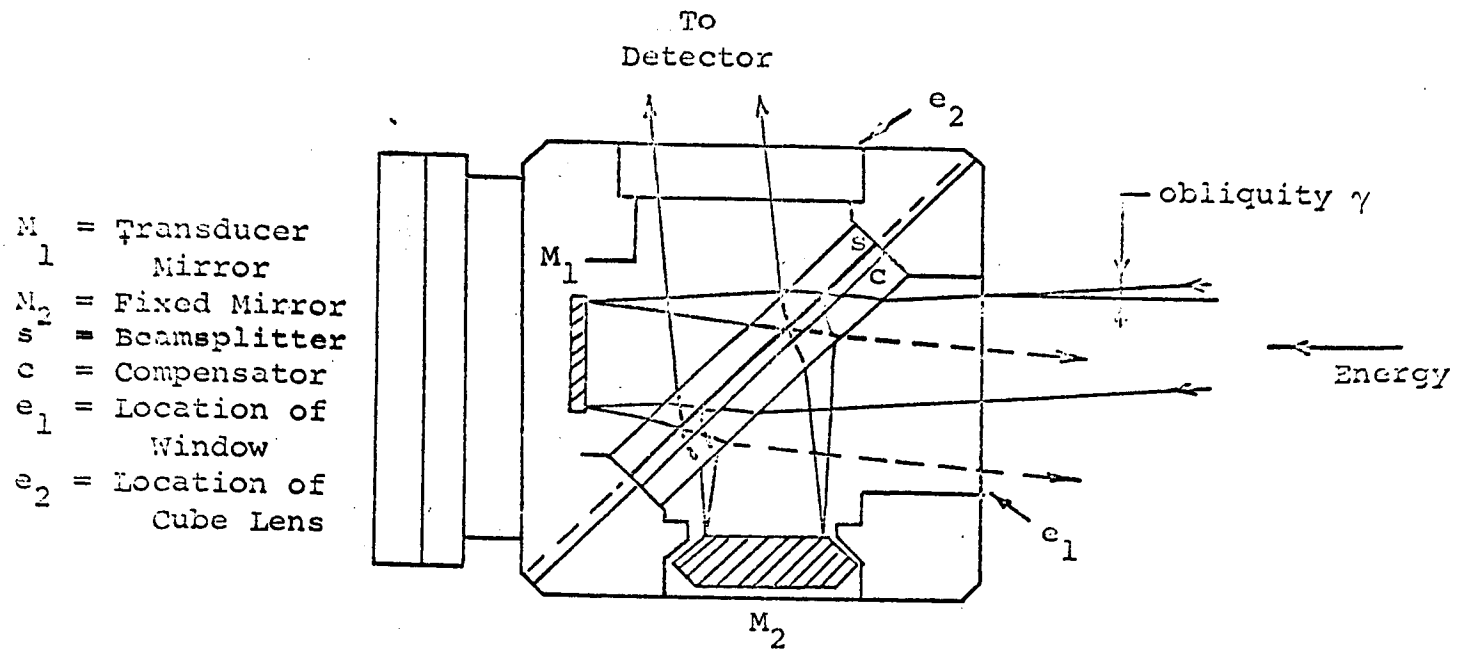

Figure 2a.
Path of an Oblique
Parallel Bundle.

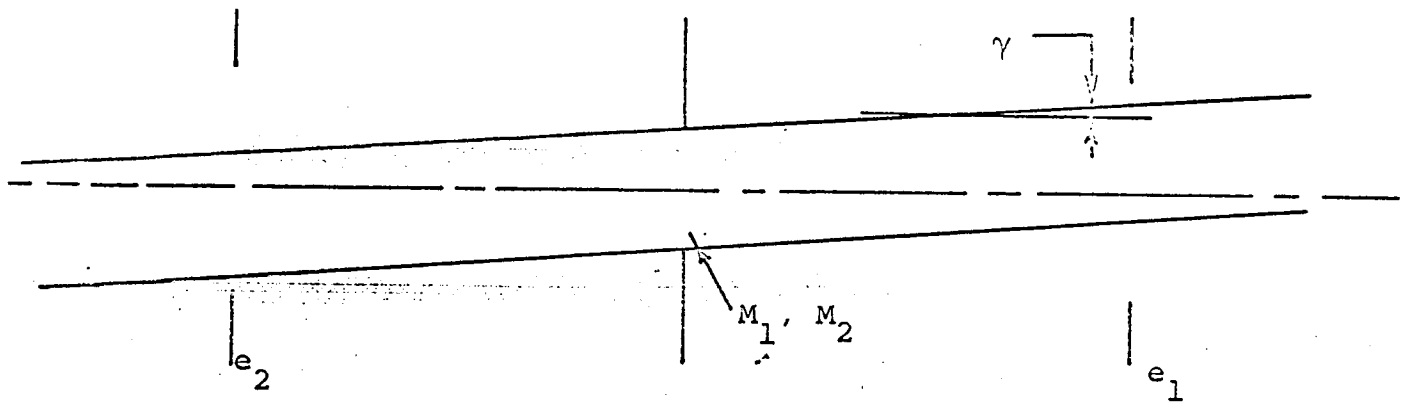

Figure 1

Optical Equivalent to Show Ray Paths

the splitter, the light transmitted toward the detector from leg M_2 is transmitted with a second incremental shift of $\pi/2$ and the ray from leg M_1 with a shift of π. The sums of the phase shifts of the rays in both legs are $3\pi/2$ and, being equal, the waves reinforce each other. On the other hand, the exit ray from the spectrometer requires the ray from leg M_2 to be reflected again with a second shift of π and the ray from leg M_1 to be transmitted with a shift of $\pi/2$. The sum of the phase shifts in leg M_2 is 2π and in leg M_1 is π. Since the rays in this case differ in phase by an increment of π, there is destructive interference. The result of this is that all the light entering the spectrometer when the legs are of equal length is transmitted to the detector, this producing a bright central fringe.

This explanation is somewhat simplified since it does not account for effects such as absorption, but the same general argument holds in a more rigorous treatment. The same treatment is also valid for Michelson interferometers which use dielectric beamsplitters, (e.g., a thin germanium film), except that the phase changes are difference with the result that the central fringe is black fro zero retardation.

As we have just seen, when the optical path lengths of the M_1 leg and the M_2 leg are equal, all of the original light energy which reaches the detector via route M_1 is in phase with that arriving via route M_2. If, however, we cause the M_1 mirror to be displaced an amount Δx, we find that the phase of the light arriving at the detector via route M_1 is retarded by an amount $2\ \Delta x$ from that arriving via route M_2. For monochromatic light of wavelength λ, a displacement $\Delta x = \lambda/4$ will cause a retardation of $2x = 2\lambda/4 = \lambda/2$. The two equal amplitude light fractions will

therefore reach the detector an increment of π out of phase, cancellation will result, and the net signal of wavelength λ to the detector will be zero. The detector signal will, in fact, be zero for all displacements Δx which are odd multiples of $\lambda/4$ ($\pm \lambda/4$, $\pm 3\lambda/4$, $\pm 5\lambda/4$, etc.) and will be equal to the total input energy (minus absorptions) for all even multiples of $\lambda/4$ beginning with zero (0, $\pm \lambda/2$, $\pm \lambda$, $\pm 3/2\lambda$, $\pm 2\lambda$, etc.), where the plus and minus signs denote displacements on both sides of zero retardation corresponding to increased or decreased optical path lengths (retardations) respectively.

If the displacement of mirror M_1 is slowly changed, we find that the energy at the detector goes through a series of maxima and minima (light and dark "fringes") as the retardation of the optical path lengths of the two legs differs by integral numbers of wavelengths, according to the expression

$$I = 0.5\ I_o\ (1 + \cos 2\pi\ \nu\ Bt/T) \qquad (17)$$

where ν is the wavenumber of the incident radiation in cm^{-1}, and $Bt/2T$ is the instantaneous displacement, x, of the mirror moving a distance B/2 in time T. In other words, the frequency of the energy transmitted to the detector is a joint function of the wavenumber of the input radiation and the mirror velocity B/2T.

Since the optical retardation, B, is twice the mirror displacement, then,

$$f_\nu = 2 \cdot \nu \cdot \frac{B}{2T} = \nu \cdot \frac{B}{T} \qquad (18)$$

Increased mirror velocity yields higher output frequencies.

In an interferometer the movable mirror is mounted on the armature of an electromagnet and is displaced by changing the

d.c. current through the armature. Figure 3 is a plot of the mirror position in time showing the linear mirror displacement.

Clearly, the audio frequency range to which the incident radiation is heterodyned can be changed by varying the sweep velocity. For instance, if T is halved while B is kept the same, the resulting audio frequency (for a given monochromatic input) will double. Also, if two (or more) light frequencies are present in the input radiation, there will be two (or more) uniquely corresponding audio frequencies present in the audio output spectrum.

The capability of a practical instrument to resolve two neighboring frequencies is specified in terms of the smallest increment of wavelength, $\Delta\lambda$, which can be distinguished at the output (or alternatively, in terms of wavenumber, $\Delta\nu$). It can be shown that the limit of spectral resolution is a constant dependent only on the maximum internal retardation, B, according to $\Delta\nu = K/B$ where K is determined by the amount of refraction at the entrance aperture. For our instrument, K = 1, approximately, so that $\Delta\nu = \frac{1}{B}$.

Since the interferometer looks at all component frequencies of the spectrum of interest all the time instead of one small wavelength bandpass at a time as with conventional monochromators, it is apparent that the interferometer offers an advantage in its more efficient use of the scan time interval. Reference 1 discussed this advantage as follows: "A simple argument allows one to prodict the order of magnitude of gain that can be expected. If with an exploring dispersive <u>spectrometer</u> it is desired to measure M spectral elements during time T, each element is observed during time T/M; with a spectrograph or a multiplex method, each element is observed during the whole time T. In the case where

the fluctuations have a spectrum of uniform frequency and where the background noise is not increased by the simultaneous arrival of all spectral elements, the precision varies as the square root of the exploration time. The gain in sensitivity is therefore of the order of $\sqrt{M}$. Hence, in the infrared where photon noise is negligible compared with receiver noise, the spectroscopic method using Fourier transformation is the most powerful, no matter what may be the desired resolution, and it is all the more interesting because the spectrum studied contains more spectral elements. This gain in sensitivity can be expressed in several ways:

--the signal/noise ratio can be multiplied by $\sqrt{M}$ if the duration of the measurement is the same as in the classical method;

--for equal signal/noise ratio, the duration of the measurement is divided by M;

--finally, for a given s/n ratio and measurement time, one can obtain an increase in resolution and thus treat some problems inaccessible by any other method."

In general, interferometer spectrometers are run as d.c. systems: that is, the input is not chopped and rectified but rather the scanning of the interferometer modulates the frequency of the signal which is picked up by the detector. The response time constant of the detector sets an upper bound to the rate T^{-1} at which the instrument may be scanned for any given ν maximum according to $f\nu = \nu B/T$. Problems of the detector drift and of time variation of the target radiation set a lower bound. In general, it is found that optimum scan rates fall within the range of 0.5 to 8 sec^{-1}.

The interferometer has a size advantage as well over comparably sensitive dispersive instrument due to the use of a large aperture hole rather than flux-limiting slits; it intercepts more spectral power from the target. In particular, if the target fills the field of view, the collected spectral power P is independent of the distance from the source and is a function only of the aperture stop and focal ratio of the optical system. This function is called through (θ) and is equal to the product of acceptance solid angle (Ω) and the aperture stop area (A),

$$\theta = A\ \Omega$$

In the interferometer spectrometer the aperture stop is typically about 200 mm^2 whereas the aperture stop (slit area) of a comparable dispersive instrument would be on the order 2 mm^2. Moreover, the interferometer's focal ratio is f/3.8, rather fast for a dispersive instrument, which would by typically f/6, a factor in solid angle of about 3. Together, these given the interferometer an advantage in throughput (and hence in signal to noise ratio) of from 100 to 1000. This, added to the above discussed advantage (in the instrument noise limited case) of $\sqrt{M}$ where M is the number of resolution elements, usually on the order of 100, will yield an overall advantage of 10^3 to 10^4 in signal to noise in one scan over a comparable dispersive instrument. A classical method of achieving increased sensitivity is to scan slower, i.e. to increase the system's time integration. Since this is impractical in the interferometer spectrometer, a special purpose time averaging computer has been designed (called a "Coadder") which samples the input interferogram repeatedly, at a rate which, for meaningful results, should be more than twice

TEMPERATURE ACCURACY AND PROBE REQUIREMENTS

FINAL REPORT

Prepared By

Gerald Auth

Approved By

A.L. Lavery

Prepared Under

Purchase Order 39705

Account Number 46219

Submitted To

TEXACO EXPERIMENT INC.

P. O. BOX 1-T

RICHMOND, VIRGINIA 23202

7 February 1966

Submitted By

BLOCK ENGINEERING, INC.
19 Blackstone Street
Cambridge, Massachusetts 02139

Appendix II

TEMPERATURE ACCURACY AND PROBE REQUIREMENTS

LUNAR EXPERIMENT LIST

A. MAGNETIC MEASUREMENTS

1. Components of Field

   a. Total intensity
   b. Vertical intensity
   c. Horizontal intensity
   d. Declination
   e. Horizontal gradient
   f. Vertical gradient

2. Instruments

   a. Flux-gate magnetometer
   b. Proton precessional magnetometer (Varian)
   c. Rubidium vapor magnetometer (Varian)
   d. Modified Magnetron (Arnoux Corp.)
   e. Metastable Helium Magnetometer (T.I.)

3. Subsurface Magnetic

B. GRAVITY MEASUREMENTS

1. Gravity Component

   a. Single point measurement
   b. Gravity surveys
   c. Relative acceleration
   d. Vertical gradient
   e. Horizontal gradient
   f. Geodetic
   g. Downhole measurement
   h. Absolute

2. Instrumentation

a. Gravimeter
b. Vertical gradiometers
c. Torsion balances
d. Pendulums
e. Tidal gravity meters
f. Falling weight

C. SEISMIC MEASUREMENTS

1. Natural
2. Induced

a. Refraction
b. Reflection
c. Sonic velocity

D. ELECTRICAL MEASUREMENTS

1. Surface

a. Resistivity
b. Telluric currents
c. Self potential
d. Equipotential line
e. Induced polarization
f. Inductive field
g. Electromagnetic field intensity (RF antenna, antenna impedance, wave transmission)
h. Magnetic susceptibility
i. Electrostatic potential gradient
j. Spontaneous polarization
k. Potential drop
l. Electromagnetic induction
m. Electromagnetic galvanic
n. Electric field meter
o. Dielectric constant

2. Subsurface

a. Induction log

b. Magnetic susceptibility
c. Scratcher type

(1) Spontaneous potential
(2) Resistivity (normal and lateral)
(3) Resistivity (laterlog)
(4) Resistivity (microlog)
(5) Resistivity (microlaterlog)

d. Induced polarization
e. Permittivity
f. Dipmeter
g. Self potential

E. NUCLEAR MEASUREMENTS

1. Surface

a. Energetic neutron activation
b. Thermal neutron activation
c. Gamma-gamma (density)
d. Neutron-neutron
e. Natural radioactivity (alpha, beta, gamma)
f. Gamma ray spectrometer
g. Charged particle spectrometer
h. Alpha particle mass spectrometer
i. Alpha and proton backscattering spectrometer
j. X-ray diffractometer
k. X-ray fluorescence spectrometer
l. Alpha activation
m. Deuteron activation
n. Radioactive dating
o. Neutron phoswich detector
p. Radiological equipment

(1) Integrating personal dosimeter
(2) Portable survey dose rate meter

q. Solar and cosmic radiation

(1) Solar X-rays

(2) Solar plasma spectrometer
(3) Solar winds
(4) Solar flares
(5) Solar energetic particles
(6) Heavy primary cosmic rays

r. Secondary radiation (neutrons from surface, etc.)

2. Subsurface

a. Conventional (natural) gamma
b. Spectra gamma
c. Conventional neutron
d. Neutron-neutron
e. Gamma-gamma
f. Neutron activation
g. Natural alpha and beta

F. THERMAL AND RADIATION SPECTRA

1. Surface

a. Infrared absorption and reflectance surveys
b. Temperature
c. Thermal conductivity
d. Heat flux measurements
e. Thermal diffusivity and thermal inertia
f. Differential thermal analysis
g. Heat flow
h. Single crystal IR probe (water detector)
i. Visible, IR, UV Spectrometer

2. Subsurface Thermal

a. Thermal conductivity
b. Heat flow from interior
c. Permanent and semi-permanent temperature probe
d. Temperature

(1) Mercury-in-glass thermometer
(2) Thermocouple

(3) Resistance thermometer
(4) Thermistor
(5) Quartz crystal
(6) Nuclear resonance

G. ATMOSPHERIC PRESSURE AND GAS ANALYSIS

1. Gas Pressure

   a. Neutral particle pressure
   b. Total ion concentration
   c. Directed ion flux
   d. Ion mass spectrum
   e. Total gas pressure
   f. Redhead pressure gage

2. Mass Spectrometer

   a. Magnetic
   b. Quadrupole
   c. Time-of-Flight
   d. Coincidence time-of-flight

3. Gas Chromatograph

H. SOIL MECHANICS AND SOIL PROPERTIES

1. Bearing Strength
2. Penetration Resistance
3. Shear Strength
4. Porosity
5. Permeability
6. Texture
7. Drillability
8. Density

I. METEROID DETECTION (ENERGY, MOMENTUM, FLUX)

1. Primary
2. Secondary

K. TELEVISION AND PHOTOGRAPHY (REGULAR AND IR)

L. BOREHOLE CALIPER

M. WET CHEMICAL ANALYSIS

N. CLASSICAL AND RADIO ASTRONOMY

O. BIOSCIENCE AND BIOENGINEERING

1. Physiologic Performance
2. Psychomotor Performance
3. Dimensional Studies
4. Organic Chemistry
5. Microbiological

P. MISCELLANEOUS EXPERIMENTS

1. Chemical Reactivity Detector
2. Atomic Absorption
3. Hydrogen Lyman-alpha Detector
4. Photometric Albedo and Polarization
5. Spectrophotometer